

**THESE DE DOCTORAT DE L'ETABLISSEMENT UNIVERSITE BOURGOGNE FRANCHE-COMTE
PREPAREE A L'UMR 6282 - BIOGEOSCIENCES**

Ecole doctorale n°554

Ecole doctorale Environements-Santé

Doctorat de Géodynamique des enveloppes supérieures

Par

M. Perron Paul

Tectonique et architecture des bassins intracratoniques Paléozoïques :
Impact sur l'enregistrement sédimentaire et la géométrie des réservoirs associés.
Exemple de la marge Nord Gondwanienne

Thèse présentée et soutenue à Dijon le 27/06/2019

Composition du Jury :

Mme Moretti Isabelle	Chercheur associé, Université de Pau, Sorbonne Université	Président
Mr Cloetingh Sierd	Professeur, Université d'Utrecht	Rapporteur
Mr Eschard Rémi	Ingénieur géologue, TOTAL	Rapporteur
Mr Portier Eric	Ingénieur réservoir, NEPTUNE Energy	Examinateur
Mme Le Pourhiet Laetitia	Professeur, Sorbonne Université	Examinatrice
Mr Guiraud Michel	Professeur, Université de Bourgogne Franche-Comté	Directeur de thèse
Mme Vennin Emmanuelle	Professeur, Université de Bourgogne Franche-Comté	Codirecteur de thèse
Mr Pagnoux Bruno	Ingénieur réservoir, NEPTUNE Energy	Invité

UNIVERSITÉ DE BOURGOGNE FRANCHE-COMTE

UFR Sciences Vie Terre Environnement
École doctorale Environnement Santé

THÈSE

Pour l'obtention du grade de

Docteur de l'Université de Bourgogne Franche-Comté

Discipline : SCIENCES DE LA TERRE - GÉOLOGIE

par

Paul PERRON

-2019-

**Tectonique et architecture des bassins intracratoniques
Paléozoïques : Impact sur l'enregistrement sédimentaire et la
géométrie des réservoirs associés.
*Exemple de la marge Nord Gondwanienne***

**Architecture and tectonic of Paleozoic intracratonic Basins: Impact on the
sedimentary record and associated geometries. Example of peri-Hoggar
Basins (North Gondwana marge)**

Composition du jury :

Isabelle MORETTI (chercheur associé, Sorbonne Université)	Présidente
Sierd CLOETINGH (professeur, Université d'Utrecht)	Rapporteur
Rémi ESCHARD (ingénieur géologue, TOTAL)	Rapporteur
Éric PORTIER (ingénieur réservoir, NEPTUNE Energy)	Examinateur
Laetitia LE POURHIET (professeur, Sorbonne Université)	Examinatrice
Michel GUIRAUD (professeur, UBFC)	Directeur de thèse
Emmanuelle VENNIN (professeur, UBFC)	Codirectrice de thèse
Bruno PAGNOUX (ingénieur réservoir, NEPTUNE Energy)	Invité



ABSTRACT

The Paleozoic Saharan platform including the peri-Hoggar Basins (i.e. Murzuq, Illizi, Mouydir, Ahnet, Reggane and Tim Mersoï basins) are defined as intracraonic basins. Their histories have been dominated by slow long-wavelength vertical motions leading to overall low subsidence rate (i.e ca. 10 m/Ma to 50 m/Ma) and accumulation of an extensive cover of platformal sediments (i.e. shallow deposits environments), rhythmized by pulsatile periods of increasing and decreasing rate probably triggered by regional geodynamic events. The vertical motions of the platform produced several arches also called domes, swells, highs, ridges (e.g. the Tihemboka, Amguid El Biod, Arak-Foum Belrem and Azzel Matti Arches) and basins (syncline-shaped) with different wavelengths going from several hundred to more than a thousand kilometres. The persistence of a rather uniform pattern of vertical motions seems to control the architecture of the basins indicating a large-scale control (i.e. lithospheric). This latter controls spatially and temporally the deposition and the erosion dynamics. Several major erosion events significantly truncated the pre-existing sediments over wide areas, producing regional unconformities, especially restricted and amalgamated on arches, which separate the platformal cover into divisions. Through an original multidisciplinary integrated approach going from a geological basin analysis, coupling the substrate and the basin architecture to a numerical thermo-mechanical modelling of the lithosphere, this study has led to decipher the forcing factors of the intracratonic basins of the Saharan platform.

The Arches-Basins architecture is highlighted through the identification of tectono-sedimentary structures (growth strata, truncatures...). This architecture is featured by thickness variation and facies portioning, organized by sub-vertical planar normal faults (sometimes blind faults) forming horst-graben systems associated with forced folding in the cover. Connected and nucleated to major mega-shear zones, horst-graben systems are inverted (positive inversion) or reactivated (forced folds) during successive geodynamic events (e.g. Cambro-Ordovician extension, Ordo-Silurian glacial rebound, Siluro-Devonian "Caledonian" extension/compression, late Devonian extension/compression and "Hercynian" compression).

Formed under a Precambrian lithosphere of accretionary type, inherited during several paleo-orogenies (e.g. Eburnean, Pan-African), a substrates zonation of the Arches-Basins framework is described, where the Archean to Paleoproterozoic terranes are forming the structural highs and the Meso-Neoproterozoic terranes the structural lows.

Based on these geological observations and the hypothesis of conserved differential densities (implying an isostatic potential) between the inherited different accreted terranes in the lithosphere (i.e. archean and proterozoic terranes), a 2D thermo-mechanical numerical model is proposed. The first and second order forcing factors, respectively recorded in the subsidence rate pattern by the low long-lived and by their cyclic deviations, are well constrained reconciling the singular Arches-Basins tectono-stratigraphic architecture. The different simulations have shown the importance of thermal anomaly, tectonics (weak strain rate) and external sediment supply on the dynamic of these intracratonic basins. Where, sediment flux controls the speed and the duration of basin infill until achievement of the isostatic equilibrium. The thermal anomaly and the tectonics compel the tectono-stratigraphic complexification such as the arches framework (intra-arches, boundary secondary arches...) and the stratigraphy architecture (wedges, diachronic unconformities).

Furthermore, by comparing the basins architecture and the signature of the subsidence and the thermal pattern between numerical model and geological data from peri-Hoggars Basins, we see that all the forcing parameters associated can be linked to geodynamic events such as glaciation/deglaciation, global warming, rifting, intra-plate volcanism, and local deformation, probably triggered by far field stresses.

Finally, an original classification is proposed based on the best fit of each peri-Hoggars Basins with different thermomechanical numerical models and their forcing factors dominance (tectonics dominated, thermal anomaly dominated, sediment flux dominated and/or different combination of these latter).

Keywords: Saharan platform, peri-Hoggars Basins, Arches-Basins, Precambrian structural heritages, lithosphere heterogeneity, terranes, thermo-mechanical, far field stresses, density, potential isostatic equilibrium.

RESUME

La plate-forme Saharienne paléozoïque, comprenant les bassins péri-Hoggar (Murzuq, Illizi, Mouydir, Ahnet, Reggane et Tim Mersoï) sont définies comme des bassins intracratoniques. Ils ont été dominés par des mouvements verticaux lents et à grande longueur d'onde, conduisant à de faible vitesse de subsidence (c'est-à-dire environ 10 m/Ma à 50 m/Ma) et à l'accumulation d'une couverture sédimentaire étendue de type plate-forme (environnements de dépôts peu profonds), rythmée par des périodes pulsatiles d'augmentation et de diminution du taux de subsidence probablement déclenchées par des événements géodynamiques régionaux. Les mouvements verticaux de la plate-forme ont créé plusieurs arches également appelés dômes, paléo-topographies (par exemple les arches de la Tihemboka, d'Amguid El Biod, d'Arak-Foum Belrem et de l'Azzel Matti) et des bassins (en forme de synclinal) de différentes longueurs d'onde allant de plusieurs centaines à plus de milliers kilomètres. La persistance d'un ensemble assez uniforme de mouvements verticaux semble contrôler l'architecture des bassins, ce qui semble indiquer un contrôle à grande échelle (i.e. lithosphérique). Ce dernier contrôle spatialement et temporellement la dynamique sédimentaire de dépôt et d'érosion. Plusieurs périodes d'érosion majeures ont considérablement tronqué les sédiments préexistants sur de vastes zones, produisant des discordances régionales, restreintes et amalgamées sur les arches, qui séparent la couverture sédimentaire de la plateforme. À travers une approche intégrée multidisciplinaire originale allant d'une analyse géologique de bassin, associant le substrat et l'architecture de bassin à une modélisation thermomécanique numérique de la lithosphère, cette étude a permis de décrypter les facteurs de forçage des bassins intracratoniques de la plate-forme saharienne (bassins péri-Hoggar).

L'architecture en Arches-Bassins est mise en évidence par l'identification de structures tectono-sédimentaires (onlap divergents, troncatures...). Cette architecture se caractérise par des variations d'épaisseur et des partitionnements de faciès, organisés par des failles normales planes sub-verticales formant des systèmes d'horst-graben souvent associés à des plis forcés dans la couverture. Connectés et nucléés aux grandes zones de méga-cisaillement, les systèmes d'horst-graben sont inversés (inversion positive) ou réactivés (plis forcés) au cours d'événements géodynamiques successifs (par exemple : extension cambro-ordovicienne, rebond glaciaire ordo-silurien, extension/ compression Siluro-Dévonien «Calédonienne», extension/compression du dévonien tardif et compression «hercynienne»).

Formée sous une lithosphère précambrienne de type accrécionistaire héritées de plusieurs paléorogénèses (e.g. Eburnéenne, Panafricaine), une zonation des substrats sous l'architecture en Arches-Bassins est observée : Les terranes Archéen à Paléoprotozoïque se situent sous les hauts structuraux et les terranes méso-néo-protozoïques sous les dépressions.

Sur la base de ces observations géologiques et de l'hypothèse de densités différentielles conservées (impliquant un potentiel isostatique) entre les différents terranes accrétées héritées (i.e. les terranes archéennes et protozoïques) dans la lithosphère, un modèle numérique thermo-mécanique 2D est proposé. Les facteurs de forçage du premier et du second ordre, respectivement caractérisés par de faible taux de subsidence et par leurs déviations cycliques pendant de longues durées (250 Ma), sont bien contraint par le modèle réconciliant aussi l'architecture tectono-stratigraphique singulière en Arches-Bassins. Les différentes simulations ont montré l'importance des anomalies thermiques, de la tectonique (faible taux de déformation) et de l'apport externes en sédiments sur la dynamique de ces bassins intracratoniques. Le flux sédimentaire contrôle la vitesse et la durée de remplissage du bassin jusqu'à l'équilibre isostatique. L'anomalie thermique et la tectonique entraînent la complexification de l'architecture stratigraphique des bassins (onlaps divergents, discordances diachroniques) mais aussi tectonique avec la mise place de structures tels que des arches intrabassins et des arches secondaires bordières inter-bassins...

Par ailleurs, en comparant l'architecture des bassins, la signature thermique et les courbes de subsidence entre les modèles numériques et les données géologiques des bassins péri-Hoggar, nous voyons que tous les paramètres de forçage associés peuvent être liés à des événements géodynamiques tels que les glaciations/déglaciations, réchauffement global, rifting, volcanisme intra-plaque et déformation locale, probablement provoqués par des contraintes de champ lointain.

Finalement, une classification originale est proposée basée sur la meilleure correspondance de chaque bassin péri-Hoggar avec différents modèles numériques thermomécaniques et leurs différents facteurs de forçage (à dominance tectonique, à dominance thermique, à dominance flux sédimentaire et/ou combinaison différente de ces derniers).

Mots-clés: Plate-forme saharienne, Bassins péri-Hoggar, Arches-Bassins structures, héritages structuraux précambriens, hétérogénéité de la lithosphère, terranes, thermo-mécaniques, champs de contraintes lointaines, densité, potentiel isostatique.

ACKNOWLEDGMENTS – REMERCIEMENTS

Les remerciements sont sûrement l'une des parties la plus importante du manuscrit, enfin, tout au moins la plus lue. Il s'agirait donc de ne pas se louper... Un exercice difficile, donc s'il y a des oublis ou des maladresses, j'espère que vous ne m'en tiendrez pas trop rigueur. Ceci dit, il ne me reste plus qu'à commencer :

Tout d'abord, je souhaite remercier les différents rapporteurs **Sierd Cloetingh** et **Rémi Eschard** d'avoir accepté de rapporter mon travail et de faire partie de mon jury de thèse. C'est une chance de pouvoir faire apprécier son travail par des spécialistes dans leurs domaines que cela soit sur la modélisation thermomécanique ou la géologie de l'Afrique du Nord...

Je tiens à remercier très vivement **Michel Guiraud** pour avoir accepté de m'encadrer dans le cadre de cette thèse. Il fut tout au long de ces années (du master 2 à la thèse), d'un très grand soutien et d'une aide précieuse sur de nombreux aspects. Ce n'est pas peu dire que sans Michel, je ne serais pas là aujourd'hui. Sa vision globale, intégrative et novatrice de la géologie m'a toujours apparu passionnante. Sous ses explications tout apparaît simple (malgré la complexité) et marcher « diaboliquement » bien. Même s'il y a encore du travail, il m'a permis de devenir le géologue que je suis aujourd'hui. J'ai pu améliorer mes connaissances en géologie de bassin et sur bien d'autres domaines (rigueur etc...). Je remercie aussi très chaleureusement **Emmanuelle Vennin** d'avoir également accepté de m'encadrer dans cette thèse. Elle m'a été d'une très grande aide et soutien durant ces années. Emmanuelle fut toujours compréhensive et disponible tout au long des diverses problématiques rencontrées. Grâce à elle, j'ai grandement amélioré mes connaissances en sédimentologie, stratigraphie séquentielle et bien d'autres domaines. En définitive, je ne remercierai jamais assez Michel et Emmanuelle pour leur gentillesse et leur accompagnement... Je leur serai toujours reconnaissant...

Un grand merci à **Eric Portier** pour son encadrement, son soutien, sa bonne humeur et son aide qu'elle soit technique ou humaine depuis que l'on se connaît. Nous avons souvent eu des discussions captivantes (scientifiques ou non) sur de nombreux sujets (en lien ou non avec la géologie). Eric a toujours été un chercheur passionné de géologie dans le corps d'un ingénieur. Je suis heureux de voir qu'aujourd'hui il est pleinement les deux. Même si notre grande déception restera à tous les deux de n'avoir pas pu faire du terrain, j'espère qu'un jour nous

pourrons aller voir ensemble ces magnifiques falaises (glaciaire...) du Tassili en Algérie ou tout du moins au Maroc. Parce que Google Earth est un outil génial mais ne suffit pas. Je remercie également **Isabelle Moretti** d'avoir également accepté de m'encadrer tout au long de ma thèse. Merci pour son soutien et son aide, notamment au cours de la modélisation numérique thermomécanique de mes bassins. Les diverses discussions scientifiques à ce sujet ont grandement participé à une meilleure compréhension des différentes problématiques. Pour finir, je remercie fortement Isabelle et Eric pour m'avoir fait confiance et de m'avoir accueilli chaleureusement dans les bureaux d'ENGIE... Par l'intermédiaire de ces deux personnes, c'est également l'entreprise Netptune Energy que je tiens à remercier pour le financement des recherches entreprises pendant ces années de thèse.

Un très grand merci à **Laetitia Le Pourhiet** d'avoir également accepté de m'encadrer après la tragique disparition de **Evgueni Burov** en début de thèse. Je la remercie également de son accueil dans le laboratoire de l'ISTEP de Sorbonne Université. Elle fut une personne majeure et déterminante, notamment sur la modélisation numérique thermomécanique. Sa vision de la modélisation et de la géologie est captivante et bien loin de ce que j'imaginai en premier lieu. Moi qui ne savais rien, merci d'avoir grandement contribué à devenir l'apprenti « modélisateur » que je suis aujourd'hui (même s'il y a encore beaucoup de travail). Merci pour sa bonne humeur, son aide, ses conseils et tant d'autres choses précieuses qui au cours de ces années m'ont permis d'avancer. J'ai toujours apprécié nos discussions scientifiques ou non autour d'un verre ou d'un kebab...

Je voudrais aussi remercier grandement **Mary Ford** et **Olivier Bourgeois** qui ont accepté de faire partie de mon comité de thèse pendant ces années. Leurs observations et discussions m'ont permis de mieux identifier et caractériser les difficultés rencontrées. Cela m'a permis de mieux contraindre et orienter mon sujet. Je les remercie pour leur regard extérieur sur mon sujet qui fut d'une aide précieuse.

Je remercie l'ensemble des membres du **département E&P et NA d'Engie** (nouvellement Neptune) pour leur aide et leur soutien technique tout au long de ma thèse. Je remercie spécialement l'ensemble des data managers pour leur aide afin d'acquérir, traiter etc... les diverses données sismiques et puits. Je remercie aussi **Guy Desaubliaux** pour les discussions géologiques et la bibliographie sur l'Algérie. Merci aussi à **Marie Sarre** et **Aurèlie Galvani**.

Mes remerciements s'adressent également à tous les membres du **laboratoire Biogéosciences**, enseignants chercheurs et **personnels de l'UMR** que j'ai pu côtoyer tout au long de ces années à l'Université de Bourgogne. Merci pour les diverses discussions mais aussi pour les différentes aides.

Je remercie également les membres du personnel **Sayens**, notamment **Julie Parel**, **Cécile Pélissier**, **Frédérique Dementin** et **Odette Heisler** pour leurs différentes aides (administratives, commandes, frais de mission...). Je tiens à remercier tout particulièrement **Catherine Guillemin** pour son aide et son soutien sans qui je ne serais pas là...

Pour finir, je tiens à remercier tous les amis (Dijonnais, Parigos, Montpelliérain, Beauvaisien), les thésards (UB et Jussieu), et la famille (Lamifa) pour leur soutien physico-amico-dermato-anthropo-rigolo-morito-vino-alcool-racletto-pizzailo-etc-chouette tout au long de ces années... Je ferais ici une liste non exhaustive des amis thésards et de master (et plus et affinité) de l'UB que je citerai par désordre chrono-typologique : P-A (15 cm), Titine (la couturière), Didine (la diabolique), Axelle (la Ch'ti biloute), Anthonio (el stromator), Morgane², Paulette, Margot (princesse), Cédric (Aka Sergueï), Salomé (ça pique), Gwénaël (le martien et best co-bureau ever), Fabou, Marco (spaghetti), Aurélie (push up), Estelle (l'américaine), Agathe (de feeling), Elise (Lucet), Etienne, Jessica, Alexandre, Lucie...

Même méthode pour les collègues de Jussieu qui m'ont accueilli charitablement : Benjamin, Manf, Anouk, Sepideh, Max, Julien, Marie, Eloïse, Alexi (pegmatite man), Marianne (la polak), Ella (elle l'a, tu l'as ?), Anthony, Léa, Laurella...

La même mais en mieux (toi-même tu sais) pour les potos qui se demandent ce que je fais à part lécher des « cailloux ». Ils m'ont permis d'égayer notamment mes weekends : Tos (monaute), Tic (o'tacais), LN (petite chatte), Small, Marion (bordel), Co (conuts), Manuelito (Tchi-tchies por la banda), Flow (le roi du camping), Loïc (Anarchie et piraterie), (la grosse) Caro, Paul², Nico (le roi de la rési), Ben (hostis de tabernakle), P-A (15 cm), Alison (milf1), Léna (milf2), Marion (milf3), Val (9c), Albus (2000), Annaëlle (anal), Cha (tertone), Manon (vegano), Bozzal (apèral), Malou, Sophie (chanchan), Sophie (ca), David, Paulette, Amandouce (tête dure), les amis des Lentillères, de Paname city (Brissou, Mathieu, Romain...), de

Montpellier (Manu, Charlotte², Rico, Tcharly, Pico, Aurélie, Josy, Hélène, Béreng, Mathilde...) et d'ailleurs... Et un gros bisou à mon fillot Noé qui grandit à toute berzingue !

Big bisou en scred oklm à ma petite douceur des îles, Claire qui a supporté mes complaints durant la dernière ligne droite (pas tant que ça...) ...

Enfin un dernier petit mot pour ma famille. Merci à tous, et surtout merci à mes parents de m'avoir toujours soutenu dans la « life » et essayer de comprendre ce que je faisais (même si ce n'est pas évident). Merci à ma sœurette Mimidou et à mon frangin Clém (il est ou Paul ?) de me supporter, de m'avoir souvent fourni un toit, à manger ou à boire, lors de mes nombreux squattages à Paname. Et le meilleur pout la fin, un gros bisou à mon petit filleul Léo (el famoso nuevo Perron).

*En face de cet énorme horizon de toutes parts, sans obstacles pour la vue, dominant tout, de l'est à l'ouest, du Sud au nord, montagnes, ville, oasis et désert, que je passe mes meilleures heures, celles qui seront un jour pour moi les plus regrettables. J'y suis le matin, j'y suis à midi j'y retourne le soir ; j'y suis seul et je n'y vois personne... **Eugène Fromentin, Un été dans le Sahara.***

TABLE OF CONTENTS

ABSTRACT	3
RESUME	5
ACKNOWLEDGMENTS – REMERCIEMENTS	7
TABLE OF CONTENTS	11
CHAPTER I. INTRODUCTION AND CONTEXT OF STUDY	17
1 <i>Intracratonic basins main characteristics</i>	21
2 <i>Basin mechanisms and processes of formation</i>	24
3 <i>Arches and Basins architecture and basins wavelengths</i>	25
4 <i>Precambrian heritage of continental lithosphere (Archean to Proterozoic terranes)</i>	29
4.1 <i>Paleo-orogenies and orogenic style: Continental lithosphere assembly</i>	30
4.2 <i>Rheological properties of inherited accretionary lithosphere</i>	34
5 <i>Questions and problematics</i>	36
6 <i>The case of the Paleozoic Saharan platform (peri-Hoggar basins)</i>	37
7 <i>Manuscript construction</i>	38
CHAPTER II. MATERIALS AND METHODS OF AN INTEGRATED MULTIDISCIPLINARY APPROACH	41
1 <i>Characterization of syn-sedimentary structures of Arch-Basin architecture (WPI)</i>	44
1.1 <i>GIS integration of data and software</i>	44
1.2 <i>Geological mapping and satellite images interpretations</i>	44
1.3 <i>Stratal sedimentary geometries and structural style (satellite images and seismic analysis)</i>	45
1.4 <i>Sedimentology, sequence stratigraphy, electro-facies and well correlation</i>	46
1.5 <i>Biostratigraphic calibration and flattening</i>	48
1.6 <i>Backstripping (software and methods)</i>	50

2	<i>Characterization of basement heritage (WP2)</i>	50
2.1	Radiochronological datation compilation	51
2.2	Geophysics and terranes geometries.....	52
3	<i>Lithospheric thermo-mechanical numerical modelling (WP3)</i>	52
4	<i>Comparison with analogues (WP5)</i>	53

CHAPTER III. GEOLOGICAL CONTEXT OF PERI-HOGGAR INTRACRATONIC BASINS (SAHARAN PLATFORM)55

1	<i>Geographic localization of peri-Hoggar Basins</i>	58
2	<i>Geological settings of the Saharan platform</i>	61
2.1	Historical and Previous works	64
2.2	Main characteristics of the Saharan platform.....	67
2.2.1	Paleozoic area.....	67
2.2.2	Sediment thickness and low long-lived subsidence rate.....	67
2.2.3	Main terrigenous sedimentation.....	71
2.2.4	Facies homogeneity.....	71
2.2.5	The NNW paleocurrents of the Saharan platform.....	71
2.2.6	Maturity and homogeneity of the mineralogy.....	72
2.2.7	Major widespread unconformities.....	72
2.2.8	Association of Arches and Basins shape	72
2.3	Structural framework of the Saharan platform.....	73
2.3.1	The West African Craton.....	73
2.3.2	The East Saharan Craton	73
2.3.3	The Tuareg Shield.....	75
2.3.3.1	Western Part (Pharusian)	76
2.3.3.2	Central Part (LATEA)	77
2.3.3.3	Eastern Part	79
2.3.4	Deep geophysic structures of the Saharan lithosphere	82
2.4	Geodynamic and unconformities of the Saharan platform.....	83
2.4.1	The Eburnean Orogeny (c. 2000 Ma).....	83
2.4.2	The Pan-African orogeny (c. 900-600 Ma).....	84
2.4.3	The infra-Cambrian extension and Pan-African collapse (c. 1000-525 Ma)	86
2.4.4	The peneplanation (Infratassilian surface fm.) and start of subsidence (c. 525 Ma)	88
2.4.5	Cambro-Ordovician extension (c. 525-418 Ma)	88
2.4.6	“Taconic” phase (c. 445 Ma)	90
2.4.7	Hirnantian major glaciation (c. 445-444 Ma)	93

2.4.8	Deglaciation and isostatic rebound (c. 444 Ma).....	94
2.4.9	Silurian subsidence (c. 444-418 Ma).....	96
2.4.10	Early Devonian Caledonian compression (418-398 Ma)	96
2.4.11	Middle to Late Devonian extension (c. 398-359 Ma)	101
2.4.12	The early Pre-Hercynian compression (c. 359-305 Ma).....	103
2.4.13	The Carboniferous-Early Permian Hercynian Orogeny (c. 305-270 Ma).....	103
2.4.14	Mesozoic extension: Tethys and Atlantic opening (c. 270-130 Ma).....	106
2.4.15	Alpine and Austrian orogeny (c. 130-23 Ma).....	106
2.4.16	Eocene-Miocene uplift (c. 35-23 Ma to present day).....	107
2.5	Basin heat flow and thermal activity of the Saharan basins.....	108
2.6	Paleozoic sedimentary, stratigraphic and biostratigraphic context.....	109
2.6.1	The infra-Cambrian molasses series.....	112
2.6.2	The fluvio-conglomerates Cambrian series	112
2.6.3	The fluvial to marine of pre-glacial Ordovician series.....	112
2.6.4	The syn-glacial Ordovician series	113
2.6.5	The Silurian marine series	115
2.6.6	The fluvial to marine series of Lower Devonian (Lochkovian to Emsian).....	115
2.6.7	The carbonates marine series of Middle Devonian (Eifelian and Givetian)	116
2.6.8	The marine series of Upper Devonian (Frasnian and Famennian).....	116
2.6.9	The Carboniferous deltaic to marine series	117
2.6.10	Biostratigraphic data and zonation.....	117
2.7	Petroleum systems.....	120
2.8	Evidence of tectono-sedimentary structures from bibliography.....	120
3	<i>Conclusion</i>	123

CHAPTER IV. INFLUENCE OF BASEMENT HETEROGENEITY ON THE ARCHITECTURE OF LOW SUBSIDENCE RATE PALEOZOIC INTRACRATONIC BASINS (REGGANE, AHNET, MOUYDIR AND ILLIZI BASINS, HOGGAR MASSIF)

125

1	<i>Summary and objectives</i>	127
2	<i>Reminder of some concepts for the study of syn-sedimentary tectono-stratigraphic structures</i>	127
2.1	Compressional and extensional structures	128
2.2	Inversion and reactivation structures.....	130
2.3	Syn-tectonic structures (growth strata).....	131
3	<i>Published article in Solid Earth</i>	132

CHAPTER V. TECTONO-STRATIGRAPHIC CHARACTERIZATION OF THE PALEOZOIC PERI-HOGGAR BASINS: EVIDENCING ARCHES AND BASINS ARCHITECTURE – UNPUBLISHED SUPPLEMENTARY DATA173

1 Summary and objectives 175

2 Major structural elements (Arches-Basins)..... 175

3 Tectono-sedimentary structures analyses (satellite images and seismic profiles interpretation) 179

 3.1 Synsedimentary syncline-shaped basin delimited by arches..... 185

 3.2 Evidence of syn-sedimentary extensional markers..... 187

 3.3 Evidence of syn-sedimentary compressional and strike-slip markers 188

 3.4 Stratigraphy and lapout..... 207

 3.4.1 Pan-African unconformity..... 207

 3.4.2 Hirnantian glaciation..... 207

 3.4.3 Silurian transgression..... 207

 3.4.4 Hercynian unconformity..... 208

 3.5 Lithological and rheological framework..... 209

 3.6 Structural style and implications..... 210

 3.7 Precambrian inherited basement faults structures 211

 3.8 Synthesis of the chronologic tectonic kinematics and strata lapout geometries 212

4 Stratigraphy and sedimentology 214

 4.1 Facies association, depositional environments and well-log pattern 215

 4.2 Paleozoic regional well-log correlation and cross section 218

5 Conclusion 230

CHAPTER VI. LITHOSPHERIC THERMOMECHANICAL NUMERICAL MODELLING: CONTROL OF INHERITED ACCRETED LITHOSPHERIC HETEROGENEITY ON THE ARCHITECTURE AND THE LOW LONG-LIVED SUBSIDENCE RATE OF INTRACRATONIC BASINS231

1 Summary and objectives 233

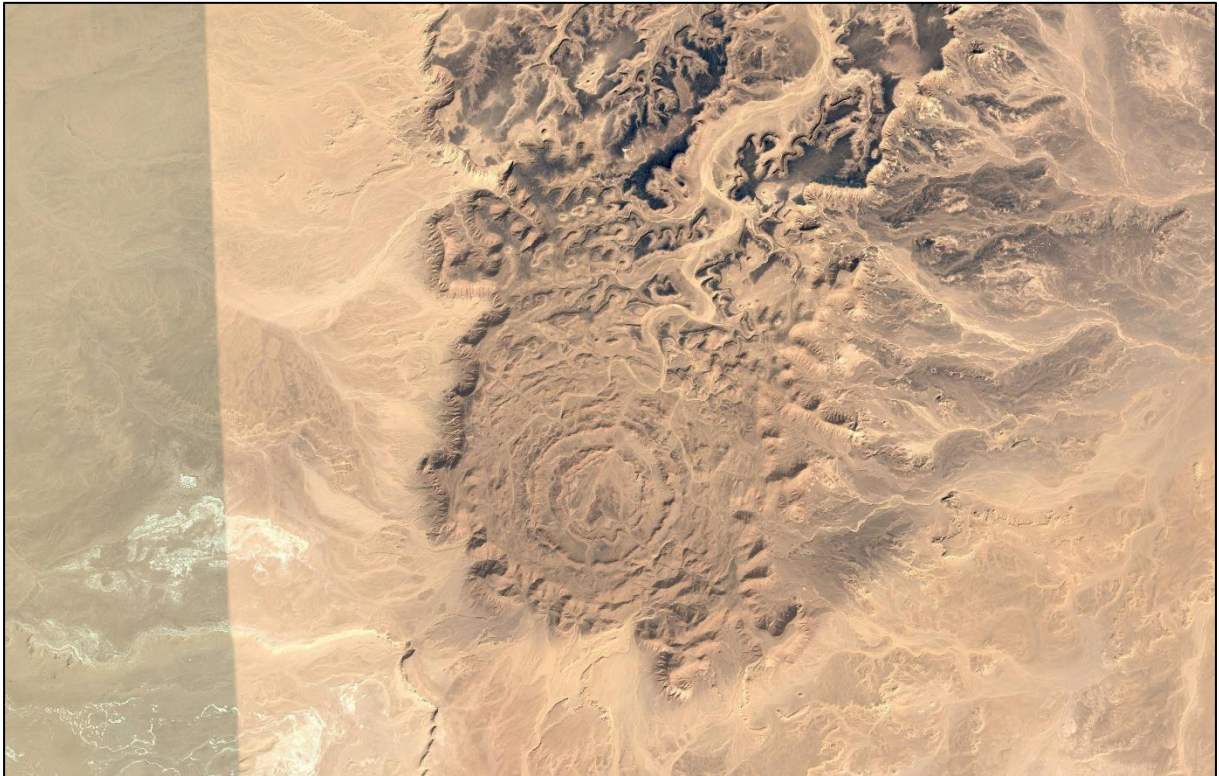
2 Notions of lithospheric thermo-mechanical numerical modelling..... 234

3 Submitted article at Basin Research 235

4	<i>Introduction</i>	237
5	<i>Working hypotheses</i>	239
5.1	Arches and basins in accretionary type lithosphere.....	239
5.2	Initial models setups and boundary conditions	242
6	<i>Accretionary vs homogeneous lithosphere</i>	245
6.1	Impact of thermal anomaly	245
6.2	Impact of far field stresses (tectonics).....	247
6.3	Interplay between tectonic and thermal anomalies.....	249
7	<i>Architecture of basins in accretionary lithosphere</i>	251
7.1	Covering the arches: Impact lateral sediment supply	251
7.2	More complex models.....	253
7.3	Basins evolution: key to deciphering past geodynamics.....	254
8	<i>Discussion</i>	258
9	<i>Conclusions</i>	259
10	<i>Appendix A: Calculation of isostatic potential between Archean and Proterozoic terranes (cf. Figure VI-4)</i>	260
11	<i>Appendix B: Numerical method</i>	261
	CHAPTER VII. DECIPHERING THE ORIGIN OF FORCING FACTORS CONTROLLING THE ARCHITECTURE OF PALEOZOIC INTRACRATONIC PERI-HOGGAR BASINS: LINK WITH GEODYNAMIC HISTORY – APPLICATION AND CLASSIFICATION	263
1	<i>Summary and objectives</i>	265
2	<i>Article in preparation</i>	265
3	<i>Introduction</i>	267
4	<i>Geological and geophysical settings</i>	269
5	<i>Methods and modelling inputs</i>	278

<i>6 Geological constrains of the numerical models M and link of forcing factors with geodynamics of peri-Hoggar Basins</i>	<i>280</i>
6.1 Lithosphere heterogeneities: Control of long-lived low rate subsidence and Arches/Basins architecture	281
6.2 Far field tectonics: Impact on tectono-stratigraphic architecture	284
6.3 Thermal activity, magmatism, and heat flux.....	288
6.4 Sourcing of sediments: Impact of sediment flux and width of the erosional surface.....	290
<i>7 Application of the numerical models M to geological data of peri-Hoggar Basins</i>	<i>291</i>
7.1 The Tasmena Basin: Example of syncline-shaped starved Basin.....	291
7.2 The Mouydir and the Tim Mersoï Basins: Example of a syncline-shaped filled Basins	294
7.3 The Ahnet Basin: Example of a complex-shaped filled Basin.....	298
<i>8 Classification of peri-Hoggar Basins in function of their forcing factors dominance....</i>	<i>302</i>
<i>9 Conclusion and perspective</i>	<i>303</i>
CHAPTER VIII. CONCLUSION AND PERSPECTIVES	305
<i>1 Temporal geological synthesis of the Paleozoic peri-Hoggar Basins</i>	<i>307</i>
<i>2 Conclusion (Question responses).....</i>	<i>311</i>
<i>3 Perspectives and comparison with intracratonic basins possible analogues (Case of Paraná Basin)</i>	<i>315</i>
LIST OF FIGURES.....	319
LIST OF TABLES.....	345
BIBLIOGRAPHIC REFERENCES	349

CHAPTER I. INTRODUCTION AND CONTEXT OF STUDY



Ring complex of Tin Bider (Google-Earth view; 27°36'05" N, 5°06'41" E)



Intracratonic basins also called “cratonic basins”, “interior cratonic basins” or “intracontinental sags” (Allen and Allen, 2013; Allen and Armitage, 2011; Heine et al., 2008) have a widespread repartition in the world (cf. Figure I-1 and Figure I-2). They host most of fresh water aquifers, minerals resources and hydrocarbons (61%) reserves of the world. They have been a renewed interest for these basins following non-conventional petroleum exploration. By their position in continents interior (see Figure I-1 and Figure I-2) and so, their stability through time (i.e. away from recycling area), they constitute an extraordinary record of the earth history. They preserve sediments in sinks (depressions) recording changes in climatic and tectonic processes occurring on the surface of the earth (Allen and Allen, 2013). They also expose relic of deep structures (Goodwin, 1996), which are witnesses of unsuspected geodynamic cycle and internal compositions of the earth constituting their substrate (i.e. basement).

Consequently, in the light of this remarks, intracratonic basins represent amazing areas allowing to both study the contents (i.e. basin substrates) and the container (i.e. sediments infill).

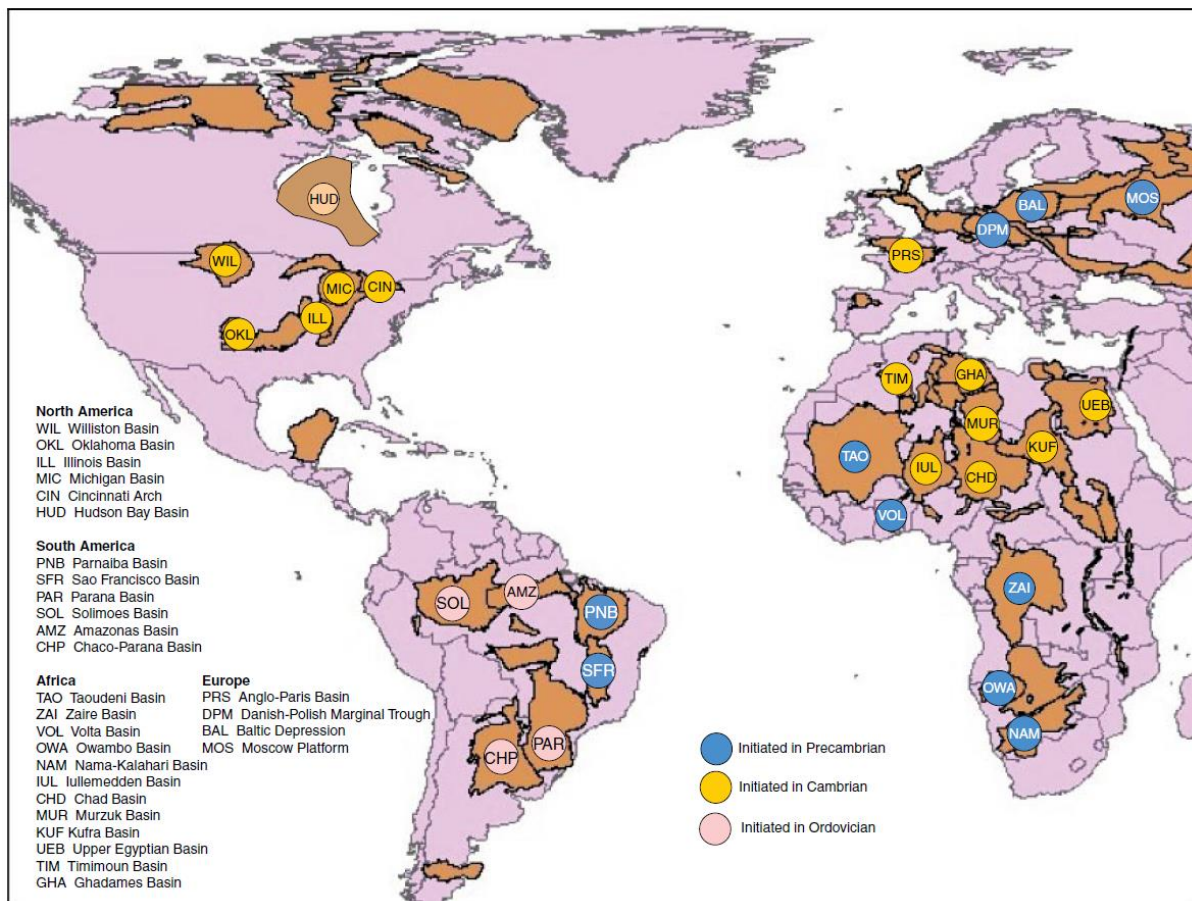


Figure I-1: Distribution of intracratonic basins on the continents surrounding the Atlantic Ocean, with typical cratonic basins highlighted. Other basins shown are commonly

unequivocally associated with extensional tectonics. Selected basins are color-coded according to the timing of initiation. Source: Base map and basin outlines provided by Trond Torsvik from Allen and Armitage, (2011).

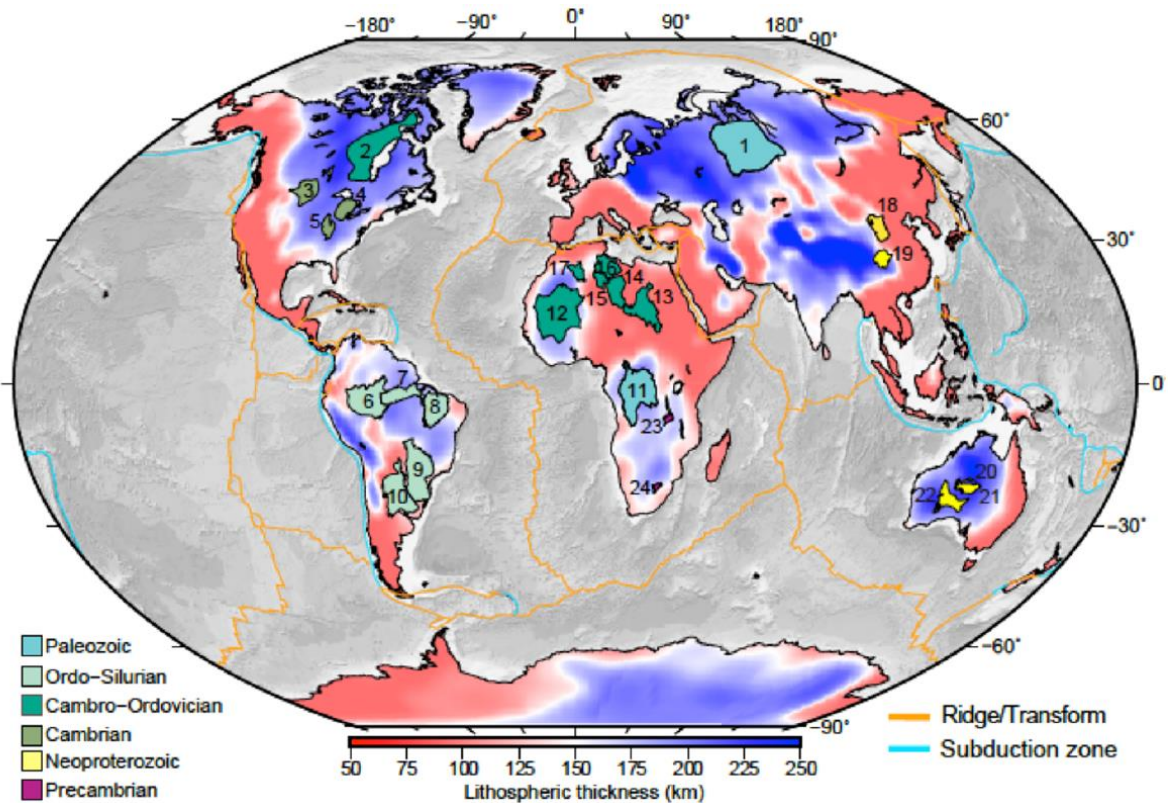


Figure I-2: Map showing the location of 24 cratonic basins overlain on a map of lithospheric thickness derived from surface wave tomography (Priestley and McKenzie, 2013). The basins are colour-coded by their age of initiation. 1: Southern West Siberian basin; 2: Hudson basin; 3: Williston basin; 4: Michigan basin; 5: Illinois basin; 6: Solimoes basin; 7: Amazon basin; 8: Parnaíba basin; 9: Paraná basin; 10: Chaco basin; 11: Congo basin; 12: Taoudenni basin; 13: Kufra basin; 14: Murzuq basin; 15: Illizi basin; 16: Ghadames basin; 17: Tindouf basin; 18: Ordos basin; 19: Sichuan basin; 20: Georgina basin; 21: Amadeus basin; 22: Officer basin; 23: Mporokoso basin; 24: Witswatersrand basin. Figure from published paper (Daly et al., 2018a).

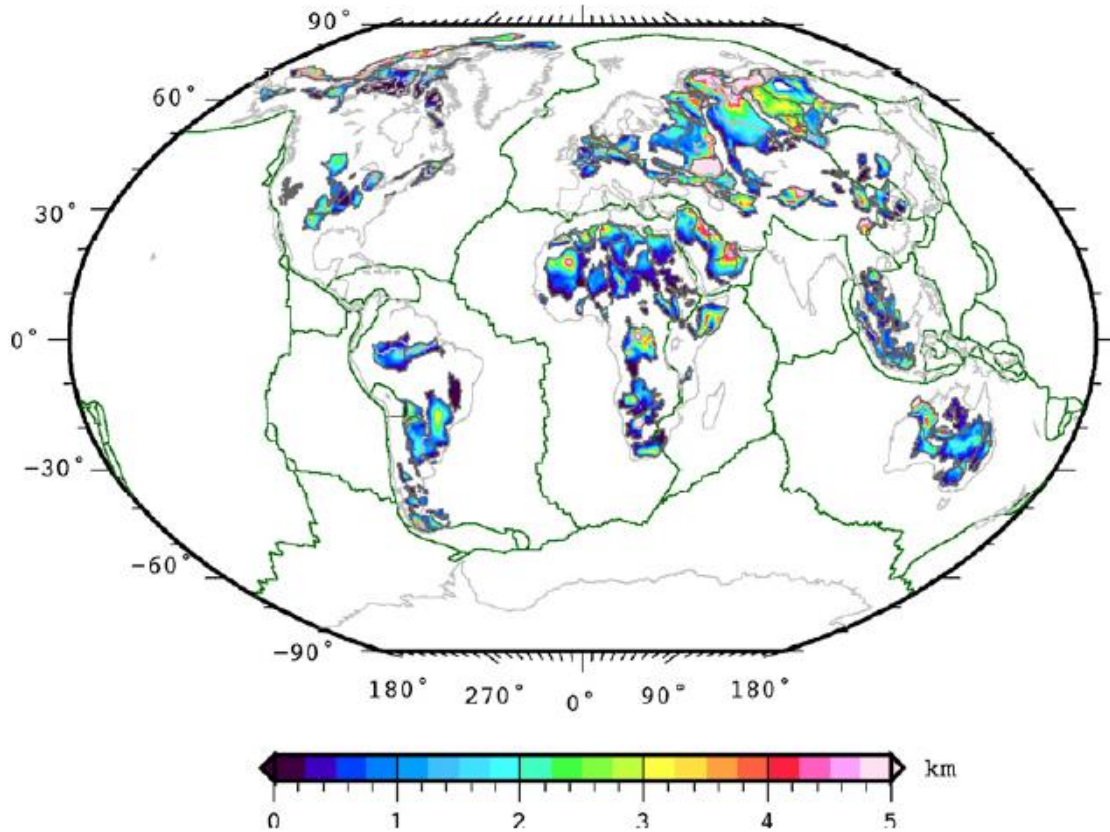


Figure I-3: Localization and thickness of intracratonic basins in the world from Heine et al., (2008).

1 Intracratonic basins main characteristics

Intracratonic basins are situated in the interior of a continent, far from any active margins upon stable lithosphere area, weakly deformed (low reliefs), there are characterized by several common features (see Allen and Allen, 2013; Allen and Armitage, 2011; Armitage and Allen, 2010 and references therein):

- They are characterized by geometries large circular, elliptical, saucer-shaped to oval-shaped (see Figure I-2 and Figure I-3);
- The basins are mainly filled with shallow-water and continental sediments, and relatively simple layer-cake stratigraphy separated by unconformities, giving superimposed mega-sequences;
- The rate and duration of subsidence are respectively slow and long-lived (Figure I-4);
- The structural framework is featured by the reactivation of structures and emergence of arches/domes/swells/highs/ridges (e.g. Figure I-7).

The compilation of backstripped tectonic curves of intracratonic basins in the world (Figure I-4) shows prolonged, often marked by an initial stage of relatively fast subsidence, followed by a period of decreasing subsidence rate (Allen and Armitage, 2011; Nunn and Sleep, 1984; Xie and Heller, 2009), somewhat similar to that of passive margins ocean basins (Sleep, 1971; Xie and Heller, 2009). They are approximately exponential in shape, following the shape and magnitude of seafloor subsidence, but with longer decay constants (Xie and Heller, 2009). Presence of deviations from idealized thermal subsidence is notable in Figure I-4. These deviations are more pronounced than those seen in passive margins and suggest that tectonic reactivation characterizes many intracontinental basins (Xie and Heller, 2009). The shape of the curve of well W17 in the Ahnet Basin localized in the Saharan platform (the area of study) is coherent with the other curves (number 12 in red; Figure I-4).

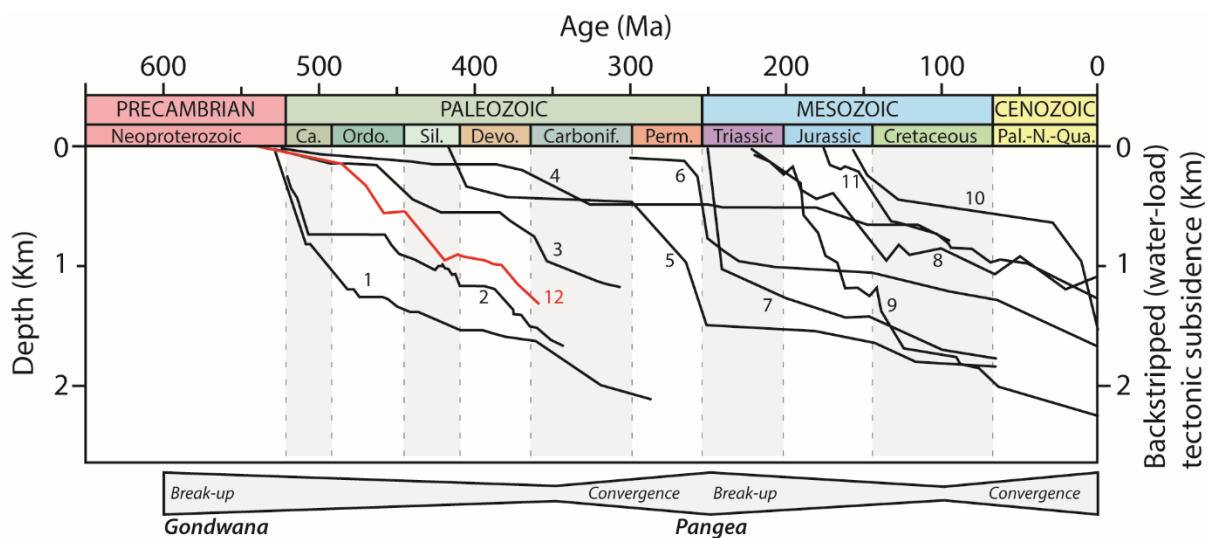


Figure I-4: Example of tectonic subsidence in intracratonic basins through the world modified from literature (Allen and Armitage, 2011; Xie and Heller, 2009). 1: Illinois Basin (Bond and Kominz, 1984); 2: Michigan Basin (Bond and Kominz, 1984); 3: Williston Basin, North Dakota (Bond and Kominz, 1984); 4: Williston Basin, Saskatchewan (Fowler and Nisbet, 1985); 5: Paraná Basin, Brazil, CB-3 well (Oliveira, 1987 from Allen and Armitage, 2011); 6: Northeast German Basin (Scheck and Bayer, 1999); 7: Southwest Ordos Basin (Xie, 2007 from Xie and Heller, 2006); 8: Paris Basin (Priyac et al., 2000); 9: West Siberian Basin, Russia, Urengoy well (Saunders et al., 2005); 10: West Siberian Basin, Russia, Samotlar-39 well (Saunders et al., 2005); 11: Paraná Basin (Zalan et al., 1990); 12: Well W17 in Ahnet Basin (Perron et al., 2018).

The distribution and the thickness of intracratonic basin are typically less than 5 km (Figure I-3). They rarely reach <6-7 km as in the West Siberian, Illinois and Paraná basins (e.g. Allen and Armitage, 2011). They are commonly regularly spaced with their centers located about 10^3 km apart (Allen and Allen, 2013; Allen and Armitage, 2011).

Contrary to others main basins (i.e. extensional rift basin, passive margin, foreland basin), the repartition of subsidence in these basins is mainly asymmetrical with irregular growth (Figure I-4). They often involve other processes and mechanisms of control.

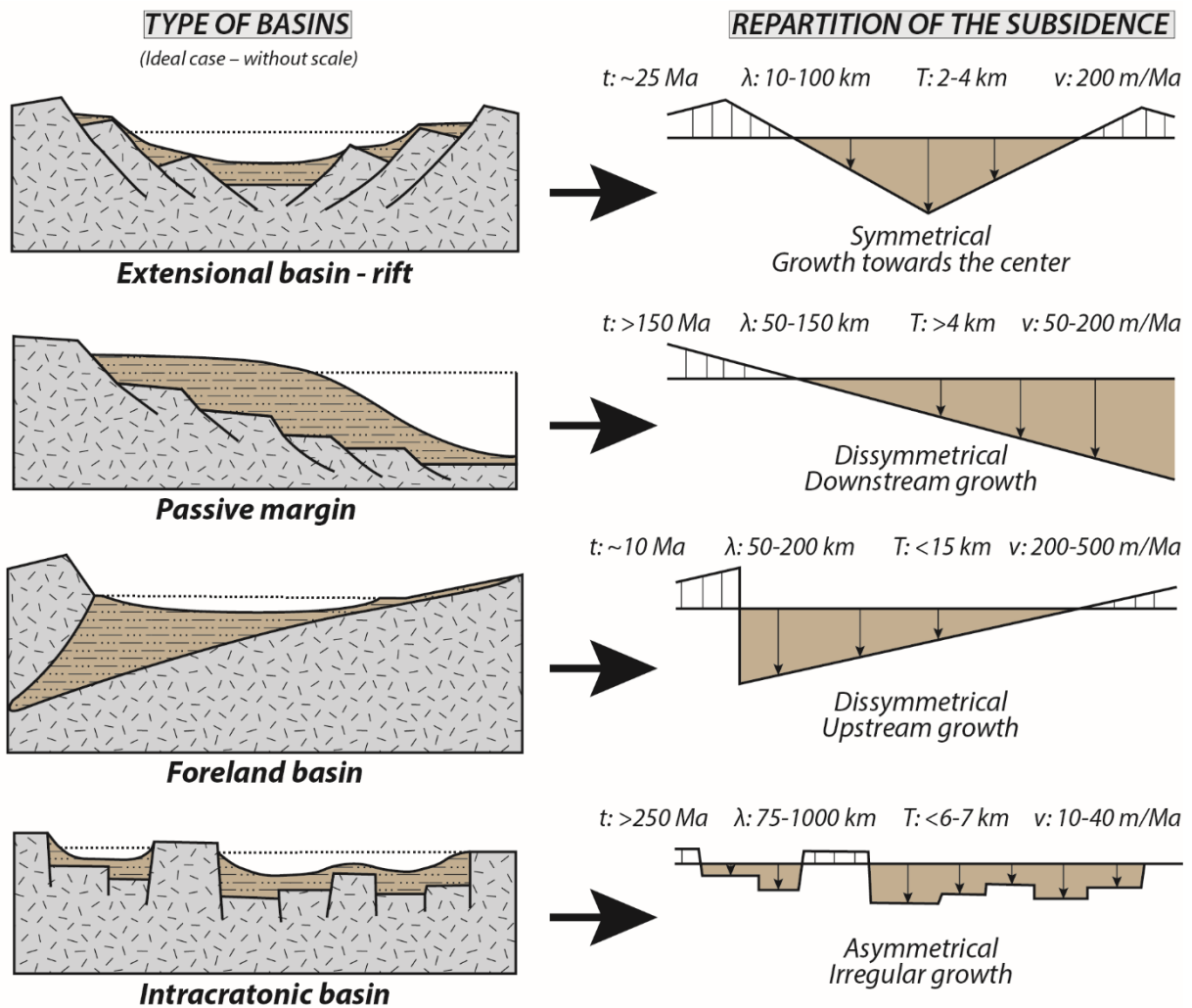


Figure I-5: Subsidence repartition in different types of basin modified from Lafont, (1994). t : basin duration of subsidence; T : thickness of the basin; λ : wavelength of the basin; v : range of subsidence rate. Values from Allen and Allen, (2013).

2 Basin mechanisms and processes of formation

Three generic basin forming mechanisms, under which the majority of basin forming mechanisms fall are proposed in the literature (Allen and Allen, 2013): Lithospheric stretching/thinning, cooling and flexural loading (Figure I-6A). When we are compared classical basins to an intracratonic basin (e.g. Figure I-5), neither of these basins looks similar either in size (geometries), in magnitude or in subsidence rate.

Consequently, multiple alternative hypotheses and models have been invoked to explain mechanism of formation of intracratonic basins (see Allen and Armitage, 2011 and references therein or; Hartley and Allen, 1994) such as thermal contraction, underplating or dynamic topography (Figure I-6B). They are also the following (not limited):

- An excess mass within the lower crust which isn't isostatically compensated. This may be either due to a phase change to a dense mineral assemblage such as eclogite (Artyushkov, 1992) or emplacement of igneous underplating (DeRito et al., 1983; Stel et al., 1993).
- Thermal contraction subsidence following heating by a plume (Kaminski and Jaupart, 2000), the emplacement of anorogenic granites (Klein and Hsui, 1987) or extension at depth which only thins the lithosphere (Xie and Heller, 2009).
- Reactivation of older structures which underlie the basin possibly due to a change of the stress field of the basin (Guiraud et al., 2005; Zalan et al., 1990; Ziegler et al., 1995).
- Reactivation of pre-existing sags under in-plane stress or flexural loading (Beaumont et al., 1988; Quinlan, 1987; Quinlan and Beaumont, 1984).
- Subsidence due to dynamic topography, over a region of downwelling in the convecting mantle beneath (Hartley and Allen, 1994; Heine et al., 2008) or related to the subduction of cold oceanic slabs (Burgess et al., 1997; Mitrovica et al., 1989).
- Extension at the surface caused by magmatic upwelling (Lüning et al., 1999; Neumann et al., 1992).
- Extremely slow rifting at low strain rates (10^{-16} s^{-1}) caused by a change in the stress field to extension associated with supercontinent break up (Armitage and Allen, 2010).

Moreover, due to the very long-lived characteristic, it is not uncommon that several mechanisms occur through time (Allen and Armitage, 2011). Other authors (e.g. Klein and Hsui, 1987) have suggested some combination of the above (models are overlapping). Knowing

that some processes are either explicit or implicit in many models (e.g. Kaminski and Jaupart, 2000; Sleep and Snell, 1976). This makes the classification of these basins often rather hard (Kingston et al., 1983; Klemme, 1980).

The more time is spent, the more complicated it seems to find evidence and clues of these processes. Besides, they are not always obvious to decipher in the geological record. It can be the presence of paleo-rift (Armitage and Allen, 2010), mantle plume (Kaminski and Jaupart, 2000) or underplating (DeRito et al., 1983; Stel et al., 1993).

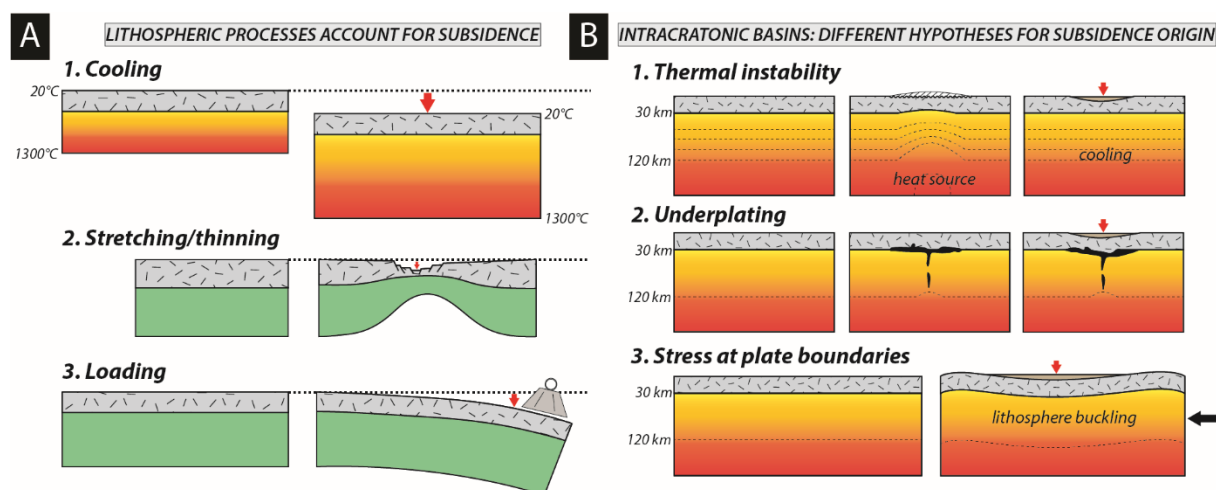


Figure I-6: (A) The three lithospheric processes account for subsidence. Any sedimentary basin subsidence results from one of these three processes or a combination of them (Allen and Allen, 2013). (B) Different hypotheses for subsidence origin of intracratonic basins (Allen and Armitage, 2011).

3 Arches and Basins architecture and basins wavelengths

We have seen that arch and (syncline-shaped) basin architectures is a common feature (Figure I-7) in intracratonic basins. In the world, it is highlighted by tectono-stratigraphic particularities (thickness changes, onlap, truncatures...), documented by numerous studies in South-America (de Brito Neves et al., 1984; Daly et al., 2014, 2018b; Milani and Zalan, 1999; Soares et al., 1978; Watts et al., 2018; Zalan et al., 1990), North-Africa (Coward and Ries, 2003; Eschard et al., 2010; Perron et al., 2018), Europa (Eyer, 2012), Russia (Alekseev et al., 1996; Vyssotski et al., 2012), Australia (Harris, 1994; Lindsay and Leven, 1996; Mory et al., 2017), Arabia (al-Laboun, 1986; Tavakoli-Shirazi et al., 2013; Vennin et al., 2015), North-America (Beaumont et al., 1988; Burgess, 2008; Burgess et al., 1997; Dineley, 1971; Pinet et al., 2013; Quinlan, 1987; Quinlan and Beaumont, 1984; Watts et al., 2018) and Asia (Thomas et al., 1999).

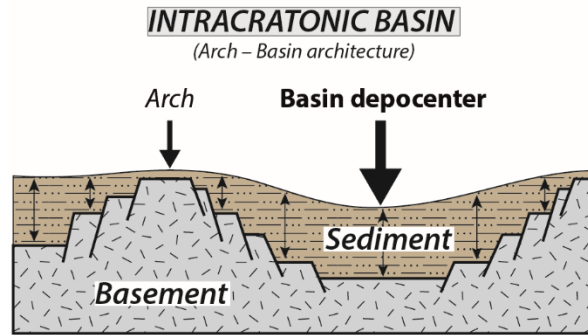


Figure I-7: The arch and syncline-shaped basin architecture, a common characteristic of intracratonic basins inspired from Seyfert, (1987).

The presence of arch and basin architectures is mainly neglected in the different models proposed in the literature (see previous part Chapter I.2). The authors habitually focus their study on the low long-lived subsidence particularities. Nevertheless, this arch-basin framework can be explained by intraplate source such as topography dynamic (Burgess et al., 1997; Burgess and Gurnis, 1995; François et al., 2013; Heine et al., 2008), lithospheric folding (Figure I-9) (Cloetingh and Burov, 2011), mantle plume (Burov and Cloetingh, 2009; Koptev et al., 2016), far field stresses (e.g. Cloetingh, 1988; Ziegler et al., 1995), local increase of the geotherm (Neves et al., 2008) or traction induced from the mantle below the deformation (Hillis et al., 2008).

λ \ e	Nulle	Weak	Middle	Strong
> 500 km	Oceanic Basin	Continental Plateform		Extension mountain chain
500 to 300 km		Buckle of the lithosphere		
300 to 30 km		Flexure of the lithosphere	Continent. rifts	Passive Margin
<30 km	Very high diversity, function of heterogeneities and level of decoupling in fragile upper crust			

Figure I-8: Relation between basins wavelength and the thickness of deformed unit. Characteristic sizes of some major types of sedimentary basins as a function of deformation intensity. Figure modified from Brun, (1999).

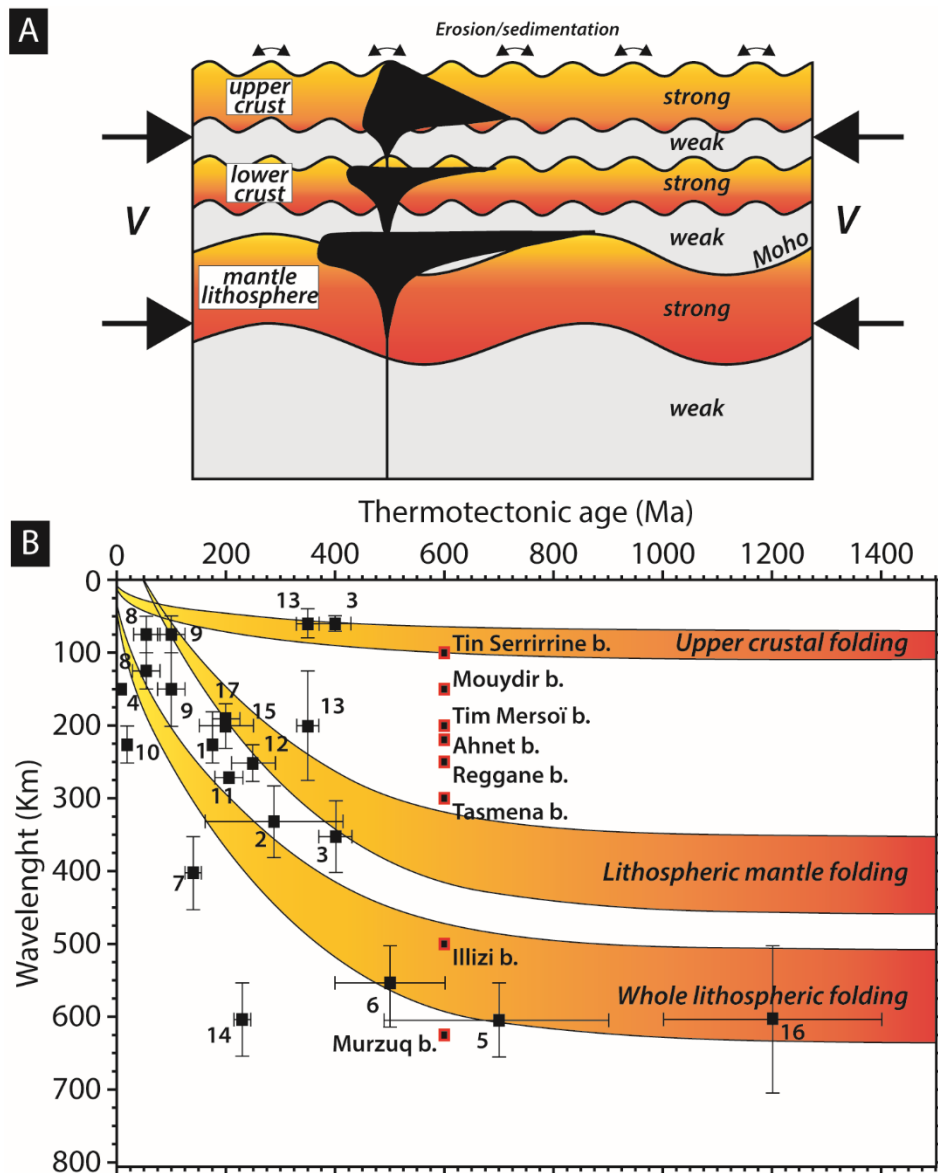


Figure I-9: Characteristics of lithospheric folding. (A) Poly-harmonic folding concept: due to rheological stratification, the lithosphere can develop different folding wavelength in response to tectonic compression. Surface topography will reflect superposition of different wavelengths. (B) Theoretically predicted wavelengths as function of thermo-tectonic age (for different lithospheric layers as well as whole-lithosphere folding. Model is compared to the observed wavelengths (Cloetingh et al., 1999). 1: Tien Shan; 2: Western Goby; 3: Central Asia; 4: Himalayan syntaxis belt; 5: Central Australia; 6: Russian platform; 7: South Caspian Basin; 8: Eastern Black Sea; 9: Western Black Sea; 10: Pannonian Basin System; 11: NW European platform; 12: Brittany; 13: Iberia; 14: Barents Sea; 15: Canadian Arctic; 16: Transcontinental Arch of North America; 17: Laramide foreland (USA). Figure modified from Cloetingh and Burov, (2011). Paleozoic peri-Hoggar Basins based on this study data (last major thermotectonic event: Pan-African orogeny dated around 600 Ma e.g. Guiraud et al., (2005).

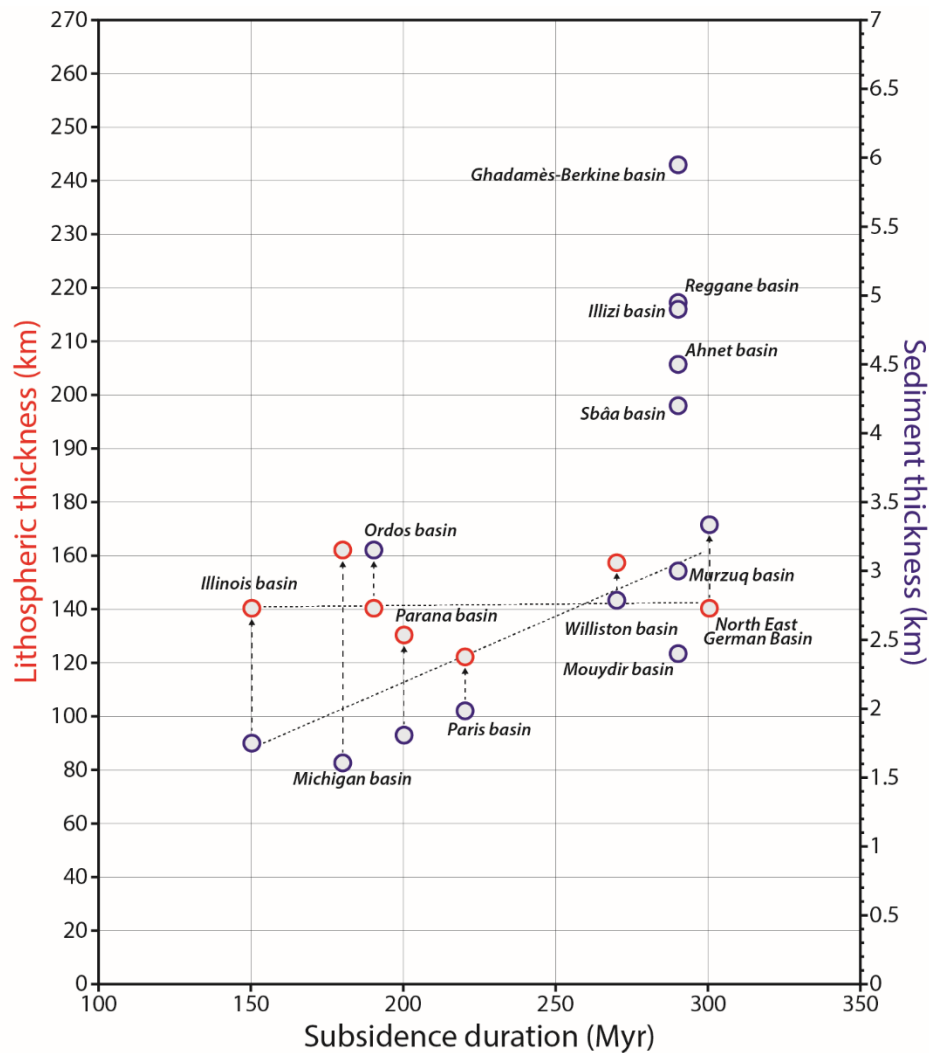


Figure I-10: Schematic diagram illustrating the relationship between the duration of subsidence and the configurations of the lithosphere and of the sedimentary infill at specific intracontinental basins modified from Cacace and Scheck-Wenderoth, (2016). Lithospheric thickness data are after (Artemieva, 2006), sediment thickness after (Heine et al., 2008), and subsidence duration after (Xie and Heller, 2009). The observed lack of correlation between equilibrium lithospheric thickness (red circles) and subsidence duration strongly suggests that subsidence in these basins cannot be exclusively explained by differences in the initial lithospheric configuration of the respective basins. In contrast, preserved sediments thickness (light blue circles) provides a better fit to the duration of subsidence, thus supporting the existence of a dynamic and structural relation between sedimentation pattern and history and resulting subsidence history. Placement of some Paleozoic peri-Hoggar Basins based on this study data.

Even if deciphering the processes of formation of intracratonic basins (and arch-basin architectures) is not always easy to decipher, the magnitude of wavelengths suggests a large-scale control (see Figure I-8 and Figure I-9), according to some authors (Brun, 2002; Burov and Cloetingh, 2009). They link the relationship between the wavelength of the basin and the thickness of the deformed unit. Indeed, when we replace the Paleozoic Saharan intracratonic basins in Figure I-9, the range of control between different basins is disparate. Therefore, it suggests for the Paleozoic basins a lithospheric scale control by buckling or flexure (see Figure I-8 and Figure I-9).

When, we observe the emplacement of the worldwide intracratonic basins, there is no relation with the lithospheric thickness (Figure I-2). Indeed, some basins can be situated upon rather thick or thin lithosphere. Knowing that, the resolution used cannot highlight local variation and heterogeneities. According to Cacace and Scheck-Wenderoth, (2016), correlation between equilibrium lithospheric thickness and subsidence duration is not clear (Figure I-10). They suggest that subsidence in these basins cannot be exclusively explained by differences in the initial lithospheric configuration of the respective basins but more probably the preserved sediments thickness provides a better fit to the duration of subsidence. Nevertheless, when we replace some Paleozoic Saharan intracratonic basins this correlation is neither obvious (Figure I-10). For the same duration of subsidence, the thickness between basins are different suggesting a local variability.

As a consequence, according to these observations the mechanism of control of intracratonic basins and their architecture seems to be rather more complex than expected. And it is often the results of combination of several parameters. In order to reconcile both the wavelength and the local variation of thickness of these basins, we should probably also take to account the influence of paleo-structures heritage (basement rheologic heterogeneities). A forcing factor which stays in the same magnitude and shouldn't be neglected.

4 Precambrian heritage of continental lithosphere (Archean to Proterozoic terranes)

Intracratonic basins are located on a variety of crustal substrates, irrespective of whether they are crystalline shields *sensu stricto*, accreted terranes, or ancient fold-belts and rift systems (Allen and Armitage, 2011).

Many authors have documented the influence of pre-existing structures, such as prior fault populations, shear zones and terrane suture zones throughout the lithosphere on the geometry and evolution of upper-crustal framework systems forming during later tectonic events (e.g. Audet and Bürgmann, 2011; Bellahsen et al., 2013, 2013; Bird et al., 2015; Bladon et al., 2015; de Brito Neves et al., 1984; Brune et al., 2017; Caravaca et al., 2017; Daly et al., 1989; Doré et al., 1997; Neves et al., 2008; Peace et al., 2018; Phillips et al., 2018; Rostirolla et al., 2003; Salomon et al., 2015).

Therefore, the basement features (i.e. rheology, thermicity...) resulting from a complex assemblage is a key factor to understand the basin arrangement and his framework.

However, the geometry and chemical-physical properties of deep structures in lithosphere are less well constrained, with information provided primarily by whole crust to lithosphere imaging geophysical methods such as seismic tomography, deep seismic reflection surveys, seismic refraction surveys and potential field imaging. Although, we are able to image these structures to substantial depths, such techniques are relatively low resolution, thereby limiting ability to interpret the geological origin of such structures and thus hampering efforts to examine how they may influence the structural style and kinematics of later formed structural architecture systems. That's why, clues of this influence are certainly to find in the analysis of the origins of continental lithosphere, the paleo-orogenies and their heritage during the "old" Precambrian times.

4.1 Paleo-orogenies and orogenic style: Continental lithosphere assembly

The Precambrian refers to the period of geological time between 4.6 Ga and 541 Ma where the Archean (i.e. 4 Ga to 2.5 Ga) and the Paleoproterozoic (i.e. 2.5 Ga to 1.6 Ga) are key epochs in world framework. Both periods are characterized by high mantle activity, high crustal accretion, and profound changes in geodynamic processes, tectonic style and architecture, paleoatmospheric and paleobiological conditions. These changes have certainly had a considerable impact on the formation of the world sedimentary basins.

Geochemical and geochronological studies show that about 60% of the current crust is formed before 2.7 Ga (Cawood et al., 2009; Taylor and McLennan, 1995). According to the models, most of the Archean and Paleoproterozoic crustal growth is operated continuously, or during periods of high growth (Condie, 1998; Reymer and Schubert, 1984; Taylor and McLennan, 1995) corresponding to periods of significant mantle activity (Campbell et al., 1989; Reymer

and Schubert, 1984). Some authors match these peaks of crustal growth with periods of supercontinent formation (Aspler et al., 2001; Eriksson et al., 2005). Three supercontinents would have existed between the end of the Archean and the Neoproterozoic. They are referenced as the Kenorland dated approximately between 2.65 and 2.4 Ga (Williams et al., 1991), the Columbia between 2.2 and 1.8 Ga (Rogers and Santosh, 2002) and the Rodinia around 1.2 Ga (Rogers et al., 1995). The existence of the first two supercontinents, their organization and their location are still very much disputed by the scientific community. However, Condie, (1998) emphasizes the importance of Archaean and Paleoproterozoic magma production. He estimates that about 39% and 35% continental crust were produced respectively during the Archean and Paleoproterozoic.

Two processes are proposed to explain the formation of continental crusts at the Archean and the Paleoproterozoic. On the one hand there is the lateral magmatic accretion involving the subduction process, and on the other hand the vertical accretion involving a massive underplating of mantle materials (Condie, 1980, 1998; Kroner, 1985; Kröner and Layer, 1992).

The deformation style during crustal thickening (orogenic) or during crustal thinning (formation of sedimentary basins) of the earth's crust depends strongly on the rheology, i.e. the mechanical behavior of the lithosphere. Knowing that the rheological behavior of Earth's lithosphere is mainly controlled by the temperature, the evolution of the geothermal gradient as a function of depth and as a function of time (Turcotte and Schubert, 2014). Indeed, in the Archean and Paleoproterozoic, continental and oceanic crusts (juvenile crusts) as well as the upper lithospheric mantle were marked by higher temperatures than in the Phanerozoic (Richter, 1988). It will impact their tectonic style.

Through the world and geological time, different orogenic styles-types are recognized and classified (Figure I-11; Cagnard et al., 2011; Chardon et al., 2009). They are the following:

- The ultra-hot Archean orogens are featured by the domes and basins structures (Figure I-11A; Cagnard et al., 2011; Chardon et al., 2009). They are characterized by a sagduction-type vertical deformation, associated with mantle convection phenomena and the establishment of "sag basins". These structures show a succession of domes of granitoid of TTG type and gneiss often migmatitic of variable size between which are placed basins of supracrustal rocks, belts of green rocks or "greenstones belts" (Figure I-11A). There are documented in the Indian craton (Bouhallier et al., 1993, 1995; Chardon et al., 1998), in the West African craton (Vidal et al., 2009), in the North-

American craton (Hoffman et al., 1989), in the Australian craton (Nijman et al., 2010) and in the Chinese craton (Zhao et al., 2001).

- The hot Paleoproterozoic orogens are defined by transpressive sigmoid accretionary structures (Figure I-11B; Cagnard et al., 2011; Chardon et al., 2009). They are organized into major lithospheric faults associated with SC shear structures (Choukroune et al., 1987) forming spectacular anastomosed network identified in worldwide continents (Figure I-11D and E). This type of orogens is experienced in the world such as in the West African craton (Baratoux et al., 2011; Perrouty et al., 2012) and in the Antarctica craton (Pelletier et al., 2002).
- The Neo-Proterozoic to Phanerozoic collisional modern cold orogens (Figure I-11C) are demarcated by essentially thrusting and “classical” tectonics (Cagnard et al., 2011).

Each of these events are associated with the set of rocks with different chemical and physical properties (Figure I-11).

The Paleoproterozoic constitutes a pivotal period of Earth's history marked by a significant change in the rheology of the whole lithosphere complex (Figure I-11). This change is characterized by the decline of mantle magmatism, the strong growth of the continental crustal surface and the transition between sagduction type geodynamics and peri-oceanic subduction processes and intracontinental associated with "cold" lithospheric plate tectonics (Cagnard et al., 2011; Chardon et al., 2009; Condie, 1998; Gapais et al., 2014).

Modern collision chains are characterized by thrusting of crustal scale. The juvenile lithospheres, on the other hand associated with a higher geothermal gradient, show a weaker mechanical resistance and appear essentially controlled by vertical forces of volume (Cagnard et al., 2011; Chardon et al., 2009; Condie, 1998; Gapais et al., 2014). Choukroune et al., (1995) show, however, that some structural features are common to both the present and Precambrian mountain ranges. Thus, some structures involved in continental deformation such as thrusting sheets, domes in the broad sense, and strike-slips, but also evolution of the metamorphic facies characterize the Precambrian or Phanerozoic orogens (Choukroune et al., 1995).

Both the Archean domes and basins (Bertrand and Caby, 1978; Haddoum et al., 1994; Ouzegane et al., 2003a) and the Paleoproterozoic accretionary structures types (Bertrand and Caby, 1978; Latouche and Vidal, 1974) are detected in the Hoggar massif (Figure I-11). They define a structural heritage that will forced and constrained further orogens (e.g. Pan-African; Black et al., 1994; Caby, 2003; Haddoum et al., 2013; Liégeois et al., 2003).

These different paleo-orogenies have led to the collage and the suturing of terranes of different Precambrian age and rheologies. It will change in deep the structure of the lithosphere and the surface behavior through time.

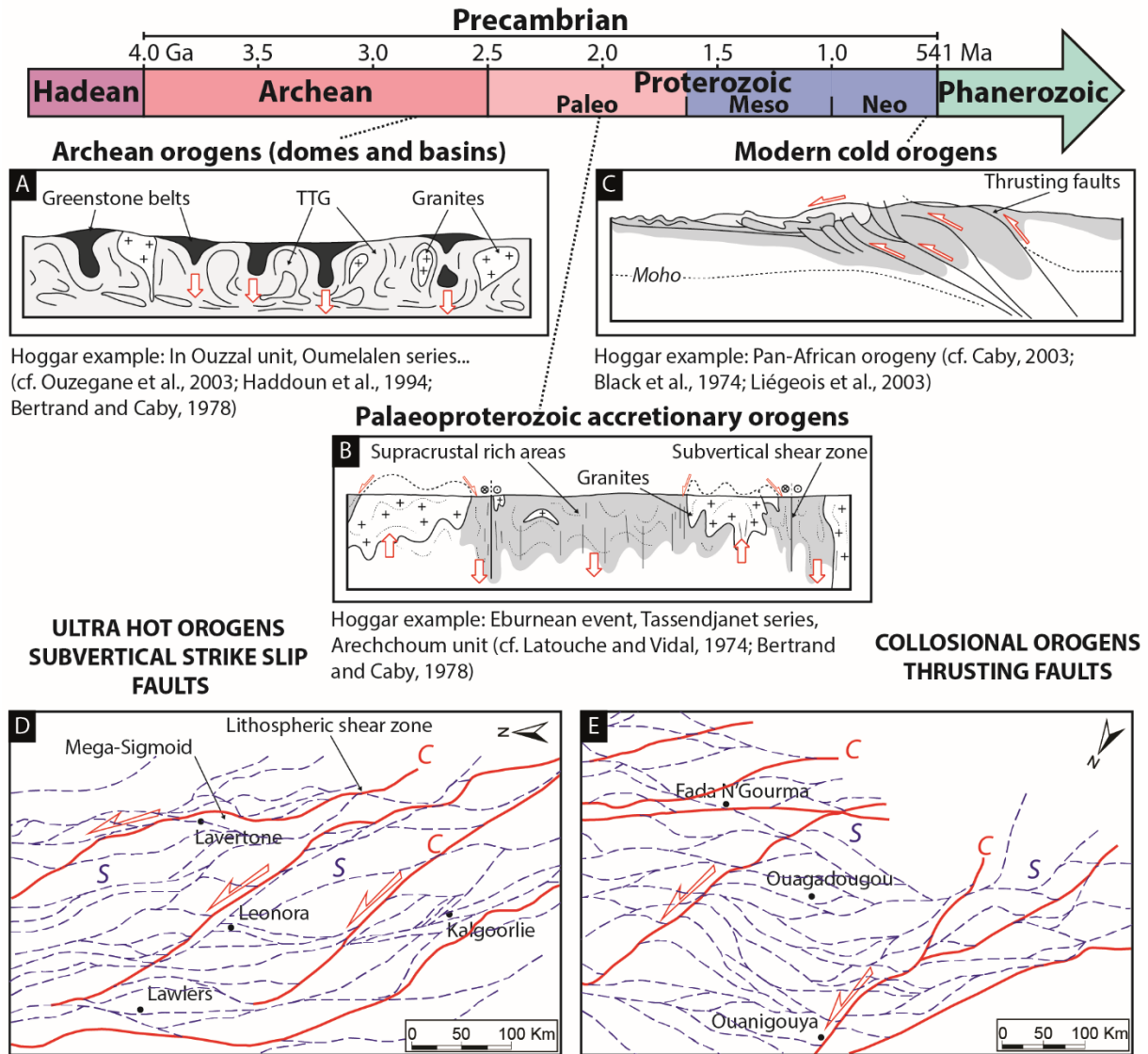


Figure I-11: Schematic cross section illustrating different orogenic styles developed through time modified from Cagnard et al., (2011). (A) Archean domes and basins orogens, (B) Paleoproterozoic accretionary orogens, (C) Modern cold orogens characterized by thrusting style tectonics. Example of regional-scale shear zone patterns and sigmoidal structures in accretionary Precambrian orogens. (D) The Eastern Goldfield province, Yilgam craton, Australia modified from Chardon et al., (2009); (E) The Birrimian orogen, West African Craton, Burkina Faso modified from Chardon et al., (2009).

4.2 Rheological properties of inherited accretionary lithosphere

We have seen that Precambrian orogenies could have assembled and put together multiple terranes of different ages and origins. Where, the terrane has been defined as: a piece of crust that broke off a tectonic plate and accreted or sutured in or on a continental platform or craton of another tectonic plate and having a different geological history than its surrounding formations. These accretionary continental lithospheres formed during accretionary orogen comprise a range of oceanic or continental lithospheric substrates of various age and composed of mafic to silicic igneous rocks and their sedimentary derivatives (Cawood, 2009; Cawood et al., 2009; Condie, 2007).

The enhanced survivability of continental cratonic lithosphere, because of nearly zero rate of lithosphere recycling since the late Archean allows their stabilization and the anticipation of their geochemical and geophysical properties through time (Artemieva, 2006). Nevertheless, they can be remobilized during major tectonic events, hence the concept of “metacraton”, that could lead to decratonization, but retaining relics and/or isotopic inheritance of the former craton (Abdelsalam et al., 2002). It is still recognizable dominantly through its rheological, geochronological and isotopic characteristic.

The analysis of continental lithospheric rheologic properties such as strength, depth, heat flux and density displays a strong relation and dependence to tectono-thermal age (Artemieva, 2009; Artemieva and Mooney, 2001; Djomani et al., 2001; Kaban et al., 2014). According to Artemieva and Mooney, (2001), an important segregation in rheological behavior exists between Neo-Meso-Proterozoic juvenile lithosphere (<1.8 Ga) and Archean-Paleoproterozoic lithosphere (Figure I-12). Each of these continental lithospheres (i.e. Archean, Proterozoic, Phanerozoic) are featured by different thickness, lithological, geochemical, thermal and rheological properties (Figure I-13). These dissimilarities between Precambrian to Phanerozoic continental lithospheres have been documented by many studies (Artemieva, 2009; Artemieva and Mooney, 2002; Cherepanova and Artemieva, 2015; Djomani et al., 2001; Durrheim and Mooney, 1994; Griffin et al., 2003; King, 2005; McKenzie and Priestley, 2008, 2016; Michaut et al., 2009; Nyblade and Pollack, 1993; Petitjean et al., 2006; Sleep, 2003, 2005).

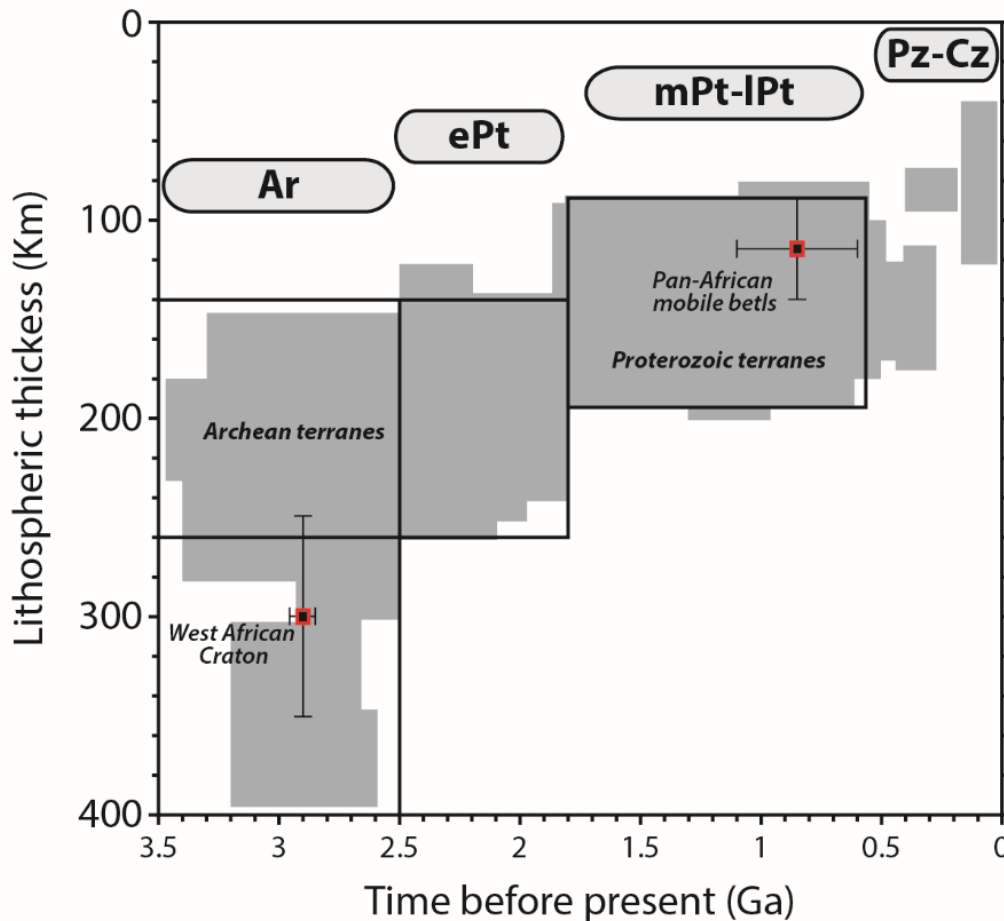


Figure I-12: Lithospheric thermal thickness versus geologic age of the continental lithosphere. The Archean lithosphere has bimodal thickness distribution centered at 350 and 220 km. Gray area shows the lithospheric thickness estimates derived from thermal data from Artemieva and Mooney, (2002). Key: Ar—Archean; ePt, mPt, lPt—early, middle and late Proterozoic, respectively; Pz—Paleozoic; Cz—Cenozoic. Placement of the West African Craton (WAC) and the Pan-African mobile belts (Central African) from Artemieva, (2006).

They especially propose differential densities and thicknesses between Archean, Proterozoic and Phanerozoic continental lithospheres (e.g. Figure I-13). Besides, statistical analysis of lithospheric geotherms reveals a striking correlation between the age of terranes and their thermal regime: the lithospheric thermal thickness linearly decreases with time from Mesoarchean to present (Artemieva, 2006). A consequence of these features is highlighted in the Siberian Craton (Cherepanova and Artemieva, 2015): its tectonic structure shows heterogeneities due to accreted Archean-Paleoproterozoic terranes separated by Proterozoic suture zones. They show a strong correlation between heterogeneous density assemblies and tectonic settings, where the deepest intracratonic sedimentary basins (the Varnavar and the Viluy Basins) are underlined by a high-density structure.

The paradigm pointing the heterogenic structures of continental lithosphere as a controlling factor could be an interesting path to understand intracratonic basins framework.

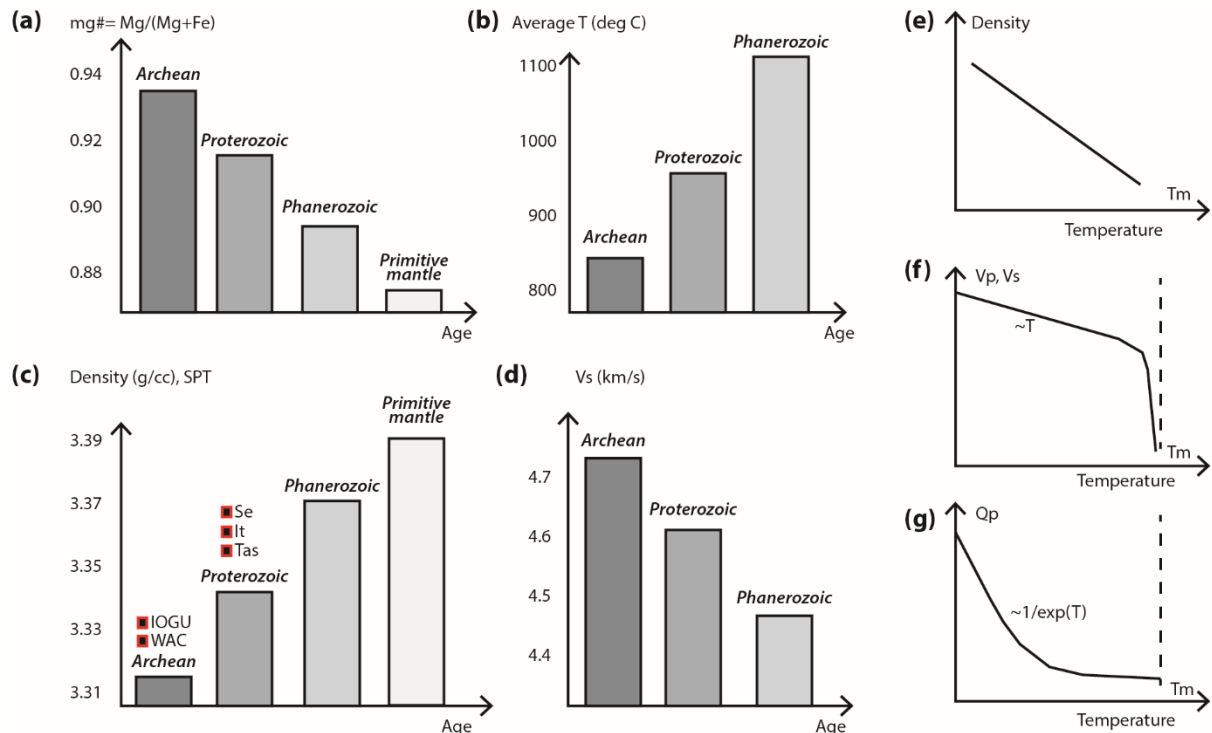


Figure I-13: Secular variations in average physical properties of the continental lithospheric mantle (CLM) due to compositional and temperature variations modified from Artemieva, (2009): (a) forsterite content, (b) average temperature in the CLM, (c) density at standard, i.e. room, P - T conditions, (d) S -wave seismic velocity. Primitive mantle (of pyrolite composition) is shown for a comparison. Right column illustrates the effect of temperature on: (e) density, (f) seismic velocities, and (g) inverse seismic attenuation. Placement of Archean terranes (WAC: West African Craton, IOGU: In Ouzal Granulites Unit) and Proterozoic terranes (Se: Serouenout, It: In Teidini, Tas: Tassendjanet).

5 Questions and problematics

To summarize, the intracratonic basins situated in continental interiors are sensitive to the substrate, which depends on the rheological parameters of the underlying terranes assembled through several different type of paleo-orogenies during Archean, Proterozoic and/or Phanerozoic. The contrast resulting from these accreted different lithospheric entities (i.e. terranes) could be an interesting approach to better understand basins infilling and so, intracratonic basins specificities. In particular, in the case of the Saharan platform, where the

different orogenies have putted together Archean type terranes (e.g. WAC) and Proterozoic type terranes (e.g. Pan-African mobile belt) with their own rheologic properties (Figure I-12).

In the light of this introduction, main features of these intracratonic basins are not well characterized and are still debated. Among the objectives of this project, the goal is to answer to questions need as follows:

- (1) What are the working mechanisms of these slow subsidence basins?
- (2) How can we characterize crustal and lithospheric deformations?
- (3) What is the nature of the apparently permanent lithospheric & rheological heterogeneities through 250 Ma?
- (4) What is the control and trigger of the regular uplifts of inherited paleohighs/arches and extensive & coeval unconformities/hiatuses?
- (5) What are the controlling factors of the sedimentary record, the reservoir architecture and facies distribution?
- (6) What is the impact on the Silurian/Devonian Hot Shales and other source rocks deposits?

The objective of this PhD project is to characterize factors controlling the architecture and the low-rate subsidence of the selected intracratonic Paleozoic basins

6 The case of the Paleozoic Saharan platform (peri-Hoggar basins)

For this purpose, we have selected the case of the Paleozoic basins of the Saharan platform. These basins initiated at the Cambrian are classified as intracratonic basins i.e. sag basin (Figure I-1). They are also often referred as intercratonic or intercontinental basins (Holt, 2012; Holt et al., 2010).

We will see how these Paleozoic basins (of Gondwana especially) regroup all the main singularities of intracratonic basins described previously. We will highlight their slow subsidence, typical large wavelength of a few 100's km, regular rejuvenation of paleohighs not easily related to global geodynamic cycles, frequent extensive unconformities, and subtle and complex facies partitioning (architecture).

The industrial application of this study is complete: The petroleum system associated to these basins are among the most prolific, either as conventional plays, or as more challenging plays, like stratigraphic traps and shales gas (oil) (Boote et al., 1998; Burke et al., 2003, 2003; Logan

and Duddy, 1998; Macgregor, 1996; MacGregor et al., 1998; Purdy and MacGregor, 2003). Following that, they remain a significant geo-strategic issue for worldwide energetic procurement.

7 Manuscript construction

The research work undertaken during this thesis allowed the writing of three scientific articles published, submitted and in preparation in international scientific journals:

- **Article 1.** Perron, P., Guiraud, M., Vennin, E., Moretti, I., Portier, É., Le Pourhiet, L., Konaté, M., 2018. Influence of basement heterogeneity on the architecture of low subsidence rate Paleozoic intracratonic basins (Reggane, Ahnet, Mouydir and Illizi basins, Hoggar Massif). *Solid Earth* 9, 1239–1275. <https://doi.org/10.5194/se-9-1239-2018>. **(Published)**.
- **Article 2.** Perron, P., Le Pourhiet, L., Guiraud, M., Vennin, E., Moretti, I., Portier, É., Konaté, M. Control of inherited accreted lithospheric heterogeneity on the architecture and the low long-lived subsidence rate of intracratonic basins. **(Submitted to Basin Research)**.
- **Article 3.** Perron, P., Le Pourhiet, L., Guiraud, M., Vennin, E., Portier, É., Moretti, I., Konaté, M. Deciphering the origin of forcing factors controlling the architecture of Paleozoic intracratonic peri-Hoggar basins of low subsidence rate: Link with geodynamic history. **(In preparation)**.

The thesis manuscript is divided into eight chapters which are based on scientific articles but also on original data. They organize themselves as follows:

- **Chapter I: “Introduction and problematics”.**

This chapter initiates the subjects by introducing intracratonic main characteristics and their mechanisms and processes of formation. A discussion is especially led on the Arches and Basins architecture and of Precambrian heritage of accretionary lithospheres. Finally, questions and problematics of the studied area are called. The calendar of execution of the different tasks is revealed.

- **Chapter II: “Materials and methods of an integrated multidisciplinary approach”.**

This chapter presents the general approach of the manuscript as well as the different methods and tools used from the characterization of both inherited structures and basins architecture to lithospheric thermo-mechanical numerical modelling.

- **Chapter III: “Geological context of peri-Hoggar Basins (Saharan platform)”.**

This chapter presents a complete synthesis of the geology of peri-Hoggar Basins. After a brief localization of the studied area, and his main singularities, the structural, geodynamic, thermal stratigraphic and sedimentary framework is described as well as the occurring petroleum systems. At the end, evidence of tectono-sedimentary structures from bibliography pointing out the arches-basins architecture is synthetized.

This part establishes a state of art of the bibliography on the studied area permitting the introduction of the following chapter.

- **Chapter IV: “Influence of basement heterogeneity on the architecture of low subsidence rate Paleozoic intracratonic basins (Reggane, Ahnet, Mouydir and Illizi basins, Hoggar Massif)”.**

After a brief reminder of some concepts in order to study syn-sedimentary tectono-stratigraphic structures, the article published in Solid Earth journal is introduced. This paper presents an integrated multidisciplinary method using satellite images, seismic and well-logs data. A sedimentologic synthesis (i.e. depositional environments and electrofacies) of the Saharan platform is done. The tectonic calendar is specified and linked to subsidence pattern. The structural style and deformation kinematics models are highlighted. Finally, a conceptual geological model integrating both the basement nature (terranes) and the architecture of the arches-basins features is established.

- **Chapter V: “Tectono-stratigraphic characterization of peri-Hoggar Basins: Evidencing Arches and Basins architecture – Unpublished supplementary data”.**

This chapter brings unpublished supplementary data helping the better characterization the tectono-stratigraphic architecture of peri-Hoggar Basins through essentially satellite images, seismic and well logs. These observations and interpretations permit a better constrain at the regional scale the architecture and the tectonic history of the Saharan platform. Regional cross sections of the Paleozoic series are also shown. This part is supported by the previous chapter

especially for the sedimentologic part where depositional environments and electrofacies were already defined.

- **Chapter VI: “Lithospheric thermo-mechanical numerical modelling: Control of inherited accreted lithospheric heterogeneity on the architecture and the low long-lived subsidence rate of intracratonic basins”.**

This chapter starts with a brief reminder of some basic concepts of lithospheric thermo-mechanical numerical modelling and finishes by the presentation of the article submitted to Basin Research. Starting from the two previous chapter, this part treats of the viability of the conceptual geological model proposed by testing it through lithospheric thermo-mechanical numerical modelling. Different simulations are launched to exam the hypothesis of an uncompensated lithosphere due to heterogenic density inherited from accreted terranes of different age (Archean and Proterozoic). A parametrization of the model and forcing factors is done.

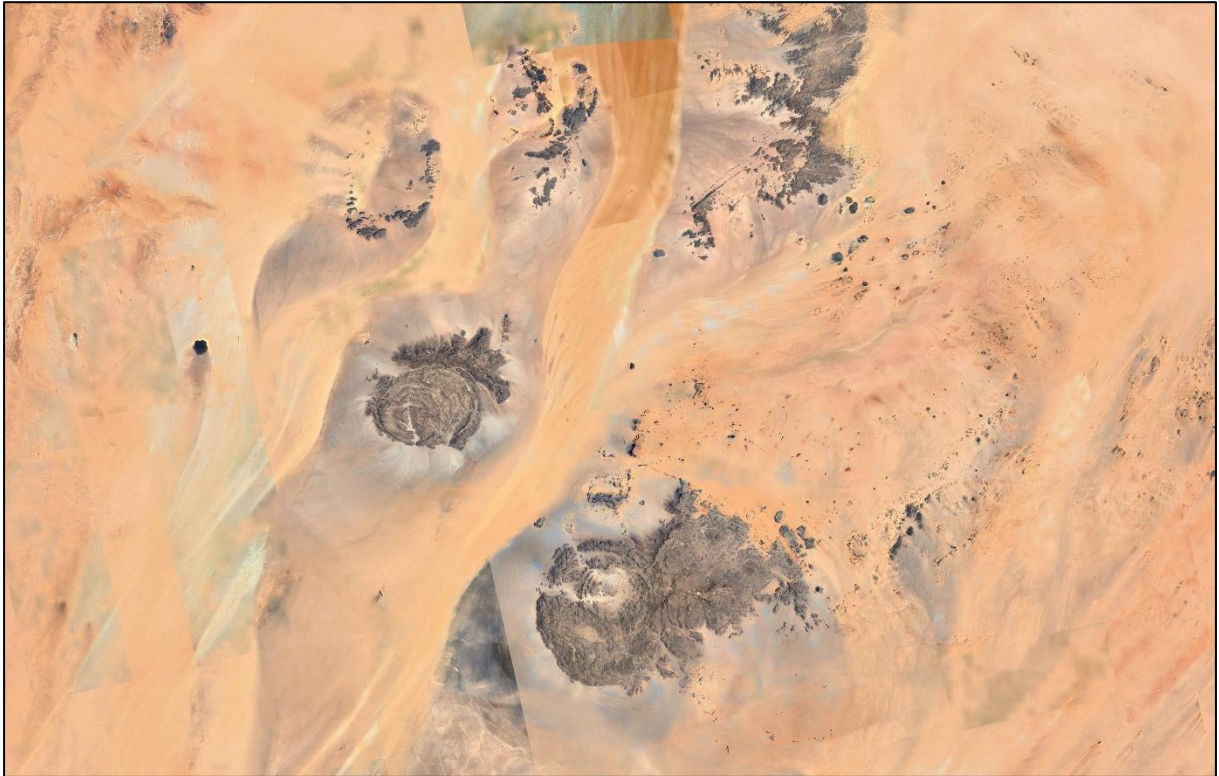
- **Chapter VII: “Deciphering the origin of forcing factors controlling the architecture of Paleozoic intracratonic peri-Hoggar basins: Link with geodynamic history – Application and calibration”.**

This chapter makes the junction between chapter IV-V proposing a geological conceptual model and chapter VI testing numerical lithospheric modelling. The numerical model is applied to peri-Hoggar Basins and calibrated/validated by geological data. The origins of the forcing factors are identified and linked to the geodynamic history of the Gondwana (eustatic and/or tectonic, climatic). This chapter loop the whole integrated study of this manuscript.

- **Chapter VIII: “Conclusion and perspectives”.**

In this final chapter, the main results of these different studies will be synthesized and the answers to the various questions formulated above will be made in the conclusion. The implications of these results in the academic and industrial fields will be presented and will help to define the perspectives opened up by this research work.

CHAPTER II. MATERIALS AND METHODS OF AN INTEGRATED MULTIDISCIPLINARY APPROACH



Ring complex of Jebel Arkenu-Uweinat (Google-Earth view; 22°10'23" N, 25°01'25" E)



The method used in this study is based on an integration of different multidisciplinary tools, technics (i.e. satellite images interpretation, sequence stratigraphy, seismic interpretation...) and datas (i.e. satellite images data, sedimentologic data, well-log data, biostratigraphic data, geochronologic data, geophysics data...). The realization of a four dimensions Geographic Information System (GIS) integrated database (satellites images data, well-log data, geophysics data, geochronologic data) allowed to characterize the architecture of the basin and the role of the basement (structural, sedimentary bodies...) in structuration of the basin. The purpose is to better understand controlling factors of these basins and to construct a model of basin. The whole method used in this study is schematically synthetized in Figure II-1. This method constitutes the unfolding of the different chapters of the thesis.

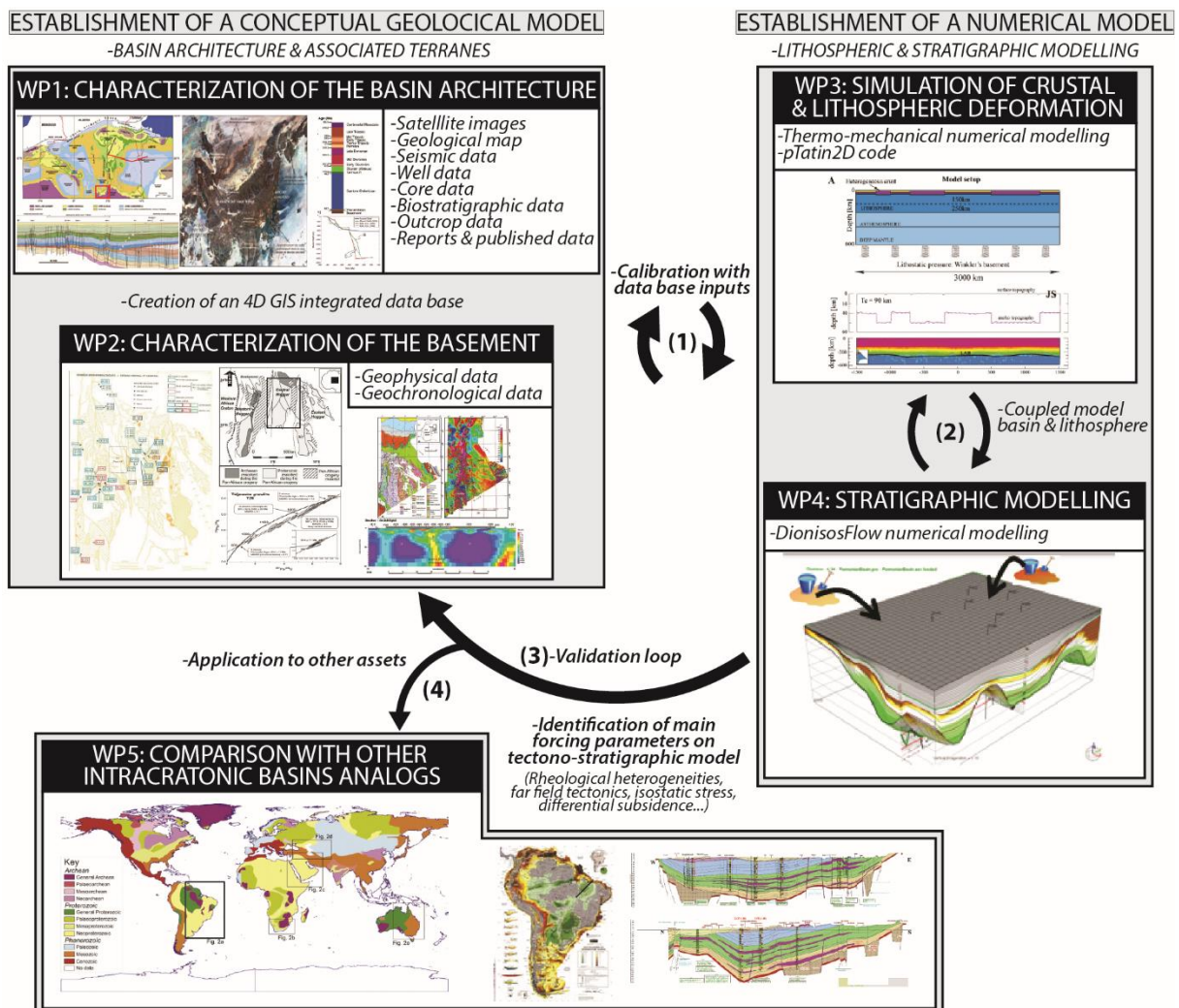


Figure II-1: Method of integrated multidisciplinary characterization of intracratonic basins used in this study. Notice that WP4 (Stratigraphic modelling) workflow is not under the scope of this manuscript. It represents an interesting perspective of work for the future.

1 Characterization of syn-sedimentary structures of Arch-Basin architecture (WP1)

The first step of our approach is to characterize the basin tectono-stratigraphic architecture (WP1; Figure II-1). It consists of characterizing the structural style, the faults kinematics and the syn-sedimentary structures using satellite images and seismic profiles. In addition, the sedimentological analysis through essentially well-log data helps to identify the facies partitioning in the area and the evolution of the depositional environment through time.

1.1 GIS integration of data and software

Our workflow is mainly centered on an integration of different type of data in a GIS (geological map, field data, well data, biostratigraphy data, geochronology data...) in order to spatialize our study. GIS is grateful tool designed to collect, store, process, analyze, manage and present all types of spatial and geographic data. In this study, a combination of GLOBAL MAPPER and ARCGIS softwares was used, each with different technical qualities. Well correlation/calibration and seismic interpretation were done with PETREL and OPENDTECT softwares.

1.2 Geological mapping and satellite images interpretations

Geological map from the Beicip-Sonatrach consortium study in the 1971-1972 (Bennacef et al., 1974; Bensalah et al., 1971) and satellite images (i.e. 7ETM+ from USGS: <https://earthexplorer.usgs.gov/>) were used to map and identify sedimentary, tectonic and syn-sedimentary tectonic structures such as wedge-shaped units associated with thickness variation (i.e. progressive unconformities; Riba, 1976).

Contrary to other geophysical technics such as seismic, there is no disturbance of the geological information. Furthermore, the well outcropping conditions of the Paleozoic succession and Precambrian basement structures provide a grateful case of study.

The structural interpretation of the outcropping study area from satellites images (flash-earth, Google Earth, Landsat 7 ETM+ ...) was achieved (Figure II-2). It has permitted to characterize the main structural style of the area. It later has helped the interpretation of wells and of seismic data. It also has highlighted tectonic kinematics of Paleozoic outcrops during the Cambro-

Ordovician extension, Devonian and the Hercynian compression and identify thickness variations, evidence of syn-tectonic sedimentation.

In fact, the field work remains regrettably very difficult in the last fifteen years because of the insecurity. Consequently, satellite images are really grateful tools to understand the geology of these areas.

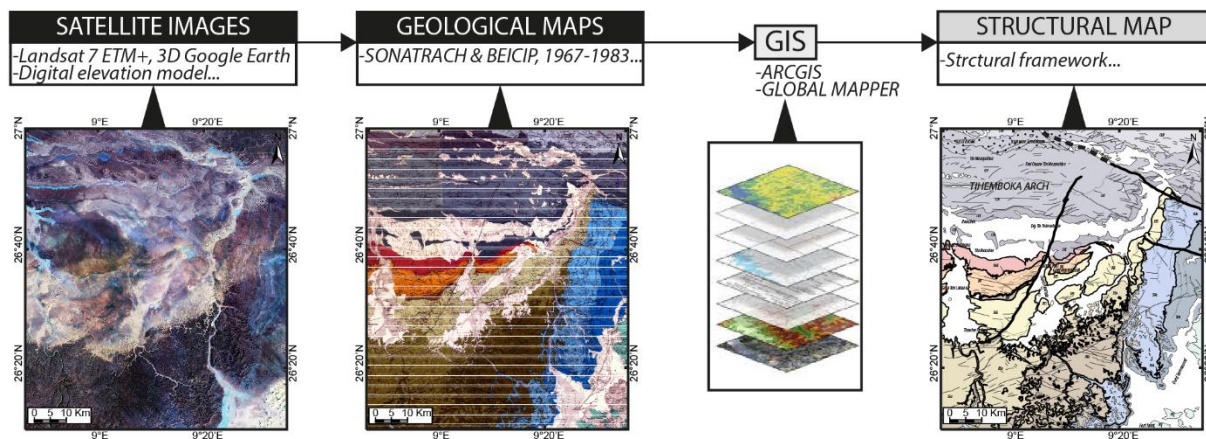


Figure II-2: Methodology of satellite images analysis and re-interpretation from Landsat 7 ETM+ (USGS: <https://earthexplorer.usgs.gov/>) and geological maps (Bennacef et al., 1974; Bensalah et al., 1971).

1.3 Stratal sedimentary geometries and structural style (satellite images and seismic analysis)

In our study, we have derived information from multiple data sets such as satellite images and seismics in order to analysis structural styles, lapout relationship, stratal stacking patterns, stratal geometries, and geomorphology of the basins. Besides, it also has helped well-log correlation and the sequence stratigraphy analysis (Catuneanu et al., 2009). Each of these applications brings limitations.

The excellent outcropping conditions of the Paleozoic provide a favorable case of study to map and identify exhumed geologic structures (e.g. wedges, thickness variation, folds, faults...). In this purpose geological map (Bennacef et al., 1974; Bensalah et al., 1971), digital elevation model (DEM) and satellite images (i.e. 7ETM+ from USGS, Google Earth) data were used. Contrary to other geophysical technics such as seismic there is no disturbance of the geological information and have a better resolution.

Seismic data provide grateful information about geological sub-surface settings. Here, the interpretation of the key stratigraphic horizon has been done by calibration of seismic profiles from well-log data (sonic). After well-calibration and the interpretation of the seismic lines, seven key horizons have been identified: near the top Ordovician, near the top Silurian, near the top Pragian, near the top Givetian, near the top mid-Frasnian, near the top Famennian, near the base Quaternary and near the Hercynian unconformities (see Perron et al., 2018). The geometries and structural style are difficult to observe in seismic profiles because of vertical or horizontal exaggeration (Stone, 1991). It can bring geological misinterpretation (e.g. fault dip...). Furthermore, the vertical seismic resolution is around 50 m, which can make difficult the investigation of some geologic structures. That's why, we have combined in this work the interpretation of satellite images and seismic data. They provide useful and complementary surface and sub-surface information.

1.4 Sedimentology, sequence stratigraphy, electro-facies and well correlation

This part is based on integration, analysis and synthesis of core, outcrop, well-log, lithologic, sedimentologic and biostratigraphic data (Figure II-3). Our approach is founded on the model-independent concept of sequence stratigraphy (Catuneanu et al., 2009). It entails to describe the sedimentary bodies in the basin (Catuneanu et al., 2009) to complete the former satellite images and seismic interpretations. The purpose of this method is to define a characteristic gamma-ray pattern (electrofacies) of the facies associations, so as to classify sedimentary depositional environments from well-logs (see Figure 8 and 9 in Perron et al., 2018).

Lithologic and sedimentologic studies were synthesized from internal Sonatrach and IFP reports (Aissani and Bennamane, 2003, 2003; Desaubliaux et al., 2005; Dokka, 1999; Eschard et al., 1999; Robertson, 2002) and published articles (Beuf et al., 1971; Biju-Duval et al., 1968; Wendt et al., 2006). Facies description from core and outcrop of these studies were lumped into facies associations corresponding to the main dispositional environments present in the Algerian platform (see Table 1 in Perron et al., 2018).

Then, the litho-sedimentologic logs were associated and compared to their gamma-ray well-logs patterns (gamma-ray electrofacies). A synthesis is available in Figures 8 and 9 in Perron et al., (2018). The well-logs data available came from several campaigns, which were led in from 1950s to 2010s with numerous sorts of petrophysics tools (spectral, laterolog...). It implies a heterogeneous database and a normalization of the petrophysic data was led.

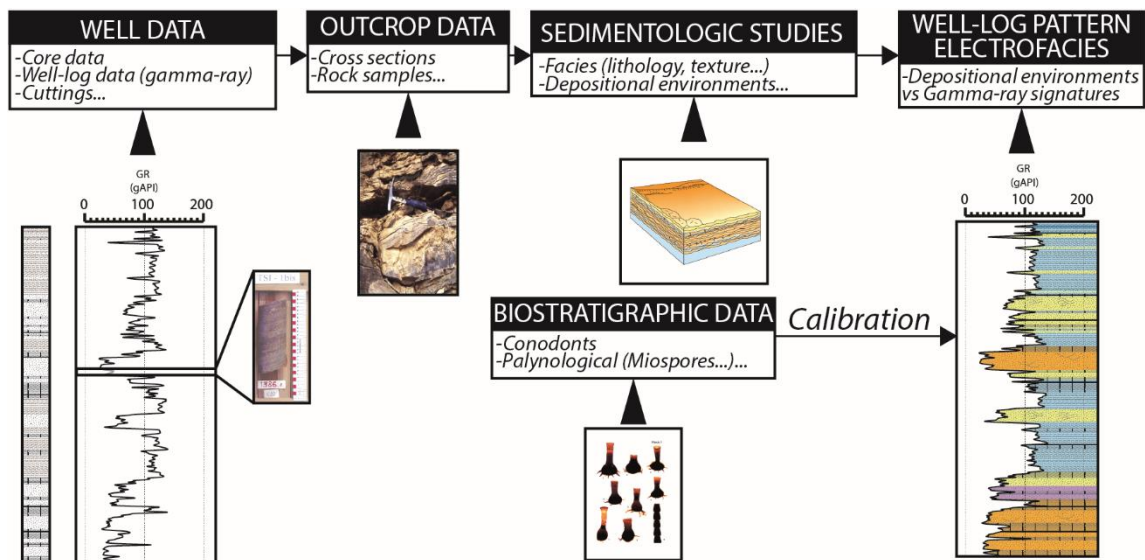


Figure II-3: Methodology of well correlation and interpretation from wireline, cuttings, core and sedimentological studies (e.g. Eschard et al., 1999).

The main tool used was the gamma-ray (GR) log and in some case when not available resistivity (RES) and spontaneous potential (SP). The gamma-ray spectrum registers the natural radioactivity of the rocks (Uranium, Thorium, and Potassium) and is sensitive to clay, K-feldspar, phosphates and organic matter. It can help to determine sand/shale ratio: increase of gamma-ray values usually indicates shales whereas decrease of this value can indicate sandstones (Serra and Serra, 2003). These features make it the most powerful tool to define lithologies. In addition, gamma-ray peaks are frequently interpreted as the maximum flooding surface (MFS) (e.g. Catuneanu et al., 2009; Galloway, 1989; Milton et al., 1990; Serra and Serra, 2003).

This method can be interrogated in littoral environments as these settings can be affected by diagenetic phenomena and glauconitic-rich facies (Hesselbo, 1996). Consequently, calibration of the gamma-ray shape curve with core or outcrop data can afford valuable information of the main sedimentary environments encountered and the stacking pattern. Besides, cuttings data were used to help interpretation and identify different lithologies (e.g. carbonates, clays).

Finally, the extrapolation of the different depositional environments, as identified from the internal, published studies and this work to the well-log patterns (electrofacies) has allowed to reconstruct with satellites images and seismic interpretation the sedimentologic-stratigraphic architecture of the peri-Hoggar Basins.

1.5 Biostratigraphic calibration and flattening

Time calibration of stratigraphic unit was applied from biostratigraphic data (Figure II-3). Knowing that macrofossil is often rare in core and cuttings sample (Legrand, 2002), calibration was mainly done from palynomorph fossils (essentially Chitinozoan and spores). Some data can be provided from cuttings sample, in this case contamination can happen.

In this study some wells present palynological data in the Cambro-Ordovician (e.g. Figure II-4) or in the Devonian (e.g. Figure II-5), which came from internal unpublished data (Abdesselam, 1990; Abdesselam-Rouighi, 1977, 1991; Azzoune, 1999; Beicip-Franlab, 1996; Bouche, 1963; Eschard et al., 1999; Futyan et al., 1996; Hassan, 1984; Khiar, 1974; Magloire and Chennaux, 1965; Robertson, 2002) and from published data (Abdesselam-Rouighi, 1986, 2003; Abdesselam-Rouighi and Boumendjel, 1992; Abdesselam-Rouighi and Coquel, 1997; Boumendjel, 2002; Coquel and Abdesselam-Rouighi, 2000; Kermadjji, 2007; Kermadjji et al., 2008, 2009; Kichou-Braïk et al., 2006; Moreau-Benoit et al., 1993; Oulebsir and Paris, 1995). A biozonation synthesis is available in Figure III-38 and Figure III-39. These data have permitted to calibrate and to date the well correlation stratigraphic sequences.

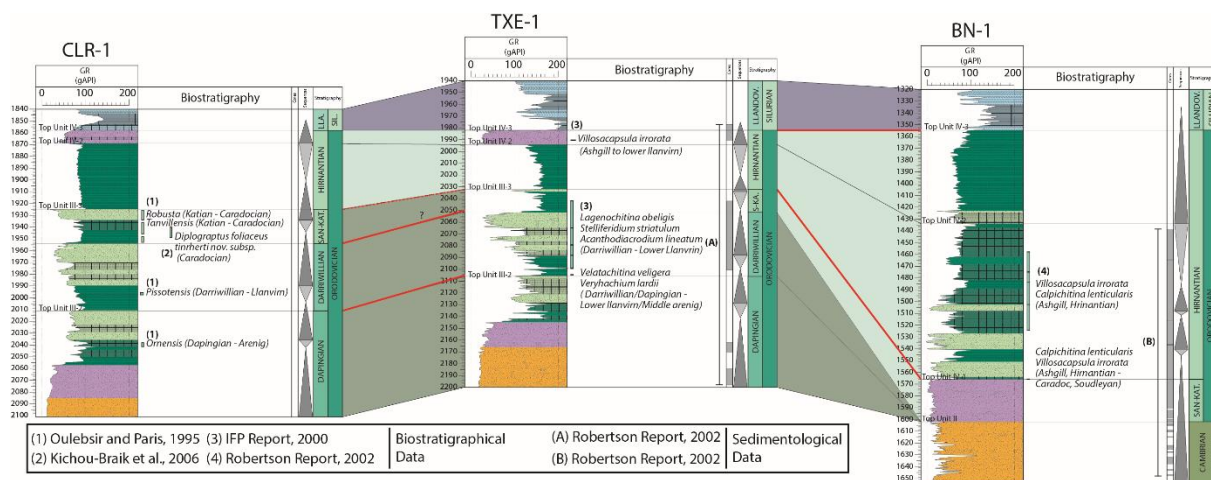


Figure II-4: Example of biostratigraphical (Palynology) correlation in the Ordovician from internal (Eschard et al., 1999; Robertson, 2002) or published data (Kichou-Braïk et al., 2006; Oulebsir and Paris, 1995).

The resolution of the biostratigraphical datations depends on the numbers of biozonations between each stratigraphic unit. Some unit are well constrained by many zonations and others are badly constrained. In addition, biostratigraphical biozonation are different between authors (Figure III-38 and Figure III-39). On the Saharan platform, the Devonian series are better

constrained than other series (e.g. Carboniferous) because of its petroleum interest. The lack of data can also be related to their heterogeneity of repartition (e.g. the Ordovician and the Devonian much more sampled than carboniferous or Cambrian).

Flattening was done at the top Pragian unit (Top C3 unit) or at the top Givetian unit which are well-preserved on the Saharan platform (Biju-Duval et al., 1968). It also corresponds to a major flooding surface on the whole Saharan platform (Carr, 2002; Eschard et al., 2005; Fekirine and Abdallah, 1998). They are also easily identified in log by a high peak of gamma-ray (shales indicator).

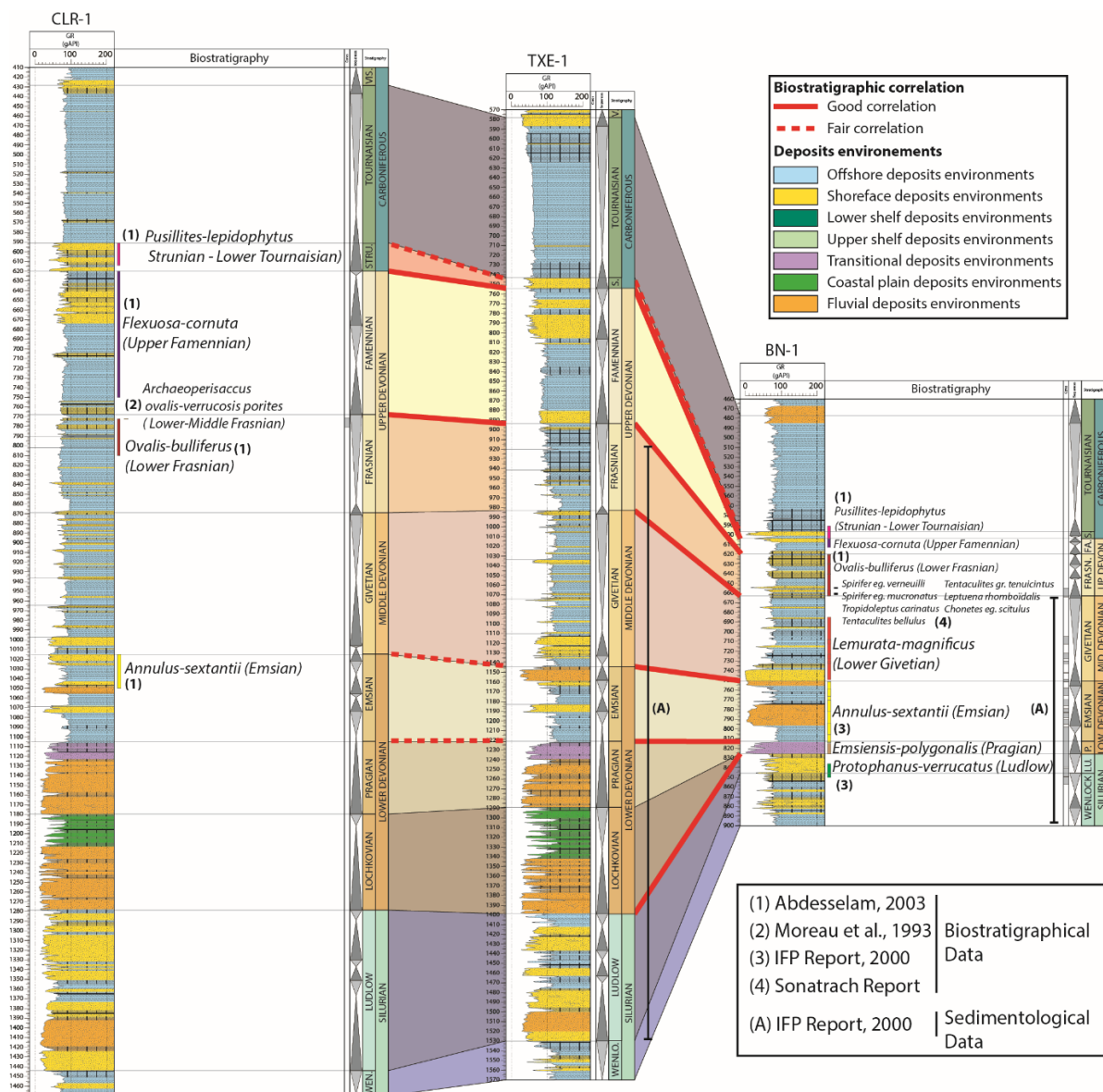


Figure II-5: Example of biostratigraphical (Palynology) good to fair correlation in the Devonian from internal (e.g. Eschard et al., 1999) or published data (e.g. Abdesselam-Rouighi, 2003; Moreau-Benoit et al., 1993).

1.6 Backstripping (software and methods)

Backstripping is a method used to restore the initial thickness (i.e. paleo-thickness) of a sedimentary column (Allen and Allen, 2005). The backstripping analysis assumes some errors and limitations which may arise from uncertainties around the data used and method (Chevalier et al., 2003; Holt et al., 2010; Lachkar et al., 2009; Xie and Heller, 2009): (1) mechanical compaction of sediments (ignoring chemical processes such as cementation); (2) accuracy of the measurement and report of the sedimentary thickness; (3) amount of erosion or non-deposition; (4) backstripping calculation; (5) paleo-bathymetry estimations; and (6) age control.

Due to resolution of wireline tools (i.e. log registering all 5 to 20 centimetre), all selected sections have been measured at a decametric scale.

Lithological compositions features have determined by interpretation of gamma-ray patterns and cuttings. Paleo-bathymetry were estimated from depositional environments. Porosity experimental data are based on (Sclater and Christie, 1980) Chrono-stratigraphical age are based on Ogg et al., (2016).

Subsidence analyses is led with OSXbackstrip software, featured by 1D Airy backstripping code after Allen and Allen, (2005) and Watts, (2001). The morphology of the backstripped curve and subsidence rates can give clues on the nature of the sedimentary basin (Xie and Heller, 2009).

2 Characterization of basement heritage (WP2)

To explore the nature of the basement (WP2; Figure II-1), a terrane map was constructed from integration of geophysics (aeromagnetic anomaly map: <https://www.geomag.us/>, Bouguer gravity anomaly map: <http://bgi.omp.obs-mip.fr/>), geologic (geologic structural map) and geochronologic data (e.g. U-Pb radiochronological).

Black et al., (1994) was the first to interpret the Hoggar massif (Tuareg Shield) as a composite of 23 terranes. To distinguish the terranes, he proposed three main working criteria for distinguish the terranes: “(1) Boundaries between terranes may be thrust fronts, some having ophiolitic remnants, or steep ductile megashear zones that acted as strike-slip faults under greenschist facies conditions during the late stage of the collision. (2) On either side of these boundaries, some features are incompatible if no large relative movements are envisioned i.e., contrasting metamorphic regimes, lithological sequences, geochronological data, vergences,

and major geologic events (e.g., anatexis). (3) Spoon-shaped thrusts at the tip of terranes, triple points indicating truncation of welded terranes by later displacement of another terrane, and molasse facies along terrane boundaries are other discriminators”. From these latter criteria proposed by Black et al., (1994), satellites images (Landsat 7 ETM+ from USGS) and published geologic maps (Berger et al., 2014; Bertrand and Caby, 1978; Black et al., 1994; Caby, 2003; Fezaa et al., 2010; Liégeois et al., 1994, 2003, 2005, 2013), we have redrawn Hoggar’s terranes boundaries and geometries.

2.1 Radiochronological datation compilation

In order to understand the rheology and the thermal age of the different terranes of geochronologic/radiochronology data from published studies have been compiled. These data were georeferenced and integrated in a GIS project to assess the thermo-tectonic age for each basement terranes (data available here: <https://doi.org/10.5194/se-9-1239-2018-supplement>, including 1177 datations points).

Thermo-tectonic ages were grouped into eight main thermo-orogenic events (see Figure 1 in Perron et al., 2018): The Liberian-Ouzzalian event (Arcehan, > 2500 Ma), the Archean, Eburnean (i.e., Paleoproterozoic, 2500–1600 Ma), the Kibarian (i.e. Mesoproterozoic, 1600–1100 Ma), the Neoproterozoic oceanization-rifting (1100–750 Ma), the syn-Pan-African orogeny (i.e. Neoproterozoic, 750–541 Ma), the post-Pan-African (i.e. Neoproterozoic, 541–443 Ma), the Caledonian orogeny (i.e. Siluro Devonian, 443–358 Ma), and the Hercynian orogeny (i.e. Carbo-Permian, 358–252 Ma). During the same time a study has published a similar compilation (Bechiri-Benmerzoug et al., 2017). This method is illustrated in Figure II-6.

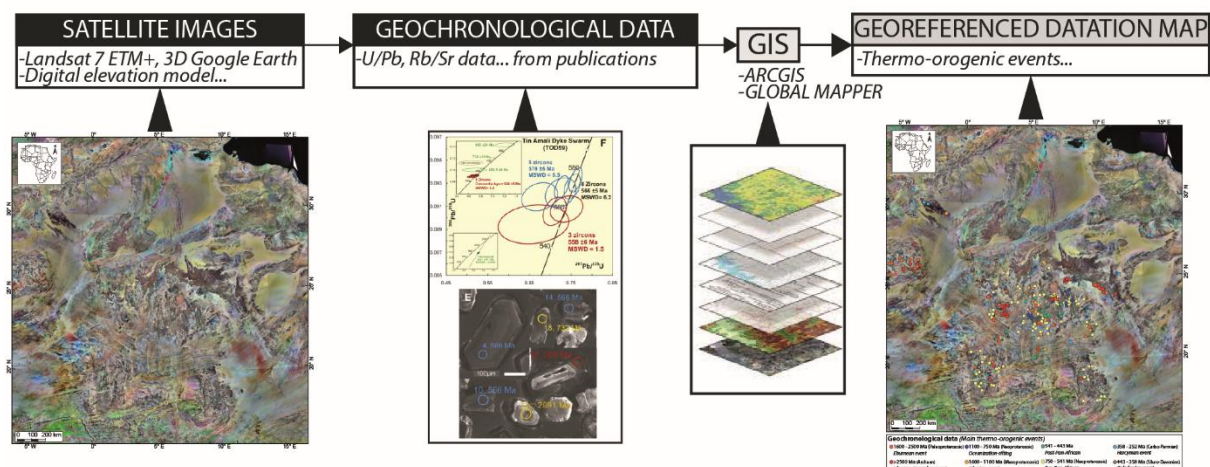


Figure II-6: Compilation and integration of radiochronology data in a SIG project.

2.2 Geophysics and terranes geometries

Aeromagnetic anomaly map (<https://www.geomag.us/>) and Bouguer gravity anomaly map (<http://bgi.omp.obs-mip.fr/>) were used to explore undercover basement structure and structural style (mega shear zone and SC sigmoidal fabrics).

Magnetic anomalies map and gravity anomalies map were integrated in the GIS project and used to detail the geometries of the basement terranes under the Paleozoic series. These tools were used in some publication in the area (Bournas et al., 2003; Brahimy et al., 2018a; Idres et al., 2011). This method is illustrated in Figure II-7 below.

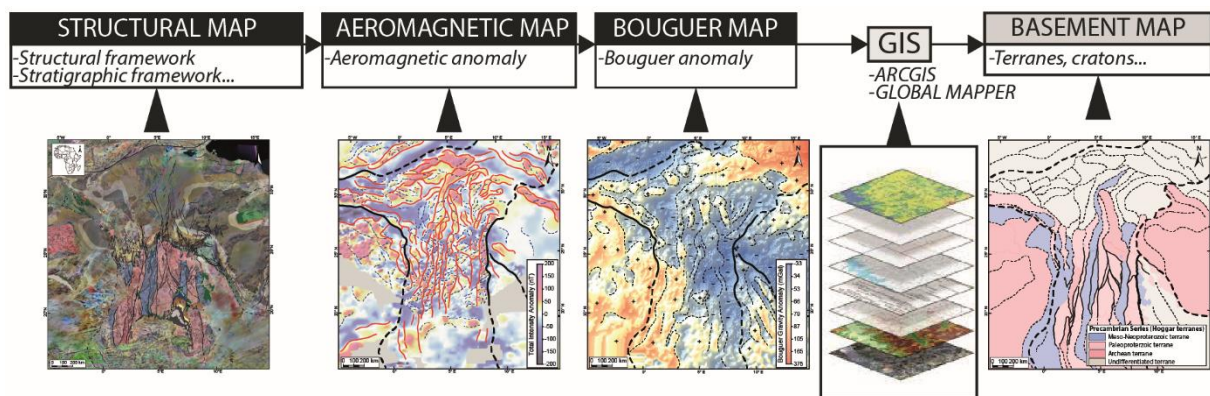


Figure II-7: Methodology characterizing the basement terranes.

3 Lithospheric thermo-mechanical numerical modelling (WP3)

In order to test our hypothesis according to our geological observations, we have used a thermo-mechanical model.

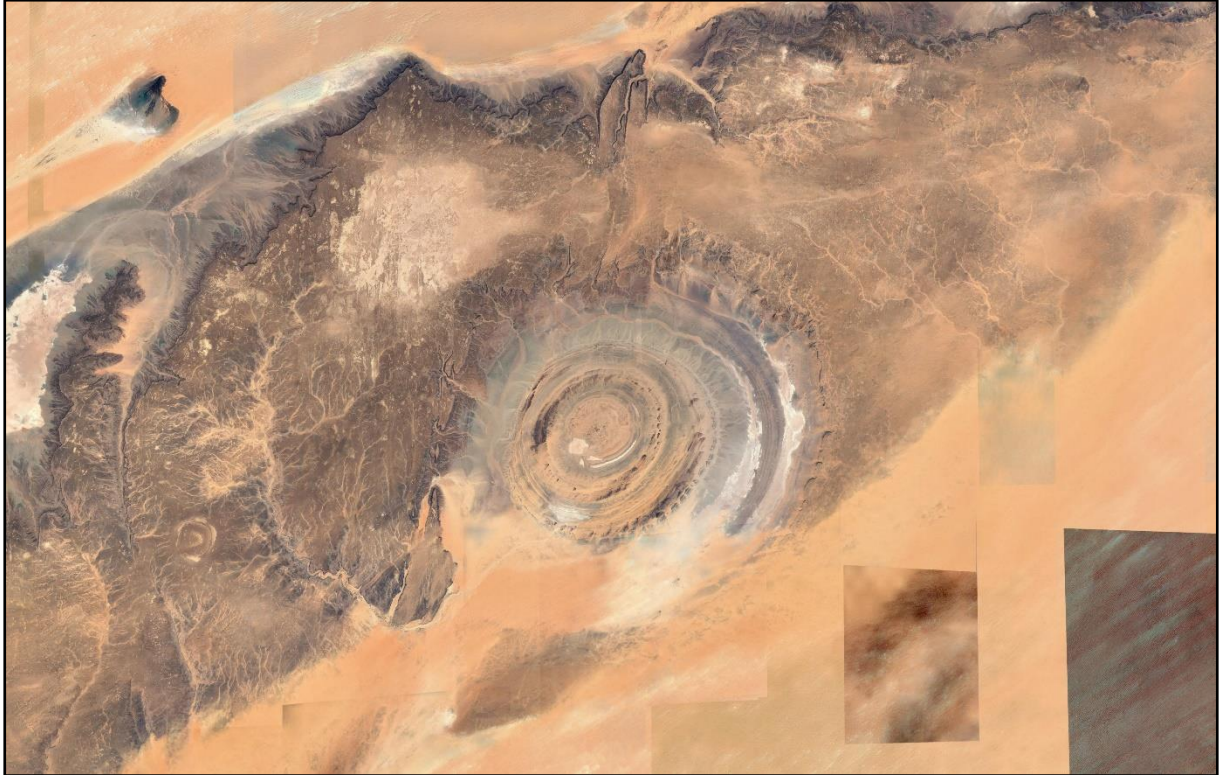
Our approach consists in using a simple numerical thermo-mechanical lithospheric model constrained by our integrated data base. In this purpose, we have used the code pTatin2D essentially developed by Laetitia Le Pourhiet from Sorbonne University. It is defined by a parallel implementation of the finite element method, which employs an Arbitrary Lagrangian Eulerian discretization, together with the material point method. Post-processing and visualization of the different calculated simulation was done via ParaView software. The forward modelled subsidence and thermal curves presented in this study are extracted with some MATLAB scripts modified from Jourdon, (2017). This workflow led to better understand controlling factors of these basins and test the viability of our models. It models the very large-scale forcing parameters and the first order mechanisms at the origins of the magnitude of

wavelength of intracratonic basins. 230 simulations were launched comprising different type of parametrization and tests.

4 Comparison with analogues (WP5)

In order to test and validate the reliability of our forward numerical models, we compare it to collected bibliographic data from other intracratonic basins elsewhere in the world. This step (WP5; Figure II-1) seeks to refine our conceptual model with other world basins. It consists essentially to assembled published literature data. This part was partially achieved and should need furthermore time to constrain our model (see Chapter VIII.3).

CHAPTER III. GEOLOGICAL CONTEXT OF PERI-HOGGAR INTRACRATONIC BASINS (SAHARAN PLATFORM)



Eye of Sahara, the Richat structure (Google-Earth view; 27°07'15" N, 11°23'57" W)



The North Africa (Figure III-1) consists of two distinct units separated by the South Atlas fault (Askri et al., 1995; Figure III-2):

- to the north, an Alpine domain marked by mountain chains of Cenozoic age resulting from the Alpine orogenesis
- to the south, the Saharan platform, a relatively stable region comprising a Precambrian basement on which thick Paleozoic (Ceno-Mesozoic too) sedimentary basins have been deposited.

The Paleozoic Saharan platform including the exposed peri-Hoggar Basins (Figure III-2) is part of the Gondwana. This history is at the origin of his actual tectonic and sedimentologic framework.

According to many authors the palaeohigh or Arches are formed above crustal mobile zones resulting from the terrane accretion during the Pan-African history (Eschard et al., 2010; Fabre, 1988, 2005; Guiraud et al., 2005). Despite this knowledge, there is still a lack of studies trying to apprehend and highlight the main singular characteristics (low rate subsidence, facies portioning, regional unconformities...) of the platform and their relationship with the heritage of Precambrian tectonic structures. Likewise, structural evolution of this intracratonic area is still poorly misunderstood.

This chapter attempts to establish a geologic synthesis of the bibliographic data available on the Paleozoic Saharan platform. We have essentially focused this study on peri-Hoggar Basins, which includes the Reggane, the Ahnet, the Mouydir, the Illizi, Murzuq and the Tim Mersoï Basins.

1 Geographic localization of peri-Hoggar Basins

The peri-Hoggar Basins, part of the northern Africa is located between Morocco at the northwest, the Tunisia at the northeast, Algeria at the center, Mali at the southwest, Niger at the southeast and Libya at the east (Figure III-1). In the south, the landscape is mainly desert environment, formed of large expanses of sand dunes (erg), gravel plains (regs) and with scattered oases islands, while on the coast in the north the climate is Mediterranean. The Eglab massif in the west and the Hoggar massif in the east expose regions of basement Precambrian rocks.

The studied area is exposed on a surface of about 2,700,000 km². The geographic localization and features of each peri-Hoggar Basins are the following:

- **The Reggane Basin**

The Reggane Basin is located in the southwestern part of Algeria at about 300 km southeast from Adrar and 100 km south from the city In Salah, at the eastern edge of the West African Craton (Figure III-1). The geometry is featured by a large asymmetric oval depression, roughly oriented North-West/South-East. It is surrounded by the Reguibat Shield (Yetti-Eglab) westwards, the Azzel Matti Arch eastwards, the Souara high (Ougarta chain) north-eastwards and the Bou Bernous Arch north-westwards. The sedimentary deposits of this basin cover a surface of approximately 140,000 km² (Figure III-2). The Paleozoic series are essentially exhumed on the edges of the basin at the vicinity of the different Arches and massif (e.g. Reguibat Shield, Ougarta Chain).

- **The Ahnet and Mouydir Basins**

The Ahnet and Mouydir Basins are located in the south-western part of Algeria and the north-west of the Hoggar massif (Figure III-1). The Ahnet-Mouydir Basins is surrounded southwards by the Hoggar massif (Tuareg Shield), westwards by the Azzel Matti Arch, eastwards by the Amguid El Biod Arch and separated between together by the Arak-Foum Belrem Arch. At the north, the Ahnet Bains is disconnected from the Timimoun Basin by the Djoua high.

In these basins, the Paleozoic deposits cover a surface of approximately 170,000 km² (Wendt et al., 2006). All the Paleozoic series are well outcropping and preserved in the area especially Carboniferous formations which have been the subject of numerous studies (e.g. Conrad, 1973, 1984; Wendt et al., 2010a). The essential of the Paleozoic formations are laid on the Hoggar

massif basement with a monoclinial dip to the north. This general dip organization is disturbed near Arches (Figure III-2).

- **The Illizi Basin**

The Illizi basin is situated in the south-eastern part of Algeria (Figure III-1). It is bordered by the Tihemboka Arch located near the south-eastern Algeria border and the south-western Libyan border and at 115 km southwest of the In Amenas gas site near the Mesozoic unconformity. The Tihemboka Arch separates the Illizi basin at the West and Murzuq basin at the East. This high associated at the East with the Atchan Arch is situated in the extension of the Djanet terrane southwards at the North-East of the Tuareg Shield.

At the West, the NE-SW Fagnoun fault delimits at the West the SE Illizi sub-basin. The surface zone studied is about 108,000 km² and the average altitude is 540 m (500-620m). Southwards, the Tassili N'Ajjer Paleozoic formations (monocline northwards of Cambrian to Devonian series) are laid on the Hoggar massif basement under significant cuesta form (Figure III-2). This zone has been subject to numerous outcrop studies related to their quality conservation (Beuf et al., 1971; Eschard et al., 2005; Zazoun, 2008).

- **The Murzuq Basin**

The Murzuq basin is mainly situated in the south-western Libya with a surface of approximately 58,000 km² (Figure III-1). The geometry is subcircular, bounded by the Tihemboka Arch westwards, the Tibesti massif eastwards, the Gargaf Arch northwards and the Djado sub-Basin southwards. Somewhere the Tihemboka Arch and the Gargaf are connected (Eschard et al., 2010). The Paleozoic outcropped series are mainly situated on the edges of the basin, near Awaynat area, near the Tihemboka Arch, bordered by the Fagnoun fault, the Gargaf Arch, the Murizidié, the Dor El Gussa area (Ghienne et al., 2013) and the Tibesti massif (Figure III-2). Some of these latter structures as well as the Tiririne high appear as lineaments that do not have significant play at the outcrop (Hallett, 2002; Sola et al., 2000). It separates the Awaynat depression at the west to the Awbari depression at the east.

- **The Tim Mersoï Basin**

The Tim Mersoï basin is situated in the north-western Niger and cover a surface of 1,500 km². It corresponds to a northward branch of the Iullemeden syncline. It extends to Algeria, where it is known as the syncline of Tin Séririne (Figure III-1). It is limited to the West by the In

Guezzam Ridge, to the East by the Air Massif and to north by the Hoggar massif (Konaté et al., 2009). The Paleozoic series, weakly deformed, are particularly well exposed on the Air massif but also on the Hoggar massif (Figure III-2), where they are laid in discordance.

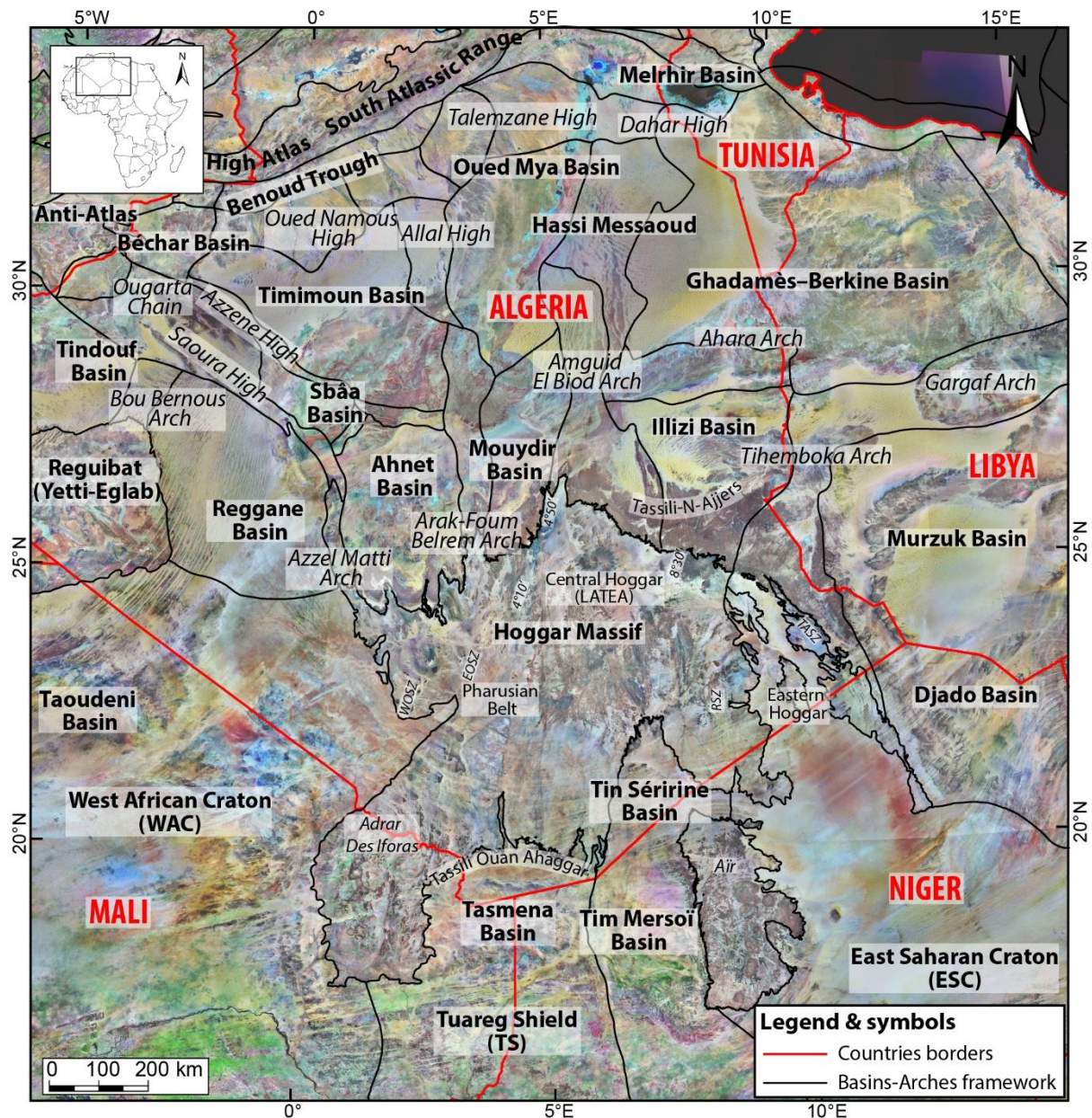


Figure III-1: Localization of peri-Hoggar basins and of the Paleozoic Saharan Platform, part of the North Gondwana (North Africa). The satellites images are from USGS Landsat 7 ETM+ (<https://earthexplorer.usgs.gov/>). Note the presence of outcropping Paleozoic series around the exhumed basement of the Hoggar Massif (800 km large).

2 Geological settings of the Saharan platform

The geological history of the Saharan platform (Figure III-2) is complex and multiphase (alternating quiescence, compressive and extensive phases; e.g. Craig et al., 2008; Fabre, 2005; Guiraud et al., 2005) This characteristic is in particular at the origin of reactivation and inversion structures. Many authors emphasize the importance of tectonic inheritance (Precambrian faults lineaments) on the architecture of current basins (Beuf et al., 1971; Craig et al., 2008; Eschard et al., 2010; Fabre, 1988, 2005; Guiraud et al., 2005).

During Phanerozoic times, the frequent rejuvenation of the fault net was responsible for the regional or local tectonic evolution, with various behaviors in response to changes in the stress fields (Coward and Ries, 2003; Craig et al., 2008). This phenomenon also influenced the development of magmatic provinces (Coward and Ries, 2003; Guiraud et al., 2005).

The fact is that for the petroleum exploration industry, the knowledge of palaeohighs uplift timing separating the Saharan craton into sub-basins is critical to our understanding of the petroleum system evolution (Eschard et al., 2010). The Azzel Matti, Arak-Foum Belrem, Amguid El Biod and Tihemboka Arches are some of these NS complexes fault systems which are at the origin of sub-basin structuring and isolation (Figure III-2 and Figure III-3).

North-Africa including Algeria, Libya and Nigeria are provinces with high petroleum potential. This explains the significant research activity in these areas. In the studied area, the main petroleum system is globally formed by the Cambro-Ordovician and Devonian sandstones (reservoirs) and the Lower Silurian “hot shales” (source rock and seal).

Furthermore, the tectonic evolution of this region is responsible of the establishment of petroleum trap system (structural traps). Indeed, the main tectonic phase that led to the current structure of the basin is undoubtedly the “Hercynian” orogeny but “Caledonian” compression with a lesser extent, also played a role, including on sedimentation (Boote et al., 1998; Coward and Ries, 2003; Eschard et al., 2010; Zazoun, 2001).

In this part, a synthesis of tectonic, geodynamic, sedimentary and geological settings is realized through the compilation of literature data.

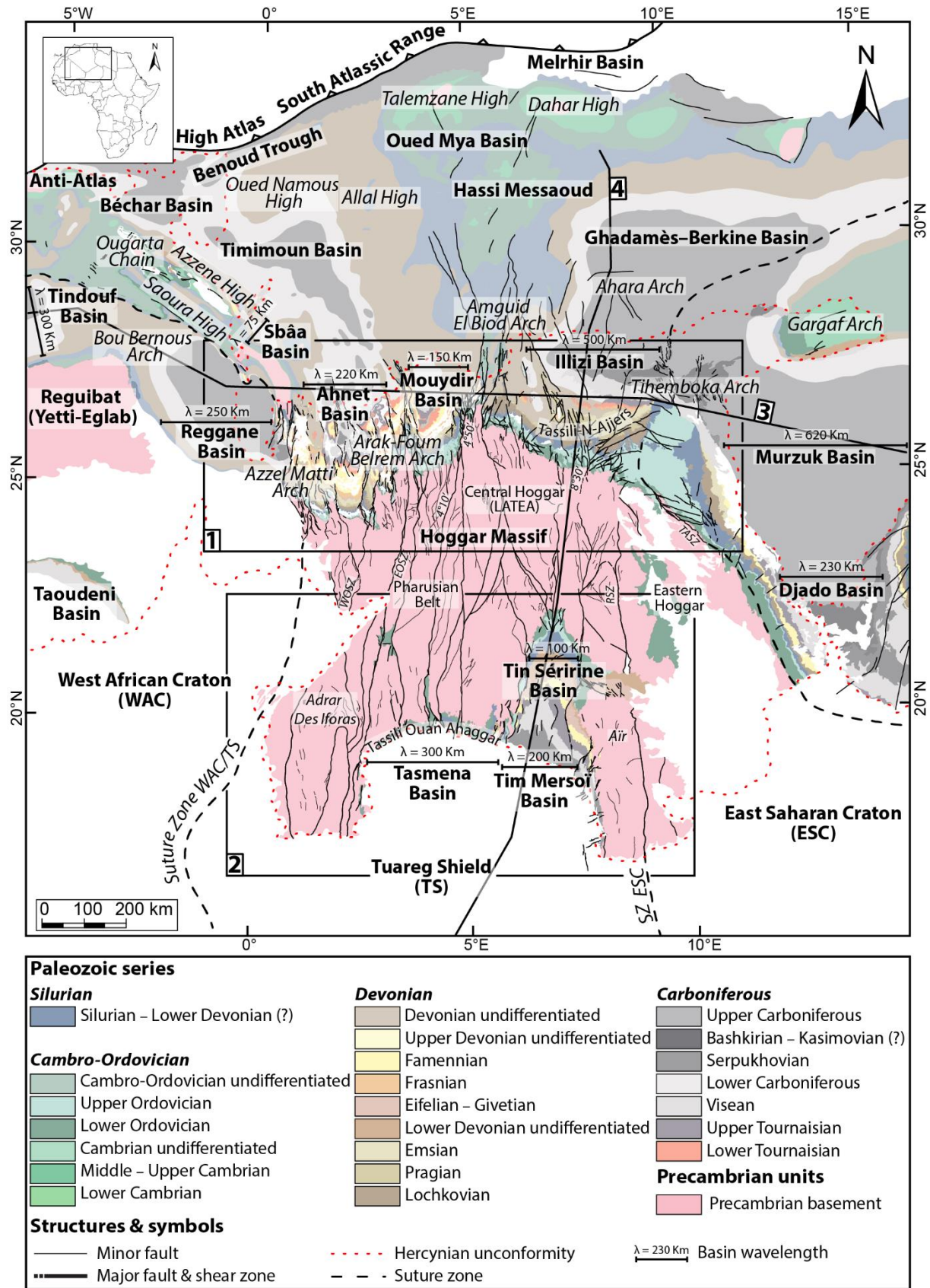


Figure III-2: Geological map of the Paleozoic North Saharan Platform (North Gondwana) georeferenced, compiled and modified from (1) Paleozoic subcrop distribution below the

Hercynian unconformity geology of the Saharan Platform (Boote et al., 1998; Galeazzi et al., 2010); (2) Geological map (1/500,000) of the Djado basin (Jacquemont et al., 1959); (3) Geological map (1/200,000) of Algeria (Bennacef et al., 1974; Bensalah et al., 1971), (4) Geological map (1/50,000) of Air (Jouliia, 1963), (5) Geological map (1/2,000,000) of Niger (Greigertt and Pougnet, 1965), (6) Geological map (1/5,000,000) of the Lower Paleozoic of the Central Sahara (Beuf et al., 1971), (7) Geological map (1/1,000,000) of Morocco (Hollard et al., 1985), (8) Geological map of the Djebel Fezzan (Massa, 1988); Shear zone and lineament names: Suture Zone East Saharan Craton (SZ ESC), West Ouzzal Shear Zone (WOSZ), East Ouzzal Shear Zone (EOSZ), Raghane Shear Zone (RSZ), Tin Amali Shear Zone (TASZ), 4°10' Shear Zone, 4°50' Shear Zone, 8°30' Shear Zone. 1: Figure III-40; 2: Figure III-41; 3: Figure III-3; 4: Figure III-4 and Figure III-34.

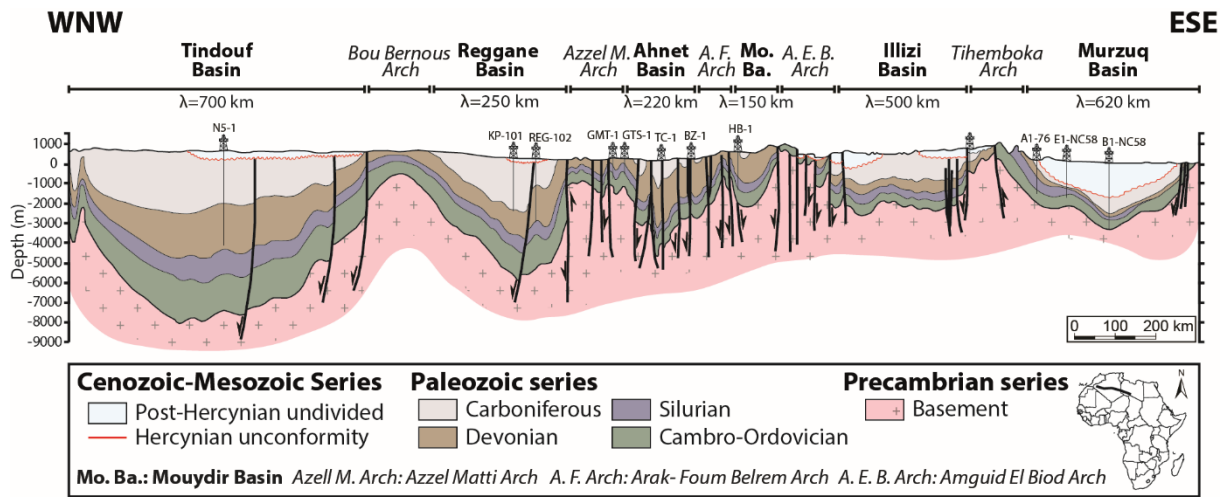


Figure III-3: EW cross section of peri-Hoggar Basins (North Gondwana Platform, North Africa) modified from Craig et al., (2006). For localization see 3 in Figure III-2.

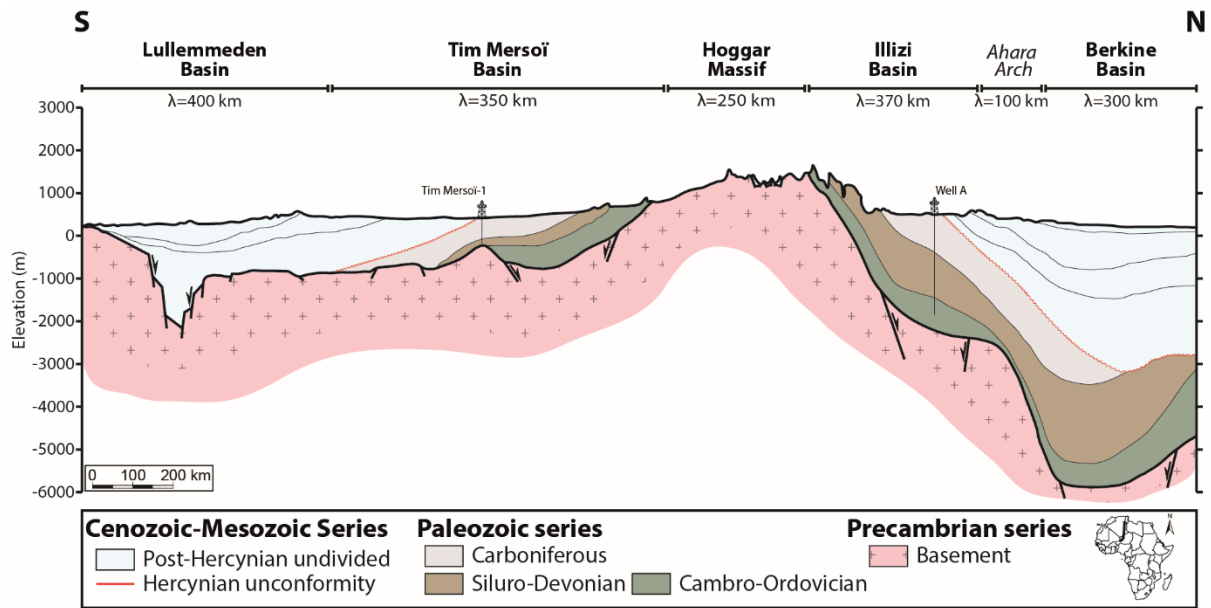


Figure III-4: NS cross section of peri-Hoggar Basins (North Gondwana Platform, North Africa) modified from English et al., (2016b). For localization see 4 in Figure III-2.

2.1 Historical and Previous works

The Saharan Platform has been the subject of several works, from the beginning of the 20th century until today (Figure III-5). Three main periods characterize the research history: (1) The first period (1900-1950) which was mainly devoted to the prospecting of coal and metals; (2) The second period (1950-1970), was oriented towards oil prospecting; and (3) the present period (after 1970) which is more diversified (Figure III-5).

(1) During the first period (1900-1950), Flamand (1911) defined the main stratigraphic lines of the Western North Sahara. Meyendorff (1928) studied Gourara, Touat, Erg Chèche, Tanezrouft and Ahnet. Killian (1925) prepared a synthesis on the geology of the central Sahara. Monod (1931-1932) carried out a geological work in the south-east of the Ahnet. From 1947 to 1957, Lapparent worked on the stratigraphy and distribution of deposits of vertebrates and invertebrates in the regions of Gourara, Touat and Tidikelt.

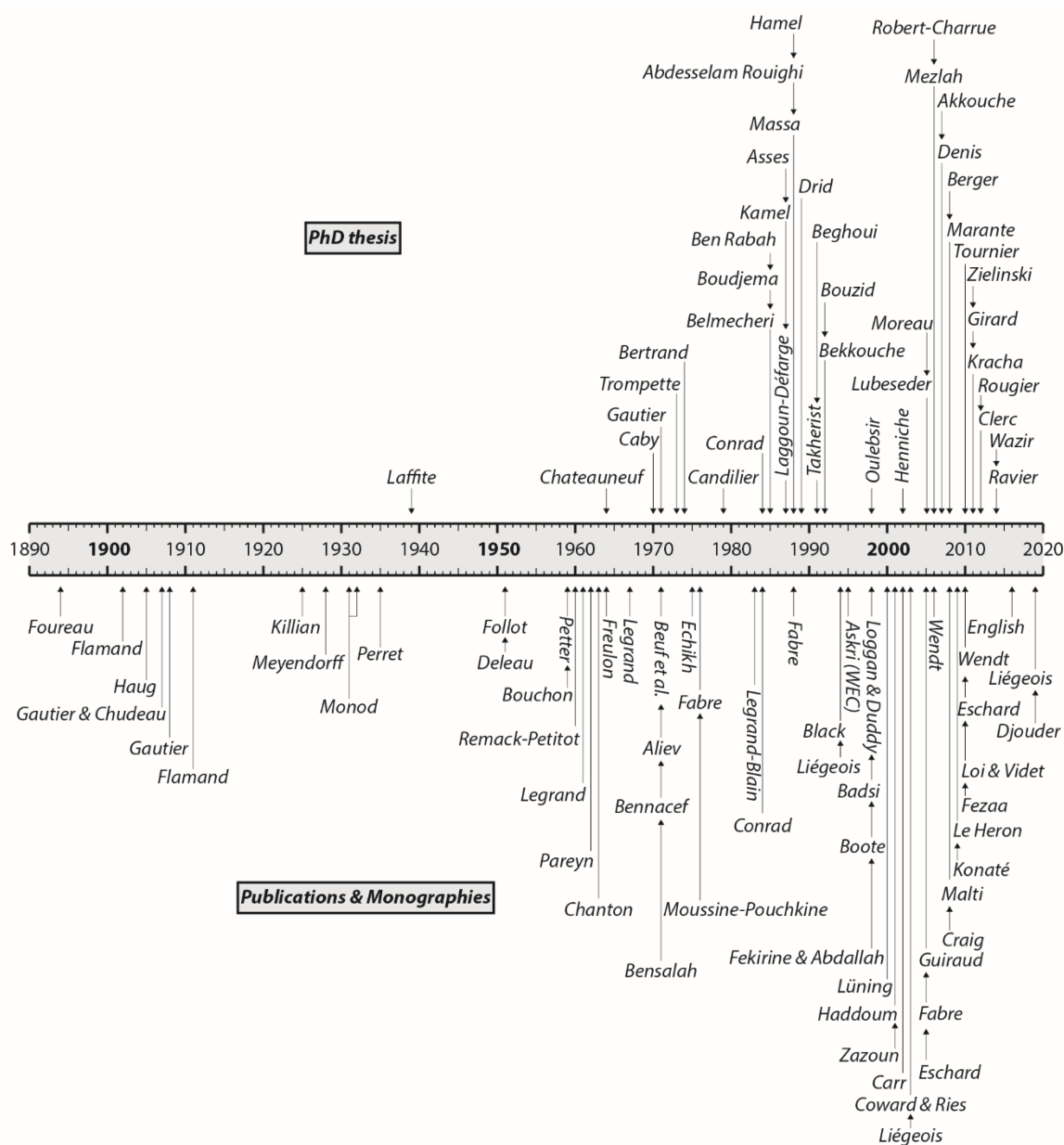


Figure III-5: Chronological repartition of major important PhD thesis, publications and monographies (not exhaustive) in the Paleozoic Saharan platform through the 20 centuries.

(2) During the second period (1950-1970), all the works were carried out by petroleum geologists. They were concerned with the establishment of lithostratigraphy and the definition of the extension of sandstone bodies which were considered as hydrocarbon reservoirs in the Sahara. Among them, we can cite: The regional monography of Follot, (1950), (1953); the Devonian Goniatites study of Petter, (1959); the structural analysis of Freulon, (1955), (1964) in the western Tassili area; the geological study of Legrand (1961-1985); the stratigraphy and the sedimentological study of the sandstones of the outer Tassili of the French Petroleum Institute (IFP) published in 1967; the produced and published lithological study of the Tassili

N'Ajjer oriental of Dubois, Beuf and Biju-Duval (1967); the Ordovician study of the Bled El Mass of Beuf (1968); the realization of the post-Hercynian continental evolution of the Algerian Sahara (Saoura, Erg Chèche, Tanezrouft, Ahnet and Mouydir) of Conrad (1969); and the new observations on the Cambro-Ordovician of Bled El Mass of Beuf, Biju-Duval, Maivier and Legrand (1969).

(3) The third period is featured by modern structural, petrographic, and geochemical works, among them we can cite the following: the remarkable published monography on the Lower Paleozoic of the Central Sahara of Beuf et al. (1971); the stratigraphic synthesis on the Paleozoic terrains of the Algerian Sahara of Aliev, (1971); the structural work carried out on the Ahnet presented by Echikh (1975) and Badsı (1998); the Saharan geological synthesis of Fabre (1976); the study of the Ordovician of Bled El Mass by Legrand (1983); the work of Conrad (1984) on the Carboniferous series; the tectonic analysis of Haddoum (1997) on the Hercynian; the study of Logan P. and Duddy I. (1998) investigating the thermal history of the Ahnet and Reggane Basins and consequences for hydrocarbon generation and accumulation; the Hercynian tectogenesis of Zazoun (2001); the major synthesis of Fabre (2005); and the recent stratigraphic work of Wendt et al., (2006) for the Devonian and the Carboniferous Wendt et al., 2010.

Associated to this period numerous PhD works were realized such as the thesis of Mezlah, (2006) on the "Mid-Devonian mud-mounds of the Ahnet and its neighboring regions"; of Kracha, (2011) on the Ordovician reservoirs in the Ahnet basin; of Candilier, (1979) on the palynology of Late Devonian Early Carboniferous of Illizi basin; of Denis, (2007) on the Glacial Ordovician in the Djado; of Lubeseder, (2005) on the Siluro-Devonian of the Sahara; of Takherist, (1991) on structural and heat flow of the platform; of Tournier, (2010) on the diagenesis of Ordovician sandstones (Sbâa Basin); of Wazir, (2014) on the diagenesis petrophysics of Ordovician sandstones (Sbâa Basin); of Laggoun-Défarage, (1987) on diagenesis organic matter (Sbâa Basin); of Moreau, (2005) on the glacial Ordovician (Murzuq Basin); of Girard, (2011) on the glacial Ordovician (Murzuq Basin, Libya); of Bekkouche, (1992) on the Siluro-Devonian sedimentology and diagenesis (Ghadamès Basin); of Akkouche, (2007) on AFTA and petroleum potential (Sbâa-Ahnet Basin); of Zielinski, (2011) on the thermal history (Ahnet-Mouydir Basin); of Clerc, (2012), on Tunnel valley of Upper Ordovician (Anti-Atlas); of Robert-Charrue, (2006) on structural inversion systems (Anti-Atlas); of Kamel, (1987) on Devono-Carboniferous tectono-sedimentary structures (Morocco); of Henniche, (2002) on the

architecture of the Illzi basin; of Marante, (2008) on the architecture and dynamic of the Saharan platform...

Concerning the exhumed basement of the Hoggar massif (formerly Ahaggar), a large quantity of works has been done since the beginning of 19 century. Conrad. Killian and others (e.g. Duveyrier, Roche, Foureau, Nieger.) were in the first to study the Hoggar. They reclaimed a big part of the understanding of this region. From this work Lelubre (1952) undertook a more precise study especially in the central part of the Hoggar but also in the In Ouzzal unit (actually called LATEA). Afterward, more recent geological, geochemical and geochronological studies were led by authors such as Black et al., (1994), Caby, (2003), Bertrand, (1974), Allègre and Othman, (1980), Berger et al., (2014), Bertrand and Lasserre, (1976), Fezaa et al., (2010), Latouche, (1972), Liégeois et al., (2013), Peucat et al., (1996), Trompette, (1973), Vialette and Vitel, (1979), Boissonnas et al., (1969), Ferrara and Gravelle, (1966), Latouche and Vidal, (1974)... They are at the origin of a better understanding of the Precambrian history of the area (see also Ouzegane et al., 2003b for the historicity).

2.2 Main characteristics of the Saharan platform

The Paleozoic Saharan Platform (North Gondwana) is characterized by eight mains singularities documented by many authors (e.g. Beuf et al., 1971; Fabre, 2005):

2.2.1 Paleozoic area

The Paleozoic is featured by an giant sedimentation area of at least 16 million km² (2000 km wide and 8000 km long) covering the Sahara and the Arabian Peninsula from central Atlantic to the Persian Gulf (Avigad et al., 2005; Beuf et al., 1971; Frizon de Lamotte et al., 2013). These deposits constitute the largest area of detrital sediments ever found on a continental crust (Burke et al., 2003).

2.2.2 Sediment thickness and low long-lived subsidence rate

The sediment thickness is low (Figure III-6) except for certain particularly area (e.g. in the Ougarta; Ghienne et al., 2007b). Indeed, these deposits often represent only a few hundred meters or a few thousand meters at most deposited around 250 Ma (Beuf et al., 1971; Eschard et al., 2005; Fabre, 1988). Furthermore, the subsidence rate is very low (Figure III-7 and Figure III-8).

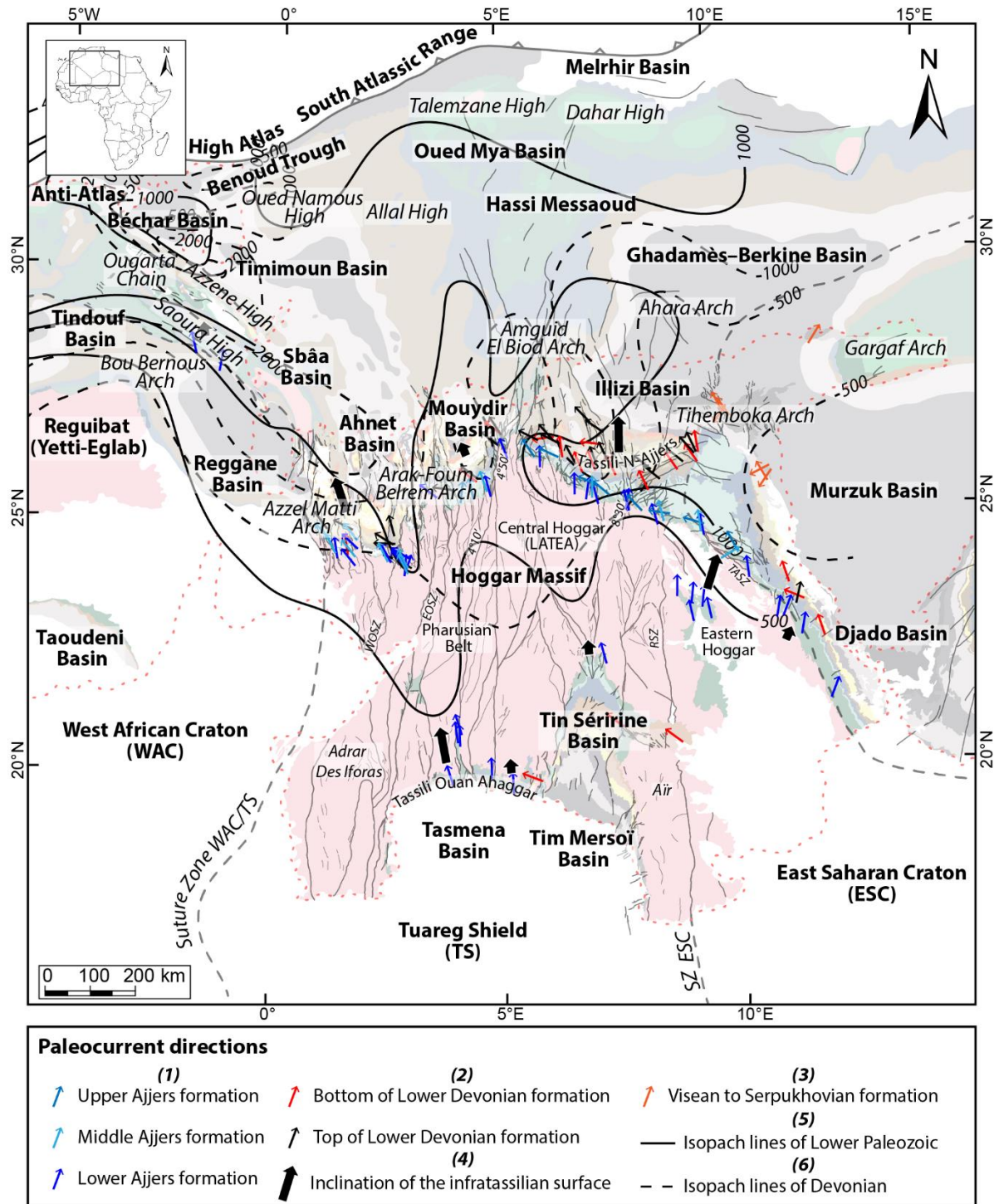


Figure III-6: Compilation of different directions of sedimentary flux and isopach maps during the Paleozoic. (1) Paleocurrent directions measured in the Ajjers formation i.e. Cambrian compiled from Beuf et al., (1971); (2) Paleocurrent directions in the Lower Devonian sandstones compiled from literature (Bennacef et al., 1971; Beuf et al., 1969, 1971); (3) Paleocurrent directions during Visean and Serpukhovian compiled from Fröhlich et al., (2010b); (4) Evidence of the inclination of the “infratassilian” surface (Pan-African surface) to the north according to the directions of the paleocurrents measured in the basic sandstones

of the Cambrian compiled from Beuf *et al.*, (1971); (5) Isopach map for the entire Lower Paleozoic in the North African platform compiled from Fabre, (1988); (6) Isopach map for the entire Devonian in the North African platform from Fabre, (1988).

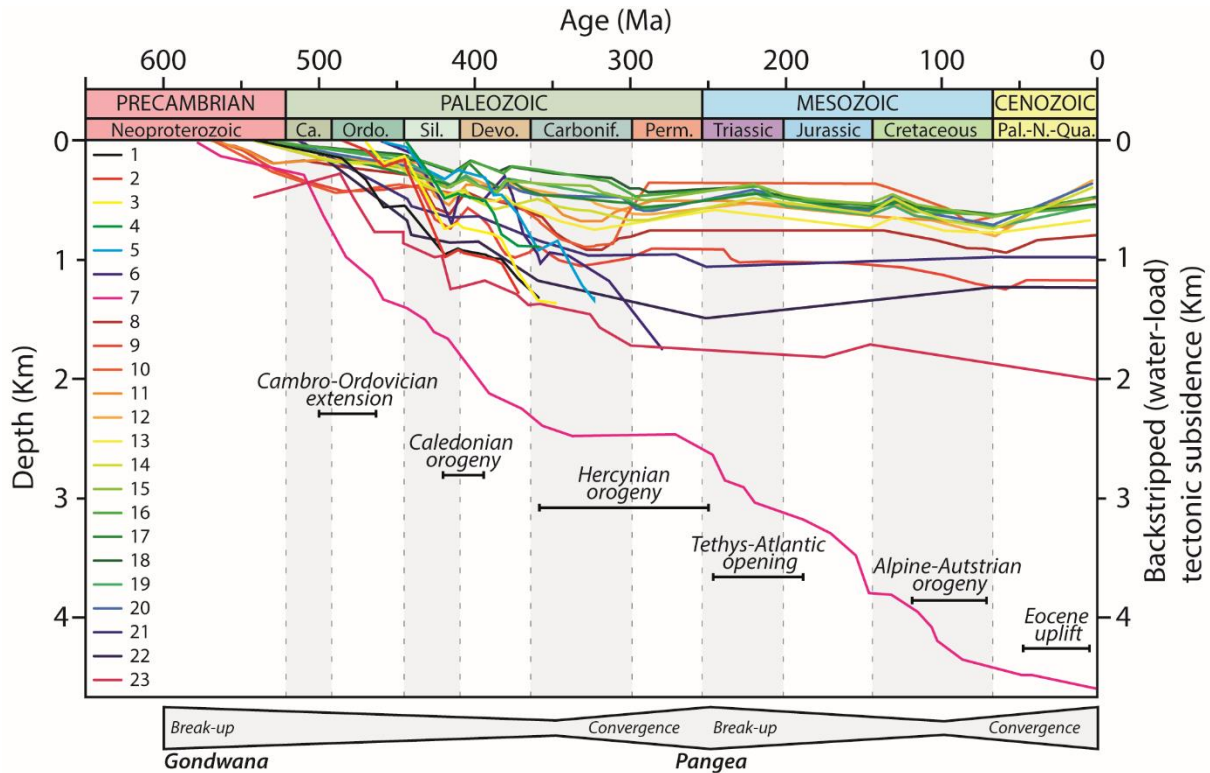


Figure III-7: Backstripped subsidence curves of the Paleozoic North Saharan Platform (peri-Hoggar basins) compiled from literature: **1**: well W17, **2**: well W5 and **3**: well W7 in Ahnet basin, **4**: well W21 in Mouydir basin, **5**: well W1 in Reggane basin (Perron *et al.*, 2018); **6**: well in Sbâa basin (Tournier, 2010); **7**: well in Ghadamès-Berkine basin (Yahi, 1999); **8**: well RPL-101 in Reggane basin, **9**: well HAD-1 in Ghadamès basin, **10**: well REG-1 in Timimoun basin, **11**: well TGE-1 in Illizi basin (Makhous and Galushkin, 2003a, 2003b); **12**: well L1-1, **13**: Pseudowell, **14**: well A1-76, **15**: well F1-NC58, **16**: well J1-NC101, **17**: well A1-77, **18**: well D1-NC58, **19**: well H1-NC58, **20**: well A1-67 in Murzuq basin (Galushkin and Eloghbi, 2014); **21**: Well B1NC43 and **22**: A1NC43 in Al Kufrah basin, **23**: composite well in Ghadames basin (Holt *et al.*, 2010).

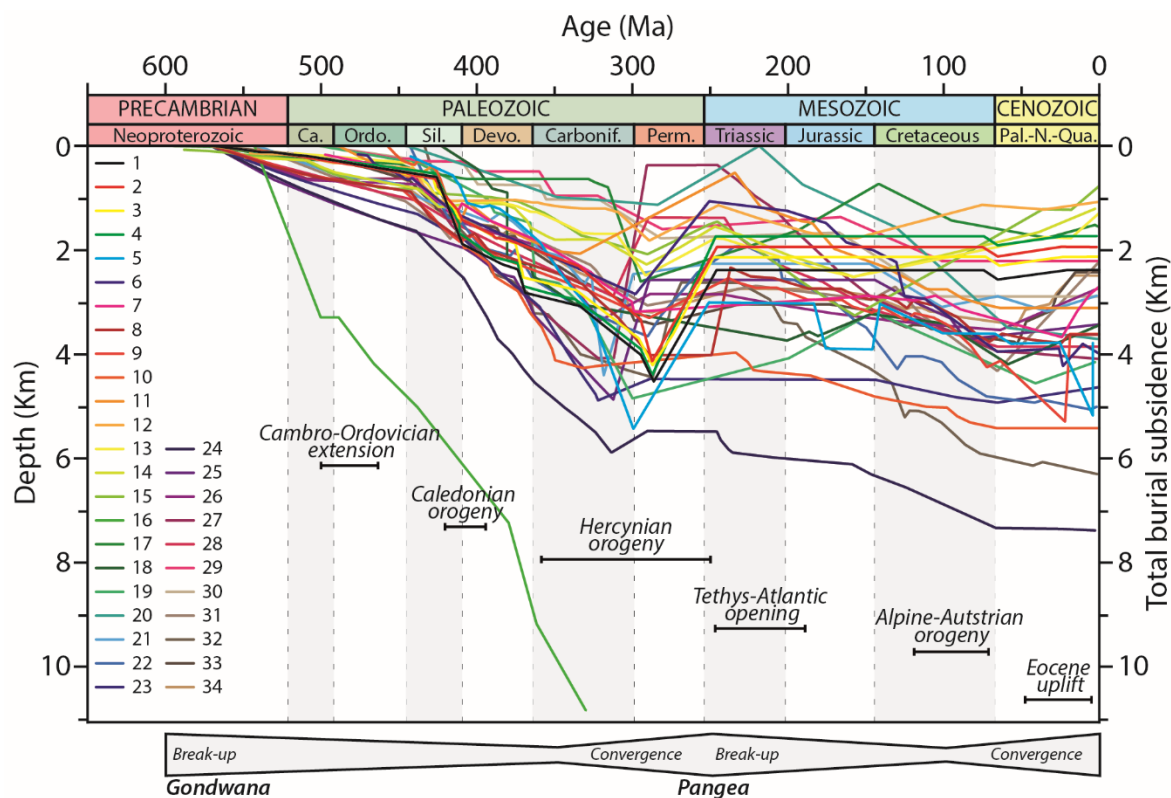


Figure III-8: Total burial subsidence curves of the Paleozoic North Saharan Platform (peri-Hoggar basins) compiled from literature: 1: well W1, 2: well W4, 3: well W7 and 4: well W9 in Ahnet basin (Kracha, 2011); 5: well KB-2 in Timimoun basin, 6: well ELA-1 in Ghadamès-Berkine basin (Kadi et al., 2013); 7: well in the Illizi basin (Wells et al., 2018); wells model 8: A and 9: B in Ghadamès-Berkine basin (Underdown et al., 2007); 10: well LD-1 and 11: well PDG-2 in Berkine-Ghadamès basin (Aissaoui et al., 2016); 12: well F3-NC174, 13: well H29-NC115, 14: well A1-NC186, 15: well A1-NC190 in Murzuq basin (Belaid et al., 2010); 16: cross section in the southwestern Anti-Atlas (Burkhard et al., 2006); 17: well OTRA-1 in the Sbâa basin, 18: well RG-3 in the Reggane basin, 19: well TEG-1 in the Timimoun basin (Logan and Duddy, 1998); 20: Hassi Messaoud field (English et al., 2017); 21: well in Sbâa basin (Tournier, 2010); 22: well in Ghadamès-Berkine basin (Yahi, 1999); 23: well RPL-101 in Reggane basin, 24: well HAD-1 in Ghadamès basin, 25: well REG-1 in Timimoun basin; 26: well TGE-1 in Illizi basin, 27: well TO-1 and 28: well KA-1 in the Dahar depression (Makhous and Galushkin, 2003a, 2003b); 29: well LT-1bis and 30: well OTLA-1 well in the Sbâa basin (Drid, 1989); 31: well LI-1 in Murzuq basin (Galushkin and Eloghbi, 2014); 32: well WT-1 in the Berkine basin (Yahi et al., 2001); 33: well G and 34: well A in the Illizi Basin (English et al., 2016a).

2.2.3 Main terrigenous sedimentation

The sediments are dominated by siliciclastic. Indeed, the Lower Paleozoic series are predominantly composed of detrital sediments, mainly siliciclastic deposited in continental to marine environments (Beuf et al., 1971; Eschard et al., 2005). Though, carbonates occurrences can be observed in the Middle-Upper Devonian to the Carboniferous series (Wendt, 1985, 1988; Wendt et al., 1993; Wendt, 1995; Wendt et al., 1997, 2006, 2009a; Wendt and Kaufmann, 1998). From the South to the North, the depositional environments progressively evolve from fluvial facies to shallow marine facies (i.e. upper to lower shoreface) and then to offshore facies (Beuf et al., 1971; Carr, 2002; Eschard et al., 2005, 2010; Fabre, 1988, 2005; Fekirine and Abdallah, 1998; Guiraud et al., 2005; Legrand, 1967a).

2.2.4 Facies homogeneity

The facies and depositional environments are featured by a great homogeneity and by very slow and subtle lateral variations over time (Beuf et al., 1971; Carr, 2002; Fabre, 1988; Guiraud et al., 2005; Legrand, 2003a; Perron et al., 2018). The homogeneity of the facies and the transitional evolution leads to a general difficulty in defining the different facies envelopes, and in particular to delimit the marine domain of the continental domain (Beuf et al., 1971).

2.2.5 The NNW paleocurrents of the Saharan platform

Measures of paleoenvironments on the Saharan platform indicate that the sediments are globally transported to the NNW (Figure III-6). During the Paleozoic, the general paleocurrent directions changes rather from NNW to NW (Beuf et al., 1969, 1971; Fabre, 1988, 2005; Fröhlich et al., 2010b; Gariel et al., 1968; Le Heron et al., 2009; Wendt, 1995). However, paleocurrent directions can be locally deviated especially near arches (e.g. see red arrows at the base of Devonian series in Figure III-6) due to tectonics events according to some authors (Beuf et al., 1968b, 1971). This main orientation over the whole Saharan domain seems to indicate an inclination of the infracambrian (or “infratassilian” or Pan-African) surface slightly dipping northwards (Beuf et al., 1971; Eschard et al., 2010; Fabre, 1988; Guiraud et al., 2005). It is validated by the South-North deposition profile and by a general thickening of all sedimentary units northward (Beuf et al., 1971; Fabre, 1988, 2005; Garfunkel, 2002; Guiraud et al., 2005). This pattern is interrupted by the presence of paleoighs such as “Arches” where thinning of some units are observed (Beuf et al., 1968b, 1971; Borocco and Nyssen, 1959; Chavand and Claracq, 1960; Eschard et al., 2010; Frizon de Lamotte et al., 2013; Wendt et al., 2006).

2.2.6 Maturity and homogeneity of the mineralogy

The mineralogical composition of the Paleozoic clastics is homogeneous and mature. There are mainly composed of quartz, few encountered micas, rare feldspars (generally altered), and heavy minerals (i.e. zircons, tourmalines and rutiles). Many articles studied the sourcing of the deposits by U-Pb detrital zircons datations (Altumi et al., 2013; Avigad et al., 2003, 2005, 2012; Linnemann et al., 2011; Meinhold et al., 2011, 2013; Morton et al., 2011). The results indicated a local provenance (West African Craton, Tuareg Shield terranes, Cadomian terranes) mainly of Neoproterozoic ages. Extreme chemical weathering and erosion led to the peneplanation of the Gondwanan supercontinent (Pan-African chains) and provided voluminous Paleozoic sandstones deposits (Avigad et al., 2003, 2005; Beuf et al., 1971).

2.2.7 Major widespread unconformities

The platform is marked by major unconformities reflecting sensitivity to climatic variations or tectonic (Beuf et al., 1971; Eschard et al., 2005, 2010; Fabre, 1988, 2005; Guiraud et al., 2005). These unconformities are related to sudden changes in environmental conditions due to global climate changes (glaciation, transgression, etc.), or to angular structures in relation to large-scale tectonic movements ("epirogenic deformations"). From the base of the Paleozoic series, four of them are relevant: (1) the infracambrian (or infratassilian) surface which marks the end of the great phases of deformations and the base of the beginning of the Paleozoic sedimentary history, (2) the discontinuity of the Upper Ordovician (Taconic discordance) resulting from global tectonic movements, and modelled by continental glaciation, (3) the erosive surface of the Silurian which marks a vast marine transgression, and (4) the basal Devonian surface (Caledonian unconformity) that materializes several phases of deformations related to the Caledonian orogeny.

2.2.8 Association of Arches and Basins shape

Arches and Basins of various wavelength (75 to 500 km) settings (Figure III-2, Figure III-3 and Figure III-4) were locally described in the literature (Beuf et al., 1968b, 1971; Chavand and Claracq, 1960; Fabre, 1988, 2005; Frizon de Lamotte et al., 2013; Guiraud et al., 2005; Wendt et al., 2006). During the Paleozoic ancient NS or NW-SE structures were rejuvenated (Beuf et al., 1968b, 1971; Boote et al., 1998; Craig et al., 2008; Dixon et al., 2010; Eschard et al., 2010; Frizon de Lamotte et al., 2013). They have induced an individualized some basins (Beuf et al., 1968b, 1971; Boote et al., 1998; Eschard et al., 2010; Frizon de Lamotte et al., 2013).

2.3 Structural framework of the Saharan platform

North Africa is composed of cratonic cores (i.e. old stable lithosphere) and surrounding accreted terranes (i.e. crustal scale lithospheric block with different geological features) (Abdelsalam et al., 2002; Black et al., 1994; Guiraud et al., 2005; Liégeois et al., 2003, 2013). Specifically, cratonic cores correspond to three main structural entities: The West African Craton, the Touareg shield (including the Hoggar massif) and the East Saharan Craton (Figure III-9; Metacraton according to Abdelsalam et al., 2002). Suture zones define the contact between these different structural units. These suture zones, although formed during the Pan-African orogeny, largely replayed during Hercynian orogens (collision between Gondwana and Africa) and Alpine/Austrian (collision between Laurasia and Europe) (Craig et al., 2008).

These different rheological domains are delimited by large North-South trending crustal shear zone forming the terranes boundaries (Abdelsalam et al., 2002; Bertrand and Caby, 1978; Caby, 2003; Fezaa et al., 2010; Liégeois et al., 2003). These N170°-N20° shear zone characterized by thrusting are more than 600 km long and 500 km large (Denis, 2007). They are marked by a sinistral movement in the western half of the Hoggar and dextral in the eastern half (Black et al., 1994; Caby, 2003; Guiraud et al., 2005; Haddoum et al., 2013).

2.3.1 The West African Craton

The West African Craton is located in the West of Northern Africa. It is consisted of an Archean to Paleoproterozoic basement covered of sediments ranging from the Neoproterozoic to the present time and entirely surrounded by Pan African or Hercynian belts (Peucat et al., 2005; Villeneuve and Cornée, 1994). Two major orogenic stages formed this craton: the Liberian orogeny (3000-2400 Ma) and the Eburnean orogeny (2200-1900 Ma) (Bertrand and Caby, 1978). It is considered stable since when and has minimally affected by recent orogens (Black et al., 1994; Fabre, 1988; Liégeois, 2019).

2.3.2 The East Saharan Craton

The East Saharan Craton is a vast region (~5,000,000 km²) located between the Tuareg Shield and the Arabian-Nubian Shield. It is composed of metamorphic and magmatic rocks and the early dating of Archean rocks in the Uweynat area (Fezaa et al., 2006, 2010, 2013). This area has first been considered as a craton and was named the Nile Craton, the northern part of the large Sahara-Congo Craton, and the Eastern Saharan Craton (Fezaa et al., 2010).

Abdelsalam et al., (2002), compiled all the geochronological and isotopic data on the region and demonstrated that if Pan-African events are largely present, protoliths are largely Paleoproterozoic or Archean in age and that the whole area share numerous pre-Neoproterozoic characteristics and behaved as a single block during the Phanerozoic. They named it “Saharan metacraton”, defining a metacraton as a craton that has been remobilized during an orogenic event but is still recognizable dominantly through its rheological, geochronological and isotopic characteristics (Abdelsalam et al., 2002; Fezaa et al., 2010; Liégeois et al., 2013). Due to the high level of force needed to destabilize rigid and thick cratonic lithosphere, it is most likely that metacratonization occurs dominantly during collisional or post-collisional events (Liégeois et al., 2013). Nevertheless, the term “metacraton” is not accepted by all authors (Bumby and Guiraud, 2005).

According to Liégeois et al., (2013), the Saharan craton was subjected, at the end of the Neoproterozoic, to important collisional events along all its margins against the Tuareg Shield (with the West African craton behind) in the west, against the Congo craton and intervening Pan-African belts to the south, against the Arabian-Nubian Shield to the east, and against an unknown continent to the north. As no tectonic escape was thus possible, the Saharan craton has been metacratonized not only on its margins but also within its interior, as described for the Djanet-Edembo terranes in Eastern Hoggar at the origin of the Murzukian episode (Fezaa et al., 2010).

These collision events might have resulted in reactivation of pre-existing zones of lithospheric weaknesses leading in some places to overgrowth of the cratonic root allowing for negative buoyancy to develop (Abdelsalam et al., 2011).

Fezaa et al., (2010), showed that the Eastern Hoggar was subjected to a late Ediacaran tectono-magmatic episode at 575–555 Ma, unlinked to the Pan-African orogeny. He proposed the existence of a Murzuk craton just to the East, below the Murzuk basin, based on geophysical and sedimentary evidences. This Murzukian intracontinental transpressive episode would be due to the indentation of the Murzuk craton, maybe in response to what occurred beyond this craton to the NE in a similar way as is the intracontinental orogeny. In that model, the Djanet Terrane would be the metacratonic boundary of the lithosphere-thick Murzuq craton (Fezaa et al., 2006, 2010, 2013).

Finally, based on surface geology and geophysical observations (Abdelsalam et al., 2011), Liégeois et al., (2013), interpreted the Western Saharan Craton as a possible composite of three

main craton remnants of the pre-Neoproterozoic: The Murzuq, Al Kufrah and Chad cratons (cf. Figure III-9).

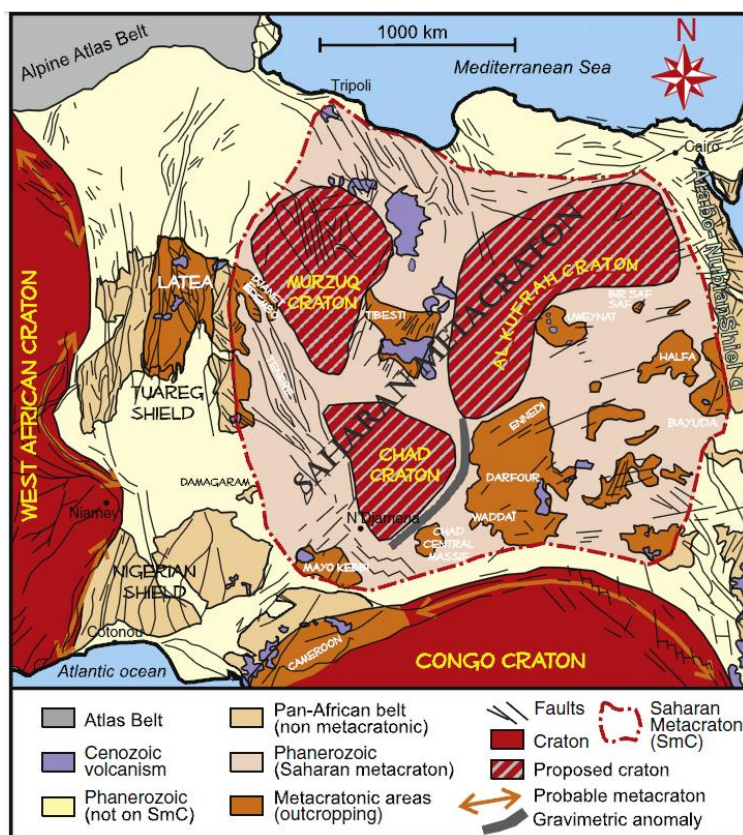


Figure III-9: Main rheological domain of Saharan Africa centered on the Saharan metacraton from Liégeois et al., (2013).

2.3.3 The Tuareg Shield

The Tuareg shield or Trans-Saharan mobile belt (Figure III-10), composed of Hoggar, Air and Iforas regions in Central Sahara was assembled during the Pan-African orogeny, at the end of the Neoproterozoic, as a result of collision between the Tuareg terranes and the West African craton (Caby, 2003; Liégeois et al., 2003, 1994, 2013; Liégeois, 2019).

The Shield Touareg is crossed by major shear zones of crustal scale, sub-vertical dip and oriented generally north-south (N170°E–N20°E) reactivated during the late-Pan-African phase (Caby, 2003; Liégeois et al., 2003, 1994, 2013). Horizontal replays are very important and are usually several hundred kilometers (Caby, 2003). Punching generated by the West African Craton in more ductile mobile zones (terrane Hoggar) resulted in a lateral expulsion of material to the north (Black et al., 1994; Caby, 2003; Coward and Ries, 2003). Thus, the direction of play of these vulnerabilities varies depending on their position in the Hoggar mountains: in the

western half, these setbacks have played in the sinistral sense, while the recesses become dextral in the eastern half of the massif (Black et al., 1994).

An earlier Neoproterozoic supercontinent of Rodinia dispersed and reassembled during the Pan-African so, typically, the Pan-African mobile belts represent full Wilson cycles (Figure III-10), exhibiting rift-related sedimentation and magmatism, passive margin sedimentation, subduction obduction, collision magmatism and tectonics (Bumby and Guiraud, 2005).

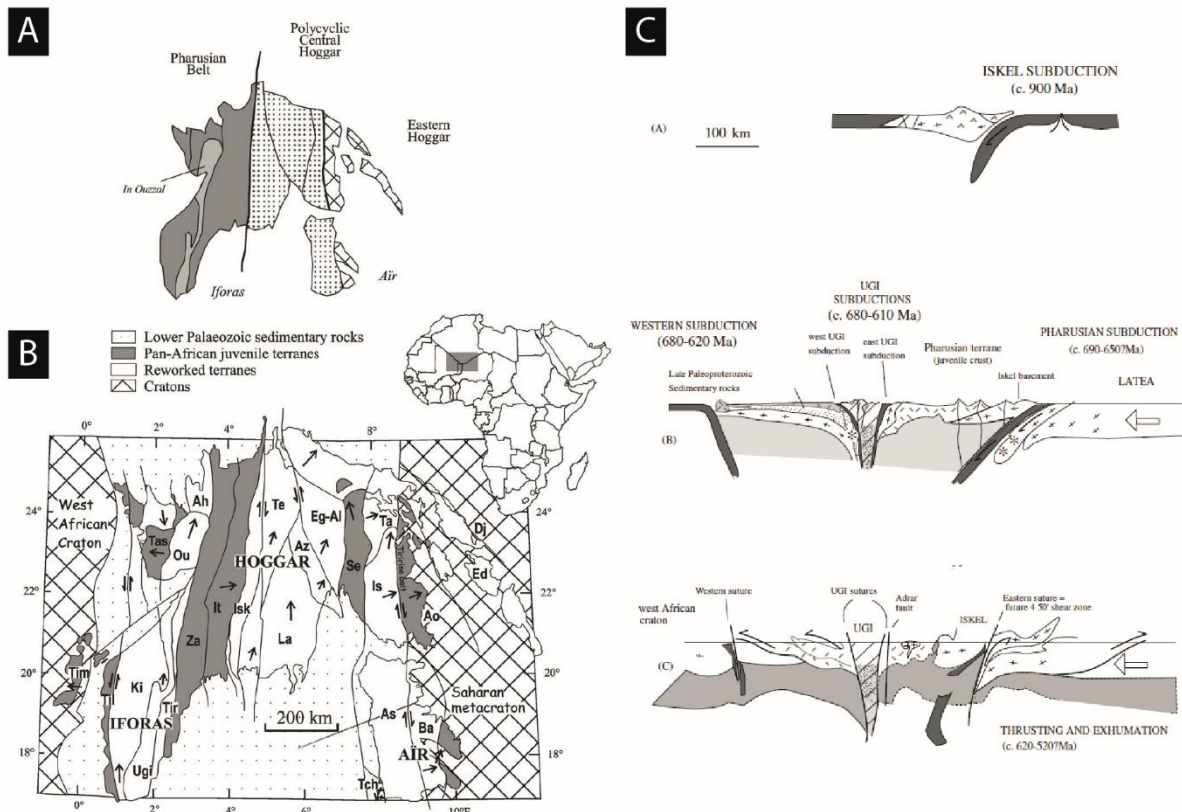


Figure III-10: (A) Historical subdivision. (B) Actual Tuareg shield terrane mapped (Liégeois et al., 2003). (C) Proposed geodynamic evolution of western and central Hoggar between 900 and 520 Ma (Caby, 2003).

2.3.3.1 Western Part (Pharusian)

The western part of the Tuareg shield (Figure III-10 and Figure III-11), instead of the In Ouzzal terrane (200 km to the west of LATEA) is dominantly constituted of terranes (Black et al., 1994; Liégeois et al., 2013). They were formed during an island arc and continental arc subduction-related events (730–630 Ma) followed by Ediacaran collisional and post-collisional events (630–580 Ma) (Berger et al., 2014; Caby, 2003; Liégeois et al., 2003).

During Cambrian times, thick molassic (i.e. dismantling of the Pan-African chain deposits) and volcanic series filled narrow grabens in the western and central parts of Hoggar. Large Paleozoic basins with thick sedimentary series were developed over the Hoggar shield since the Ordovician (Henry et al., 2007). Molasse deposits with volcanoclastic intercalations, reaching more than 6000 m thick, are found particularly in the northwest part of the shield Touareg, bordering the Pharusian chain (Djellit et al., 2002; Fabre, 1988; Henry et al., 2007). They characterize dismantling, uplift and peneplanation chain (Craig et al., 2008; Fabre, 1988, 2005; Guiraud et al., 2005).

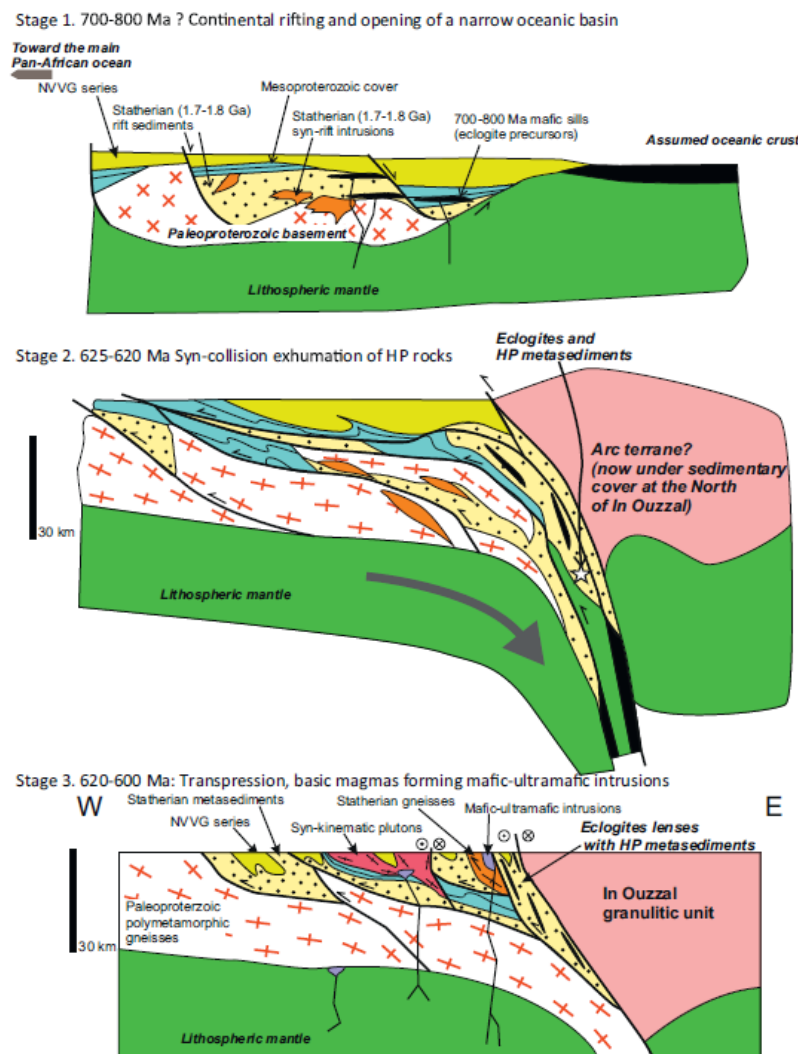


Figure III-11: Interpretative sketch summarizing the geodynamic evolution of the Tassendjanet-Tidéridjaouine terrane (western part of the Hoggar Massif) deduced from data collected on eclogite and garnetamphibolites (Berger et al., 2014).

2.3.3.2 Central Part (LATEA)

The central Hoggar (Figure III-10), historically named “Polycyclic Central Hoggar” (Caby and Andreopoulos-Renaud, 1987), located 400 km east of the suture between the Tuareg shield and the West African craton, had a different evolution. It has been shown that the four terranes constituting the Central Hoggar (Black et al., 1994) were part of a single pre-Pan-African passive margin (Liégeois et al., 2003). The acronym LATEA (from the first letters of the names of the four terranes, Laouni, Azrou-n-Fad, Tefedest, Egéré Aleksod; Figure III-10) was given to this region (Liégeois et al., 2003). LATEA was formed during the Eburnian orogeny (i.e. paleoproterozoic; Liégeois et al., 2003). It is made of Archean and Paleoproterozoic metamorphic and magmatic rocks (Black et al., 1994; Fezaa et al., 2013; Liégeois et al., 2003) behaved as a craton during the Mesoproterozoic and the Early and Middle Neoproterozoic where oceanic terranes (such as the juvenile Iskel terrane and the Tin Begane eclogite-bearing nappes) were accreted along its margins (Figure III-12) during Cryogenian and Ediacaran periods (Caby, 2003; Liégeois et al., 2003).

In the LATEA basement there is no Neoproterozoic events recorded older than 630 Ma, a time that marks the beginning of the Tuareg/West African craton collision. During that collision, the LATEA craton was dissected into several terranes and intruded by batholith largely from a preponderant Paleoproterozoic/Archean crustal source (Liégeois et al., 2003, 2013).

The partition of LATEA lithosphere was accomplished through the activation of mega-shear zones that accommodated several hundred kilometers of horizontal displacement (Liégeois et al., 2003, 2013). These shear zones are interpreted as escape roots of the northward expulsion of the Tuareg terranes as LATEA was squeezed between the West African craton to the west and the Saharan metacraton to the east (Black et al., 1994; Liégeois et al., 2013).

Furthermore, since 580 Ma, LATEA was reactivated along the same shear zones sporadically which both triggered igneous activities and volcanism episodes (Liégeois et al., 2003, 2013). Additionally, Beuf et al., (1971), exposed that these shear zones had controlled Paleozoic sedimentation (presence of large thickness variations of the Paleozoic sedimentary section across these zones). *The mega shear zones and the different types of terranes will be fundamental for the understanding of the processes associated with the evolution of the paleozoic intracratonic basins (cf. Chapter VI and Chapter VII).* The above analysis indicates that LATEA behaved as a craton during the Tonian and Cryogenian periods when there were no marked collisional orogenic events, except arc accretions not affecting the LATEA basement (Liégeois et al., 2003, 2013).

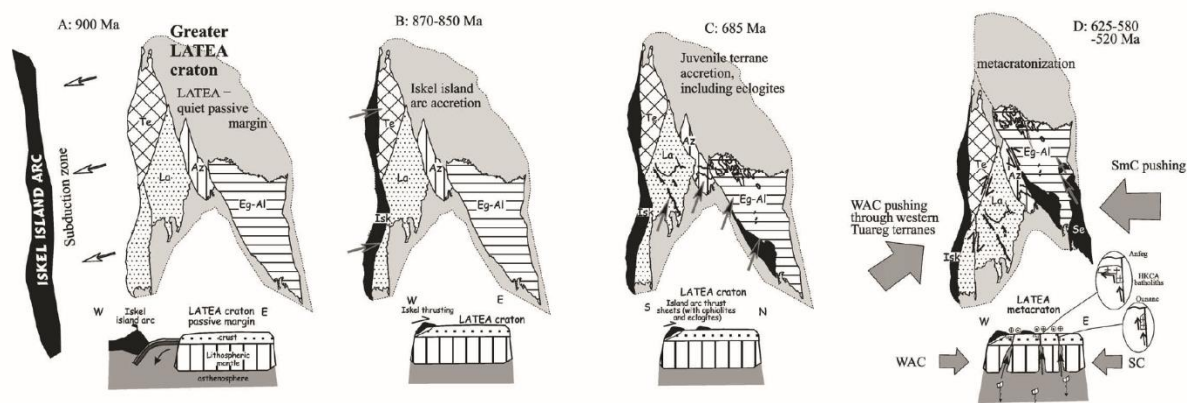


Figure III-12: Tuareg Shield formation: terranes accretion modified from Liégeois et al., (2003). (A) 900 Ma: LATEA constitutes a passive margin without any applied stress; this is the period of the building of the Iskel island arc with the subduction plane dipping away from LATEA craton; the limits of the greater LATEA craton is inferred from available drillings (Latouche, pers. observations). (B) 870–850 Ma: accretion of the Iskel island arc onto the LATEA cratonic passive margin. (C) Accretion onto LATEA of juvenile terrains represented by eclogites, ophiolites and other various oceanic lithologies, including that studied here in the Tin Begane area. (D) Period of metacratonization of LATEA: LATEA is squeezed between the West African craton (WAC) to the west and the Saharan craton (SC) or metacraton (SmC) to the east. LATEA is dissected by mega-shear zones generating linear lithospheric delamination and asthenospheric uprise.

2.3.3.3 Eastern Part

Eastern Hoggar (Figure III-13) is bounded to the west by the Raghane megashear zone (Liégeois et al., 2003, 2013), which is also the western boundary of the Saharan metacraton (Abdelsalam et al., 2002).

It is composed of three contrasted NW-SE oriented terranes (Black et al., 1994). These terranes are from west to east: The Aouzegueur terrane (Ao; eastern part of the Hoggar Massif, Figure III-10), composed of Neoproterozoic oceanic rocks thrust eastward (Fezaa et al., 2010; Liégeois et al., 2003, 2013) during the 800-650Ma period with granitic plutons intruding these structures at 600Ma; the Edembo terrane (Ed; eastern part of the Hoggar Massif, Figure III-10), composed of an amphibolite-facies metamorphic basement intruded by various granitoids and considered as an intracontinental hot belt (Liégeois et al., 2013); the Djanet Terrane, composed of greenschist-facies sediments intruded by high-K calcalkaline granites (Black et al., 1994). No

oceanic-related rocks are known in the two latter terranes (Fezaa et al., 2010; Liégeois et al., 2013).

The Djanet Group (Dj; eastern part of the Hoggar Massif, Figure III-10), equivalent to the Tiririne Group, constitutes the oldest rocks in the Djanet and Edembo terranes (Fezaa et al., 2010; Liégeois et al., 2013). During this period (600Ma), the Tuareg shield to the west of the Raghane shear zone was considered as a stable lowland craton (Black et al., 1994; Liégeois et al., 2003, 2013). However, these two terranes were affected during 575–545 Ma by metamorphic events of different metamorphic grades (Fezaa et al., 2010a).

This led Fezaa et al., (2010) to propose a distinct event called the Murzukian orogenic episode (570-550 Ma; *Figure III-13*) that affected the entire Eastern Hoggar. This orogenic event is linked with the stress induced at the western margin of a newly-discovered rigid entity to the east referred to by Fezaa et al., (2010) as the Murzuq craton.

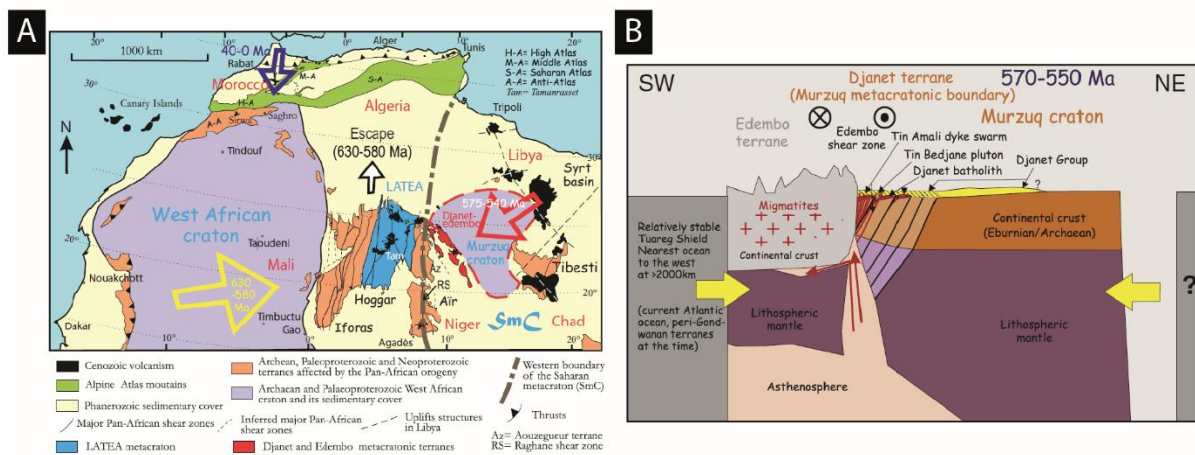


Figure III-13: (A) Main rheological domains from North-West Africa with enhancement of the LATEA metacraton and of the Djanet and Edembo metacratonic terranes (Liégeois et al., 2013). (B) Schematic model section at 570–550 Ma of the Murzuq craton. Metacratonization resulted from the intracontinental convergence of the Murzuq craton, relaying a northern unknown continent push and the relatively stable Tuareg shield, leant against the West African craton (Fezaa et al., 2010; Liégeois et al., 2013).

The late Ediacaran Murzukian (Figure III-13) event is thus an intracratonic event resulting from a convergence at plate boundaries beyond the limits of the Murzuq craton (Fezaa et al., 2010). It has been proposed that this event was due to vertical planar lithospheric delamination during transpressive movements along pre-existing weakness zones inherited from the

Paleoproterozoic evolution of these terranes as a result of the indentation of the Murzuq craton (Fezaa et al., 2010).

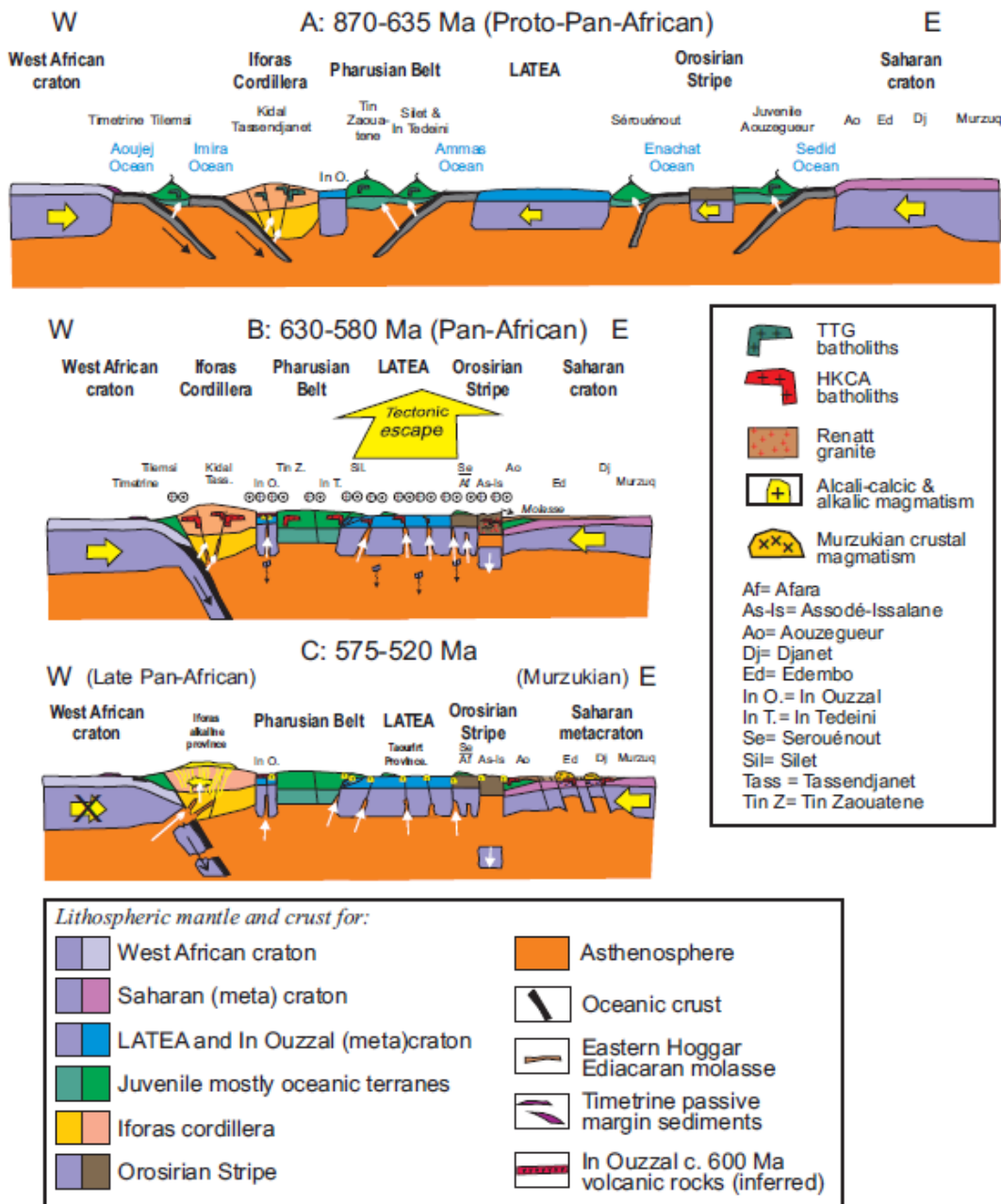


Figure III-14: Sketched E–W cross-sections through the Tuareg Shield showing terranes accretion (Liégeois, 2019).

To summarize: The Precambrian history of the Hoggar corresponds to several complete Wilson cycle (Figure III-14). The neoproterozoic Pan-African orogeny was responsible of the accretion of three types of lithospheres: the Ouzzalian-Oumelalian (>2.7 Ga; Paleoproterozoic to Archean cratons; e.g. Ferrara and Gravelle, 1966; Latouche and Vidal, 1974; Ouzegane et al., 2003a),

the older strongly metamorphic Suggarian as the equivalent of the Eburnean (~2 Ga orogeny; continental lithosphere delaminated métacratons; e.g. Ouzegane et al., 2003b; Peucat et al., 2003, 2005) or of the middle Palaeoproterozoic (2.2–1.8 Ga) and the younger slightly metamorphic Pharusian as the equivalent of the Pan-African (~0.6 Ga orogeny; oceanic lithosphere and Neoproterozoic metasediments; Berger et al., 2014; Bertrand and Lasserre, 1976; Black et al., 1994; Caby, 2003; Liégeois et al., 2003; Liégeois, 2019).

2.3.4 Deep geophysic structures of the Saharan lithosphere

Many studies have documented through geophysics tools (tomography, resistivity...) the deep structures of the Hoggar massif and the Saharan platform. Liégeois et al., (2005) has proposed a model (Figure III-15) showing through tomography the differential thickness between the diverse entities of the lithosphere. Cratons and terranes are identified and circumscribed by geophysics such as the Saharan shield (Abdelsalam et al., 2011), the terranes of Hoggar Massif (Bournas et al., 2003; Brahimy et al., 2018a; Takherist, 1991) and the West African Craton (Roussel and Lesquer, 1991). Others authors, have displayed the lithospheric scale of the shear zones identified on the massif (In Ouzzal terranes) through magnetotelluric modeling (Bouzid et al., 2008).

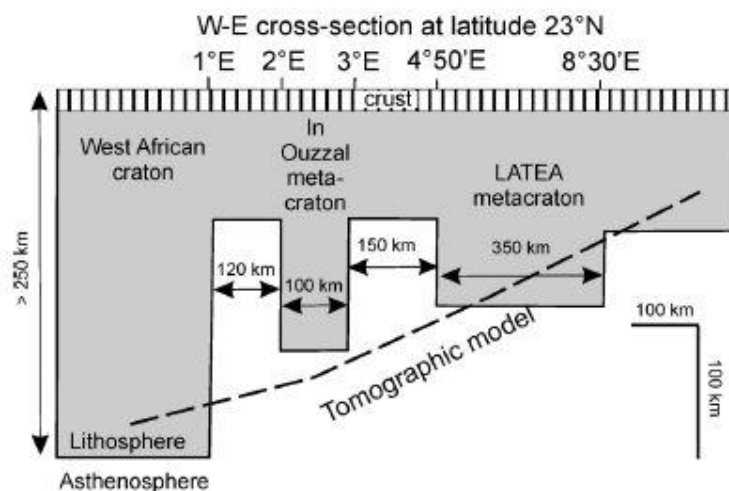


Figure III-15 Lithospheric model based on geology and tomography showing differential lithospheric thickness between terranes and cratonic cores from Liégeois et al., (2005).

2.4 Geodynamic and unconformities of the Saharan platform

North Africa is composed of three major structural entities (Figure III-2), namely the West African Craton (WAC), the Tuareg Shield (TS) and the East Saharan Craton (ESC). It has formed part of a single lithospheric plate throughout the Phanerozoic and, hence its structural development has been controlled to a large degree by intraplate processes (e.g. Holt et al., 2010; Ziegler et al., 1998). The majority of Phanerozoic tectonism and magmatism within the North African plate can be considered to have occurred along broad lineaments, which represent repeatedly reactivation and exploitation of earlier, Late Proterozoic Pan-African sutures (heterogeneity, shear zones...), and which formed generally between 720 and 550 Ma (Beuf et al., 1971; Bumby and Guiraud, 2005; Craig et al., 2008; Galeazzi et al., 2010; Guiraud and Bosworth, 1997). This featured determines the main deformation trends, especially the N-S Pan-African basement fault systems (Figure III-2; Bumby and Guiraud, 2005; Galeazzi et al., 2010; Guiraud et al., 2005). The interpretation of the formation of Phanerozoic basins is often accomplished by considering the inter-relationship between the orientations of Phanerozoic stress fields relative to the orientation of the Pan-African trends (Beuf et al., 1971; Bumby and Guiraud, 2005; Craig et al., 2008; Guiraud and Bosworth, 1997).

The Paleozoic North Saharan Platform including the peri-Hoggar basins was a part of the northern passive margin of the Gondwana supercontinent and experienced a complex and polyphase history (Boote et al., 1998; Craig et al., 2008; Fabre, 1988; Guiraud et al., 2005).

The Saharan Paleozoic intracratonic basins have experienced sixteen major tectonic phases, thus affecting sedimentation through geological time. They are the following:

2.4.1 The Eburnean Orogeny (c. 2000 Ma)

The Eburnean orogeny, or Eburnean cycle was a series of tectonic, metamorphic and plutonic events in what is now West Africa during the Paleoproterozoic era (i.e. about 2000 ± 100 Ma).

In the Hoggar massif, this event is identified in several places such as Tassendjanet, In Ouzzal (cf. Figure III-16), Aleskod and Oumelalen areas (Allegre and Caby, 1972; Bertrand and Caby, 1978; Bertrand and Lasserre, 1976; Latouche and Vidal, 1974; Ouzegane et al., 2003b, 2003a).

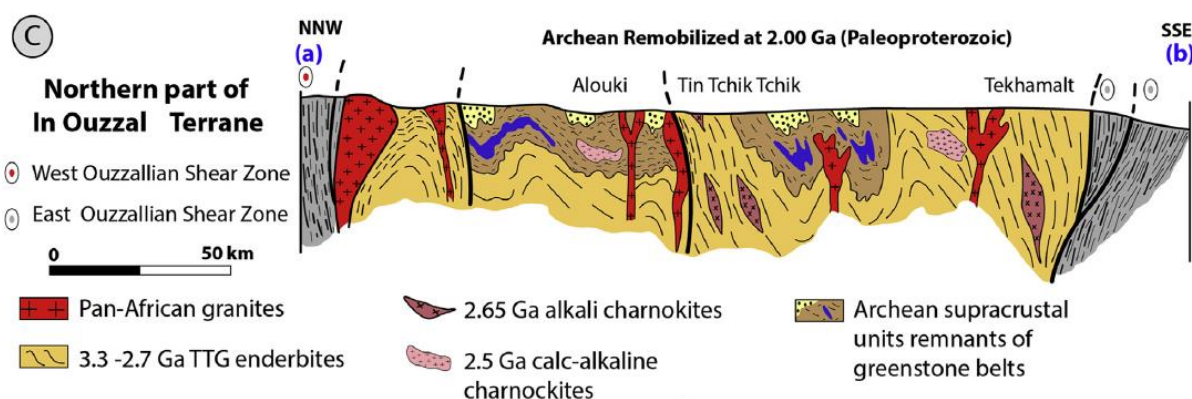


Figure III-16: Archean terrane of In Ouzal structural style in "dome and basins" reactivated during the Paleoproterozoic Eburnean orogeny via the mega shear zones (Benbatta et al., 2016).

2.4.2 The Pan-African orogeny (c. 900-600 Ma)

The Pan-African orogeny, also called Cadomian orogeny or Brasiliano (in Brazil) is a major event in the geological history of Africa (Figure III-17). It results from the collision of several tectonic plates and has led to the formation of the super-continent Pannotia (Hallett, 2002). According to Caby, (2003), these three tectonic plates are composed of Archean cratons to Paleoproterozoic (West African craton, Kalahari, Congo and Nile), the suture zones correspond to mobile zones accreted Neoproterozoic oceans (Mozambique, Adamastor and Pharusian).

The Pan-African orogeny at the origin of the Gondwana supercontinent was formed by the assembly of several continental fragments and oceanic terranes during the Neoproterozoic Pan-African orogeny (Craig et al., 2008; Guiraud et al., 2005; Unrug, 1992; Figure III-17). In the North African platform it resulted from the collision of the West African Craton (WAC) and the East Saharan Craton (ESC), between the Tuareg Shield (TS) mobile belt (Craig et al., 2008; Guiraud et al., 2005; Unrug, 1992). It is characterized by an East-West shortening direction and numerous large North-South trending faults with a very important horizontal displacements about hundred kilometers (Caby, 2003; Craig et al., 2008; Guiraud et al., 2005; Liégeois et al., 2003). This phase of convergence is followed by a period of post-orogenic thermal subsidence (<600 Ma) which favors the development of the North African Paleozoic basins (Burke et al., 2003; Coward and Ries, 2003; Fabre, 1988).

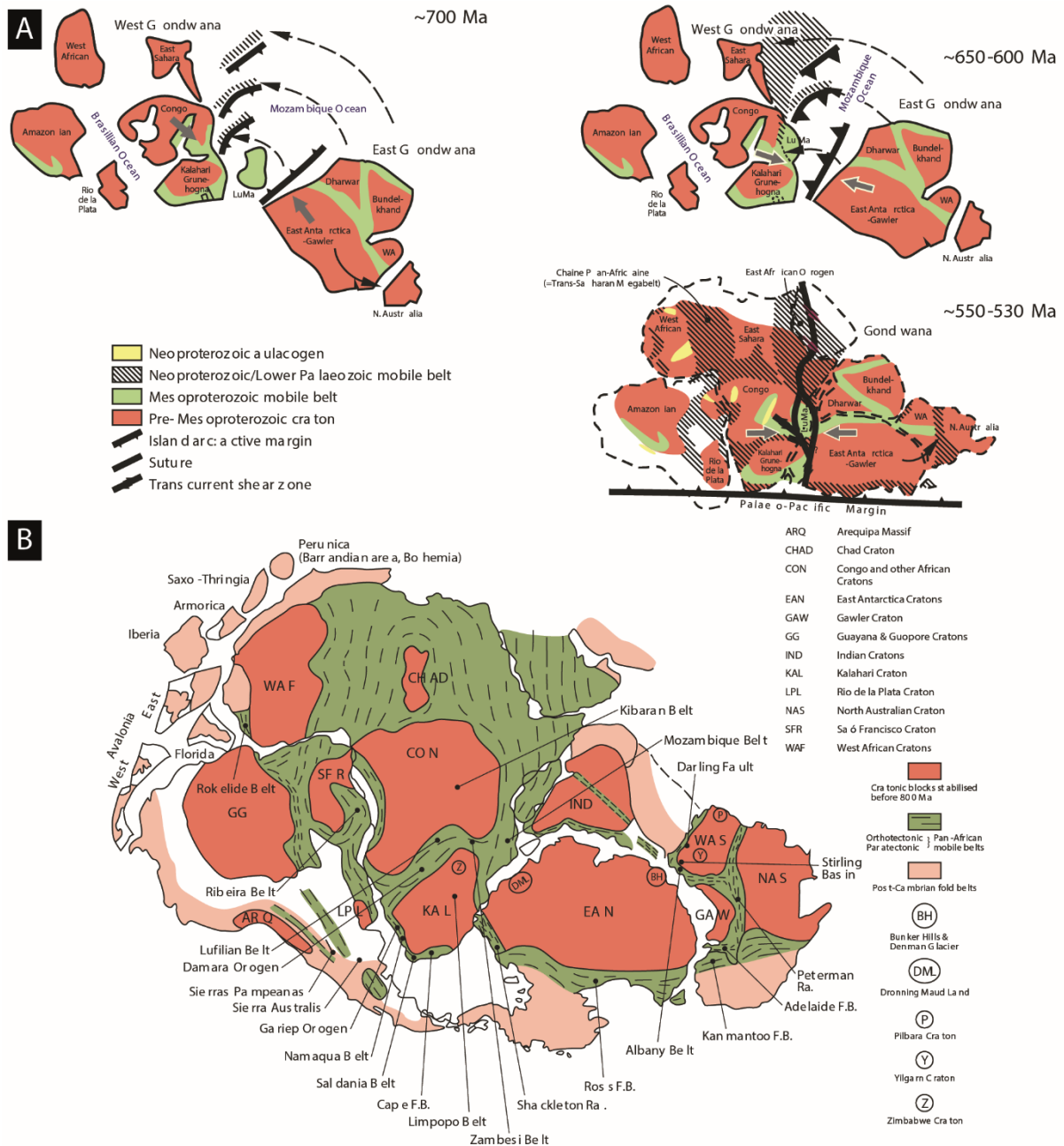


Figure III-17: (A) Evolution of North Africa during the Pan-African orogeny modified from Craig et al., (2008). (B) Paleogeographic reconstruction of the supercontinent Gondwana at the end of the Pan-African cycle relating the distribution of stable cratons and Pan-African mobile belts modified from Craig et al., (2008).

In Northern-Africa, the Pan-African orogeny results from the collision of the West African Craton (WAC) and the East Saharan Craton (ESC) between the Tuareg Shield (TS) (Figure III-17). According to Black et al., (1994), this orogeny has two main periods: a period of major collision (750-660 Ma) and a period of major shear (660-580 Ma). It led to the subduction, the collision and amalgamation of Archean and Proterozoic cratons, voluminous island arc material

as accreted terranes (23 terranes; cf. Black et al., 1994), and sub-craton sized fragments of Proterozoic continental material into a coherent supercontinental unit (Black et al., 1994; Bumby and Guiraud, 2005; Caby, 2003). It is characterized by an East-West shortening direction and numerous large North-South trending faults with a very important horizontal displacement about hundred kilometers (Caby, 2003; Craig et al., 2008; Guiraud et al., 2005; Haddoum et al., 2013; Liégeois et al., 2003, 2013).

It leads to the formation of the supercontinent Gondwana (Caby, 2003; Coward and Ries, 2003; Fabre, 1988, 2005; Liégeois et al., 2013). This collision has headed to lateral expulsion of triangular-shaped blocks of lithosphere material from the Tuareg Shield to the north and south (Black et al., 1994; Coward and Ries, 2003; Fabre, 1988, 2005). The collision of the West African Craton had the effect of producing a large-scale uplifted area across northern Africa, and also produced anastomosing patterns of both left and right-lateral strike-slip tectonics throughout northern Africa associated with subsequent tectonic escape (Coward and Ries, 2003).

Collision was accomplished by multiple phases of both east- and west-dipping paleo-subduction zones during the Neoproterozoic (Caby, 2003). The end of the Pan African orogeny was diachronous. Local timings for the last deformation vary from Late Precambrian to the Early Cambrian (Holt et al., 2010). The Pan-African structures will be reactivated during the late successive tectonic phases, illustrating the role of the Pan-African structural configuration on the evolution of North African sedimentary basins (Craig et al., 2008).

2.4.3 The infra-Cambrian extension and Pan-African collapse (c. 1000-525 Ma)

At the end of the Pan-African orogeny, after the major phase of deformation and metamorphism, an orogenic collapse of the Pan-African Mountains set place (Ahmed and Moussine-Pouchkine, 1987; Bumby and Guiraud, 2005; Caby et al., 1985; Djellit et al., 2002; Fabre, 1988, 2005).

This late-orogenic extension may have been associated with the formation of pull-apart basins and horst-graben structures infilled with Upper Precambrian-Cambrian volcano-sedimentary molasses (e.g. “Bled El Mass” series, “Pourprée” series, El Moungar conglomerate series; Figure III-18), deposited preferentially along mega lineaments (Ahmed and Moussine-Pouchkine, 1987; Bumby and Guiraud, 2005; Caby et al., 1985; Coward and Ries, 2003; Djellit

et al., 2002; Fabre, 1988). It is also recognized in the Anti-Altas, Morocco (Oudra et al., 2005; Piqué et al., 1999).

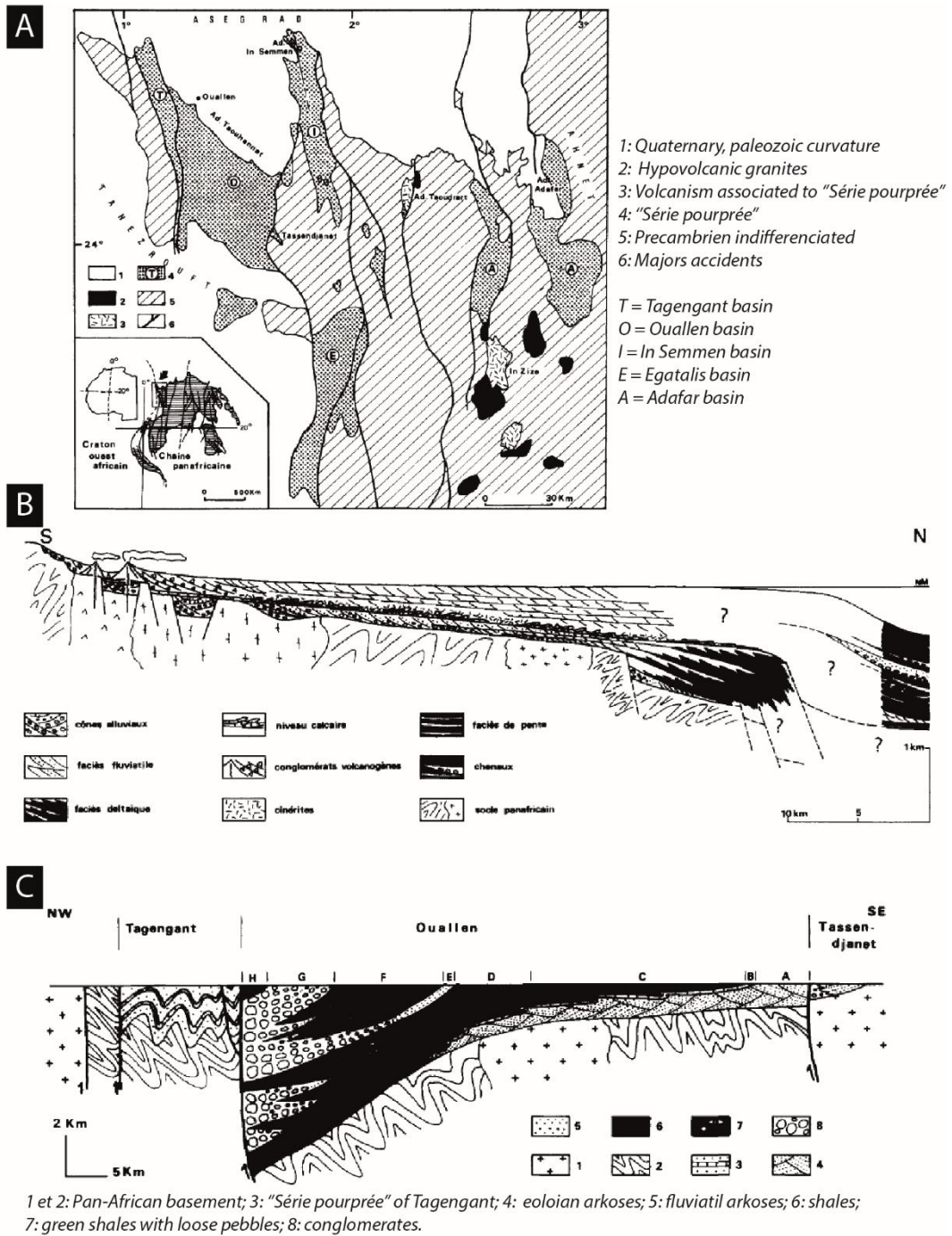


Figure III-18: Late-orogenic Pan-African molasses basins of In Semmen and of Ouallen (Ahmed and Moussine-Pouchkine, 1987).

2.4.4 The peneplanation (Infratassilian surface fm.) and start of subsidence (c. 525 Ma)

At the beginning of the Cambrian (i.e. around 530 and 500 Ma), the consolidated Pan-African orogen of North Africa was levelled and peneplaned and set the place of a relatively stable platform (Beuf et al., 1971; Fabre, 1988). The duration of this peneplanation must be restricted to several tens of millions of years (Bennacef et al., 1971; Beuf et al., 1968b; Boissonnas et al., 1969). This “Infratassilian” surface unconformity (also called Pan-African unconformity) is featured by a wide polygenic planar peneplain or pediplain surface with sometimes residual relief (i.e. inselbergs), composed of quartzite dreikanter, ferruginous levels, arenites and reworked clasts (Beuf et al., 1971; Fabre, 1988, 2005). This surface gives the start of the deposition of a vast Paleozoic mainly siliciclastic deposits (Beuf et al., 1971), experienced by a typical cratonic tectono-stratigraphic history (Beuf et al., 1971; Boote et al., 1998; Eschard et al., 2010).

2.4.5 Cambro-Ordovician extension (c. 525-418 Ma)

The Cambro-Ordovician is characterized by an extensive regime associated with the rift/split and drift of the Avalonia terrane from Gondwana, the development of the Armorica micro-continent and the opening of the Rheic Ocean (Nance et al., 2010; Stampfli and Borel, 2002; Zazoun and Mahdjoub, 2011).

There were no major plate collisions or separations at this time and local transpressional and transtensional reactivation processes dominated the region as a result of the interaction of intraplate stress fields with pre-existing fault systems of varying orientation and geometry (Craig et al., 2008). They were reactivated as normal faults or strike-slip faults, leading to the development of horst-grabens or half-graben structures (Coward and Ries, 2003). During this period the Saharan platform experienced several tectonic phase related to an oceanic opening and a tectonic tilting towards the N-NW (Beuf et al., 1971; Coward and Ries, 2003; Craig et al., 2008; Eschard et al., 2010).

By the end of the Cambrian, where a brief drop in sea level was registered a regional uplift has probably happened (Fabre, 1988). At the Early Ordovician, a tectonic activity occurs characterized by the absence of the Cambrian over the main uplifts, e.g. the Ahara Uplift and the Tihemboka Arch (Echikh, 1998; Eschard et al., 2010). During Llandeilo time (i.e. Darriwilian), a peak of activity has occurred, particularly on the southern edge of the Ghadames Basin, in Illizi and close to the Gargaf Uplift (Echikh, 1998).

The Cambrian and Lower Ordovician was a period of active uplift, with palaeohighs forming slowly rising broad horsts covered by the Cambro-Ordovician sediments before being eroded during the uplift phase (Eschard et al., 2010). They were covered by the Cambro-Ordovician sediments before being eroded during the uplift phase (Eschard et al., 2010). The Ahara (Figure III-20C-D), the Tihemboka (Figure III-20A), the Azzel Matti (Figure III-20B), the Amguid El Biod, the Ougarta range and the Arak-Foum Belrem (Figure III-19) Arches show evidences of tectonic activity during the Cambro-Ordovician (Beuf et al., 1968b; Borocco and Nyssen, 1959; Eschard et al., 2010; Fabre, 2005; Ghienne et al., 2007b; Kracha, 2011). It is documented by syn-sedimentary tectonic structures such as thickness variations, lateral facies variations, current directions variations (Figure III-19 and Figure III-20). These structures also present in the Ajjers formation are evidences of the early activity of the Arches leading to the individualization of the different basins of the Saharan platform since the Cambrian time.

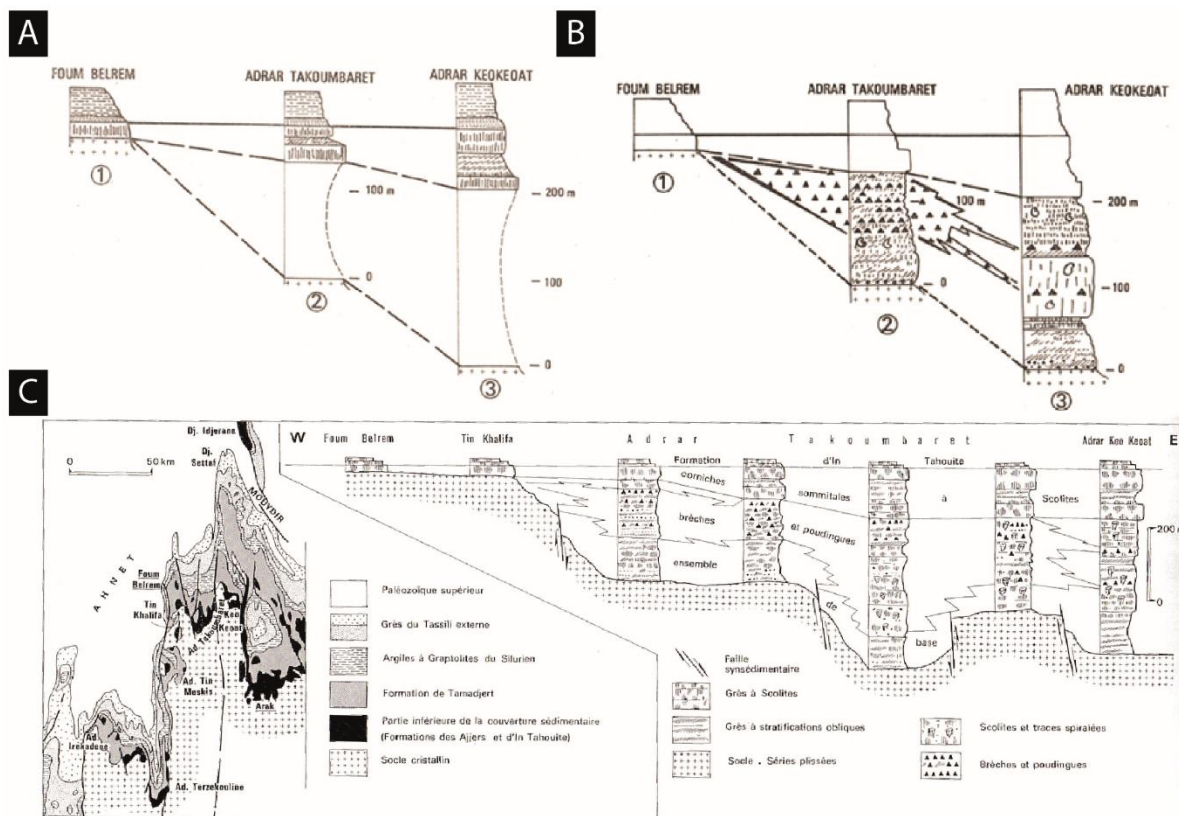


Figure III-19: (A) Thickness and facies lateral variation of Cambro-Ordovician series on the Arak-Foum Belrem Arch (Beuf et al., 1968b). (B) Syn-tectonic conglomerates in Cambro-Ordovician series on the Arak-Foum Belrem Arch (Beuf et al., 1968b). (C) Syn-tectonic conglomerates in Cambro-Ordovician series on the Arak-Foum Belrem Arch (Beuf et al., 1971).

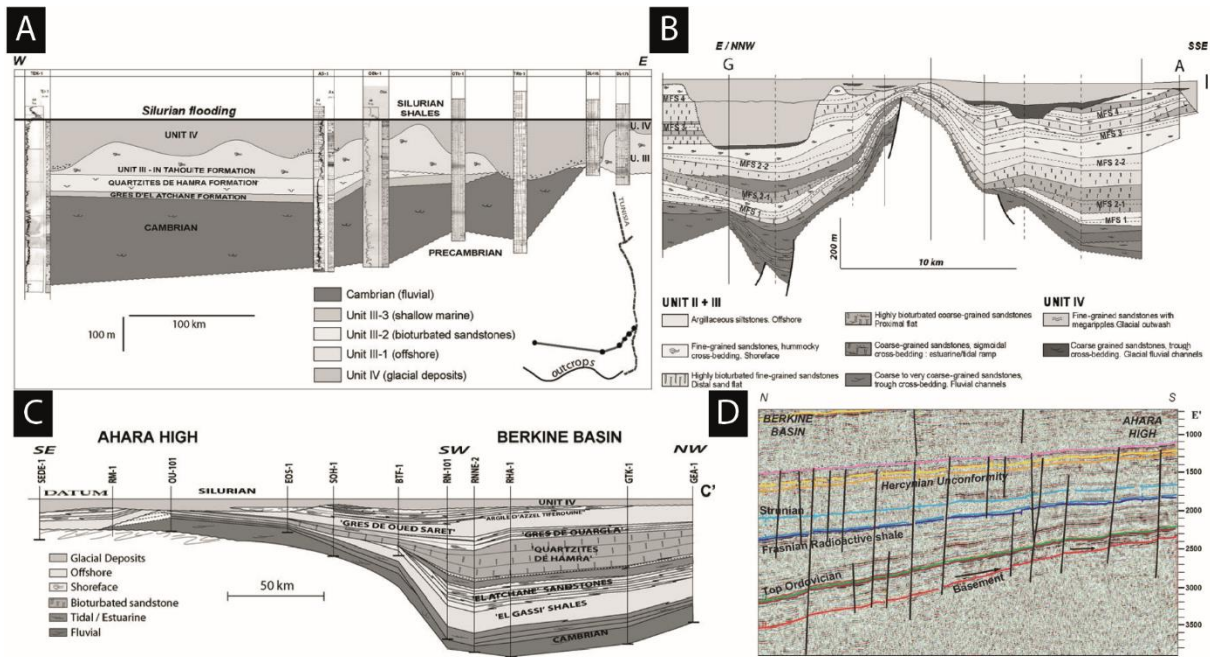


Figure III-20: (A) EW cross section on the Tihemboka Arch (Illizi Basin) showing variation of thickness, wedges strata in the Cambro-Ordovician series. (B) NNW-SSE cross section on the Ahzet Matti Arch (Ahnet Basin) showing variation of thickness, wedges strata in the Cambro-Ordovician series. (C) Cross-section between the Berkine Basin and the Ahara High, showing the stratigraphic pinchout of the Cambro-Ordovician succession on the northern flank of the Ahara High. (D) Seismic section on the southern flank of the Berkine Basin illustrating the onlap configuration of the Cambro-Ordovician, and the thickness reduction of the Silurian and Devonian succession. Images from published paper (Eschard et al., 2010).

In the Tassili-N-Ajjers (Oued Messiradjene) unconformity has been observed between Ajjers and In Tahouite formations (Bennacef et al., 1971; Beuf and Montadert, 1962). In the eastern Murzuq basin (Dor El Gussa and Murizidié location), intra-Ordovician tectonically driven unconformity were shown (Ghienne et al., 2013).

2.4.6 “Taconic” phase (c. 445 Ma)

The Taconic orogeny (or Taconian) is defined as the orogenic disturbance that occurred in eastern North America at the end of the Ordovician period (Rodgers, 1971). In the Saharan platform, the Taconic tectonic phase is featured by an moderate amplitude deformation leading to a major low-angle stratigraphic unconformity which occurred before the late Asghill glacial event and after the deposition of In Tahouite formation (Bennacef et al., 1971; Eschard et al., 2010; Fabre, 1988). Evidence of the Taconic unconformity is documented by a cross-section

near the Dhar high (cf. Figure III-21) where successive units of the Early Ordovician is pinch out and eroded associated to volcanic layers in the Brides and Illizi basin (Echikh, 1998). This magmatic intrusion is linked to Mesozoic instead by K-Ar datations (Chabou et al., 2007b). In the Adrar Tan Elak (i.e. Amguid El Biod Arch), it is described by an intra-Ordovician angular unconformity after a roughly NS direction folding phase (Borocco and Nyssen, 1959; Claracq et al., 1958). Many evidence of Late Ordovician (Caradocian? i.e. Sandbian to Katian) Taconic event were highlighted by partial or complete erosion to the basement in the Eglab and major lineament (see Pl. 27, p.422; Beuf et al., 1971) such as the Bled el Mass Arch (Beuf et al., 1968a; Eschard et al., 2010).

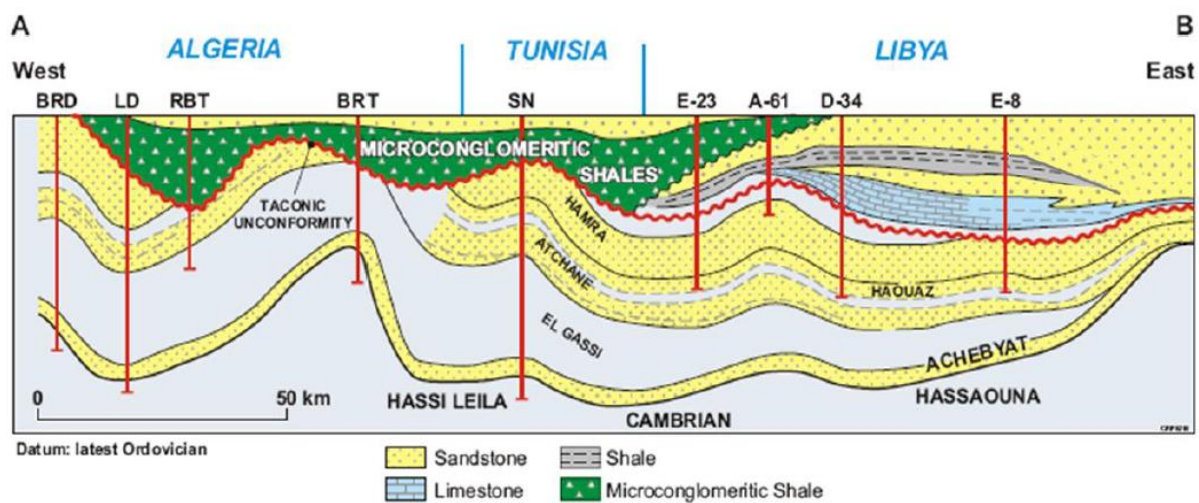


Figure III-21: Geological section of the Ordovician formations in North Africa illustrating the gully associated with the Taconic unconformity (Echikh, 1998).

During the Ashgillian (i.e. Upper Katian to Hirnantian), the isopach map of the Tamadert Formation (i.e. Syn-glacial deposits) for the Illizi basin shows the existence of the NW-SE pull-apart grabens and half-grabens basins (Figure III-22), consistent with a NE-SW extensional direction (Zazoun and Mahdjoub, 2011). In the Gargaf area, location of the main glacial valleys partly controlled by inherited Pan-African structural trends, and by the existence of glacio-isostatically induced fault-related depocentres. (Ghienne et al., 2003).

However, the origin of the Taconic unconformity remains a subject of considerable controversy when we look at regional cross-sections, the field and the seismic lines. Indeed, Late Ordovician geologic structures are complex to understand because the effects of the local uplift interfered with the Taconic unconformity (Eschard et al., 2010). According to Galeazzi et al., (2010), this unconformity show very little relation with tectonism and are most probably due to major sea level falls related to a glacial eustatic fall. For Zazoun and Mahdjoub, 2011, the Taconic

unconformity is probably a combination of traditional tectonic movements and glaciotectonics (Figure III-23).

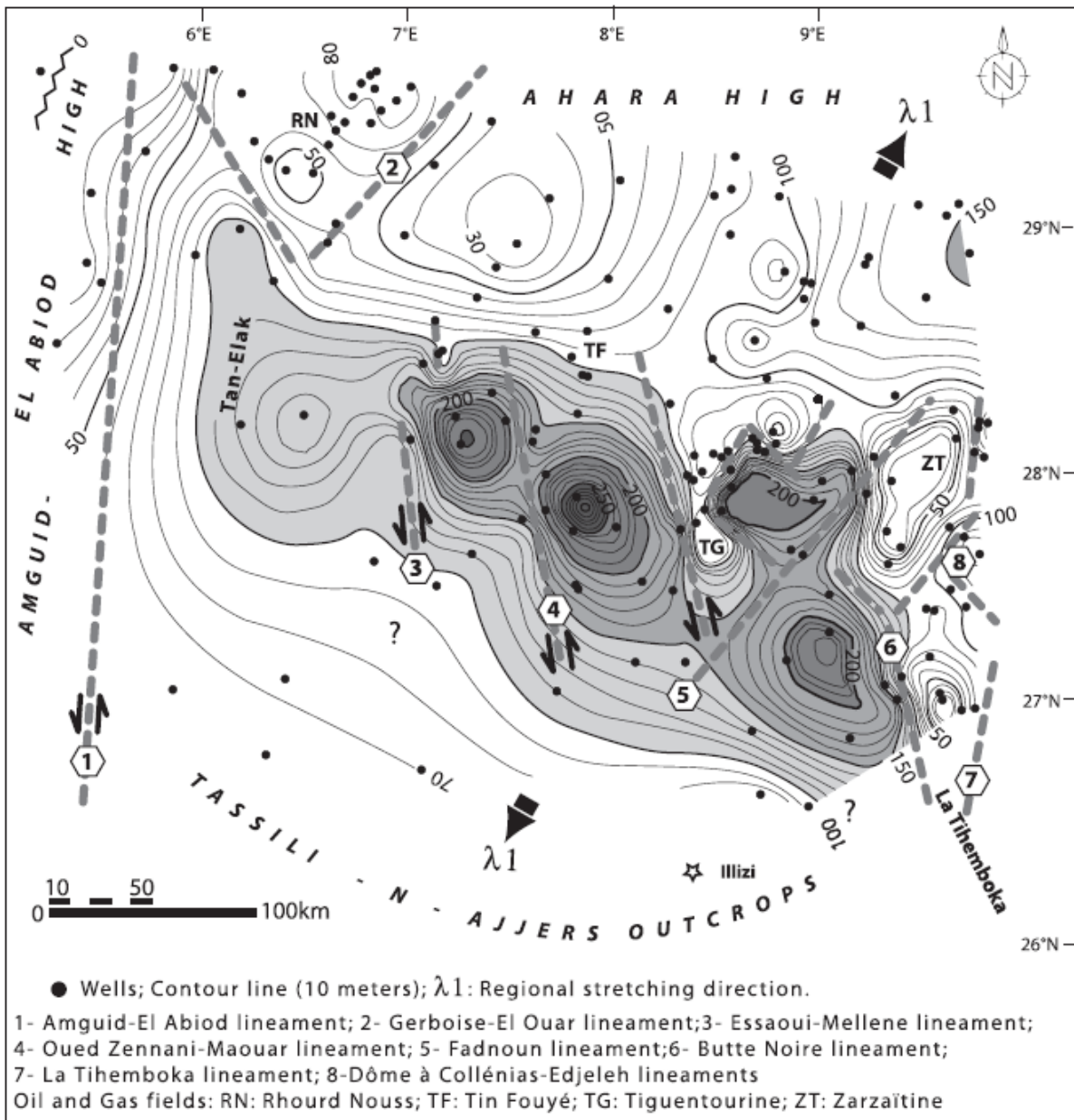


Figure III-22: Isopachs map of syn-glacial Tamadjert Formation in the Illizi basin. The geometry seems compatible with an NE–SW extensional direction resulted in a transtension along the N–S and NNW–SSE major lineaments and the formation of pull-apart basins during the deposition of the Tamadjert Formation (Zazoun and Mahdjoub, 2011).

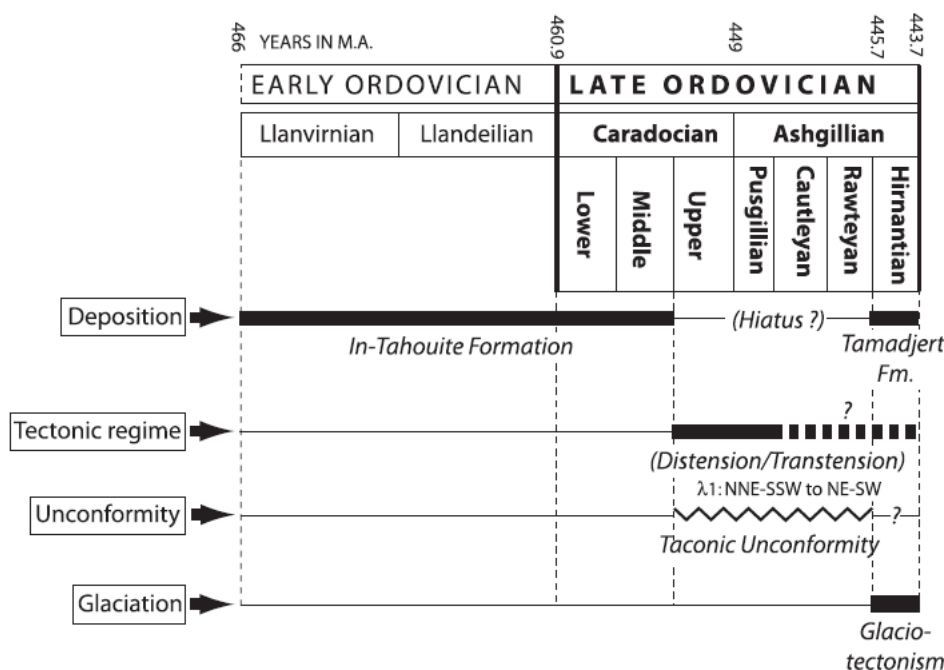


Figure III-23: Constraints regime in Cambro-Ordovician series in the Illizi basin (Zazoun and Mahdjoub, 2011).

2.4.7 Hirnantian major glaciation (c. 445-444 Ma)

Towards the end of the Ordovician, the North-Gondwana platform drifts through the South Pole. The climate was relatively warm in the lower Ordovician, becoming cold and dry towards the end of the Ordovician, favoring the installation of an ice cap covering a good part of the current Sahara (Clerc et al., 2013; Denis et al., 2007; Fabre, 2005; Ghienne et al., 2007a; Heron and Craig, 2008; Le Heron, 2007; Ravier, 2014; Scotese et al., 1999). The "maximum" hypothesis envisages the existence of a single cap, with a diameter of nearly 8000 km (Figure III-24; see also Figure III-24), which would be much greater than the size of the current Antarctic icecap. A "minimal" alternative hypothesis proposes the development of several smaller caps (Ghienne et al., 2007a). However, numerical modelling has rejected this scenarios with individual separate ice centers because of instability (Pohl et al., 2016). Still according to this study, land ice thickness simulated in their baseline runs reaches 6000 m over extensive areas.

The sedimentary architecture of glacial deposits is controlled by the repetition of periods of glacial erosion, associated with the jerky extension of the ice sheet during its growth period, and by the formation of depocentres associated with glacio-isostatic reactivation of a pre-existing fault networks (Clerc et al., 2013; Denis et al., 2007; Ghienne et al., 2003; Girard et

al., 2018; Ravier et al., 2014). Soft-sediment deformation structures in subglacial environments are also recorded (Clerc, 2012; Clerc et al., 2013; Ravier, 2014; Ravier et al., 2014). This results in discontinuous and juxtaposed sedimentary units, filling in paleotopographies. Facies of proglacial/deglaciation are documented in the Saharan platform (Clerc et al., 2013; Deschamps et al., 2013; Girard et al., 2012; Hirst et al., 2002; Le Heron et al., 2006).

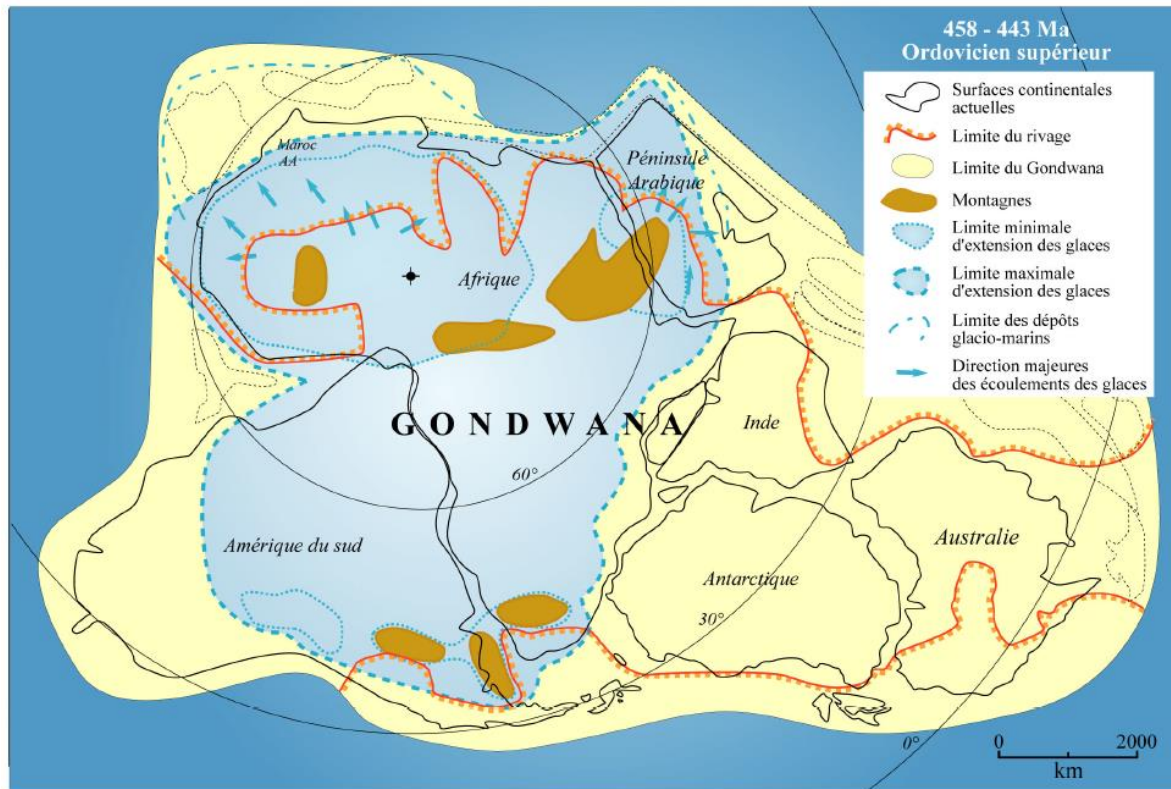


Figure III-24: Paleogeography of the Gondwana at the Upper Ordovician (Veevers, 2005). At that time, Gondwana is partly covered by a large ice cap. During the period of maximum ice extension, the ice cap covered more than half of the South American continent and the Arabian Peninsula, as well as almost the entire African continent.

2.4.8 Deglaciation and isostatic rebound (c. 444 Ma)

After a period of glaciation, the Saharan platform was partly recovered by an enormous ice-sheet (Figure III-24; Beuf et al., 1971; Le Heron et al., 2009; Heron and Craig, 2008; Ghienne et al., 2007a; Girard et al., 2012, 2018; Dixon et al., 2008a). The melting and ice retreating (Figure III-24) lead to a complex isostatic rebalancing of the basement structures which is a rapid geologic phenomena (Beuf et al., 1971; Heron and Craig, 2008; Denis, 2007; Le Heron et al., 2006; Ghienne et al., 2003; Fabre, 1988). Evidence of a positive isostatic compensations is suggested by the absence of Lower Llandovery (Imirhou formation) in the Mouydir basin

(see p.428 and table 28; Beuf et al., 1971). In the Djado, during interstadial and postglacial stages, glacio-isostatic rebound, grabens, normal faults, radial extensional micro-faults and extensional dihedrons were generated by extensional tectonics (Denis, 2007; Denis et al., 2007; Moreau, 2011). In the Murzuq basin, unconformity due to postglacial retirement were also outlined (Ghienne et al., 2013; Le Heron et al., 2006).

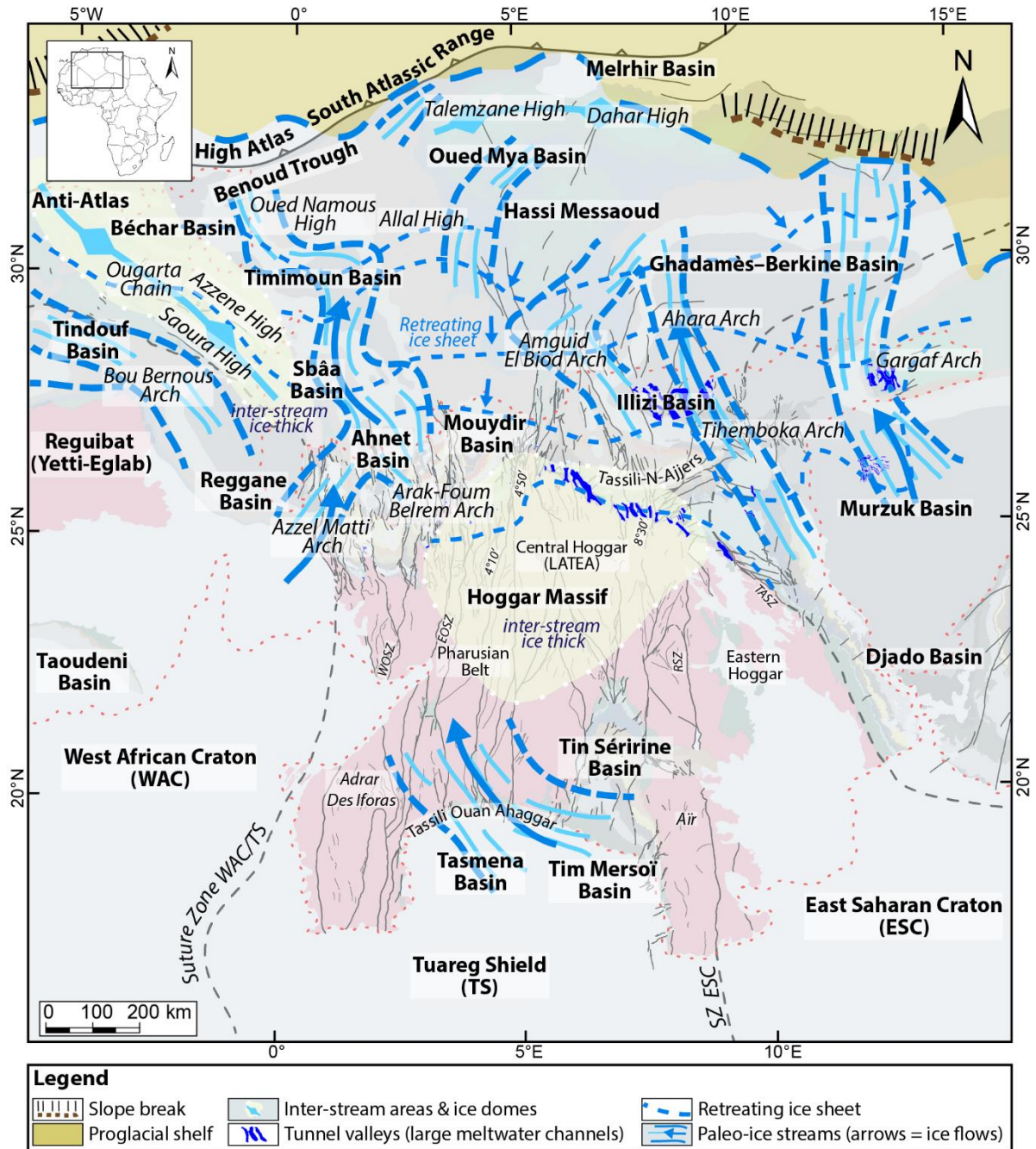


Figure III-25: Paleo-glaciological reconstructions of the Late Ordovician Saharan ice sheet modified from Heron and Craig, (2008) showing both Ice sheet configuration at glacial maximum position and during its stepwise recession.

2.4.9 Silurian subsidence (c. 444-418 Ma)

Silurian times were marked by continuous subsidence of the north Gondwanan passive margin reflecting the development of the proto-Tethyan ocean between Gondwana, Armorica and Avalonia (Craig et al., 2008; Lüning et al., 2000). It is a period of general quiescence and stability with limited uplift of all paleohighs, which were passively flooded during the Lower Silurian transgression (Eschard et al., 2010). At that time, a residual topography remained, and was overlapped by the basal part of the transgressive Silurian shales (Eschard et al., 2010). The Middle and Upper Silurian progradational sequences (Lüning et al., 2000) were deposited without being influenced by the paleohighs topography (Eschard et al., 2010). Transgression started at the east and south-east and flooded the major Arches during the Middle Llandovery (Beuf et al., 1971).

2.4.10 Early Devonian Caledonian compression (418-398 Ma)

The Caledonian orogeny is related to the convergence and collision of Laurentia, Baltica, Avalonia and intervening terranes leading to the closure of the Iapetus Ocean, occupying a time interval of around 200 Ma (Mckerrow et al., 2000). At the same time (Figure III-37), rifting/drifted of the Hun Superterrane progressively set place to the Paleotethys ocean and close the Rheic ocean between Laurussia and Gondwana (Stampfli and Borel, 2002).

In the Saharan platform, the Caledonian tectonic event, is mainly mentioned as uplifting of some trends (Figure III-26, Figure III-27 and Figure III-28), large-scale folding or blocktilting (e.g. Gargaff Arch, Tihemboka Arch, Fagnoun axis, Azell Matti Arch, Saoura-Ougarta, Air area, Tasmena area, In Ezzan area, In Guezzam area, Ahara high, Amguid El Biod Arch), associated with breaks in the series and frequent angular unconformities below Early Devonian formations (Beuf et al., 1971; Biju-Duval et al., 1968; Boote et al., 1998; Boudjema, 1987; Carruba et al., 2014; Chavand and Claracq, 1960; Collomb, 1962; Coward and Ries, 2003; Dubois et al., 1967; Dubois and Mazelet, 1964; Echikh, 1998; Eschard et al., 2010; Fabre, 2005; Frizon de Lamotte et al., 2013; Ghienne et al., 2013; Gindre et al., 2012; Legrand, 1967b, 1967a; Lessard, 1961; Massa, 1988). Already at the Wenlock epirogenic events (long wavelength deformation) have modified sedimentation conditions (see p. 102; Beuf et al., 1971). During this compressive event, large wavelength folds and paleohighs were accentuated, affecting sedimentation and facies distribution in the sedimentary basins (Eschard et al., 2010; Galeazzi

et al., 2010). Locally, paleohighs may have provided detrital material (Eschard et al., 2010; Galeazzi et al., 2010).

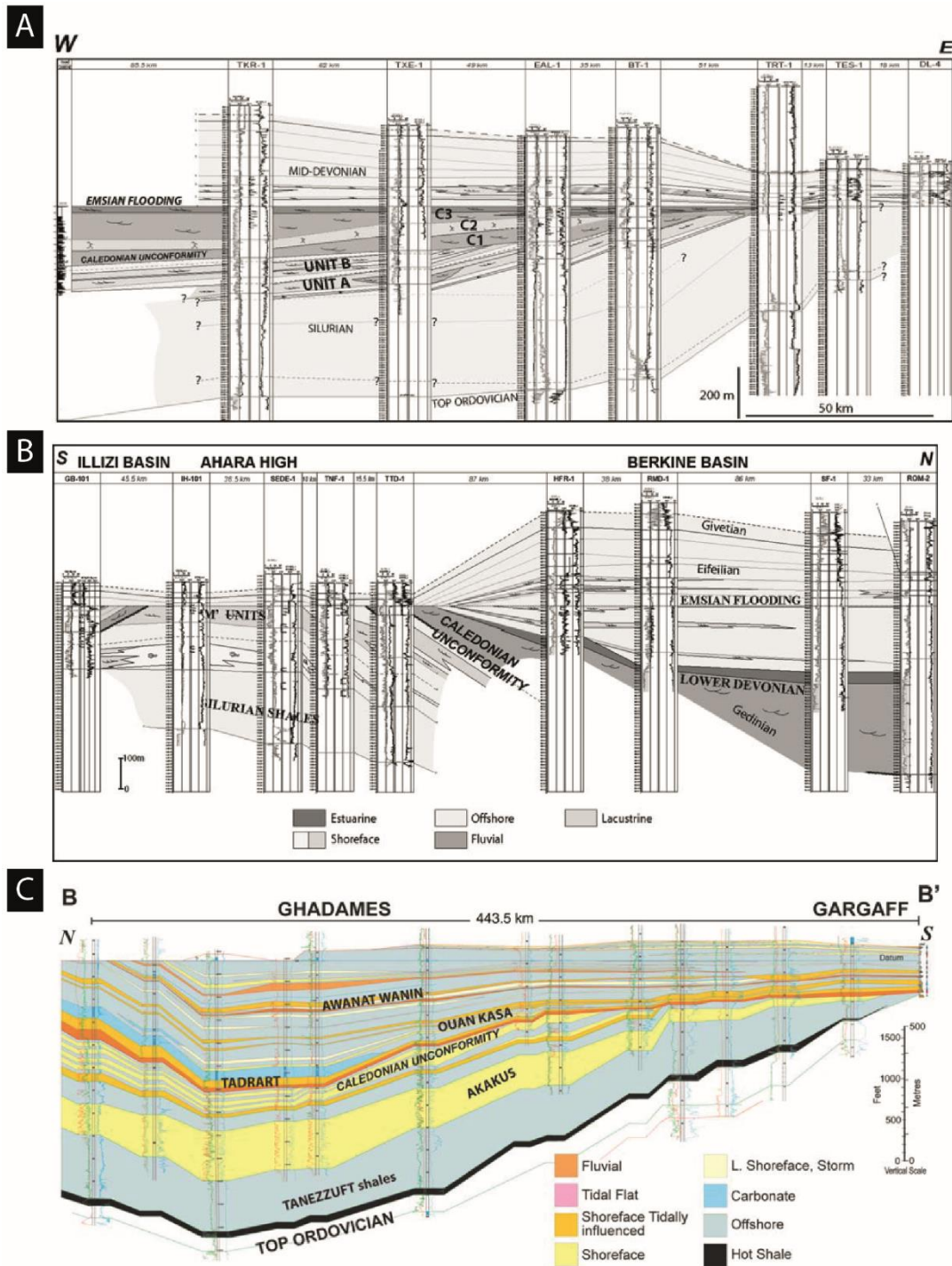


Figure III-26: (A) EW cross section in the Illizi basin and the Tihemboka Arch showing variation of thickness, angular unconformities, wedges strata in the lower Devonian series (Eschard et al., 2010). (B) Correlation of the Devonian succession on the northern flank of the Ahara High where we observe the complete pinchout of the Gedinnian fluvial unit on the flank

of the high (Eschard et al., 2010). (C) Cross-section showing the stratigraphic architecture of the Siluro-Devonian succession between the Ghadames Basin and the Gargaff Arch (Eschard et al., 2010).

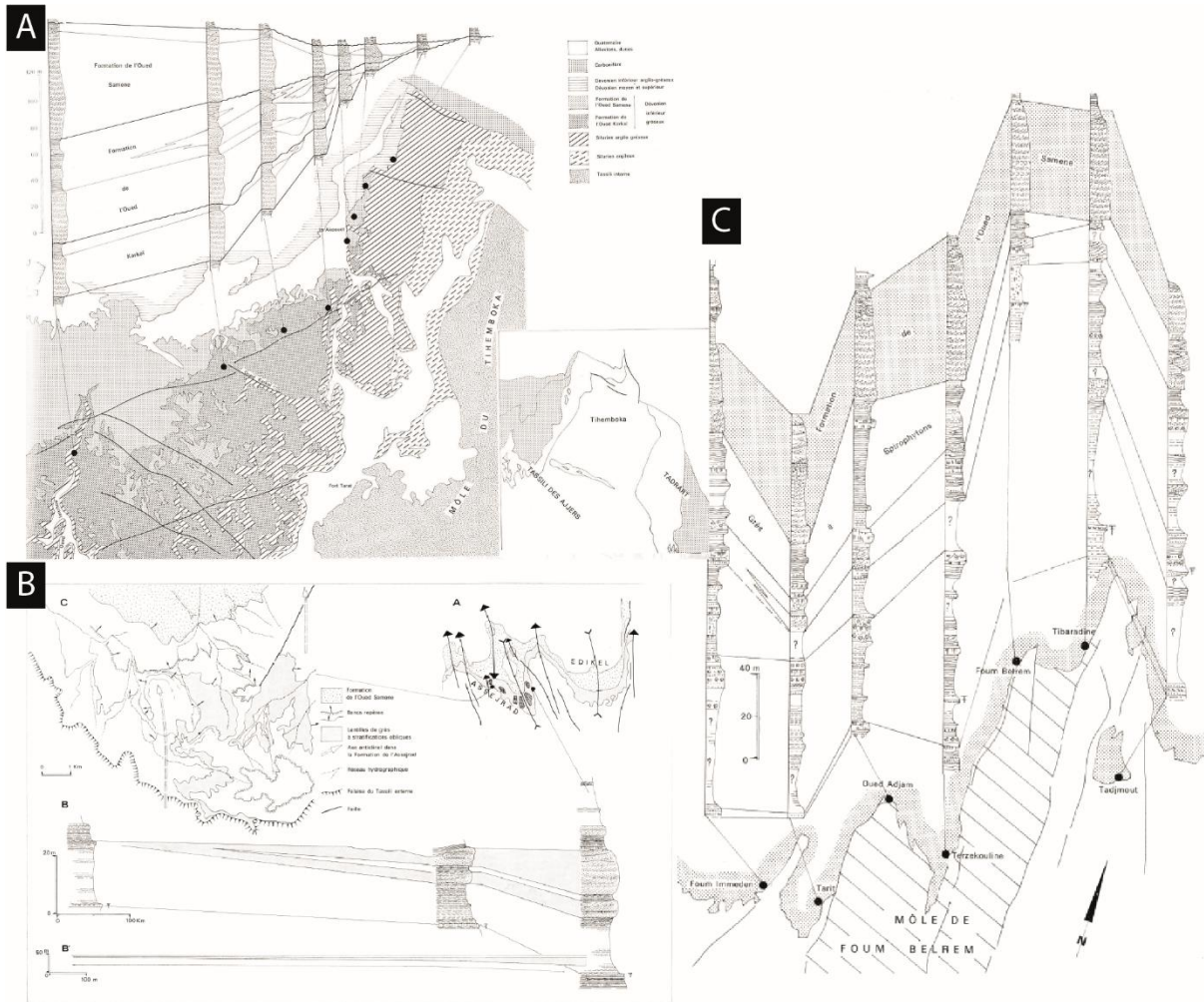


Figure III-27: (A) EW cross section on the Tihemboka Arch (Illizi basin) showing variation of thickness, angular unconformities, wedges strata in the lower Devonian series (Beuf et al., 1971). (B) Thickness variation and sandy lense (Beuf et al., 1971). (C) EW cross section through the Ahnet and Mouydir basin in the Siluro-lower Devonian series showing variation of thickness near Azzel Matti and Arak-Foum Belrem Arches (Beuf et al., 1971) see also (Biju-Duval et al., 1968).

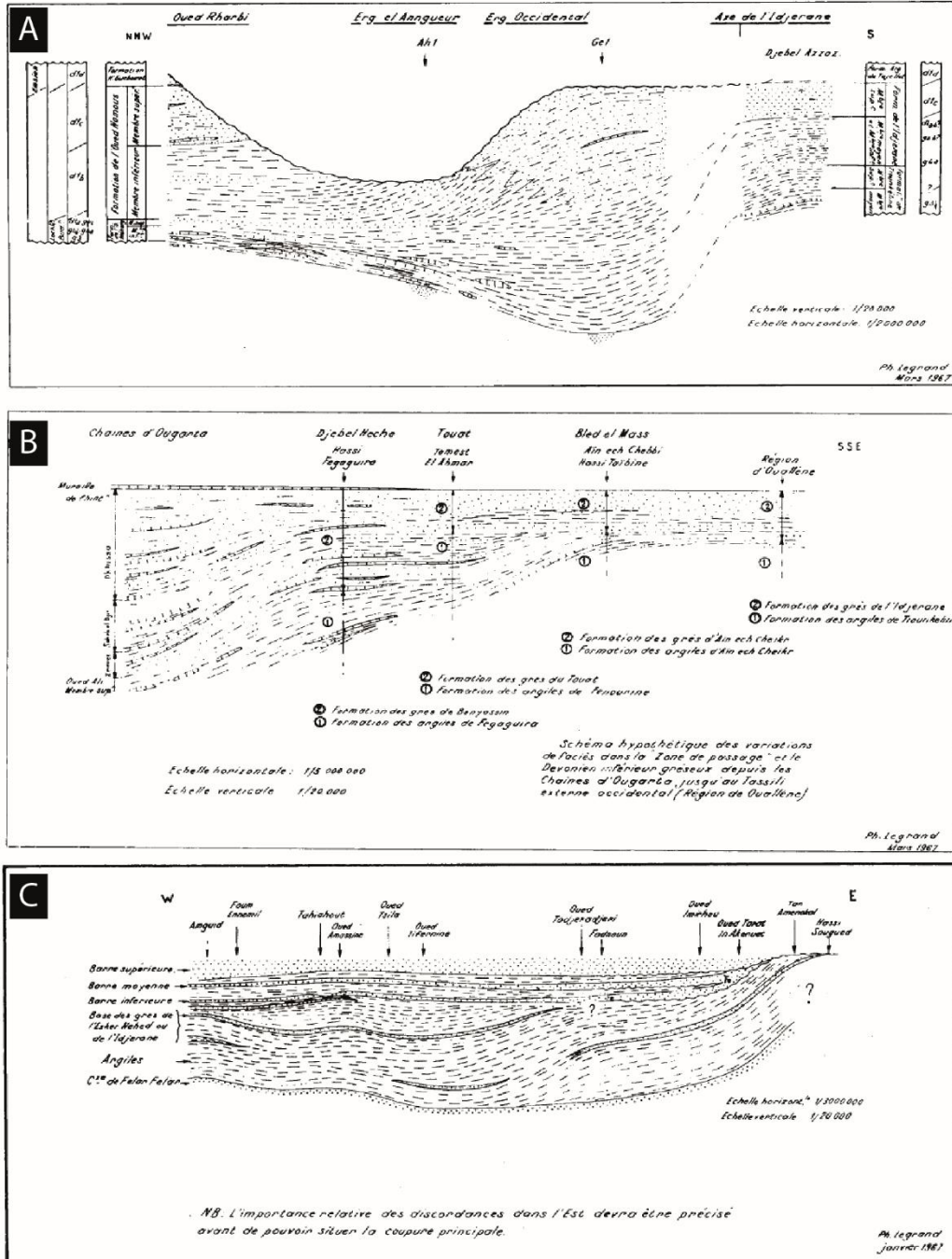


Figure III-28: (A) Thickness and facies variations of Siluro-Devonian formations on the Idjerane axis (i.e. Arak-Foum belrem Arch) (Legrand, 1967a). (B) Thickness and facies variations of Siluro-Devonian formations in the Bled El Mass area (i.e. Azzel Matti Arch) (Legrand, 1967a). (C) EW cross section in the Illizi basin and the Tihemboka Arch showing variation of thickness, angular unconformities, wedges strata in the lower Devonian series (Legrand, 1967a).

Evidence of the Caledonian event is documented, in the southwestern and southern flank of the Ghadames Basin, the Lower Devonian Tadrart formation is seen to directly overlie the Upper Silurian basal Acacus series with a progressive truncation of the Acacus (Upper Silurian) units from NE to SW on this unconformity (Echikh, 1998). In the Illizi basin, only the lowermost part of Acacus Formation is preserved (Echikh, 1998). Besides, seismic data may show folding of the Silurian section below flat-lying Devonian deposits (Echikh, 1998). Well described indications of Caledonian unconformity are also highlighted in the Murzuq basin (Ghienne et al., 2013) and Al Kufrah basin (Gindre et al., 2012). Massive sand injection associated with igneous intrusion triggered by basin-scale uplift are also described in the Murzuq basin (Moreau et al., 2012). These structural features imply NW-SE shortening, probably of moderate intensity, though much weaker than the Hercynian one (Guiraud et al., 2005). Elsewhere, in the Drâa basin, in the NW Libya and over the Al Kabir trend, there is also no sign of this event in Lower Devonian series (Echikh, 1998; Ouanaimi and Lazreq, 2008).

Moreover, a widespread near top Emsian unconformity probably triggered by regional tectonic activity has been identified in the Illizi basin (Abdesselam-Rouighi, 2003; Boudjema, 1987; Boumendjel et al., 1988; Brice and Latrèche, 1998; Moreau-Benoit et al., 1993), in the Ahnet-Mouydir basin (Wendt et al., 2006), in the Libyan Ghadames and Al Kufra basins (Bellini and Massa, 1980). It is associated to basaltic volcanism and intrusive activity in the Ahnet basin and Anti-Atlas (Belka, 1998; Wendt et al., 1997)

Many authors have correlated the Late Silurian to Early Devonian tectonism as the maximum collisional deformation of the Caledonian Orogeny (see references below). However, this event clearly relates to collisions involving far away continents and terranes where Gondwana was located thousands of kilometres to the south and separated from the collisional zone by a major ocean during this time (Craig et al., 2008; Mckerrow et al., 2000; Stampfli and Borel, 2002). Tectonic events in North Africa during post-Infracambrian-pre-Hercynian times were therefore independent of the Caledonian Orogeny. Time-descriptive terms may be preferred instead (Craig et al., 2008). This denomination is thus controversial. The origin of this intra-plate stress could be linked to far field stresses, knowing that, in continental craton compression stresses can be transmitted through distances of up to 1600 km from a collision front (Ziegler et al., 1995). The origin of Late Silurian to Early Devonian intra-plate stress in North Africa is currently unclear but is possibly associated either with a phase of rifting along the Gondwana margin (Boote et al., 1998) or with initial closure of the Iapetus Ocean (Fekirine and Abdallah,

1998). Frizon de Lamotte et al., 2013 didn't interpreted it as a far effect of the Variscan orogeny, contrary to Fabre, 2005 who associated to the beginning of it.

2.4.11 Middle to Late Devonian extension (c. 398-359 Ma)

The Middle to Late Devonian times (Figure III-37) is defined by the divergence between Gondwana and European Hunic terrane, where the latter converging (pre colliding) with Laurussia leading to the closing of the Rheic ocean (Stampfli and Borel, 2002).

The Late Devonian is the time for two contrasting large-scale tectonic processes: the onset of the Variscan Orogeny along the Gondwana-Laurussia margin on the one hand and the development of magmatism, rifting and domal basement uplift within these continents on the other hand (Frizon de Lamotte et al., 2013). The collision between Gondwana and Laurasia that ultimately produced the Hercynian Orogeny possibly first affected North Africa during the mid-Devonian, creating extension/transension pull-apart basins (Craig et al., 2008).

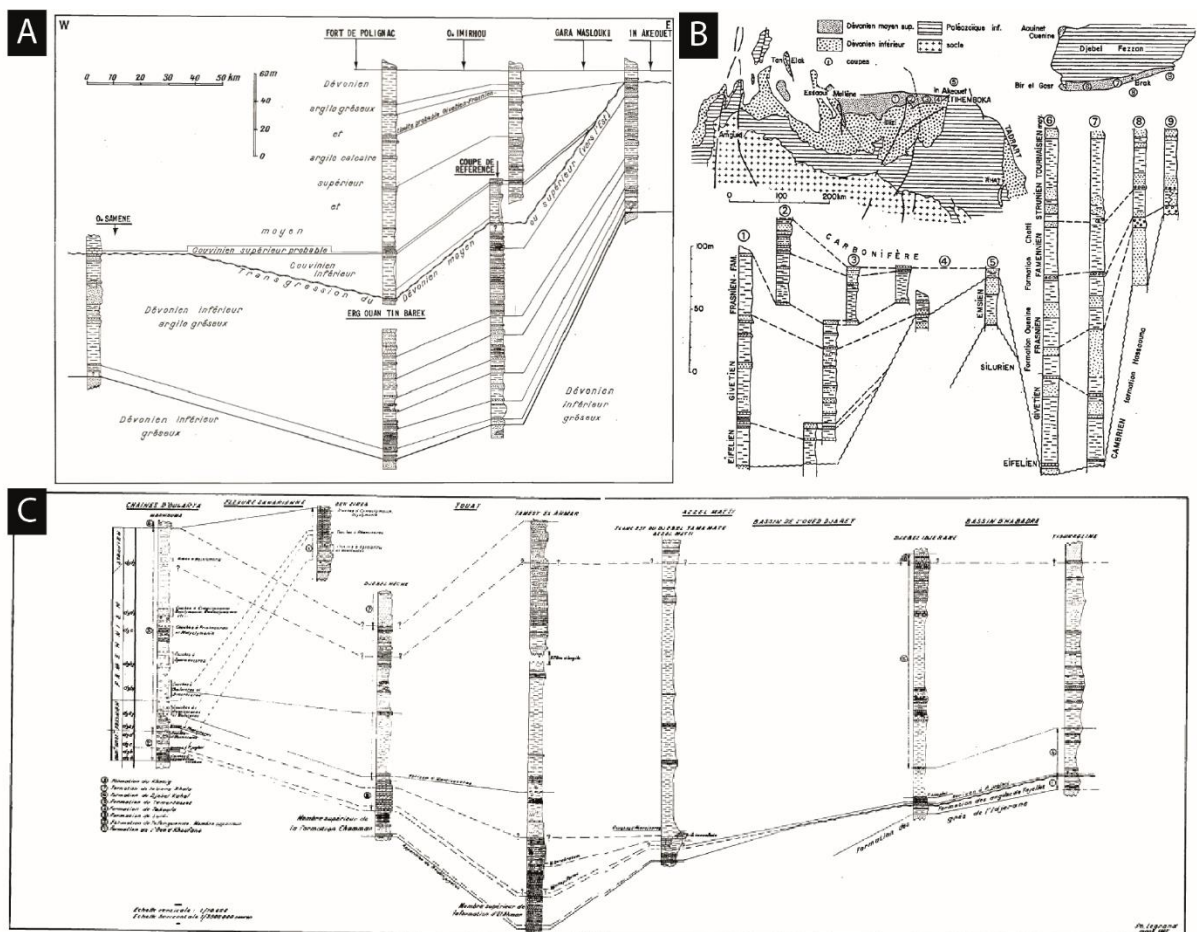


Figure III-29: (A) Pinch out of Middle-Upper Devonian series on the Tihemboka Arch (Chaumeau et al., 1961). (B) Pinch out of Middle-Upper Devonian series on the Tihemboka

and Gargaf Arches (Fabre, 2005). (C) Pinch out of Middle-Upper Devonian series on the Ougarta chain, Djebel Heche, Touat, Azzel Matti and the Ahnet basin (Legrand, 1967a).

This Devonian deformation has reactivated megashear zone systems coeval with semi-regional uplift of the Ghadames and Illizi basins and of the adjacent Tihemboka, Ahara, Gargaf and Brak-Bin Ghanimah Arches in the mid-Eifelian and at the end of the mid-Devonian (Late Givetian) and with the related development of the Frasnian Unconformity (Craig et al., 2008).

Evidence of extensional structures and/or tectonic activity during the Late Devonian, as proved by the major thickness variations of these series are documented in the Anti-Atlas (Baïdier et al., 2008; Michard et al., 2008; Wendt, 1985), in the Tihemboka (Chaumeau et al., 1961; Fabre, 2005; Legrand, 1967a), in the Tasmena basin (Derycke and Goujet, 2011; Fabre, 1976; Lessard, 1961), in the Gargaff Arch (Collomb, 1962; Fabre, 2005; Massa, 1988), in the Azzel Matti Arch (Legrand, 1967a; Wendt et al., 2006), in the Foug Belrem Arch (Wendt et al., 2006), in the Amguid El Biod Arch (Wendt et al., 2009b), in the northern Africa and in Arabia platform (Frizon de Lamotte et al., 2013). Example are imaged in Figure III-29 and Figure III-30.

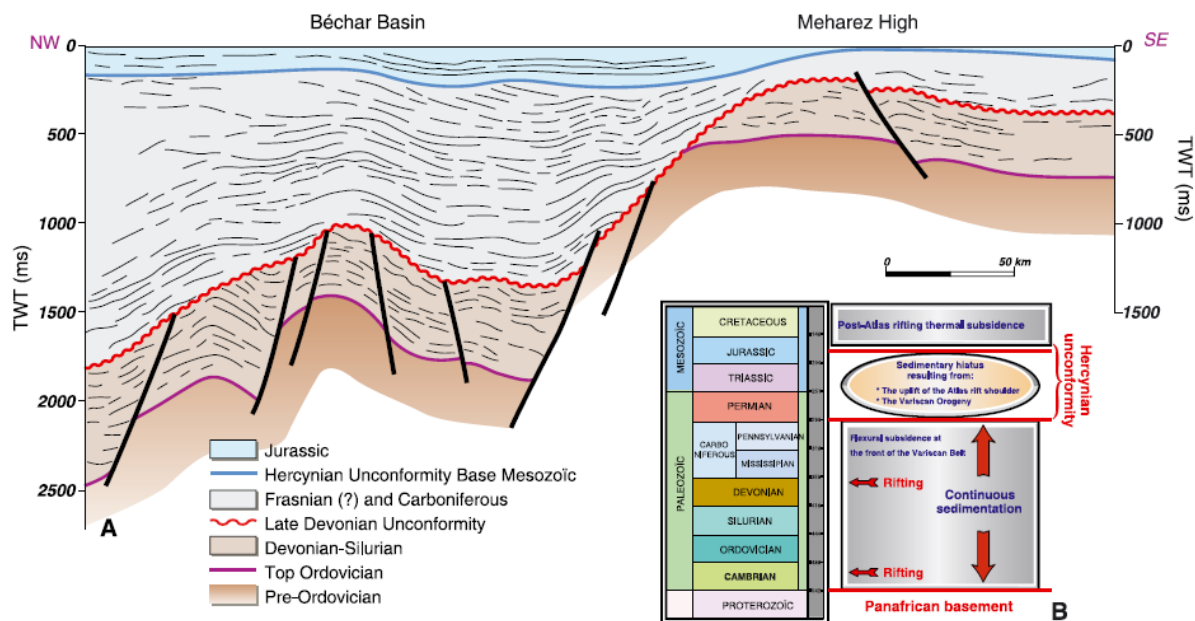


Figure III-30: The structural context of the Bechar Basin (Algeria) (Frizon de Lamotte et al., 2013). (a) Line drawing illustrating the geometry of the Bechar Basin at depth; notice that the tilted blocks at depth were folded during the Variscan Orogeny together with the Upper Devonian (?)–Carboniferous infilling of the Bechar Basin. (b) Schematic diagram synthesizing the tectonic history of the Bechar Basin during the Paleozoic and Mesozoic.

This event corresponds to a major collapse and even “disintegration” of the north-western Gondwana margin prior to the Variscan Orogeny (Wendt, 1985). While, the activity of the palaeohighs (e.g. Ahara, Gargaff and Tihemboka High) almost ceased during the Frasnian times, with marine shales onlapping different elements of the Paleozoic succession below and sealing most of the palaeohighs (Eschard et al., 2010).

2.4.12 The early Pre-Hercynian compression (c. 359-305 Ma)

Prior to the main Hercynian orogeny, the compressive event started from Late Devonian, resulting in the reactivation of basement faults, and the development of pull-apart basins, strike-slip faults (Craig et al., 2008). Tournaisian to Lower Visean sediments have also been partially eroded from the hanging wall of local structures in the Tihemboka Arch (Boudjema, 1987). Late Devonian and Carboniferous were marked by a complete reorganization of the depocentres on the craton, in relation to the beginning of the Hercynian compression, except for the Gargaff High, which continuously grew to the present day (Eschard et al., 2010). Biostratigraphic data indicate that Early Tournaisian strata are absent over most of the area of the Ghadames and Illizi basins (Echikh, 1998). In the Ahnet-Mouydir basins, two major gaps, one during the middle Tournaisian, the other during the middle Visean to Serpukhovian were identified and related to tectonic pulses (Wendt et al., 2009a).

2.4.13 The Carboniferous-Early Permian Hercynian Orogeny (c. 305-270 Ma)

The Hercynian orogeny is centred around the Carboniferous-Early Permian and led to the formation of the supercontinent Pangea (Stampfli and Borel, 2002). It is associated with the closure of the Iapetus Ocean between Laurentia and Baltica (thus creating Laurussia) and subsequent collision between Laurussia and Gondwana by closure of the Paleotethys (Bumby and Guiraud, 2005; Stampfli and Borel, 2002).

In the Saharan Platform, evidence of this deformation is documented as an uplift phase and major erosion clearly recorded, corresponding to intense folding, strike-slip faulting (Coward and Ries, 2003; Craig et al., 2008; Haddoum, 2009; Haddoum et al., 2001; Zazoun, 2001, 2008). Two main compression phases with different of shortening are documented (Craig et al., 2008; Haddoum et al., 2001; Zazoun, 2001): A Tournaisian to Lower Visean compressive phase, oriented N40°, resulting in the development of NW-SE folding trend and a post-Namurian compressive phase, oriented N120°.

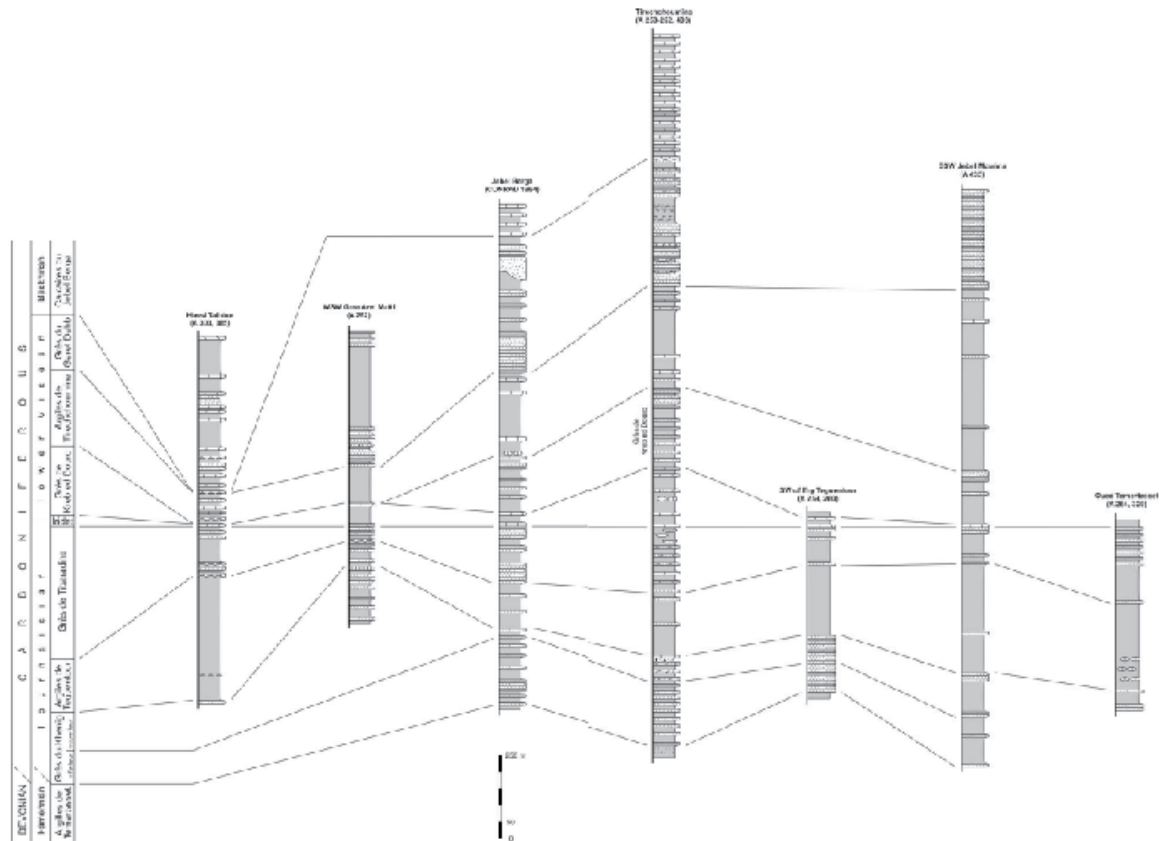


Figure III-31: EW cross section in the Ahnet and Mouydir basins in the Carboniferous series showing variation of thickness near Azzel Matti and Arak-Foum Belrem Arches (Wendt et al., 2010b).

The present-day configuration of the Saharan platform is essentially inherited from this major tectonic event (Coward and Ries, 2003; Guiraud et al., 2005). Folding, strike-slip faulting and reverse faulting occurred by the latest Paleozoic, resulting in the development of structures which are unconformably sealed by Mesozoic formations (Boote et al., 1998; Coward and Ries, 2003; Haddoum et al., 2001). Once again, it is very likely that the Pan-African fault pattern had influenced the Hercynian deformation (Boote et al., 1998; Coward and Ries, 2003; Haddoum et al., 2001).

The intensity of Hercynian deformation decreases eastwards across North Africa away from the collision zone (Craig et al., 2008). This compressive deformation increased during the Carboniferous, inducing a migration of the depocentres: the Ahara High started to subside and the Tihemboka High was sealed by the Carboniferous sediments (Eschard et al., 2010). In the Tim Mersoï basin, litho-stratigraphic correlation shows variation of thickness between the center of the basin and the Air basement (Coquel et al., 1995; Fabre, 2005)

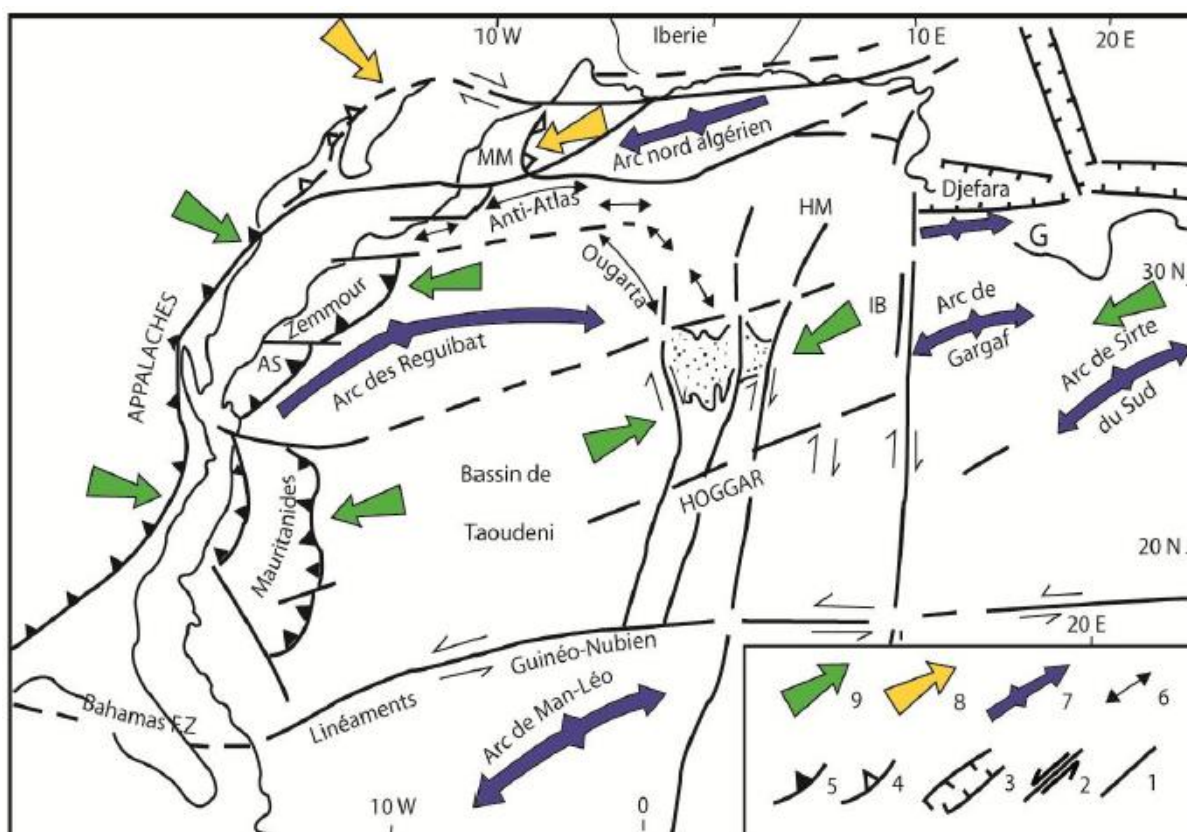


Figure III-32: Permo-Carboniferous intra-plate deformation of the Sahara Platform forming the foreland of the Mauretaniides-Atlas orogen. Arrows indicate axes of major Arches. Schematic evolutionary diagram of Ougarta trough modified from Dallmeyer and Lécorché, (1991); Ziegler et al., (1995). Ti = Tinduff basin, Ta = Taoudeni basin, Tm = Timimoun basin, Gh = Cihadames basin, MO = Mourzouk basin. (1) major faults, (3) rift, (4) Late Carboniferous thrusting, (5) Lower Permian thrusting, (6) Lower Permian-Late Carboniferous folded chain, (7) major extruded Arches, (8) terminal Carboniferous shortening direction, (9) terminal Permian shortening direction.

In the Ahnet and the Mouydir basins, the folding and faulting have occurred around the Carboniferous/Permian transition or, more probably, during the Early Permian (Haddoum et al., 2001). Thickness variations of Carboniferous series are also observed at the vicinity of Arches (Figure III-31). Moreover, inversion or reactivation of former structure are identified in the Ghadamès basin (Abudeif, 2015) and in the Ahnet basin (Badsı et al., 1999). The Figure III-32 illustrates the impact of the Hercynian orogeny on the Saharan platform.

2.4.14 Mesozoic extension: Tethys and Atlantic opening (c. 270-130 Ma)

During the Mesozoic, the Pangea break-up and the opening of the Central Atlantic and Tethys is accompanied by an extensive tectonic regime (Craig et al., 2008; Guiraud et al., 2005a; Guiraud and Maurin, 1992). This event is recorded in North-Africa by the initiation of rifting processes and the development of magmatic provinces (Craig et al., 2008). In the Illizi Basin, the NE-SW fault system is reactivated as normal fault system with a NW-SE lengthening direction, leading to local bloc tilting (Figure III-33).

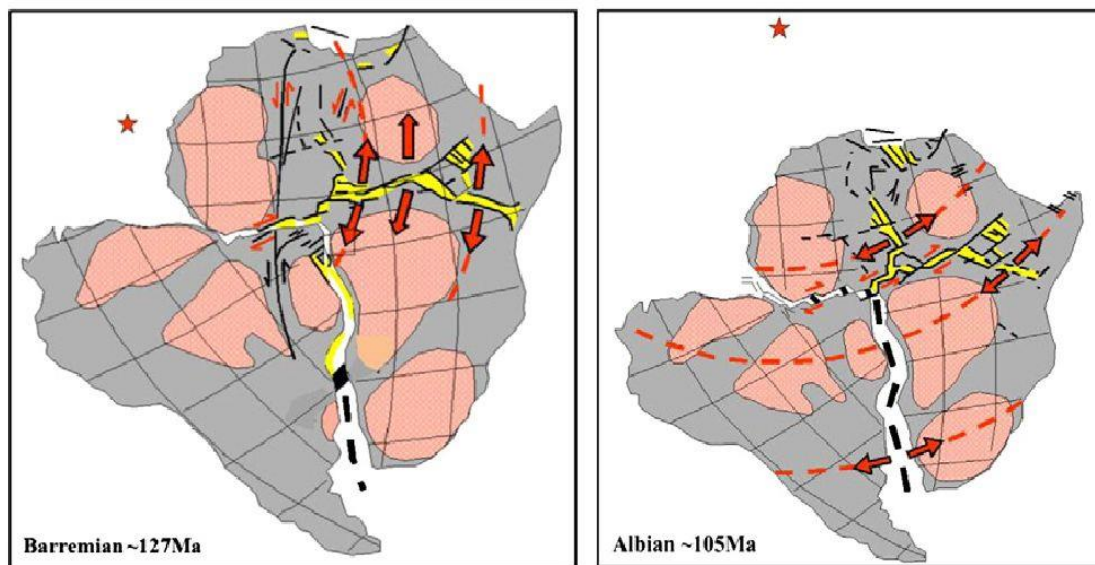


Figure III-33: Main extension phases during the Tethys and Atlantic opening reactivating major ancient faults lineaments (Fairhead et al., 2013).

2.4.15 Alpine and Austrian orogeny (c. 130-23 Ma)

The collision between European and African tectonic plate resulted in the closure of the Tethys and the Alpine orogeny (Bumby and Guiraud, 2005; Craig et al., 2008; Guiraud et al., 2005a). In Africa, this event is recorded through compressive pulses starting at the late Cretaceous. The first phase (Austrian) is an E-W compression phase leading to the development of folds along the N-S reactivated faults, as well as wrench reactivation of NE-SW faults with “en-échelons” folds. Most of the deformation is accommodated by the Atlasic domain, although limited deformation could be affecting the Illizi Basin (tilting blocs).

2.4.16 Eocene-Miocene uplift (c. 35-23 Ma to present day)

Since the Miocene, the Hoggar Massif was uplifted (4000-5000 meters) resulting in the exhumation of the Paleozoic series in the southern part of the Illizi Basin (Tassilli N’Ajjers). This uplift is associated with the reactivation of Pan-African and Paleozoic faults (Liégeois et al., 2005), rifting processes associated with the opening of Central Atlantic, thermal anomaly beneath the Hoggar and the presence of a potential hot-spot (Craig et al., 2008; Guiraud et al., 2005).

Nevertheless, a new study based on thermochronology methods (Apatite fission tracks) revealed evidence of a widespread exhumation of the Touareg Shield during the Late Eocene, before the establishment of the first 35 Ma volcanic edifices (English et al., 2016b; Rougier, 2012; Rougier et al., 2013; Ye et al., 2017).

Furthermore, it indicated that if there was reactivation of Pan-African shear zones, they were only minor and did not affect exhumation of the basement. Thermochronological data suggest burial of the Hoggar and Reguibat shields (English et al., 2016b; Leprêtre, 2015; Leprêtre et al., 2015; Rougier et al., 2013), consistently with subsidence under the Saharan basins before late Eocene exhumation (Figure III-34). Rougier, (2012) also presented that the Touareg Shield may have been buried under a sedimentary cover of 1 to 2.5 km thick.

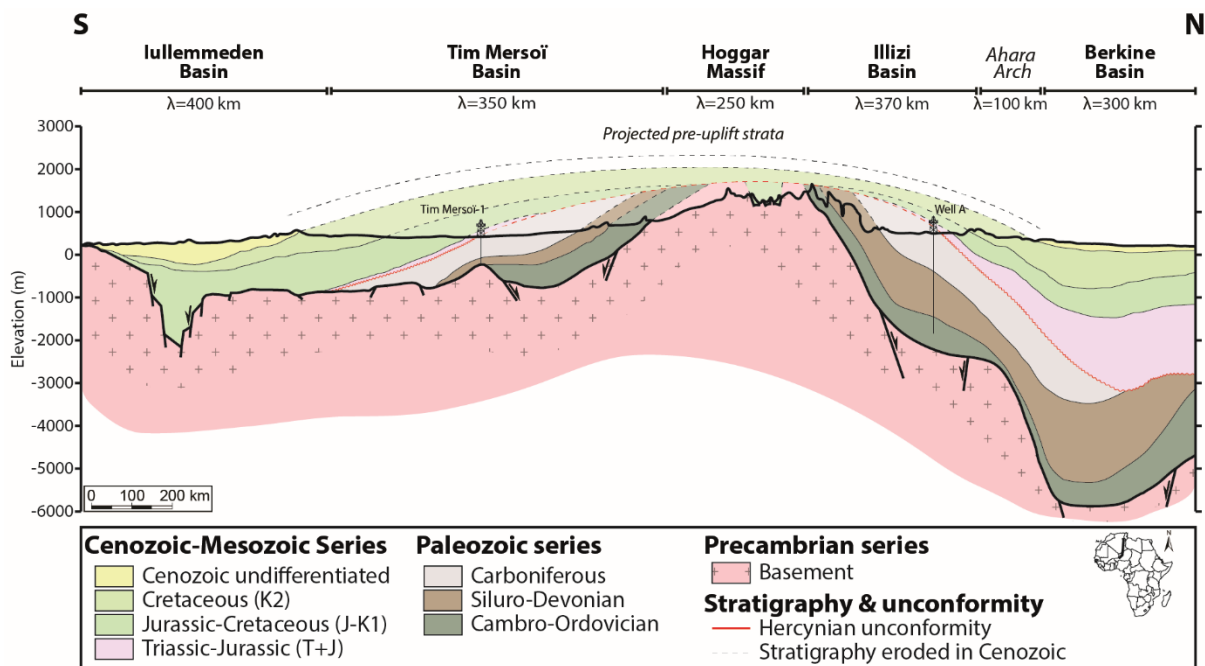


Figure III-34: Schematic structural section across the Hoggar Massif from the Berkine Basin in the north to the Iullemeden Basin in the south from English et al., (2016b). Note that the

Hoggar had an earlier history of uplift with significant erosion of the Paleozoic sequence during the Hercynian orogeny. For localization see 4 in Figure III-2.

2.5 Basin heat flow and thermal activity of the Saharan basins

Overviews of the tectonic development and thermal activity of the north African basin were published by many authors (Badalini et al., 2002; Boote et al., 1998; Coward and Ries, 2003; Craig et al., 2008; Logan and Duddy, 1998; Zielinski, 2011; Zieliński, 2012). A compilation of thermal curves is presented below (Figure III-35). Heat production of the actual Sahara are documented by some authors (Lesquer et al., 1989; Takherist, 1991; Takherist and Lesquer, 1989).

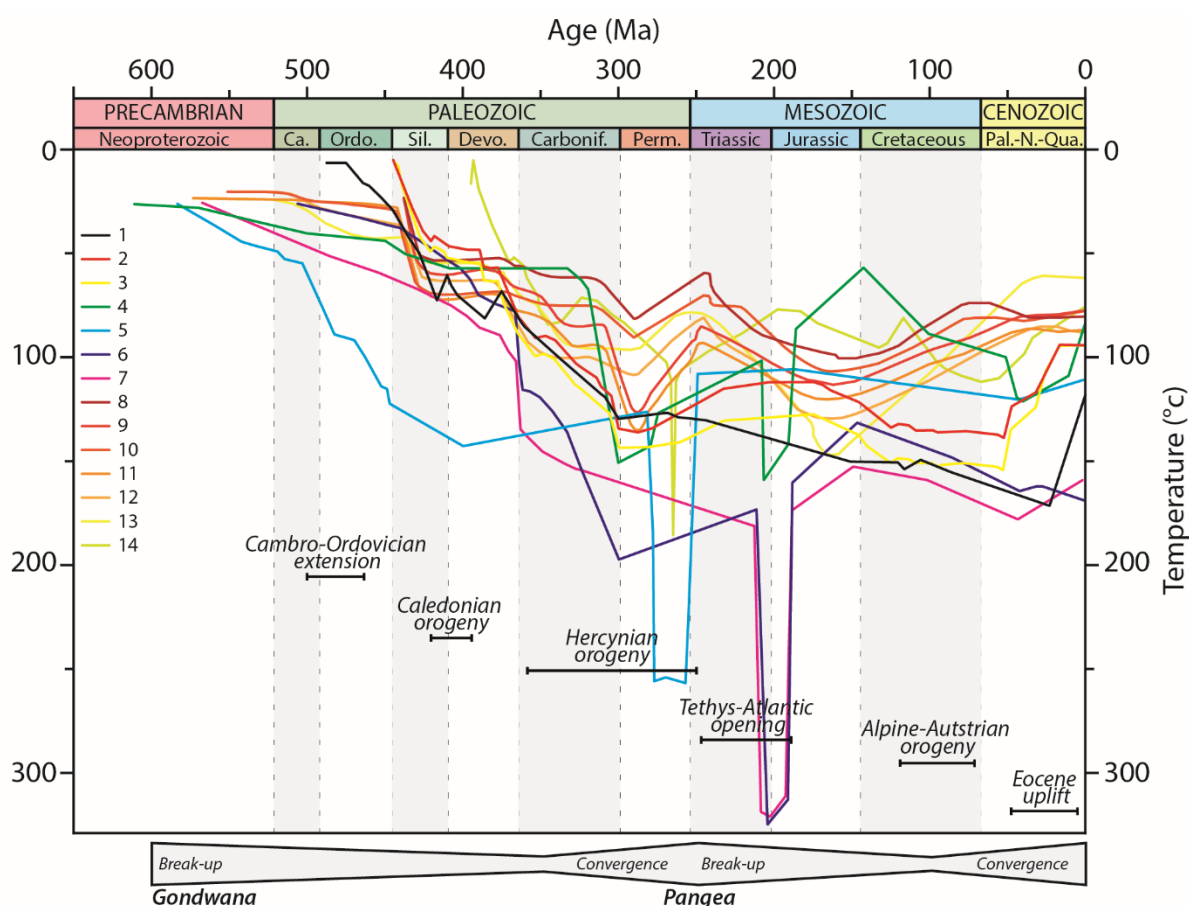


Figure III-35: Thermal history curves of the Paleozoic North Saharan Platform (peri-Hoggar basins) compiled from literature: 1: well in the Illizi basin (Wells et al., 2018); 2: well model A and 3: G in Ghadamès-Berkine basin (Underdown et al., 2007); 4: well OTRA-1 in the Sbâa basin, 5: well RG-3 in the Reggane basin, 6: well TEG-1 in the Timimoun basin, 7: well in the eastern Ahnet basin (Logan and Duddy, 1998); 8: well F3-NC174, 9: well H29-NC115, 10:

well NC-174, 11: well NC-115, 12: well NC-186, 13: well NC-190 in Murzuq basin (Belaid et al., 2010); 14: well A-76 well in Murzuq basin (Galushkin and Eloghbi, 2014).

2.6 Paleozoic sedimentary, stratigraphic and biostratigraphic context

The Paleozoic represents about 290 Ma (541-251 Ma, Ogg et al., 2016) which are divided into six periods: Cambrian, Ordovician, Silurian, Devonian, Carboniferous and Permian. The first three constitute the Lower Paleozoic (541-419 Ma), the last three the Upper Paleozoic (419-251 Ma). During the Paleozoic, two great orogenic cycles take place, the New Caledonian cycle and the Hercynian cycle, respectively attributed to the Lower and Upper Paleozoic.

These cycles, marked by several orogenic phases (for example for the New Caledonian cycle: Sardinian, Taconic and Caledonian), each comprise three major phases: sedimentation, orogenesis and peneplanation. The base of the cycles is thus materialized by large surfaces of major discordances.

As already mentioned, the set of proposed Paleozoic reconstructions (Blakey, 2008; Stampfli et al., 2002; Stampfli and Borel, 2002; Torsvik et al., 2012; Torsvik and Cocks, 2011, 2013; Veevers, 2005) show that during this period of the Earth was marked by the presence of a super-continent called Gondwana which formed a huge continental area (see also Figure III-37).

The principal paleogeographic characteristics of North and Central Africa during the Paleozoic were the permanency of large exposed lands over central Africa, surrounded by northerly and northwesterly dipping pediplanes episodically flooded by epicontinental seas related to the Paleotethys Ocean (Beuf et al., 1971; Eschard et al., 2010; Guiraud et al., 2005). This configuration, in combination with eustatic sea-level fluctuations, had a strong influence on facies distributions. Significant transgressions occurred during the Early Cambrian, Tremadocian, Llandovery, Middle to Late Devonian, Early Carboniferous, and Moscovian (Fabre, 1988, 2005; Guiraud et al., 2005). During Paleozoic times, the sedimentation conditions in the Gondwana platform were profoundly influenced by three main factors: The colonization of the earth by vegetation, a contrasted climatic cyclicity and low gradients in continental and shallow marine environments (Guiraud et al., 2005).

Figure III-36 is a summary of the Paleozoic litho-stratigraphic, sequence stratigraphy and tectonic framework context on the peri-Hoggar Basins. It regroups the Reggane, the Ahnet, the Mouydir, the Illizi (with the Tassili), the Murzuq and the Tim Mersoï Basins.

CHAPTER III – GEOLOGICAL CONTEXT OF PERI-HOGGAR BASINS

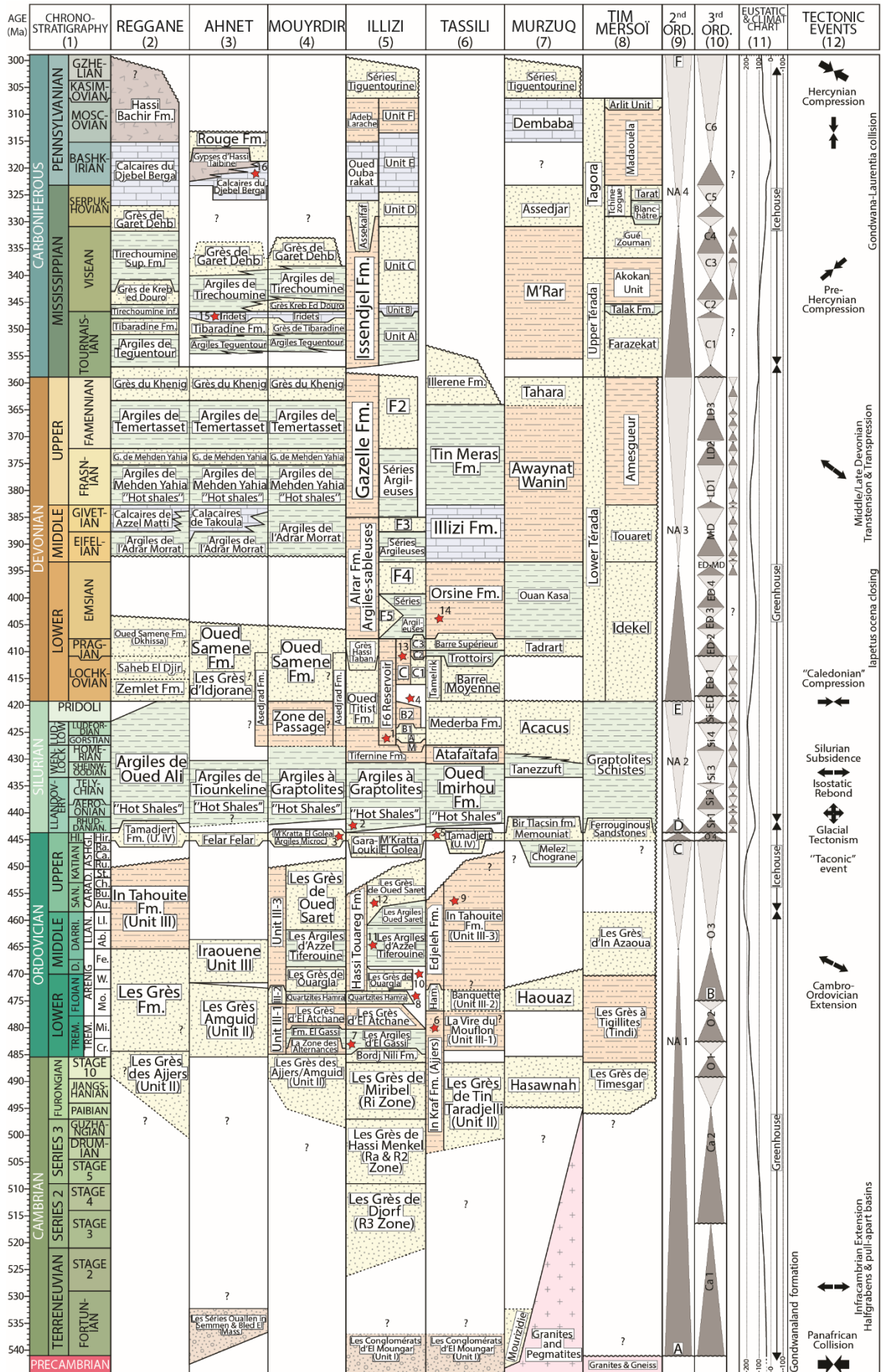


*Figure III-36: Paleozoic litho-stratigraphic, sequence stratigraphy and tectonic framework of the Peri-Hoggar basins (North African Saharan Platform) compiled from (1) Chronostratigraphic chart (Ogg et al., 2016), (2) The Cambrian–Silurian (Askri et al., 1995) and the Devonian–Carboniferous stratigraphy of the Reggane basin (Cózar et al., 2016; Lubeseder, 2005; Lubeseder et al., 2010; Magloire, 1967; Wendt et al., 2006), (3) The Cambrian–Silurian (Paris, 1990; Wendt et al., 2006) and the Devonian–Carboniferous stratigraphy of the Ahnet basin (Beuf et al., 1971; Conrad, 1973, 1984; Legrand-Blain, 1985; Wendt et al., 2006, 2009a), (4) The Cambrian–Silurian (Askri et al., 1995; Paris, 1990; Videt et al., 2010) and the Devonian–Carboniferous stratigraphy of the Mouydir basin (Askri et al., 1995; Beuf et al., 1971; Conrad, 1973, 1984; Wendt et al., 2006, 2009a), (5) The Cambrian–Silurian (Eschard et al., 2005; Fekirine and Abdallah, 1998; Jardiné and Yapaudjian, 1968; Videt et al., 2010) and the Devonian–Carboniferous stratigraphy of the Illizi basin (Eschard et al., 2005; Fekirine and Abdallah, 1998; Jardiné and Yapaudjian, 1968), (6) The Cambrian–Silurian (Dubois, 1961; Dubois and Mazelet, 1964; Eschard et al., 2005; Henniche, 2002; Videt et al., 2010) and the Devonian–Carboniferous stratigraphy of the Tassili-N-Ajers (Dubois et al., 1967; Eschard et al., 2005; Henniche, 2002; Wendt et al., 2009a), (7) The whole stratigraphy of the Murzuq basin (Echikh and Sola, 2000), (8) The whole stratigraphy of the Tim Mersoï basin (Coquel et al., 1995; Denis et al., 2007; Joulia, 1963), (9) 2nd order sequence stratigraphy of the Saharan Platform (Carr, 2002; Eschard et al., 2005; Fekirine and Abdallah, 1998), (10) 3rd order sequence stratigraphy of the Saharan Platform (Djouder et al., 2018; Eschard et al., 2005; Fröhlich et al., 2010b; Lubeseder, 2005; Lubeseder et al., 2010; Wendt et al., 2006), (11) Eustatic and climatic chart (Haq and Schutter, 2008; Scotese et al., 1999), (12) Tectonic events (Boudjema, 1987; Coward and Ries, 2003; Craig et al., 2008; Guiraud et al., 2005; Lüning, 2005); (A) Infra-Tassilian (Pan-African) unconformity, (B) Intra-Arenig unconformity, (C) “Taconic” and glacial unconformity, (D) Isostatic rebound unconformity, (E) Caledonian unconformity, (F) Hercynian unconformity. *16: Conrad, (1984) and Wendt et al., (2009a) dated the formation Carboniferous; *15: Iridet Dalle dated Late Touraisian Early-Visean by ammonoids (Korn et al., 2010a); *14: Orsine fm. dated Emsian by abundant microfauna (Eschard et al., 2005); *13: Unit C2 dated Pragian by palynomorphs (Eschard et al., 2005); *12: Oued Saret sandstones dated Lower Llandeilo (Oulebsir and Paris, 1993; Paris et al., 2000a); *11: Azzel-Tiferouine shales dated Arenig to Llandeilo (Paris et al., 2000a); *10: Ouargla sandstones dated Arenig (Oulebsir and Paris, 1993); *9: In Tahouite fm. dated Arenig by brachiopods and lamellibranches (Legrand, 1964); *8: Hamra’s Quartzite/Unit III-2 dated Arenig (Eschard et al., 2005); *7: El Gassi shales/Unit III-1 dated Tremadoc by*

*Graptolites and Chitinozoan (Legrand, 1964; Paris et al., 2000a); *6: Vire du Mouflon dated Lower Ordovician by brachiopods and lamellibranches (Legrand, 1964); *5: Unit IV /Tamadjert fm. dated Late Ashgill (Oulebsir and Paris, 1993); *4: Unit B Dalle dated Pridoli (Henniche, 2002); *3: M'Kratta Dalle dated Late Ordovician (Oulebsir and Paris, 1993); *2: Graptolites shales dated from Llandovery to Upper Ludlow (Legrand, 1964); *1: Unit M dated Wenlock to Ludlow (Boumendjel et al., 1988; Henniche, 2002).*

2.6.1 The infra-Cambrian molasses series

The Infra-Cambrian is mainly composed of crystalline rocks formed during the Pan-African orogeny (e.g. Fabre, 2005). Locally, it is possible to find molasses (e.g. Western Hoggar), whose thickness can reach 6000 m, which were deposited in extensive basins formed during the Pan-African late-orogenic extension phase (Djellit et al., 2002).

2.6.2 The fluvio-conglomerates Cambrian series

The Cambrian starts at the base with volcano-sedimentary (i.e. molasses) and conglomerates facies respectively corresponding to the formation of El Mouggar in the Illizi-Tassili basins, the “Pourrée” series in the Ahnet basin and the Ouallen in Semmen-Bled El Mass series in the Mouydir basin, equivalent to the unit I in subsurface. The top is featured by fluvial sandstones facies corresponding to the Tin Taradjelli in the Tassili, Ajjers-Hassi Leila in the Illizi basin, the Ajjers-Amguid in the Mouydir basin, the Ajjers-Azzel Matti in the Ahnet basin, the Ajjers in the Reggane, which is equivalent to the unit II in subsurface (Figure III-36).

2.6.3 The fluvial to marine of pre-glacial Ordovician series

The pre-glacial Ordovician succession comprises all the series deposited between the fluvial Cambrian and the polyphase glacial erosion surface of the Hirnantian glacial episode (Figure III-36). The base is mainly composed of clastic sediments going through fluvial to shallow marine (estuarine to upper shoreface) environments matching at the base to the Formation of “Vire du Mouflon” in the Tassili and Alternation Zone, El Gassi and El Atchane in the Ahnet-Mouydir-Illizi basins equivalent to the unit III-1 (Eschard et al., 2005, 2010; Videt et al., 2010). In the middle, the Formation of “Banquette” in the Tassili is principally defined by a bioturbated clastic ramp corresponding to the Hamra quartzite in the Ahnet-Mouydir-Illizi basins and equivalent to the unit III-2. At the top, the In Tahouite Formation in the Tassili or Reggane basin also called Hassi Touareg in the Illizi basin is composed by the Ouargla (shoreface facies),

the Azzel Tiferouine offshore shales facies, the tidal ramp Oued Saret entities forming the unit III-3 (Figure III-36).

16 main cycles, high frequency (Videt et al., 2010) and five to six transgressive-regressive, low frequency depositional sequences (Eschard et al., 2005; Ghienne et al., 2007b) have been differentiated on the northern Gondwana platform.

2.6.4 The syn-glacial Ordovician series

The syn-glacial Ordovician (i.e. late Ashgill or Hirnantian glaciation) is stratigraphically characterized by the Tamadjert Formation in the Tassili also called the Felar-Felar Formation and equivalent to the unit IV (Figure III-36). The succession comprises all the series deposited between the glacial irregular deeply incising unconformity and isostatic rebound erosional surface resulting from ice melting sediments filling (e.g. Deschamps et al., 2013; Hirst et al., 2002). It is composed of microconglomerates shales and El Golea sandstones Formations (Figure III-36). At this time Northwestern Africa was located in the paleo South Pole area and glacial deposits were registered both in continental and marine domains (Guiraud et al., 2005; Scotese et al., 1999). The ice kinematics is characterized by migrating ice fronts during successive phases of ice advance and recession (Ghienne, 2003). It is recorded by in the form of glaciotectonic deformation structures within unconsolidated glacial sediments (e.g. complex subglacial shear zones, decametre- scale sediment diapirs, load-structures and plurikilometric composite thrust and fold systems) (Beuf et al., 1971; Clerc et al., 2013; Denis, 2007; Denis et al., 2007; Ghienne, 2003; Le Heron et al., 2005; Ravier et al., 2014, 2015).

The number of glacial cycles preserved in North Gondwana is controversial and varies between 2 and 5 (Ghienne, 2003; Le Heron et al., 2006, 2009; Loi et al., 2010). The duration of this icehouse event was short (i.e. 1 million years to 2 million years) and most of western Gondwana was buried under a thick continental ice-sheet, centered above Central Africa (Figure III-37), implying coalescent synchronous glaciers (Ghienne et al., 2007a; Le Heron et al., 2009; Sutcliffe et al., 2000). New numerical modelling helped to respond to circumscribe this glaciation (Pohl et al., 2016). At the end of the Ordovician a major diachronous flooding take place on the all Saharan domain due to deglaciation processes (diachronous), paleo-topography and differential isostatic readjustment (Beuf et al., 1971). The progressive retreat of ice sheet set place to periglacial deposits (Beuf et al., 1971).

GONDWANA PALEOGEOGRAPHY

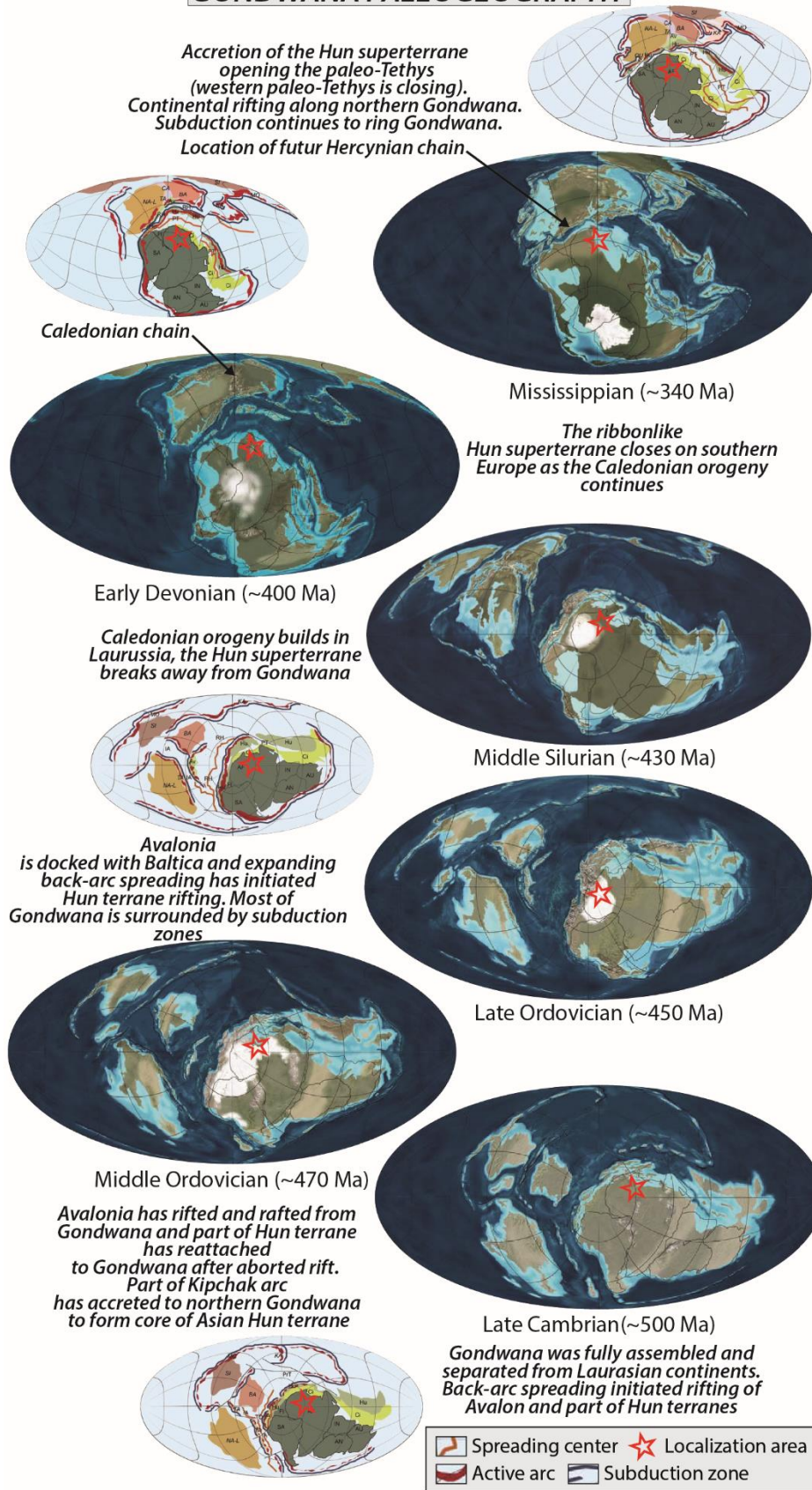


Figure III-37: Paleozoic plate reconstruction of the north Gondwana modified from Blakey, (2008).

2.6.5 The Silurian marine series

The Silurian starts with the M'Kratta Dalle characterized by bioturbated tidal sandstones post-glacial deposits (deglaciation) and rich organic radioactive shales "Hot Shales" deposited in offshore. The rest of the succession is dominated by offshore shale marine facies respectively corresponding to the Oued Imirhou in the Tassili, the Graptolites shales in the Illizi-Mouydir basins, the Tioukeline in the Ahnet basin, the Oued Ali formations in the Reggane basin. The top Silurian is composed of shoreface to fluvio-estuarine sandstones respectively corresponding to the Formation Atafaitafa-Mederba in the Tassili, the Tifernine-Oued Titist in the Illizi basin, equivalent to the F6 in subsurface (divided by M, A, B1 and B2 units), the "Passage zone" or Lower Assejrad in the Ahnet-Mouydir basin. The lower part of the Silurian is marked by a prograding transgressive sequence up to the offshore deposits followed by at the top a regressive succession. Silurian marine shales with graptolites shows transgression diachronism depending on region between lower Llandovery with an early partial melt and a middle Llandovery general melt of the ice-sheet (Beuf et al., 1971).

2.6.6 The fluvial to marine series of Lower Devonian (Lochkovian to Emsian)

The lower Devonian is stratigraphically featured by the Talmerik Middle bar, the Sidewalks, the Upper Bar and the Osirine Formations in the Tassili. In the Illizi basin, it is marked by Oued Tifidist, the Hassi Tabankort, the Alrar shaly-Sandstones equivalent to the F6 reservoirs (divided by C1 to C3 units), the F5 and the F4 reservoirs. It is defined by the Oued Samene or Asjerad or Idjorane Sandstones formations in the Ahnet-Mouydir basins (Figure III-36). It is identified by the Zemlet, the Saheb El Djir and Oued Samene (Dkhissa) Formations in the Reggane basin. It is marked by continental/fluvial sandstones systems in the south, passing into deltaic/shallow marine sandstones with argillaceous intercalations towards the north and northwest (Beuf et al., 1971; Djouder et al., 2015, 2018; Dubois et al., 1967; Eschard et al., 2005; Henniche, 2002; Wendt et al., 2006). More precisely, it is characterized by a gradual transition from a continental fluvial environment in the central and eastern part of the Tassili N'Ajjers/Illizi basin, across a continental marine zone in the western part of the Tassili N'Ajjers/Illizi basin and the Mouydir basin, into a predominantly marine regime in the Ahnet basin (Beuf et al., 1971; Dubois et al., 1967; Eschard et al., 2005; Henniche, 2002; Wendt et al., 2006). Paleocurrents show mainly S-N to SE-NW directions (Beuf et al., 1969). The Silurian-Devonian boundary, defined by the flat low-angle tectonic unconformity, called the 'Caledonian unconformity' is linked with a tectonic event and a major relative sea-level fall

which affected most of the Gondwanan margin (Beuf et al., 1971; Eschard et al., 2005, 2010; Henniche, 2002). The late Early Devonian registered a brief marine transgression during the Emsian, with the occurrence of shallow marine sandstones to offshore marine mudstones all along the North African platform (Guiraud et al., 2005).

2.6.7 The carbonates marine series of Middle Devonian (Eifelian and Givetian)

The Middle Devonian is stratigraphically marked by the Illizi Formations in the Tassili, Alrar shaly-Sandstones equivalent to the F3 reservoirs and Shale series in the Illizi basin, the Adrar Morrat shales in the Mouydir-Ahnet-Reggane basins, evolving to Takoula limestones and Azzel Matti limestones in the Ahnet-Reggane basins (Wendt et al., 2006, 2009b; Figure III-36). During the early Givetian, spectacular carbonate mud mounds were constructed in this area (Mezlah, 2006; Wendt et al., 1993, 1997, 2006). In the Middle Devonian (Figure III-37), plate reconstruction of this part of Gondwana locates it at about 45°S (Golonka, 2002), at about 50°S (Scotese et al., 1999) or at about 60°S (Torsvik and Cocks, 2011).

2.6.8 The marine series of Upper Devonian (Frasnian and Famennian)

The Late Devonian were initiated by deposition of organic-rich shales (Guiraud et al., 2005; Lüning et al., 2000, 2004), evolving to shale facies and finishing with fluvio-deltaic to nearshore sandstones deposits (Conrad, 1984; Conrad et al., 2010; Eschard et al., 2010; Wendt et al., 2006). The succession comprises the Tin Meras Formation, the Illerene Formation in the Tassili. The Illerene Formation is diachron (Attar et al., 1980; Latreche and Coquel, 1996): In the south, its age is essentially Famennian, whereas on the Ahara uplift its age is mainly Strunian.

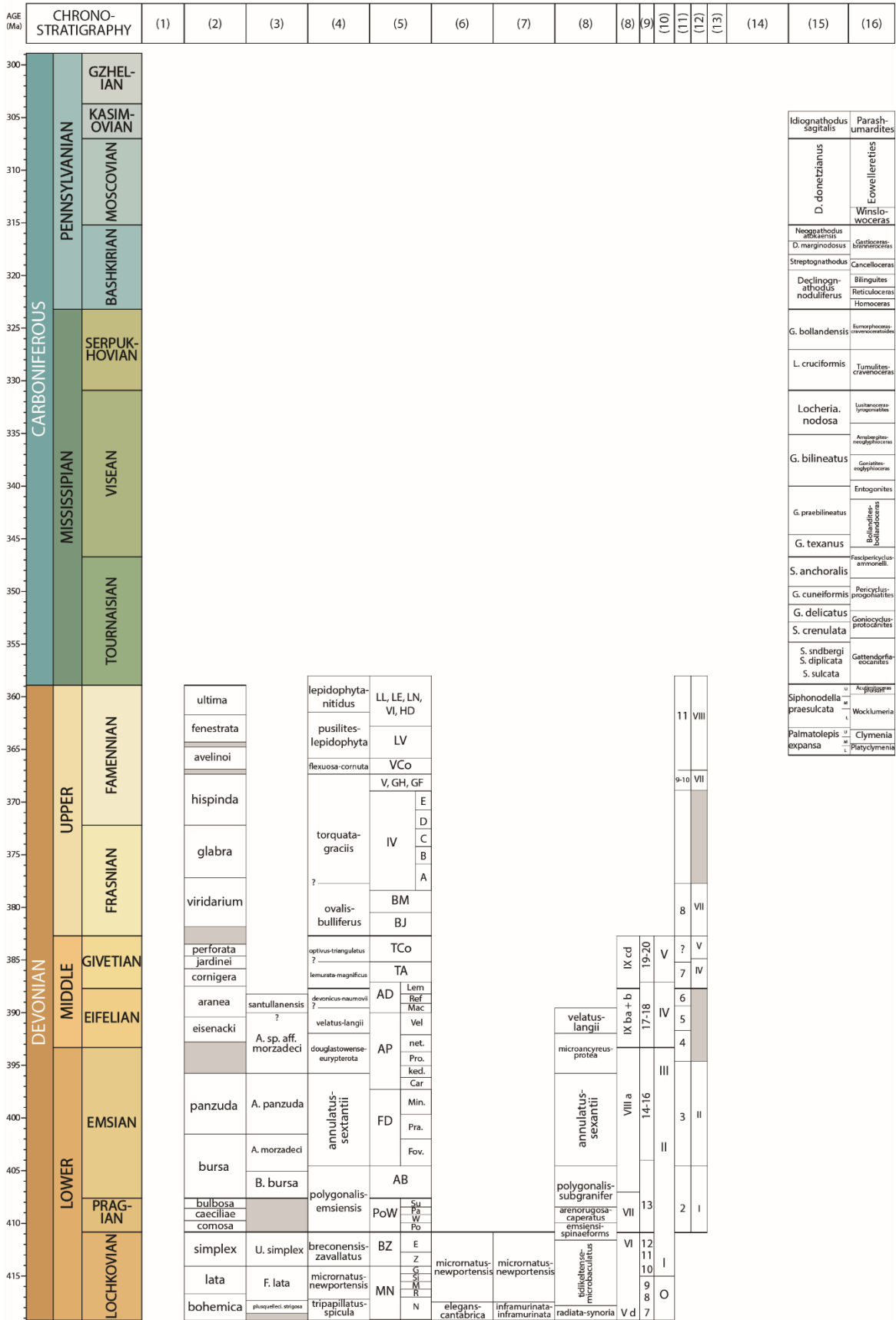
It is defined by the Gazelle formation equivalent to the shale Series and F2 reservoirs in the Illizi basin. It is featured by the Meden Yahia Formation (shales and Sandstones), the Temertasset Formation and the Khenig Formations in the Reggane-Ahnet-Mouydir basins (Figure III-36). In the Late Devonian (Figure III-37), after the northward drift and clockwise rotation of Gondwana (Aifa et al., 1990), the palaeolatitude of this area has shifted to about 30°S (Golonka, 2002). The Late Devonian is generally considered as a period of major environmental and biotic crises (the Frasnian-Famennian and Devonian-Carboniferous boundary crises) and by the onset of a long-term cooling event (the Upper Paleozoic Icehouse stage) (e.g. Copper, 1986; Streel et al., 2000). The Late Devonian was initiated by deposition of transgressive deposits. Three main transgressive-regressive low frequency cycles can be identified (Wendt et al., 2006).

2.6.9 The Carboniferous deltaic to marine series

The Carboniferous strata were deposited under open-marine, deltaic, shallow-subtidal, fluvial, and continental environments (Conrad, 1972, 1973, 1984; Wendt et al., 2009a). It is characterized from the bottom to the top by the Khenig, the Teguentour Shales, the Tibaradine, the Iridets, the Kreb El Douro, the Tirechoumine Shales, the Djebel Berga, the Hassi Taibine and the Red Formations in the Ahnet-Mouydir basins. In the Reggane basin, from the bottom to the top the Carboniferous is composed by the Khenig, the Teguentour Shales, the Tibaradine, the Lower Tirechoumine, the Kreb Ed Douro, the upper Tirechouline, the Gart Dehb, the Djebel Berga and the Hassi Bachir Formations (Figure III-36). In the Early Carboniferous (Figure III-37), plate reconstruction of this sector of Gondwana situates it at about 30°S (Golonka, 2002) and at about 45° S (Scotese et al., 1999). In Late Carboniferous, after the northward drift and clockwise rotation of Gondwana (Aïfa et al., 1990), the palaeolatitude of this area shifted to about 15° S (Golonka, 2002) or more southerly at 18-24°S (Derder et al., 2001) or even more southerly at 50° S (Torsvik and Cocks, 2011) based on a compilation of palaeomagnetic and faunal/floral data. It is subdivided in four transgressive–regressive cycles (Wendt et al., 2009a). Two major gaps were identified, one during the middle Tournaisian, the other during the middle Viséan to Serpukhovian (Wendt et al., 2009a). Absent in the Tassili, in the Illizi basin, the Carboniferous is stratigraphically marked the Issendjel, the Assekaifaf, the Oued Oubarakat, the Adeb Larache and the Tiguentourine formations equivalent to the A to F units in subsurface.

2.6.10 Biostratigraphic data and zonation

In this part, a synthesis of biostratigraphical data and zonation of different fossils have been done in the Saharan platform. According to Lubeseder, (2005), a revision of these early results is necessary because one or more of the following problems is usually encountered: a) the early works refer to old stage schemes and differ from today's standards (e.g. old Siegenian vs. new Pragian/(new) Emsian); b) stage boundary definitions have changed, with new index-fossils or their correlatives; c) only taxa have been listed in a publication without an age proposal; d) previous index taxa are now known to have a different range; e) recent reviews show that previous taxa determinations may be erroneous because the fauna was compared to the wrong faunal type province (e.g. brachiopods, Jansen, 2001; graptolites, Legrand, 1985); f) different fossil groups in one location and level indicate different ages. In addition, a regional chronostratigraphic correlation requires a common biozone reference standard. These are the graptolite zones for the Silurian and the conodont zones for the Devonian. All other formation



Idiognothodus sagittalis	Parashumardites
D. donetzianus	Eowellierites
Neognothodus affinis	Winskiwocheras
D. marginodosus	Gastoceras
Streptognothodus	Cancelloceras
Declinognothodus noduliferus	Blinguites
	Reticuloceras
	Homoceras
G. bollandensis	Emmerphaceros
	Tumulticeras
L. cruciformis	Tumulticeras
	Locheria nodosa
	Lunaticeras
	G. bilineatus
	G. praebilineatus
	G. texanus
	S. anchoralis
	G. cuneiformis
	G. delicatus
	S. crenulata
	S. snidbergi
	S. duplicata
	S. sulcata
Siphonodella praesulcata	Wocklumenia
Palmatolepis expansa	Clymenia
	Platyclymenia

Figure III-39: Devono-Carboniferous synthesis of biostratigraphic zonation compiled from bibliography. (1) Time slices. (2) Chitizonooan biozones of North Gondwana (Paris, 1990; Paris

et al., 2000b; Videt *et al.*, 2010). (3) *Chitizonoan biozones of Illizi* (Eschard *et al.*, 1999; Paris *et al.*, 2000b). (4) *Miospores biozones* (Richardson and McGregor, 1986). (5) *Miospores biozones* (Streel *et al.*, 1987). (6) *Miospores biozones* (Richardson and McGregor, 1986). (7) *Miospores biozones* (Rubinstein and Steemans, 2002). (8) *Miospores biozones* (Kermandji, 2007, 2012; Kermandji *et al.*, 2008, 2009). (9) *Miospores biozones* (Boumendjel, 1987). (10) *Miospores biozones* (Massa, 1988). (11) *Miospores biozones* (Moreau-Benoit *et al.*, 1993). (12) *Miospores biozones* (Abdesselam-Rouighi, 1986, 2003, 2003). (13) *Acritaches biozones* (Jardiné *et al.*, 1974). (14) *Graptolites biozones* (Videt *et al.*, 2010). (15) *Conodontes biozones* (Wendt *et al.*, 2010b). (16) *Ammonites zonations* (Korn *et al.*, 2007, 2010a, 2010b).

2.7 Petroleum systems

Paleozoic deposits of the Saharan platform (North Africa) is a highly productive petroleum system with a long exploration history in Algeria, Libya and Tunisia from the late 1950s to present day (Boote *et al.*, 1998; Burke *et al.*, 2003, 2003; Logan and Duddy, 1998; Macgregor, 1996; MacGregor *et al.*, 1998; Purdy and MacGregor, 2003). The Lower Silurian and Frasnian “hot shales” are considered as the main hydrocarbon source rocks (respectively 80-90% and 10%) and seals (Boote *et al.*, 1998; Lüning *et al.*, 2000, 2004). The Cambro-Ordovician and Lower Devonian sandstones are known as the main reservoirs (Boote *et al.*, 1998; Craig *et al.*, 2008; Eschard *et al.*, 2005, 2010). A general description of the petroleum systems in the North Africa province can be found in (Burke *et al.*, 2003; Macgregor, 1996; MacGregor *et al.*, 1998), more precisely for the Ahnet-Reggane province in (Logan and Duddy, 1998) and for the Ghadames-Illizi province in (Dixon *et al.*, 2010). An overview of the Illizi-Berkine petroleum area (Eastern part of the Saharan Platform) was published by Galeazzi *et al.*, 2010.

2.8 Evidence of tectono-sedimentary structures from bibliography

In this part, a synthesis of bibliographic geologic cross sections is presented showing evidence of stratigraphic and sedimentary structures (see Chapter III.2.4). They are often evidence of Arches and Basins geometries. All the cross sections collected in the literature are georeferenced in Figure III-40 for the north peri-Hogggar basins and in Figure III-41 for the south peri-Hogggar basins. They range from years 1950 to 2010. They document thickness variations, growth strata, stratal lapout lateral facies variations, current directions variations related to tectono-sedimentary structures. They can be evidences of extensional or compressional kinematics during the Paleozoic on the Saharan Platform such the Cambro-

Ordovician extension, the Caledonian event, the Middle to Late Devonian event and the Hercynian compression (see Chapter III.2.4).

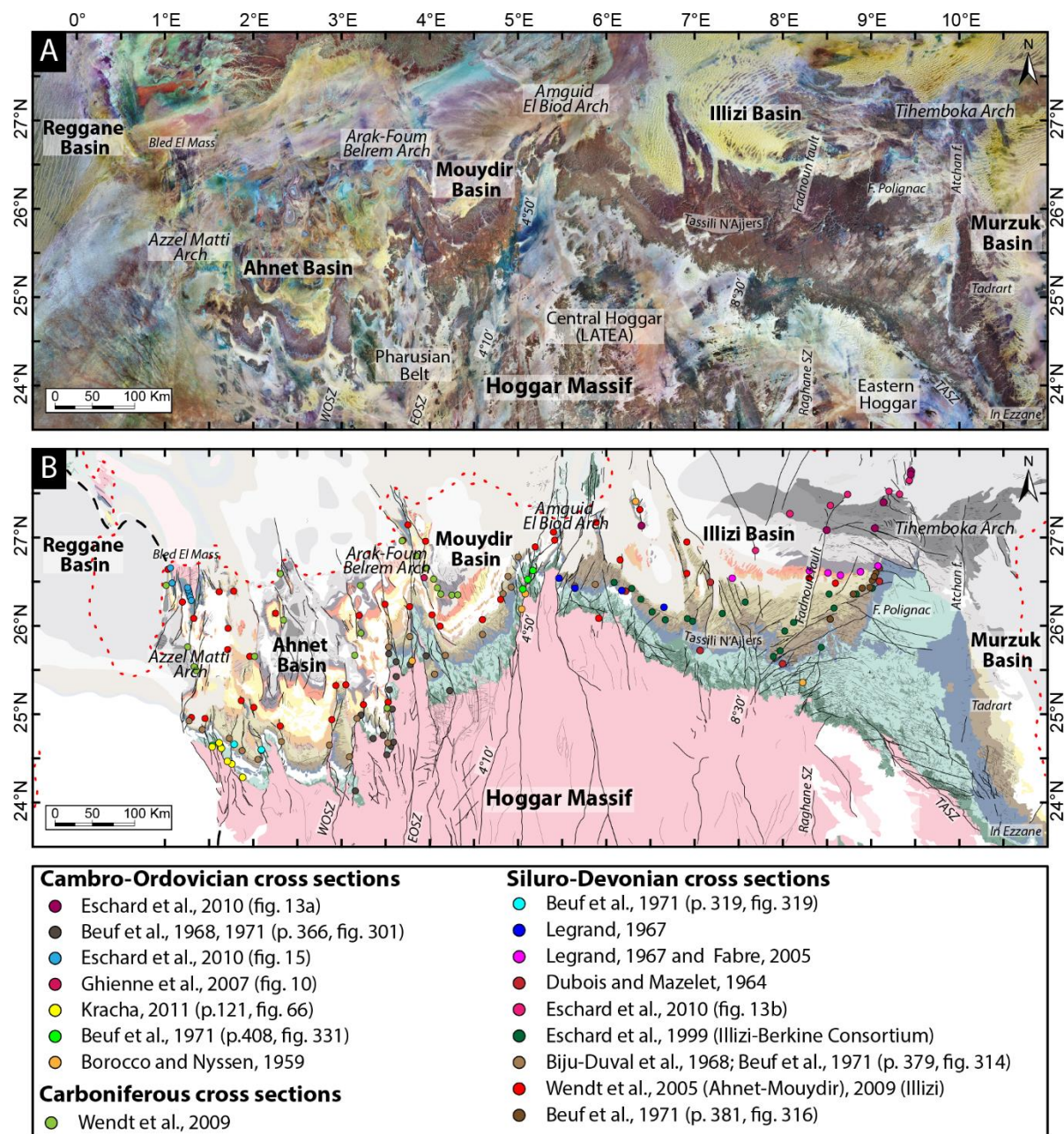


Figure III-40: Localization of different cross sections of north peri-Hoggar Basins georeferenced and compiled from bibliography. See Figure III-2 for geological legend and localization.

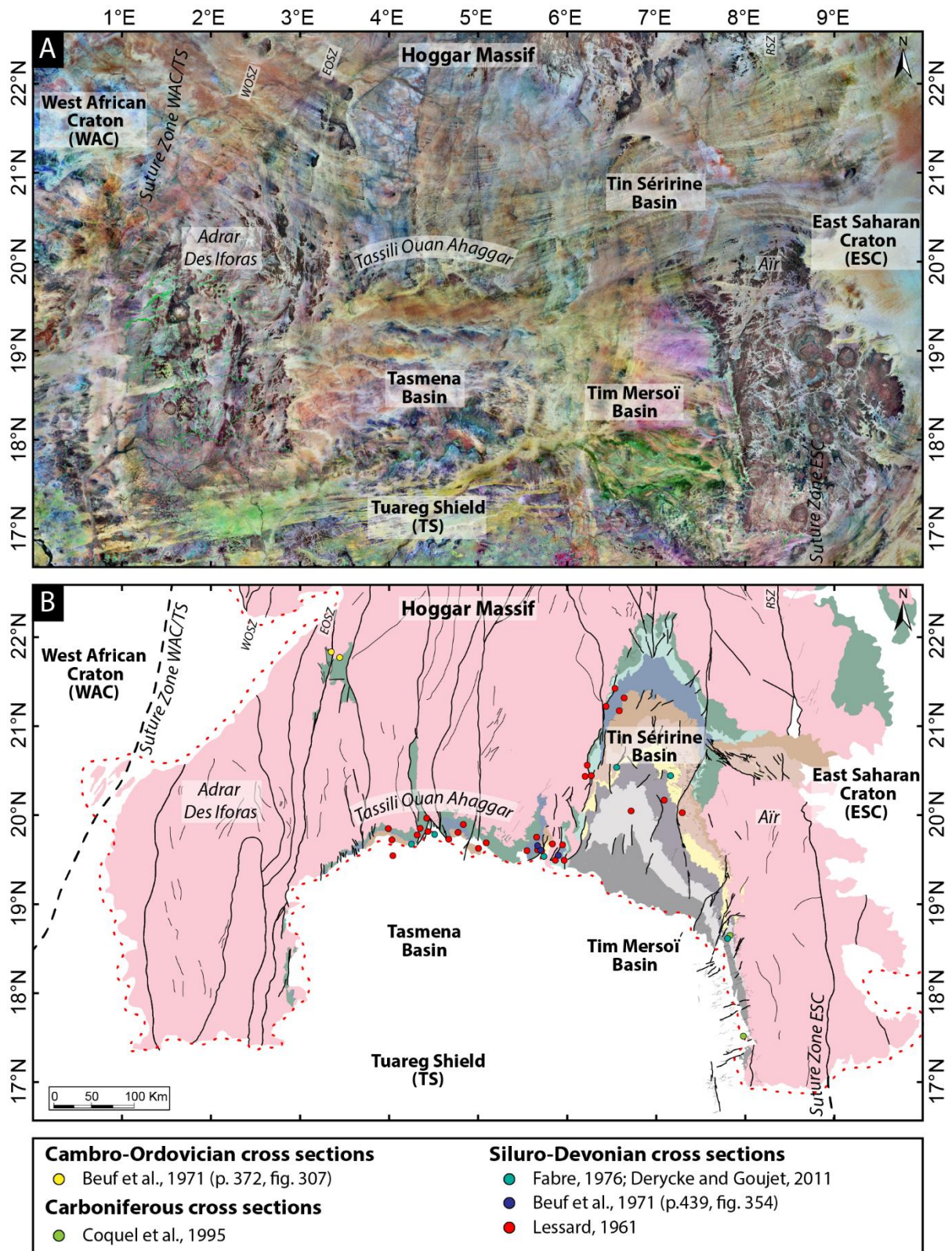


Figure III-41: Localization of different cross sections of south peri-Hoggar Basins georeferenced and compiled from bibliography. See Figure III-2 for geological legend and localization.

3 Conclusion

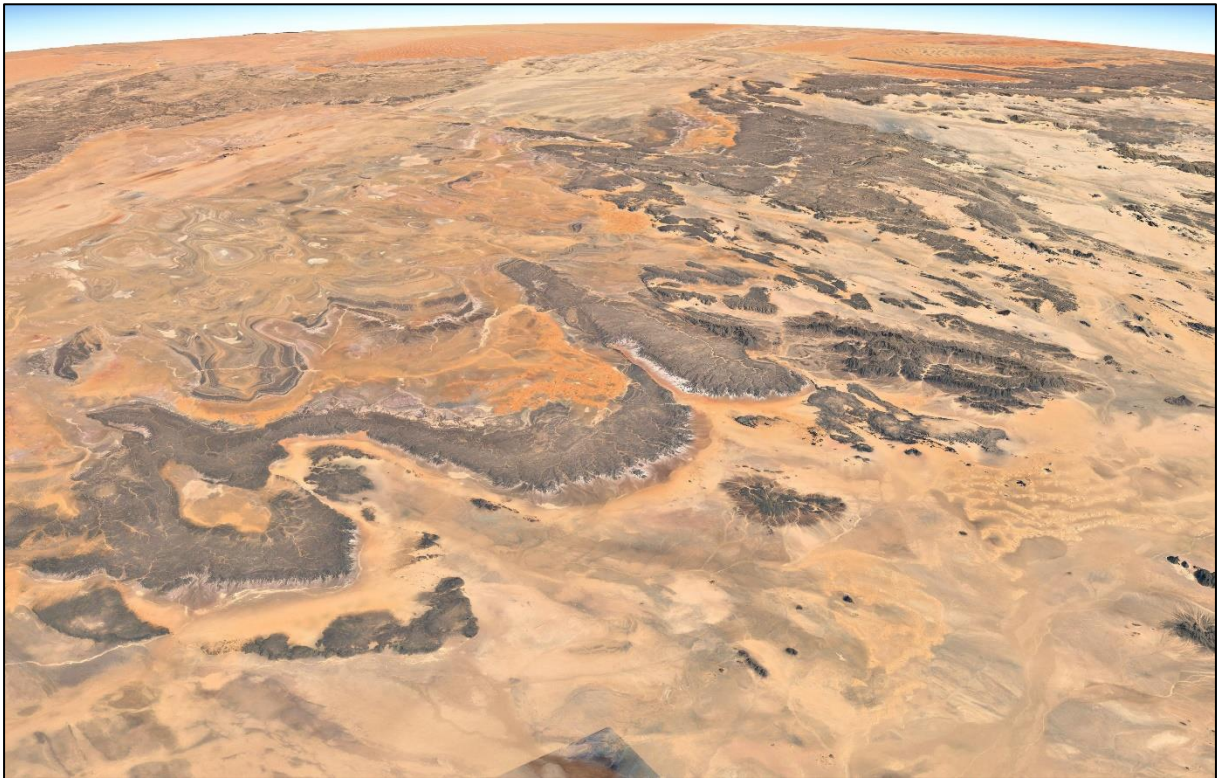
According to this literature review, the Paleozoic (North Gondwana) intracratonic basins of the Saharan platform history have been dominated by *slow long-wavelength vertical motions* leading to overall *low rate subsidence* and accumulation of an extensive cover of platformal sediments (i.e. shallow deposits environments), with occasional tectonic pulsatile events such as rifting, intra-plate volcanism, and local deformation, probably triggered by far field stresses.

The vertical motions of the platform produced *several Arches* (i.e. domes, swells, highs, ridges) and *basins (synclines) with different wavelengths* going from several hundred to more than a thousand kilometres. This latter may control spatially and temporally the deposition and the erosion dynamics. Many studies have documented *tectono-sedimentary structures* such as thickness variations, onlaps and truncatures at the vicinity of enigmatic Arches. Several *major erosion events* significantly truncated the pre-existing sediments over wide areas, producing regional unconformities that separate the platformal cover into divisions.

The persistence of a rather *uniform pattern of vertical motions* seems to control the architecture of these basins. This architectural pattern of the Saharan platform and his associated Arches and Basins (sub-basins), which is often *identified in the literature as basement related*, seems to point out a large-scale control (i.e. lithospheric).

As a consequence, integrate Precambrian substrate studies and architectural tectono-sedimentologic analysis, seems to be crucial to build a coherent and viable conceptual geological model. These two domains of study are often led separately, at least in our area, because of partitioning of the different disciplines.

**CHAPTER IV. INFLUENCE OF BASEMENT
HETEROGENEITY ON THE ARCHITECTURE OF LOW
SUBSIDENCE RATE PALEOZOIC INTRACRATONIC
BASINS (REGGANE, AHNET, MOUYDIR AND ILLIZI
BASINS, HOGGAR MASSIF)**



North peri-Hoggar basins (Google-Earth view; 25°28' N, 3°10' E)



1 Summary and objectives

The last chapter has presented a state of art of bibliography data available on the Saharan platform and peri-Hoggar Basins. The many years of previous works has highlighted the main singularities of these intracratonic Basins. It forms an important base of knowledge, indispensable for a better understanding and characterization of the studied area.

The purpose of this part, which have been published into Solid Earth, is to the establish a conceptual geological model based on the integration of multidisciplinary data such as satellite images, seismic profiles, well logs, Bouguer anomaly maps and aeromagnetic anomaly maps. The study is essentially focus on the Reggane, the Ahnet, the Mouydir and the Illizi Basins for characterization of the basin architecture, and the Hoggar massif for the analysis of the basement. This chapter starts with a brief reminder of concepts of syn-sedimentary tectono-sedimentary structures. It will help the reader on some tectono-sedimentary notions used in the paper.

In more details, the main objectives are the following:

- Elaborated a multidisciplinary integrated methodology;
- Observe, describe and interpret tectono-stratigraphic structures (structural style, stratal geometries);
- Synthetize sedimentologic, depositional environments studies and their associated well logs pattern;
- Define sequence stratigraphy and facies partitioning calibrated by biostratigraphy;
- Found a geological model integrating basement and tectono-stratigraphic architecture characterization of Arches-Basins.

2 Reminder of some concepts for the study of syn-sedimentary tectono-stratigraphic structures

In this part, an inventory of tectonics literature is proposed in order to help the identification and the analysis of syn-tectonic structures in the studied area.

2.1 Compressional and extensional structures

The recognition of faults kinematics is based on literature of fault-related folding in extensional terrains (Grasemann et al., 2005; Reches and Eidelman, 1995; Schlische, 1995; Withjack et al., 1990, 2002). These authors identify the emplacement of footwall anticlines and hanging-wall synclines by investigating fault-propagation folds or drag forced folds (Figure IV-1). The half-graben basin with a roll-over anticline (i.e. reverse drag) is the most common geometrical model used in extensional settings (Cosgrove and Ameen, 1999; Grasemann et al., 2005; Schlische, 1995) (Figure IV-2). Nevertheless, half-graben basin models with normal drags have also been described in extensional settings (Grasemann et al., 2005; Khalil and McClay, 2002; Schlische, 1995; Withjack et al., 2002; Withjack and Callaway, 2000). In this framework, the geometry of the extensional forced folds and their associated fault patterns depend on the thickness and viscosity of the viscous layer, the thickness of the cover sequence, the strength and ductility of the cover sequence, the dip, the magnitude and the rate of displacement along the underlying master normal fault (Patton and Fletcher, 1995; Withjack et al., 1990; Withjack and Callaway, 2000). Furthermore, the fact that folds associated to the strain are asymmetrical, it is characteristic of forced folds mechanisms (Cosgrove and Ameen, 1999).

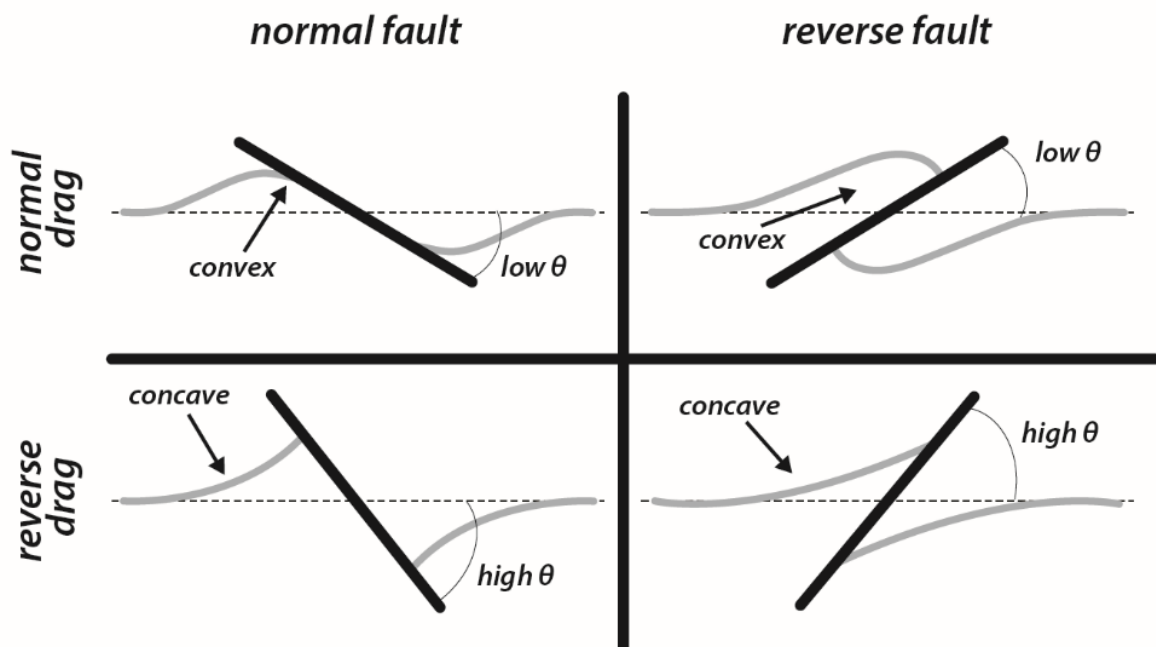


Figure IV-1: Fault drag of a central marker along normal and reverse (thrust) faults. Normal drag refers to markers that are convex in the direction of slip and reverse drag to markers that are concave in the direction of slip. The angle θ is the acute angle measured from the fault to

the undeformed central marker (anticlockwise angles are positive). The presented work demonstrates that low angles favor normal drag and high angles favor reverse drag modified from Grasemann et al., (2005).

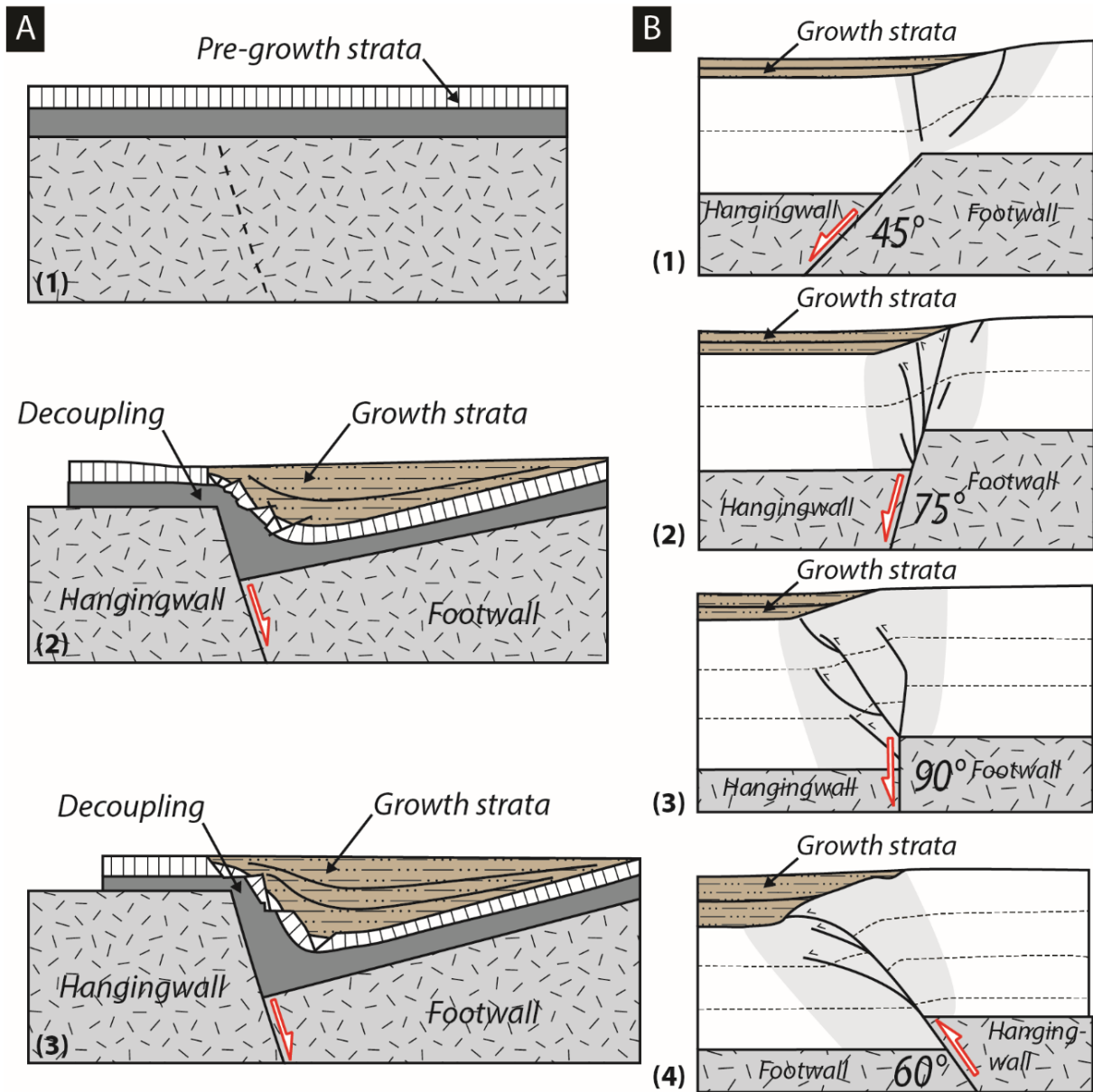


Figure IV-2: (A) Development of a syn-depositional syncline during extensional tectonics modified from Guiraud and Seguret, (1985). The syncline develops on a tilted basement block overlain by a competent-incompetent layer. (B) Fold and fault patterns associated with extensional/compressional forced folding modified from Patton and Fletcher, (1995) and Withjack et al., (1990). (1-2) normal, (3) vertical, and (4) reverse fault basement.

2.2 Inversion and reactivation structures

Many authors have studied influence (Figure IV-3), reactivation and inversion of pre-existing tectonic structures in different context (Bellahsen and Daniel, 2005; Bonini et al., 2012; Buchanan and McClay, 1991; Butler, 1989; Casas et al., 2001; Dooley and Schreurs, 2012; Soto et al., 2007; Ustaszewski et al., 2005; Viola et al., 2004). They mainly show that inherited structural features represent a key factor in controlling strain distribution and localization of deformation as long as a pre-existing fault remains mechanically weaker than its surroundings. Indeed, surfaces of pre-existing faults usually display lower cohesive strength and friction coefficient than intact rocks. They demonstrate that heterogeneities such as pre-existing faults should be included in models designed to understand the behavior and the tectonic evolution of sedimentary basins.

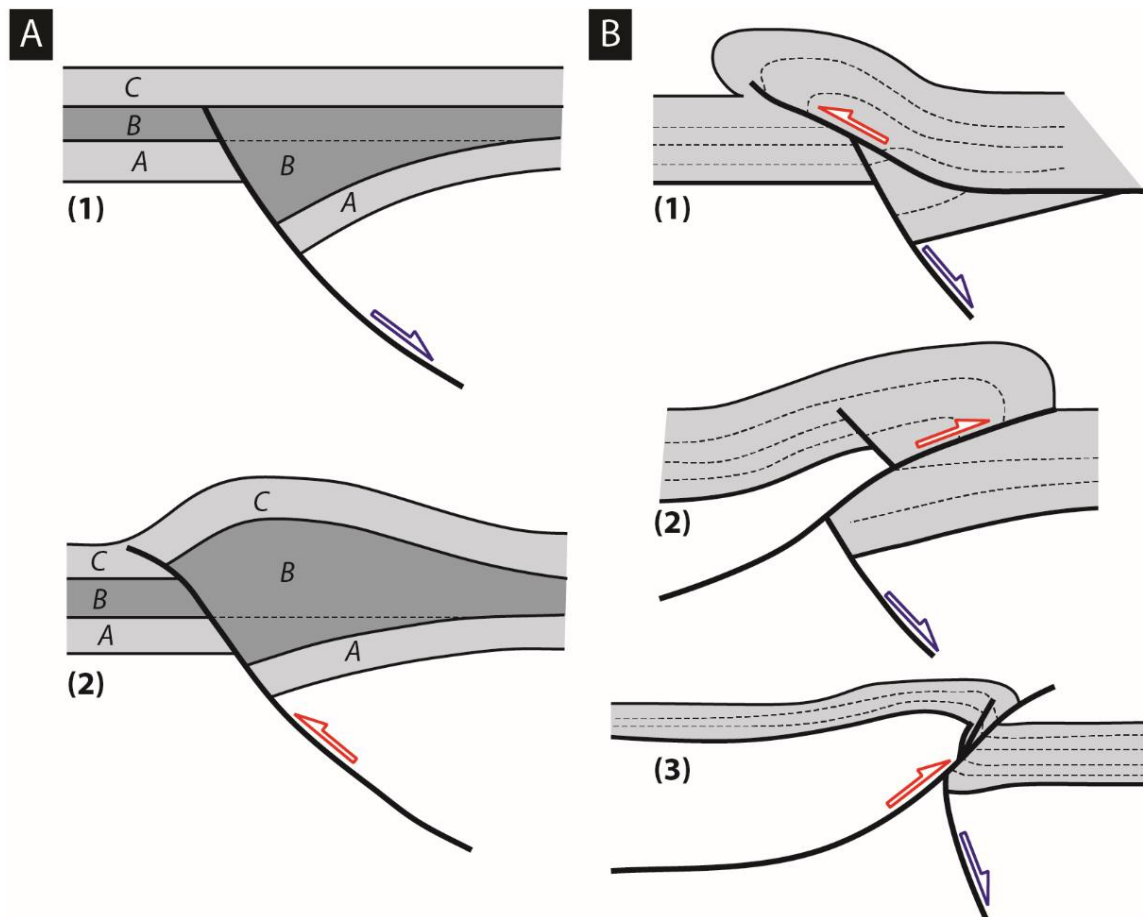


Figure IV-3: (A) Schematic diagram of a classical positive inversion structure; A, B and C are stratigraphic sequences. A, prerift; B, synrift; C, postrift sequence modified from Williams et al., (1989). (B) Deformation styles of shortened (inverted) normal fault systems: (1) normal

fault localizing thrust-ramp; (2-3) thrust ramp decapitating an early normal fault modified from Bonini et al., (2012).

To summarize, the behavior of faulted rock is determined by its geometric, kinematic, rheological, historical characteristics (inherited mechanical weakness) and its orientation relative to the new stress field. Besides, the dip of basement inherited structures have an direct influence on the geomorphology of the forced folds associated in surface (Johnson and Johnson, 2002; Patton and Fletcher, 1995; Withjack et al., 1990).

2.3 Syn-tectonic structures (growth strata)

The syn-sedimentary structuring of a basin results from sedimentation disturbances in the space and time. The signatures of these syn-sedimentary tectonic markers are: syn-sedimentary fault, progressive unconformities (growth structure), variations in thickness series and/or changes in facies and the distribution of current directions. They are records of tectonic activities. The term progressive unconformity was first defined by Briot (1937). It characterized by the provision of sediments in the vicinity range of an active fault (i.e. syn-sedimentary). Many examples of progressive unconformities (Figure IV-4), especially associated with folds or thrusting, have been described (Casas-Sainz et al., 2005; Riba, 1976; Suppe et al., 1992). Progressive unconformities frequently associated with intra-formational angular unconformity result in significant lateral variation thickness.

Growth or syntectonic strata (Figure IV-4) are stratigraphic intervals that were deposited during deformation (Shaw et al., 2005). The timing of deformations is thus determined by the ages of the growth strata (Shaw et al., 2005). The geometries of growth structures (i.e. growth fold patterns) are controlled principally by the folding mechanism and the relative rates of sedimentation and uplift (Shaw et al., 2005).

Syn-sedimentary fault-related folding has been documented in the Gulf of Suez (Khalil and McClay, 2002; Lewis et al., 2015), in the North Sea (Kane et al., 2010; Lewis et al., 2013) and from analogue models (Withjack et al., 1990) or numerical trishear model (Jin and Groshong, 2006). In fault-related folds, growth strata are typically thin across fold limbs toward structural highs (Shaw et al., 2005).

Sedimentation rate in a basin depends on the space available (i.e. accommodation) and weathering/erosion mechanism (i.e. climate conditions). It is controlled by the base level variation (i.e. the lowest level to which a land surface can be eroded by streams, which is,

ultimately, sea level or a level where they can be deposition). This variation is governed by internal forcing (tectonic) and external forcing (glacio-eustatic). It implies that during a period of strong tectonic there is a lot of accommodation for sedimentation. Reflectors structures such as onlaps, toplaps, truncation or offlaps can be evidence of these activities.

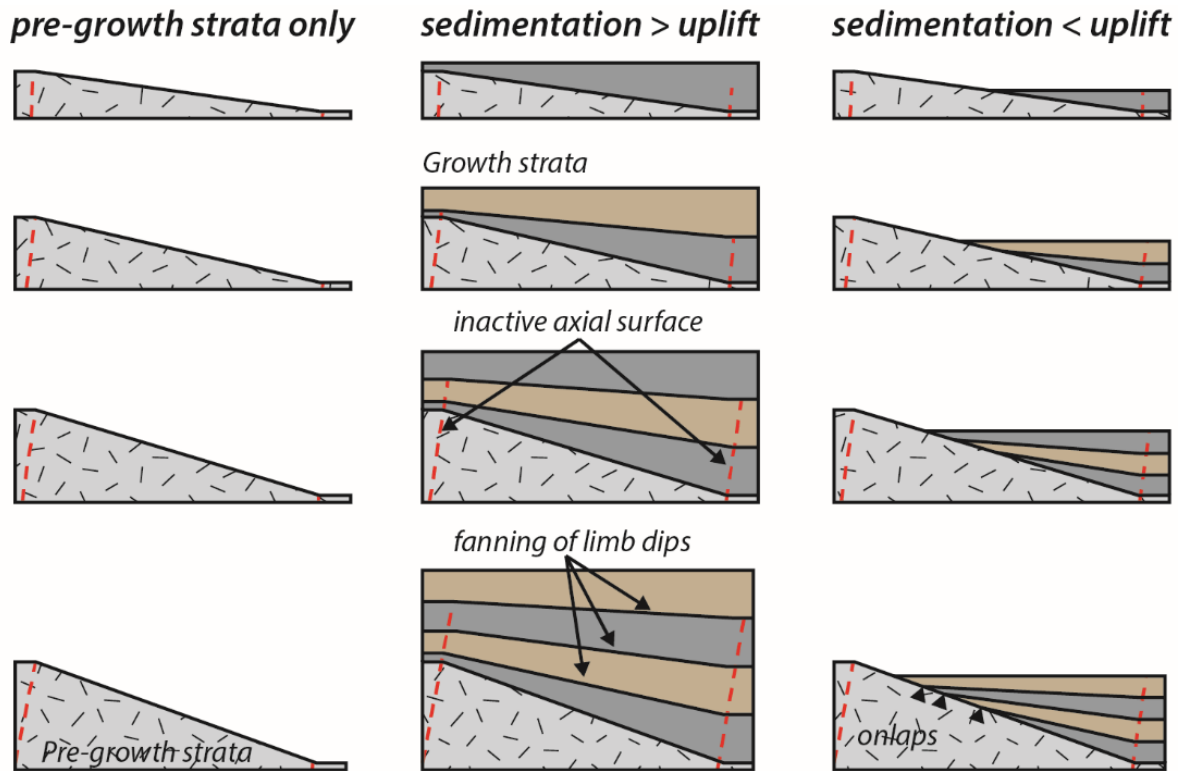


Figure IV-4: Growth strata as records of fold kinematics (folding by progressive limb rotation) modified from Shaw et al., (2005).

3 Published article in Solid Earth

Abstract (Français)

La plateforme intracratonique paléozoïque nord-africaine est caractérisée par une association d'arches (rides, dômes, ou paléo-hauts structuraux) et de bassins synclinaux à faible taux de subsidence de différentes longueurs d'onde (75 à 620 km). Les bassins de Reggane, d'Ahnet, de Mouydir et d'Illizi sont délimités successivement d'est en ouest par les arches d'Amguid El Biod, d'Arak-Foum Belrem et d'Azzel Matti.

Grâce à l'analyse de nouvelles données géologiques non publiées (images satellitaires, diagraphies de puits, lignes sismiques), on peut voir que les dépôts associés à ces arches et bassins synclinaux présentent des variations d'épaisseur et des modifications de faciès allant

des environnements continentaux aux environnements marins. Les arches sont caractérisées par de minces dépôts avec des surfaces érosionnelles amalgamées et condensées, tandis que les bassins synclinaux présentent des successions plus épaisses et bien conservées. De plus, la succession de faciès verticaux évolue de dépôts minces du Silurien au Givétien en sédiments épais au Dévonien supérieur.

Les structures synsédimentaires et les discordances majeures sont liées à plusieurs événements tectoniques, tels que l'extension cambro-ordovicienne, le rebond glaciaire ordo-silurien, l'extension/compression «Calédonienne» siluro-dévonienne, la compression/extension «tardi-dévonienne» et la compression «Hercynienne».

Localement, la déformation est caractérisée par des failles normales planes presque verticales responsables de la structuration en horst et graben associée en surface au plissement au cours de la période cambrienne-ordovicienne-silurienne. Ces structures peuvent avoir été inversées ou réactivées lors de la compression dévonienne (i.e. calédonienne, du dévonien moyen à tardif) et du carbonifère (i.e. pré-hercynien à l'hercynien).

La caractérisation du socle à partir de données géologiques et géophysiques (cartes aéromagnétiques et gravimétriques) montre une zonation structurale des arches et bassins en fonction de l'âge des terranes délimitées par des méga zones de cisaillement. Les "anciennes" terranes (Archéennes et Paléoprotérozoïques) sont situées sous les arches tandis que les "jeunes" terranes (Néo-Mésoprotérozoïques) sont situées sous les dépôcentres des bassins. Ce cadre structural résulte de l'accrétion de terranes archéennes et protérozoïques hérités d'orogénèses précédentes (e.g. l'orogénèse panafricaine 900-520 Ma). Ainsi, le modèle de remplissage sédimentaire paléozoïque et la nature de la déformation résultent de la réactivation lente et répétée des terranes précambriennes liés par des systèmes de failles lithosphériques sub-verticales. Les périodes d'alternance entre quiescence tectonique et accélération de la faible subsidence en association avec la tectonique d'extension et d'inversion locale apparaissent synchrones d'événements géodynamiques paléozoïques (e.g. orogénèses lointaines, glaciation...).

Mots-clés: Bassin intracratonique, paléozoïque, arches, faible taux de subsidence, héritage tectonique, terranes, Sahara central.

Les principaux résultats de l'article :

Les analyses multi-échelles et multidisciplinaires effectuées dans cette étude nous permettent d'établir un modèle des bassins intracratoniques Paléozoïque du Sahara Central couplant l'architecture de bassin et les structures du socle. Bien que nous ne fournissions pas d'explication quantitative de la dynamique de ces bassins, notre synthèse souligne que leur mécanisme de subsidence n'est pas le résultat d'un processus unique. Nous essayons de faire ici une liste des propriétés indispensables à la formation de ces bassins tels que :

- L'association de grands bassins synclinaux et d'arches avoisinantes (i.e. paléo-reliefs). Le cadre structural montre une association étroite des bassins synclinaux, des arches inter-bassins principales à secondaires et d'arches secondaires intra-bassins ;
- Par une architecture de horst et graben constituée par des failles normales sub-verticales planes associées à des structures de plis forcés. Localement, cette tectonique d'extension est perturbée par des structures d'inversion positive ou des failles normales transportées ;
- Un faible taux de subsidence compris entre 5 et 50 m.Ma⁻¹ ;
- Les longues périodes d'extension et de quiescence tectonique sont interrompues par de brèves périodes de compression ou de glaciation/déglaciation (Beuf et al., 1971; Denis et al., 2007; Le Heron et al., 2006). Ces périodes de compression peuvent être liées à des compressions intraplaques corrélées à des orogénèses lointaines tels que les événements calédonien et Hercynien (Frizon de Lamotte et al., 2013) ou à un soulèvement intraplaque des arches due au magmatisme (Derder et al., 2016; Fabre, 2005; Frizon de Lamotte et al., 2013; Moreau et al., 1994) ;
- Des onlaps divergents synsédimentaires et discordances locales sont identifiés à partir des données sismiques, des images satellites et des données de puits. Les périodes d'activités tectoniques sont caractérisées par une réactivation normale à inverse des failles bordières, la mise en place de prismes d'accrétions sédimentaires et de discordances au voisinage des arches ;
- L'architecture stratigraphique présente une variation latérale de faciès et un partitionnement des faciès entre les faciès marins distaux remplissant les centres des bassins intracratoniques (i.e. dépôts marin offshore) et les faciès amalgamés proximaux (i.e. fluvio-marin, littoral) associées à des hiatus stratigraphiques importants et à des discordances érosionnelles à proximité des arches ;

- Un lien étroit est mis en évidence entre la période de déformation tectonique et la présence de discordances. En revanche, les périodes de quiescences et d'extensions tectoniques sont caractérisées par de faibles variations latérales des faciès, des dépôts épais et l'absence de surfaces d'érosion ;
- L'héritage précambrien correspond aux terranes Archéennes à Paléoprotérozoïque identifiées dans le massif du Hoggar et réactivées au cours du cycle panafricain Méso-Néoprotérozoïque. L'hétérogénéité lithosphérique précambrienne illustrée par les différentes caractéristiques des terranes précambriennes (longueur d'onde, âge, nature, zones de faille) contrôle spatialement la mise en place des bassins synclinaux intracratoniques reposant sur les terranes océaniques Méso-Néoprotérozoïque et les arches situées sous les terranes continentales Archéen à Paléoprotérozoïque. De nombreux auteurs suggèrent que le contrôle de la fabrique du socle est hérité de l'orogénèse panafricaine dans les bassins sahariens (Beuf et al., 1968b, 1971; Boote et al., 1998; Carruba et al., 2014; Coward and Ries, 2003; Eschard et al., 2010; Guiraud et al., 2005; Sharata et al., 2015).

Solid Earth, 9, 1239–1275, 2018
<https://doi.org/10.5194/se-9-1239-2018>
 © Author(s) 2018. This work is distributed under
 the Creative Commons Attribution 4.0 License.



Influence of basement heterogeneity on the architecture of low subsidence rate Paleozoic intracratonic basins (Reggane, Ahnet, Mouydir and Illizi basins, Hoggar Massif)

Paul Perron¹, Michel Guiraud¹, Emmanuelle Vennin¹, Isabelle Moretti², Éric Portier³, Laetitia Le Pourhiet⁴, and Moussa Konaté⁵

¹Université de Bourgogne Franche-Comté, Centre des Sciences de la Terre, UMR CNRS 6282 Biogéosciences, 6 Bd Gabriel, 21000 Dijon, France

²ENGIE SA, 1, place Samuel de Champlain, Faubourg de l'Arche, 92930 Paris La Défense, France

³Neptune Energy International S.A., 9-11 Allée de l'Arche – Tour EGEE – 92400 Courbevoie, France

⁴Sorbonne Université, CNRS-INSU, Institut des Sciences de la Terre Paris, ISTeP UMR 7193, 75005 Paris, France

⁵Département de Géologie, Université Abdou Moumouni de Niamey, BP:10662, Niamey, Niger

Correspondence: Paul Perron (paul.perron@u-bourgogne.fr, paul.perron@hotmail.fr)

Received: 30 May 2018 – Discussion started: 27 June 2018

Revised: 28 September 2018 – Accepted: 4 October 2018 – Published: 7 November 2018

Abstract. The Paleozoic intracratonic North African Platform is characterized by an association of arches (ridges, domes, swells, or paleo-highs) and low subsidence rate syncline basins of different wavelengths (75–620 km). The Reggane, Ahnet, Mouydir and Illizi basins are successively delimited from east to west by the Amguid El Biod, Arak-Foum Belrem, and Azzel Matti arches. Through the analysis of new unpublished geological data (i.e., satellite images, well logs, seismic lines), the deposits associated with these arches and syncline basins exhibit thickness variations and facies changes ranging from continental to marine environments. The arches are characterized by thin amalgamated deposits with condensed and erosional surfaces, whereas the syncline basins exhibit thicker and well-preserved successions. In addition, the vertical facies succession evolves from thin Silurian to Givetian deposits into thick Upper Devonian sediments. Synsedimentary structures and major unconformities are related to several tectonic events such as the Cambrian–Ordovician extension, the Ordovician–Silurian glacial rebound, the Silurian–Devonian “Caledonian” extension/compression, the late Devonian extension/compression, and the “Hercynian” compression. Locally, deformation is characterized by near-vertical planar normal faults responsible for horst and graben structuring associated with folding during the Cambrian–Ordovician–

Silurian period. These structures may have been inverted or reactivated during the Devonian (i.e., Caledonian, Mid–Late Devonian) compression and the Carboniferous (i.e., pre-Hercynian to Hercynian). Additionally, basement characterization from geological and geophysics data (aeromagnetic and gravity maps), shows an interesting age-dependent zonation of the terranes which are bounded by mega-shear zones within the arches–basins framework. The “old” terranes are situated under arches while the “young” terranes are located under the basins depocenter. This structural framework results from the accretion of Archean and Proterozoic terranes inherited from former orogeny (e.g., Pan-African orogeny 900–520 Ma). Therefore, the sedimentary infilling pattern and the nature of deformation result from the repeated slow Paleozoic reactivation of Precambrian terranes bounded by subvertical lithospheric fault systems. Alternating periods of tectonic quiescence and low-rate subsidence acceleration associated with extension and local inversion tectonics correspond to a succession of Paleozoic geodynamic events (i.e., far-field orogenic belt, glaciation).

Published by Copernicus Publications on behalf of the European Geosciences Union.

1 Introduction

Paleozoic deposits fill numerous intracratonic basins, which may also be referred to as “cratonic basins”, “interior cratonic basins”, or “intracontinental sags”. Intracratonic basins are widespread around the world (Heine et al., 2008) and exploration for nonconventional petroleum has revived interest in them. They are located in “stable” lithospheric areas and share several common features (Allen and Armitage, 2011). Their geometries are large circular, elliptical, and/or saucer-shaped to oval. Their stratigraphy is filled with continental to shallow-water sediments. Their subsidence rate is low (5 to 50 m Ma⁻¹) and long (sometimes more than 540 Myr). Their structural framework shows the reactivation of structures and emergence of arches also referred to in the literature as “ridges”, “paleo-highs”, “domes”, and “swells”. Multiple hypotheses and models have been proposed to explain how these slowly subsiding, long-lived intracratonic basins formed and evolved (see Allen and Armitage, 2011 and references therein or Hartley and Allen, 1994). However, their tectonic and sedimentary architectures are often poorly constrained.

The main specificities of intracratonic basins are found on the Paleozoic North Saharan Platform. The sedimentary infilling during ca. 250 Myr is relatively thin (i.e., around a few hundred to a few thousand meters), of great lateral extent (i.e., 9 million km²), and is separated by major regional unconformities (Beuf et al., 1968a, 1971; Carr, 2002; Eschard et al., 2005, 2010; Fabre, 1988, 2005; Fekirine and Abdallah, 1998; Guiraud et al., 2005; Kracha, 2011; Legrand, 2003a). Depositional environments were mainly continental to shallow-marine and homogeneous. Very slow and subtle lateral variations occurred over time (Beuf et al., 1971; Carr, 2002; Fabre, 1988; Guiraud et al., 2005; Legrand, 2003a). The Paleozoic North Saharan Platform is arranged (Fig. 1) into an association of long-lived broad synclines (i.e., basins or subbasins) and anticlines (i.e., arches) of different wavelengths (λ : 75–620 km). Burov and Cloetingh (2009) report deformation wavelengths of the order of 200–600 km when the whole lithosphere is involved and of 50–100 km when the crust is decoupled from the lithospheric mantle. This insight suggests that the inherited basement fabric influences intracratonic basin architecture at a large scale. In addition, pre-existing structures, such as shear zones and terrane suture zones, are present throughout the lithosphere, affecting the geometry and evolution of upper-crustal structural framework forming during later tectonic events (Peace et al., 2018; Phillips et al., 2018).

In this study of the Reggane, Ahnet, Mouydir, and Illizi basins, a multidisciplinary workflow involving various tools (e.g., seismic profiles, satellite images) and techniques (e.g., photogeology, seismic interpretation, well correlation, geophysics, geochronology) has enabled us to (1) make a tectono-sedimentary analysis, (2) determine the spatial arrangement of depositional environments calibrated by bio-

stratigraphic zonation, (3) characterize basin geometry, and (4) ascertain the inherited architecture of the basement and its tectonic evolution. We propose a conceptual coupled model explaining the architecture of the intracratonic basins of the North Saharan Platform. This model highlights the role of basement heritage heterogeneities in an accreted mobile belt and their influence on the structure and evolution of intracratonic basins. It is a first step towards a better understanding of the factors and mechanisms that drive intracratonic basins.

2 Geological setting: the Paleozoic North Saharan Platform and the Reggane, Ahnet, Mouydir, and Illizi basins

The Reggane, Ahnet, Mouydir and Illizi basins (Figs. 1 and 2) are located in southwestern Algeria, north of the Hoggar Massif (Ahaggar). They are depressions filled by Paleozoic deposits. The basins are bounded to the south by the Hoggar Massif (Tuareg Shield) and they are separated one another by the Azzel Matti, the Arak-Foum Belrem, and the Amguid El Biod arches.

Figure 3 synthesizes the lithostratigraphy, the large-scale sequence stratigraphic framework delimited by six main regional unconformities (A to F), and the tectonic events proposed in the literature (cf. references under Fig. 3) affecting the Paleozoic North Saharan Platform.

During the Paleozoic, the Reggane, Ahnet, Mouydir and Illizi basins were part of a set of the supercontinent Gondwana (Fig. 1). This supercontinent resulted from the collision of the West African Craton (WAC) and the East Saharan Craton (ESC), which sandwiched the Tuareg Shield (TS) mobile belt during the Pan-African orogeny (Craig et al., 2008; Guiraud et al., 2005; Trompette, 2000). This orogenic cycle followed by the chain’s collapse (ca. 1000–525 Ma) was also marked by phases of oceanization and continentalization (ca. 900–600 Ma) giving rise to the heterogeneous terranes in the accreted mobile belt (Trompette, 2000). The Hoggar Massif is composed of several accreted, sutured, and amalgamated terranes of various ages and compositions resulting from multiple phases of geodynamic events (Bertrand and Caby, 1978; Black et al., 1994; Caby, 2003; Liégeois et al., 2003). Twenty-three well preserved terranes were identified in the Hoggar Massif and grouped into Archean, Paleoproterozoic, and Mesoproterozoic–Neoproterozoic juvenile Pan-African terranes (see legend in Fig. 1). In the West African Craton, the Reguibat Shield is composed of Archean terrains in the west and of Paleoproterozoic terranes in the east (Peucat et al., 2003, 2005).

Then, there is evidence of a complex and polyphased history throughout the Paleozoic (Fig. 3), with alternating periods of quiescence and tectonic activity, individualizing and rejuvenating ancient N–S, NE–SW, or NW–SE structures in arch and basin configurations (Badalini et al., 2002; Boote et al., 1998; Boudjema, 1987; Coward and Ries, 2003; Craig

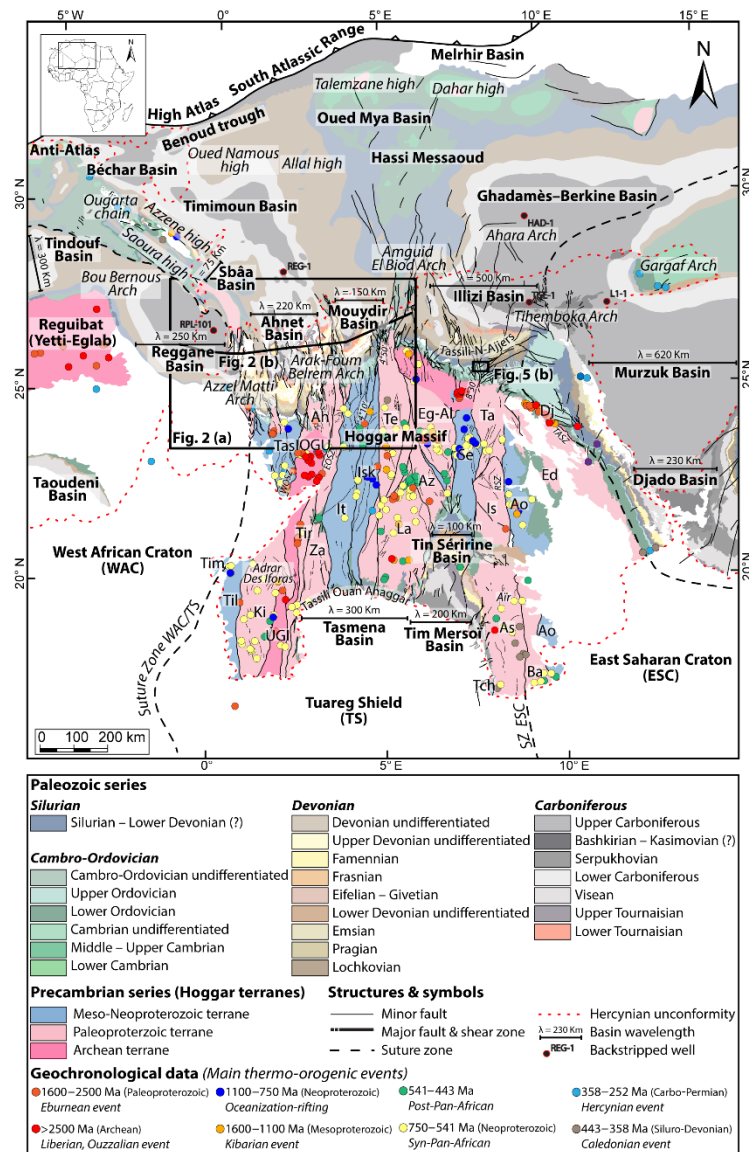


Figure 1. Geological map of the Paleozoic North Saharan Platform (North Gondwana) georeferenced, compiled and modified from (1) a Paleozoic subcrop distribution below the Hercynian unconformity geology of the Saharan Platform (Boote et al., 1998; Galeazzi et al., 2010), (2) a geological map (1/500 000) of the Djado Basin (Jacquemont et al., 1959), (3) a geological map (1/200 000) of Algeria (Bennacef et al., 1974; Bensalah et al., 1971), (4) a geological map (1/50 000) of Air (Jouliat, 1963), (5) a geological map (1/2 000 000) of Niger (Greigert and Pougnet, 1965), (6) a geological map (1/5 000 000) of the Lower Paleozoic of the central Sahara (Beuf et al., 1971), (7) a geological map (1/1 000 000) of Morocco (Hollard et al., 1985), (8) a geological map of the Djebel Fezzan (Massa, 1988), and (9) a basement characterization of the different terranes from geochronological data compilation (see Supplement) and geological maps (Berger et al., 2014; Bertrand and Caby, 1978; Black et al., 1994; Caby, 2003; Fezaa et al., 2010; Liégeois et al., 1994, 2003, 2005, 2013). Terrane names and abbreviations: Tassendjanet (Tas), Tassendjanet nappe (Tas n.), Ahnet (Ah), In Ouzzal Granulitic Unit (IOGU), Iforas Granulitic Unit (UGI), Kidal (Ki), Timétrine (Tim), Tilemsi (Til), Tirek (Tir), In Zaoutane (Za), In Teidini (It), Iskel (Isk), Tefedest (Te), Laoui (La), Azrou-n-Fad (Az), Egéré-Aleskod (Eg-Al), Serouenout (Se), Tazat (Ta), Issalane (Is), Assodé (As), Barghot (Ba), Tchilit (Tch), Aouzegueur (Ao), Edembo (Ed), and Djanet (Dj). Shear zone and lineament names and abbreviations: suture zone East Saharan Craton (SZ ESC), west Ouzzal shear zone (WOSZ), east Ouzzal shear zone (EOSZ), Raghane shear zone (RSZ), Tin Amali shear zone (TASZ), 4° 10' shear zone, 4° 50' shear zone, and 8° 30' shear zone.

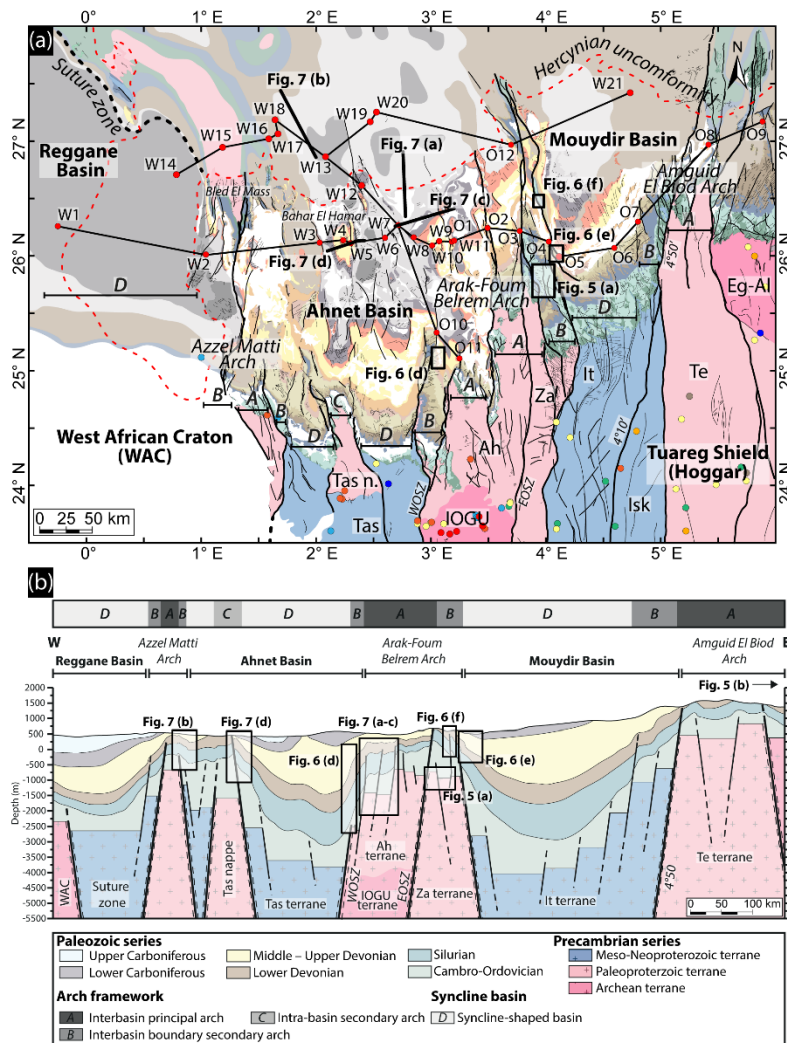


Figure 2. (a) Geological map of the Paleozoic of the Reggane, Ahnet, and Mouydir basins. For the legend and references see Fig. 1. (b) An E–W cross section of the Reggane, Ahnet, and Mouydir basins associated with the different terranes and highlighting the classification of the different structural units. Localization of the interpreted sections (seismic profiles and satellite images). W represents well and O represents outcrop. See Fig. 1 for location of the geological map A and cross section B.

et al., 2008; Guiraud et al., 2005; Logan and Duddy, 1998; Lüning, 2005). The Paleozoic successions of the North Saharan Platform are predominantly composed of siliciclastic detrital sediments (Beuf et al., 1971; Eschard et al., 2005). They form the largest area of detrital sediments ever found on continental crust (Burke et al., 2003), dipping gently NNW (Beuf et al., 1971, 1969; Fabre, 1988, 2005; Fröhlich et al., 2010; Gariel et al., 1968; Le Heron et al., 2009). Carbonate deposits are observed from the Middle–Late Devonian to the Carboniferous (Wendt, 1985, 1988, 1995; Wendt et al., 1993, 1997, 2006, 2009a; Wendt and Kaufmann, 1998). From south

to north, the facies progressively evolve from continental fluvial to shallow marine (i.e., upper to lower shoreface) and then to offshore facies (Beuf et al., 1971; Carr, 2002; Eschard et al., 2005; Fabre, 1988; Fekirine and Abdallah, 1998; Legrand, 1967a).

3 Data and methods

A multidisciplinary approach was used in this study integrating new data (i.e., satellite images, seismic lines and well-

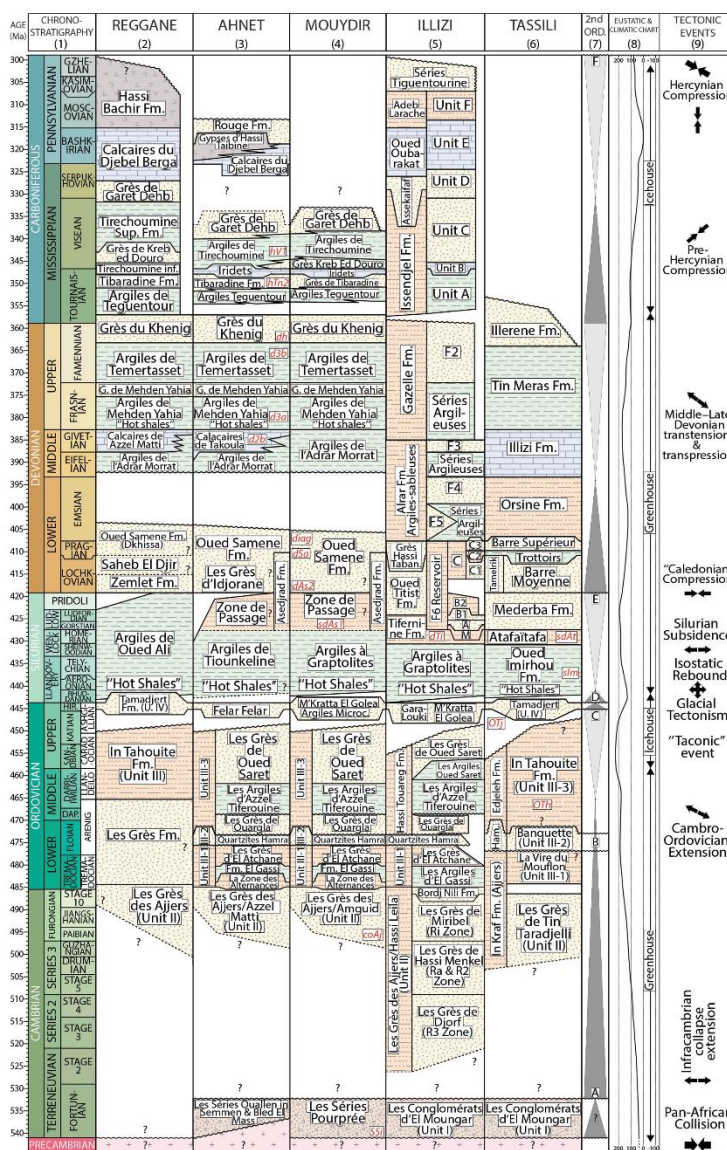


Figure 3. Paleozoic litho-stratigraphic, sequence stratigraphy, and tectonic framework of the north peri-Hoggar basins (North African Saharan Platform) compiled from (1) a chronostratigraphic chart (Ogg et al., 2016), (2) the Cambrian–Silurian (Askri et al., 1995) and the Devonian–Carboniferous stratigraphy of the Reggane Basin (Cózar et al., 2016; Lubeseder, 2005; Lubeseder et al., 2010; Magloire, 1967; Wendt et al., 2006), (3) the Cambrian–Silurian (Paris, 1990; Wendt et al., 2006) and the Devonian–Carboniferous stratigraphy of the Ahnet Basin (Beuf et al., 1971; Conrad, 1973, 1984; Legrand-Blain, 1985; Wendt et al., 2006, 2009a), (4) the Cambrian–Silurian (Askri et al., 1995; Paris, 1990; Videt et al., 2010) and the Devonian–Carboniferous stratigraphy of the Mouydir Basin (Askri et al., 1995; Beuf et al., 1971; Conrad, 1973, 1984; Wendt et al., 2006, 2009a), (5) the Cambrian–Silurian (Eschard et al., 2005; Fekirine and Abdallah, 1998; Jardiné and Yapaudjian, 1968; Videt et al., 2010) and the Devonian–Carboniferous stratigraphy of the Illizi Basin (Eschard et al., 2005; Fekirine and Abdallah, 1998; Jardiné and Yapaudjian, 1968), (6) the Cambrian–Silurian (Dubois, 1961; Dubois and Mazelet, 1964; Eschard et al., 2005; Henniche, 2002; Videt et al., 2010) and the Devonian–Carboniferous stratigraphy of the Tassili-N-Ajjers (Dubois et al., 1967; Eschard et al., 2005; Henniche, 2002; Wendt et al., 2009a), (7) the sequence stratigraphy of the Saharan Platform (Carr, 2002; Eschard et al., 2005; Fekirine and Abdallah, 1998), (8) a eustatic and climatic chart (Haq and Schutter, 2008; Scotese et al., 1999), and (9) tectonic events (Boudjema, 1987; Coward and Ries, 2003; Craig et al., 2008; Guiraud et al., 2005; Lüning, 2005). (A) Infra-Tassilian (Pan-African) unconformity, (B) intra-Arenig unconformity, (C) Taconic and glacial unconformity, (D) isostatic rebound unconformity, (E) Caledonian unconformity, and (F) Hercynian unconformity.

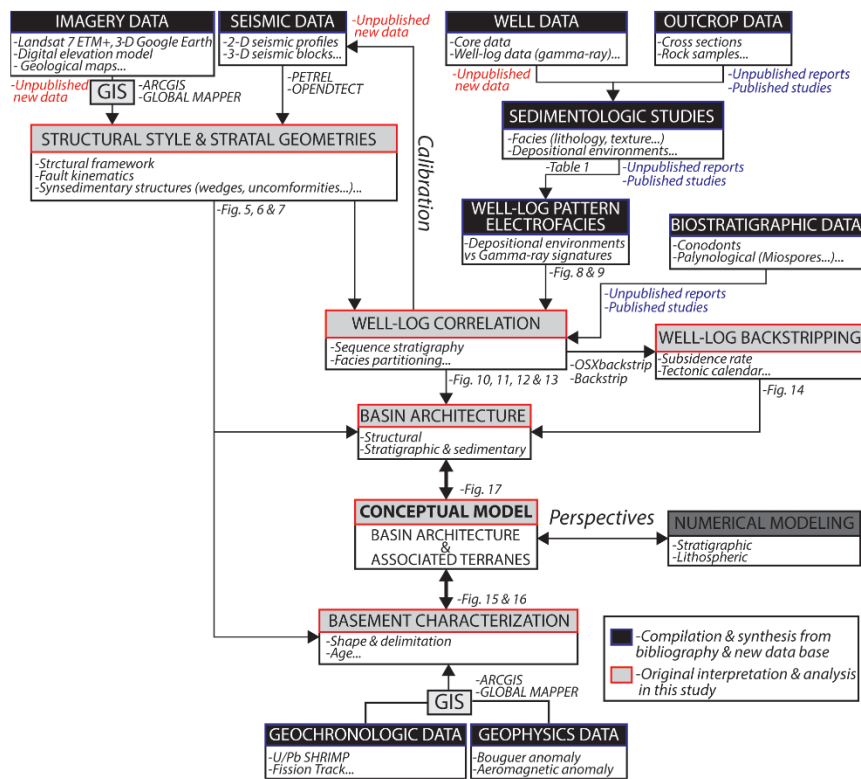


Figure 4. Schematic synthesis of the integrated method of basin analysis in this study.

logs data) in particular from the Reggane, Ahnet, Mouydir, and Illizi basins and the Hoggar Massif (Fig. 4).

The Paleozoic series of the Ahnet and Mouydir basins are well-exposed over an area of approximately 170 000 km² and are well observed in satellite images (Google Earth and Landsat from USGS). Furthermore, a significant geological database (i.e., wells, seismic records, geological reports) has been compiled in the course of petroleum exploration since the 1950s. The sedimentological dataset is based on the integration and analysis of cores, outcrops, well logs, and of lithological and biostratigraphic data. They were synthesized from internal SONATRACH (Dokka, 1999), IFP-SONATRACH consortium reports (Eschard et al., 1999), and published articles (Beuf et al., 1971; Biju-Duval et al., 1968; Wendt et al., 2006). Facies described from cores and outcrops of these studies were grouped into facies associations corresponding to the main depositional environments observed on the Saharan Platform (Table 1). Characteristic gamma-ray (GR) patterns (electrofacies) are proposed to illustrate the different facies associations. The gamma-ray peaks are commonly interpreted as the maximum flooding surfaces (MFS) (e.g., Catuneanu et al., 2009; Galloway, 1989; Milton et al., 1990; Serra and Serra, 2003). Time calibration

of well logs is based on palynomorphs (essentially Chitinozoans and spores) and outcrops on conodonts, goniatites, and brachiopods (Wendt et al., 2006). Palynological data of wells (W1, W7, W12, W19 and W20) from internal unpublished data (Abdesselam-Roughi, 1991; Azzoune, 1999; Hassan, 1984; Khier, 1974) are based on biozonations from Magloire (1967) and Boumendjel et al. (1988). Well W18 is supported by palynological data and biozonations from Kermandji et al. (2008).

Synsedimentary extensional and compressional markers are characterized in this structural framework based on the analyses of satellite images (Figs. 5 and 6), seismic profiles (Fig. 7), 21 wells (W1 to W21), and 12 outcrop cross sections (O1 to O12). Wells and outcrop sections are arranged into three E–W sections (Figs. 10, 11 and 12) and one N–S section (Fig. 13). Satellite images (Figs. 5 and 6) and seismic profiles (Fig. 7) are located at key areas (i.e., near arches) illustrating the relevant structures (Fig. 2). The calibration of the key stratigraphic horizon on seismic profiles (Fig. 7) was settled by sonic well-log data using Petrel and OpendTect software. Nine key horizons easily extendable at the regional scale are identified and essentially correspond to major depositional unconformities: near top

Table 1. Synthesis of facies associations (AF1 to AF5), depositional environments, and electrofacies in the Devonian series compiled from internal (Eschard et al., 1999) and published studies (Beuf et al., 1971; Biju-Duval et al., 1968; Wendt et al., 2006).

Facies associations	Criteria & characteristics			Formations	Depositional environments
	Textures/lithology	Sedimentary structures	Biotic/non-biotic grains		
AF1	Conglomerates, mid to coarse sandstones, siltstones, shales	Trough cross-bedding, mud clasts, lag deposits, flutinal and overturn structures, imbricated grains, lenticular laminations, oblique stratification	Rare oolitic intercalations, imbricated pebbles, sandstones, ironstones, phosphorites, corroded quartz grains, calcareous matrix, brachiopod coquinas, phosphatized pebbles, hematite, azurite, quartz	Oued Samene Fm., Barre Supérieur, Barre Moyenne	Fluvial Continental (fluvial)
AF2	Silt to argillaceous fine sandstone	Current ripples, climbing ripples, crevasse splay, root traces, paleosols, plant debris	Nodules, ferruginous horizon	Oued Samene Fm., Barre Supérieur, Barre Moyenne	Flood plain
AF3a	Fine to coarse sandstones, argillaceous siltstones, shales (heterolithic)	Trough cross-bedding, some planar bedding, flaser bedding, mud clasts, mud drapes, root trace, desiccation cracks, water escape, wavy bedding, shale pebble, sigmoidal cross-bedding	Brachiopods, trilobites, tentaculites, graptolites	Oued Samene Fm., Grès du Khenig, Barre Supérieur, Barre Moyenne	Delta/estuarine channels Coastal Plain (transitional marine/continental)
AF3b	Very coarse-grained poorly sorted sandstone	Trough cross-bedding, sigmoidal cross-bedding, abundant mud clasts and mud drapes	Increasing upward bioturbation <i>Skolithos</i> (SK)	Oued Samene Fm., Grès du Khenig, Barre Supérieur, Barre Moyenne	Fluvial/tidal distributary channels
AF3c	Fine-grained to very coarse-grained heterolithic sandstone	Sigmoidal cross-bedding with multidirectional tidal bundles, wavy, lenticular, flaser bedding, occasional current and oscillation ripples, occasional mud cracks	Intense bioturbation, <i>Skolithos</i> (SK), <i>Planolites</i> , (PI), <i>Thalassinoides</i> (Th)	Talus à Trigillites	Tidal sand flat
AF3d	Mudstones, varicolored shales, thin sandstone layers	Occasional wave ripples, mud cracks, horizontal lamination, rare multidirectional ripples	Absence of ammonoids, goniatites, calymenoids, pelecypod molds, brachiopods coquinas	Oued Samene Fm., Grès du Khenig, Atafatafa Fm.	Lagoon/rundflat
AF4a	Silty mudstone associated with coarse to very coarse argillaceous sandstone, poorly sorted, heterolithic silty mudstone	Sigmoidal cross-bedding, abundant mud clasts, wavy, lenticular cross-bedding and flaser bedding, abundant current and oscillation ripples, mud drapes	Shell debris (crinoids, brachiopods)	Oued Samene Fm., Talus à Trigillites	Subtidal Shoreface
AF4b	Fine- to mid-grained sandstones interbedded with argillaceous siltstone and mudstone, bioclastic carbonates sandstones, brownish sandstones and clays, silts	Oscillation ripples, swaley cross-bedding, bidirectional bedding, flaser bedding, rare hummocky cross-bedding, mud cracks (syneresis), convolute bedding, wavy bedding, combined flow ripples, planar cross low angle stratification, cross-bedding, ripple marks, centimetric bedding, shale pebbles	Ooids, crinoids, bryozoans, conal clasts, fossil debris, stromatopores, tabulates, colonial mose corals, myriad pelagic stylonids, neritic tentaculitids, brachiopods, iron ooliths, abundant micas	Atafatafa Fm., Zone de passage, Grès de Mehden Yahia, Calcaires d'Azzel Matti	Open marine-upper shoreface

Table 1. Continued.

Facies associations	Textures/lithology	Criteria & characteristics			Formations	Depositional environments
		Sedimentary structures	Biotic/non-biotic grains	Ichnofacies		
AF4c	Silty shales to fine sandstones (heterolithic)	Hummocky cross-bedding, planar bedding, combined flow ripples, convolute bedding, dish structures, mud drapes, remnant ripples, flat lenses, slumping	Intense bioturbation, <i>Cruziana</i>	<i>Thalassinoides</i> (Th), <i>Planolites</i> (Pl), <i>Skolithos</i> (Sk), <i>Diplocraterion</i> (Dip), <i>Teichichnus</i> (Te), <i>Chondrites</i> (Ch), <i>Roggenella</i> (Ro), <i>Climacichnites</i> (Cl)	Atakataka Fm., Zone de passage, Grès de Méhden Yaha, Calcaires d'Azze! Matu	Lower shoreface
AF5a	Grey silty-shales, bundles of skeletal wackestones, silty greenish shale interlayers fine grained sandstones, calcareous mudstones, black shales, polychrome clays (black, brown, grey, green, red, pink), grey and reddish shales	Lenticular sandstones, rare hummocky cross-bedding, mud mounds, mud buildups, low-angle cross-bedding, tempestite bedding, slumping, deep groove marks	Intensive burrowing, bivalve debris, horizontal burrows, skeletal remains (goniatites, orthoconic, nautiloids, siphonolites, trilobites, crinoids, solitary rugose, corals). Limestones nodules, ironstone nodules and layers	<i>Zoophycos</i> (Z), <i>Teichichnus</i> (Te), <i>Planolites</i> (Pl)	Argiles à Graptolites, Orsine Fm., Argiles de Méhden Yaha, Argiles de Temtrasset	Upper offshore Offshore
AF5b	Black silty-shales (mudstones), bituminous mudstones-wackestones, packstones	Rare structures	Parallel-aligned siphonolites, goniatites, orthoconic nautiloids, pelagic pelicypod <i>Bachia</i> , anoxic conditions. Limestone nodules, goniatites, <i>Bachia</i> , <i>temaculinitis</i> , ostracods and rare fish remains, <i>Tornoceras</i> , <i>Aulacoceras</i> , <i>Lobococeras</i> , <i>Mantoceras</i> , <i>Costamantoceras</i> and <i>Virginoeras</i> , graptolites	<i>Zoophycos</i> (Z)	Argiles à Graptolites, Orsine Fm., Argiles de Méhden Yaha, Argiles de Temtrasset	Lower offshore

infra-Cambrian, near top Ordovician, near top Silurian, near top Pragian, near top Givetian, near top mid-Frasnian, near top Famennian, near base Quaternary and near Hercynian unconformities (Fig. 7). The stratigraphic layers are identified by the integration of satellite images (Google Earth and Landsat USGS: <https://earthexplorer.usgs.gov/>, last access: 29 November 2016), digital elevation models (DEM), and the 1 : 200 000 geological maps of Algeria (Bennacef et al., 1974; Bensalah et al., 1971).

Subsidence analysis characterizes the vertical displacements of a given sedimentary depositional surface by tracking its subsidence and uplift history (Van Hinte, 1978). The resulting curve details the total subsidence history for a given stratigraphic column (Allen and Allen, 2005; Van Hinte, 1978). Backstripping is also used to restore the initial thicknesses of a sedimentary column (Allen and Allen, 2005; Angevine et al., 1990). Lithologies and paleobathymetries have been defined using facies analysis or literature data. Porosity and the compaction proxy are based on experimental data from (Sclater and Christie, 1980). In this study, subsidence analyses were performed on sections using OSXBackstrip software performing 1D Airy backstripping (following Allen and Allen, 2005; Watts, 2001); available at: <http://www.uis.no/nesstor/work/programs.html>, last access: 5 January 2017).

The 800 km² outcrop of basement rocks of the Hoggar Massif provides an exceptional case study of an exhumed mobile belt composed of accreted terranes of different ages. To reconstruct the nature of the basement, a terrane map (Figs. 15 and 16) was put together by integrating geophysical data (aeromagnetic anomaly map: <https://www.geomag.us/>, last access: 1 December 2016, Bouguer gravity anomaly map: <http://bgi.omp.obs-mip.fr/>, last access: 1 December 2016), satellite images (7ETM+ from Landsat USGS: <https://earthexplorer.usgs.gov/>, last access: 29 November 2016) data, geological maps (Berger et al., 2014; Bertrand and Caby, 1978; Black et al., 1994; Caby, 2003; Fezaa et al., 2010; Liégeois et al., 1994, 2003, 2005, 2013), and geochronological data (e.g., U/Pb radiochronology, see Supplement data 1). Geochronological data from published studies were compiled and georeferenced (Fig. 1). Thermo-tectonic ages were grouped into eight main thermo-orogenic events (Fig. 1): The Liberian-Ouzzalian event (Archean, > 2500 Ma), the Archean, Eburnean (i.e., Paleoproterozoic, 2500–1600 Ma), the Kibarian (i.e., Mesoproterozoic, 1600–1100 Ma), the Neoproterozoic oceanization-rifting (1100–750 Ma), the syn-Pan-African orogeny (i.e., Neoproterozoic, 750–541 Ma), the post-Pan-African (i.e., Neoproterozoic, 541–443 Ma), the Caledonian orogeny (i.e., Siluro-Devonian, 443–358 Ma), and the Hercynian orogeny (i.e., Carbo-Permian, 358–252 Ma).

4 Structural framework and tectono-sedimentary structure analyses

The structural architecture of the North Saharan Platform is characterized by mostly circular to oval shaped basins structured by major faults frequently associated with broad asymmetrical folds displayed by three main trends (Fig. 1): (1) near-N–S, varying from 0 to 10 or 160° N, (2) from 40 to 60° N, and from (3) 100 to 140° N (Figs. 1, 3a, and 4). These fault zones are about 100 km (e.g., faults F1 and F2, Fig. 5) to tens of kilometers long (e.g., faults F3 to F8, Fig. 5). They correspond to the mainly N–S Azzel-Matti, Arak-Foum Belrem, Amguid El Biod, and Tihemboka arches, the NE–SW Bou Bernous, Ahara, and Gargaf arches, and the NW–SE Saoura and Azzene arches (Fig. 1).

4.1 Synsedimentary extensional markers

Extensional markers are characterized by the settlement of steeply westward or eastward-dipping basement normal faults associated with colinear syndepositional folds of several kilometers in length (e.g., Figs. 6a to e and 7a), represented by footwall anticline and hanging wall syncline-shaped forced folds. They are located in the vicinity of different arches (Fig. 2) such as the Tihemboka Arch (Figs. 5b and 6a, b), Arak-Foum Belrem Arch (Figs. 5a, 6c to f and 7a, c), Azzel Matti Arch (Fig. 7b), and Bahar El Hamar area intrabasin arch (Fig. 7d). These tectonic structures can be featured by basement blind faults (e.g., fault F1 in Fig. 7a). The deformation pattern is mainly characterized by brittle faulting in Cambrian–Ordovician series down to the basement and fault-damping in Silurian series (e.g., faults F1 to F6 in Fig. 7b). The other terms of the series (i.e., Silurian to Carboniferous) are usually affected by folding except (see F1 faults in Figs. 6d, 7b, d, and c) where the brittle deformation can be propagated to the Upper Devonian (due to reactivation and/or inversion as suggested in the next paragraph).

In association with the extensional markers, thickness variations and tilted divergent onlaps of the sedimentary series (i.e., wedge-shaped units, progressive unconformities) in the hanging wall syncline of the fault escarpments are observed (Figs. 6 and 7). These are attested using photogeological analysis of satellite images (Fig. 6) and are marked by a gentler dip angle of the stratification planes away from the fault plane (i.e., fault core zone). The markers of syndepositional deformation structures are visible in the hanging-wall synclines of Precambrian to Upper Devonian series (Figs. 6 and 7).

The footwall anticline and hanging-wall syncline-shaped forced folds recognized in this study are very similar to those described in the literature by Grasemann et al. (2005), Khalil and McClay (2002), Schlische (1995), Stearns (1978), Withjack et al. (1990, 2002), and Withjack and Callaway (2000). The wedge-shaped units (DO0 to DO3; Figs. 5, 6, and 7) associated with the hanging-wall synclines are interpreted as

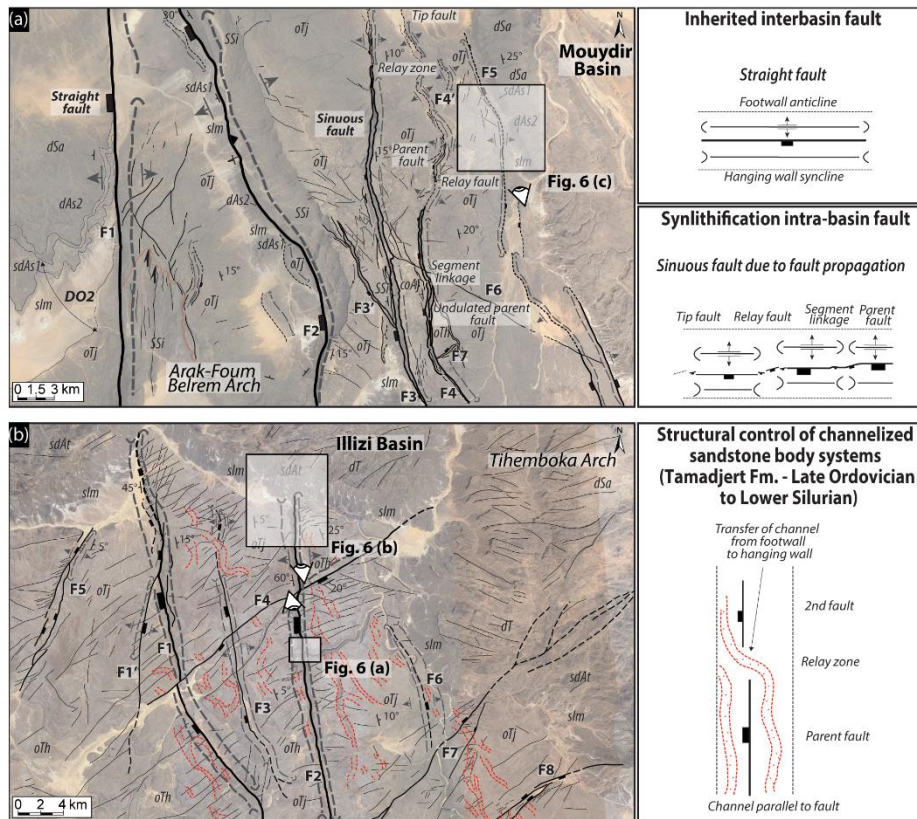


Figure 5. (a) Typology of different types of faults (inherited straight faults vs. sinuous short synlithification propagation faults) in the Cambrian–Ordovician series of the Djebel Settaf (Arak-Foum Belrem Arch; interbasin boundary secondary arch between the Ahnet and Mouydir basins). (b) Structural control of channelized sandstone bodies in Late Ordovician series of South Adrar Assaouatene, Tassili-N-Ajjers (Tihemboka interbasin boundary secondary arch between the Illizi and Murzuq basins). The dotted red line represents Tamadjert Fm. channelized sandstone bodies. The abbreviations used in the figure are as follows: *OTh* – In Tahouite Fm. (Early to Late Ordovician, Floian to Katian); *OTj* – Tamadjert Fm. (Late Ordovician, Hirnantian); *slm* – Imirhou Fm. (Early Silurian); *sdAs1* – Asedjrad Fm. 1 (Late Silurian to Early Devonian); *dAs2* – Asedjrad Fm. 2 (Early Devonian, Lochkovian); *dSa* – Oued Samene Fm. (Lower Devonian, Pragian). See Fig. 2 for map and cross-section location.

synsedimentary normal fault-related folding. The whole tectonic framework forms broad extensional horsts and grabens related to synsedimentary forced folds controlling basin shape and sedimentation.

Following Khalil and McClay (2002), Lewis et al. (2015), Shaw et al. (2005), and Withjack et al. (1990), we use the ages of the growth strata (i.e., wedge-shaped units) to determine the timing of the deformation. The main four wedge-shaped units identified (DO0 to DO3) are indicative of the activation and/or reactivation of the normal faults (extensional settings) during the Neoproterozoic (DO0), the Cambrian–Ordovician (DO1), the Early to Mid-Silurian (DO2), and the Middle to Late Devonian (DO3) times.

In planar view, straight (F1 in Fig. 5a) and sinuous faults (F2, F3, F3', F4, F4', and F5 in Fig. 5a) can be identified.

The sinuous faults are arranged “en echelon” into several segments with relay ramps. These faults are ten to several tens of kilometers long with vertical throws of hundreds of meters that fade rapidly toward the fault tips. The sinuous geometry of normal undulated faults as well as the rapid lateral variation in fault throw are controlled by the propagation and the linkage of growing parent and tip synsedimentary normal faults (Marchal et al., 2003, 1998). We use the stratigraphic age of impacted layers (here Tamadjert Fm.) to date (re)activation of the faults.

According to Holbrook and Schumm (1999), river patterns are extremely sensitive to tectonic structure activity. Here we find that the synsedimentary activity of the extensional structures is also evidenced by the influence of the fault scarp on the distribution and orientation of sinuous channelized sand-

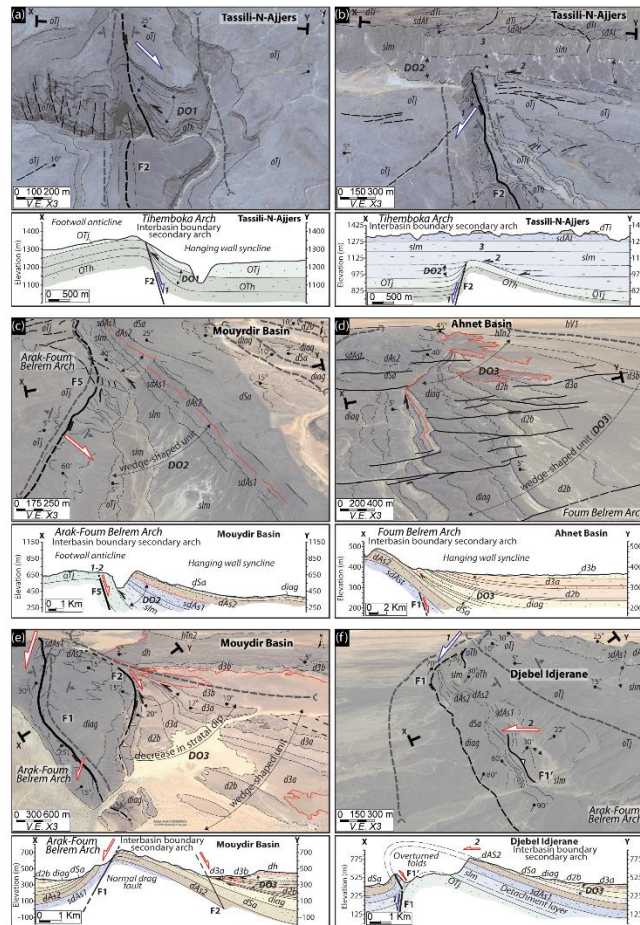


Figure 6. (a) Normal fault (F2) associated with a footwall anticline and a hanging wall syncline with divergent onlaps (i.e., wedge-shaped unit DO1) in the Early to Late Ordovician In Tahouite series (Tassili-N-Ajjers, Tihemboka interbasin boundary secondary arch between the Illizi and Murzuq basins). (b) Ancient normal fault (F2) escarpment reactivated and sealed during Silurian deposition (poly-historic paleo-reliefs) linked to thickness variation, divergent onlaps (DO2) in the hanging wall synclines, and onlaps on the fold hinge anticline (Tassili-N-Ajjers, Tihemboka interbasin boundary secondary arch between the Illizi and Murzuq basins). 1: Early to Late Ordovician extension, 2: Late Ordovician to Early Silurian extension, and 3: Middle to Late Silurian sealing (horizontal drape). (c) Normal fault (F5) associated with forced fold with divergent strata (syncline-shaped hanging wall syncline and associated wedge-shaped unit DO2) and truncation in the Silurian–Devonian series of Djebel Settaf (Arak-Foum Belrem Arch; interbasin boundary secondary arch between the Mouydir and Ahnet basins). 1: Cambrian–Ordovician extension and 2: Silurian–Devonian extensional reactivation (Caledonian extension). (d) Blind basement normal fault (F1) associated with forced fold with in the hanging wall syncline divergent onlaps of the Lower to Upper Devonian series (wedge-shaped unit DO3) and intra-Emsian truncation (Arak-Foum Belrem Arch; interbasin boundary secondary arch between the Mouydir and Ahnet basins). (e) N170° normal blind faults F1 and F2 forming a horst and graben system associated with a forced fold with Lower to Upper Devonian series divergent onlaps (wedge-shaped unit DO3) and intra-Emsian truncation in the hanging-wall syncline (in the Mouydir Basin near Arak-Foum Belrem Arch, eastward interbasin boundary secondary arch). (f) Inherited normal fault (F1) transported from footwall to hanging wall associated with an inverse fault (F1') and accommodated by a detachment layer in the Silurian shales series (thickness variation of Imirhou Fm. between the footwall and hanging wall) and spilled dip strata markers of overturned folding (Djebel Idjerane, Arak-Foum Belrem Arch, eastwards interbasin boundary secondary arch). 1: Cambrian–Ordovician extension and 2: Middle to Late Devonian compression. The abbreviations used in the figure are as follows: *OTh* – In Tahouite Fm. (Early to Late Ordovician, Floian to Katian); *OTj* – Tamadjert Fm (Late Ordovician, Hirnantian); *slm* – Imirhou Fm. (Early to Mid-Silurian); *sdAr* – Atafaitafa Fm. (Middle Silurian); *dti* – Tifernine Fm. (Middle Silurian); *sdAs1* – Asedjrad Fm. 1 (Late Silurian to Early Devonian); *dAs2* – Asedjrad Fm. 2 (Early Devonian, Lochkovian); *dSa* – Oued Samene Fm. (Early Devonian, Pragian); *diag* – Oued Samene shaly-sandstones Fm. (Early Devonian, Emsian?); *d2b* – Givetian; *d3a* – Mehden Yahia Fm. (Late Devonian, Frasnian); *d3b* – Mehden Yahia Fm. (Late Devonian, Famennian); *dh* – Khenig sandstones (late Famennian to early Tournaisian); *hTn2* – late Tournaisian; *hV1* – early Visean. The red line represents unconformity. See Figs. 1, 2, and 5 for map and cross-section location.

www.solid-earth.net/9/1239/2018/

Solid Earth, 9, 1239–1275, 2018

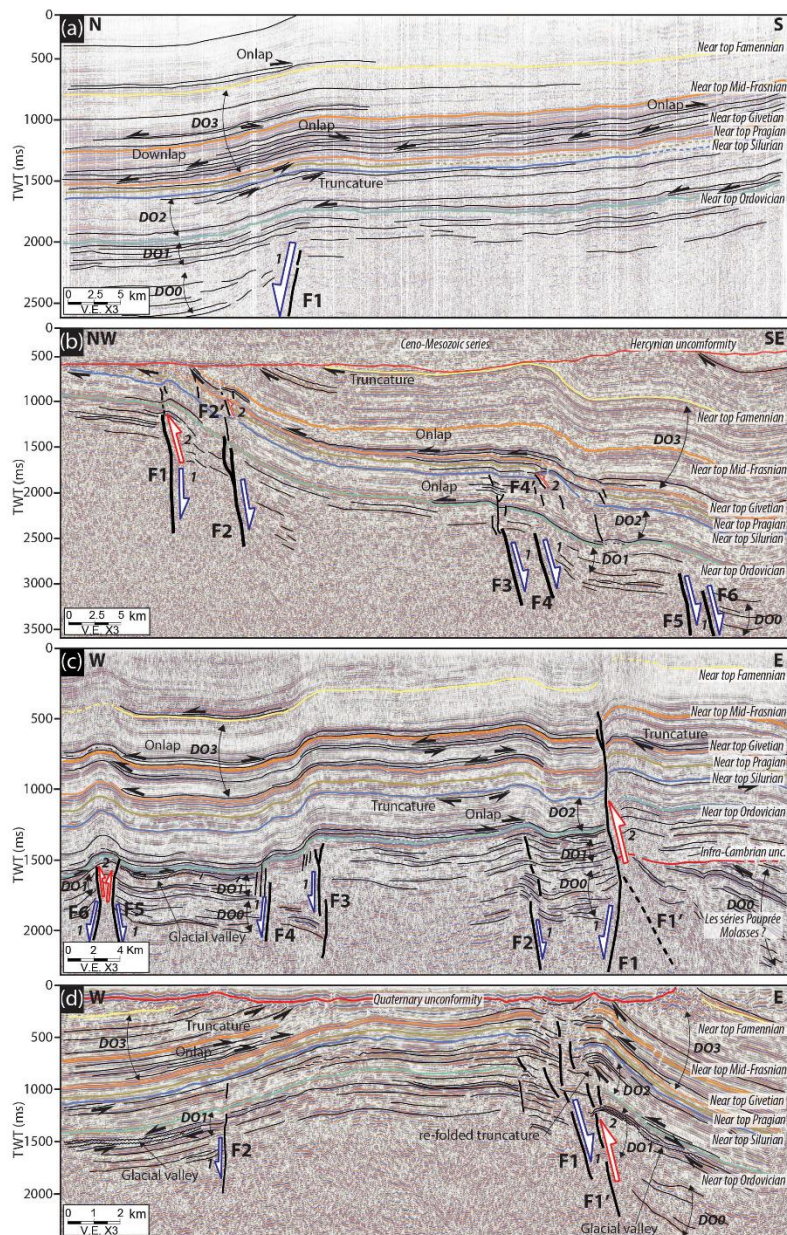


Figure 7. (a) N–S interpreted seismic profile in the Ahnet Basin near Erg Tegumentour (near Arak-Foum Belrem Arch, westward interbasin boundary secondary arch) showing steeply dipping northward basement normal blind faults associated with forced folding. (b) NW–SE interpreted seismic profile of near Azzel Matti Arch (interbasin principal arch) showing steeply dipping southeastward basement normal blind faults associated with forced folds. The westernmost structures are featured by reverse fault related propagation fold. (c) W–E interpreted profile of the Ahnet Basin (Arak-Foum Belrem Arch, westward interbasin boundary secondary arch) showing horst and graben structures influencing Paleozoic tectonics associated with forced folds. (d) W–E interpreted seismic profile of Bahar el Hammar in the Ahnet Basin (Ahnet intra-basin secondary arch) showing steeply dipping normal faults F1 and F2 forming a positively inverted horst associated with folding. Multiple activation and inversion of normal faults are correlated with divergent onlaps (wedge-shaped units): DO0 infra-Cambrian extension, DO1 Cambrian–Ordovician extension, DO2 Silurian extension with local Silurian–Devonian positive inversion, and DO3 Frasnian–Famennian extension–local compression. See Fig. 2 for map and cross-section location.

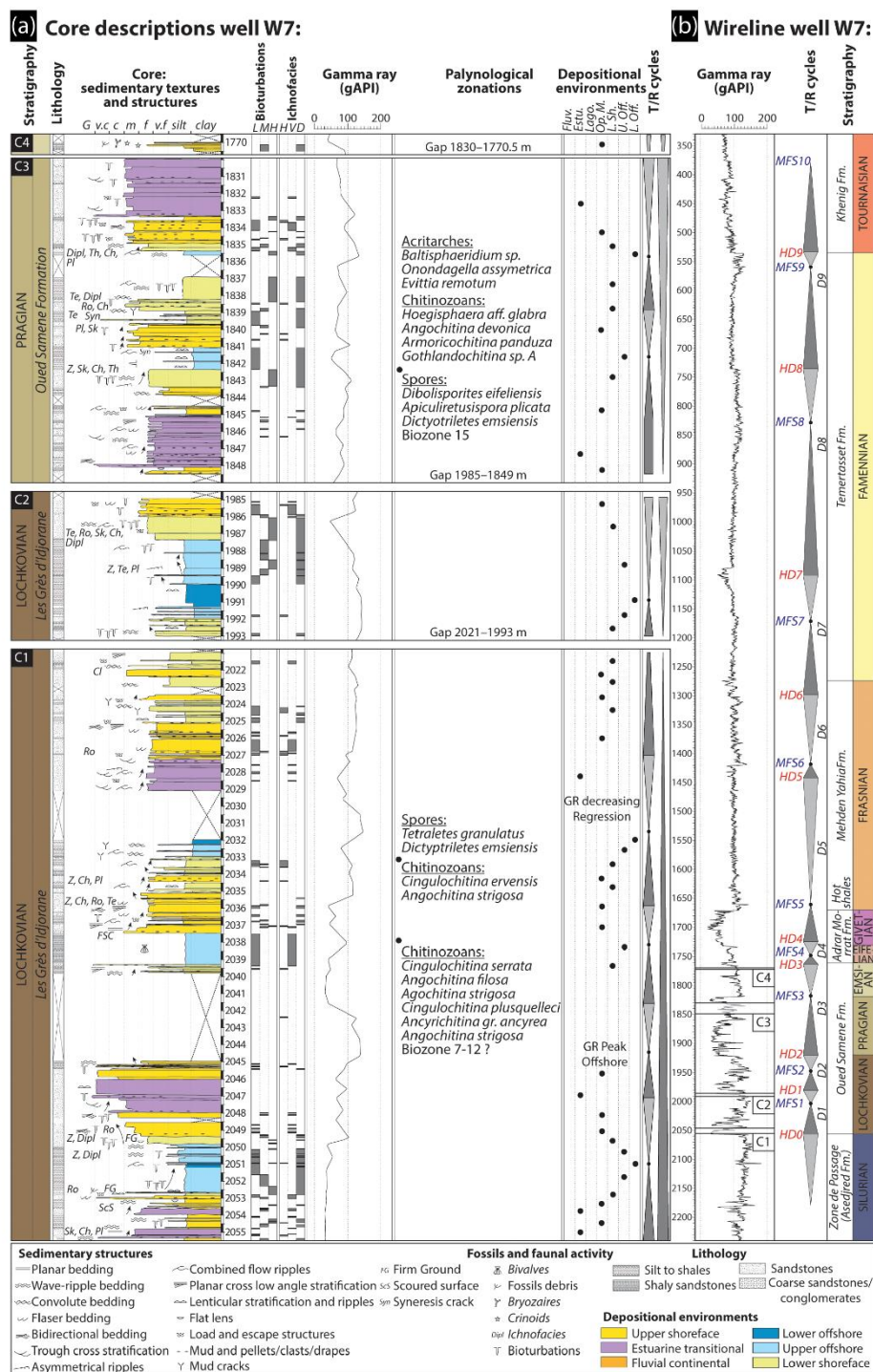


Figure 8. (a) Core description, palynological calibration, and gamma-ray signatures of well W7 modified from an internal core description report (Dokka, 1999) and an internal palynological report (Azzoune, 1999). (b) Devonian sequential stratigraphy of well-log W7. For the location of well W7 see Fig. 2a.

stone body systems (dotted red lines in Fig. 5b). It highlights the (re)activation of the faults during the deposition of these channels, i.e., Late Hirnantian dated by (Girard et al., 2012).

4.2 Synsedimentary compressional markers (inversion tectonics)

After the development of the extensional tectonism described previously, evidence of synsedimentary compressional markers can be identified. These markers are located and preferentially observable near the Arak-Foum Belrem Arch (Fig. 6f; F2 in Fig. 7c), the Azzel Matti Arch (2 in Fig. 7v), and the Bahar El Hamar area intra-basin arch (2 in Fig. 7d). The tectonic structures take the form of inverse faulting reactivating former basement faults (F1' in Fig. 6f, F1 in Fig. 7c, F1' in Fig. 7d, F1 in Fig. 7b). The synsedimentary inverse faulting is demonstrated by the characterization of asymmetric anticlines and is especially observable in satellite images and restricted to the fault footwalls (Fig. 5a along F1–F2).

Landsat image analysis combined with the line drawing of certain seismic lines reveals several thickness variations reflecting divergent onlaps (i.e., wedge-shaped units) which are restricted to the hanging-wall asymmetric anticlines (2 in Figs. 6f, 7b, c and d). The compressional synsedimentary markers clearly post-date extensional divergent onlaps at hanging-wall syncline-shaped forced folds (1 in Figs. 7c, c and d). This architecture is very similar to classical positive inversion structures of former inherited normal faults (Bellahsen and Daniel, 2005; Bonini et al., 2012; Buchanan and McClay, 1991; Ustaszewski et al., 2005). Tectonic transport from the paleo-graben hanging wall toward the paleo-horst footwall (F1, F2–F2', F4–F4' in Fig. 7b; F1–F1' in Fig. 7d) is evidenced. Further positive tectonic inversion architecture is identified by tectonic transport from the paleo-horst footwall to the paleo-graben hanging wall (F1–F1' in Fig. 6f; F1, F5, and F6 in Fig. 7c). This second type of tectonic inversion is very similar to the transported fault models defined by Butler (1989) and Madritsch et al. (2008). The local positive inversions of inherited normal faults occurred during Silurian–Devonian (F4' Fig. 7b) and Middle to Late Devonian times (Figs. 7b, c and d). A late significant compression event between the end of the Carboniferous and the Early Mesozoic was responsible for the exhumation and erosion of the tilted Paleozoic series. This series is related to the Hercynian angular unconformity surface (Fig. 7b).

5 Stratigraphy and sedimentology

The whole sedimentary series described in the literature is composed of fluvial to braid-deltaic plain Cambrian, not only fluvial (e.g., Brahmaputra River analogue), with a transitional facies from continental to shallow marine (Beuf et al., 1968a, b, 1971; Eschard et al., 2005, 2010; Sabaou et al., 2009), Upper Ordovician glaciogenic deposits (Beuf

et al., 1968a, b, 1971; Eschard et al., 2005, 2010), argillaceous deep marine Silurian deposits (Djouder et al., 2018; Eschard et al., 2005, 2010; Legrand, 1986, 2003b; Lüning et al., 2000), and offshore to embayment Carboniferous deposits (Wendt et al., 2009a). In this complete sedimentary succession, we have focused on the Devonian deposits as they are very sensitive to and representative of basin dynamics. The architecture of the Devonian deposits allows us to approximate the main forcing factors controlling the sedimentary infilling of the basin and its synsedimentary deformation. Eleven facies associations organized into four depositional environments (Table 1) are defined to reconstruct the architecture and the lateral and vertical sedimentary evolution of the basins (Figs. 10, 11, 12 and 13).

5.1 Facies association, depositional environments, and erosional unconformities

Based on the compilation and synthesis of internal studies (Eschard et al., 1999), and published papers on the Saharan Platform (Beuf et al., 1971; Eschard et al., 2005, 2010; Henriche, 2002) and on the Ahnet and Mouydir basins (Biju-Duval et al., 1968; Wendt et al., 2006), eleven main facies associations (AF1 to AF5) and four depositional environments are proposed for the Devonian succession (Table 1). They are associated with their gamma-ray responses (Figs. 8 and 9). They are organized into two continental fluvial (AF1 to AF2), four transitional coastal plain (AF3a to AF3d), three shoreface (AF4a to AF4c), and two offshore (AF5a to AF5b) sedimentary environments.

5.1.1 Continental fluvial environments

This depositional environment features the AF1 (fluvial) and the AF2 (flood plain) facies association (Table 1). Facies association AF1 is mainly characterized by a thinning-up sequence with a basal erosional surface and trough cross-bedded intraformational conglomerates with mud clast lag deposits, quartz pebbles, and imbricated grains (Table 1). It passes into medium to coarse trough cross-bedded sandstones, planar cross-bedded siltstones, and laminated shales. These deposits are associated with rare bioturbation (except at the surface of the sets), ironstones, phosphorites, corroded quartz grains, and phosphatized pebbles. Laterally, facies association AF2 is characterized by horizontally laminated and very poorly sorted silt to argillaceous fine sandstones. They contain frequent root traces, plant debris, well-developed paleosols, bioturbation, nodules, and ferruginous horizons. Current ripples and climbing ripples are associated in prograding thin sandy layers.

In AF1, the basal erosional reworking and high energy processes are characteristic of channel-filling of fluvial systems (Allen, 1983; Owen, 1995). Eschard et al. (1999) identify three fluvial systems (see A, B, and C in Fig. 9) in the Tassili-N-Ajers outcrops: braided dominant (AF1a), meandering

dominant (AF1b), and straight dominant (AF1c). They differentiate them by their different sinuosity, direction of accretion (lateral or frontal), the presence of mud drapes, bioturbation, and giant epsilon cross-bedding. Gamma-ray signatures of these facies associations (A, B, and C in Fig. 9) are cylindrical with an average value of 20 gAPI. The gamma-ray shapes are largely representative of fluvial environments (Rider, 1996; Serra and Serra, 2003; Wagoner et al., 1990). The bottom is sharp with high value peaks and the tops are frequently fining-up, which may be associated with high values caused by argillaceous flood plain deposits and roots (Eschard et al., 1999). AF2 is interpreted as humid flood-plain deposits (Allen, 1983; Owen, 1995) with crevasse splays or preserved levees of fluvial channels (Eschard et al., 1999). Gamma-ray curves of AF2 (D, Fig. 9) show a rapid succession of low to very high peak values, ranging from 50 to 120 gAPI. AF1 and AF2 are typical of the Pragian “Oued Samene” Formation (Wendt et al., 2006). In the Illizi Basin, these facies are mainly recorded in the Ajjers Formation (dated Upper Cambrian? to Ordovician, see Fabre, 2005; Vecoli, 2000; Vecoli et al., 1995, 1999, 2008; Vecoli and Playford, 1997) and the Lochkovian to Pragian “Barre Moyenne” and “Barre Supérieure” formations (Beuf et al., 1971; Eschard et al., 2005).

5.1.2 Transitional coastal plain environments

This depositional environment comprises facies associations AF3a (delta/estuarine), AF3b (fluvial/tidal distributary channels), AF3c (tidal sand flat), and AF3d (lagoon/mudflat) (Table 1). AF3a is mainly dominated by sigmoidal cross-bedded heterolithic rocks with mud drapes. It is also characterized by fine to coarse, poorly sorted sandstones and siltstones often structured by combined flow ripples, flaser bedding, wavy bedding, and some rare planar bedding. Mud clasts, root traces, desiccation cracks, water escape features, and shale pebbles are common. The presence of epsilon bedding is attested, which is formed by lateral accretion of a river point bar (Allen, 1983). The bed surface sets are intensively bioturbated (*Skolithos* and *Planolites*) indicating a shallow marine subtidal setting (Pemberton and Frey, 1982). Faunas such as brachiopods, trilobites, tentaculites, and graptolites are present. AF3b exhibits a fining-up sequence featured by a sharp erosional surface, trough cross-bedded, very coarse-grained, poorly sorted sandstone at the base and sigmoidal cross-bedding at the top (Figs. 8 and 9). AF3c is formed by fine-grained to very coarse-grained sigmoidal cross-bedded heterolithic sandstones with multidirectional tidal bundles. They are also structured by lenticular, flaser bedding and occasional current and oscillation ripples with mud cracks. They reveal intense bioturbation composed of *Skolithos* (Sk), *Thalassinoides* (Th), and *Planolites* (Pl) ichnofacies indicating a shallow marine subtidal setting (Frey et al., 1990; Pemberton and Frey, 1982). AF4d is characterized by horizontally laminated mudstones associated with varicolored shales

and fine-grained sandstones. They exhibit mud cracks, occasional wave ripples, and rare multidirectional current ripples. These sedimentary structures are poorly preserved because of intense bioturbation composed of *Skolithos* (Sk), *Thalassinoides* (Th), and *Planolites* (Pl). The fauna includes ammonoids (rare), goniatites, calymenids, pelecypod molds, and brachiopod coquinas.

In AF3a, both tidal and fluvial systems in the same facies association can be interpreted as an estuarine system (Dalrymple et al., 1992; Dalrymple and Choi, 2007). The gamma-ray signature is characterized by a convex bell shape with rapidly alternating low to mid values (30 to 60 gAPI) due to the mud draping of the sets (see E Fig. 9). These forms of gamma ray are typical of fluvial–tidal influenced environments with upward-fining parasequences (Rider, 1996; Serra and Serra, 2003; Wagoner et al., 1990). AF3a is identified at the top of the Pragian “Oued Samene” Formation and in Famennian “Khenig” Formation (Wendt et al., 2006) in the Ahnet and Mouydir basins. In the Illizi Basin, AF3a is mostly recorded at the top Cambrian of the Ajjers Formation, in the Lochkovian “Barre Moyenne”, and at the top Pragian of the “Barre Supérieure” Formation (Beuf et al., 1971; Eschard et al., 2005). The AF3b association can be characterized by a mixed fluvial and tidal dynamic based on criteria such as erosional basal contacts, fining-upward trends, or heterolithic facies (Dalrymple et al., 1992; Dalrymple and Choi, 2007). They are associated with abundant mud clasts, mud drapes, and bioturbation indicating tidal influences (Dalrymple et al., 1992, 2012; Dalrymple and Choi, 2007). The major difference with the estuarine facies association (AF3a) is the slight lateral extent of the channels which are only visible in outcrops (Eschard et al., 1999). The gamma-ray pattern is very similar to the estuarine electrofacies (see F Fig. 9). AF3c is interpreted as a tidal sand flat laterally present near a delta (Lessa and Masselink, 1995) and associated with an estuarine environment (Leuven et al., 2016). The gamma-ray signature (see G Fig. 9) is distinguishable by its concave funnel shape with alternating low and mid peaks (25 to 60 gAPI) due to the heterogeneity of the deposits and rapid variations in the sand/shale ratio. These facies are observed in the “Talus à Tigillites” Formation of the Illizi Basin (Eschard et al., 2005). In AF4d, both ichnofacies and facies are indicative of tidal mudflat/lagoonal depositional environments (Dalrymple et al., 1992; Dalrymple and Choi, 2007; Frey et al., 1990). The gamma-ray signature has a distinctively high value (80 to 130 gAPI) and an erratic shape (see H Fig. 9). AF4d is observed in the “Atafaitafa” Formation and in the Emsian prograding shoreface sequence of the Illizi Basin (Eschard et al., 2005). It is also recorded in the Lochkovian “Oued Samene” Formation and the Famennian “Khenig” sandstones (Wendt et al., 2006).

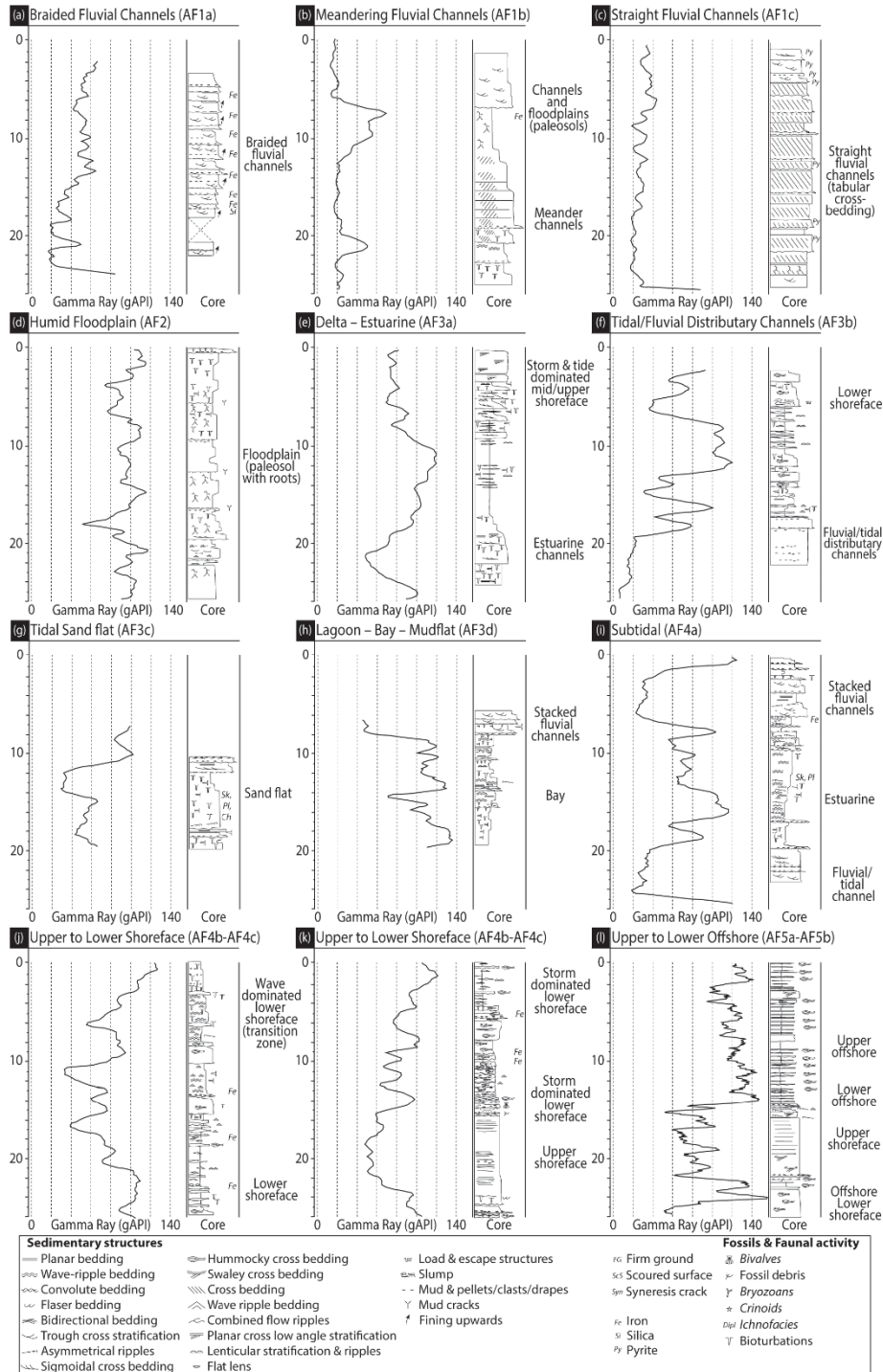


Figure 9. The main depositional environments (a–l) and their associated electrofacies (i.e., gamma-ray patterns) modified and compiled from Eschard et al. (1999).

5.1.3 Shoreface environments

This depositional environment is composed of AF4a (subtidal), AF4b (upper shoreface), and AF4c (lower shoreface) facies associations (Table 1). AF4a is characterized by the presence of brachiopods, crinoids, and diversified bioturbations, by the absence of emersion, and by the greater amplitude of the sets in a dominant mud lithology (Eschard et al., 1999). AF4b is heterolithic and composed of fine to medium-grained sandstones (brownish) interbedded with argillaceous siltstones and bioclastic carbonated sandstones. Sedimentary structures include oscillation ripples, swaley cross-bedding, flaser bedding, cross-bedding, convolute bedding, wavy bedding, and low-angle planar cross-stratification. Sediments were affected by moderate to highly diversified bioturbation by *Skolithos* (Sk), *Cruziana*, *Planolites*, (Pl) *Chondrites* (Ch), *Teichichnus* (Te), *Spirophytons* (Sp) and are composed of ooids, crinoids, bryozoans, stromatoporoids, tabulate and rugose corals, pelagic styliolinids, neritic tentaculitids, and brachiopods. AF4c can be distinguished by a low sand/shale ratio, thick interbeds, abundant hummocky cross-stratification (HCS), deep groove marks, slumping, and intense bioturbation (Table 1).

AF4a is interpreted as a lagoonal shoreface. The gamma-ray pattern (see I Fig. 9) is characterized by a concave bell shape influenced by a low sand/shale ratio with values fluctuating between 100 and 200 gAPI. AF4a is identified in the “Talus à Tigillites” Formation and the Emsian sequence of the Illizi Basin (Eschard et al., 2005) and in the Lochkovian “Oued Samene” Formation (Wendt et al., 2006). AF4b is interpreted as a shoreface environment. The presence of swaley cross-bedding produced by the amalgamation of storm beds (Dumas and Arnott, 2006) and other cross-stratified beds is indicative of upper shoreface environments (Loi et al., 2010). The gamma-ray pattern (see J and K Fig. 9) displays concave erratic egg shapes with a very regularly decreasing-upward trend and ranging from offshore shale with mid values (80 to 60 gAPI) to clean sandstone with lower values at the top (40 to 60 gAPI). AF4b is observed in the “Atafaitafa” Formation corresponding to the “Zone de passage” Formation of the Illizi Basin (Eschard et al., 2005). AF4c is interpreted as a lower shoreface environment (Dumas and Arnott, 2006; Suter, 2006). The gamma-ray pattern displays the same features as the upper shoreface deposits with higher values (i.e., muddier facies) ranging from 100 to 80 gAPI (see J and K Fig. 9).

5.1.4 Offshore marine environments

This depositional environment is composed of AF5a and AF5b facies associations (Table 1). AF5a is mainly defined by wavy to planar-bedded heterolithic silty-shales interlayered with fine-grained sandstones. It also contains bundles of skeletal wackestones and calcareous mudstones. The main sedimentary structures are lenticular sandstones, HCS,

mud mounds, low-angle cross-bedding, tempestite bedding, slumping, and deep groove marks. Sediments can present rare horizontal bioturbation such as *Zoophycos* (Z), *Teichichnus* (Te), and *Planolites* (Pl). AF5b is characterized by an association of black silty shales with occasional bituminous wackestones and packstones. It is composed of graptolites, goniatites, orthoconic nautiloids, pelagic pelecypods, limestone nodules, tentaculitids, ostracods, and rare fish remains. Rare bioturbation such as *Zoophycos* (Z) is visible.

In AF5a, the occurrence of HCS, the decrease in sand thickness and grain size, and the bioturbation and the florofaunal associations indicate a deeper marine environment under the influence of storms (Aigner, 1985; Dott and Bourgeois, 1982; Reading and Collinson, 2009). AF5a is interpreted as upper offshore deposits (i.e., offshore transitional). The gamma-ray pattern is serrated and erratic with values well grouped around high values from 120 to 140 gAPI (see L Fig. 9). Positive peaks may indicate siltstone to sandstone ripple beds. AF5b is interpreted as lower offshore deposits (Aigner, 1985; Stow et al., 2001; Stow and Piper, 1984). Here again the gamma-ray signature is serrated and erratic with values well grouped around 140 gAPI (see L Fig. 9). Hot shales with anoxic conditions are characterized by gamma-ray peaks (> 140 gAPI). These gamma-ray patterns are typical of offshore environments dominated by shales (Rider, 1996; Serra and Serra, 2003; Wagoner et al., 1990). AF5a and AF5b are observed in the Silurian “Argiles à Graptolites” Formation and the Emsian “Orsine” Formation of the Illizi Basin (Beuf et al., 1971; Eschard et al., 2005; Legrand, 1986, 2003b). The “Argiles de Mehden Yahia” and “Argiles de Temertasset” shales have the same facies (Wendt et al., 2006).

5.2 Sequential framework and unconformities

The high-resolution facies analysis, depositional environments, stacking patterns, and surface geometries observed in the Devonian succession reveal at least two different orders of depositional sequences (large and medium scale, Fig. 8) considered as transgressive/regressive (T/R) (Catuneanu et al., 2009). The sequential framework proposed in Fig. 8b results from the integration of the vertical evolution of the main surfaces (Fig. 8a) and the gamma-ray pattern (Fig. 9). The Devonian series under focus exhibits 9 medium-scale sequences (D1 to D9, Fig. 8; Figs. 10, 11, 12, and 13) bounded by 10 major sequence boundaries (HD0 to HD9), and 9 major flooding surfaces (MFS1 to MFS9). The correlation of the different sequences at the scale of the different basins and arches is used to build three cross sections – two E–W (Figs. 10, 11 and 12) and one N–S (Fig. 13).

The result of the analysis of the general pattern displayed by the successive sequences reveal two major patterns (Figs. 10, 12 and 13) limited by a major flooding surface MFS5. The first pattern extends from the Oued Samene to Adrar Morrat formations and is dated from the Lochko-

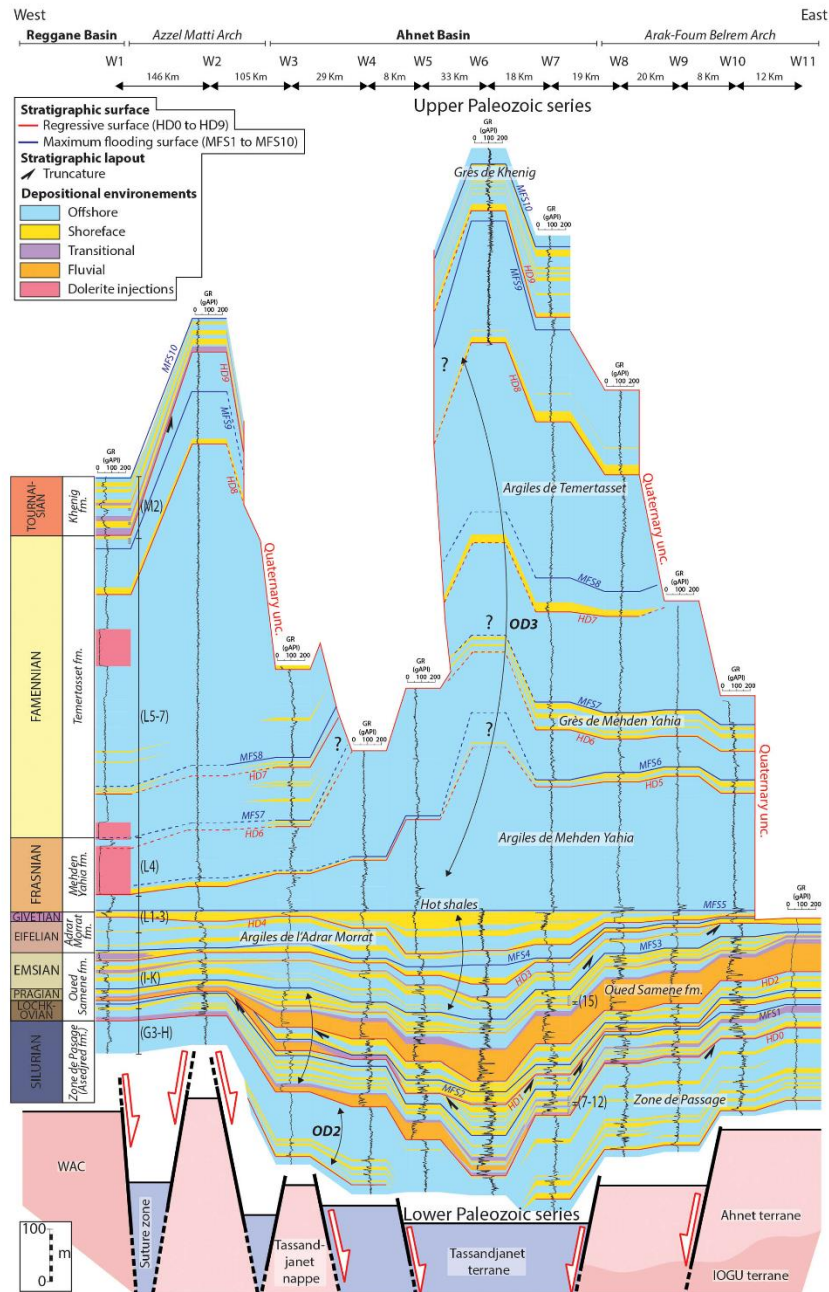


Figure 10. SE–W cross-section between the Reggane Basin, the Azzel Matti Arch, the Ahnet Basin, the Arak-Foum Belrem Arch, the Mouydir Basin, and the Amguid El Biod Arch (well locations in Fig. 3). The well W1 biozone calibration is from Hassan (1984) and the internal report is based on the Magloire (1967) classification: biozone G3-H (Wenlock–Ludlow, Upper Silurian), biozone I-K (Lochkovian–Emsian, Lower Devonian), biozone L1-3 (Eifelian–Givetian, Middle Devonian), biozone L4 (Frasnian, Upper Devonian), biozone L5-7 (Famennian, Upper Devonian), and biozone M2 (Tournaisian–Lower Carboniferous). The well W7 biozone calibration is from Azzoune (1999) and the internal report is based on the Boumendjel (1987) classification: biozone 7–12 (Lochkovian, Lower Devonian) and biozone 15 (Emsian, Lower Devonian). Interpretation of the basement is based on Figs. 1, 2, and 15. Well location is in Fig. 2.

vian to Givetian. D1 to D5 medium-scale sequences indicate a general proximal clastic depositional environment (dominated by fluvial to transitional and shoreface facies) with intensive lateral facies evolution. This first pattern is thin (from 500 m in the basin depocenter to 200 m around the basin rim) and with successive amalgamated surfaces on the edge of the arches between the “Zone de passage” and “Oued Samene” formations (e.g., Figs. 10 and 13). It is delimited at the bottom by the HD0 surface corresponding to the Silurian–Devonian boundary. D1 to D3 are composed of T/R sequences with a first deepening transgressive trend indicative of a transition from continental to marine deposits bounded by a major MFS and evolving into a second shallowing trend from deep marine to shallow marine depositional environments. D1 to D3 thin progressively toward the edge and the continental deposits, in the central part of the basin, pass laterally into a major unconformity. The amalgamation of the surfaces and lateral variations of facies between the Ahnet Basin and Azzel Matti and Arak-Foum Belrem arches demonstrate a tectonic control related to the presence of subsiding basins and paleo-highs (i.e., arches).

D4 and D5 display the same T/R pattern with a reduced continental influence and upward decrease in lateral facies variations and thicknesses where the MFS4 marks the beginning of a marine-dominated regime in the entire area. It is identified as the Early Eifelian transgression defined by Wendt et al. (2006). The D5 sequence is mainly composed of shoreface carbonates. Evidence of mud mounds preferentially located along faults are well-documented in the area for that time (Wendt et al., 1993, 1997, 2006; Wendt and Kaufmann, 1998). This change in the general pattern indicates reduced tectonic influence.

MFS5, at the transition between the two main patterns, represents a major flooding surface on the platform and is featured worldwide by deposition of “hot shales” during the early Frasnian (Lüning et al., 2003, 2004; Wendt et al., 2006).

The second pattern extends from the “Mehden Yahia”, “Temertasset” to the “Khenig” formations dated Frasnian to Lower Tournaisian. This pattern is composed of part of D5–D9 medium-scale sequences. It corresponds to homogeneous offshore depositional environments with no lateral facies variations. However, local deltaic (fluvio–marine) conditions are observed during the Frasnian at the Arak Foum Belrem Arch (“Grès de Mehden Yahia” in Fig. 12). A successive alternation of shoreface and offshore deposits is organized into five medium-scale sequences (part of D5, and D6 to D9; Figs. 10, 11 and 12). They, in particular, show some regressive phases with the deposition of both “Grès de Mehden Yahia” and “Grès du Khnig” sandstones (bounded by HD6 and HD9). This pattern (i.e., part of D5 to D9) corresponds to the general maximum flooding (Lüning et al., 2003, 2004; Wendt et al., 2006) under eustatic control with no tectonic influences.

6 Subsidence and tectonic history: an association of low rate extensional subsidence and positive inversion pulses

The backstripping approach (Fig. 14) was applied to five wells (W1, W5, W7, W17, and W21). The morphology of the backstripped curve and subsidence rates can provide clues as to the nature of the sedimentary basin (Xie and Heller, 2009). In intracratonic basins, reconstructed tectonic subsidence curves are almost linear to gently exponential in shape, similar to those of passive margins and rifts (Xie and Heller, 2009). The compilation of tectonic backstripped curves from several wells in peri-Hoggar basins (Fig. 14a, see Fig. 1 for location) and from wells in the study area (Fig. 14b) display low rates of subsidence (from 5 to 50 m Myr⁻¹) organized in subsidence patterns of: inversion of the low rate subsidence (ILRS type c, red line, Fig. 14c), deceleration of the low rate subsidence (DLRS type b, black line), and acceleration of the low rate subsidence (ALRS type a, blue line).

Each period of ILRS, DLRS, and ALRS may be synchronous among the different wells studied (see B1 to J, Fig. 14b) and some wells from published data (see D to J Fig. 14a).

The Saharan Platform is marked by a rejuvenation of basement structures, around arches (Figs. 1, 2, and 3), linked to regional geodynamic pulses during Neoproterozoic to Paleozoic times (Fig. 14). A compilation of the literature shows that the main geodynamic events are associated with discriminant association of subsidence patterns:

- a. Late Pan-African compression and collapse (patterns a, b, and c, A Fig. 14a). The infra-Cambrian (i.e., top Neoproterozoic) is characterized by horst and graben architecture associated with wedge-shaped unit DO0 in the basement (Fig. 7). This structuring, probably related to Pan-African post-orogenic collapse, is illustrated by intracratonic basins infilled with volcano-sedimentary molasses series (Ahmed and Moussine-Pouchkine, 1987; Coward and Ries, 2003; Fabre et al., 1988; Oudra et al., 2005).
- b. Cambrian–Ordovician geodynamic pulse (Fig. 14). Highlighted by the wedge-shaped units DO1 (Figs. 6a and 7), the horst and graben system is correlated with deceleration (DLRS pattern a, B1) and with local acceleration of the subsidence (ALRS pattern b, B2). The Cambrian–Ordovician extension is documented on arches (Arak-Foum Belrem, Azzel Matti, Amguid El Biod, Tihemboka, Gargaf, Murizidié, Dor El Gussa, etc.) of the Saharan Platform by synsedimentary normal faults, reduced sedimentary successions (Bennacef et al., 1971; Beuf et al., 1968a, b, 1971; Beuf and Montadert, 1962; Borocco and Nyssen, 1959; Claracq et al., 1958; Echikh, 1998; Eschard et al., 2010; Fabre, 1988; Ghienne et al., 2003, 2013; Zazoun and Mahdjoub, 2011), and by stratigraphic hiatuses (Mélou et al.,

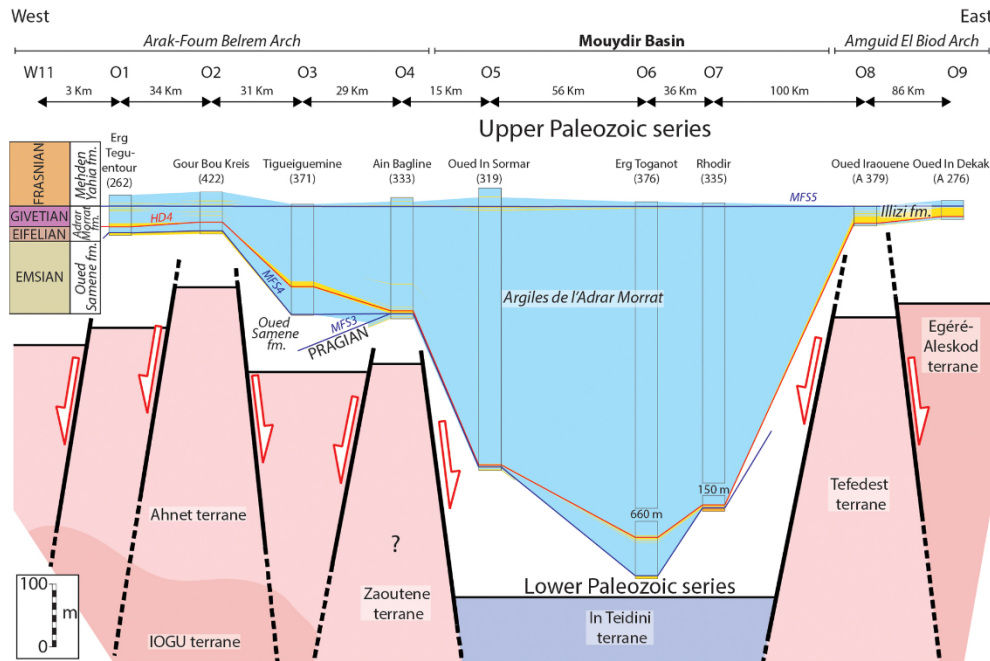


Figure 11. SE–W cross section between the Arak-Foum Belrem Arch, the Mouydir Basin, and the Amguid El Biod Arch. Outcrop cross-section correlations and biostratigraphic calibrations are based on the compilation of published papers (Wendt et al., 2006, 2009b). Interpretation of the basement is based on Figs. 1, 2, and 15. Outcrop location is in Fig. 2.

1999; Oulebsir and Paris, 1995; Paris et al., 2000; Vecoli et al., 1995, 1999).

- c. Late Ordovician geodynamic pulse (i.e., Hirnantian glacial and isostatic rebound; Fig. 14). Late Ordovician incisions mainly situated at the hanging walls of normal faults (Fig. 7c and d) are interpreted as Hirnantian glacial-paleovalleys (Le Heron, 2010; Smart, 2000) and followed by local inversion of low rate subsidence (ILRS of type c, C in Fig. 14).
- d. Silurian extensional geodynamic pulse (D, Fig. 14). The Silurian post-glaciation period is featured by the reactivation and sealing of the inherited horst and graben fault system (i.e., wedge-shaped unit DO2; Figs. 6b, c, 7a and b). It is linked to an acceleration of the subsidence (ALRS of pattern b in Fig. 14). This tectonic extension is documented in seismic records (Najem et al., 2015) and is associated with the Silurian major transgression on the Saharan Platform (e.g., Eschard et al., 2005; Lüning et al., 2000).
- e. Late Silurian to Early Devonian geodynamic pulse (Caledonian compression; E Fig. 14). Late Silurian times are marked by reactivation and local positive inversion of the former structures (Figs. 6c and 7b);

this occurs due to truncations located at fold hinges (Figs. 6c and 7) and due to a major shift from marine to fluvial/transitional environments (e.g., Fig. 10). Back-stripped curves register an inversion of the subsidence (ILRS of pattern c, in Fig. 14). The Caledonian event is mentioned as related to large-scale folding or uplifted arches (e.g., the Gargaff, Tihemboka, Ahara, Murizid-Dor el Gussa and Amguid El Biod arches) and it is associated with breaks in the series and with angular unconformities (Beuf et al., 1971; Biju-Duval et al., 1968; Boote et al., 1998; Boudjema, 1987; Boumendjel et al., 1988; Carruba et al., 2014; Chavand and Claracq, 1960; Coward and Ries, 2003; Dubois and Mazelet, 1964; Echikh, 1998; Eschard et al., 2010; Fekirine and Abdallah, 1998; Follot, 1950; Frizon de Lamotte et al., 2013; Ghienne et al., 2013; Gindre et al., 2012; Legrand, 1967a, b; Magloire, 1967).

- f. Early Devonian tectonic quiescence (F Fig. 14). This is characterized by a deceleration of the low rate subsidence (DLRS of pattern a, F in Fig. 14). During this period, we have detected Emsian truncation from satellite images (Fig. 6d and e) and erosion and pinch out of Upper Emsian to Eifelian series from well cross sections (Figs. 10, 12 and 13). In previous works, these hiatuses/gaps (i.e., Upper Lochkovian, Lower Pragian,

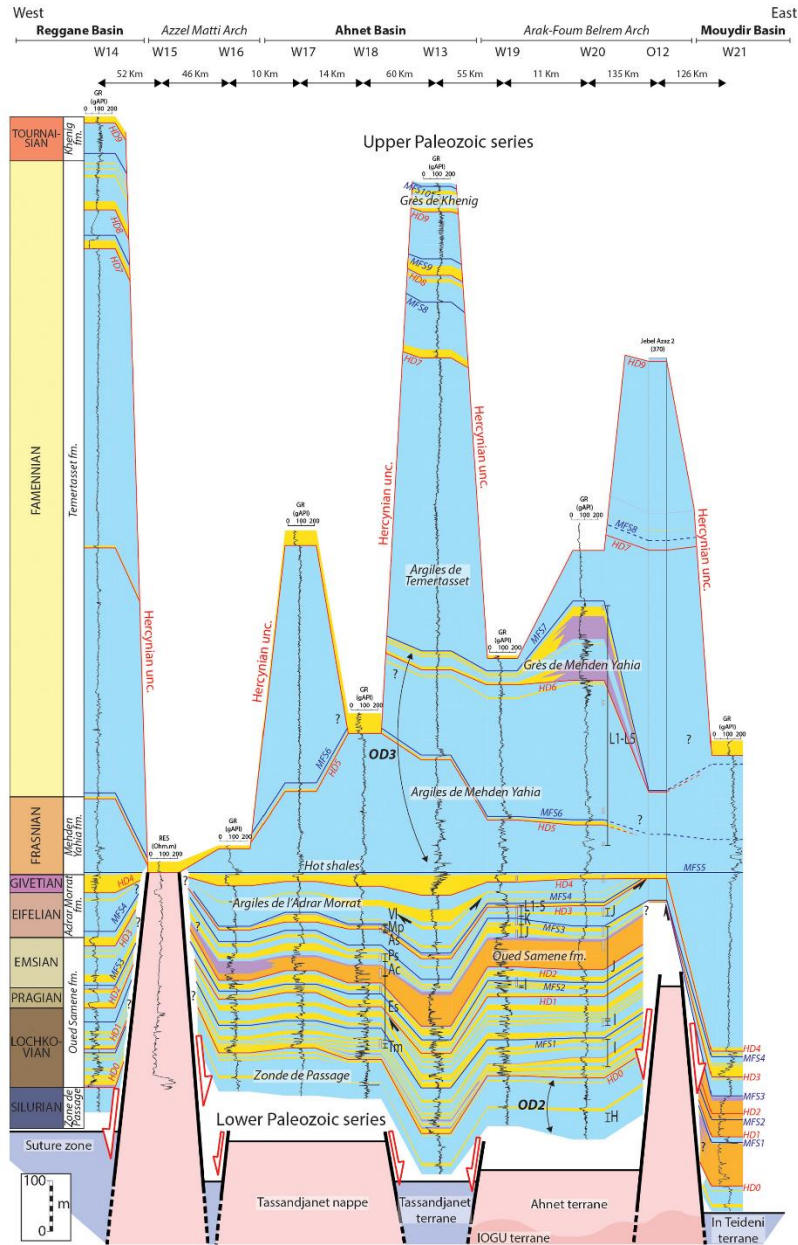


Figure 12. NE–W cross section between the Reggane Basin, the Azzel Matti Arch, the Ahnet Basin, the Arak-Foum Belrem Arch, the Mouydir Basin, and the Amguid El Biod Arch. The well W18 biozone calibration is based on Kermadjji et al. (2009): biozone (Tm) *tidikeltense microbaculatus* (Lochkovian, Lower Devonian), biozone (Es) *emsiensis spinaeformis* (Lochkovian–Pragian, Lower Devonian), biozone (Ac) *arenorugosa caperatus* (Pragian, Lower Devonian), biozone (Ps) *poligonalis subgranifer* (Pragian–Emsian, Lower Devonian), biozone (As) *annulatus svalbardiae* (Emsian, Lower Devonian), biozone (Mp) *microancyreus protea* (Emsian–Eifelian, Lower to Middle Devonian), and biozone (Vl) *velatus langii* (Eifelian, Middle Devonian). The well W19 and W20 biozones calibration from internal reports (Abdesselam-Rouighi, 1991; Khiar, 1974) is based on the Magloire (1967) classification: biozone H (Pridoli, Upper Silurian), biozone I (Lochkovian, Lower Devonian), biozone J (Pragian, Lower Devonian), biozone K (Emsian, Lower Devonian), and biozone L1–5 (Middle Devonian to Upper Devonian). Interpretation of the basement is based on Figs. 1, 2, and 15. Outcrop and well location is in Fig. 2.

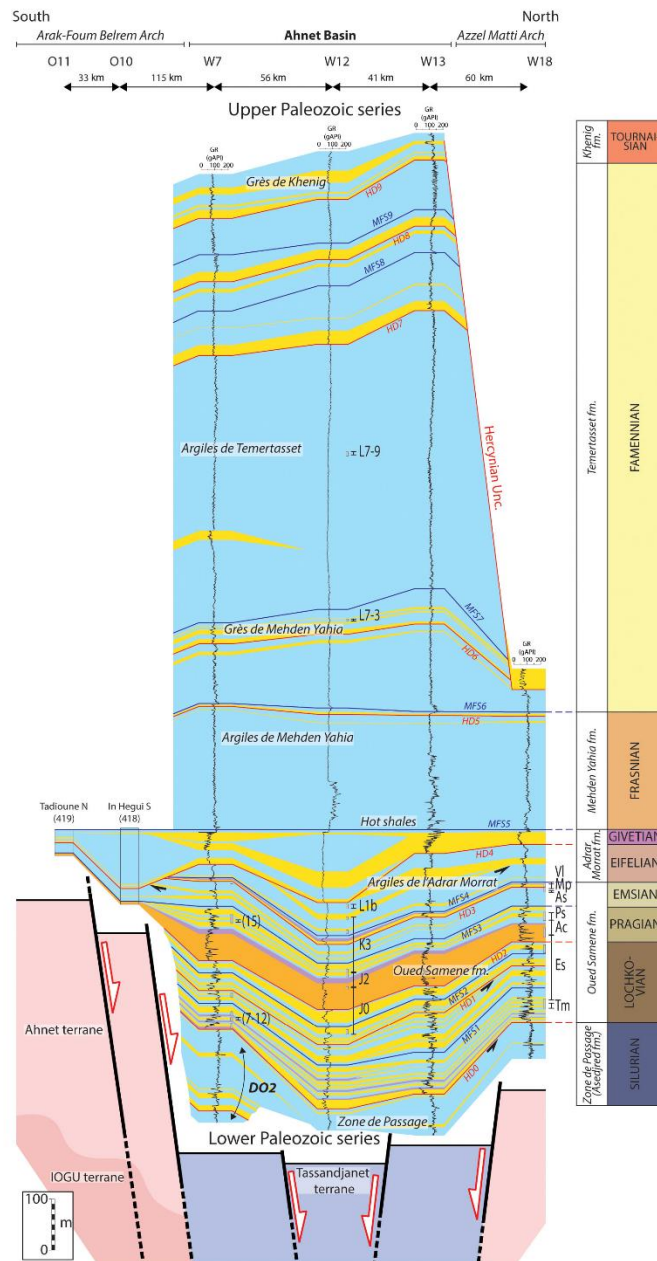


Figure 13. N–S cross section in the Ahnet Basin between Azzel Matti Arch and Arak-Foum Belrem Arch; well W7 biozone calibration from Azzoune, (1999) internal report based on the Boumendjel (1987) classification: biozones 7–12 (Lochkovian, Lower Devonian), biozone 15 (Emsian, Lower Devonian). Well W18 biozone calibration is based on Kermadji et al. (2009): biozone (Tm) *tidikeltense microbaculatus* (Lochkovian, Lower Devonian), biozone (Es) *emsiensis spinaeformis* (Lochkovian–Pragian, Lower Devonian), biozone (Ac) *arenorugosa caperatus* (Pragian, Lower Devonian), biozone (Ps) *poligonalis subgranifer* (Pragian–Emsian, Lower Devonian), biozone (As) *amulatus svalbardiae* (Emsian, Lower Devonian), biozone (Mp) *microancyreus protea* (Emsian–Eifelian, Lower to Middle Devonian), and biozone (VI) *velatus langii* (Eifelian, Middle Devonian). The well W12 biozone calibration from Abdesselam-Rouighi (1977) internal report is based on the Boumendjel (1987) classification: biozone J (Pragian, Lower Devonian), biozone K (Emsian, Lower Devonian), biozone L1 (Eifelian, Middle Devonian), and biozone L7-3, L7-9 (Frasnian–Famennian, Upper Devonian). Interpretation of the basement is based on Figs. 1, 2, and 15. Outcrop and well location is in Fig. 2.

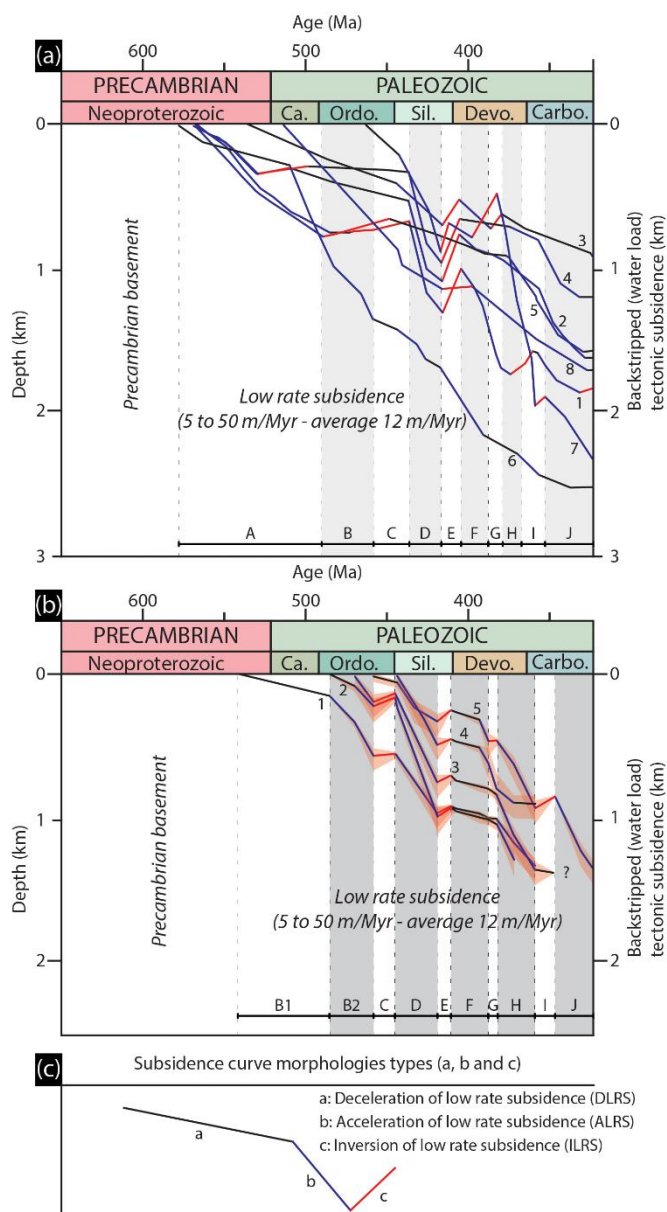


Figure 14. (a) Tectonic backstripped curves of the Paleozoic North Saharan Platform (peri-Hoggar basins) compiled from literature. 1: HAD-1 well in Ghadamès Basin (Makhous and Galushkin, 2003b); 2: well RPL-101 in Reggane Basin (Makhous and Galushkin, 2003b); 3: L1-1 well in Murzuq Basin (Galushkin and Eloghbi, 2014); 4: TGE-1 in Illizi Basin (Makhous and Galushkin, 2003a); 5: REG-1 in Timimoun Basin (Makhous and Galushkin, 2003b); 6: Ghadamès-Berkine Basin (Allen and Armitage, 2011; Yahy, 1999); 7: well in Sbâa Basin (Tournier, 2010); and 8: well B1NC43 in Al Kufrah Basin (Holt et al., 2010). (b) Tectonic backstripped curves of wells in the study area 1: well W17 in Ahnet Basin; 2: well W5 in Ahnet Basin; 3: well W7 in Ahnet Basin; 4: well W21 in Mouydir Basin; and 5: well W1 in Reggane Basin. (c) Typologies of subsidence curves morphologies. A: Late Pan-African compression and collapse (type a, b, and c subsidence), B: undifferentiated Cambrian–Ordovician (type a, b, and c subsidence), B1: Cambrian–Ordovician tectonic quiescence (type a subsidence), B2: Cambrian–Ordovician extension (type b subsidence), C: Late Ordovician glacial and isostatic rebound (type c subsidence), D: Silurian extension (type b subsidence), E: Late Silurian Caledonian compression (type c subsidence), F: Early Devonian tectonic quiescence (type a subsidence), G–H: Middle to late Devonian extension with local compression (i.e., inversion structures, type b and c subsidence), I: Early Carboniferous extension with local tectonic pre-Hercynian compression (type c and b subsidence), and J: Middle Carboniferous tectonic extension (type b subsidence).

- Upper Pragian, Upper Emsian, Lower Eifelian) are observed in the Ahnet Basin (Kermadjji, 2007; Kermadjji et al., 2003, 2008, 2009; Wendt et al., 2006), in the Illizi (Boudjema, 1987) and in the Reggane (Jäger et al., 2009).
- g., h. Middle to late Devonian geodynamic pulse (extension and local inversions, G and H Fig. 14). The Middle to Late Devonian period is characterized by large wedge hiatuses and truncations associated with the reactivation of horst and graben structures and local positive inversion (OD3 in Figs. 6d, e, f, 7 and 10 to 13). This period is characterized by inversion and acceleration of low rate subsidence (patterns c and b: ILRS – ALRS, Fig. 14). Some of the Middle to Late Devonian syntectonic structures and hiatuses (e.g., Givetian/Frasnian) are noticed in the Ahnet Basin (Wendt et al., 2006), on the Amguid Ridge (Wendt et al., 2009b), in the Illizi Basin (Boudjema, 1987; Chaumeau et al., 1961; Eschard et al., 2010; Fabre, 2005; Legrand, 1967a), on the Gargaf (Carruba et al., 2014; Collomb, 1962; Fabre, 2005; Massa, 1988) and elsewhere on the platform (Frizon de Lamotte et al., 2013).
- i., j. Pre-Hercynian to Hercynian geodynamic pulses (I and J Fig. 14). This period is organized in Early Carboniferous pre-Hercynian (I, Fig. 14) to Late Carboniferous–Early Permian Hercynian compressions limited by Mid Carboniferous tectonic quiescence/extension (J, Fig. 14). The Carboniferous period is characterized by a normal reactivation and local positive inversion of the previous structural patterns involving reverse faults, overturned folds, transpressional flower structures along strike-slip fault zones (Figs. 6f, 7b, c and d). The major Carboniferous tectonic event on the Saharan Platform impacted all arches and it is mainly controlled by near-vertical basement faults with a strike-slip component (Boote et al., 1998; Caby, 2003; Carruba et al., 2014; Haddoum et al., 2001, 2013; Liégeois et al., 2003; Wendt et al., 2009a; Zazoun, 2001, 2008). According to these authors basement fabric features exerted a very strong control on the structural evolution during the Hercynian deformation. Two major hiatuses (i.e., Mid Tournaisian to Mid Viséan–Serpukhovian) are recognized (Wendt et al., 2009a).

The geodynamic pulses attest to the reactivation of the terranes and associated lithospheric fault zones. This observation questions the nature of the Precambrian basement and associated structural heritage.

7 Basement characterization: Precambrian structural heritage

Geochronological data show that the different terranes were reworked during several main thermo-orogenic events. The

two main events deduced from geochronological data are the Neoproterozoic (i.e., Pan-African) and Paleoproterozoic (i.e., Eburnean) episodes (Bertrand and Caby, 1978). Aeromagnetic anomaly surveys are commonly used to analyze geological features such as rock types and fault zones (e.g., Turner et al., 2007). A similar study was led in the meantime showing similar interpretations (Bournas et al., 2003; Brahimi et al., 2018). In this study, these data highlight the geometries and the extension of the different terranes under the sedimentary cover. Four main domains can be identified from the aeromagnetic anomaly map, delimited by contrasted magnetic signatures and interpreted as suture zones (thick black lines, Fig. 15a). The study area is bounded to the south by the Tuareg Shield (TS), to the north by the south Atlantic Range, to the west by the West African Craton (WAC), and to the east by the East Saharan Craton (ESC) or Saharan Metacraton (Abdelsalam et al., 2002).

The magnetic disturbance features (Fig. 15a) show three main magnetic trends. A major N–S sinuous fabric and two minor sinuous 130–140° E and N45° E trends. The major N–S lineaments coincide with terrane boundaries and mega-shear zones (e.g., 4°50', 4°10', WOSZ, EOSZ, 8°30', RSZ shear zones; Fig. 1). Sigmoidal-shaped terranes 200 to 500 km long and 100 km wide are characterized (red lines in Fig. 15a). The whole assemblage forms a typical SC-shaped shear fabric (Choukroune et al., 1987) associated with vertical mega-shear zones and suture zones (e.g., WOSZ, EOSZ, 4°10', 4°50' or 8°30' Hoggar shear zones in Fig. 1). The SC fabrics combined with subvertical lithospheric shear zones (Fig. 16b and c) are typical features of the Paleoproterozoic accretionary orogens (Cagnard et al., 2011; Chardon et al., 2009). This architecture is concordant with the Neoproterozoic collage of the Tuareg Shield (i.e., mobile belt) between the West African Craton and the East Saharan Craton (i.e., cratonic blocks) described by (Coward and Ries, 2003; Craig et al., 2008).

The gravimetric anomaly map (Fig. 15b) shows a correlation between gravimetric anomalies and tectonic architecture (intracratonic syncline-shaped basin and neighboring arches). Positive anomalies (> 66 mGal) are mainly associated with arches, whereas negative anomalies are related to intracratonic basins (< 66 mGal). Nevertheless, negative anomaly disturbance is found in the Hoggar Massif probably due to Cenozoic volcanism and the Hoggar swell (Liégeois et al., 2005) or to Eocene Alpine intraplate lithospheric buckling (Rougier et al., 2013).

The Precambrian structural heritage is characterized by accreted lithospheric terranes limited by vertical strike-slip mega-shear zones (Fig. 16b and c). A zonation is observed between the Paleozoic basins and arches configurations and the different terranes (thermo-tectonic age). Arches are linked to Archean to Paleoproterozoic continental terranes in contrast to syncline-shaped basins which are associated with Meso-Neoproterozoic terranes (Figs. 1, 2 and 16a).

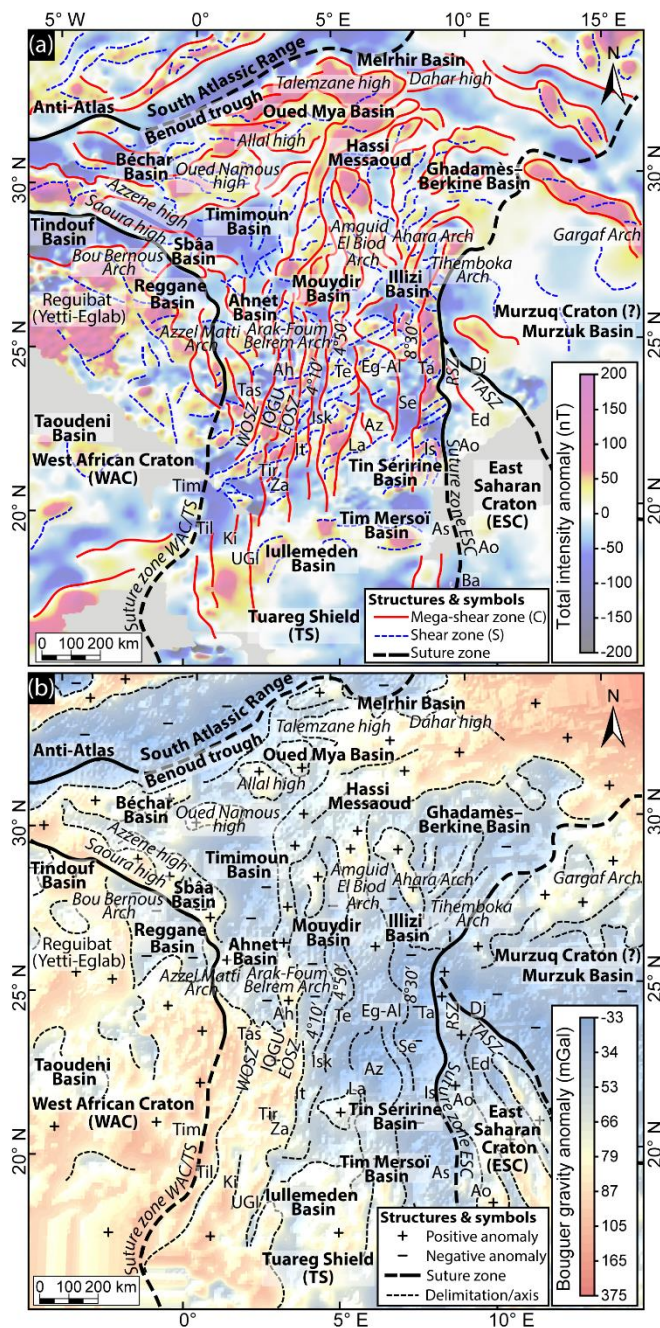


Figure 15. (a) Interpreted aeromagnetic anomaly map (<https://www.geomag.us/>, last access: 1 December 2016) of the Paleozoic North Saharan Platform (peri-Hoggar basins) showing the different terranes delimited by N–S, NW–SE, and NE–SW lineaments and megasigmoid structures (SC – shear fabrics). (b) Bouguer anomaly map (from the International Gravimetric Bureau: <http://bgi.omp.obs-mip.fr/>, last access: 1 December 2016) of the North Saharan Platform (peri-Hoggar basins) presenting evidence of positive anomalies under arches and negative anomalies under basins.

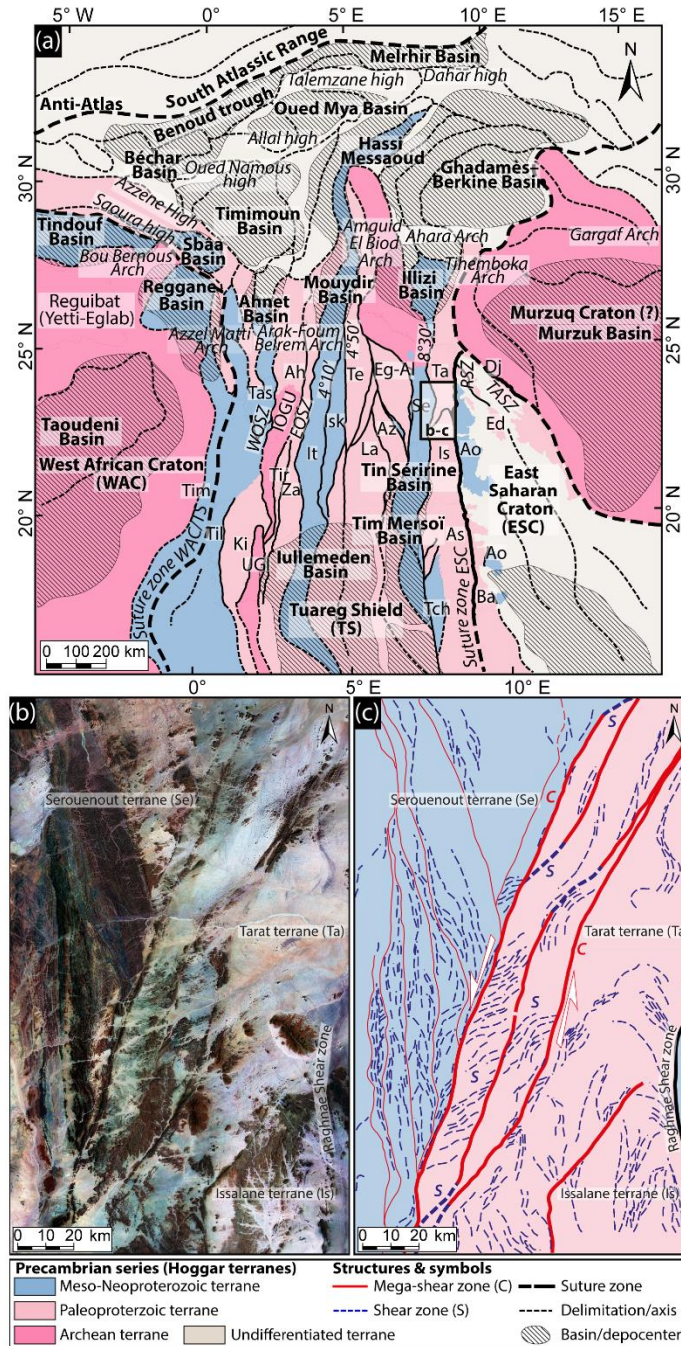


Figure 16. (a) Interpreted map of basement terranes according to their age (compilation of datasets in Fig. 1 and Supplement data 1); (b) Satellite images (7ETM+ from USGS: <https://earthexplorer.usgs.gov/>, last access: 29 October 2016) of Paleoproterozoic Issalane-Tarat terrane, central Hoggar (see C for location). (c) Interpreted satellite images of Paleoproterozoic Issalane-Tarat terrane showing sinistral sigmoid mega-structures associated with transcurrent lithospheric shear fabrics (SC).

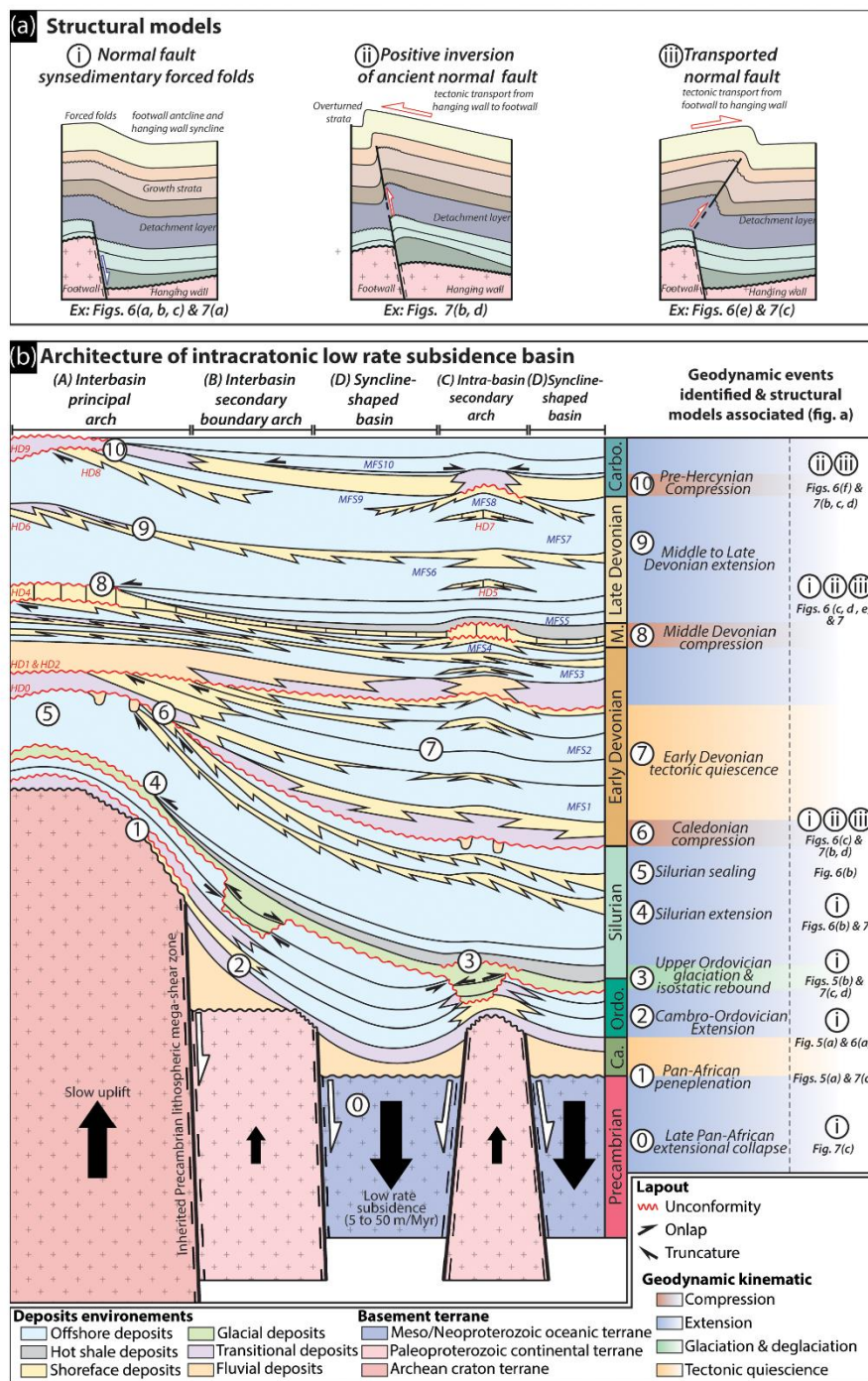


Figure 17. (a) Different structural model styles identified from the analysis of seismic profiles and from interpretation of the satellite images. (b) A conceptual model of the architecture of an intracratonic low rate subsidence basin and synthesis of the tectonic kinematics during the Paleozoic. Note that the differential subsidence between arches and basins is controlled by terrane heterogeneity (i.e., thermo-chronologic age, rheology, etc.).

8 Low subsidence rate intracratonic Paleozoic basins of the central Sahara provide a basis for an integrated modeling study

Paleozoic intracratonic basins with similar characteristics (architecture, subsidence rate, stratigraphic partitioning, alternating episodes of intraplate extension, and short duration compressions with periods of tectonic quiescence, etc.) have been documented in North America (e.g., Allen and Armitage, 2011; Beaumont et al., 1988; Burgess, 2008; Burgess et al., 1997; Eaton and Darbyshire, 2010; Pinet et al., 2013; Potter, 2006; Sloss, 1963; Xie and Heller, 2006), South America (Allen and Armitage, 2011; de Brito Neves et al., 1984; Milani and Zalan, 1999; de Oliveira and Mohriak, 2003; Soares et al., 1978; Zalan et al., 1990), Russia (Allen and Armitage, 2011; Nikishin et al., 1996) and Australia (Harris, 1994; Lindsay and Leven, 1996; Mory et al., 2017). However, the nature of the potential driving processes (lithospheric folding, far-field stresses, local increase in the geotherm, mechanical anisotropy from lithospheric rheological heterogeneity, etc.) associated with the formation of intracratonic Paleozoic basins remains highly speculative (Allen and Armitage, 2011; Armitage and Allen, 2010; Braun et al., 2014; Burgess and Gurnis, 1995; Burov and Cloetingh, 2009; Cacace and Scheck-Wenderoth, 2016; Célérier et al., 2005; Gac et al., 2013; Heine et al., 2008; Leeder, 1991; Vauchez et al., 1998).

The multiscale and multidisciplinary analysis performed in this study enable us to document a model of Paleozoic intracratonic central Saharan basins that couples basin architecture and basement structures (Fig. 17). While we do not provide any quantitative explanations for the dynamics of these basins, our synthesis highlights that their subsidence is not the result of a single process and we attempt to make a check-list here of the properties that a generic model of formation of such basins must capture:

- a. The association of syncline-shaped wide basins and neighboring arches (i.e., paleo-highs). The structural framework shows a close association of syncline-shaped basins, interbasin principal to secondary arches, and intra-basin secondary arches (see Fig. 2).
- b. By local horst and graben architecture linked to steep-dipping planar normal faults and associated with normal fault-related fold structures (i.e., forced folds; a, Fig. 17a). Locally, the extensional structures are disrupted by positive inversion structures (b, Fig. 17a) or transported normal faults (c, Fig. 17a).
- c. A low rate of subsidence ranging between 5 to 50 m Myr⁻¹ (Fig. 14).
- d. Long periods of extension and tectonic quiescence are interrupted by brief periods of compression or glaciation/deglaciation events (Beuf et al., 1971; Denis et al.,

2007; Le Heron et al., 2006). These periods of compression are possibly related to intraplate compression linked to distal orogenies (i.e., Late Silurian Caledonian event, Late Carboniferous Hercynian, (Frizon de Lamotte et al., 2013) or to intraplate arch uplift related to magmatism (Derder et al., 2016; Fabre, 2005; Frizon de Lamotte et al., 2013; Moreau et al., 1994).

- e. Synsedimentary divergent onlaps and local unconformities are identified from integrated seismic data, satellite images, and borehole data (Figs. 5, 6, 7 and 10 to 13). The periods of tectonic activity are characterized by normal to reverse reactivation of border faults, emplacement of wedge-shaped units, and erosional unconformities neighboring the arches.
- f. The stratigraphic architecture displays a lateral facies variation and partitioning between distal marine facies infilling the intracratonic basins (i.e., offshore deposits) and proximal amalgamated facies (i.e., fluvio-marine, shoreface) associated with prominent stratigraphic hiatus and erosional unconformities in the vicinity of the arches.
- g. A close connection is evidenced between the period of tectonic deformation and the presence of erosional unconformities (i.e., 2, 3, 6, 8, 10 geodynamic events in Fig. 17b). By contrast, the periods of tectonic quiescence and extension are characterized by low lateral facies variations, thin deposits, and the absence of erosional surfaces.
- h. The Precambrian heritage corresponds to Archean to Paleoproterozoic terranes identified in the Hoggar Massif and reactivated during the Meso-Neoproterozoic Pan-African cycle (Fig. 1). The Precambrian lithospheric heterogeneity illustrated by the different characteristics of Precambrian terranes (wavelength, age, nature, fault zones) spatially control the emplacement of the syncline-shaped intracratonic basins underlain by Meso-Neoproterozoic oceanic terranes and the arches underlain by Archean to Paleoproterozoic continental terranes (Figs. 1, 2 and 16). Many authors suggest control of the basement fabrics is inherited from the Pan-African orogeny in the Saharan basins (Beuf et al., 1968b, 1971; Boote et al., 1998; Carruba et al., 2014; Coward and Ries, 2003; Eschard et al., 2010; Guiraud et al., 2005; Sharata et al., 2015).

9 Conclusions

Our integrated approach using both geophysical (seismic, gravity, aeromagnetic, etc.) and geological (well, seismic, satellite images, etc.) data has enabled us to decrypt the characteristics of the intracratonic Paleozoic Saharan basins and the control of the heterogeneous lithospheric heritage of the

horst and graben architecture, low rate subsidence, and the association of long-lived broad synclines and anticlines (i.e., arches swells, domes, highs or ridges) with very different wavelengths (λ) (tens to hundreds of kilometers). A coupled basin architecture and basement structures model is proposed (Fig. 17).

This study highlights a tight control of the heterogeneous lithosphere zonation over the structuring of the intracratonic central Saharan Basin. This particular type of basin is characterized by a low rate of subsidence and fault activation controlling the homogeneity of sedimentary facies and the distribution of the main unconformities. The low rate activation of vertical mega-shear zones bounding the intracratonic basin during Paleozoic times contrasts markedly with classic rift kinematics and architecture. Three different periods of tectonic compressional pulses (i.e., Caledonian, Middle to Late Devonian, and pre-Hercynian), extension, and quiescence are identified and controlled the sedimentary distribution (Fig. 17). An understanding of tectono-sedimentary interaction is key to understanding the distribution of the Paleozoic petroleum reservoirs of this first-order oil province.

Data availability. Seismic and well log data analysed in this study are part of the Neptune Energy/SONATRACH internal database. Unfortunately, they are not publicly available. Nonetheless, satellite images and geophysical data are all available (see data and methods).

Supplement. The Supplement related to this article is available online at: <https://doi.org/10.5194/se-9-1239-2018-supplement>.

Author contributions. The structural seismic and photogeology interpretation as well as the basement interpretation and analyses throughout this study were mainly undertaken by PP and MG. Interpretations of the well logs, the sedimentology, and the sequence stratigraphy were primarily carried out by PP and EV. Backstripping was led by PP and controlled by IM and EP. The paper was written by PP, with additional input and scientific editing from MG and EV. All authors contributed to the technical interpretation, extensive discussions, and ideas throughout the study and the writing of the paper.

Competing interests. The authors declare that they have no conflict of interest.

Acknowledgements. We are most grateful to Neptune Energy and ENGIE which provided the database used in this paper and funded the work. Special thanks to the data management service of Neptune Energy (especially Aurelie Galvani) for their help with the database. Thanks also go to Jobst Wendt, Réda Samy Zazoun, and

Fabio Lottaroli for detailed reviews/comments, along with a short comment from Alexander Peace, which considerably enriched and improved this paper.

Edited by: Mark Allen

Reviewed by: Reda Samy Zazoun, Fabio Lottaroli, and Jobst Wendt

References

- Abdelsalam, M. G., Liégeois, J.-P., and Stern, R. J.: The saharan metacraton, *J. Afr. Earth Sci.*, 34, 119–136, 2002.
- Abdesselam-Rouighi, F.: Etude palynologique du sondage Sebkhel El Melah (unpublished), Entreprise nationale Sonatrach division hydrocarbures direction Laboratoire central des hydrocarbures, Boumerdès, 1977.
- Abdesselam-Rouighi, F.: Résultats de l'étude palynologiques des sondages Garet El Guefoul Bassin de l'Ahnet-Mouydir (unpublished), Entreprise nationale Sonatrach division hydrocarbures direction Laboratoire central des hydrocarbures, Boumerdès, 1991.
- Ahmed, A. A.-K. and Moussine-Pouchkine, A.: Lithostratigraphie, sédimentologie et évolution de deux bassins molassiques intramontagneux de la chaîne Pan-Africaine: la Série pourprée de l'Ahnet, Nord-Ouest du Hoggar, Algérie, *J. Afr. Earth Sci.*, 6, 525–535, 1987.
- Aigner, T.: Storm depositional systems: dynamic stratigraphy in modern and ancient shallow-marine sequences, *Lect. Notes Earth Sci. Berl. Springer Verl.*, 3, 1–158, 1985.
- Allen, J. R. L.: Studies in fluvial sedimentation: bars, bar-complexes and sandstone sheets (low-sinuosity braided streams) in the Brownstones (L. Devonian), Welsh Borders, *Sediment. Geol.*, 33, 237–293, 1983.
- Allen, P. A. and Allen, J. R.: Subsidence and thermal history, in *Basin analysis: Principles and applications*, 349–401, Wiley-Blackwell, Oxford, 2005.
- Allen, P. A. and Armitage, J. J.: Cratonic Basins, in *Tectonics of Sedimentary Basins*, edited by: Busby, C. and Azor, A., 602–620, John Wiley & Sons, Ltd., 2011.
- Angevine, C. L., Heller, P. L., and Paola, C.: Quantitative sedimentary basin modeling, *American Association of Petroleum Geologists*, 1990.
- Armitage, J. J. and Allen, P. A.: Cratonic basins and the long-term subsidence history of continental interiors, *J. Geol. Soc.*, 167, 61–70, <https://doi.org/10.1144/0016-76492009-108>, 2010.
- H. Askri, A. Belmecheri, B. Benrabah, A. Boudjema, K. Boumendjel, M. Daoudi, M. Drid, T. Ghalem, A. M. Docca, H. Ghandriche, A. Ghomari, N. Guellati, M. Khennous, R. Lounici, H. Naili, D. Takherist, and M. Terkmani: Geology of Algeria, in *Well Evaluation Conference Algeria*, 1–93, Schlumberger-Sonatrach., 1995.
- Azzoune, N.: Analyse palynologique de trois (03) échantillons de carottes du sondages W7, Sonatrach (unpublished), Entreprise nationale Sonatrach division hydrocarbures direction Laboratoire central des hydrocarbures, Boumerdès, 1999.
- Badalini, G., Redfern, J., and Carr, I. D.: A synthesis of current understanding of the structural evolution of North Africa, *J. Petrol. Geol.*, 25, 249–258, 2002.

- Beaumont, C., Quinlan, G., and Hamilton, J.: Orogeny and stratigraphy: Numerical models of the Paleozoic in the eastern interior of North America, *Tectonics*, 7, 389–416, 1988.
- Bellahsen, N. and Daniel, J. M.: Fault reactivation control on normal fault growth: an experimental study, *J. Struct. Geol.*, 27, 769–780, <https://doi.org/10.1016/j.jsg.2004.12.003>, 2005.
- Bennacef, A., Beuf, S., Biju-Duval, B., de Charpal, O., Gariel, O., and Rognon, P.: Example of Cratonic Sedimentation: Lower Paleozoic of Algerian Sahara, *AAPG Bull.*, 55, 2225–2245, 1971.
- Bennacef, A., Attar, A., Froukhi, R., Beuf, S., Philippe, G., Schmerber, G., and Vermeire, J. C.: Cartes Géologiques d'Iherir-Dider (NG-32-IX), Iherir (NG-32-X), Illizi (NG-32-XV), Aharhar (NG-32-VIII), Oued Samène (NG-32-XIV), Erg Tihodaine (NG-32-VII), Tin Alkoun (NG-32-V), Djanet (NG-32-IV), Ta-N-Mellet (NG-32-XIII), Ta-N-Elak (NG-32-XIX), Fort Tarat (NG-32-XVI), Tilmas El Mra (NG-31-XXIV), Ers Oum El Lil (NG-31-XXII), Amguid (NG-31-XVIII), 1/200000 Sonatrach-Ministère de l'Industrie et des Mines, Algérie, 1974.
- Bensalah, A., Beuf, S., Gabriel, O., Philippe, G., Lacot, R., Paris, A., Basseto, D., Conrad, J., and Moussine-Pouchkine, A.: Cartes Géologiques de Khanguet El Hadid (NG-31-XVII), Ain Tidjoubar (NG-31-XVI), Oued Djaret (NG-31-XV), Aoulef El Arab (NG-31-XIV), Reggane (NG-31-XIII), Ifetessene (NG-31-IX), Arak (NG-31-X et NG-31-IV), Meredoua (NG-31-XIII), Tanezrouft (NG-31-VII et NG-31-I), In Heguis (NG-31-IX), Tin Senasset (NG-31-III), Ouallene (NG-31-II) 1/200000 Sonatrach-Ministère de l'Industrie et des Mines, Algérie, 1971.
- Berger, J., Ouzegane, K., Bendaoud, A., Liégeois, J.-P., Kié-nast, J.-R., Bruguier, O., and Caby, R.: Continental subduction recorded by Neoproterozoic eclogite and garnet amphibolites from Western Hoggar (Tassendjanet terrane, Tuareg Shield, Algeria), *Precambrian Res.*, 247, 139–158, <https://doi.org/10.1016/j.precamres.2014.04.002>, 2014.
- Bertrand, J. M. L. and Caby, R.: Geodynamic evolution of the Pan-African orogenic belt: A new interpretation of the Hoggar shield (Algerian Sahara), *Geol. Rundsch.*, 67, 357–388, <https://doi.org/10.1007/BF01802795>, 1978.
- Beuf, S. and Montadert, L.: Géologie-sur une discordance angulaire entre les unités II et III du Cambro-Ordovicien au sud-est de la plaine de Dider (Tassili des Ajjers), *Compte Rendus Hebd. Séances L'Académie Sci.*, 254, 1108–1109, 1962.
- Beuf, S., Biju-Duval, B., Mauvier, A., and Legrand, P.: Nouvelles observations sur le “Cambro-Ordovicien” du Bled El Mass (Sahara central), *Publ. Serv. Géologique Algér. Bull.*, 38, 39–51, 1968a.
- Beuf, S., Biju-Duval, B., De Charpal, O., Gariel, O., Bennacef, A., Black, R., Arene, J., Boissonnas, J., Chachau, F., and Guérangé, B.: Une conséquence directe de la structure du bouclier africain: L'ébauche des bassins de l'Ahnet et du Mouydir au Paléozoïque inférieur, *Publ. Serv. Géologique L'Algérie Nouv. Sér. Bull.*, 38, 105–134, 1968b.
- Beuf, S., Biju-Duval, B., De Charpal, O., and Gariel, O.: Homogénéité des directions des paléocourants du Dévonien inférieur au Sahara central, *Comptes Rendus L'Académie Sci. Sér. D*, 268, 2026–2029, 1969.
- Beuf, S., Biju-Duval, B., de Charpal, O., Rognon, P., Gabriel, O., and Bennacef, A.: Les grès du Paléozoïque inférieur au Sahara: Sédimentation et discontinuités évolution structurale d'un craton, *Technip.*, Paris., 1971.
- Biju-Duval, B., de Charpal, O., Beuf, S., and Bennacef, A.: Lithostratigraphie du Dévonien inférieur dans l'Ahnet et le Mouydir (Sahara Central), *Bull. Serv. Géologique Algérie*, 38, 83–104, 1968.
- Black, R., Latouche, L., Liégeois, J. P., Caby, R., and Bertrand, J. M.: Pan-African displaced terranes in the Tuareg shield (central Sahara), *Geology*, 22, 641–644, 1994.
- Bonini, M., Sani, F., and Antonielli, B.: Basin inversion and contractional reactivation of inherited normal faults: A review based on previous and new experimental models, *Tectonophysics*, 522–523, 55–88, <https://doi.org/10.1016/j.tecto.2011.11.014>, 2012.
- Boote, D. R. D., Clark-Lowes, D. D., and Traut, M. W.: Palaeozoic petroleum systems of North Africa, *Geol. Soc. Lond. Spec. Publ.*, 132, 7–68, <https://doi.org/10.1144/GSL.SP.1998.132.01.02>, 1998.
- Borocco, J. and Nyssen, R.: Nouvelles observations sur les “gres inferieurs” cambro-ordoviciens du Tassili interne (Nord-Hoggar), *Bull. Société Géologique Fr.*, S7-I, 197–206, <https://doi.org/10.2113/gssgfbull.S7-I.2.197>, 1959.
- Boudjema, A.: Evolution structurale du bassin pétrolier “triasique” du Sahara nord oriental (Algérie), *Doctoral dissertation*, Paris 11, France, 1987.
- Boumendjel, K.: Les chitinozoaires du silurien supérieur et du dévonien du Sahara algérien (cadre géologique, systématique, biostratigraphie), *Doctoral dissertation*, Rennes 1, France, 1987.
- Boumendjel, K., Loboziak, S., Paris, F., Steemans, P., and Streel, M.: Biostratigraphie des Miospores et des Chitinozoaires du Silurien supérieur et du Dévonien dans le bassin d'Illizi (S.E. du Sahara algérien), *Geobios*, 21, 329–357, [https://doi.org/10.1016/S0016-6995\(88\)80057-3](https://doi.org/10.1016/S0016-6995(88)80057-3), 1988.
- Bournas, N., Galdeano, A., Hamoudi, M., and Baker, H.: Interpretation of the aeromagnetic map of Eastern Hoggar (Algeria) using the Euler deconvolution, analytic signal and local wavenumber methods, *J. Afr. Earth Sci.*, 37, 191–205, <https://doi.org/10.1016/j.jafrearsci.2002.12.001>, 2003.
- Brahimi, S., Liégeois, J.-P., Ghienne, J.-F., Munsch, M., and Bourmatte, A.: The Tuareg shield terranes revisited and extended towards the northern Gondwana margin: Magnetic and gravimetric constraints, *Earth-Sci. Rev.*, 185, 572–599, <https://doi.org/10.1016/j.earscirev.2018.07.002>, 2018.
- Braun, J., Simon-Labric, T., Murray, K. E., and Reiners, P. W.: Topographic relief driven by variations in surface rock density, *Nat. Geosci.*, 7, 534–540, <https://doi.org/10.1038/ngeo2171>, 2014.
- Buchanan, P. G. and McClay, K. R.: Sandbox experiments of inverted listric and planar fault systems, *Tectonophysics*, 188, 97–115, [https://doi.org/10.1016/0040-1951\(91\)90317-L](https://doi.org/10.1016/0040-1951(91)90317-L), 1991.
- Burgess, P. M.: Phanerozoic evolution of the sedimentary cover of the North American craton, in: *Sedimentary Basins of the World*, 5, 31–63, Elsevier, 2008.
- Burgess, P. M. and Gurnis, M.: Mechanisms for the formation of cratonic stratigraphic sequences, *Earth Planet. Sc. Lett.*, 136, 647–663, [https://doi.org/10.1016/0012-821X\(95\)00204-P](https://doi.org/10.1016/0012-821X(95)00204-P), 1995.
- Burgess, P. M., Gurnis, M., and Moresi, L.: Formation of sequences in the cratonic interior of North America by interaction between mantle, eustatic, and stratigraphic processes, *Geol. Soc. Am. Bull.*, 109, 1515–1535, 1997.
- Burke, K., MacGregor, D. S., and Cameron, N. R.: Africa's petroleum systems: four tectonic “Aces” in the past 600 million years, *Geol. Soc. Lond. Spec. Publ.*, 207, 21–60, 2003.

- Burov, E. and Cloetingh, S.: Controls of mantle plumes and lithospheric folding on modes of intraplate continental tectonics: differences and similarities, *Geophys. J. Int.*, 178, 1691–1722, <https://doi.org/10.1111/j.1365-246X.2009.04238.x>, 2009.
- Butler, R. W. H.: The influence of pre-existing basin structure on thrust system evolution in the Western Alps, *Geol. Soc. Lond. Spec. Publ.*, 44, 105–122, <https://doi.org/10.1144/GSL.SP.1989.044.01.07>, 1989.
- Caby, R.: Terrane assembly and geodynamic evolution of central-western Hoggar: a synthesis, *J. Afr. Earth Sci.*, 37, 133–159, <https://doi.org/10.1016/j.jafrearsci.2003.05.003>, 2003.
- Cacace, M. and Scheck-Wenderoth, M.: Why intracontinental basins subside longer: 3-D feedback effects of lithospheric cooling and sedimentation on the flexural strength of the lithosphere: Subsidence at Intracontinental Basins, *J. Geophys. Res.-Sol. Ea.*, 121, 3742–3761, <https://doi.org/10.1002/2015JB012682>, 2016.
- Cagnard, F., Barbey, P., and Gapais, D.: Transition between “Archaean-type” and “modern-type” tectonics: Insights from the Finnish Lapland Granulite Belt, *Precambrian Res.*, 187, 127–142, <https://doi.org/10.1016/j.precamres.2011.02.007>, 2011.
- Carr, I. D.: Second-Order Sequence Stratigraphy of the Palaeozoic of North Africa, *J. Petrol. Geol.*, 25, 259–280, <https://doi.org/10.1111/j.1747-5457.2002.tb00009.x>, 2002.
- Carruba, S., Perotti, C., Rinaldi, M., Bresciani, I., and Bertozzi, G.: Intraplate deformation of the Al Qarqaf Arch and the southern sector of the Ghadames Basin (SW Libya), *J. Afr. Earth Sci.*, 97, 19–39, <https://doi.org/10.1016/j.jafrearsci.2014.05.001>, 2014.
- Catuneanu, O., Abreu, V., Bhattacharya, J. P., Blum, M. D., Dalrymple, R. W., Eriksson, P. G., Fielding, C. R., Fisher, W. L., Galloway, W. E., Gibling, M. R., Giles, K. A., Holbrook, J. M., Jordan, R., Kendall, C. G. S. C., Macurda, B., Martinsen, O. J., Miall, A. D., Neal, J. E., Nummedal, D., Pomar, L., Posamentier, H. W., Pratt, B. R., Sarg, J. F., Shanley, K. W., Steel, R. J., Strasser, A., Tucker, M. E., and Winker, C.: Towards the standardization of sequence stratigraphy, *Earth-Sci. Rev.*, 92, 1–33, <https://doi.org/10.1016/j.earscirev.2008.10.003>, 2009.
- Célérier, J., Sandiford, M., Hansen, D. L., and Quigley, M.: Modes of active intraplate deformation, Flinders Ranges, Australia, *Tectonics*, 24, 1–17, <https://doi.org/10.1029/2004TC001679>, 2005.
- Chardon, D., Gapais, D., and Cagnard, F.: Flow of ultrahot orogens: A view from the Precambrian, clues for the Phanerozoic, *Tectonophysics*, 477, 105–118, <https://doi.org/10.1016/j.tecto.2009.03.008>, 2009.
- Chaumeau, J., Legrand, P., and Renaud, A.: Contribution à l'étude du Couvinien dans le bassin de Fort-de-Polignac (Sahara), *Bull. Société Géologique Fr.*, S7-III, 449–456, <https://doi.org/10.2113/gssgfbull.S7-III.5.449>, 1961.
- Chavand, J. C. and Claracq, P.: La disparition du Tassili externe à l'E de Fort-Polignac (Sahara central), *CR Soc Géol Fr*, 1959, 172–174, 1960.
- Choukroune, P., Gapais, D., and Merle, O.: Shear criteria and structural symmetry, *J. Struct. Geol.*, 9, 525–530, [https://doi.org/10.1016/0191-8141\(87\)90137-4](https://doi.org/10.1016/0191-8141(87)90137-4), 1987.
- Claracq, P., Fabre, C., Freulon, J. M., and Nougarede, F.: Une discordance angulaire dans les “Grès inférieurs” de l'Adrar Tan Elak (Sahara central), *C. r. Somm. Séances Soc. Géologique Fr.*, 309–310, 1958.
- Collomb, G. R.: Étudé géologique du Jebel Fezzan et de sa bordure paléozoïque, *Compagnie française des pétroles*, 1962.
- Conrad, J.: Les grandes lignes stratigraphiques et sédimentologiques du Carbonifère de l'Ahnet-Mouydir (Sahara central algérien), *Rev. Inst. Fr. Pétrole*, 28, 3–18, 1973.
- Conrad, J.: Les séries carbonifères du Sahara central algérien: stratigraphie, sédimentation, évolution structurale, Doctoral dissertation, Université Aix-Marseille III, France, 1984.
- Coward, M. P. and Ries, A. C.: Tectonic development of North African basins, *Geol. Soc. Lond. Spec. Publ.*, 207, 61–83, <https://doi.org/10.1144/GSL.SP.2003.207.4>, 2003.
- Cózar, P., Somerville, I. D., Vachard, D., Coronado, I., García-Frank, A., Medina-Varea, P., Said, I., Del Moral, B., and Rodríguez, S.: Upper Mississippian to lower Pennsylvanian biostratigraphic correlation of the Sahara Platform successions on the northern margin of Gondwana (Morocco, Algeria, Libya), *Gondwana Res.*, 36, 459–472, <https://doi.org/10.1016/j.gr.2015.07.019>, 2016.
- Craig, J., Rizzi, C., Said, F., Thusu, B., Luning, S., Asbali, A. I., Keeley, M. L., Bell, J. F., Durham, M. J., and Eales, M. H.: Structural styles and prospectivity in the Precambrian and Palaeozoic hydrocarbon systems of North Africa, *Geol. East Libya*, 4, 51–122, 2008.
- Dalrymple, R. W. and Choi, K.: Morphologic and facies trends through the fluvial-marine transition in tide-dominated depositional systems: A schematic framework for environmental and sequence-stratigraphic interpretation, *Earth-Sci. Rev.*, 81, 135–174, <https://doi.org/10.1016/j.earscirev.2006.10.002>, 2007.
- Dalrymple, R. W., Zaitlin, B. A., and Boyd, R.: A conceptual model of estuarine sedimentation, *J. Sediment. Petrol.*, 62, 1130–1146, 1992.
- Dalrymple, R. W., Mackay, D. A., Ichaso, A. A., and Choi, K. S.: Processes, Morphodynamics, and Facies of Tide-Dominated Estuaries, in *Principles of Tidal Sedimentology*, 79–107, Springer, Dordrecht, 2012.
- de Brito Neves, B. B., Fuck, R. A., Cordani, U. G., and Thomaz, F., A.: Influence of basement structures on the evolution of the major sedimentary basins of Brazil: A case of tectonic heritage, *J. Geodyn.*, 1, 495–510, [https://doi.org/10.1016/0264-3707\(84\)90021-8](https://doi.org/10.1016/0264-3707(84)90021-8), 1984.
- Denis, M., Buoncristiani, J.-F., Konaté, M., Ghienne, J.-F., and Guiraud, M.: Hirnantian glacial and deglacial record in SW Djado Basin (NE Niger), *Geodin. Acta*, 20, 177–195, <https://doi.org/10.3166/ga.20.177-195>, 2007.
- de Oliveira, D. C. and Mohriak, W. U.: Jaibaras trough: an important element in the early tectonic evolution of the Parnaíba interior sag basin, Northern Brazil, *Mar. Petrol. Geol.*, 20, 351–383, [https://doi.org/10.1016/S0264-8172\(03\)00044-8](https://doi.org/10.1016/S0264-8172(03)00044-8), 2003.
- Derder, M. E. M., Maouche, S., Liégeois, J. P., Henry, B., Amenna, M., Ouabadi, A., Bellon, H., Bruguier, O., Bayou, B., Bestandji, R., Nouar, O., Bouabdallah, H., Ayache, M., and Beddiaf, M.: Discovery of a Devonian mafic magmatism on the western border of the Murzuq basin (Saharan metacraton): Paleomagnetic dating and geodynamical implications, *J. Afr. Earth Sci.*, 115, 159–176, <https://doi.org/10.1016/j.jafrearsci.2015.11.019>, 2016.
- Djouder, H., Lüning, S., Da Silva, A.-C., Abdallah, H., and Boulvain, F.: Silurian deltaic progradation, Tassili n'Ajjer plateau, south-eastern Algeria: Sedimentology, ichnology and sequence stratigraphy, *J. Afr. Earth Sci.*, 142, 170–192, 2018.
- Dokka, A. M.: Sedimentological core description WELL: W7, Block – 340, (District – 3) (unpublished), Core description,

- Sonatrach division exploration direction des opérations département assistance aux opérations service géologique, Algérie, 1999.
- Dott, R. H. and Bourgeois, J.: Hummocky stratification: Significance of its variable bedding sequences, *Geol. Soc. Am. Bull.*, 93, 663–680, [https://doi.org/10.1130/0016-7606\(1982\)93<663:HSSOIV>2.0.CO;2](https://doi.org/10.1130/0016-7606(1982)93<663:HSSOIV>2.0.CO;2), 1982.
- Dubois, P.: Stratigraphie du Cambro-Ordovicien du Tassili n'Ajjer (Sahara central), *Bull. Société Géologique Fr.*, S7-III, 206–209, <https://doi.org/10.2113/gssgfbull.S7-III.2.206>, 1961.
- Dubois, P. and Mazelet, P.: Stratigraphie du Silurien du Tassili N'Ajjer, *Bull. Société Géologique Fr.*, S7-VI, 586–591, <https://doi.org/10.2113/gssgfbull.S7-VI.4.586>, 1964.
- Dubois, P., Beuf, S., and Bijou-Duval, B.: Lithostratigraphie du Dévonien inférieur gréseux du Tassili n'Ajjer, in *Symposium on the Lower Devonian and its limits*: Bur. Recherche Geol. et Minières Mem, 227–235, 1967.
- Dumas, S. and Arnott, R. W. C.: Origin of hummocky and swaley cross-stratification – the controlling influence of unidirectional current strength and aggradation rate, *Geology*, 34, 1073–1076, 2006.
- Eaton, D. W. and Darbyshire, F.: Lithospheric architecture and tectonic evolution of the Hudson Bay region, *Tectonophysics*, 480, 1–22, <https://doi.org/10.1016/j.tecto.2009.09.006>, 2010.
- Echikh, K.: Geology and hydrocarbon occurrences in the Ghadames basin, Algeria, Tunisia, Libya, *Geol. Soc. Lond. Spec. Publ.*, 132, 109–129, 1998.
- Eschard, R., Desaubliaux, G., Deschamps, R., Montadert, L., Ravenne, C., Bekkouche, D., Abdallah, H., Belhaouas, S., Benkouider, M., Braïk, F., Henniche, M., Maache, N., and Mouaici, R.: Illizi-Berkine Devonian Reservoir Consortium (unpublished), Institut Française du Pétrole – Sontrach, Algérie, 1999.
- Eschard, R., Abdallah, H., Braïk, F., and Desaubliaux, G.: The Lower Paleozoic succession in the Tassili outcrops, Algeria: sedimentology and sequence stratigraphy, *First Break*, 23, 27–36, 2005.
- Eschard, R., Braïk, F., Bekkouche, D., Rahuma, M. B., Desaubliaux, G., Deschamps, R., and Proust, J. N.: Palaeohighs: their influence on the North African Palaeozoic petroleum systems, *Pet. Geol. Mature Basins New Front. 7th Pet. Geol. Conf.*, 707–724, 2010.
- Fabre, J.: Les séries paléozoïques d'Afrique: une approche, *J. Afr. Earth Sci. Middle East*, 7, 1–40, [https://doi.org/10.1016/0899-5362\(88\)90051-6](https://doi.org/10.1016/0899-5362(88)90051-6), 1988.
- Fabre, J.: Géologie du Sahara occidental et central, Musée royal de l'Afrique centrale, 2005.
- Fabre, J., Kaci, A. A., Bouïma, T., and Moussine-Pouchkine, A.: Le cycle molassique dans le Rameau trans-saharien de la chaîne panafricaine, *J. Afr. Earth Sci.*, 7, 41–55, [https://doi.org/10.1016/0899-5362\(88\)90052-8](https://doi.org/10.1016/0899-5362(88)90052-8), 1988.
- Fekirine, B. and Abdallah, H.: Palaeozoic lithofacies correlates and sequence stratigraphy of the Saharan Platform, Algeria, *Geol. Soc. Lond. Spec. Publ.*, 132, 97–108, <https://doi.org/10.1144/GSL.SP.1998.132.01.05>, 1998.
- Fezaa, N., Liégeois, J.-P., Abdallah, N., Cherfouh, E. H., De Waele, B., Bruguier, O., and Ouabadi, A.: Late Ediacaran geological evolution (575–555Ma) of the Djanet Terrane, Eastern Hoggar, Algeria, evidence for a Murzukian intracontinental episode, *Precambrian Res.*, 180, 299–327, <https://doi.org/10.1016/j.precamres.2010.05.011>, 2010.
- Follot, J.: Sur l'existence de mouvements calédoniens au Mouydir (Sahara Central), *Compte Rendus Hebd. Séances L'Académie Sci.*, 230, 2217–2218, 1950.
- Frey, R. W., Pemberton, S. G., and Saunders, T. D.: Ichnofacies and bathymetry: a passive relationship, *J. Paleontol.*, 64, 155–158, 1990.
- Frizon de Lamotte, D., Tavakoli-Shirazi, S., Leturmy, P., Averbuch, O., Mouchot, N., Raulin, C., Leparmentier, F., Blanpied, C., and Ringenbach, J.-C.: Evidence for Late Devonian vertical movements and extensional deformation in northern Africa and Arabia: Integration in the geodynamics of the Devonian world: Devonian evolution Northern Gondwana, *Tectonics*, 32, 107–122, <https://doi.org/10.1002/tect.20007>, 2013.
- Fröhlich, S., Petitpierre, L., Redfern, J., Bodin, S., and Lang, S.: Sedimentological and sequence stratigraphic analysis of Carboniferous deposits in western Libya: Recording the sedimentary response of the northern Gondwana margin to climate and sea-level changes, *J. Afr. Earth Sci.*, 57, 279–296, <https://doi.org/10.1016/j.jafrearsci.2009.09.007>, 2010.
- Gac, S., Huismans, R. S., Simon, N. S. C., Podladchikov, Y. Y., and Faleide, J. I.: Formation of intracratonic basins by lithospheric shortening and phase changes: a case study from the ultra-deep East Barents Sea basin, *Terra Nova*, 25, 459–464, <https://doi.org/10.1111/ter.12057>, 2013.
- Galeazzi, S., Point, O., Haddadi, N., Mather, J., and Druésne, D.: Regional geology and petroleum systems of the Illizi-Berkine area of the Algerian Saharan Platform: An overview, *Mar. Petrol. Geol.*, 27, 143–178, <https://doi.org/10.1016/j.marpetgeo.2008.10.002>, 2010.
- Galloway, W. E.: Genetic Stratigraphic Sequences in Basin Analysis I: Architecture and Genesis of Flooding-Surface Bounded Depositional Units, *AAPG Bull.*, 73, 125–142, 1989.
- Galushkin, Y. I. and Eloghbi, S.: Thermal history of the Murzuq Basin, Libya, and generation of hydrocarbons in its source rocks, *Geochem. Int.*, 52, 486–499, <https://doi.org/10.1134/S0016702914060032>, 2014.
- Gariel, O., de Charpal, O., and Bennacef, A.: Sur la sédimentation des gres du Cambro-Ordovicien (Unité II) dans l'Ahnet et le Mouydir (Sahara central): Algeria, *Serv. Geol. Bull N Ser*, 38, 7–37, 1968.
- Ghienne, J.-F., Deynoux, M., Manatschal, G., and Rubino, J.-L.: Palaeovalleys and fault-controlled depocentres in the Late-Ordovician glacial record of the Murzuq Basin (central Libya), *C. R. Geosci.*, 335, 1091–1100, <https://doi.org/10.1016/j.crte.2003.09.010>, 2003.
- Ghienne, J.-F., Moreau, J., Degermann, L., and Rubino, J.-L.: Lower Palaeozoic unconformities in an intracratonic platform setting: glacial erosion versus tectonics in the eastern Murzuq Basin (southern Libya), *Int. J. Earth Sci.*, 102, 455–482, <https://doi.org/10.1007/s00531-012-0815-y>, 2013.
- Gindre, L., Le Heron, D., and Bjørnseth, H. M.: High resolution facies analysis and sequence stratigraphy of the Siluro-Devonian succession of Al Kufrah basin (SE Libya), *J. Afr. Earth Sci.*, 76, 8–26, <https://doi.org/10.1016/j.jafrearsci.2012.08.002>, 2012.
- Girard, F., Ghienne, J.-F., and Rubino, J.-L.: Channelized sandstone bodies (“cordons”) in the Tassili N'Ajjer (Algeria & Libya): snapshots of a Late Ordovician proglacial out-

- wash plain, *Geol. Soc. Lond. Spec. Publ.*, 368, 355–379, <https://doi.org/10.1144/SP368.3>, 2012.
- Grasemann, B., Martel, S., and Passchier, C.: Reverse and normal drag along a fault, *J. Struct. Geol.*, 27, 999–1010, <https://doi.org/10.1016/j.jsg.2005.04.006>, 2005.
- Greigert, J. and Pougnet, R.: Carte Géologique du Niger, 1/2000000, BRGM, République du Niger, 1965.
- Guiraud, R., Bosworth, W., Thierry, J., and Delplanque, A.: Phanerozoic geological evolution of Northern and Central Africa: An overview, *J. Afr. Earth Sci.*, 43, 83–143, <https://doi.org/10.1016/j.jafrearsci.2005.07.017>, 2005.
- Haddoum, H., Guiraud, R., and Moussine-Pouchkine, A.: Hercynian compressional deformations of the Ahnet–Mouydir Basin, Algerian Saharan Platform: far-field stress effects of the Late Palaeozoic orogeny, *Terra Nova*, 13, 220–226, 2001.
- Haddoum, H., Mokri, M., Ouzegane, K., Ait-Djaffer, S., and Djemai, S.: Extrusion de l'In Ouzal vers le Nord (Hoggar occidental, Algérie): une conséquence d'un poinçonnement panafricain, *J. Hydrocarb. Mines Environ. Res. Vol.*, 4, 6–16, 2013.
- Haq, B. U. and Schutter, S. R.: A Chronology of Paleozoic Sea-Level Changes, *Science*, 322, 64–68, <https://doi.org/10.1126/science.1161648>, 2008.
- Harris, L. B.: Structural and tectonic synthesis for the Perth basin, Western Australia, *J. Petrol. Geol.*, 17, 129–156, 1994.
- Hartley, R. W. and Allen, P. A.: Interior cratonic basins of Africa: relation to continental break-up and role of mantle convection, *Basin Res.*, 6, 95–113, 1994.
- Hassan, A.: Etude palynologique Paléozoïque du sondage Razzal-Allah-Nord (unpublished), Entreprise nationale Sonatrach division hydrocarbures direction Laboratoire central des hydrocarbures, Boumerdès, 1984.
- Heine, C., Dietmar Müller, R., Steinberger, B., and Torsvik, T. H.: Subsidence in intracontinental basins due to dynamic topography, *Phys. Earth Planet. Int.*, 171, 252–264, <https://doi.org/10.1016/j.pepi.2008.05.008>, 2008.
- Henniche, M.: Architecture et modèle de dépôts d'une série sédimentaire paléozoïque en contexte cratonique, Rennes 1, France, 2002.
- Holbrook, J. and Schumm, S. A.: Geomorphic and sedimentary response of rivers to tectonic deformation: a brief review and critique of a tool for recognizing subtle epeirogenic deformation in modern and ancient settings, *Tectonophysics*, 305, 287–306, 1999.
- Holland, H., Choubert, G., Bronner, G., Marchand, J., and Sougy, J.: Carte géologique du Maroc, scale 1: 1 000 000, Serv. Carte Géol. Maroc., 260, 1985.
- Holt, P. J., Allen, M. B., van Hunen, J., and Bjørnseth, H. M.: Lithospheric cooling and thickening as a basin forming mechanism, *Tectonophysics*, 495, 184–194, <https://doi.org/10.1016/j.tecto.2010.09.014>, 2010.
- Jacquemont, P., Jutard, G., Plauchut, B., Grégoire, J., and Mouflard, R.: Etude du bassin du Djado, *Bur. Rech. Pétroles Rapp.*, 1215, 1959.
- Jäger, H., Lewandowski, E., and Lampart, V.: Palynology of the upper Silurian to middle Devonian in the Reggane Basin, southern Algeria, *Ext. Abstr. DGMK-Tagungsbericht 2009-1 DGMKÖGEW Spring Meet. Celle*, 47–51, 2009.
- Jardiné, S. and Yapaudjian, L.: Lithostratigraphie et palynologie du Dévonien-Gothlandien gréseux du Bassin de Polignac (Sahara), *Rev. L'Institut Fr. Pétrole*, 23, 439–469, 1968.
- Jouliá, F.: Carte géologique de reconnaissance de la bordure sédimentaire occidentale de l'Air au 1/500 000, Éditions BRGM Orléans Fr., 1963.
- Kermandji, A. M.: Silurian–Devonian miospores from the western and central Algeria, *Rev. Micropaléontol.*, 50, 109–128, <https://doi.org/10.1016/j.revmic.2007.01.003>, 2007.
- Kermandji, A. M. H., Kowalski, M. W., and Pharissat, A.: Palynologie et séquences de l'Emsien de la région d'In Salah, Sahara central Algérien, *Bull. Société D'Histoire Nat. Pays Montbél.*, 301–306, 2003.
- Kermandji, A. M. H., Kowalski, W. M., and Touhami, F. K.: Miospore stratigraphy of Lower and early Middle Devonian deposits from Tidikelt, Central Sahara, Algeria, *Geobios*, 41, 227–251, <https://doi.org/10.1016/j.geobios.2007.05.002>, 2008.
- Kermandji, A. M. H., Touhami, F. K., Kowalski, W. M., Abbés, S. B., Boularak, M., Chabour, N., Laifa, E. L., and Hannachi, H. B.: Stratigraphie du Dévonien Inférieur du Plateau du Tidikelt d'In Salah (Sahara Central Algérie), *Commun. Geológicas*, 96, 67–82, 2009.
- Khalil, S. M. and McClay, K. R.: Extensional fault-related folding, northwestern Red Sea, Egypt, *J. Struct. Geol.*, 24, 743–762, 2002.
- Khiar, S.: Résultats palynologiques du sondage Garet El Guefoul (unpublished), Entreprise nationale Sonatrach division hydrocarbures direction Laboratoire central des hydrocarbures, Alger, 1974.
- Kracha, N.: Relation entre sédimentologie, fracturation naturelle et diagénèse d'un réservoir à faible perméabilité application aux réservoirs de l'Ordovicien bassin de l'Ahnet, Sahara central, Algérie, Doctoral dissertation, Université des sciences et technologies de Lille, France, 2011.
- Le Heron, D. P.: Interpretation of Late Ordovician glaciogenic reservoirs from 3-D seismic data: an example from the Murzuq Basin, Libya, *Geol. Mag.*, 147, 28–41, <https://doi.org/10.1017/S0016756809990586>, 2010.
- Le Heron, D. P., Craig, J., Sutcliffe, O. E., and Whittington, R.: Late Ordovician glaciogenic reservoir heterogeneity: An example from the Murzuq Basin, Libya, *Mar. Petrol. Geol.*, 23, 655–677, <https://doi.org/10.1016/j.marpetgeo.2006.05.006>, 2006.
- Le Heron, D. P., Craig, J., and Etienne, J. L.: Ancient glaciations and hydrocarbon accumulations in North Africa and the Middle East, *Earth-Sci. Rev.*, 93, 47–76, <https://doi.org/10.1016/j.earscirev.2009.02.001>, 2009.
- Leeder, M. R.: Denudation, vertical crustal movements and sedimentary basin infill, *Geol. Rundsch.*, 80, 441–458, <https://doi.org/10.1007/BF01829376>, 1991.
- Legrand, P.: Le Devonien du Sahara Algérien, *Can. Soc. Pet. Geol.*, 1, 245–284, 1967a.
- Legrand, P.: Nouvelles connaissances acquises sur la limite des systèmes Silurien et Dévonien au Sahara algérien, *Bull. Bur. Rech. Géologiques Minières*, 33, 119–37, 1967b.
- Legrand, P.: The lower Silurian graptolites of Oued In Djerane: a study of populations at the Ordovician–Silurian boundary, *Geol. Soc. Lond. Spec. Publ.*, 20, 145–153, <https://doi.org/10.1144/GSL.SP.1986.020.01.15>, 1986.

- Legrand, P.: Late Ordovician-early Silurian paleogeography of the Algerian Sahara, *Bull. Société Géologique Fr.*, 174, 19–32, 2003a.
- Legrand, P.: Silurian stratigraphy and paleogeography of the northern African margin of Gondwana, in: *Silurian Lands and Seas: Paleogeography Outside of Laurentia*, edited by: Landing, E. and Johnson, M. E., 59–104, New York, 2003b.
- Legrand-Blain, M.: Dynamique des Brachiopodes carbonifères sur la plate-forme carbonatée du Sahara algérien: paléoenvironnements, paléobiogéographie, évolution, Doctoral dissertation, Université de Bordeaux I, France, 1985.
- Lessa, G. and Masselink, G.: Morphodynamic evolution of a macrotidal barrier estuary, *Mar. Geol.*, 129, 25–46, 1995.
- Leuven, J. R. F. W., Kleinhans, M. G., Weisscher, S. A. H., and van der Vegt, M.: Tidal sand bar dimensions and shapes in estuaries, *Earth-Sci. Rev.*, 161, 204–223, <https://doi.org/10.1016/j.earscirev.2016.08.004>, 2016.
- Lewis, M. M., Jackson, C. A.-L., Gawthorpe, R. L., and Whipp, P. S.: Early synrift reservoir development on the flanks of extensional forced folds: A seismic-scale outcrop analog from the Hadahid fault system, Suez rift, Egypt, *AAPG Bull.*, 99, 985–1012, <https://doi.org/10.1306/12011414036>, 2015.
- Liégeois, J. P., Latouche, L., Boughrara, M., Navez, J., and Guiraud, M.: The LATEA metacraton (Central Hoggar, Tuareg shield, Algeria): behaviour of an old passive margin during the Pan-African orogeny, *J. Afr. Earth Sci.*, 37, 161–190, <https://doi.org/10.1016/j.jafrearsci.2003.05.004>, 2003.
- Liégeois, J.-P., Black, R., Navez, J., and Latouche, L.: Early and late Pan-African orogenies in the Air assembly of terranes (Tuareg Shield, Niger), *Precambrian Res.*, 67, 59–88, 1994.
- Liégeois, J.-P., Benhallou, A., Azzoumi-Sekkal, A., Yahiaoui, R., and Bonin, B.: The Hoggar swell and volcanism: Reactivation of the Precambrian Tuareg shield during Alpine convergence and West African Cenozoic volcanism, *Geol. Soc. Am. Spec. Pap.*, 388, 379–400, <https://doi.org/10.1130/0-8137-2388-4.379>, 2005.
- Liégeois, J.-P., Abdelsalam, M. G., Ennih, N., and Ouabadi, A.: Metacraton: Nature, genesis and behavior, *Gondwana Res.*, 23, 220–237, <https://doi.org/10.1016/j.gr.2012.02.016>, 2013.
- Lindsay, J. F. and Leven, J. H.: Evolution of a Neoproterozoic to Palaeozoic intracratonic setting, Officer Basin, South Australia, *Basin Res.*, 8, 403–424, <https://doi.org/10.1046/j.1365-2117.1996.00223.x>, 1996.
- Logan, P. and Duddy, I.: An investigation of the thermal history of the Ahnet and Reggane Basins, Central Algeria, and the consequences for hydrocarbon generation and accumulation, *Geol. Soc. Lond. Spec. Publ.*, 132, 131–155, 1998.
- Loi, A., Ghienne, J.-F., Dabard, M. P., Paris, F., Botquelen, A., Christ, N., Elaouad-Debbaj, Z., Gorini, A., Vidal, M., Videt, B., and Destombes, J.: The Late Ordovician glacio-eustatic record from a high-latitude storm-dominated shelf succession: The Bou Ingarf section (Anti-Atlas, Southern Morocco), *Palaeogeogr. Palaeoclimatol., 296*, 332–358, <https://doi.org/10.1016/j.palaeo.2010.01.018>, 2010.
- Lubeseder, S.: Silurian and Devonian sequence stratigraphy of North Africa; Regional correlation and sedimentology (Morocco, Algeria, Libya), Doctoral dissertation, University of Manchester, UK, 2005.
- Lubeseder, S., Redfern, J., Petitpierre, L., and Fröhlich, S.: Stratigraphic trapping potential in the Carboniferous of North Africa: developing new play concepts based on integrated outcrop sedimentology and regional sequence stratigraphy (Morocco, Algeria, Libya), in: *Geological Society, London, Petroleum Geology Conference series*, 7, 725–734, Geological Society of London, 2010.
- Lüning, S.: North African Phanerozoic, in: *Phanerozoic in the Northern African basins*, *Encyclopedia of Geology*, 152–172, Elsevier, 2005.
- Lüning, S., Craig, J., Loydell, D. K., Štorch, P., and Fitches, B.: Lower Silurian “hot shales” in North Africa and Arabia: regional distribution and depositional model, *Earth-Sci. Rev.*, 49, 121–200, [https://doi.org/10.1016/S0012-8252\(99\)00060-4](https://doi.org/10.1016/S0012-8252(99)00060-4), 2000.
- Lüning, S., Adamson, K., and Craig, J.: Frasnian organic-rich shales in North Africa: regional distribution and depositional model, *Geol. Soc. Lond. Spec. Publ.*, 207, 165–184, <https://doi.org/10.1144/GSL.SP.2003.207.9>, 2003.
- Lüning, S., Wendt, J., Belka, Z., and Kaufmann, B.: Temporal-spatial reconstruction of the early Frasnian (Late Devonian) anoxia in NW Africa: new field data from the Ahnet Basin (Algeria), *Sediment. Geol.*, 163, 237–264, [https://doi.org/10.1016/S0037-0738\(03\)00210-0](https://doi.org/10.1016/S0037-0738(03)00210-0), 2004.
- Madritsch, H., Schmid, S. M., and Fabbri, O.: Interactions between thin-and thick-skinned tectonics at the northwestern front of the Jura fold-and-thrust belt (eastern France), *Tectonics*, 27, 1–31, <https://doi.org/10.1029/2008TC002282>, 2008.
- Magloire, L.: Étude stratigraphique, par la Palynologie, des dépôts argilo-gréseux du Silurien et du Dévonien inférieur dans la Région du Grand Erg Occidental (Sahara Algérien), *Can. Soc. Pet. Geol.*, 2, 473–491, 1967.
- Makhous, M. and Galushkin, Y. I.: Burial history and thermal evolution of the northern and eastern Saharan basins, *AAPG Bull.*, 87, 1623–1651, <https://doi.org/10.1306/04300301122>, 2003a.
- Makhous, M. and Galushkin, Y. I.: Burial history and thermal evolution of the southern and western Saharan basins: Synthesis and comparison with the eastern and northern Saharan basins, *AAPG Bull.*, 87, 1799–1822, 2003b.
- Marchal, D., Guiraud, M., Rives, T., and van den Driessche, J.: Space and time propagation processes of normal faults, *Geol. Soc. Lond. Spec. Publ.*, 147, 51–70, <https://doi.org/10.1144/GSL.SP.1998.147.01.04>, 1998.
- Marchal, D., Guiraud, M., and Rives, T.: Geometric and morphologic evolution of normal fault planes and traces from 2D to 4D data, *J. Struct. Geol.*, 25, 135–158, [https://doi.org/10.1016/S0191-8141\(02\)00011-1](https://doi.org/10.1016/S0191-8141(02)00011-1), 2003.
- Massa, D.: Paléozoïque de Libye occidentale?: stratigraphie et paléogéographie, Doctoral dissertation, Université de Nice, France, 1988.
- Mélou, M., Oulebsir, L., and Paris, F.: Brachiopodes et chitinozoaires ordoviéciens dans le NE du Sahara algérien: Implications stratigraphiques et paléogéographiques, *Geobios*, 32, 822–839, [https://doi.org/10.1016/S0016-6995\(99\)80865-1](https://doi.org/10.1016/S0016-6995(99)80865-1), 1999.
- Milani, E. J. and Zalan, P. V.: An outline of the geology and petroleum systems of the Paleozoic interior basins of South America, *Episodes*, 22, 199–205, 1999.
- Milton, N. J., Bertram, G. T., and Vann, I. R.: Early Palaeogene tectonics and sedimentation in the Central North Sea, *Geol. Soc. Lond. Spec. Publ.*, 55, 339–351, 1990.

- Moreau, C., Demaiffe, D., Bellion, Y., and Boullier, A.-M.: A tectonic model for the location of Palaeozoic ring complexes in Air (Niger, West Africa), *Tectonophysics*, 234, 129–146, 1994.
- Mory, A. J., Zhan, Y., Haines, P. W., Hocking, R. M., Thomas, C. M., and Copp, I. A.: A paleozoic perspective of Western Australia, Geological Survey of Western Australia, 2017.
- Najem, A., El-Arnauti, A., and Bosmina, S.: Delineation of Paleozoic Tecto-stratigraphic Complexities in the Northern Part of Murzuq Basin-Southwest Libya, in SPE North Africa Technical Conference and Exhibition, Society of Petroleum Engineers, 2015.
- Nikishin, A. M., Ziegler, P. A., Stephenson, R. A., Cloetingh, S., Furne, A. V., Fokin, P. A., Ershov, A. V., Bolotov, S. N., Korotaev, M. V., and Alekseev, A. S.: Late Precambrian to Triassic history of the East European Craton: dynamics of sedimentary basin evolution, *Tectonophysics*, 268, 23–63, 1996.
- Ogg, J. G., Ogg, G., and Gradstein, F. M.: Introduction, in *A Concise Geologic Time Scale: 2016*, p. 3, Elsevier, 2016.
- Oudra, M., Beraouz, H., Ikenne, M., Gasquet, D., and Soulaïmani, A.: La Tectonique Panafricaine du Secteur d'Igherm: Implication des dômes extensifs tardifs à post-orogéniques (Anti-Atlas occidental, Maroc), *Estud. Geológicas*, 61, 177–189, 2005.
- Oulebsir, L. and Paris, F.: Chitinozoaires ordoviciens du Sahara algérien: biostratigraphie et affinités paléogéographiques, *Rev. Palaeobot. Palyno.*, 86, 49–68, [https://doi.org/10.1016/0034-6667\(94\)00098-5](https://doi.org/10.1016/0034-6667(94)00098-5), 1995.
- Owen, G.: Senni Beds of the Devonian Old Red Sandstone, Dyfed, Wales: anatomy of a semi-arid floodplain, *Sediment. Geol.*, 95, 221–235, 1995.
- Paris, F.: The Ordovician chitinozoan biozones of the Northern Gondwana domain, *Rev. Palaeobot. Palyno.*, 66, 181–209, [https://doi.org/10.1016/0034-6667\(90\)90038-K](https://doi.org/10.1016/0034-6667(90)90038-K), 1990.
- Paris, F., Bourahrouh, A., and Hérissé, A. L.: The effects of the final stages of the Late Ordovician glaciation on marine palynomorphs (chitinozoans, acritarchs, leiospheres) in well NI-2 (NE Algerian Sahara), *Rev. Palaeobot. Palyno.*, 113, 87–104, [https://doi.org/10.1016/S0034-6667\(00\)00054-3](https://doi.org/10.1016/S0034-6667(00)00054-3), 2000.
- Peace, A., McCaffrey, K., Imber, J., van Hunen, J., Hobbs, R., and Wilson, R.: The role of pre-existing structures during rifting, continental breakup and transform system development, offshore West Greenland, *Basin Res.*, 30, 373–394, 2018.
- Pemberton, S. G. and Frey, R. W.: Trace fossil nomenclature and the Planolites-Palaeophycus dilemma, *J. Paleontol.*, 56, 843–881, 1982.
- Peucat, J. J., Drareni, A., Latouche, L., Deloule, E., and Vidal, P.: U–Pb zircon (TIMS and SIMS) and Sm–Nd whole-rock geochronology of the Gour Oumelalen granulitic basement, Hoggar massif, Tuareg shield, Algeria, *J. Afr. Earth Sci.*, 37, 229–239, <https://doi.org/10.1016/j.jafrearsci.2003.03.001>, 2003.
- Peucat, J.-J., Capdevila, R., Drareni, A., Mahdjoub, Y., and Kahoui, M.: The Eglab massif in the West African Craton (Algeria), an original segment of the Eburnean orogenic belt: petrology, geochemistry and geochronology, *Precambrian Res.*, 136, 309–352, <https://doi.org/10.1016/j.precamres.2004.12.002>, 2005.
- Phillips, T. B., Jackson, C. A.-L., Bell, R. E., and Duffy, O. B.: Oblique reactivation of lithosphere-scale lineaments controls rift physiography – the upper-crustal expression of the Sorgenfrei-Tornquist Zone, offshore southern Norway, *Solid Earth*, 9, 403–429, <https://doi.org/10.5194/se-9-403-2018>, 2018.
- Pinet, N., Lavoie, D., Dietrich, J., Hu, K., and Keating, P.: Architecture and subsidence history of the intracratonic Hudson Bay Basin, northern Canada, *Earth-Sci. Rev.*, 125, 1–23, <https://doi.org/10.1016/j.earscirev.2013.05.010>, 2013.
- Potter, D.: Relationships of Cambro-Ordovician Stratigraphy to Paleotopography on the Precambrian Basement, Williston Basin, *Sask. Geol. Soc.*, 63–73, 2006.
- Reading, H. G. and Collinson, J. D.: *Clastic coasts, in Sedimentary environments: processes, facies, and stratigraphy*, 154–231, John Wiley & Sons, Oxford; Cambridge, Mass., 2009.
- Rider, M. H.: Facies, Sequences and Depositional Environments from Logs, in *The geological interpretation of well logs*, 226–238, Whittles Publishing, Caithness, Scotland, 1996.
- Rougier, S., Missenard, Y., Gautheron, C., Barbarand, J., Zeyen, H., Pinna, R., Liégeois, J.-P., Bonin, B., Ouabadi, A., Derder, M. E.-M., and Lamotte, D. F. de: Eocene exhumation of the Tuareg Shield (Sahara Desert, Africa), *Geology*, 41, 615–618, <https://doi.org/10.1130/G33731.1>, 2013.
- Sabaou, N., Ait-Salem, H., and Zazoun, R. S.: Chemostratigraphy, tectonic setting and provenance of the Cambro-Ordovician clastic deposits of the subsurface Algerian Sahara, *J. Afr. Earth Sci.*, 55, 158–174, <https://doi.org/10.1016/j.jafrearsci.2009.04.006>, 2009.
- Schlische, R. W.: Geometry and origin of fault-related folds in extensional settings, *AAPG Bull.*, 79, 1661–1678, 1995.
- Sclater, J. G. and Christie, P. A. F.: Continental stretching: An explanation of the Post-Mid-Cretaceous subsidence of the central North Sea Basin, *J. Geophys. Res.-Sol. Ea.*, 85, 3711–3739, <https://doi.org/10.1029/JB085iB07p03711>, 1980.
- Scotese, C. R., Boucot, A. J., and McKerrow, W. S.: Gondwanan palaeogeography and paleoclimatology, *J. Afr. Earth Sci.*, 28, 99–114, [https://doi.org/10.1016/S0899-5362\(98\)00084-0](https://doi.org/10.1016/S0899-5362(98)00084-0), 1999.
- Serra, O. and Serra, L.: Well logging, facies, sequence and environment, in *Well logging and geology*, 197–238, Technip Editions, France, 2003.
- Sharata, S., Röth, J., and Reicherter, K.: Basin evolution in the North African Platform, *Geotecton. Res.*, 97, 80–81, <https://doi.org/10.1127/1864-5658/2015-31>, 2015.
- Shaw, J. H., Connors, C. D., and Suppe, J.: Recognizing growth strata, in *Seismic interpretation of contractional fault-related folds: an AAPG seismic atlas*, 53, 11–14, American Association of Petroleum Geologists, Tulsa, Okla, USA, 2005.
- Sloss, L. L.: Sequences in the cratonic interior of North America, *Geol. Soc. Am. Bull.*, 74, 93–114, 1963.
- Smart, J.: Seismic expressions of depositional processes in the upper Ordovician succession of the Murzuq Basin, SW Libya, in: *Geological Exploration in Murzuq Basin*, edited by: Sola, M. A. and Worsley, D., 397–415, Elsevier Science B.V., Amsterdam, 2000.
- Soares, P. C., Landim, P. M. B., and Fulfaro, V. J.: Tectonic cycles and sedimentary sequences in the Brazilian intracratonic basins, *GSA Bull.*, 89, 181–191, [https://doi.org/10.1130/0016-7606\(1978\)89<181:TCASSI>2.0.CO;2](https://doi.org/10.1130/0016-7606(1978)89<181:TCASSI>2.0.CO;2), 1978.
- Stearns, D. W.: Faulting and forced folding in the Rocky Mountains foreland, Laramide Fold. Assoc. Basement Block Faulting West, *US Geol. Soc. Am. Mem.*, 151, 1–37, 1978.
- Stow, D. A. V. and Piper, D. J. W.: Deep-water fine-grained sediments: facies models, *Geol. Soc. Lond. Spec. Publ.*, 15, 611–646, <https://doi.org/10.1144/GSL.SP.1984.015.01.38>, 1984.

- Stow, D. A. V., Huc, A.-Y., and Bertrand, P.: Depositional processes of black shales in deep water, *Mar. Petrol. Geol.*, 18, 491–498, [https://doi.org/10.1016/S0264-8172\(01\)00012-5](https://doi.org/10.1016/S0264-8172(01)00012-5), 2001.
- Suter, J. R.: Facies models revisited: clastic shelves, *Spec. Publ.-SEPM*, 84, 339–398, 2006.
- Tournier, F.: Mécanismes et contrôle des phénomènes diagénétiques en milieu acide dans les grès de l'Ordovicien glaciaire du bassin de Sbaa, Algérie, Doctoral dissertation, Université de Paris 11, France, 2010.
- Trompette, R.: Gondwana evolution; its assembly at around 600 Ma, *Comptes Rendus Académie Sci.-Ser. IIA-Earth Planet. Sci.*, 330, 305–315, 2000.
- Turner, G. M., Resson, J. L., and Reeves, C. V.: Observation and Measurement Techniques, in *Treatise on Geophysics*, 5, edited by: Schubert, G., 33–75, Blackwell Pub, Malden, MA., 2007.
- Ustaszewski, K., Schumacher, M., Schmid, S., and Nieuwland, D.: Fault reactivation in brittle–viscous wrench systems—dynamically scaled analogue models and application to the Rhine–Bresse transfer zone, *Quaternary Sci. Rev.*, 24, 363–380, <https://doi.org/10.1016/j.quascirev.2004.03.015>, 2005.
- Van Hinte, J. E.: Geohistory analysis—application of micropaleontology in exploration geology, *AAPG Bull.*, 62, 201–222, 1978.
- Vauchez, A., Tommasi, A., and Barruol, G.: Rheological heterogeneity, mechanical anisotropy and deformation of the continental lithosphere, *Tectonophysics*, 296, 61–86, [https://doi.org/10.1016/S0040-1951\(98\)00137-1](https://doi.org/10.1016/S0040-1951(98)00137-1), 1998.
- Vecoli, M.: Palaeoenvironmental interpretation of microphytoplankton diversity trends in the Cambrian–Ordovician of the northern Sahara Platform, *Palaeogeogr. Palaeoclimatol.*, 160, 329–346, [https://doi.org/10.1016/S0031-0182\(00\)00080-8](https://doi.org/10.1016/S0031-0182(00)00080-8), 2000.
- Vecoli, M. and Playford, G.: Stratigraphically significant acritarchs in uppermost Cambrian to basal Ordovician strata of Northwestern Algeria, *Grana*, 36, 17–28, <https://doi.org/10.1080/00173139709362585>, 1997.
- Vecoli, M., Albani, R., Ghomari, A., Massa, D., and Tongiorgi, M.: Précisions sur la limite Cambrien–Ordovicien au Sahara Algérien (Secteur de Hassi-Rmel), *Comptes Rendus Académie Sci. Sér. 2 Sci. Terre Planètes*, 320, 515–522, 1995.
- Vecoli, M., Tongiorgi, M., Abdesselam-Roughi, F. F., Benzarti, R., and Massa, D.: Palynostratigraphy of upper Cambrian–upper Ordovician intracratonic clastic sequences, North Africa, *Boll.-Soc. Paleontol. Ital.*, 38, 331–342, 1999.
- Vecoli, M., Videt, B., and Paris, F.: First biostratigraphic (palynological) dating of Middle and Late Cambrian strata in the subsurface of northwestern Algeria, North Africa: Implications for regional stratigraphy, *Rev. Palaeobot. Palynol.*, 149, 57–62, <https://doi.org/10.1016/j.revpalbo.2007.10.004>, 2008.
- Videt, B., Paris, F., Rubino, J.-L., Boumendjel, K., Dabard, M.-P., Loi, A., Ghienne, J.-F., Marante, A., and Gorini, A.: Biostratigraphical calibration of third order Ordovician sequences on the northern Gondwana platform, *Palaeogeogr. Palaeoclimatol.*, 296, 359–375, <https://doi.org/10.1016/j.palaeo.2010.03.050>, 2010.
- Wagoner, J. C. V., Mitchum, R. M., Campion, K. M., and Rahmanian, V. D.: Siliciclastic Sequence Stratigraphy in Well Logs, Cores, and Outcrops: Concepts for High-Resolution Correlation of Time and Facies, *AAPG Methods Explor. Ser. No 7*, 174, III–55, 1990.
- Watts, A. B.: *Isostasy and Flexure of the Lithosphere*, Cambridge University Press, Oxford University, 2001.
- Wendt, J.: Disintegration of the continental margin of northwestern Gondwana: Late Devonian of the eastern Anti-Atlas (Morocco), *Geology*, 13, 815–818, 1985.
- Wendt, J.: Facies Pattern and Paleogeography of the Middle and Late Devonian in the Eastern Anti-Atlas (Morocco), *Can. Soc. Pet. Geol.*, 1, 467–480, 1988.
- Wendt, J.: Shell directions as a tool in palaeocurrent analysis, *Sediment. Geol.*, 95, 161–186, [https://doi.org/10.1016/0037-0738\(94\)00104-3](https://doi.org/10.1016/0037-0738(94)00104-3), 1995.
- Wendt, J. and Kaufmann, B.: Mud buildups on a Middle Devonian carbonate ramp (Algerian Sahara), *Geol. Soc. Lond. Spec. Publ.*, 149, 397–415, <https://doi.org/10.1144/GSL.SP.1999.149.01.18>, 1998.
- Wendt, J., Belka, Z., and Moussine-Pouchkine, A.: New architectures of deep-water carbonate buildups: Evolution of mud mounds into mud ridges (Middle Devonian, Algerian Sahara), *Geology*, 21, 723–726, 1993.
- Wendt, J., Belka, Z., Kaufmann, B., Kostrewa, R., and Hayer, J.: The world's most spectacular carbonate mud mounds (Middle Devonian, Algerian Sahara), *J. Sediment. Res.*, 67, 424–436, <https://doi.org/10.1306/D426858B-2B26-11D7-8648000102C1865D>, 1997.
- Wendt, J., Kaufmann, B., Belka, Z., Klug, C., and Lubeseder, S.: Sedimentary evolution of a Palaeozoic basin and ridge system: the Middle and Upper Devonian of the Ahnet and Mouydir (Algerian Sahara), *Geol. Mag.*, 143, 269–299, <https://doi.org/10.1017/S0016756806001737>, 2006.
- Wendt, J., Kaufmann, B., Belka, Z., and Korn, D.: Carboniferous stratigraphy and depositional environments in the Ahnet Mouydir area (Algerian Sahara), *Facies*, 55, 443–472, <https://doi.org/10.1007/s10347-008-0176-y>, 2009a.
- Wendt, J., Kaufmann, B., and Belka, Z.: Devonian stratigraphy and depositional environments in the southern Illizi Basin (Algerian Sahara), *J. Afr. Earth Sci.*, 54, 85–96, <https://doi.org/10.1016/j.jafrearsci.2009.03.006>, 2009b.
- Withjack, M. O. and Callaway, S.: Active normal faulting beneath a salt layer: an experimental study of deformation patterns in the cover sequence, *AAPG Bull.*, 84, 627–651, 2000.
- Withjack, M. O., Olson, J., and Peterson, E.: Experimental models of extensional forced folds, *AAPG Bull.*, 74, 1038–1054, 1990.
- Withjack, M. O., Schlische, R. W., and Olsen, P. E.: Rift-basin structure and its influence on sedimentary systems, *Soc. Sediment. Geol. Spec. Publ.*, 73, 57–81, 2002.
- Xie, X. and Heller, P.: Plate tectonics and basin subsidence history, *Geol. Soc. Am. Bull.*, 121, 55–64, <https://doi.org/10.1130/B26398.1>, 2009.
- Yahi, N.: Petroleum generation and migration in the Berkine (Ghadames) Basin, Eastern Algeria: an organic geochemical and basin modelling study, Doctoral dissertation, Forschungszentrum, Zentralbibliothek, Jülich, 1999.
- Zalan, P. V., Wolff, S., Astolfi, M. A. M., Vieira, I. S., Concelcao, J. C. J., Appi, V. T., Neto, E. V. S., Cerqueira, J. R., and Marques, A.: The Parana Basin, Brazil: Chapter 33: Part II. Selected Analog Interior Cratonic Basins: *Analog Basins*, 134, 681–708, 1990.
- Zazoun, R. S.: Hercynian deformation in the western Ahnet Basin and Bled El-Mass area, Algerian Sahara: a continuous strain, *J. Afr. Earth Sci.*, 32, 869–887, 2001.

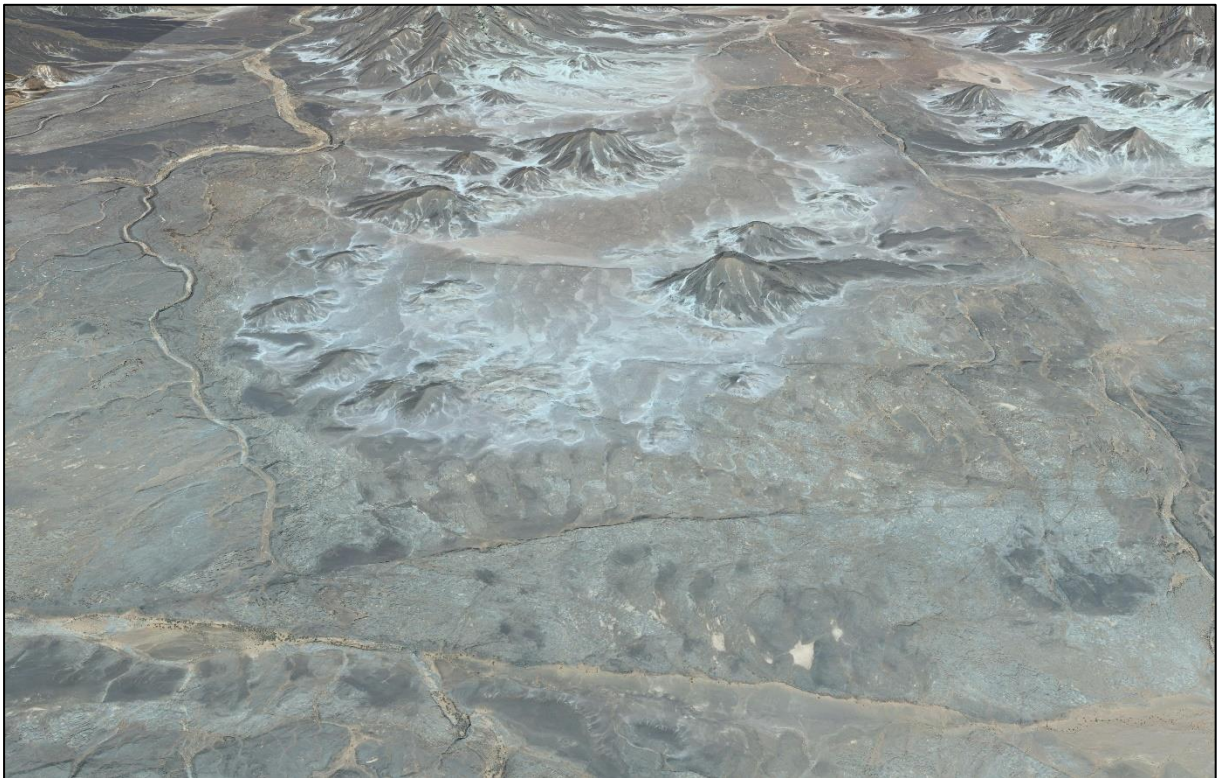
P. Perron et al.: Influence of basement heterogeneity on the architecture

1275

Zazoun, R. S.: The Fadnoun area, Tassili-n-Azdjer, Algeria: Fracture network geometry analysis, *J. Afr. Earth Sci.*, 50, 273–285, <https://doi.org/10.1016/j.jafrearsci.2007.10.001>, 2008.

Zazoun, R. S. and Mahdjoub, Y.: Strain analysis of Late Ordovician tectonic events in the In-Tahouite and Tamadjert Formations (Tassili-n-Ajjers area, Algeria), *J. Afr. Earth Sci.*, 60, 63–78, <https://doi.org/10.1016/j.jafrearsci.2011.02.003>, 2011.

**CHAPTER V. TECTONO-STRATIGRAPHIC
CHARACTERIZATION OF THE PALEOZOIC PERI-
HOGGAR BASINS: EVIDENCING ARCHES AND BASINS
ARCHITECTURE – UNPUBLISHED SUPPLEMENTARY
DATA**



*Late Ordovician sandstones mega-dunes in the Tassili-N-Ajjers (Google-Earth view;
25°38'50" N, 8°57'09" E)*



1 Summary and objectives

In the last chapter, we have seen that the Saharan Paleozoic peri-Hoggar basins display stratigraphic architecture and structural styles typical of intracratonic basins, characterized by relatively thin and laterally extensive sedimentary series that contain major regional unconformities and are arranged in broad synclines and anticlines, affected by regional basement-involved faults, and crustal buckling. Where, this framework is closely linked to terranes zonation. The distribution is preferentially organized by “old” terranes forming the substrates of the Arches and the “young” ones the substrates of the basins depocenter. Regional highs and faults are usually long-lived features that separate basins, and some are organized in strike-slip fault belts. Faults are often reactivated through time as a response to tectonic events developed either close to the area or more often to relatively distant plate-boundary events.

In this chapter supplementary observations and interpretation are presented of the Saharan Paleozoic peri-Hoggar Basins based on satellite images, seismic profiles and well logs data. They bring further additional data validating the model proposed previously in the published paper and some new geological elements.

The different objectives of this chapter are the following:

- Bring further observations and interpretations from satellite images, seismic profiles (local and regional) and well logs (regional correlation);
- Improve the structural style, the lithological rheologic framework and highlight the syn-sedimentary extensional and compressional markers;
- Link with Precambrian inherited basement faults;
- Analyze the stratigraphy, sedimentologic and the sequence stratigraphy of regional cross sections;
- Better characterized the tectono-sedimentary architecture of the peri-Hoggar Basins, especially the Arches-Basins framework.

2 Major structural elements (Arches-Basins)

The Saharan platform (Figure V-1) is structured by three major faults lineaments trends: Sub-meridian (varying from NS to NNW-SSE or NNE-SSW), NW-SE and NE-SW directions. There are mainly associated to NS, NNW-SSE, NNE-SSW, NW-SE and NE-SW broad

asymmetrical folds. These trends are often linked to basement structures (i.e. mega-shear zones and sutures zones) outcropping in the Hoggar massif (Figure V-1).

The Saharan platform and peri-Hoggar Basins (Figure V-1) is characterized by an association of synclines (i.e. basins) and anticlines (i.e. arches, domes, high area) with different wavelength (λ). The wavelength of the basins (Figure V-1) can vary from 620 km in the Murzuq basin to 75 km in the Sbâa basin going through the Tindouf basin (300 km), the Reggane (250 km), the Ahnet basin (220 km), the Mouydir basin (150 km), the Illizi basin (500 km), the Djado basin (230 km), the Iullemeden basin (300 km), the Tin Séririne basin (100 km) and the Tim Mersoï basin (200 km). They are limited with each other by the Azzel-Matti, the Arak-Foum Belrem, the Amguid El Biod and the Tihemboka arches mainly oriented NS, the Bou Bernou, the Ahara, and the Gargaf arches-oriented NE-SW, the Saoura and the Azzene arches-oriented NW-SE. Consequently, a large wave-length and low amplitude flexural deformation characterizes Paleozoic times on the Gondwana shield

We have seen that the basins are principally circular to oval shaped constrained by arches framework (Figure V-1). The whole describes a sort of fan-shaped with orientation of arches and basins going from NW-SE westwards to NE-SW eastwards. This is concordant with the squeeze of Tuareg Shield (i.e. mobile belt) between the West African Craton and the East Saharan Craton (i.e. cratonic blocks) described by many authors (Coward and Ries, 2003; Craig et al., 2008).

In the Saharan platforms (Figure V-1), we have presented a complex classification of Arches-Basins framework characterized by inter-basin principal arch, inter-basin boundary secondary arch, intra-basin secondary arch and syncline-shaped basin (cf. Chapter IV). This structural outline can also be observed and identified in regional seismic profiles in the Reggane, the Ahnet, the Sbâa and the Timimoun Basins around the Azell Matti Arch, the Arak-Foum Belrem Arch and the Azzene High (Figure V-2 and Figure V-3). These structures are formed by large broad horst and grabens systems with planar faults associated with forced folds. Diminution of thickness of the different series are observed at the vicinity of the Arches.

In the next part, we will see that these singular structures are re-activated or inverted during the Paleozoic, evidenced by syn-sedimentary tectonic markers. They are identified by the study of seismic profiles and satellite images.

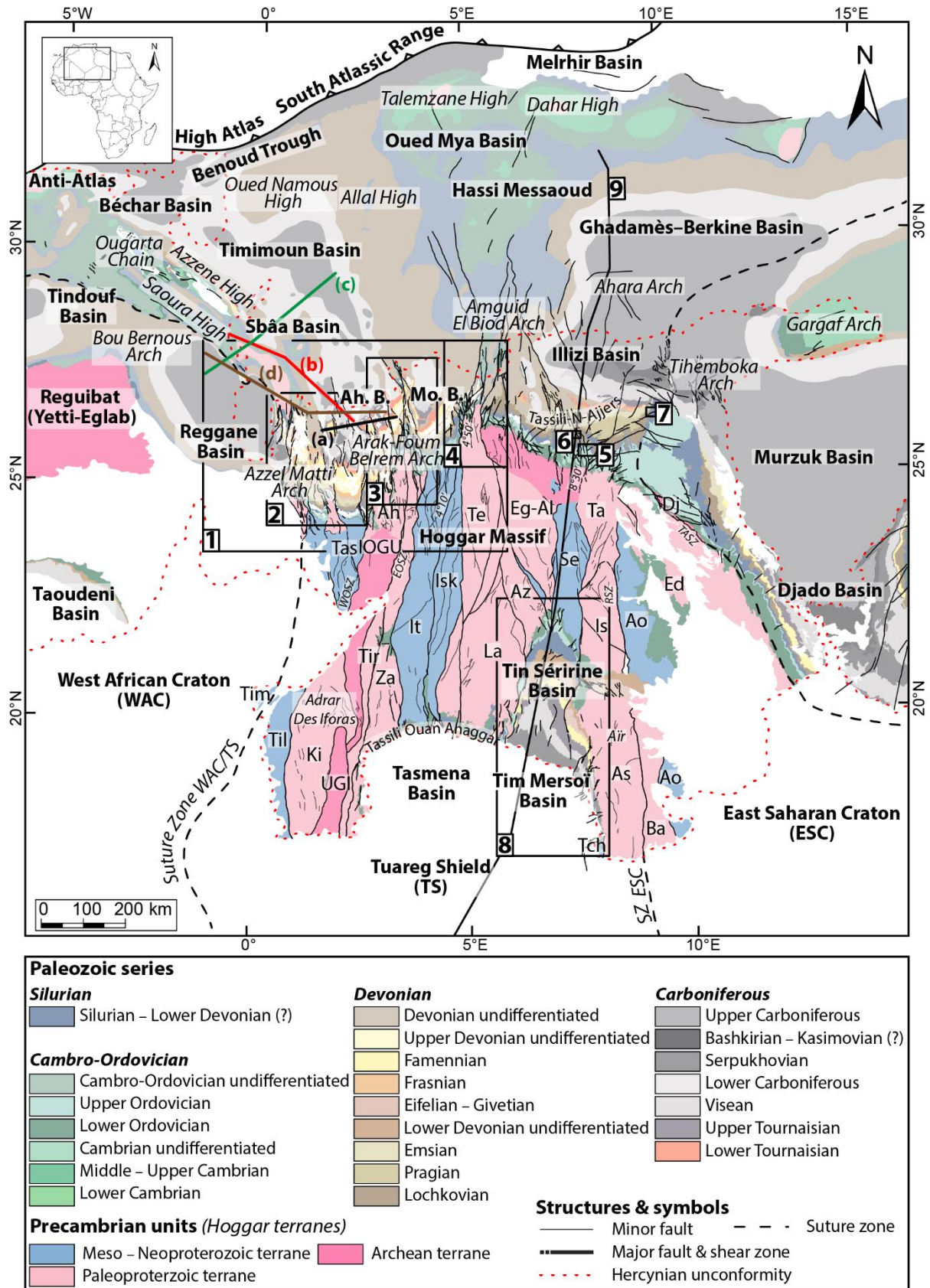


Figure V-1: Geological map of the Paleozoic North Saharan Platform (North Gondwana) showing the localization of geological map zooms, structural interpretations zooms and

regional seismic cross sections. 1: Figure V-4; 2: Figure V-5; 3: Figure V-6; 4: Figure V-7; 5: Figure 5b in (Perron et al., 2018); 6: Figure V-14B; 7: Figure V-17A; 8: Figure VII-12; 9: Figure V-8. (a): Figure V-2A; (b): Figure V-2B; (c): Figure V-3A; (d): Figure V-3B. Ah. B.: Ahnet Basin; Mo. B.: Mouydir Basin.

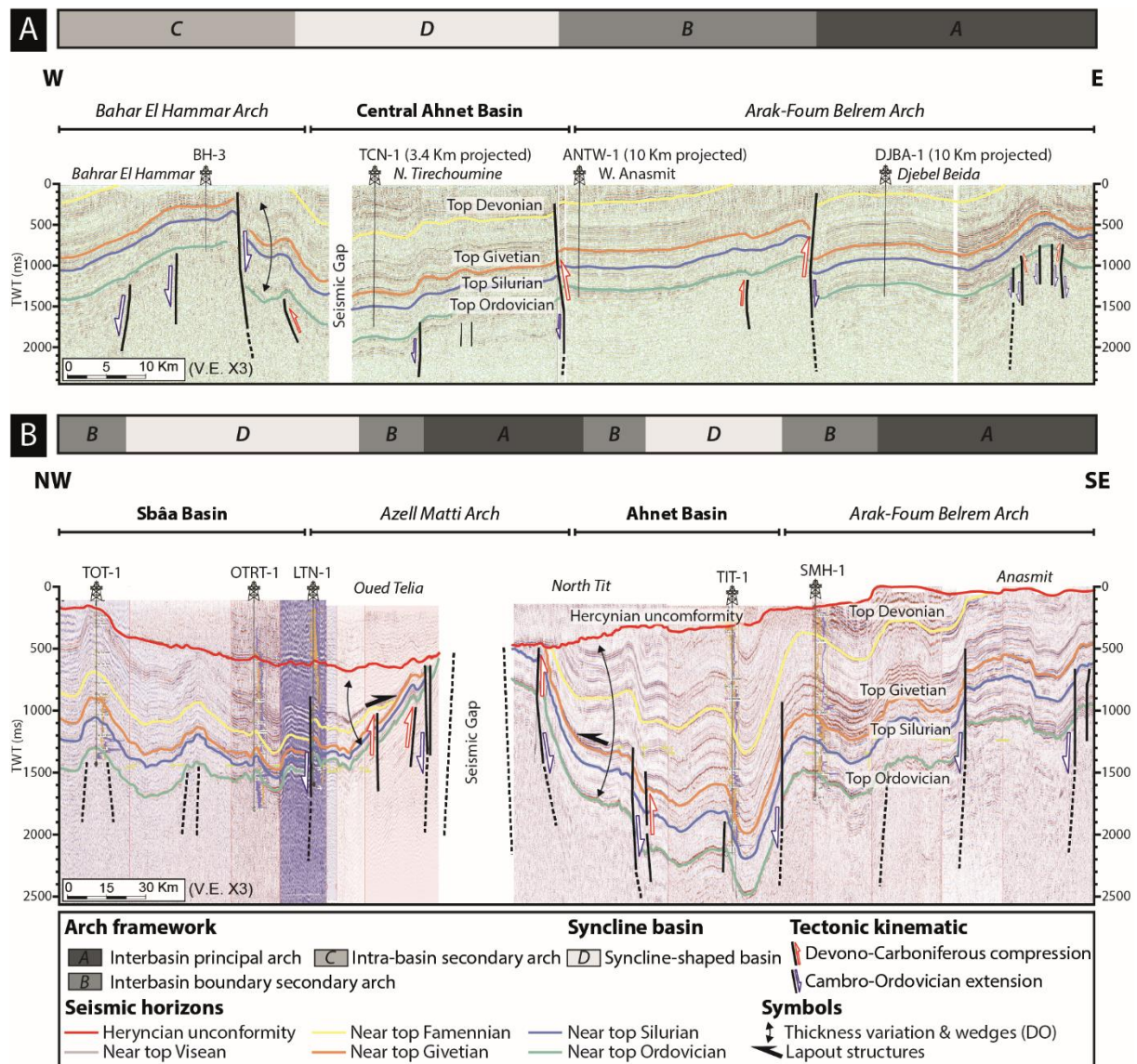


Figure V-2: (A) EW seismic profile of Ahnet Basin showing Arches and basins architectures between Bahar El Hammar intra-arches and Fom Belrem interbasin boundary secondary arch. (B) NW-SE seismic cross section from Sbâa to Ahnet Basins going through the Azzel Matti Arch and Ara-Foum Belrem Arch. See (a) and (b) in Figure V-1 for localization.

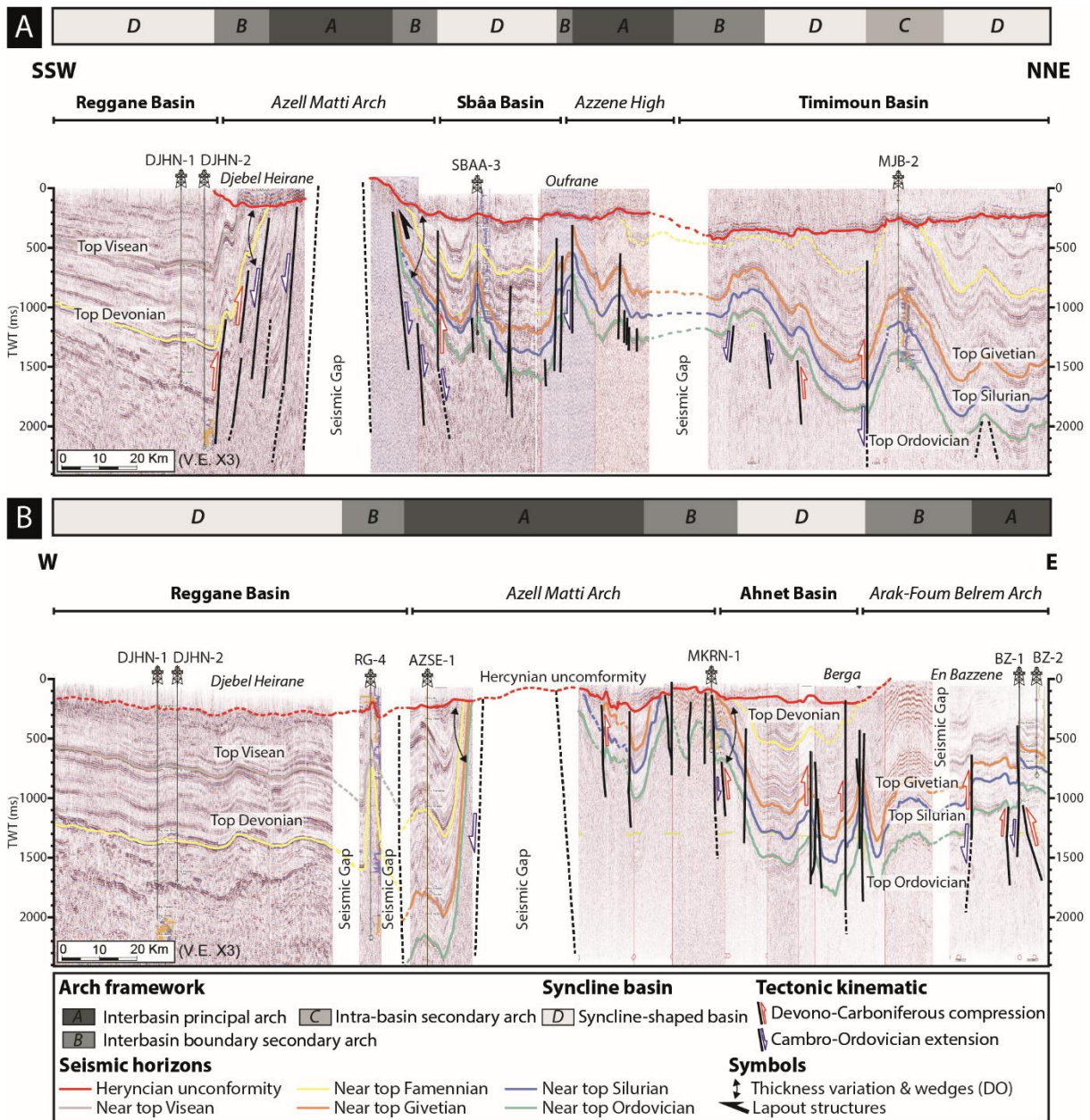


Figure V-3: (A) SSW-NNE seismic cross section through the Reggane, the Sbâa and the Timimoun Basins showing Arches and basins architectures. (B) W-E seismic cross section from the Reggane to the Ahnet Basins separated by Azzel Matti Arch and Arak-Foum Belrem Arch. See (c) and (d) in Figure V-1 for localization.

3 Tectono-sedimentary structures analyses (satellite images and seismic profiles interpretation)

On the Saharan platform, the sedimentation occurred in wide sags and sub-basins over a stable cratonic domain, the sub-basins being separated by tectonic arches episodically uplifted and eroded (Eschard et al., 2005). The difficulty is that the facies and thickness evolutions are very

progressive in these low subsiding basins and depositional. Furthermore, the wedge geometry can then be rather complex when local progressive unconformities interfered with more global regional unconformities (Eschard et al., 2010). However, according to many authors, rapid facies and thickness variations can be expected when approaching the arches which were active during sedimentation (Beuf et al., 1971; Eschard et al., 2005).

We have seen that subsequently, flexural intracratonic sub-basins were created on the Saharan platform, the sub-basins being separated by Arches forming highs on which sedimentary series are thinning. The structuration of the Arches was not continuous but reactivated during specific periods and each sub-basin also had a specific subsidence regime. The highs can be passively onlapped by sediments or actively uplifted and eroded. The mechanism of such deformation is still poorly known, and probably resulted from a lithospheric buckling and the reactivation of Precambrian structures.

It is often difficult to discriminate if the arches and highs actually observed at a regional scale were contemporaneous from the Paleozoic sedimentation or if they correspond to more recent uplifts and truncations.

Through the analysis of satellite images (Figure V-5, Figure V-6 and Figure V-7) and seismic profiles (Figure V-4), the aim of this study is to understand structural style, the tectonic kinematic evolution (i.e. compressive and extensive alternating periods) and accommodation of the deformation during the Paleozoic. Besides, the object is also to better circumscribe the role of heritage on the establishment of current faults patterns. Notice that this part adds supplementary observations and interpretation shown in the Chapter IV (i.e. Perron et al., 2018).

Several seismic profiles (Figure V-4) and satellite images zoom (Figure V-5, Figure V-6 and Figure V-7) are selected in order to highlight evidence of syn-tectono-sedimentary structures (e.g. wedges strata, growth strata, onlaps, thickness variations, angular unconformities, progressive unconformities). Some of these structures are located at vicinity of inter-basin arch and intra-basin arch.

Three tectonic events are shown by identifying the kinematics and the timing of the faults and folds through the analysis of the syn-sedimentary structures. They are the following on the structural maps (Figure V-5, Figure V-6 and Figure V-7): the Cambro-Ordovician (blue), the Siluro-Devonian (red) and the Carboniferous (green).

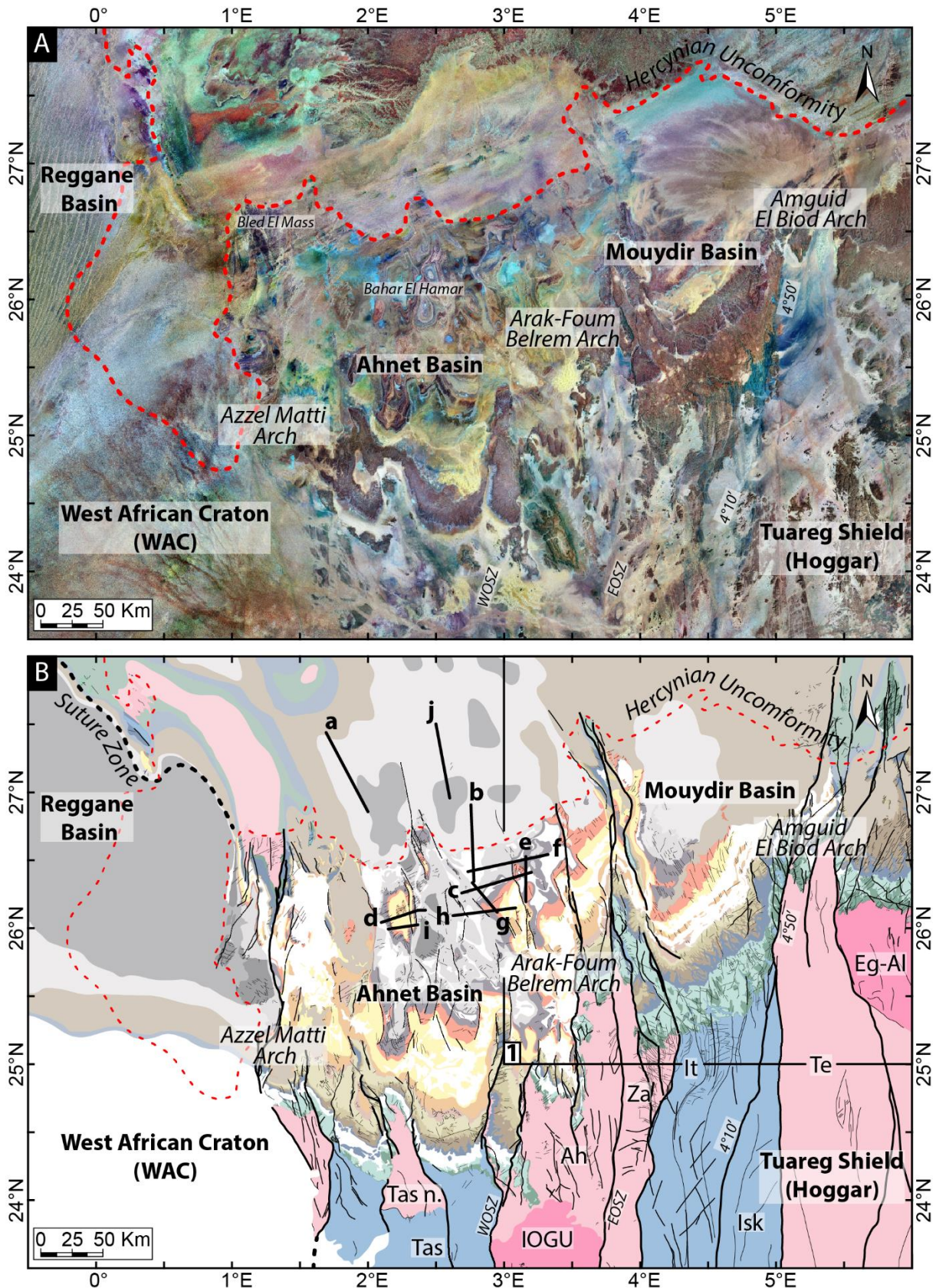


Figure V-4: (A) Satellite images of the Reggane, Ahnet, and Mouydir Basins (Landsat 7 ETM + from USGS database). (B) Geological map of the Paleozoic of the Reggane, Ahnet, and Mouydir Basins associated with the different terranes. For the legend and references see Figure

V-1. Localization of map 1: Figure VII-13 and Figure V-9. Localization of the interpreted seismic profiles **a**: Figure 7b in (Perron et al., 2018); **b**: Figure 7a in (Perron et al., 2018); **c**: Figure 7c in (Perron et al., 2018); **d**: Figure 7d in (Perron et al., 2018); **e**: Figure V-26; **f**: Figure V-19; **g**: Figure V-20; **h**: Figure V-21; **i**: Figure V-25; **j**: Figure V-18.

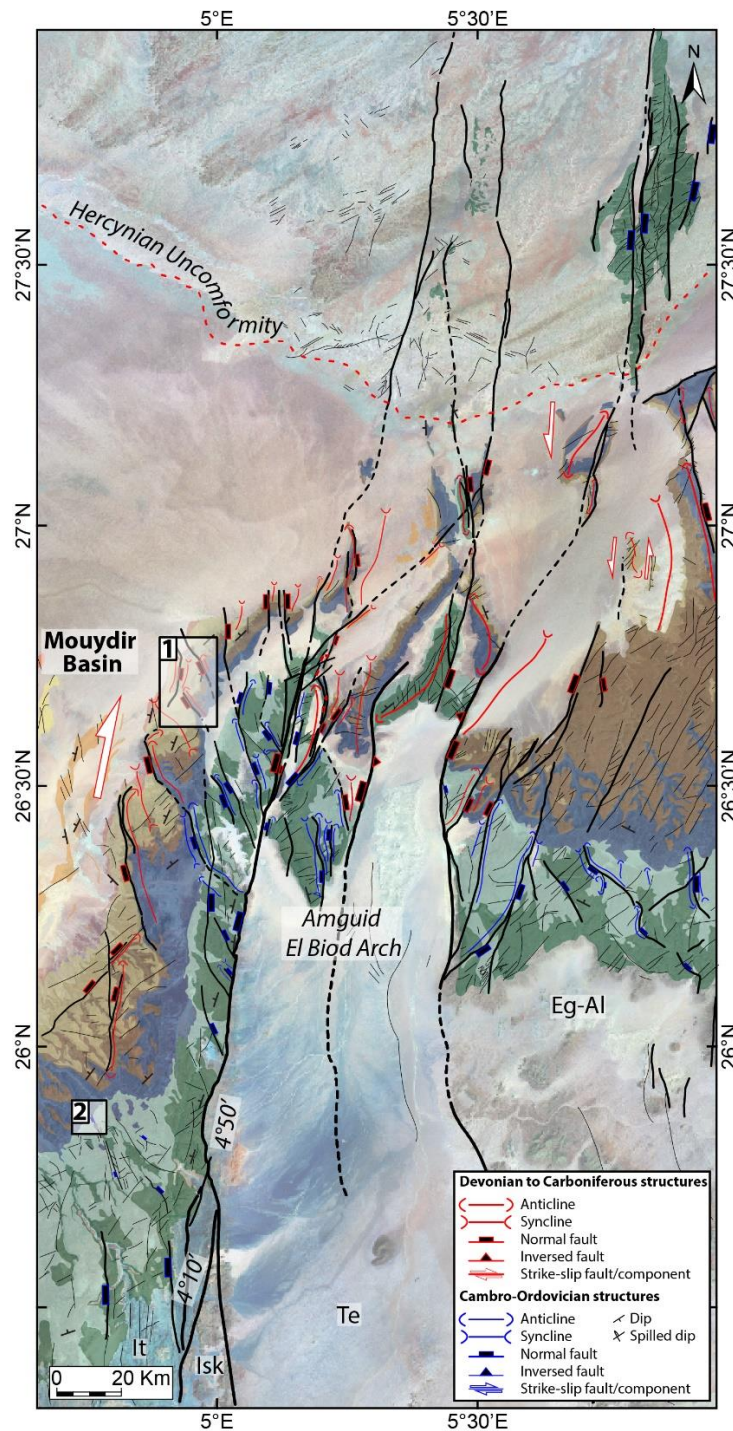


Figure V-5: Structural map of Amguid El Biod Arch. The blue and red colors corresponding respectively to Cambro-Ordovician structures and Devonian structures (to Carboniferous?). 1: Figure V-16A; 2: Figure V-14A. For localization of the map see Figure V-1.

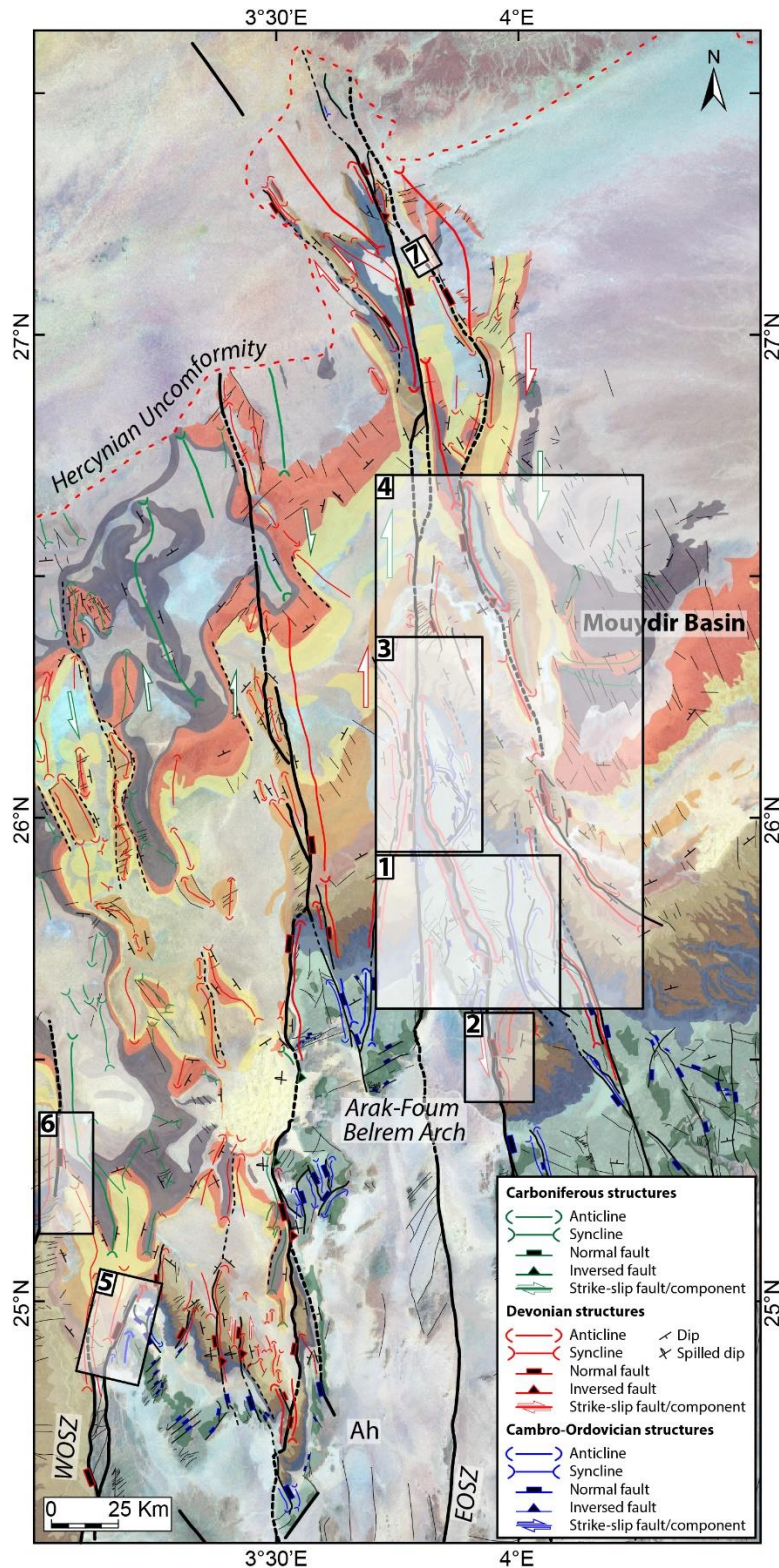


Figure V-6: Structural map of Arak-Foum Belrem Arch. The blue, red and green colors corresponding respectively to Cambro-Ordovician structures, Devonian structures and Carboniferous (Hercynian). 1: Figure 5a in (Perron et al., 2018); 2: Figure V-15; 3: Figure V-13; 4: Figure V-22; 5: Figure V-11A; 6: Figure 6d in (Perron et al., 2018); 7: Figure V-11B. For localization of the map see Figure V-1.

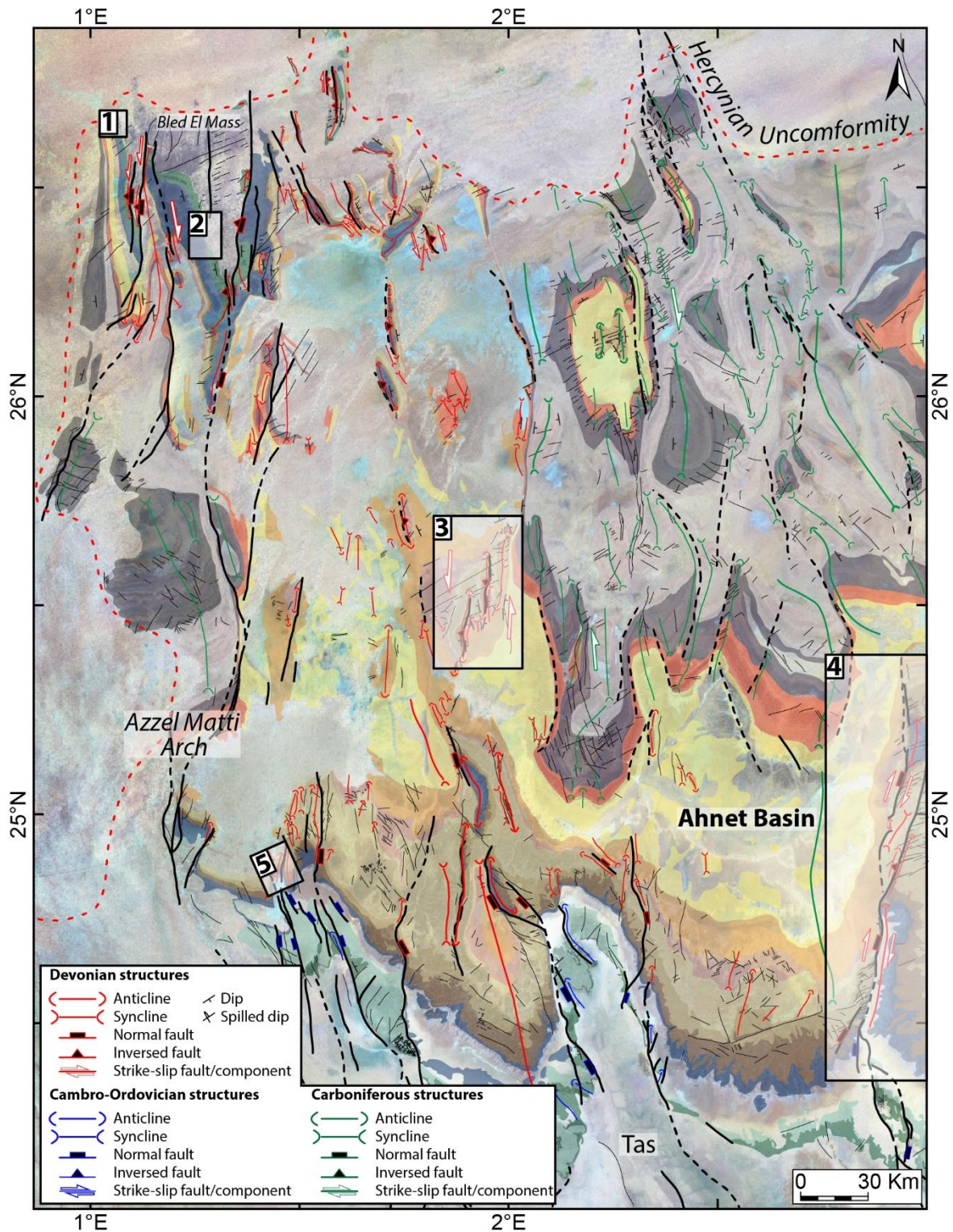


Figure V-7: Structural map of Ahnet Basin and Azzel Matti Arch. The blue, red and green colors corresponding respectively to Cambro-Ordovician structures, Devonian structures and Carboniferous (Hercynian). 1: Figure V-12A; 2: Figure V-12B; 3: Figure V-23; 4: Figure V-24; 5: Figure V-17B. For localization of the map see Figure V-1.

3.1 Synsedimentary syncline-shaped basin delimited by arches

At the large scale, the peri-Hoggar Basins is characterized by the Arches-Basins architecture. It is demarcated by arches (i.e. anticlines) delimiting syncline-shaped basins (see example of Mouydir Basin in Figure V-9).

In the last part (Chapter IV), we have seen that mainly all the series are thin when approaching arches while they thicken at center of the basin (depocenter). This differential subsidence between arches and the basin implies a more or less constant relative uplift of arches likened to basin depocenter.

Notice that we can also observe this main feature with satellite images i.e. 2D plan (Figure V-9B). It is due to the two major tectonic events during the Phanerozoic (Hercynian and Late Eocene swell) which are at the origin of the exhumation and the tilting of the Paleozoic series actually presented in the Saharan Platform (English et al., 2016b; Rougier, 2012; Rougier et al., 2013; Ye et al., 2017). These events allow us to interpret in section the series visible in maps (Figure V-8). Following that, we can perceive in 2D map the architecture of the Saharan platform such as thickness variations between arches and basins.

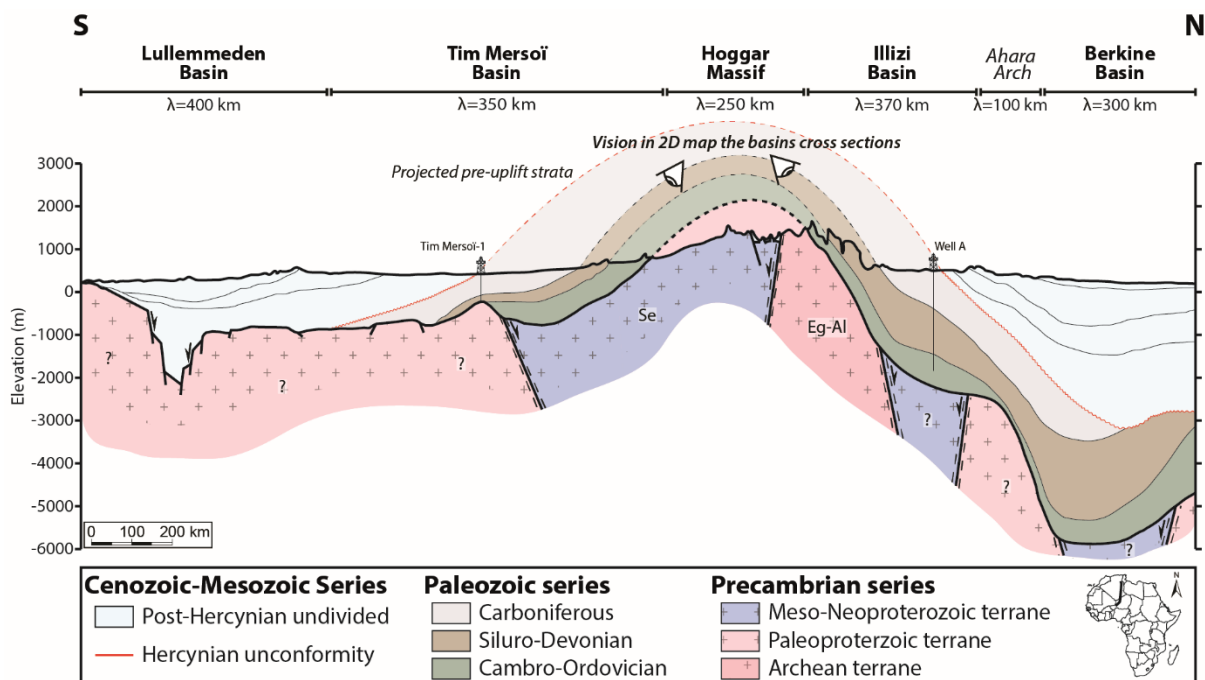


Figure V-8: Schematic structural section across the Hoggar Massif and the peri-Hoggar Basins showing in 2D map projection the architecture of the basins modified from English et al., (2016b). Note that the Hoggar had two history of uplift with significant erosion of the Paleozoic sequence during the Hercynian orogeny and the Late Eocene. For localization see Figure V-1.

Besides, we can see clearly the zonation of the terranes between arches-basins systems and the thickness variations (wedges) associated (Figure V-8).

Eschard et al., (2010) have also shown the progressive growing of arches (referred as paleohighs in the article) during the Paleozoic times. In Chapter IV, we have revealed that this pattern is not only restricted to few layers. But it is a large frequent component of these intracratonic basins. Moreover, the global low rate of subsidence can vary from acceleration, deceleration to inversion during the Paleozoic probably related to geodynamic events (Perron et al., 2018).

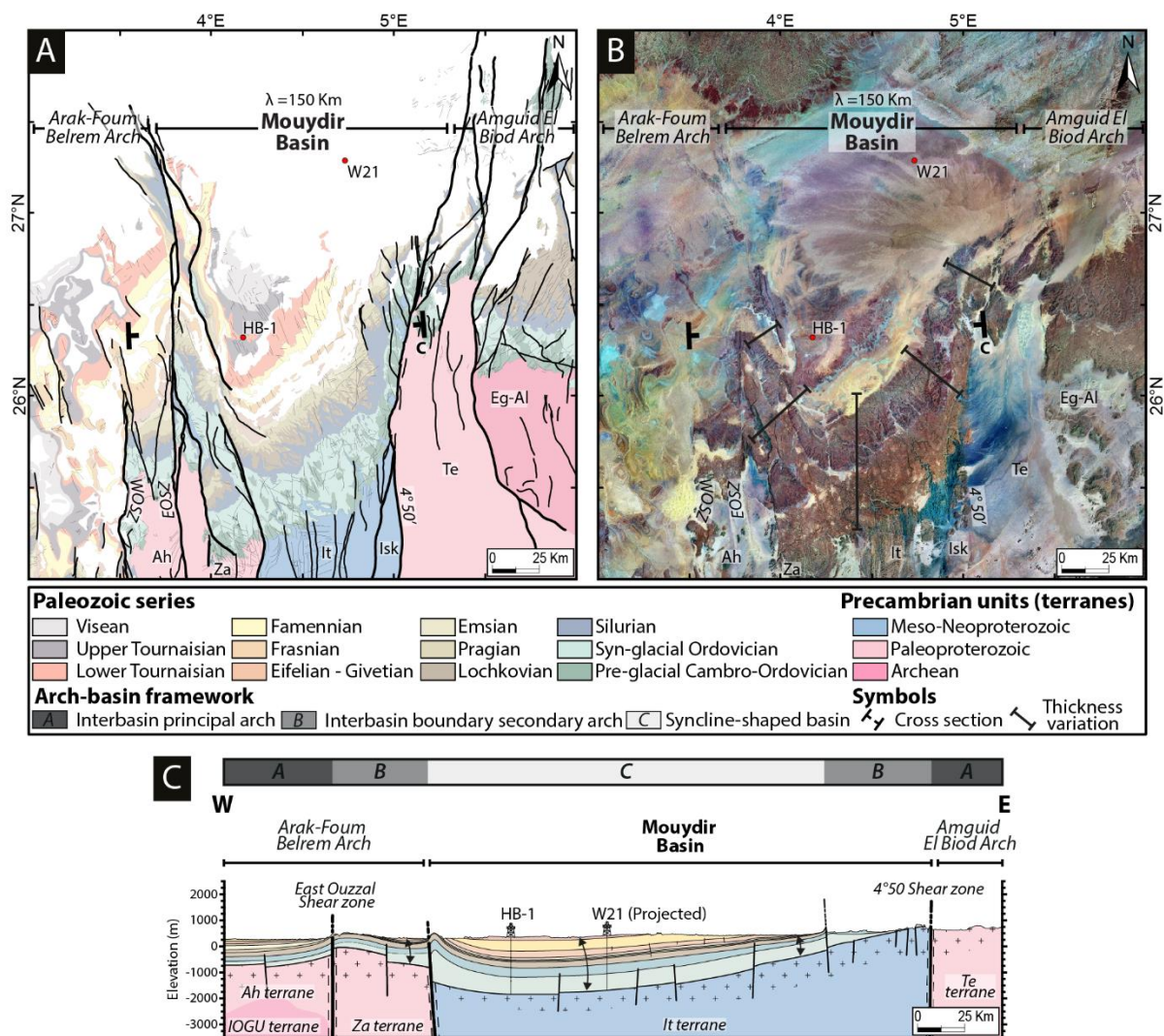


Figure V-9: Example of Mouydir Basin a synsedimentary syncline-shaped basin delimited by arches showing maximum of thickness of series at the center and reduce approaching arches. See Figure V-4 for localization.

This deconvolution of the raw tectonic signal represents the first order pattern of the peri-Hoggar Basins where the arches-basins architecture is control by the terranes repartition and

nature. However, more local signal can be identified which are also fractal evidences and guides of this latter first one (see next part with markers of synsedimentary tectonics). Knowing that, the cover fault network is mainly connected and nucleated on basement paleo-structures (i.e. shear zones). And consequently, they our control by the movements and kinematics of the basement...

3.2 Evidence of syn-sedimentary extensional markers

In the Saharan Platform (Figure V-5, Figure V-6 and Figure V-7) and according to Chapter IV, two types of geometry of faults have been observed (Figure V-13 and Figure V-22):

- There are the sinuous shaped faults (fault F2, faults F7 to F12 in Figure V-13B). They are arranged “en echelon” or sinuous shape result from normal fault propagation and linkage between isolated faults, tip faults, relay faults and parents faults (Marchal et al., 1998, 2003). The sinuous shape as well as the lateral rapid variation of fault displacement are characteristic of syn-lithification fault structures (Marchal et al., 1998, 2003). These structures are preferentially located in the boundary of arches (i.e. intra-basin and intra-terrane).
- There are the straight shaped faults showing lateral low variation of fault displacement related to post-lithification brittle faults (see reviews in Marchal et al., 1998, 2003). They are featured by discontinuous deformation cutting the Paleozoic cover (fault F1 in Figure V-13 and Figure V-22). They are preferentially situated above mega-shear zone between terrane boundaries (i.e. inter-basin). They are controlled by basement heritage and seems to be reactivated through the Paleozoic (syn to post depositional). The intensity of the deformation is the most significant.

The extensional normal faulting is associated with pluri-kilometric folding (folds collinear with faults) represented by footwall anticlines and hanging-wall synclines. The faults are steeply-dipping (sub-vertical) and planar. The folds footwall anticlines are generally asymmetric. They are mainly oriented $N0^{\circ}$ - $N10^{\circ}$ - $N170^{\circ}$, varying from $N150^{\circ}$ - $N140^{\circ}$ to $N30^{\circ}$ - $N40^{\circ}$ (Figure V-5, Figure V-6 and Figure V-7). A secondary trend can be seen perpendicularly (i.e. more or less $N90^{\circ}$ to $N120^{\circ}$ or $N50^{\circ}$ - $N60^{\circ}$) to these trends. These latter was interpreted in some area (e.g. Djado basin) as extension fault due to isostatic rebound after deglaciation event (Denis et al., 2007).

The approach for the recognition of the kinematics of the deformation is reminded in Chapter IV. The models of extensional structures, which seems to best fit to our area are described.

These markers of kinematic are detected in satellite images (Figure V-11A-B, Figure V-12A-B, Figure V-14, Figure V-15, Figure V-16 and Figure V-17B) and in seismic profiles (Figure V-18, Figure V-19, Figure V-20 and Figure V-21). They show mainly steeply-dipping normal fault decipherable by a footwall anticline and a syncline hanging wall. Normal blind faults are also identified (e.g. Figure V-18), linked to basement movement. The whole can form horst and grabens systems (cf. Figure V-15, Figure V-16, Figure V-18 and Figure V-21).

Notice in Figure V-11 and Figure V-12 an example of how stratigraphic units are identified using geological maps (Bennacef et al., 1974; Bensalah et al., 1971) which were georeferenced beforehand (see also Chapter II.1.2 and Chapter II.1.3).

The syncline hanging wall can be associated with divergent onlaps (i.e. growth strata), allowing the datation of the movement of the fault. According to these structures, several extensional events were deciphered, featured by the activation or reactivation of the normal faults. They occurred during the Infracambrian (DO0) (e.g. Figure V-18), the Cambro-Ordovician (DO1) (e.g. Figure V-12A), the Hirnantian (e.g. Figure V-25), the Silurian (DO2) (e.g. Figure V-14B) and the Mid-Late Devonian (DO3) (e.g. Figure V-12B).

All the extensional structures (faults, forced folds) identified in seismic and in satellite images imply one main stresses axis oriented N90°. In the literature, this axis can be referred to both the late Infra-Cambrian extension and the Cambro-Ordovician extensional regime (Galeazzi et al., 2010).

3.3 Evidence of syn-sedimentary compressional and strike-slip markers

After the establishment of broad horst and graben systems during Infracambrian or/and Cambro-Ordovician (described previously), compressional and inversion structures have occurred through further tectonic events (e.g. Caledonian, Hercynian) reactivating basement faults framework. These compressional markers are more easily decipherable in seismic profiles rather than in satellite images. Nevertheless, simple inversed and thrust structures can be detected in satellite images (e.g. Figure V-11B and Figure V-12A).

Two type of inversion models have been highlighted in the area (cf. Chapter IV):

- The positive inversion of paleo-normal faults model featured by inversed fault-propagation folds with a tectonic transport from hanging wall to footwall. This kind of model can be observed in the Bahar El Hammar intra-basin Arch (Figure V-25 and Figure V-2A) and near the Azzel Matti inter-basin Arch (Figure V-2B).
- The transported normal fault model characterized by inversed fault-propagation folds with a tectonic transport from footwall to hanging wall (accommodated by Silurian detachment layer). This type of model is identifiable in satellite images (Figure V-11B, Figure V-12A and Figure V-15) and in seismic (Figure V-20 and Figure V-21).

These inversion model can be thin-skinned i.e. deforming limited layers (e.g. Figure V-20) or thick-skinned i.e. involving a lot of series (e.g. Figure V-21 and Figure V-18), depending on the deformation intensity and decoupling shale layers. In the literature (e.g. Figure V-10A), these structures are well-documented and differentiated (e.g. Madritsch et al., 2008; Tozer et al., 2002).

Associated to these compressional (and previous extensional) kinematics, markers of strike-slip component are decipherable, evidenced by different type of structures such as: dextral strike slip horsetails (e.g. Figure V-24), dextral sigmoid fold (e.g. Figure V-22), sinistral lateral folds, dextral lateral folds and dextral en echelon folds (e.g. Figure V-23). These markers are more easily observable in satellite images. Nevertheless, pop-up structures connected to a flower-like faults systems are recognized (e.g. Figure V-21). In the literature (Figure V-10B-C), these structures are evidence of strike slip movement (e.g. Casas et al., 2001; Dooley and Schreurs, 2012; Sylvester, 1988). In seismic strike-slip faults are often characterized by a typical geometry called “flower” or “palmed tree structure” (Dooley and Schreurs, 2012; Fossen, 2010; Le Guerroué and Cobbold, 2006; Soto et al., 2007; Woodcock and Fischer, 1986; Woodcock and Rickards, 2003).

In general, most of real strike-slip zones have an additional component. Two main types of "flower structures" have been defined, positive and negative "flower structures" (Figure V-10C). Negative flower structures are created in an extensive context (i.e. transtensive faults). They are characterized by a depression zone established by normal faulting. While positive flowers structures are formed in shortening conditions (i.e. transpression faults). They are featured by a rising configuration in surface (i.e. “pop up”) resulting from reverse faulting

(Figure V-10D). Transpression results in combinations of wrenching and thrusting structures (e.g. Casas et al., 2001; Dooley and Schreurs, 2012; Sylvester, 1988).

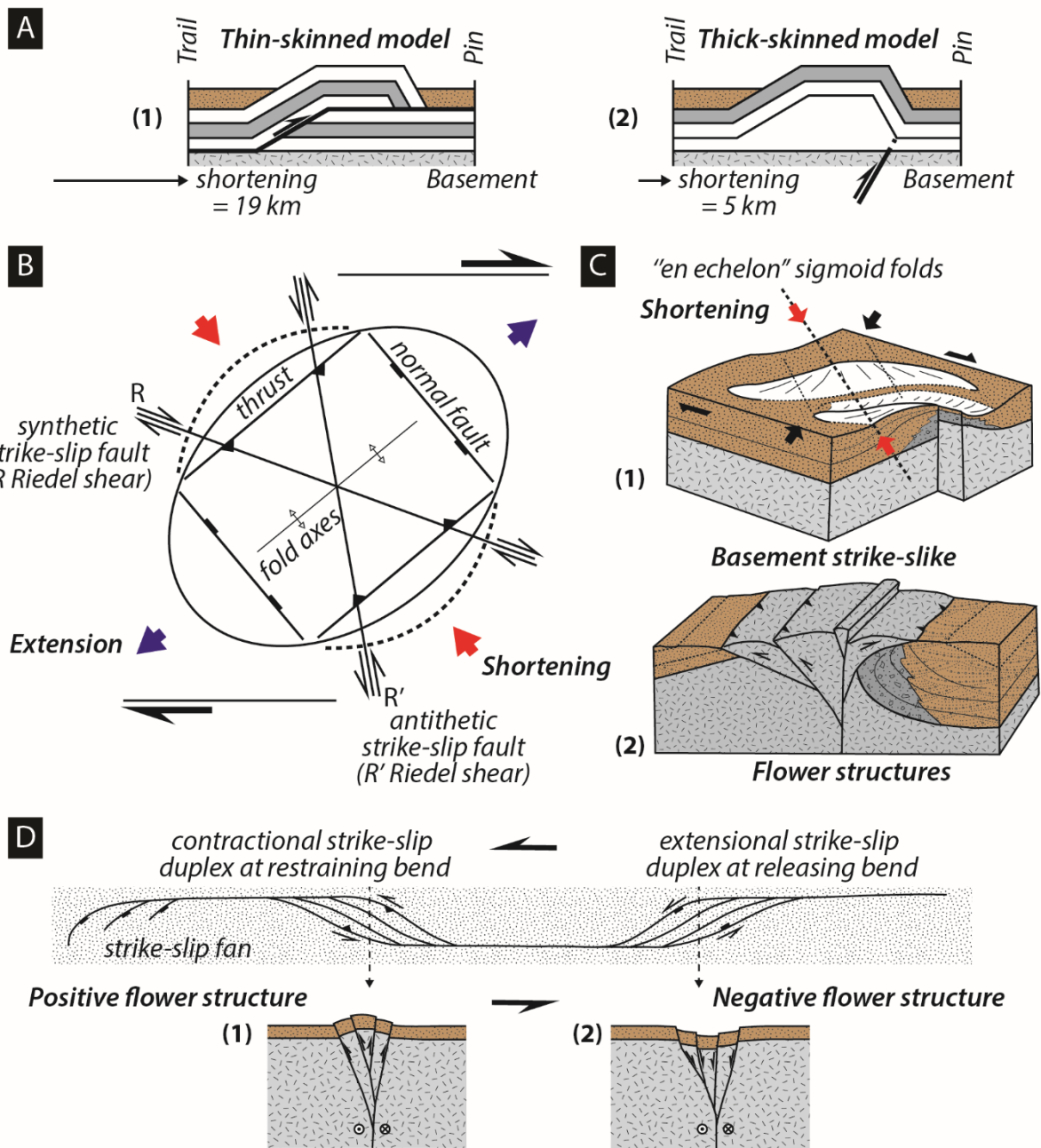


Figure V-10: (A) Thin-skinned vs thick-skinned tectonic style modified from Tozer et al., (2002); In (1) uplift and folding have resulted from thin-skinned thrusting and duplication of the stratigraphy at depth. In contrast, uplift in interpretation in (2) is due to reactivation of a pre-existing extensional fault that originally hosted an increased thickness of sediment. (B) Structural pattern of a dextral strike-slip fault (Riedel shear) modified from Sylvester, (1988). (C) Example of tectonic structures present in a strike slip zone modified from Guiraud, (1990); (1) Deformation of the sedimentary cover by folds arranged in echelon on a basement strike-

slip fault; (2) Positive flower structures associated to strike-slip component in a fault zone. (D) Map and cross-sections of a generic strike-slip fault system, showing flower structures and duplexes; (1) Positive flower structure and (2) Negative flower structure modified from Woodcock and Fischer, (1986).

Locally, strike slip faults can evolve into reverse faults propagation folds which attest of compressional kinematics. The presence of spilled dip strata along these faults forming overturned folds highlights a compression event (e.g. see fault F6 in Figure V-22 and F2 in Figure V-15). Observations which was already documented by Haddoum et al., (2001).

All these observations are clues of transpressional and transtensional tectonic kinematics during the Paleozoic. As already studied in Chapter IV, through the identification of growth strata, truncatures and thickness variation, indications of compression have essentially occurred during the Caledonian, the Mid-Late Devonian and the Hercynian.

All the compressional structures (folds, faults) identified in seismic and in satellite images imply three main stresses axes:

- One Oriented N90°. In the literature, this axis can be referred to the Caledonian compression regime (Beuf et al., 1971; Galeazzi et al., 2010).
- And two oriented N40° and N120°. They are assigned in the literature to two compression phases: N40° of Viséan age and 120° of post-Serpukhovian-ante Permian age (Haddoum et al., 2001; Zazoun, 2001).

The intensity of the deformation is not the same on the different faults. This can be explained by the orientation of the fault lineaments relative to the principal stress during the different tectonic event. It is known that in strike slip structure more the stress is perpendicular to the shear plane more the deformation will be important (Casas et al., 2001; Dooley and Schreurs, 2012). This fact will control the strike slip (wrenching, friction) dominant or the compression (thrusting) dominant of the arches.

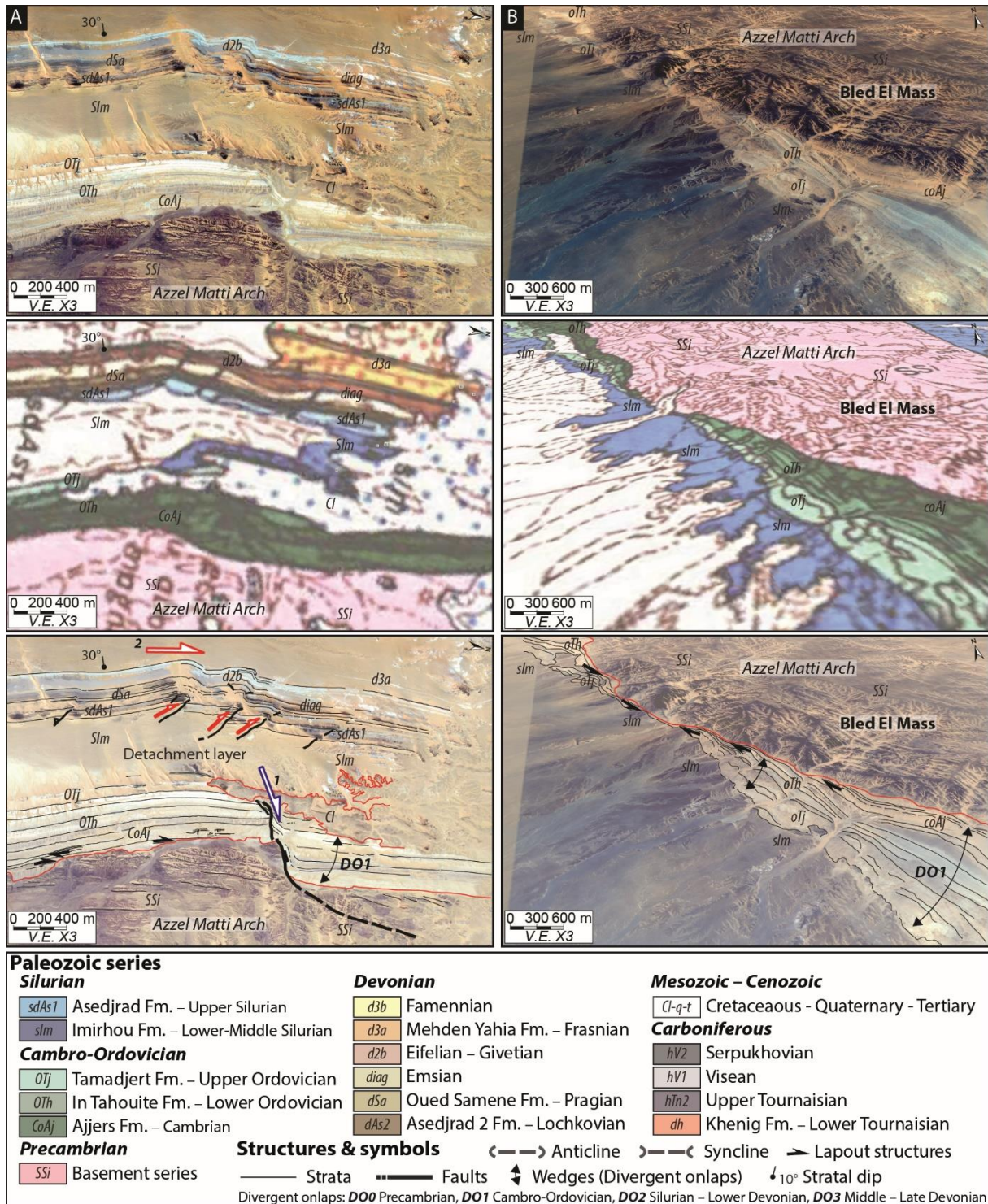


Figure V-12: (A) Syn-sedimentary normal fault in Cambro-Ordovician series and inversion of Lower Devonian on Silurian detachment layer. (B) Divergent onlaps over Azzel Matti basement (“series Pourprée”). For localization see 1 and 2 in Figure V-7.

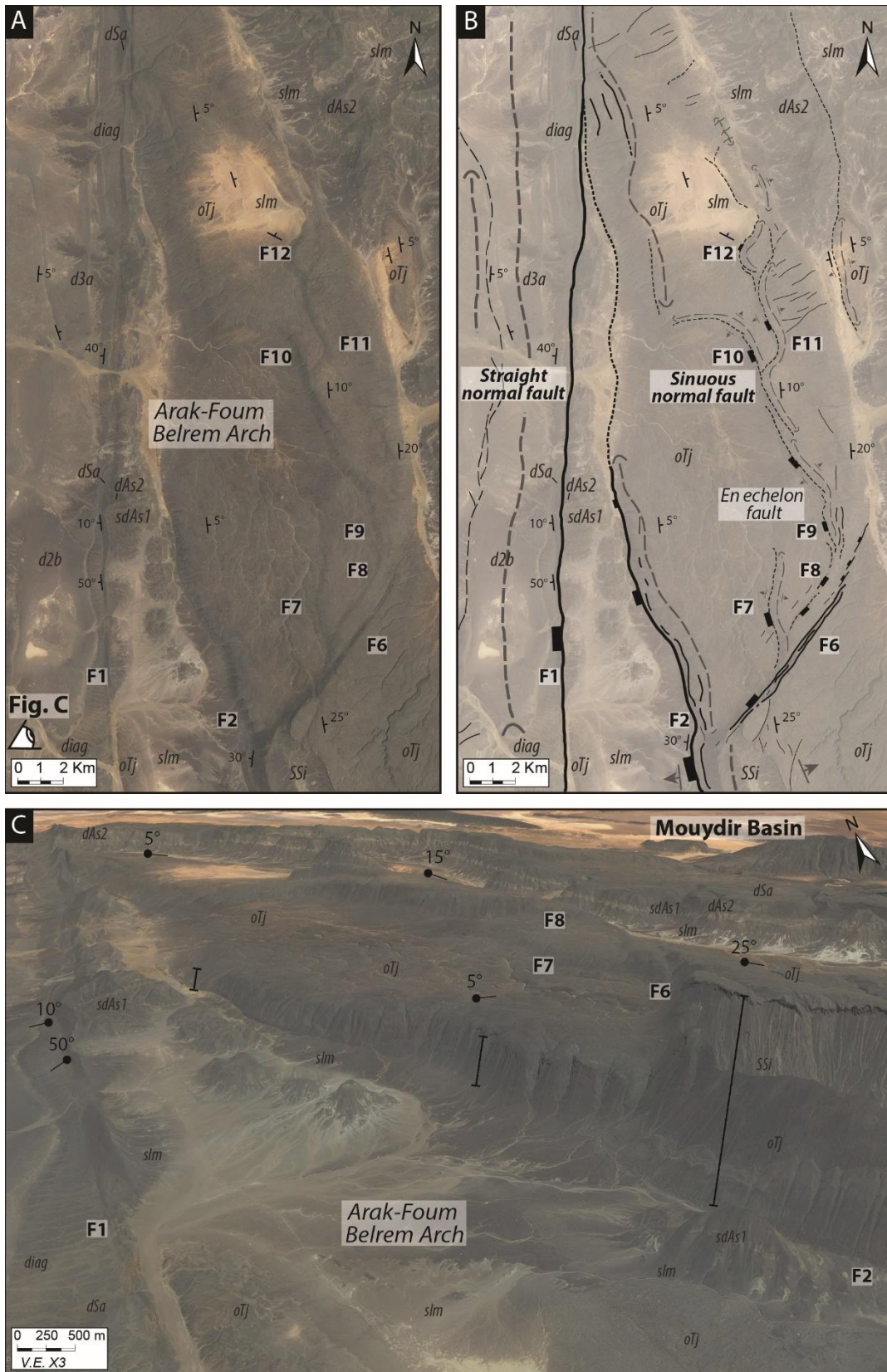


Figure V-13: (A) Not interpreted Google Earth image (B) Interpreted Google Earth image showing NS normal sinuous and straight faults in Cambro-Ordovician series (C) 3D Google Earth image showing relief. For localization see 3 in Figure V-6.

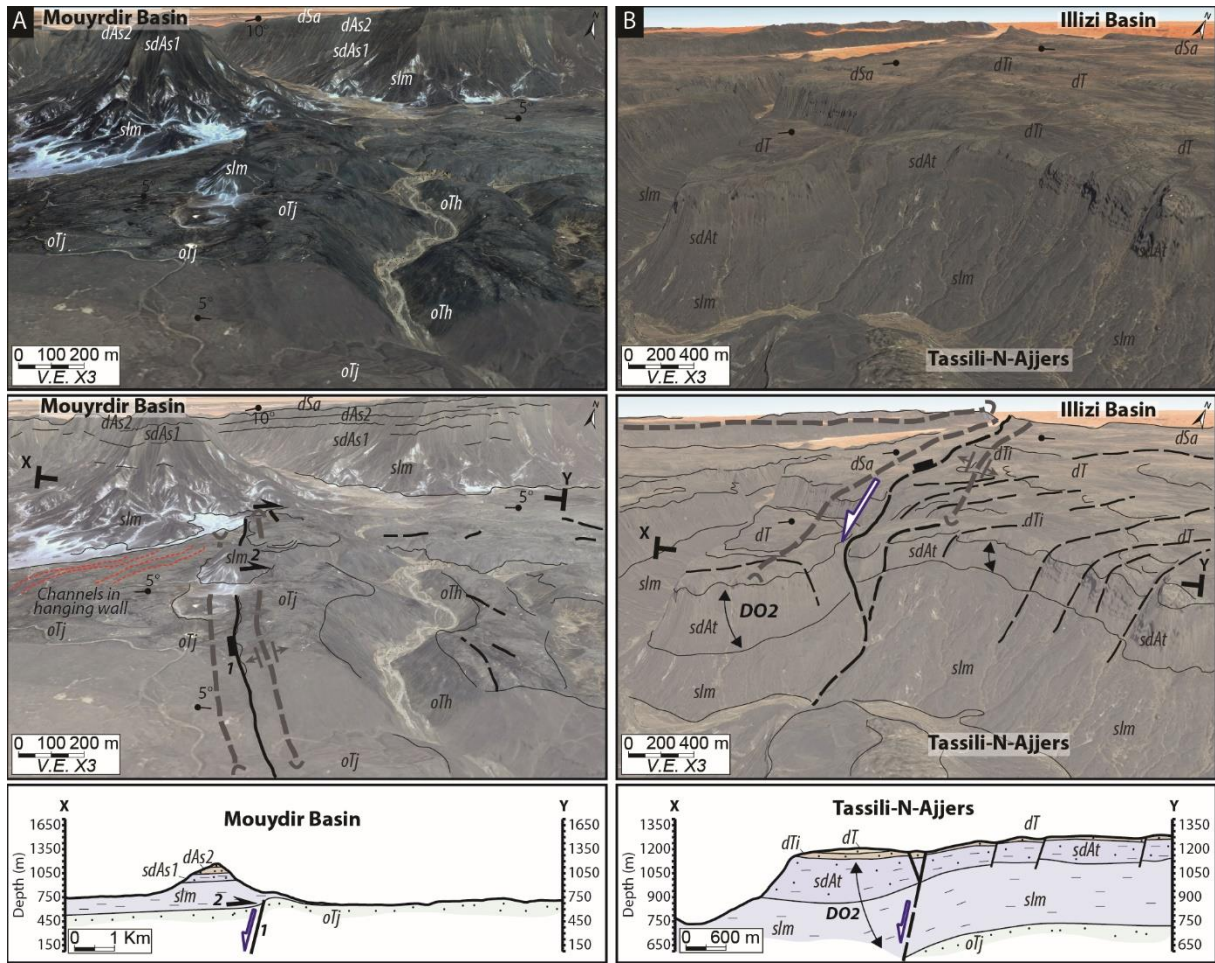


Figure V-14: (A) Structural interpretation of Google earth satellites images of Aguelman area showing poly-historic paleo-reliefs (ancient normal fault escarpment associated to a footwall anticline and a hanging wall syncline) sealed by Silurian deposits. (B) Structural interpretation of Google earth satellites images showing growth strata (wedges) in Siluro-Devonian series. OTh: In Tahouïte formation (Early to Late Ordovician, Floian to Katian), OTj: Tamadjert Formation (Late Ordovician, Hirnantian), slm: Imirhou formation (Early Silurian), sdAt: Atafaïtafa formation (Middle Silurian), dTi: Tifernine formation (Middle Silurian). 1: Cambro-Ordovician extension, 2: Silurian sealing (horizontal drape). For localization see 2 in Figure V-5 for (A) and 6 in Figure V-1 for (B).

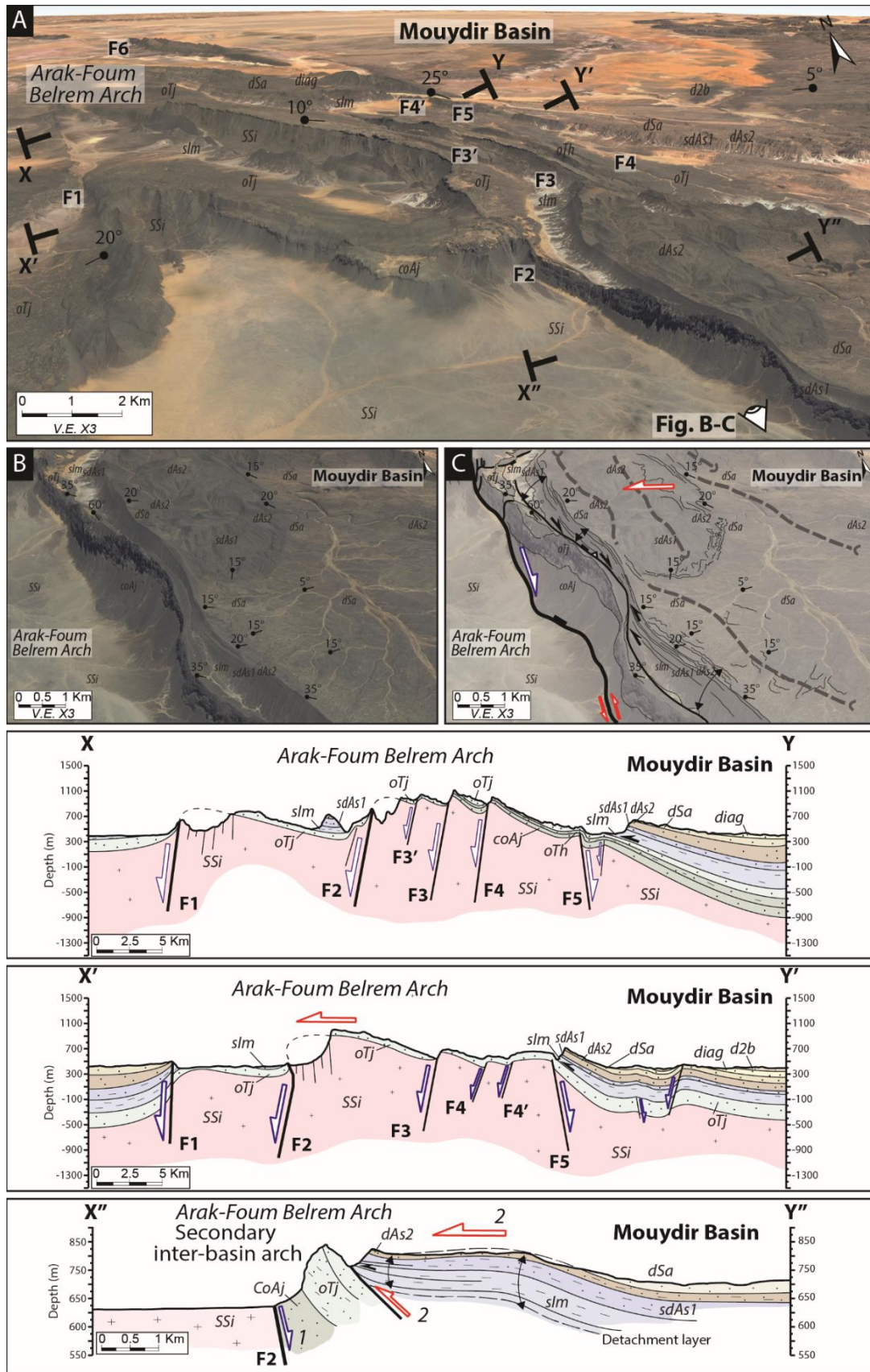


Figure V-15: (A) 3D Google Earth image of Arak-Foum Belrem Arch with localization of cross sections. (B) Google earth satellites images of Adrar Tiggad-N-Teghlamt (near Arak-Foum

Belrem Arch, eastwards inter-basin boundary secondary arch). (C) Structural interpretation Google earth satellites images showing normal fault inverted structure associated with folding (tectonic transport from hanging wall to footwall), detachment layer in Silurian shales series; Strata geometries shows divergent onlap in Silurian series in the hanging wall. (SSi: Basement and infra-Cambrian series, CoAj: Ajers formation (Late Cambrian), OTh: In Tahouite formation (Early to Late Ordovician, Floian to Katian), OTj: Tamadjert Formation (Late Ordovician, Hirnantian), sIm: Imirhou formation (Early Silurian), sdAs1: Asedjrad formation 1 (Late Silurian to Early Devonian), dAs2: Asedjrad formation 2 (Early Devonian, Lochkovian), dSa: Oued Samene formation (Early Devonian, Pragian). 1: Cambro-Ordovician extension, 2: Siluro-Devonian reactivation (Caledonian event) to Herycnian (?). For localization see 1 and 2 in Figure V-6.

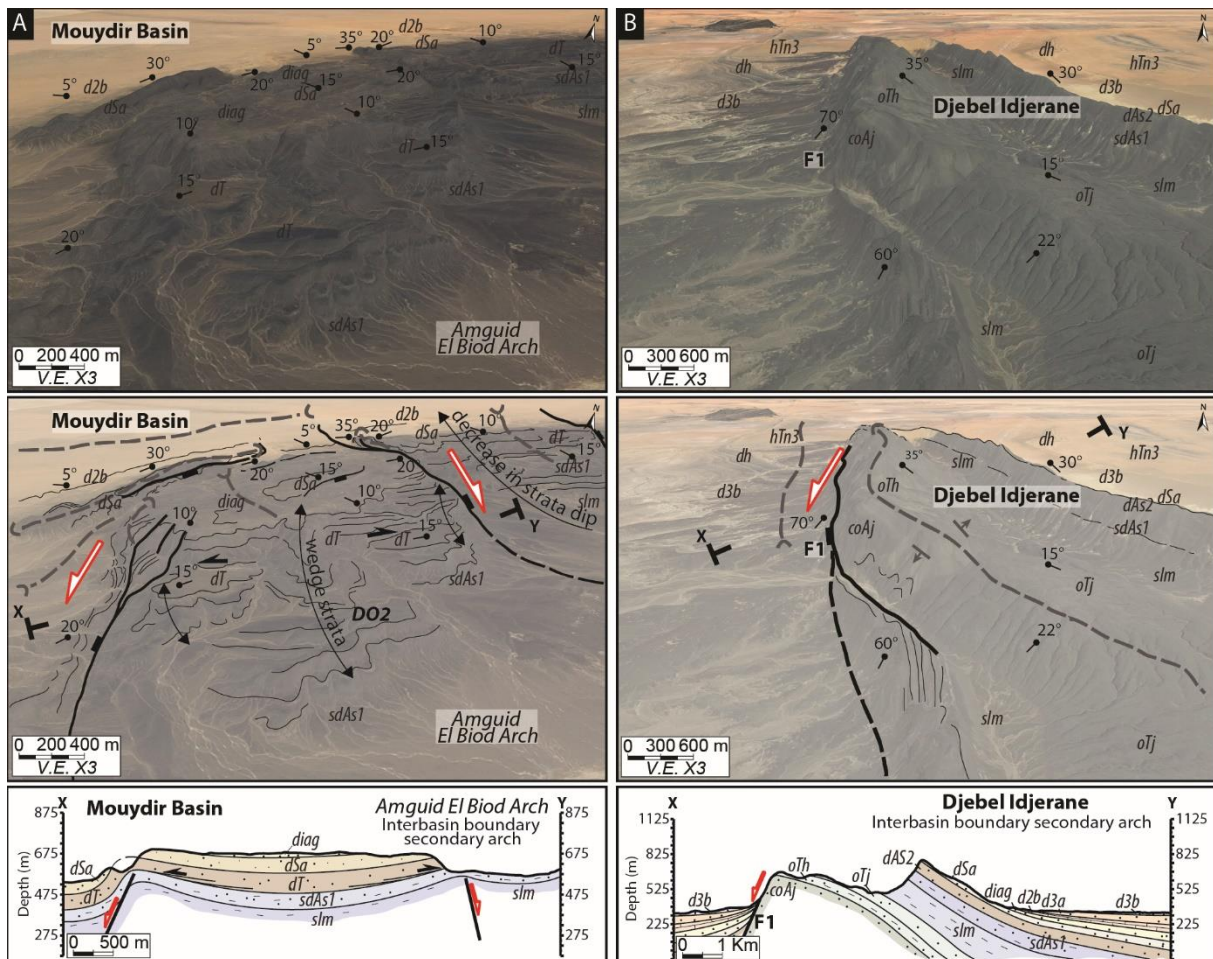


Figure V-16: (A) Structural interpretation of Google earth satellites images near Oued In Rhlem (near Amguid El Biod Arch, inter-basin boundary secondary arch) showing normal fault; Strata geometries shows divergent onlap in Lower Devonian series in the hanging wall. For localization see 1 in Figure V-5. (B) Structural interpretation of Google earth satellites

images of Djebel Idjerane in the Mouydir basin (near Arak-Foum Belrem Arch, eastwards inter-basin boundary secondary arch) showing a normal fault (footwall anticline and syncline hanging wall). Thickness variation of Imirhou formation (Early Silurian) between footwall and hanging wall. For localization see 1 in Figure V-22 and 4 in Figure V-6. OTj: Tamadjert Formation (Late Ordovician, Hirnantian), *slm*: Imirhou formation (Early Silurian), *sdAs1*: Asedjrad formation 1 (Late Silurian to Early Devonian), *dAs2*: Asedjrad formation 2 (Early Devonian, Lochkovian), *dSa*: Oued Samene formation (Early Devonian, Pragian) *d2b*: Givetian, *d3a*: Meden Yahia formation (Late Devonian, Frasnian).

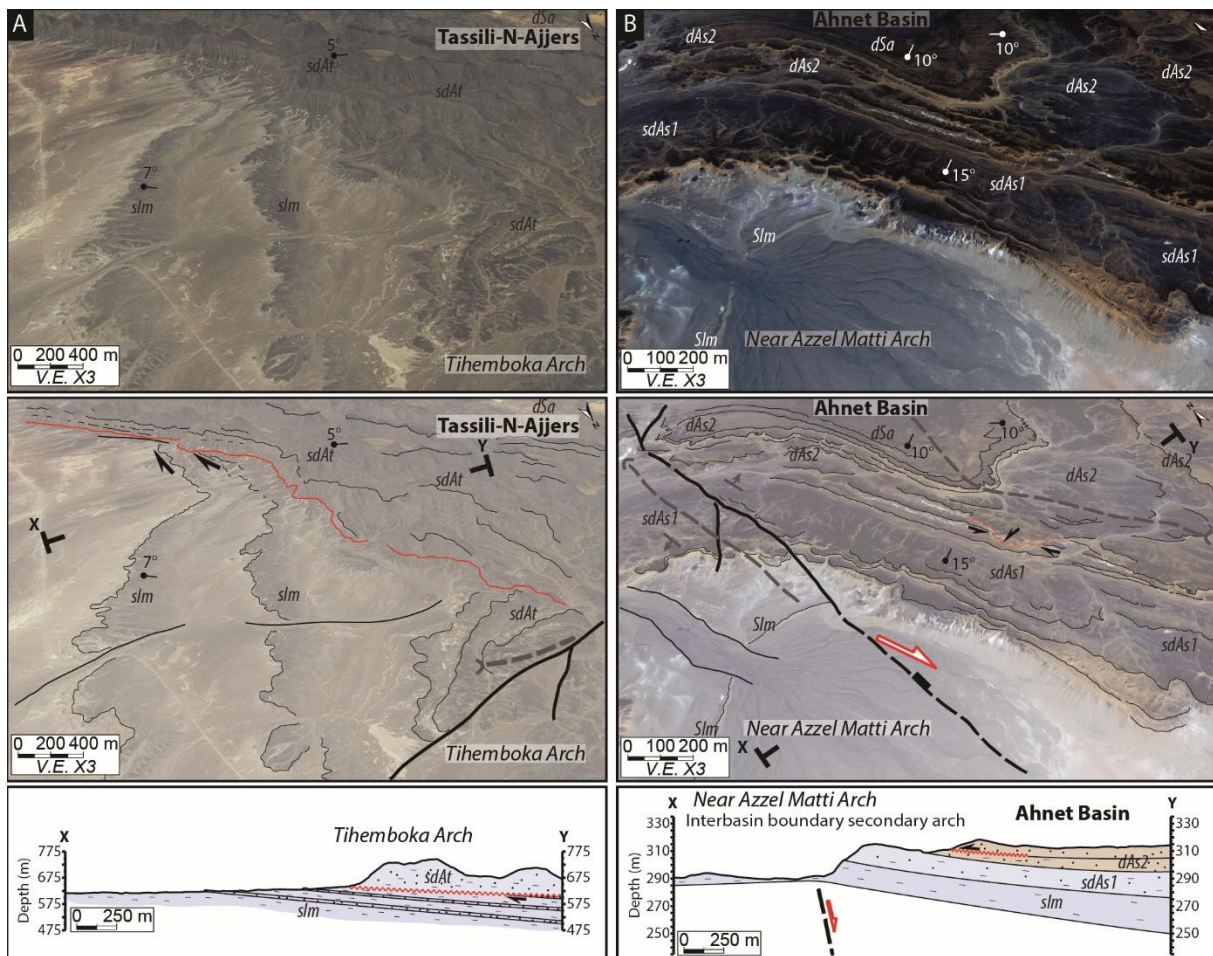


Figure V-17: (A) Structural interpretation of Google earth satellites images near Tihemboka arch (inter-basin arch) showing angular unconformity in Upper Silurian-Lower Devonian series in the hanging wall. For localization see 7 in Figure V-1. (B) Structural interpretation of Google earth satellites images near Azzel Matti Arch (inter-basin boundary secondary arch) showing normal blind fault; Strata geometries shows onlap in Lower Devonian series in the hanging wall. For localization see 5 in Figure V-7. *slm*: Imirhou formation (Early Silurian),

sdAs1: Asedjrad formation 1 (Late Silurian to Early Devonian), *dAs2*: Asedjrad formation 2 (Early Devonian, Lochkovian), *dSa*: Oued Samene formation (Early Devonian, Pragian).

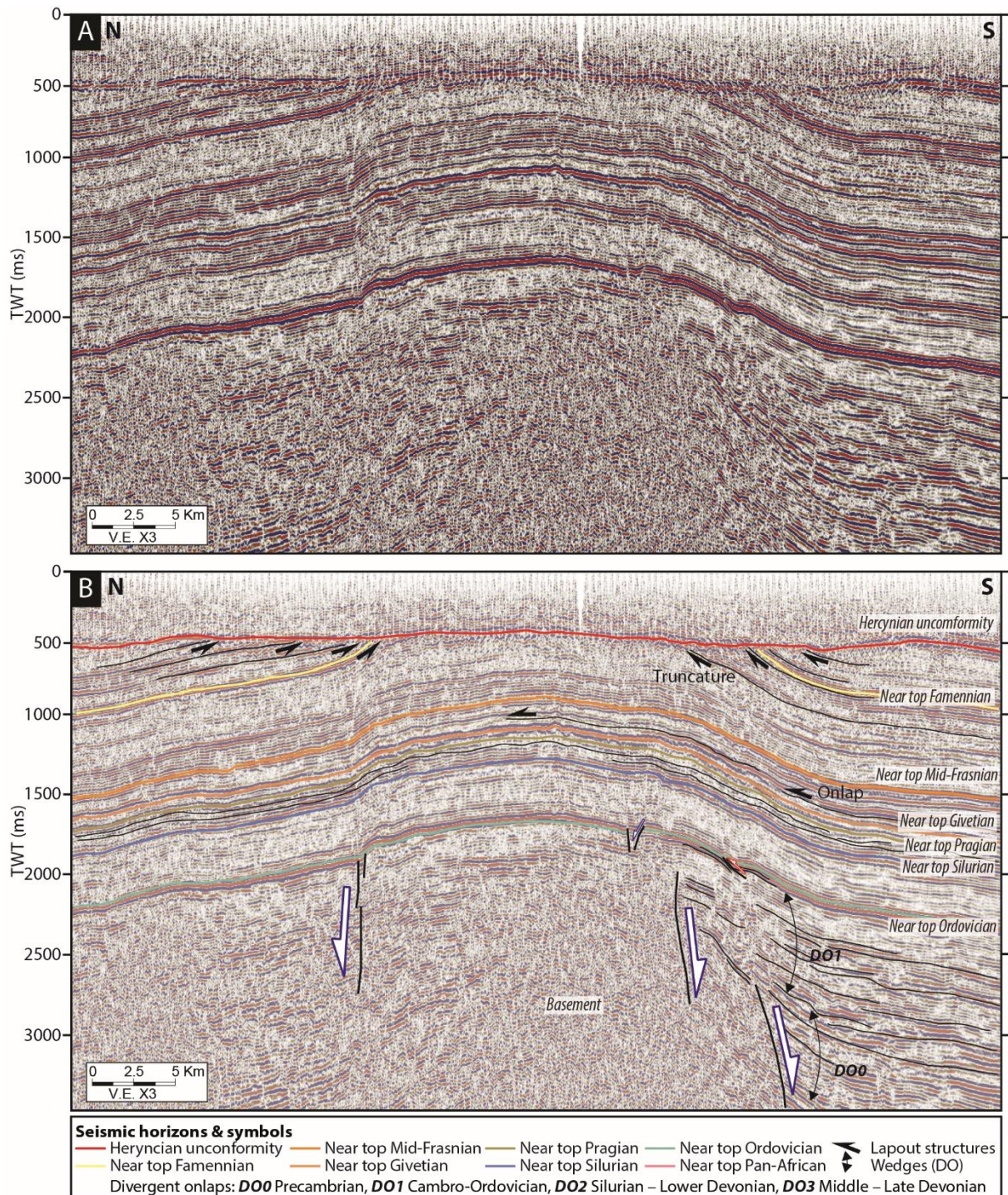


Figure V-18: (A) NS seismic profile of near Djoua arch (inter-basin arch between the Ahnet and the Timimoun basins); (B) Interpreted seismic profile showing steeply-dipping basement normal blind faults associated to forced folding forming a horst; At the south, a structures is featured by reverse fault propagation fold (inversion); Strata lapout geometries shows

Frasnian onlaps on top Givetian and diminution of Frasnian near the arch; Truncature of Paleozoic series by Mesozoic unit on Hercynian unconformity. For localization see j in Figure V-4.

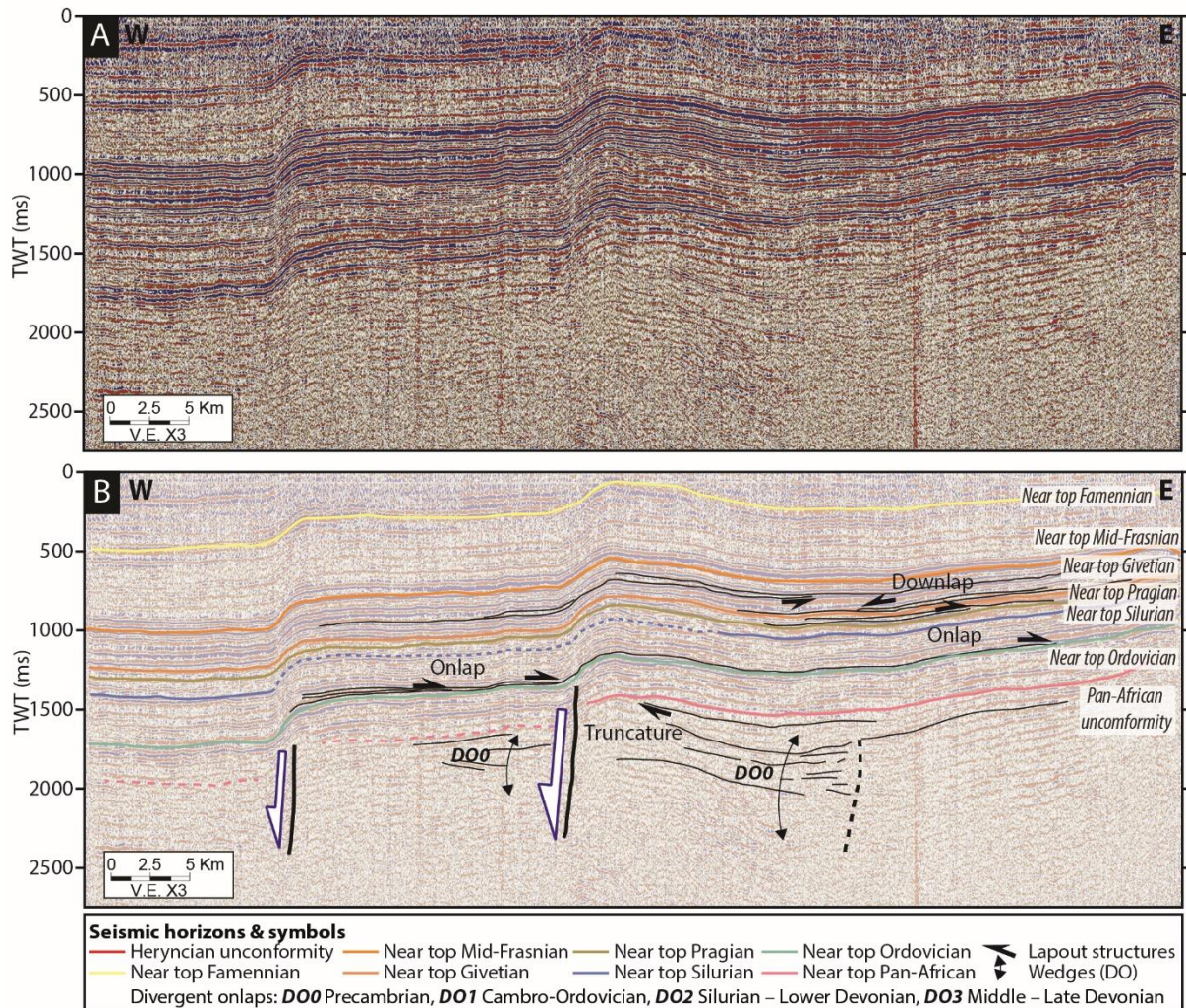


Figure V-19: (A) West-East seismic profile in the Ahnet basin near Erg Tegumentour (near Arak-Foum Belrem Arch, westwards inter-basin boundary secondary arch) (B) Interpreted seismic profile showing steeply-dipping westwards basement normal blind faults associated to forced folding; Strata lapout geometries shows lower Silurian onlaps on the top Ordovician, upper, onlaps and downlaps of Frasnian series on top Givetian unit. For localization see f in Figure V-4.

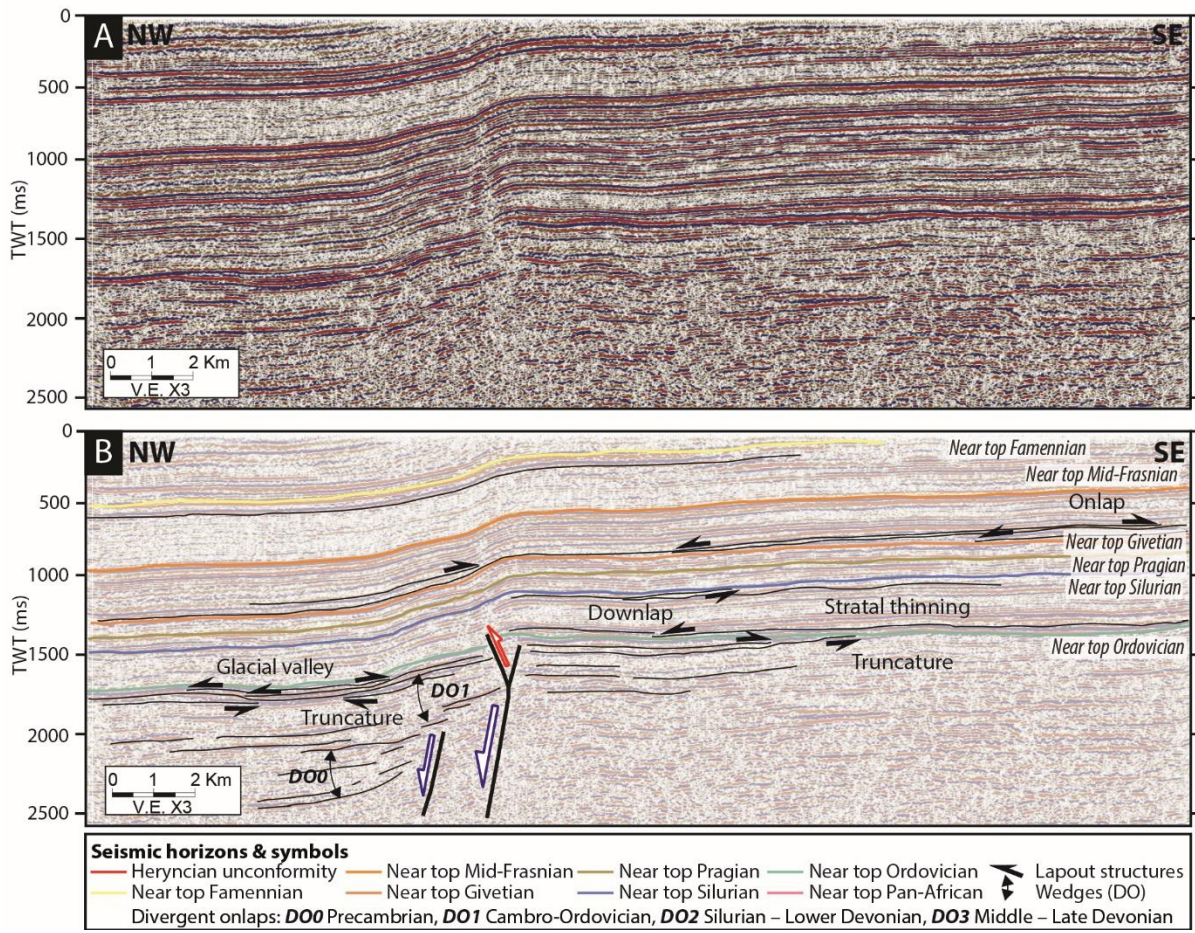


Figure V-20: (A) NW-SE seismic profile in the Ahnet basin near Erg Teguentour (near Arak-Foum Belrem Arch, westwards inter-basin boundary secondary arch) (B) Interpreted seismic profile showing steeply-dipping westwards basement normal blind faults associated to forced folding; Strata lapout geometries shows lower Silurian onlaps on the top Ordovician, glacial valley in intra-Ordovician series, onlaps and downlaps of Frasnian series on top Givetian unit. For localization see g in Figure V-4.

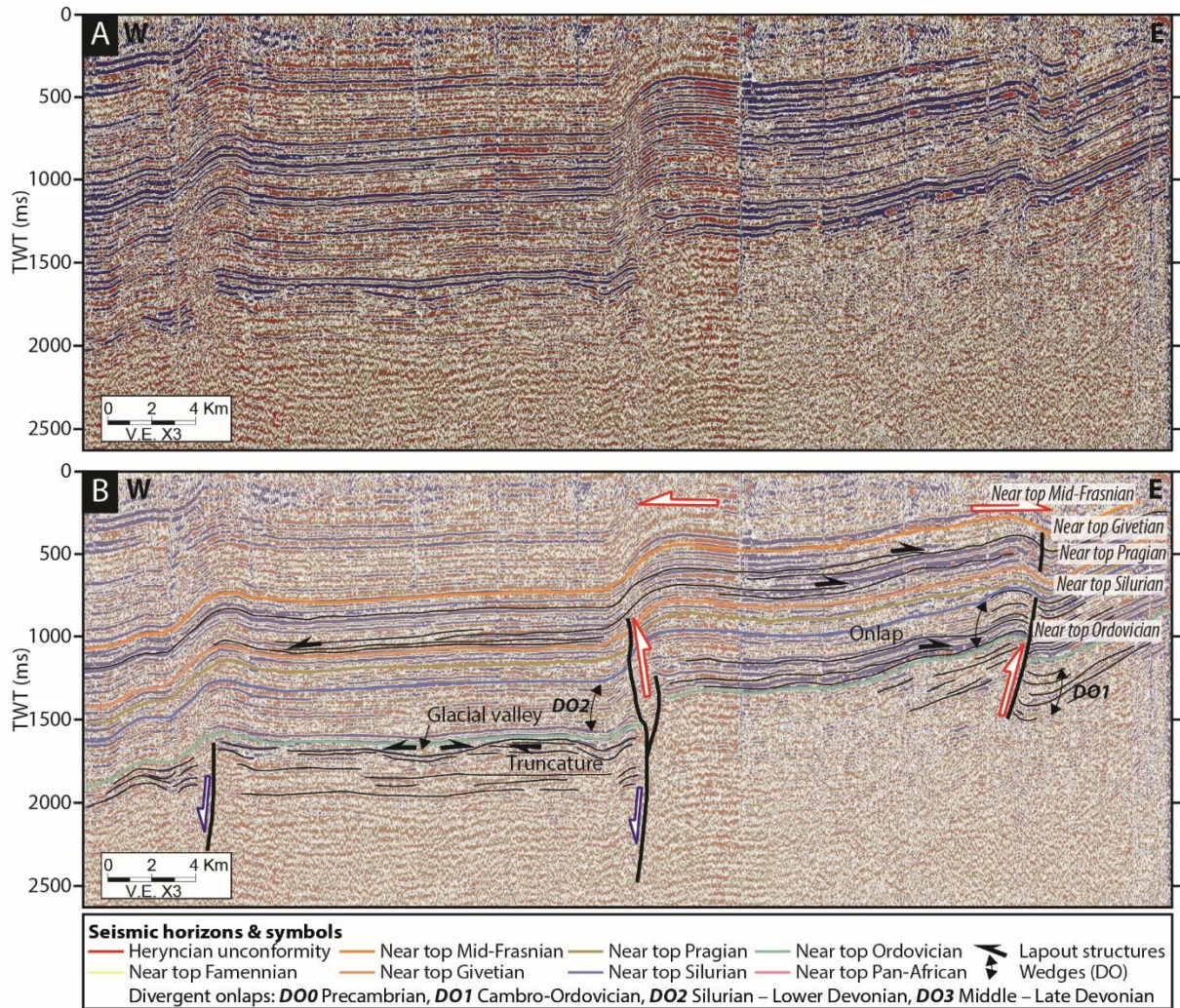


Figure V-21: (A) West-East seismic profile in the Ahnet basin near Erg Tegumentour (near Arak-Foum Belrem Arch, westwards inter-basin boundary secondary arch). (B) Interpreted seismic profile showing steeply-dipping westwards basement normal blind faults associated to forced folding; Strata lapout geometries shows lower Silurian onlaps on the top Ordovician, upper, onlaps and downlaps of Frasnian series on top Givetian unit. For localization see h in Figure V-4.

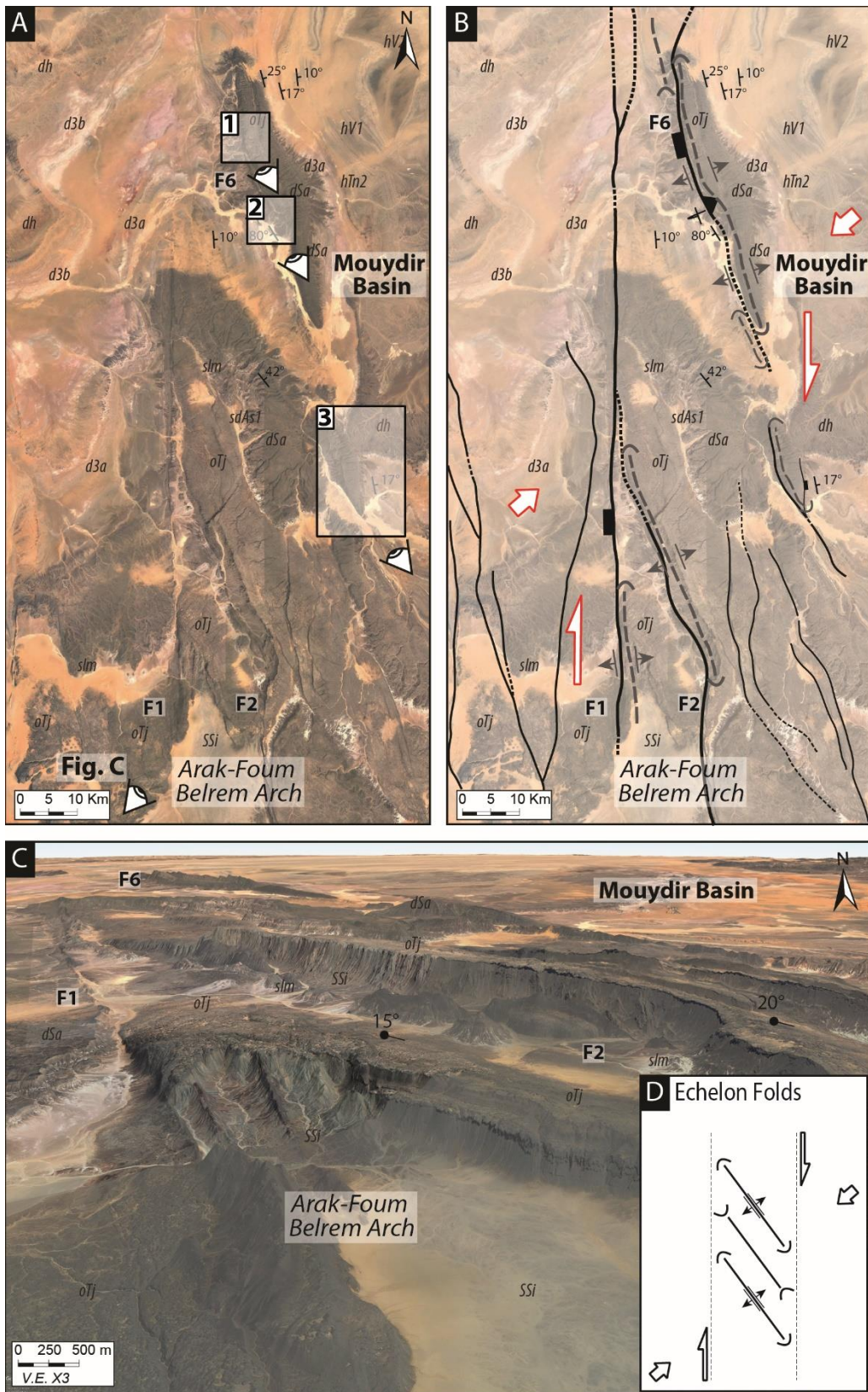


Figure V-22: (A) Not interpreted Google Earth image with localization of maps; 1: Figure V-16B; 2: Figure 6f in Perron et al., (2018); 3: Figure 6e in Perron et al., (2018). (B) Interpreted Google Earth image showing NS echelon folds in Devonian series. (C) 3D Google

Earth image showing relief. (D) Model of en echelon dextral folds. For localization see 4 in Figure V-6.

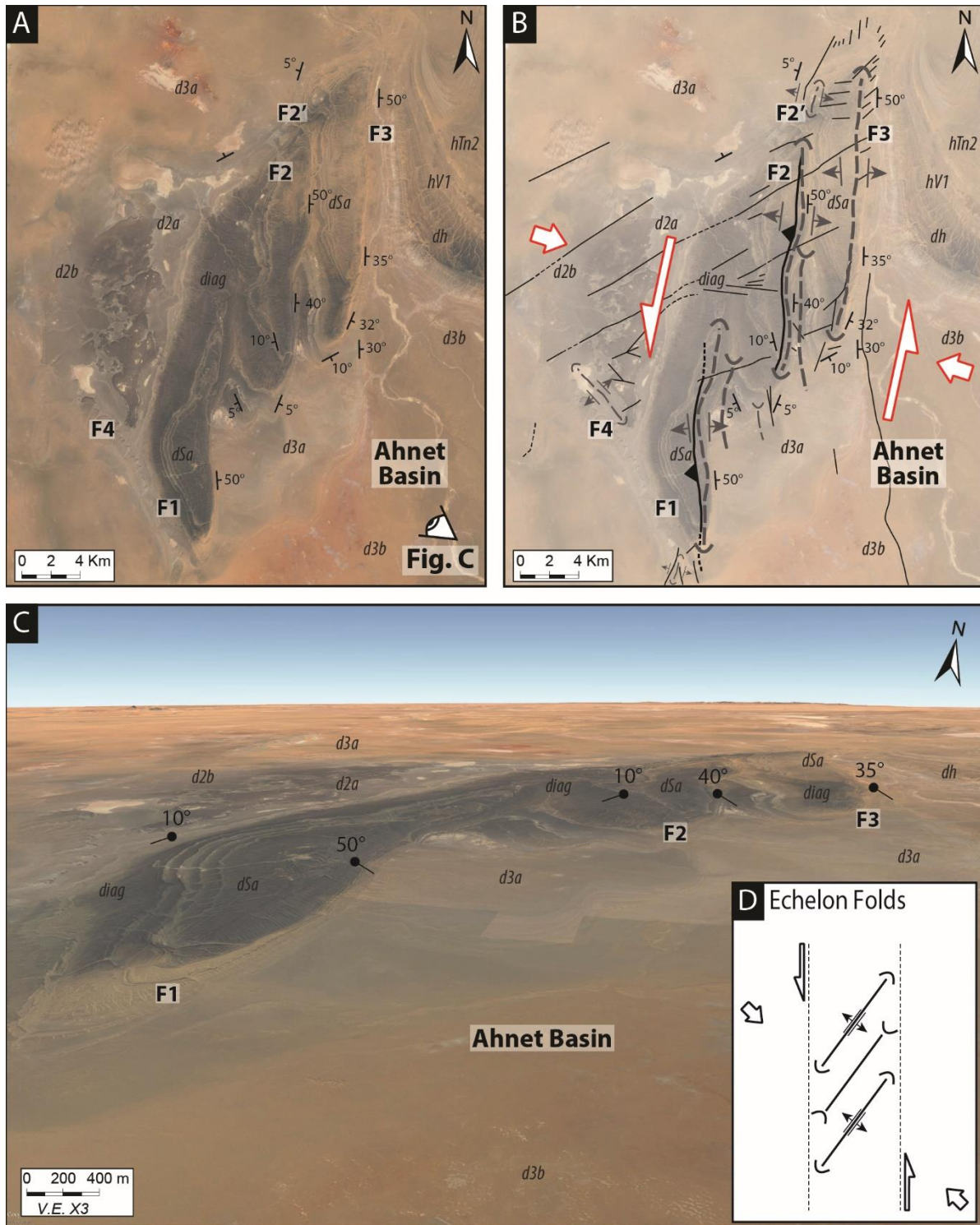


Figure V-23: (A) Not interpreted Google Earth image. (B) Interpreted Google Earth image near Azzl Matti Arch showing echelon fold with a senestral strike slip movement in Devonian series. (C) 3D Google Earth image showing relief. (D) Model of en echelon senestral folds. For localization see 3 in Figure V-7.

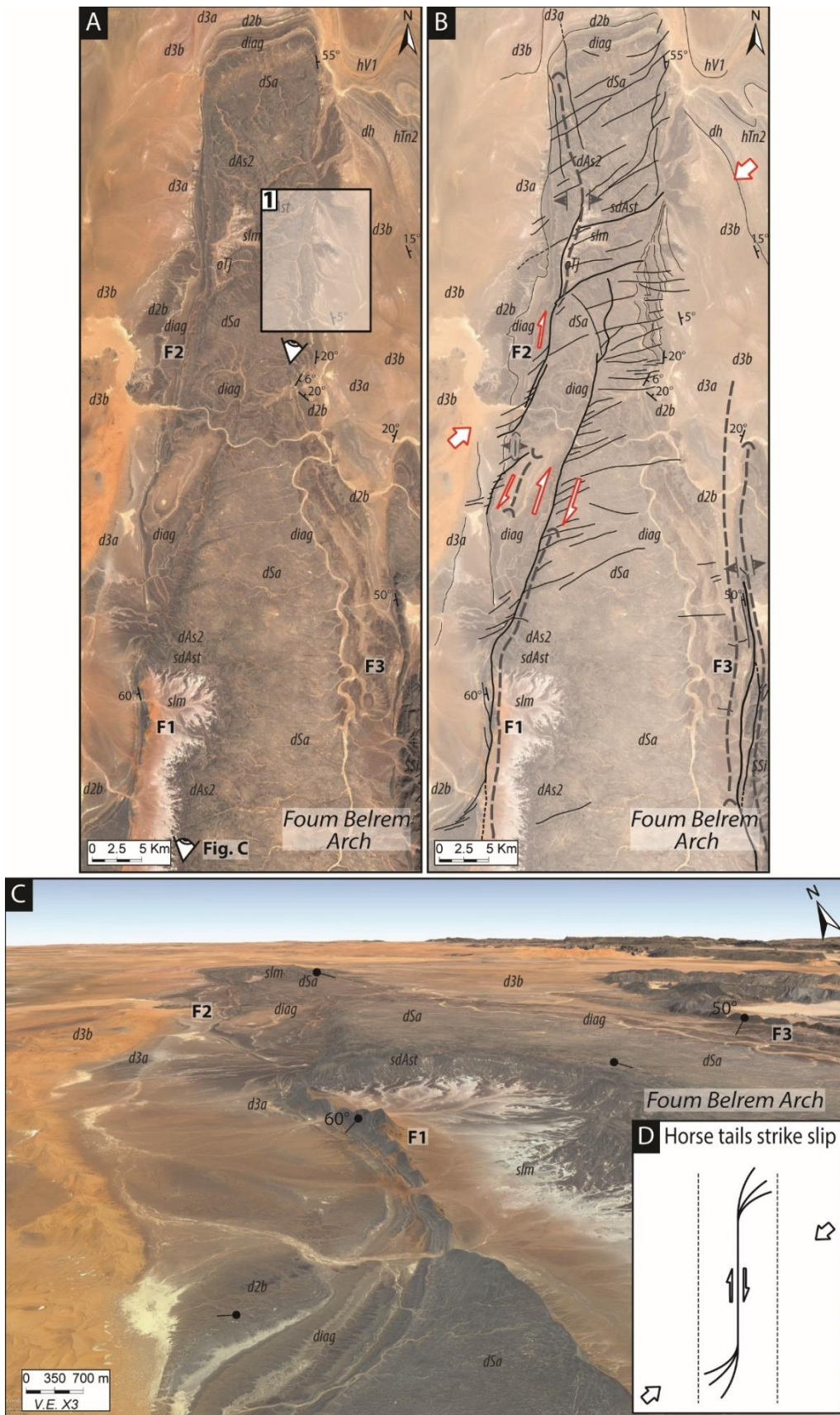


Figure V-24: (A) Not interpreted Google Earth image with localization of map; 1: Figure 6e in (Perron et al., 2018). (B) Interpreted Google Earth image showing dextral strike slip fault

associated to horse tails structures in Devonian series (C) 3D Google Earth image showing relief. (D) Model of horse tails strike slip. For localization see 4 in Figure V-7.

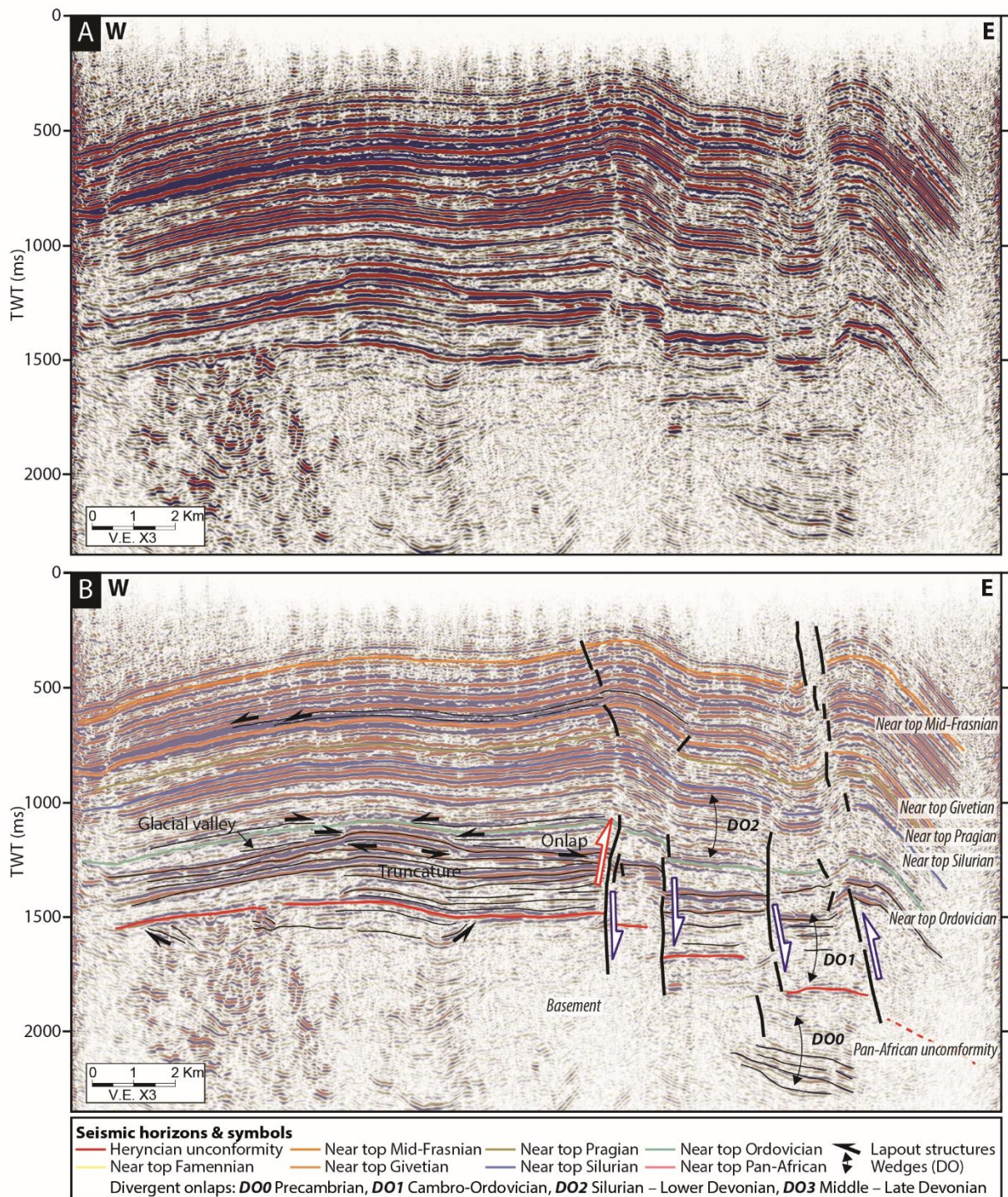


Figure V-25: (A) West-East seismic profile of Bahar el Hammar in the Ahnet basin (Ahnet intra-basin arch); (B) Interpreted seismic profile showing steeply-dipping eastwards normal fault inverted structure associated with folding (convex drag in each part of the fault); Strata lapout geometries shows glacial valley in the Ordovician series, Silurian onlaps on top

Ordovician, Silurian onlaps on top Ordovician; Frasnian onlaps on top Givetian; Polyphased events: Cambro-Ordovician extension and Devo-Carboniferous positive inversion (tectonic transport from hanging wall to footwall). For localization see i in Figure V-4.

3.4 Stratigraphy and lapout

This part is an inventory of stratigraphy and lateral termination of strata (i.e. lapout) such as onlaps, downlaps and toplaps. They were identified on both seismic and satellite images.

3.4.1 Pan-African unconformity

The Pan-African unconformity or the Infra-Cambrian (Infra-tassilian) surface can be identified on several seismic profiles (Figure V-19, Figure V-25 and Figure V-26) and satellites images (Figure V-12A-B). Tilted basement reflectors probably Precambrian series (“Les séries Pourprée”) are truncated by sub-horizontal planar Cambro-Ordovician strata forming an angular unconformity. Some of the paleo-structures observed can be sealed by Cambro-Ordovician series or reactivated in further tectonics (Figure V-25 and Figure V-26). Moreover, onlaps of Cambro-Ordovician strata are visible on Precambrian series (Figure V-12A-B), attesting of paleo-relief on the Azzel Matti Arch since the Cambrian.

3.4.2 Hirnantian glaciation

Incised valleys are observable in the hanging wall of fault (Figure V-20, Figure V-21, Figure V-25 and Figure V-26). These incised valleys are filled with onlapped reflectors and bound by truncated reflectors on the floor and the margins. They seem to be preferentially located in hanging-wall of the horst and graben systems. These seismic structures are described in the Murzuq basin and are characteristic of incised glacial valley related to Hirnantian glaciation (Smart, 2000).

3.4.3 Silurian transgression

The Silurian transgression is observed in seismic profiles (e.g. Figure V-26 and Figure V-21) and in satellite images (Figure V-14A). It is characterized by Lower Silurian onlaps and downlaps directly lay on the top Ordovician series. It can seal Cambro-ordovician fault (Figure V-14A).

3.4.4 Hercynian unconformity

The Hercynian unconformity is well identified in seismic (cf. Figure V-18). Paleozoic reflectors truncated by Cenozoic series feature it. Horizontal isopach (?) layer weakly deformed attesting of a very subtle tectonic strain after their deposition features the Cenozoic unit. Consequently, the Hercynian unconformity has sealed the Paleozoic series (Boote et al., 1998). Discordant Quaternary deposits (Quaternary unconformity) are also identified covering the whole Paleozoic series (Figure V-11A and Figure V-12A).

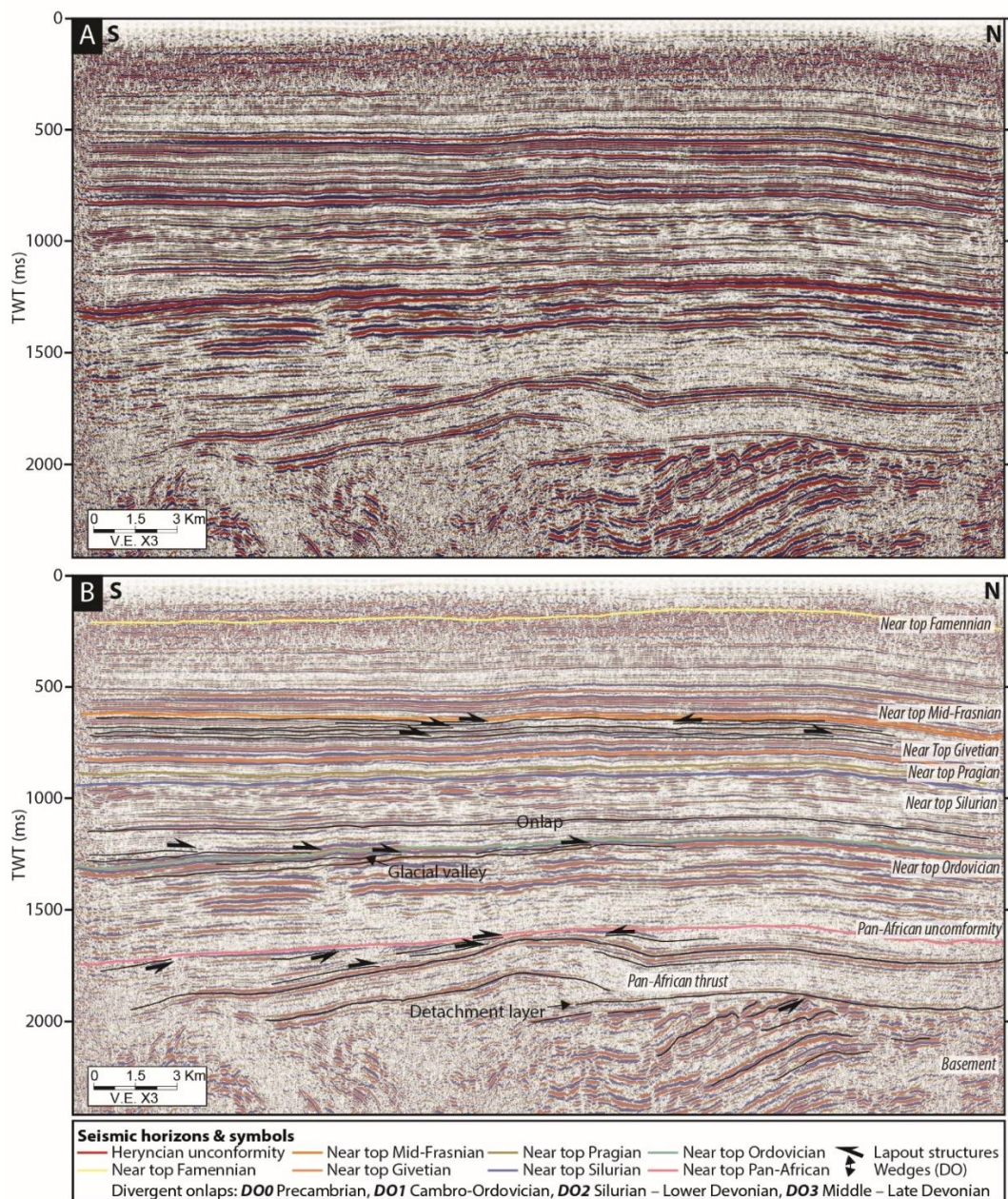


Figure V-26: (A) SN seismic profile near the Fom Belrem Arch. (B) Interpreted SN seismic profile near the Fom Belrem Arch showing glacial valley in the Ordovician series, Silurian

onlaps on the top Ordovician limit, downlaps and onlaps structures in Frasnian series on the top Givetian, Pan-African unconformity, Pan-African paleo-thrusting. For localization see e in Figure V-4.

3.5 Lithological and rheological framework

The stratigraphic succession of Paleozoic (cf. Figure III-36) displays two main contrasted types of lithologies: Thick low resistance (i.e. ductile) shales characterized by the Silurian and the Frasnian-Famennian units. High resistance (i.e. elastic) sandstones (with some limestone layers) featured by the Cambro-Ordovician, Lower Devonian and Lower Carboniferous units.

It follows that major uncouplings can be identified: Uncoupling between Cambro-Ordovician and Lower Devonian series; Uncoupling Lower Devonian and Lower Carboniferous series. Evidence of Silurian shales acting as a detachment layer uncoupling Cambro-Ordovician and Devonian series are visible such as Figure V-12A. Decoupling of Lower Devonian and Carboniferous separated by Frasnian-Famennian Shales series visible in Ahnet basin characterized by disharmony (Figure V-4). Frequency of folds is more important in the Carboniferous series than in the underlying Famennian series (i.e. Cambrian to Mid Devonian series).

Furthermore, Silurian and Frasnian-Famennian shales play an important role in the rheological behavior of Paleozoic structures. It permits in some cases to accommodate the deformation and inverted paleo-structures. The forced folds shape initiated by basement faults can be influenced by this ductile-plastic layer (Johnson and Johnson, 2002). Damping of faults often occurs in these series (e.g. Figure V-14B).

Additionally, the presence of a mechanical uncoupling can also exist between “Pourprée” series, lateritic series and the crystalline basement (Beuf et al., 1971).

Structures are discontinuously deformed (fault and folds association) and coupled with the basement. Cambro-Ordovician layers are essentially dominated by sandstone deposits (i.e. elastic rheology) while Silurian is composed of shales (i.e. plastic-ductile rheology). Whereas Silurian to Carboniferous layers are deformed continuously (folds) where Silurian plays the role of detachment layer between the two latter. The Silurian shales could be a good client for decoupling the deformation and permitting forced fold structures.

3.6 Structural style and implications

Our observations made from seismic and satellites images highlight several tectonic features: (1) heritage and reactivation/inversion of basement faults (essentially sub-vertical but presence of thrusting fault); (2) Forced fold and trishear models; (3) major uncoupling between Cambro-Ordovician series and Devonian series through Silurian detachment shale layer; (4) minor uncoupling in layer cake series such as Devonian series and Carboniferous series; (5) imply disharmonic structures/layers; (6) sub-vertical planar fault; (7) dominated by repeatedly strike slip movement.

Clearly the structural style in this Paleozoic intracratonic area is defined by basement steeply dipping tectonic structures where the deformation is accommodated mainly by strike slip movement (i.e. transpression or transtension) on sub-vertical faults. The compression component is accommodated by flexural structure (folding) and the extension component by sub-vertical planar extension faults. In case of sub-vertical planar extensional fault compensation graben occurs to accommodate the deformation (Faure and Chermette, 1989).

In surface, the deformation is characterized by folds (fault propagation fold, asymmetric uplift). The mechanical behavior (i.e. the accommodation of the deformation) of the basement and the cover seems to be different (i.e. ductile to brittle). It can be explained by the petrological heritage of these two entities: crystalline rocks for the basement and shales and sandstones for the cover. From analogical and numerical structural analysis, the thesis of detachment fold and propagation fold were privileged (Badsı et al., 1999).

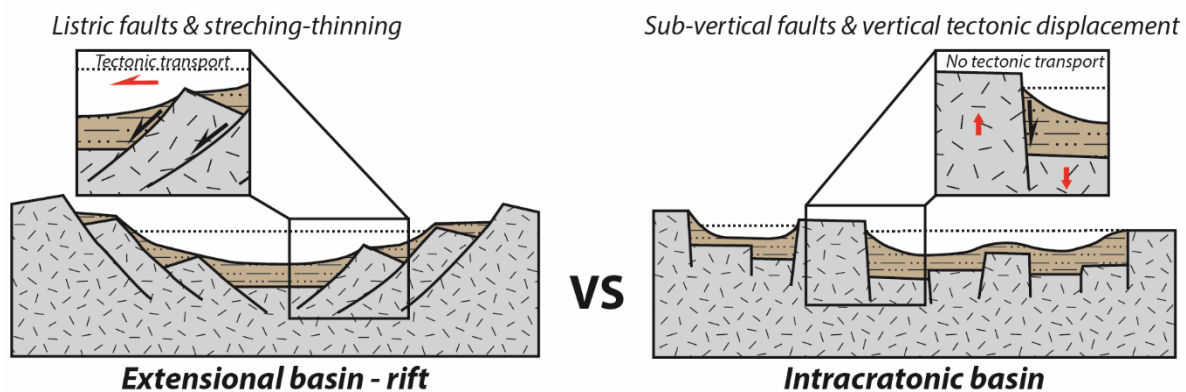


Figure V-27: Comparison between classical extensional basin and peri-Hoggar intracratonic basins structural style. Notice that faults morphologies impact the sedimentation pattern.

To summarize, the structural style is featured by vertical displacement and equilibration on major sub-vertical faults between terranes. A singular tectonic kinematics, where there is no (or weakly) stretching which can be observe in classical extensional zones such as rifts (Figure V-27).

3.7 Precambrian inherited basement faults structures

The establishment of Paleozoic tectonic structures (e.g. folds) seems to be tough to explain under simple compression without basement faults (Badsı et al., 1999; Beekman et al., 2000). The hypotheses of the presence of pre-existing basement discontinuities reactivating during Paleozoic tectonic events seems to be the key understanding (Badsı et al., 1999; Beekman et al., 2000; Haddoum et al., 2001; Zazoun, 2001). In the literature, many authors have pointed the significance of influence of basement faults on the basin structuration (e.g. Fowler and Osman, 2013). Numerous study show how weakness zone influence the geometries and structuring of strike slip fault zone (e.g. Dooley and Schreurs, 2012).

Several evidences of basement structures can be observed in seismic profiles (e.g. Figure V-18 and Figure V-26). Basement analysis of the seismic cross section doesn't permit to clearly distinguish the faults geometries. Reflectors signatures are often chaotic. Seismic survey acquisition has not been for deep structures objectives (Badsı et al., 1999). Though, the faults are mainly characterized by steeply dipping planar normal faults (to the east or to the west). It can form a horst and graben system probably inherited from the Precambrian. The lateral movement of this basement faults (i.e. wrench) is difficult to decipher in cross section, nevertheless many authors has demonstrated it (Caby, 2003; Haddoum et al., 2013; Liégeois et al., 2003). In surface satellites imagery (e.g. Figure V-22, Figure V-23 and Figure V-24), the presence of sigmoid folds, echelon folds, horse tails structures attest of the strike slip movement (see also Haddoum et al., 2001; Zazoun, 2001). Tilted series to the east is uncomfortably overlain by the Cambro-Ordovician unit (pointed out by reflectors truncatures) (e.g. Figure V-26). This structure might have been controlled by a paleo-thrusting featured in the basement by an inverse fault with a moderate dip to the east and with a tectonic transport to the west or a paleo-half graben (not visible here but possibly present eastwards) during the Precambrian. All these structures seem to be reactivated or inverted during the Paleozoic tectonic events leading to the deformation of the cover.

3.8 Synthesis of the chronologic tectonic kinematics and strata layout geometries

The main structures detectable in the subsurface by seismic interpretation and in surface by satellites images are normal faults affecting the basement and dividing it into horst and graben systems during Cambro-Ordovician (maybe earlier by Pan-African chain collapse). The reactivation or/and positive inversion of these systems, consisting of compressional gentle folds associated with reverse faults located on the pre-existing normal faults or/and extensional fault related to forced fold helped by detachment layer (i.e. Silurian and Frasnian-Famennian series) are the main structural kinematics of these basins. The extensional movement switched into a compressional one. This latter description synthesized the structural style, stratigraphic layout and the chronologic tectonic kinematics of the Saharan Platform where three main tectonic models have been identified (Figure V-28).

Contrary to the Siluro-Devonian tectonic which rejuvenated some paleo-structures the Hercynian compression has largely affected the Precambrian basement and is at the origin of the actual state of Saharan platform (Follot, 1953). Indeed, the Hercynian unconformity sealed the Paleozoic series (Boote et al., 1998). The Hercynian event is featured by a particular tectonic style. The uncoupling of the Cambro-Ordovician and Devo-Carboniferous series separated by Silurian shales is visible. This observation was already shown by Follot, (1953).

Our observation shows that the Arches and Basins association were active and rejuvenated during local or/and regional strain between the Cambrian to the Carboniferous. This characteristic framework disappear during the carboniferous according to Wendt et al., (2006). The control of basement faults inherited from Precambrian orogeny on Paleozoic covers was point out by many authors (Beuf et al., 1968b, 1971; Biju-Duval et al., 1968; Boote et al., 1998; Echikh, 1998; Eschard et al., 2010; Fabre, 2005; Frizon de Lamotte et al., 2013; Guiraud et al., 2005; Haddoum et al., 2001; Zazoun, 2001). Nevertheless, we have seen that some event describe in the literature are not easily decipherable in seismic or satellites images (e.g. Caledonian event).

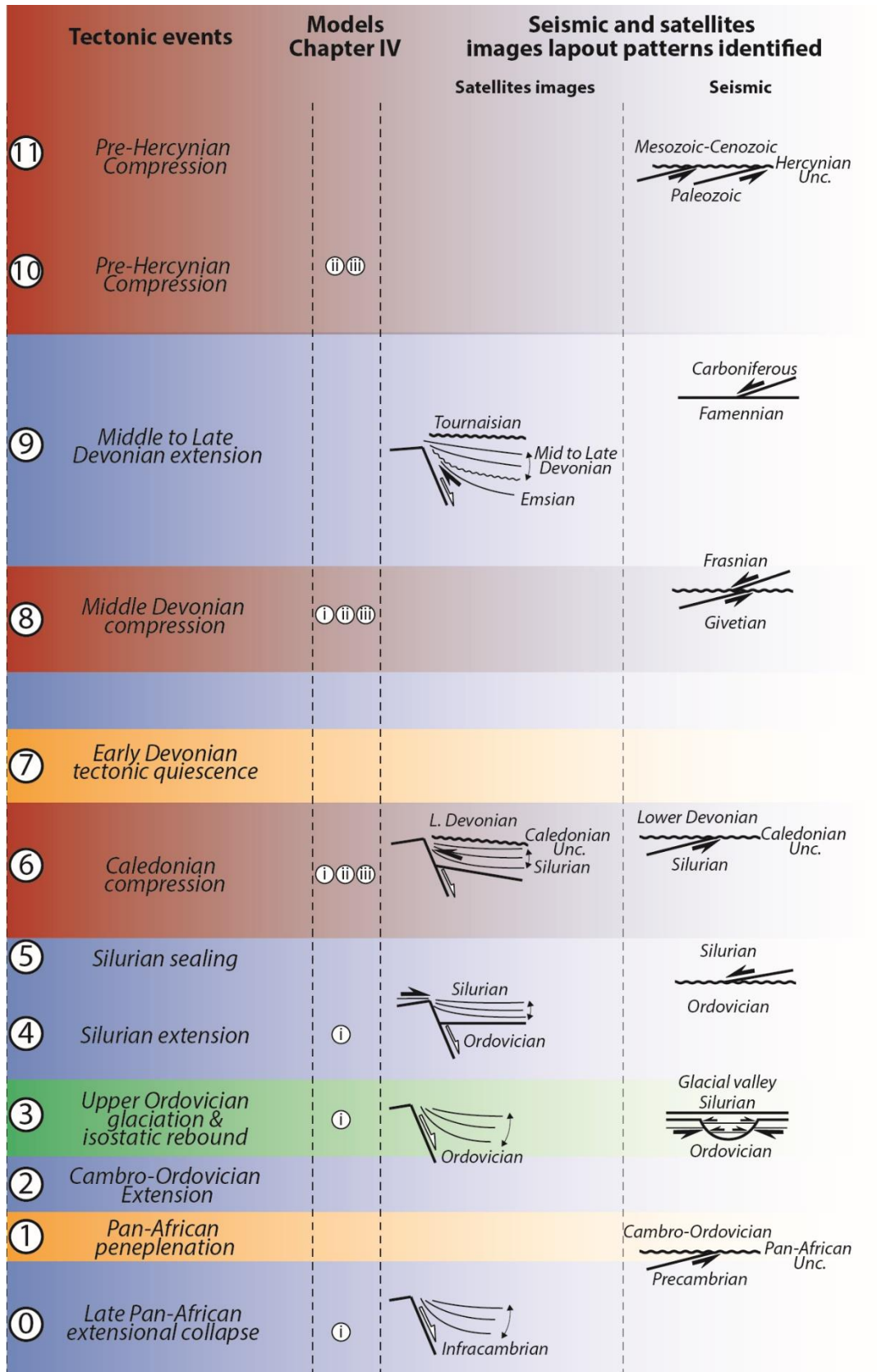


Figure V-28: Synthesis of structural model, stratigraphic lapout identified from satellite images and seismic profiles during the Paleozoic time on the Saharan Platform. (i), (ii), (iii) correspond to structural models proposed in Perron et al., 2018.

4 Stratigraphy and sedimentology

In this part, the analysis of the basin architecture of the peri-Hoggar Basins is led through the angle of well logs correlation and the facies partitioning. Regional correlations of wells (Figure V-29) are made calibrated by biostratigraphic data and guide by previous tectonic analysis.

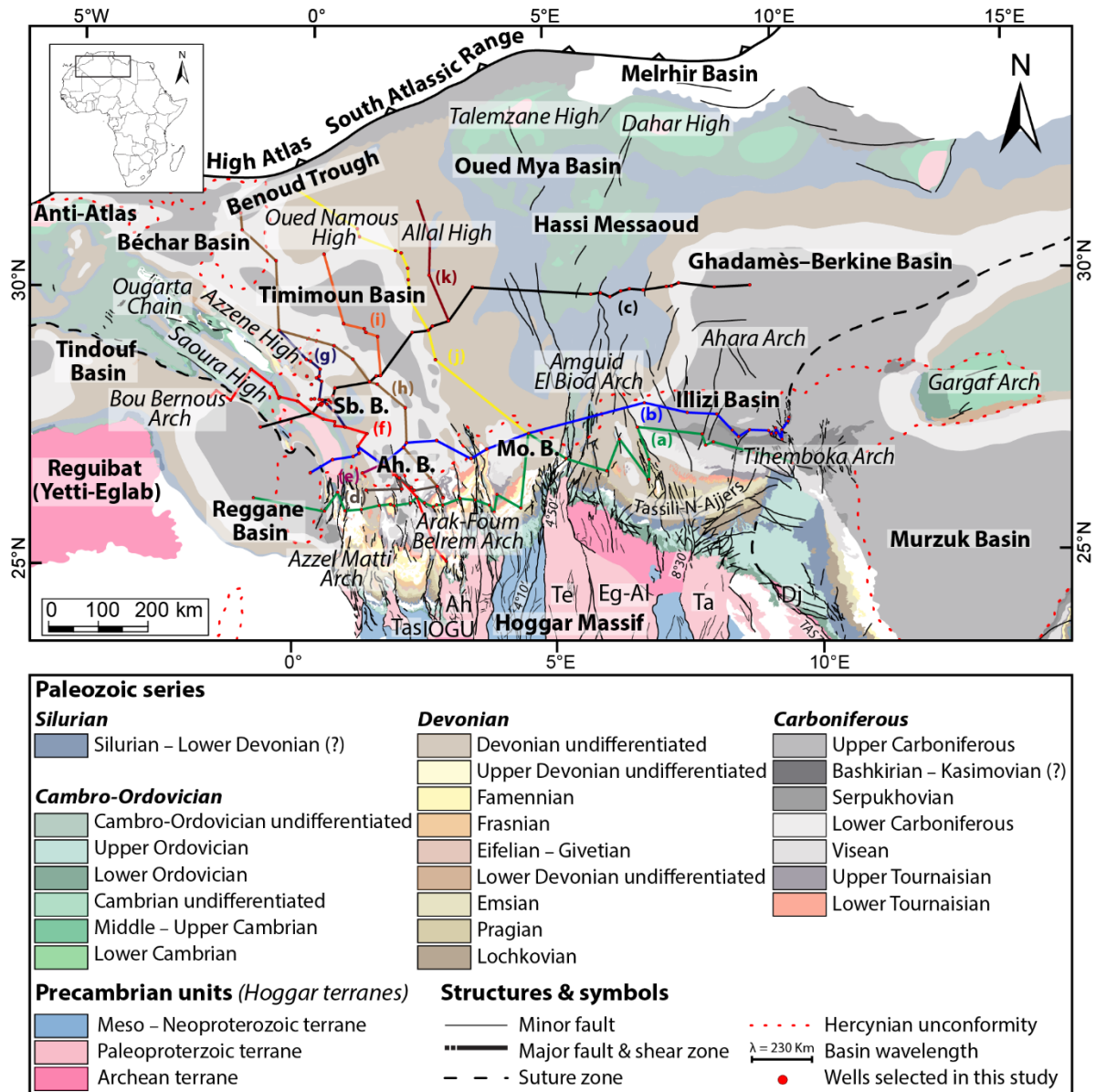


Figure V-29: Geological map of the Paleozoic North Saharan Platform (North Gondwana) showing the localization of regional wells cross sections. (a): Figure V-33; (b): Figure V-32; (c): Figure V-39; (d): Figure V-35; (e): Figure V-34; (f): Figure V-36; (g): Figure V-42; (h): Figure V-37; (i): Figure V-40; (j): Figure V-38; (k): Figure V-41. Sb. B.: Sbâa Basin; Ah. B.: Ahnet Basin; Mo. B.: Mouydir Basin.

4.1 Facies association, depositional environments and well-log pattern

The Paleozoic sedimentary series described in the literature is composed of fluvial to Braid-deltaic plain Cambrian, not only fluvial (e.g. Brahmaputra River analogue), with a transitional facies from continental to shallow marine (e.g. Beuf et al., 1968b, 1968a, 1971; Eschard et al., 2005, 2010; Sabaou et al., 2009), Upper Ordovician glaciogenic deposits (e.g. Beuf et al., 1968a, 1971; Deschamps et al., 2013; Dixon et al., 2008b, 2008a; Eschard et al., 2005, 2010; Ghienne et al., 2007a; Girard, 2011; Hirst, 2012, 2016; Lang et al., 2012; Le Heron et al., 2009), argillaceous deep marine Silurian deposits (e.g. Djouder et al., 2018; Eschard et al., 2005, 2010; Gindre et al., 2012; Legrand, 1986, 2003b; Lüning et al., 2000) and offshore to embayment Carboniferous deposits (e.g. Wendt et al., 2009). In this complete sedimentary succession, the facies associations and depositional as well as well-log pattern of the Silurian and the Carboniferous are rather similar to Cambro-Ordovician and the Devonian. As consequence, we have focused on the Cambro-Ordovician and the Devonian.

The Devonian facies association describe in Table 1 in Chapter IV related to their gamma-ray log patterns (Figure 9 in Chapter IV) are regrouped into five main depositional systems: Continental (fluvial), coastal plain, transitional (estuarine, tidal flat, lagoon, fluvial/tidal distributary channels), (upper to lower) shoreface and (upper to lower) offshore. Additional core descriptions with their gamma ray signal are presented in Figure V-31.

The Cambro-Ordovician facies association description and their gamma-ray signature are issue from internal studies (Desaubliaux et al., 2005; Robertson, 2002). After a compilation and synthesis, they are reorganized into four main depositional systems: Continental (fluvial), continental to marine transition, upper marine and lower marine shelf.

An example of stacked patterns of depositional environments associated with their gamma-ray log signature is exposed in Figure V-30. They are well representative of the Cambro-Ordovician and Devonian successions that can be experienced in the peri-Hoggar Basins. It constitutes a base for interpretation of the regional cross sections.

The depositional environment systems (based on facies succession) were established considering the lateral environments evolution and the reconstruction of paleoprofiles deposits from the stratigraphic correlations between the different sections. The interpretation of certain facies was difficult or equivocal, and sometimes the recognition of the relative position of these facies has resolved any ambiguity and offered the best interpretation.

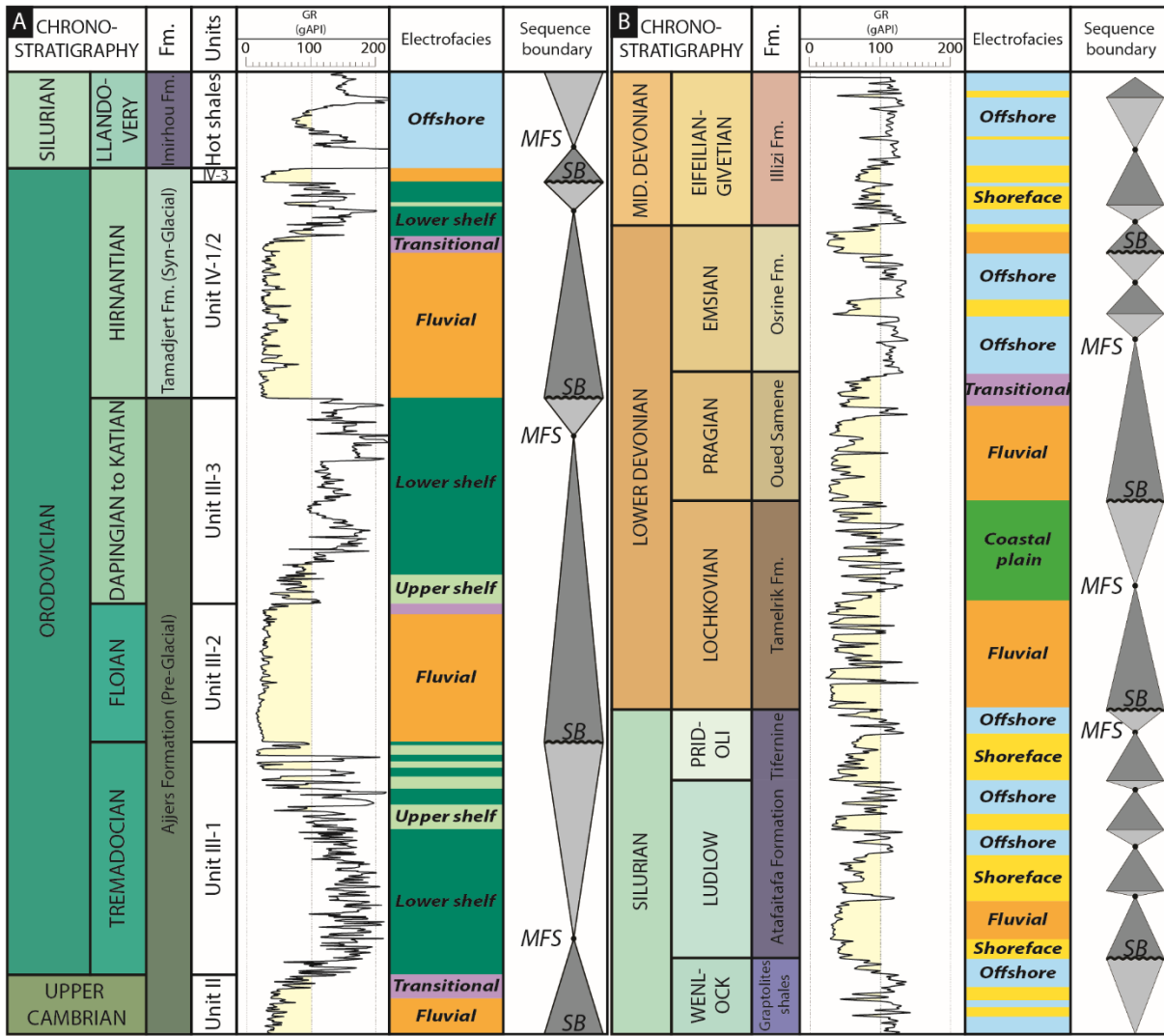


Figure V-30: Example of sequence stratigraphy limit with the depositional environments associated with their gamma-ray signature and well-logs patterns (i.e. electro-facies) in (A) the Ordovician series and (B) in the Devonian series. Example of representative electrofacies of Cambro-Ordovician and Devonian successions used as a pattern for regional well correlations of peri-Hoggar Basins.

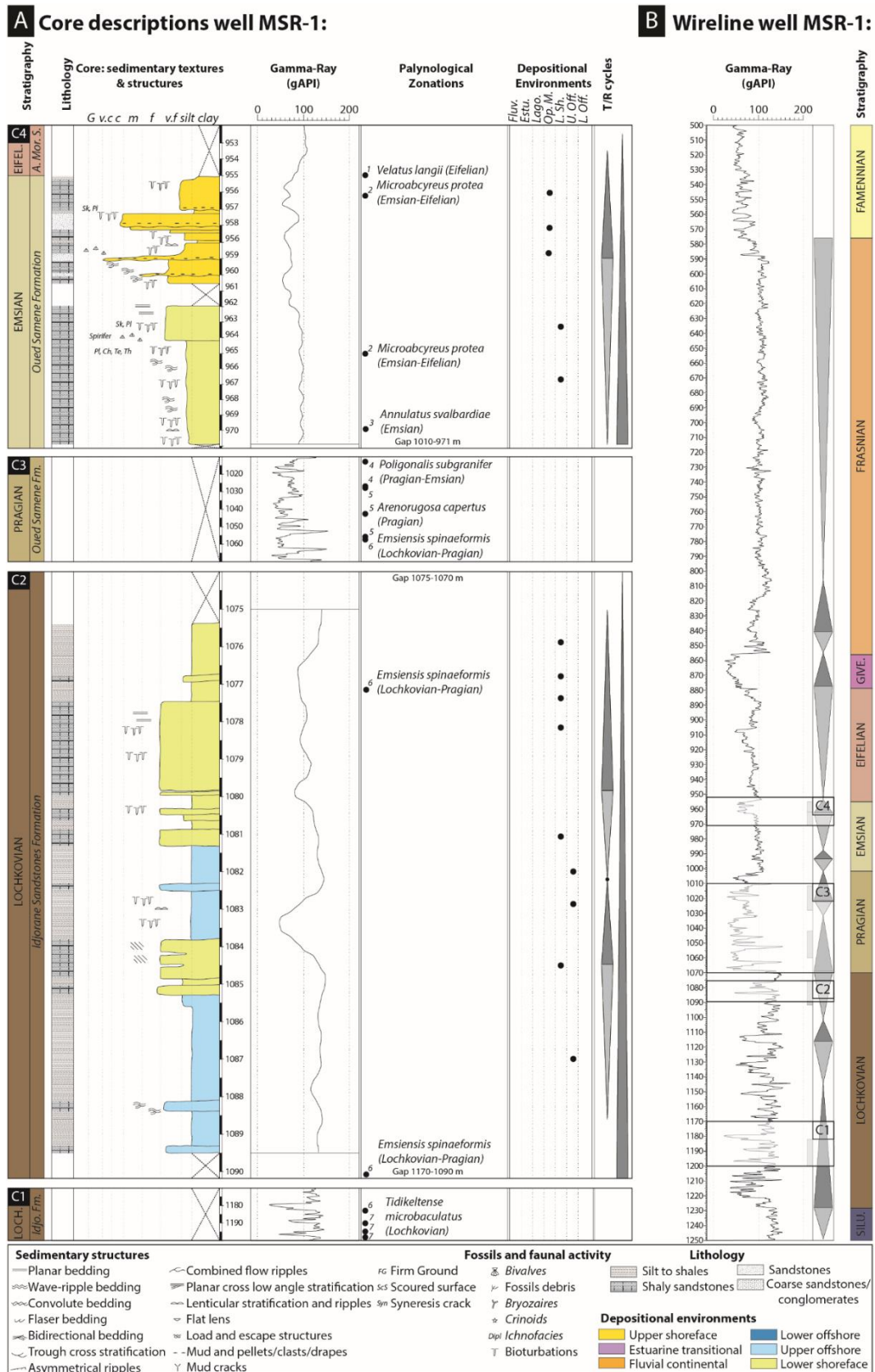


Figure V-31: Core sedimentologic description of well MSR-1 in Devonian series in Ahnet Basin. The palynological datation is from published paper (Kermandji et al., 2008) and the core description from internal study (Aissani and Bennamane, 2003).

4.2 Paleozoic regional well-log correlation and cross section

The description of the gamma-ray log patterns and trends (Figure V-30) permit the reconstitution of the geometries of the sedimentary bodies and of their vertical and lateral evolution of the Paleozoic. A parasequence is defined as a prograding succession, bounded by flooding surfaces and defining a coarsening or cleaning upward trend.

A selection of 138 wells and 15 outcrop cross section have been used to illustrate the stratigraphic architecture of the peri-Hoggar Basins (Figure V-29). They are displayed on five East-West cross sections (Figure V-32, Figure V-33, Figure V-34, Figure V-35 and Figure V-39) and one North-South cross sections (Figure V-36, Figure V-37, Figure V-38, Figure V-40, Figure V-41 and Figure V-42).

The stacking pattern of the Paleozoic successions shows multiple cycles of major regression and major transgression (Figure V-32, Figure V-33, Figure V-34, Figure V-35, Figure V-36, Figure V-37, Figure V-38, Figure V-39, Figure V-40, Figure V-41 and Figure V-42).

In the Upper Silurian to Lower Devonian series a lateral variation of facies is observe. The facies evolve from fluvial near the Tihemboka Arch to shoreface systems westwards (more and more marine influence). Spatially, we observe a deepening of facies northwards but also westwards (i.e. north-westwards trend). This feature was already observe by numerous authors (e.g. Beuf et al., 1971; Eschard et al., 2005).

Temporally, we display a shallowing downward of the different unit (i.e. Lower Devonian has more proximal facies than Upper Devonian). Moreover, the Cambro-Ordovician and the Devonian are essentially characterized by shallower facies than the Silurian and the Carboniferous

Our observation shows evidence of thickness variation and erosion between arches and basin. Some level can be condensed or eroded at proximity of the arch. Subtle facies lateral variations are also detected. It is featured by a shallowing of depositional environments at the vicinity of arches and deepening of environments in basin lows. The maximum of thickness of the Paleozoic series are observed upon Proterozoic terranes.

In this part, multiple regional cross section from internal wells data has highlighted evidence of stratigraphic and sedimentary structures. Likewise, it leads to confirm of the arches and basins architecture characteristics previously pointed out in Chapter IV.

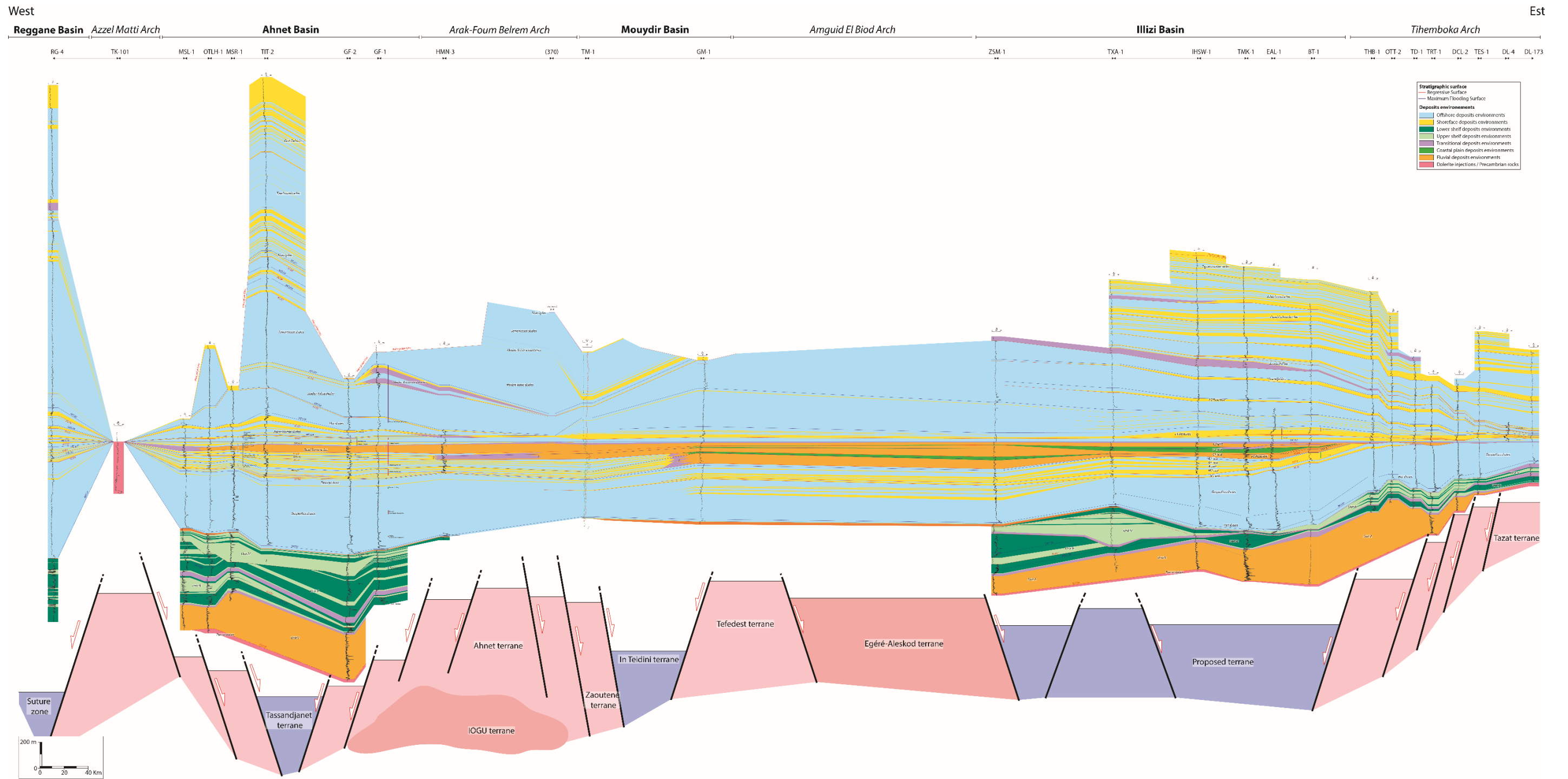


Figure V-32: North EW wells cross section of North peri-Hoggar Basins (Reggane-Ahnet-Mouydir-Illizi Basins). Horizontalization on top Pragian transgression. For localization see Figure V-29.

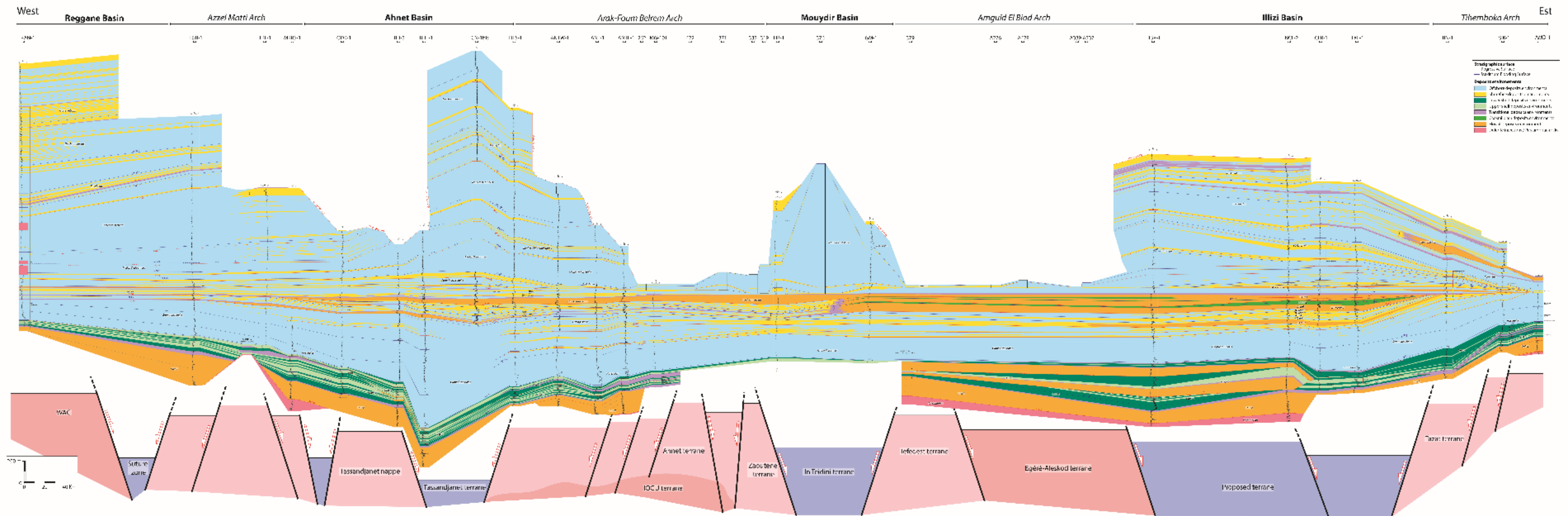


Figure V-33: South EW wells cross section of North peri-Hoggar Basins (Reggane-Ahnet-Mouydir-Illizi Basins). Horizontalization on top Pragian transgression. For localization of the cross section see Figure V-29.

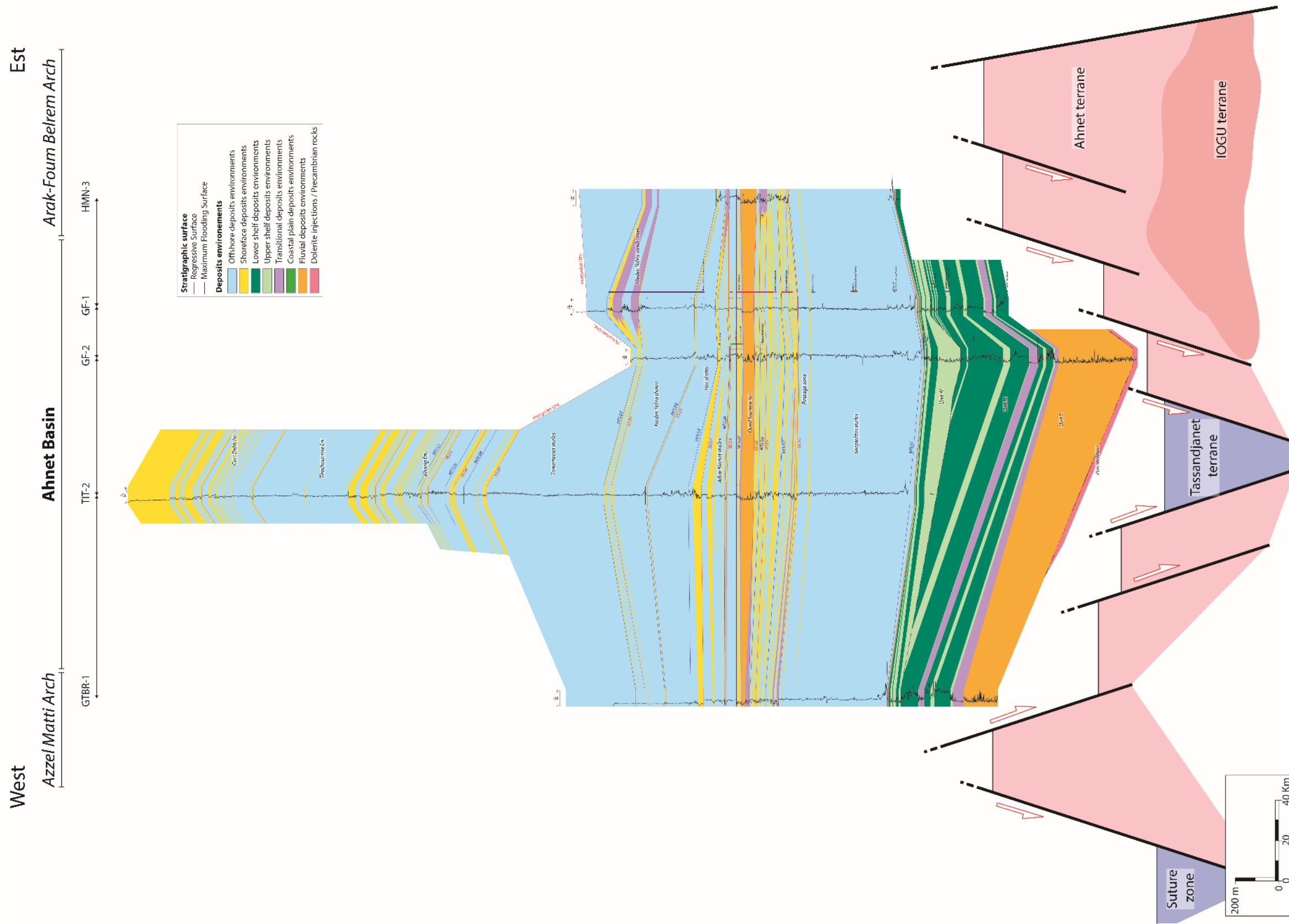


Figure V-34: EW cross wells section in the North part of the Ahnet Basin. Horizontalization on top Pragian transgression. For localization of the cross section see Figure V-29.

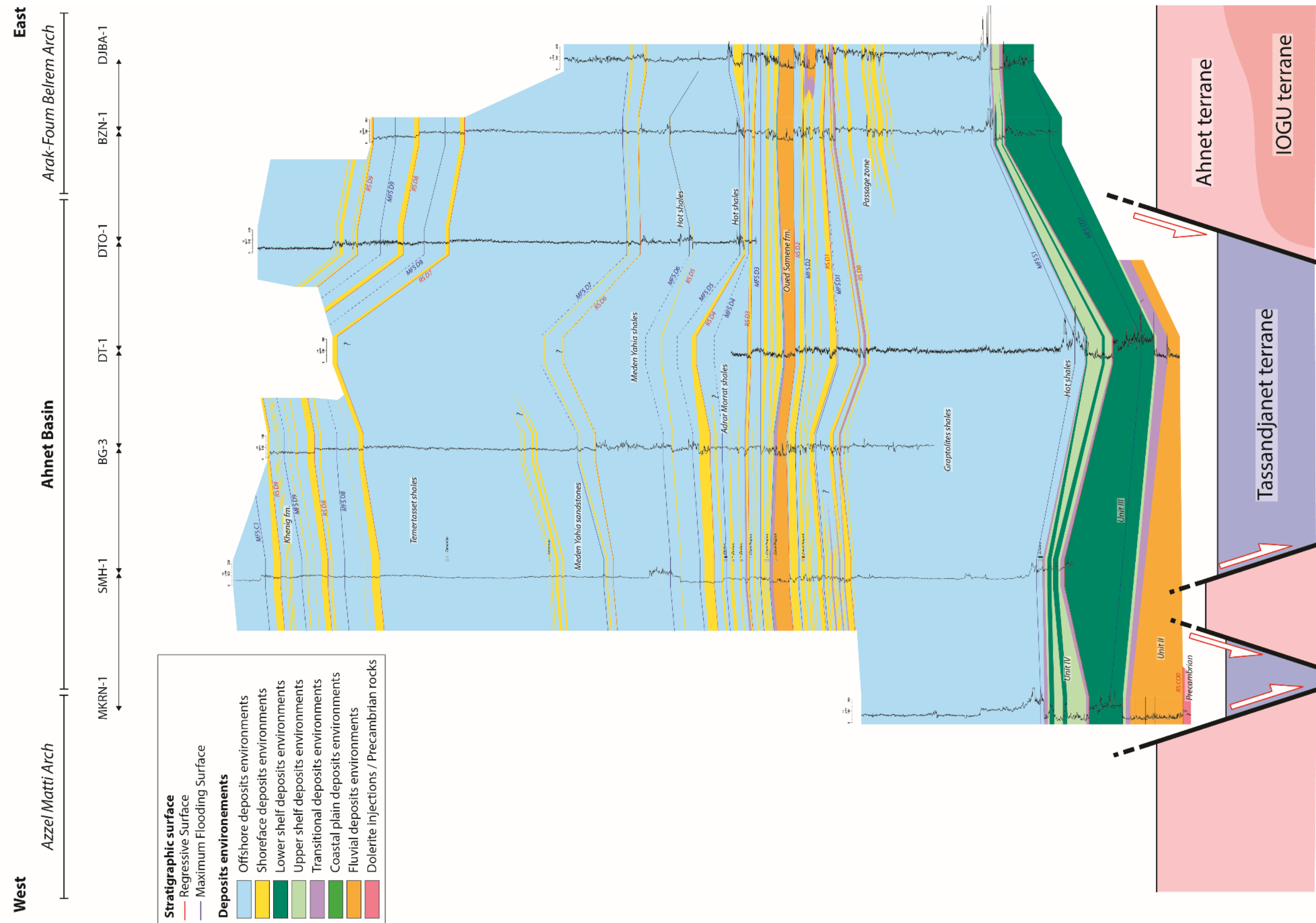


Figure V-35: EW cross wells section in the central part of the Ahnet Basin. Horizontalization on top Pragian transgression. For localization of the cross section see Figure V-29.

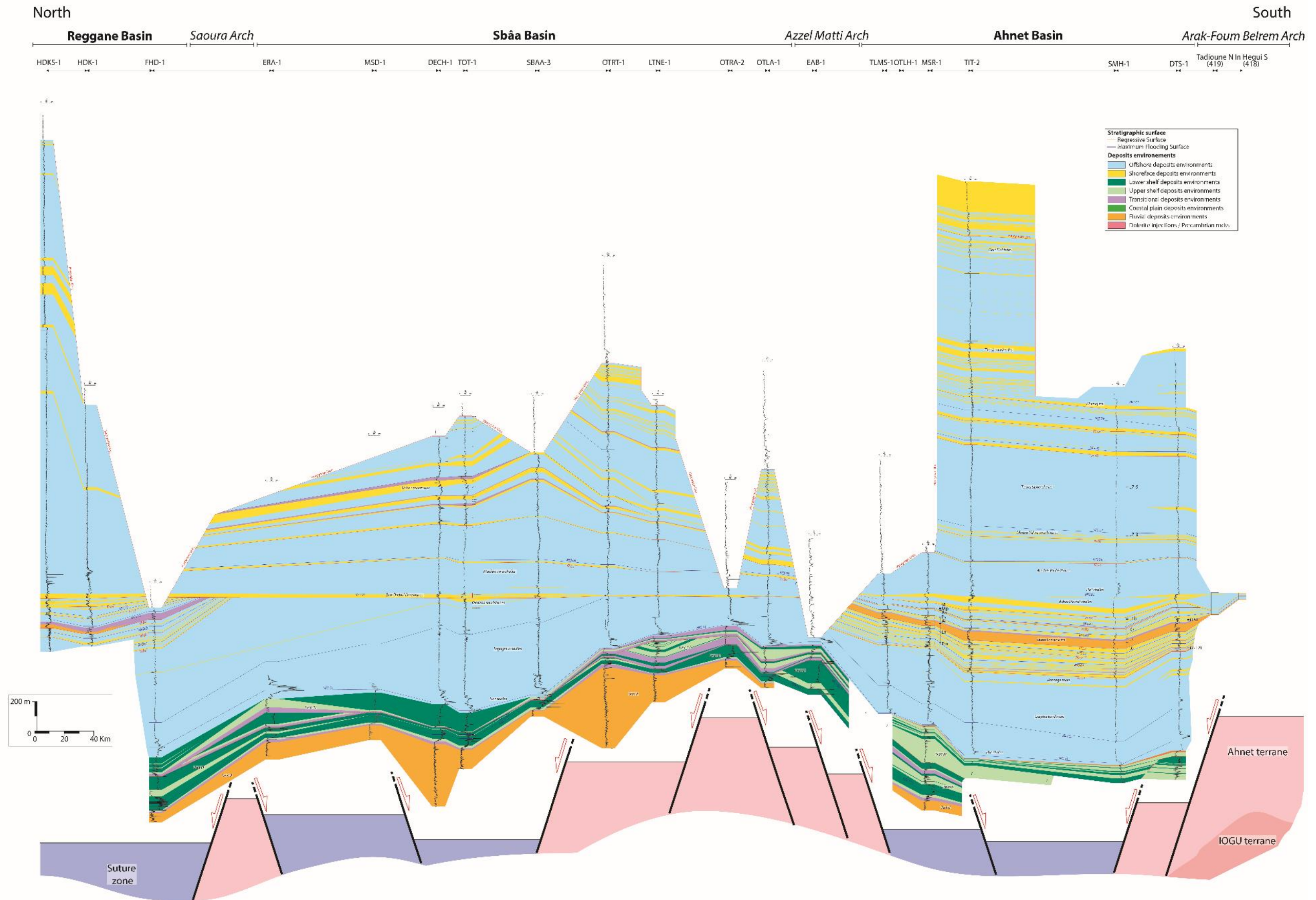


Figure V-36: NS wells cross section of North peri-Hoggar basins (Ahnet-Sbâa-Reggane Basins). Horizontalization on top Givetian transgression. For localization of the cross section see Figure V-29.

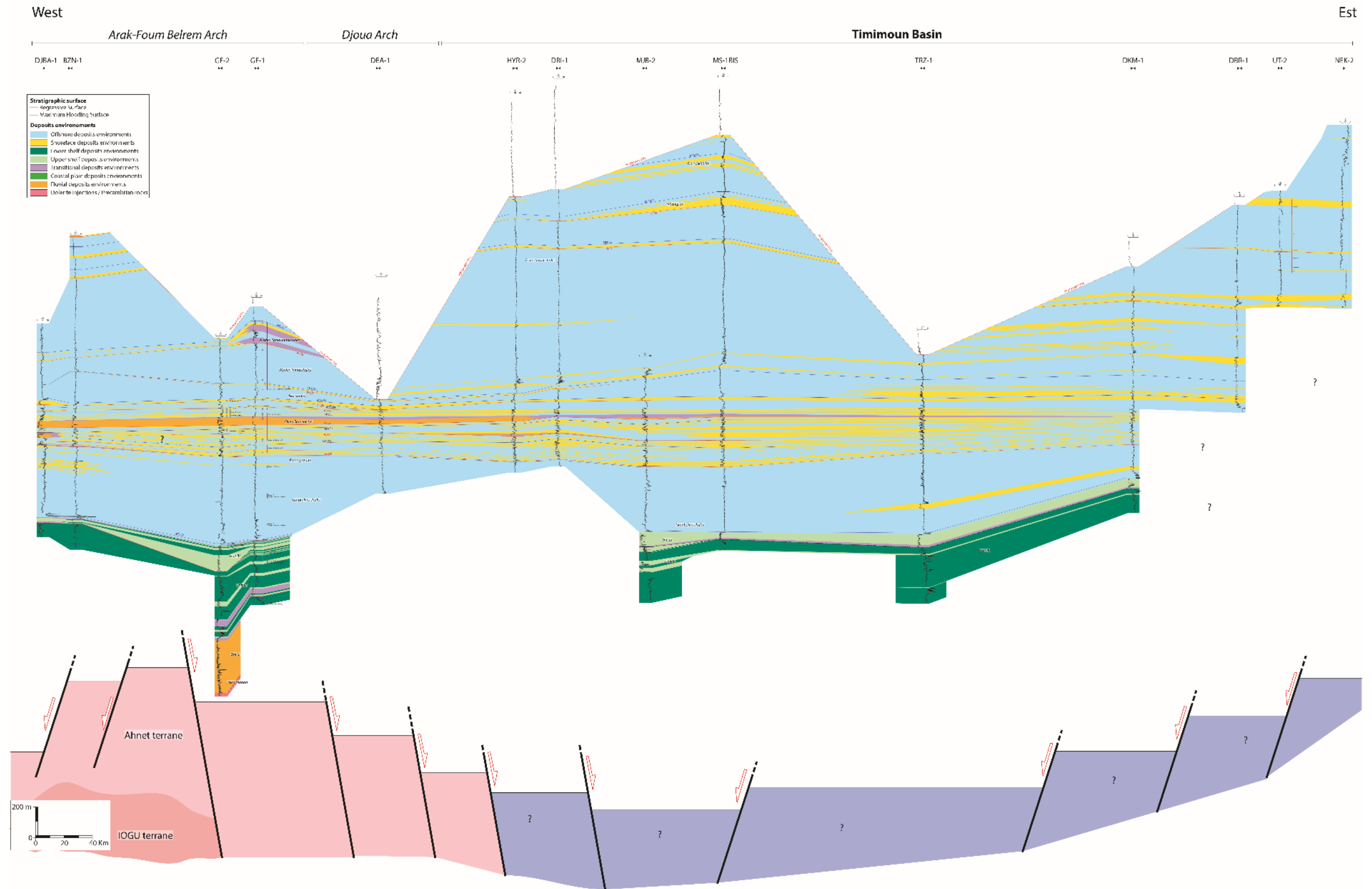


Figure V-37: NS wells cross section of North peri-Hoggar basins (Ahnet-Timimoun Basins). Horizontalization on top Pragian transgression. For localization of the cross section see Figure V-29.

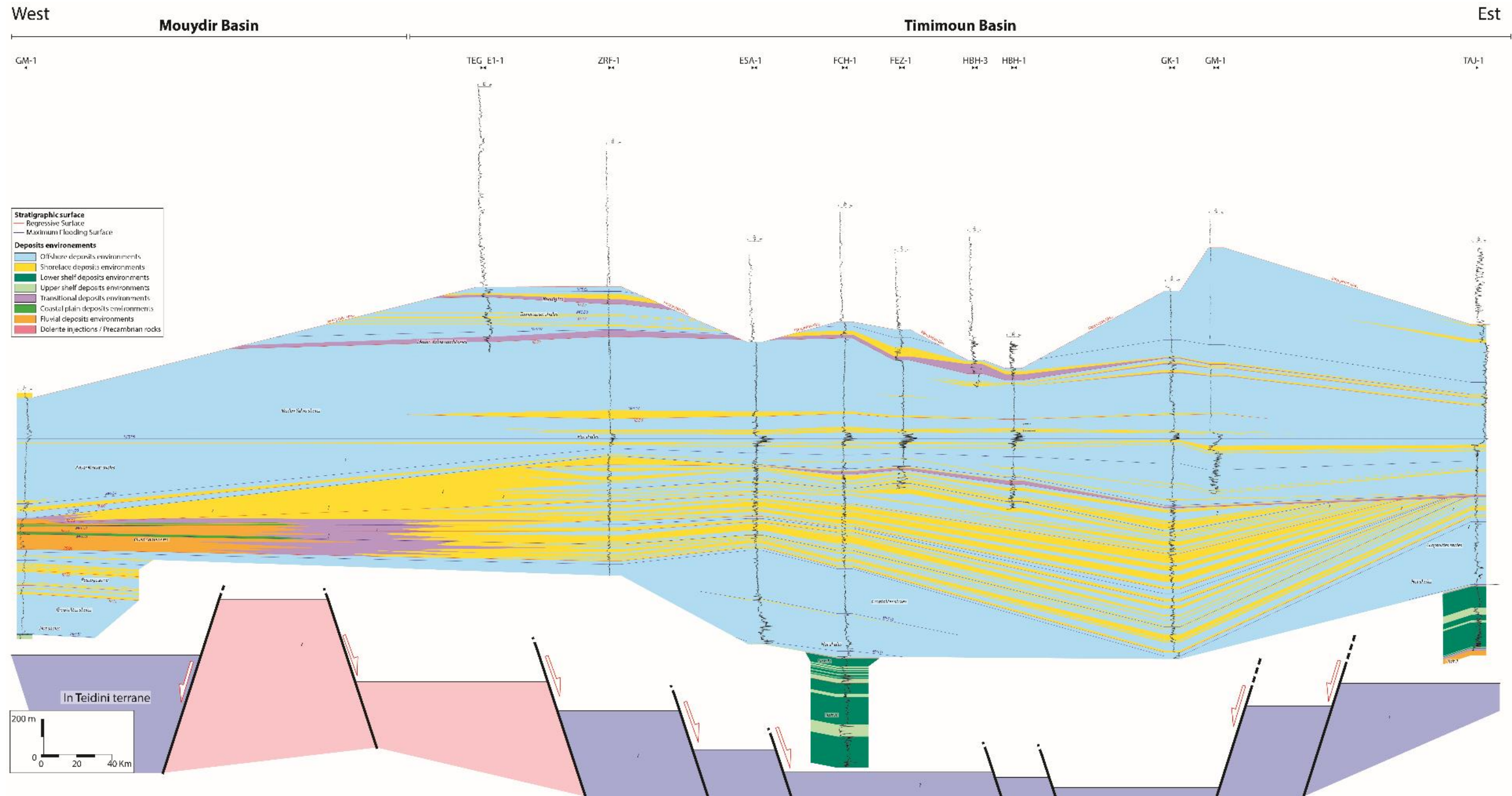


Figure V-38: NS wells cross section of North peri-Hoggar basins (Mouydir-Timimoun Basins). Horizontalization on top Givetian transgression. For localization of the cross section see Figure V-29.

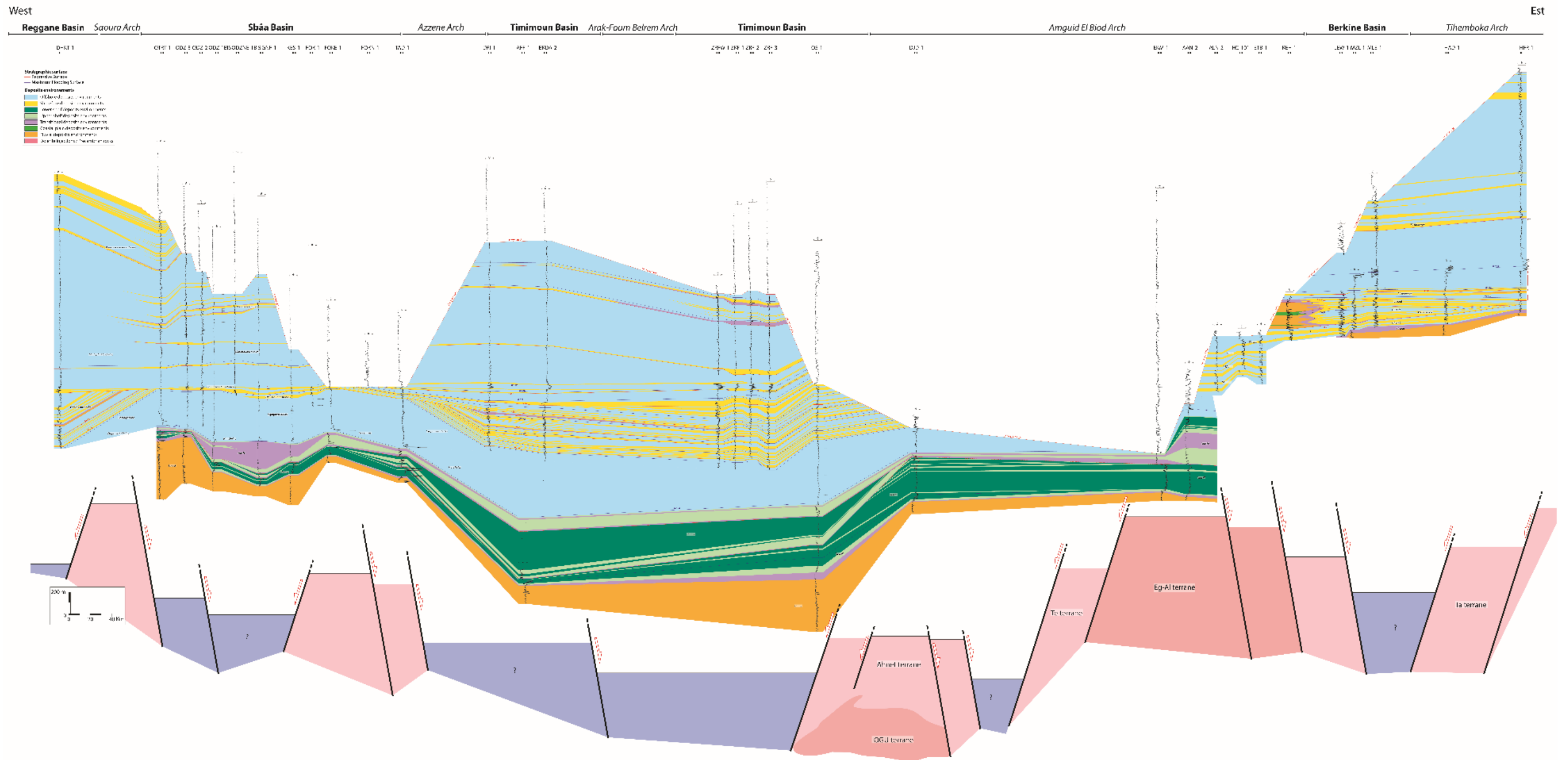


Figure V-39: EW wells cross section of North peri-Hoggar basins (Reggane-Sbâa-Timimoun Basins). Horizontalization on top Givetian transgression. For localization of the cross section see Figure V-29.

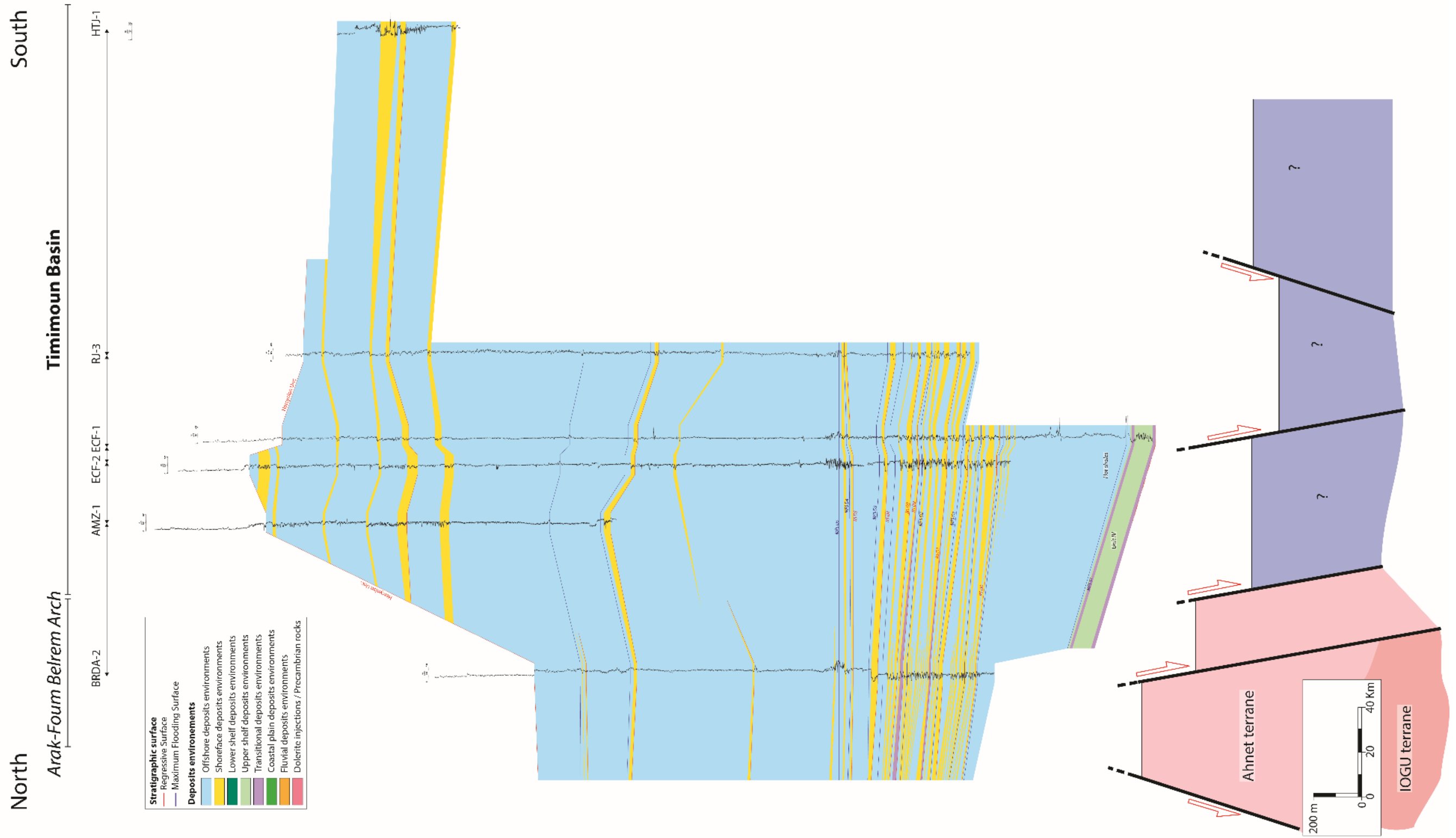


Figure V-40: NS wells cross section of North peri-Hoggar basins (Ahnet-Timimoun Basins). Horizontalization on top Givetian transgression. For localization of the cross section see Figure V-29.

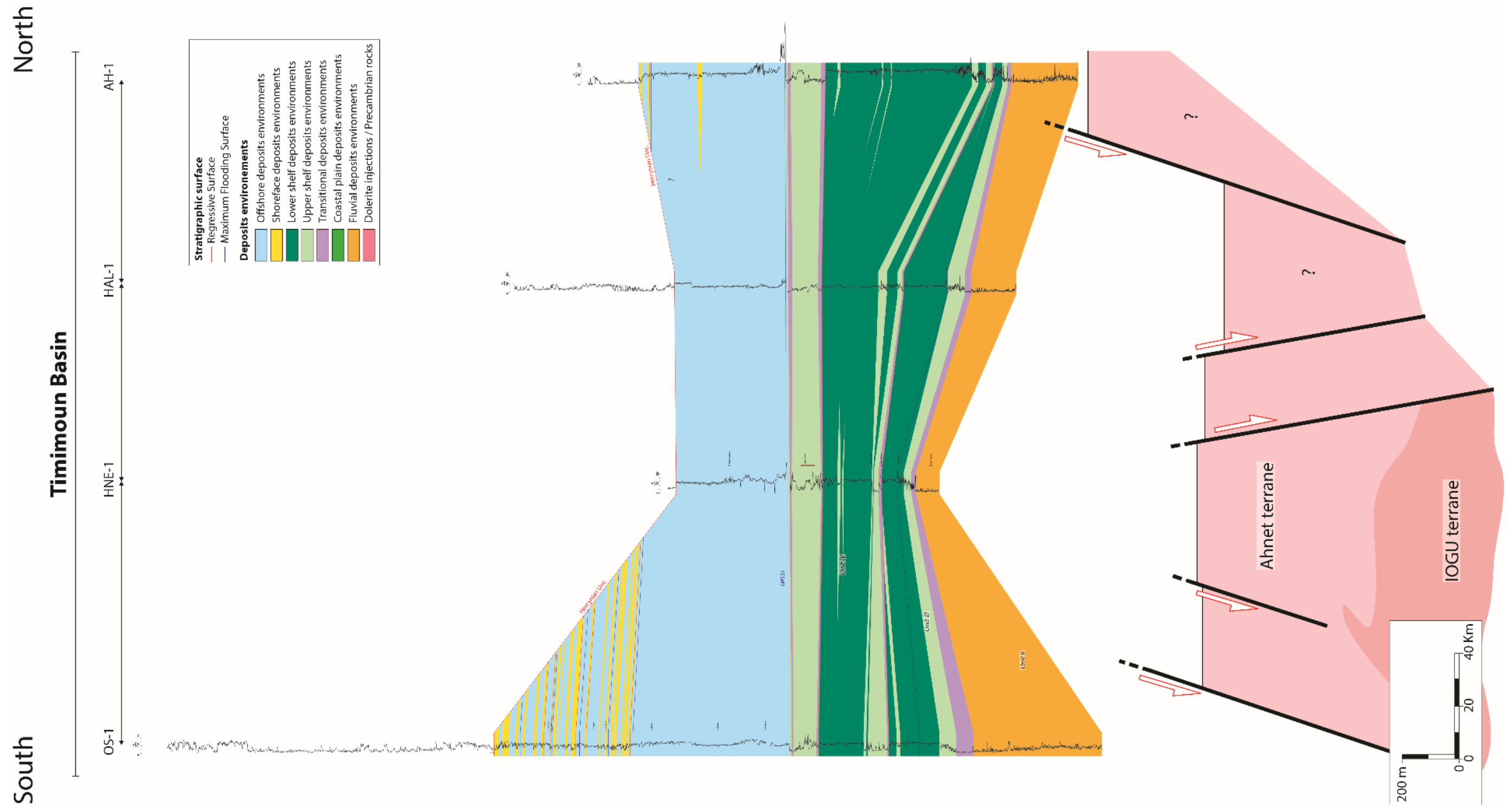


Figure V-41: NS wells cross section of North peri-Hoggar basins (Timimoun Basin). Horizontalization on Lower Silurian transgression. For localization of the cross section see Figure V-29.

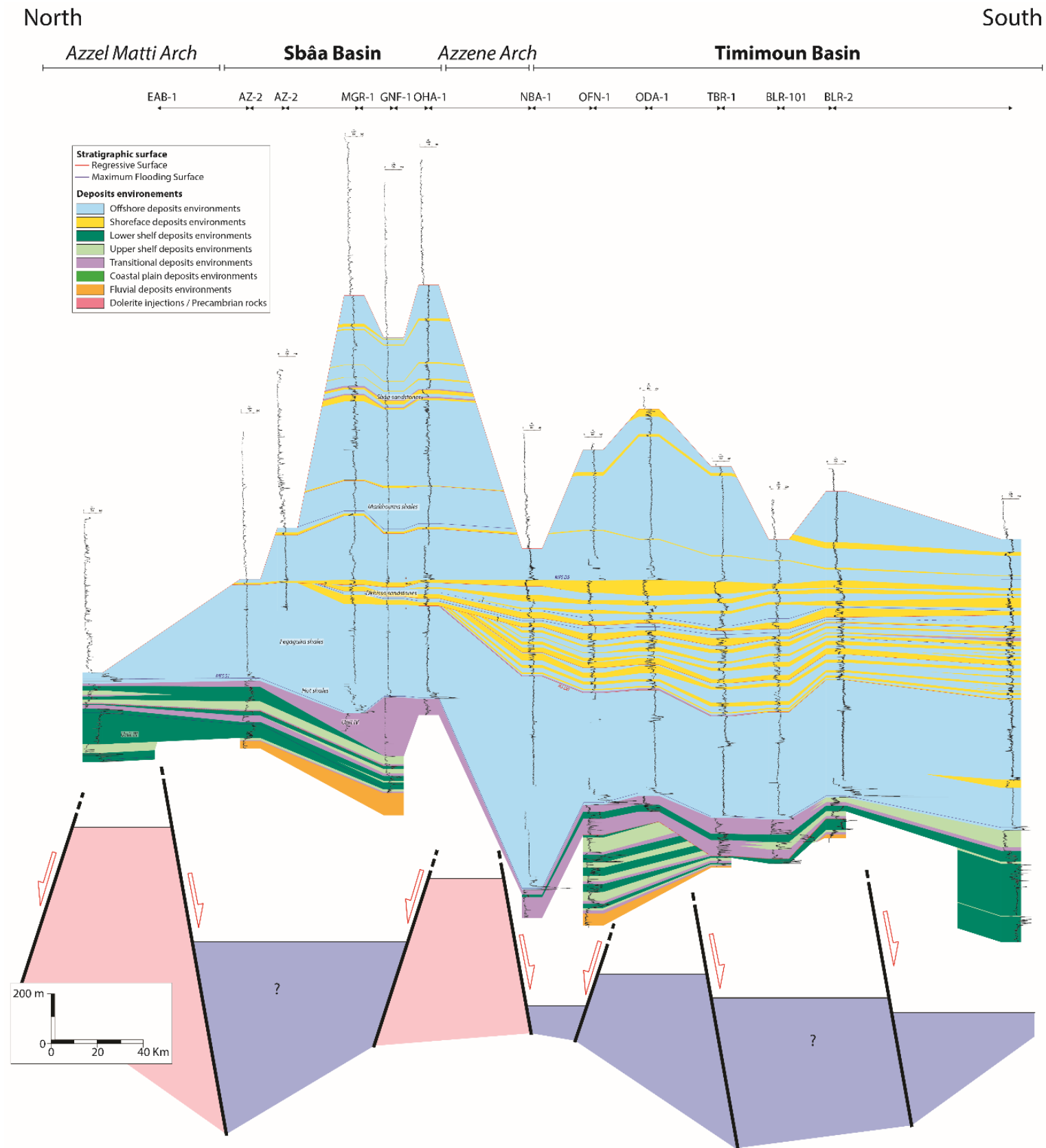


Figure V-42: NS wells cross section of North peri-Hoggar basins (Sbâa-Timimoun Basins). Horizontalization on top Givetian transgression. For localization of the cross section see Figure V-29.

5 Conclusion

The supplementary data presented previously bring new observations so as to improve the geological model proposed in Chapter IV. It confirms that the Peri-Hoggar Basins are of intracratonic basin type characterized by strong interactions with basement NS-trending horst and graben systems. This framework is inverted or/and reactivated since the late Proterozoic as a response to tectonic events (i.e. transpression or transtension) developed either close to the area or more often to relatively distant plate-boundary events according to some authors (Bumby and Guiraud, 2005; Galeazzi et al., 2010).

Indeed, local tectonism is considered to be the far-field effect of plate-tectonic processes that affected the North African plate-boundaries, such as the Caledonian and Hercynian Orogenies, the opening of the Tethys and Atlantic oceans, and the Alpine Orogeny (Galeazzi et al., 2010; Ziegler et al., 1995). These were accompanied by localized thermal mantle processes (Galeazzi et al., 2010) or igneous activity (Derder et al., 2016; Moreau et al., 1994).

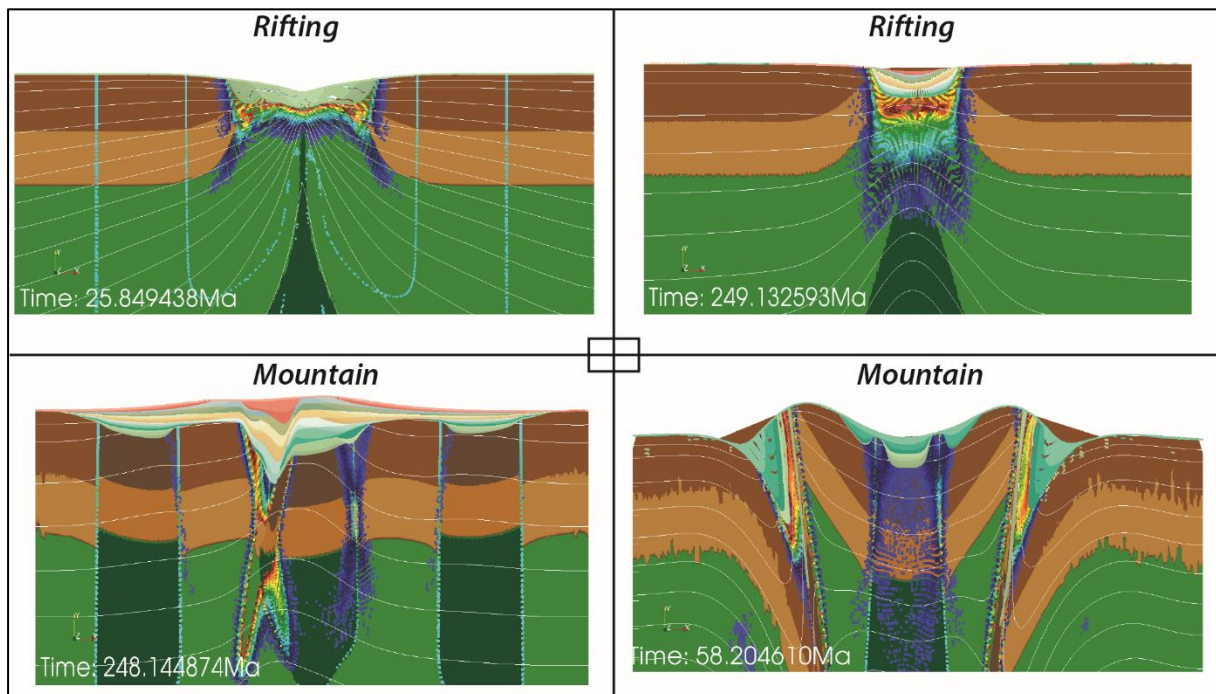
We have seen that the basement heterogeneity of the Hoggar Massif continues into the subsurface of the Saharan Platform basins and determined main Phanerozoic deformation trends. They structure the broad arches and basins architecture, partitioning the sedimentary distribution of peri-Hoggar Basins.

This part has brought supplementary data highlighting the influence of inherited substrate heterogeneities, far field tectonics and thermal anomalies on the Arches-Basins tectono-sedimentary architecture of these intracratonic basins.

However, the mechanism of such deformation and subsidence is still poorly known, and probably resulted from a lithospheric buckling and the reactivation of Precambrian structures.

As a consequence of these observations, forward numerical modelling should take to account and assimilate these geological constrains (“ingredients”) in order to build a viable model.

**CHAPTER VI. LITHOSPHERIC
THERMOMECHANICAL NUMERICAL MODELLING:
CONTROL OF INHERITED ACCRETED LITHOSPHERIC
HETEROGENEITY ON THE ARCHITECTURE AND THE
LOW LONG-LIVED SUBSIDENCE RATE OF
INTRACRATONIC BASINS**



Samples of failed 2D numerical thermo-mechanical models (mountains and rifts)



1 Summary and objectives

The Saharan Paleozoic basins display stratigraphic architecture and structural styles typical of intracratonic basins, characterized by relatively thin and laterally extensive sedimentary series that contain major regional unconformities and are arranged in broad synclines and anticlines, affected by regional basement-involved faults, and crustal buckling.

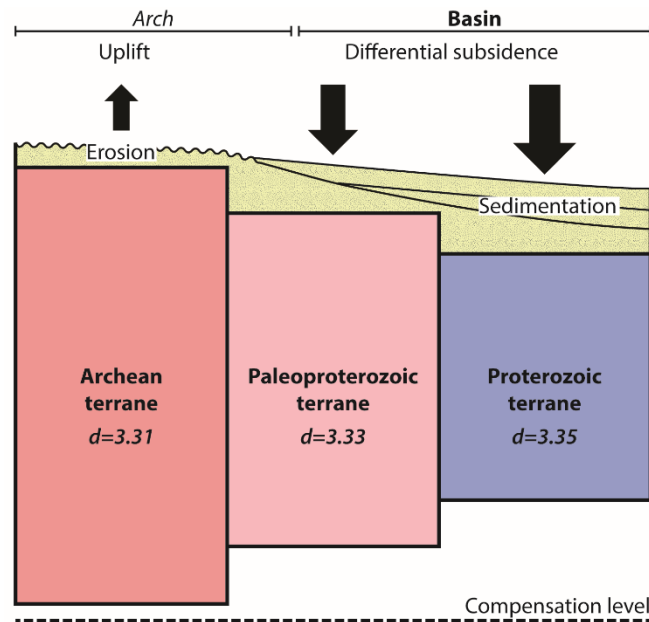


Figure VI-1: Conceptual model of the subsidence mechanism between arches and basins depocenter extracted from geological observations in previous chapter.

On the one hand, our results from analysis of satellites images, seismic profiles and well cross sections show a differential low rate subsidence, sedimentary architecture and tectonic style between arches and basins highlighting the Saharan intracratonic basins. On the other hand, the basement characterization shows a specific organization of terranes between arch and basins (Figure VI-1). All these outcomes point out a large-scale control involving the lithosphere. From these observations, many questions arise such as: What are the forcing factors and motors of the intracraonic basins? Can the heterogeneity of the lithosphere, especially due to differential density of the terranes, constrain the architecture of these basins?

The different objectives of this chapter are the following:

- Test the viability of the conceptual geological model featured by lithospheric density heterogeneities between terranes (Figure VI-1) by doing a numerical thermo-mechanical modelling;
- Parametrization and simulation of models with homogenous and heterogenous lithosphere to tectonics, sediment flux and thermal anomaly;
- Extract the basins architecture and subsidence curves of the forward models;
- Identify the different forcing factors controlling the intracratonic basins.

2 Notions of lithospheric thermo-mechanical numerical modelling

To model something is to simplify something. Any model relies on approximations on the physics. Using Newtonian mechanics instead of relativity; using a pseudo static formulation rather than a fully dynamic one and neglecting the propagation of seismic waves; neglecting the change of volume associated to variations of density by assuming incompressibility with Boussinesq approximation instead of solving for mass conservation; all these are examples of approximations. These approximations are not made by chance, and in general it is possible and even necessary to find theoretical and/or experimental justification for them. Once these hypotheses on the physics are chosen, the scientist can determine a mathematical or numerical model which allows making some predictions about the phenomenon.

Once the problem is set, i.e. the physics, the initial conditions and the boundary conditions are chosen (ingredients), it is desirable to actually be able to solve it (Figure VI-2).

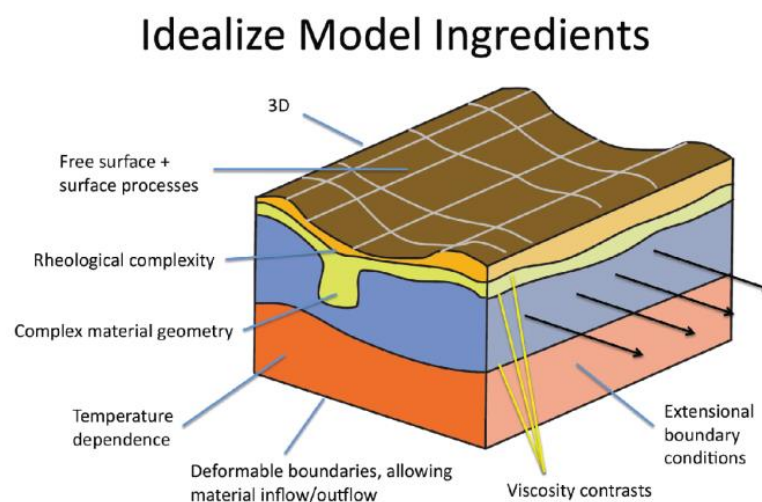


Figure VI-2: Example of idealize model ingredients for numerical physic calculation.

3 Submitted article at Basin Research

Abstract (Français)

Les bassins intracratoniques ont tendance à subsider beaucoup plus longtemps que l'échelle de temps prévue par la relaxation thermique de la lithosphère. De nombreuses hypothèses ont été suggérées pour expliquer leur longévité, mais peu ont été testées à l'aide de modèles numériques thermomécaniques quantitatifs, qui capturent la dynamique de la lithosphère. La modélisation tectono-stratigraphique de ces bassins est difficile, car ils ne présentent que quelques kilomètres de subsidence sur 1000 km au cours d'une période dépassant 250 millions d'années. Nos simulations sont conçues pour examiner le rôle relatif de l'anomalie thermique, de la tectonique et de l'hétérogénéité de la lithosphère sur la formation de bassins intracratoniques.

Les résultats des simulations numériques thermomécaniques 2D démontrent que la lithosphère continentale hétérogène accrétée permet de former des bassins plus subsidents que les bassins homogènes, qu'une anomalie thermique initiale et/ou qu'un forçage tectonique soit appliqué ou non. L'hétérogénéité de la lithosphère explique donc au premier ordre la subsidence à long terme et l'architecture arches-bassins des bassins intracratoniques. De fortes lithosphères hétérogènes maintiennent en effet un déséquilibre isostatique local pendant une très longue période. Ces variations latérales stockent l'énergie potentielle consommée par l'érosion différentielle. Pour un coefficient d'érosion relativement bien accepté de 10^{-6} m²/s, la subsidence dure plus longtemps que 250 Myr. Plus généralement, la quantité de sédiments disponible contrôle la durée de l'affaissement.

Les résultats montrent également que le forçage tectonique de champ lointain peut expliquer la tendance du second ordre, telle que l'accélération, la décélération et l'inversion du taux de subsidence. De légers changements dans les champs de contraintes lointains lors de la subsidence complexifient l'architecture tectono-stratigraphique (arches intra-bassins, sous-bassins) de ces bassins et provoquent un diachronisme dans la subsidence, ce qui entraîne des modifications du signal stratigraphique entre différents bassins voisins (discordances et diachronismes).

Mots clés: Bassin intracratonique, zone mobile accrétée hétérogène, compensation isostatique, subsidence potentiel, tectonique de champs de contraintes lointains.

Les principaux résultats de l'article :

Grâce à une modélisation thermomécanique 2D, nous avons appliqué des facteurs de forçage externes (mécanisme d'érosion/déposition et de flux sédimentaire à vitesse constante) et de forçage internes (anomalie thermique, tectonique) à des lithosphères homogènes et à des lithosphères accrétées (Archéen et Protérozoïque). À partir de l'analyse des simulations, nous pouvons affirmer que :

- La présence d'une anomalie thermique n'est pas suffisante pour créer des bassins avec des subsidences de longues durées. Même avec les processus d'érosion/sédimentation, la subsidence thermique cesse après 150 Ma ;
- Les arches et les bassins peuvent émerger de la géométrie des terranes grâce à la compensation isostatique verticale et différentielles des terranes archéennes et Protérozoïques avec de différentes rhéologies/densités ;
- Les taux de sédimentation contrôlent la durée de subsidence, généralement elle peut être supérieure à 250 Ma dans un contexte intracontinental où il n'y a pas de chaînes de montagnes pouvant fournir un apport important de sédiments ;
- En raison de la distance par rapport aux sources et des changements paléoclimatiques (alternance de phases arides et humides), les vitesses de sédimentation peuvent varier dans ces grandes zones intrac Continentales subsistantes, ce qui entraîne la complexité à interpréter les architectures sédimentaires (hiatus, troncatures, onlaps...) même si les conditions aux limites sont assez simples et identiques pour les différents bassins ;
- Un flux sédimentaire latéral (externe) est nécessaire pour couvrir les arches, augmenter l'épaisseur et la température des bassins ;
- La tectonique conduit à des bassins plus asymétriques/complexes et permettent la formation d'arches intra-bassins et d'arches bordières secondaires interbassins délimités par des failles formant des sous-bassins (grabens). Ils peuvent expliquer les différences de remplissage sédimentaire entre les bassins voisins ainsi que la présence de discordances dans les dépo-centres des sous-bassins ;
- L'effet de la tectonique est amplifié lorsqu'une anomalie thermique profonde affaiblit la lithosphère.

Abstract (English)

Intracratonic basins tend to subside much longer than the timescale predicted by thermal relaxation of the lithosphere. Many hypotheses have been suggested to explain their longevity, yet few have been tested using quantitative thermo-mechanical numerical models, which capture the dynamic of the lithosphere. Tectono-stratigraphic modelling of these basins is challenging since they display only few kilometers of subsidence over 1000 of km during period that exceed 250 Myr. The simulations are designed to examine the relative role of thermal anomaly, tectonics and heterogeneity of the lithosphere on the formation of intracratonic basins.

Results of the 2D thermo-mechanical numerical simulations demonstrate that heterogeneous accretionary continental lithosphere allows forming deeper basins than homogeneous one whether an initial thermal anomaly and/or tectonic forcing are applied or not. Heterogeneity of the lithosphere therefore explains to first order long-term subsidence and the arches-basins architecture of the intracratonic basins. Strong heterogeneous lithospheres indeed maintain local isostatic disequilibrium for very long period of time. These lateral variations store potential energy that is consumed by differential erosion. For relatively well-accepted coefficient of erosion of 10^{-6} m²/s, the subsidence last longer than 250 Myr. More generally, the quantity of sediments available controls the subsidence duration.

The results also highlight that far field tectonic forcing can account for the second order trend, such as acceleration, deceleration and inversion of subsidence rate. Slight changes in far field stress during subsidence complexify the tectono-stratigraphic architecture (intra-basin arches, sub-basins) of these basins and causes subsidence diachronism, which results in stratigraphic unconformities between different neighboring basins.

Key words: Intracratonic basin, heterogenous accreted mobile belt, isostatic compensation, potential subsidence, far field tectonic.

4 Introduction

Intracratonic basins also called “cratonic basins”, “interior cratonic basins” or “intracontinental sags” have a widespread distribution in the world (see fig. 6 from Heine et al., 2008). They host most of fresh water aquifers, minerals resources and hydrocarbons reserves of the world. They possess several common features (see Allen and Armitage, 2011 and references therein). They are located in the interior of a continent, far from any active margins (stretch or convergent)

upon stable continental lithosphere area. They are usually large (>150,00 km² in area) circular, elliptical to oval-shaped in plan and saucer-shaped in cross section. They display a low topographic relief and an elevation close to present-day sea level and are filled with continental to shallow-water sedimentation. Their structural framework can be characterized by the emergence of the association of arches in a broad sense and basins of different kilometric wavelengths reactivated through time (de Brito Neves et al., 1984; Perron et al., 2018; Quinlan, 1987; Seyfert, 1987). Yet, their stretching factors are very low (Armitage and Allen, 2010; Allen and Allen, 2013). They experience low subsidence rate (5 to 50 m/Ma) during a long period (>250 Myr) characterized by curves with sublinear to gently exponential shape (Figure VI-3).

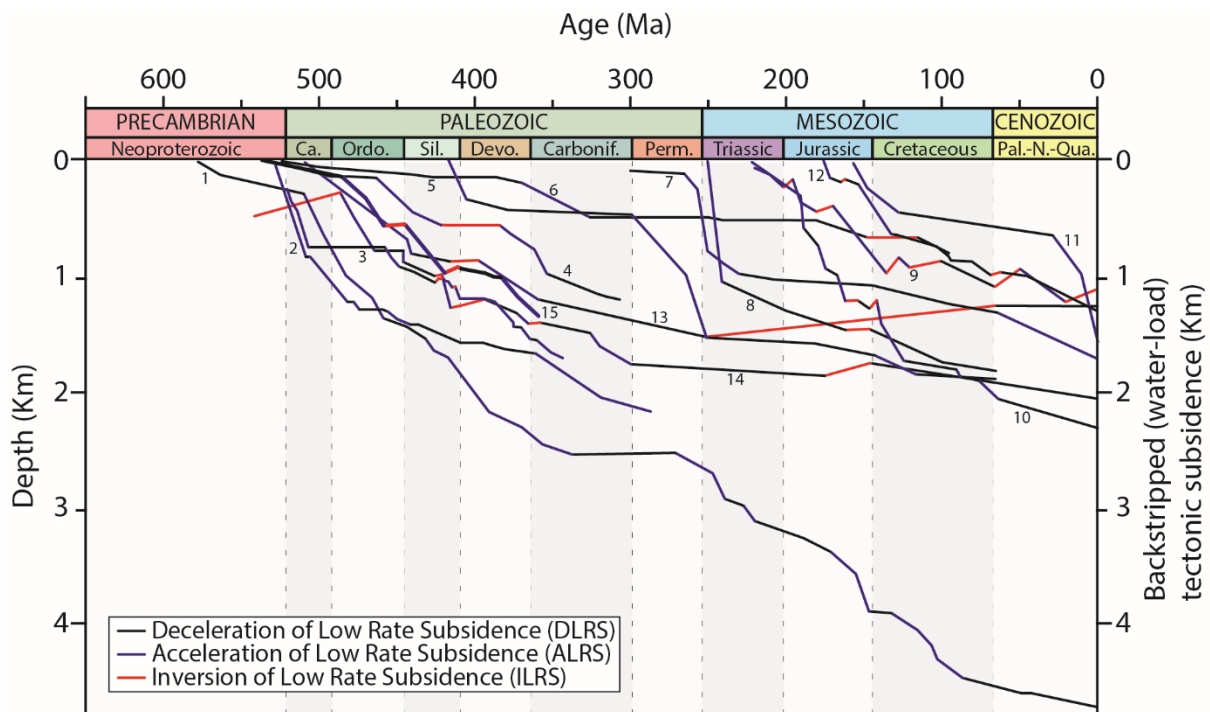


Figure VI-3: Compilation of backstripped tectonic subsidence of intracratonic basins modified from literature (Allen and Armitage, 2011; Xie and Heller, 2009) showing periods of acceleration (ALRS), deceleration (DLRS) and inversion (ILRS) of the low rate subsidence. 1: Ghadames/Berkine Basin, Algeria (Yahi, 1999); 2: Illinois Basin (Bond and Kominz, 1984); 3: Michigan Basin (Bond and Kominz, 1984); 4: Williston Basin, North Dakota (Bond and Kominz, 1984); 5: Williston Basin, Saskatchewan (Fowler and Nisbet, 1985); 6: Paraná Basin, Brazil, CB-3 well (Oliveira, 1987 from Allen and Armitage, 2011); 7: Northeast German Basin (Scheck and Bayer, 1999); 8: Southwest Ordos Basin (Xie, 2007 from Xie and Heller, 2006); 9: Paris Basin (Prijac et al., 2000); 10: West Siberian Basin, Russia, Urengoy well (Saunders et al., 2005); 11: West Siberian Basin, Russia, Samotlar-39 well (Saunders et al., 2005); 12:

Paraná Basin (Zalan et al., 1990); 13: AINC43 Al Kufrah basin (Holt et al., 2010); 14: Ghadamès basin (Holt et al., 2010); 15: Well W17 in Ahnet Basin (Perron et al., 2018).

Multiple hypotheses and models have been invoked to explain the dynamics of these slow subsiding long-lived intracratonic basins (see Allen and Armitage, 2011 and references therein or Hartley and Allen, 1994). The preservation of the low subsidence rate in these basins together with the long exponential decay of subsidence with time (Fig. 1) has led many authors to propose essentially a thermal decay subsidence origin for these basins (Armitage and Allen, 2010; Cacace and Scheck-Wenderoth, 2016; Haxby et al., 1976; Holt et al., 2015; Howell and van der Pluijm, 1999; McKenzie, 1978; Nunn, 1994; Nunn et al., 1984; Nunn and Sleep, 1984; Xie and Heller, 2009). This first order trend of idealized thermal-driven subsidence does not explain the long geological time scale (i.e. >250 Myr) over which these basins subside. Indeed, the thermal relaxation of the lithosphere should be mainly achieved in 50 Ma (Moretti and Froidevaux, 1986). Moreover, it does not explain the alternation of periods of quiescence (i.e. deceleration; DLRS: Deceleration of the Low Rate Subsidence), acceleration (ALRS: Acceleration of the Low Rate subsidence) and inversion (ILRS: Inversion of the Low Rate Subsidence) of the subsidence curves (Figure VI-3).

Using numerical simulations of lithospheric deformation, the aim of this study is to circumscribe what first-order mechanisms can maintain the low long-lived subsidence rate of the intracratonic basins through the geological time and what second-order forcing can explain local acceleration and inversion of subsidence. Part 2 outlines our working hypothesis before describing and justifying the adopted modelling scheme. Part 3 deals with the role of internal forcing due to lateral variation in lithology, initial geotherm and tectonics. Part 4 focuses on the tectono-stratigraphic architecture of basins and explores the effects of erosion-deposition processes and lateral sediment. We finally compare and discuss the subsidence pattern resulting from the experiments to previously proposed models.

5 Working hypotheses

5.1 Arches and basins in accretionary type lithosphere

Considering the lithospheres as homogenous simplifies the conceptual models but it might sometimes be fundamentally incorrect. Continental lithospheres are indeed the result of a complex blocks assembly even in old cratonic areas (de Wit et al., 1992). Intracontinental basins (Holt, 2012; Holt et al., 2010, 2015) are often basins formed upon an inherited heterogeneous

lithosphere assembled during different former geodynamic events (Cawood, 2009; Cawood et al., 2009; Condie, 2007). According to many authors (de Brito Neves et al., 1984; Daly et al., 2018b; Peace et al., 2018; Perron et al., 2018; Phillips et al., 2018), the basement inherited heterogeneities (i.e. terranes) separated by shear zones structures are connected to arches and basins features, constraining their shape and architecture through time and tectonic activity. For instance, in North Africa, Perron et al. (2018) have described the correlation between the zonation of terranes age and the location of arches and basins.

Accretionary type lithospheres are the result of the collage of different types of lithospheric column along vertical shear zones (Figure VI-4) inherited from former orogenies. The tectonic orogenic style of the Archean (i.e. ultra-hot orogens) and the Proterozoic (i.e. accretionary to collisional orogens) is different from modern orogenies (Cagnard et al., 2011; Chardon et al., 2009). Accretionary orogens indeed display sub-vertical shear zones rather than mega-thrust observed in contemporary orogens. These vertical shear zones are often involved in further tectonic events (Audet and Bürgmann, 2011; Peace et al., 2018; Perron et al., 2018). Many studies stress the importance of these paleo-weaknesses in the basement on structural framework developed later on (Célérier et al., 2005). Whether this inheritance is related to the weakness of the shear zone or the rheological contrast between the different blocks remains a question in the framework of intracratonic basins. Modelling studies have shown that strength contrast are often more likely to be reactivated than fault zones (Ranalli, 2000; Buitter and Pfiffner, 2003; Pourhiet et al., 2004; Lafosse et al., 2016; von Tscharner et al., 2016).

In any cases, the dissimilarities between Archean and the Proterozoic lithospheres that typically constitutes cratonic areas is well agreed (Artemieva, 2009; Artemieva and Mooney, 2002; Cherepanova and Artemieva, 2015; Djomani et al., 2001; Durrheim and Mooney, 1994; Griffin et al., 2003; King, 2005; McKenzie and Priestley, 2008, 2016; Michaut et al., 2009; Nyblade and Pollack, 1993; Petitjean et al., 2006; Sleep, 2003, 2005). Difference in thickness, lithology, geochemical content, thermal regime and rheological properties have been evidenced using both geological and geophysical arguments on all continents such as Africa (Brahimi et al., 2018; de Wit and Linol, 2015; Fishwick and Bastow, 2011; Hartley et al., 1996; Hartley and Allen, 1994), Russia (Cherepanova et al., 2013; Cherepanova and Artemieva, 2015), but also in North-America (Caravaca et al., 2017; Daly et al., 2018b; Eaton and Darbyshire, 2010; Frederiksen et al., 2013; Gaschnig et al., 2013; Haxby et al., 1976; Lyatsky et al., 2006; Tesauro et al., 2015), South-America (Cordani and Teixeira, 2007; Dallmeyer, 1989; Daly et al., 2014, 2018b; Heilbron et al., 2008; James and Assumpção, 1996; Mantovani et al., 2005; Nunn and

Aires, 1988; Padilha et al., 2014; Pérez-Gussinyé et al., 2007; Tozer et al., 2017), and Asia (Ratheesh-Kumar et al., 2014).

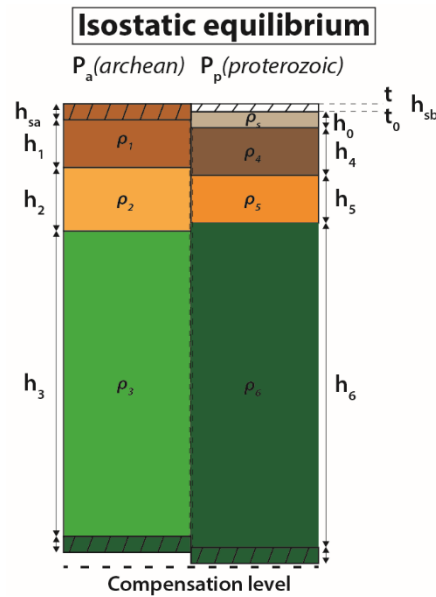


Figure VI-4: Isostasy equilibrium potential by an Airy calculation between Archean and Proterozoic terranes (see Appendix A).

Another parameter that is often overlooked in study of inheritance at fast deforming plate boundaries but might become important in slow deforming plate interiors is the contrast in density between Proterozoic lithosphere and Archean ones. In some case, geophysical data (e.g. map of Bouguer anomaly, free air anomaly, isostatic anomaly) point out that these lithospheric columns are still not locally isostatically compensated (Gwavava et al., 1996; Perron et al., 2018). Besides, isostatically uncompensated ancient mass excess related to ancient rift zone (DeRito et al., 1983) or dense body in the lower crust (Haxby et al., 1976; Howell and Pluijm, 1990; Howell and van der Pluijm, 1999; Nunn and Sleep, 1984) are recognized to drive subsidence. These buried loads indeed trigger downward surface flexure, which can be filled by sediments as long as isostatic compensation mass excess is not achieved.

These geological and geophysical observations constrained our heterogeneous theoretical initial lithospheric models (Figure VI-5). We hypothesis that the isostatic disequilibrium inherited from the accretion of terranes of different density together with differential erosion/deposition could potentially cause the prolonged subsidence of intracratonic basins. Using a simple Airy isostatic balance model (e.g. Allen and Allen, 2013), it is possible to calculate the potential of space creation in the basins knowing the initial topography. We than compare this driver with external forcing such as far field tectonic loading and massive sediment influx.

5.2 Initial models setups and boundary conditions

In order to test whether the isostatic potential is a valid working hypothesis, we use thermo-mechanical simulations. The model box is 300 deep and 1600 km long. The mesh is refined to enable modelling large-scale dynamics over 250 Myr with a resolution of 500×500 m at the surface in reasonable computing time. This surface resolution allows us to visualize and constrain the tectono-stratigraphic architecture of the synthetic basins.

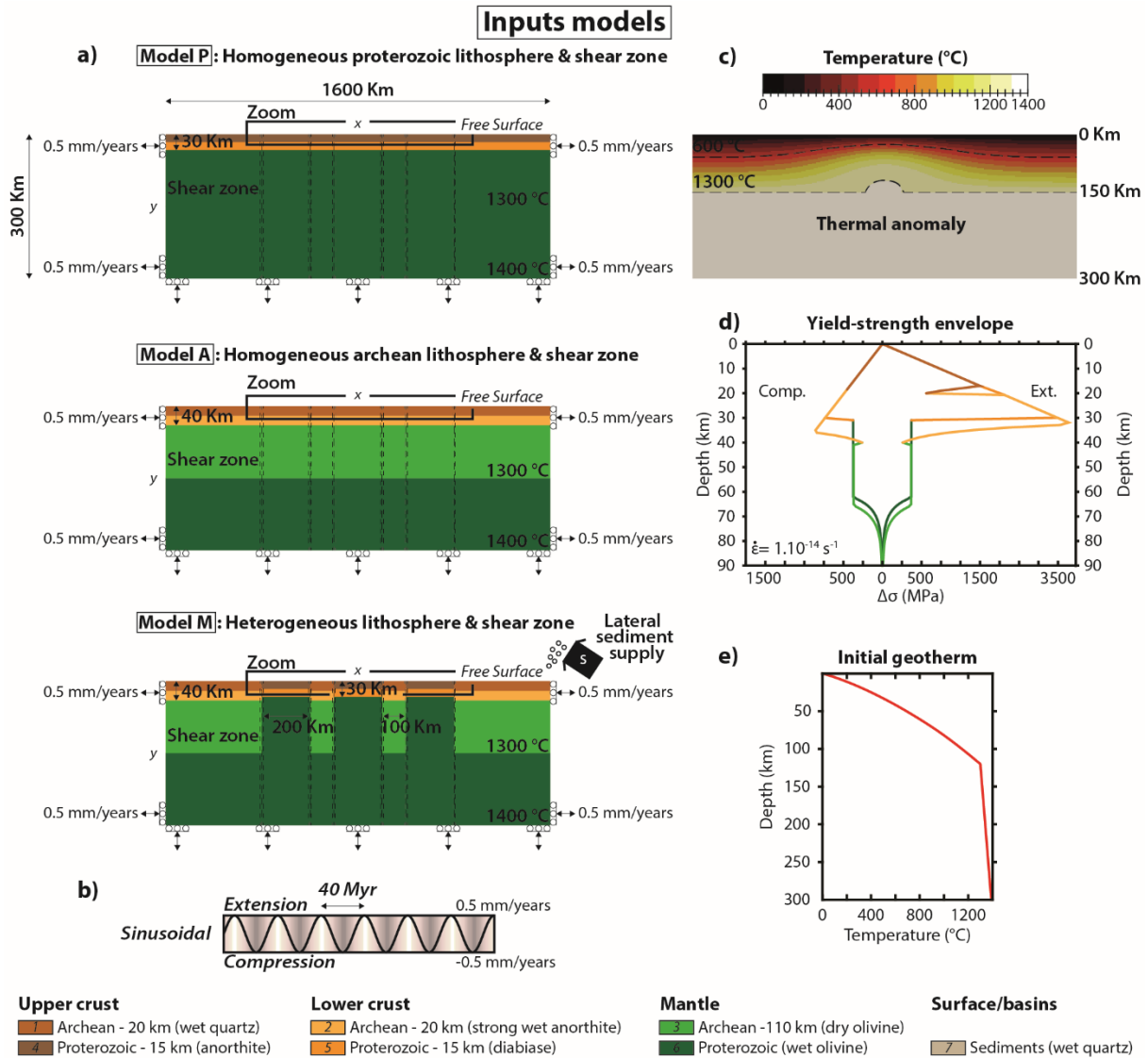


Figure VI-5: a) Inputs models (model P, A and M) of the different simulations with the different parameters applied in experiments such as b) the far fields stresses (sinusoidal extension-compression 40 Myr) and c) the thermal anomaly. d) Yield-strength envelopes of the simulated materials calculated for a strain rate of $1.5 \cdot 10^{-11} s^{-1}$. $\Delta\sigma$ represents the deviatoric stress,

positive values under extension and negative values under compression. e) Initial temperature state of the lithosphere for all the simulations presented.

The thermal structure of the continental lithosphere is computed for a plate thickness of 120 km, a thermal age of 400 Myr and a surface radiogenic heat production of $3 \cdot 10^{-9} \text{ W} \cdot \text{kg}^{-1}$ with an exponential decay characteristic depth of 10 km using the formula in Burov and Diament, (1995). For the asthenosphere, an adiabatic gradient of $0.5^\circ\text{K}/\text{km}$ is used. Temperatures are fixed at the top and base of the model at 0°C and 1400°C respectively, and a null heat flux is assumed on the model lateral boundaries (Figure VI-5e).

In order to test the effect of thermal subsidence, some of the simulations are affected by a thermal anomaly. In that case, the thermal age follows a gaussian distribution from 50 Myr at the center of the model to 400 Myr on the borders with a standard deviation of 600 km (Figure VI-5c).

The effect of thermal anomaly is compared to isostatic rebalancing using two types of lithospheric columns: Archean and Proterozoic and three initial geometries (Figure VI-5a). Model P is composed of a homogenous Proterozoic lithosphere. The model A is defined by a homogenous Archean lithosphere. The model M (i.e mixed) is composed of two types of lithosphere (Archean cratonic and Proterozoic terranes). The Archean terranes have a 40 km crust (20+20 km) and a lighter mantle lithosphere that reflects their high magnesium number. The Proterozoic terranes have a 30 km thick crust (15+15 km) and their mantle is of the same density as the asthenosphere. The rheological parameters of the Archean and Proterozoic lithosphere are consigned in Table 1 and their associated yield-strength envelope in Figure 2d. All initial geometries include vertical low friction zones to mimic inherited weak shear zones from ancient orogenies.

Model M is largely inspired from the geodynamic setting of the Saharan platform (Perron et al., 2018). It consists of three 200 km wide Proterozoic terranes separated by two Archean terranes of 100 km in width sandwiched in between two 400 km wide Archean cratons. Model M is therefore by no mean in local isostatic equilibrium in the initial conditions. According to initial density parameters (Table 1), initial model inputs (Figure VI-4) and an initial topography of 500 m, we estimated a potential basin filling of around 5 km, when the isostatic compensation is achieved (see Appendix A).

All the models use a free upper boundary surface subject to constant erosion – sedimentation allowing the development of sedimentary basins. These surface processes (erosion and sedimentation) are modelled using Culling's, (1965) law with a diffusivity (κ) of $1.10^{-6} \text{ m}^2 \cdot \text{s}^{-1}$. Lateral inflow of sediments follows the same kind of modelling used in Jourdon et al., (2018). The vertical velocity at the base of the model is computed in order to compensate for horizontal stretching or shortening applied on the vertical sides.

	Archean upper crust	Archean lower crust	Archean Mantle	Proterozoic upper crust	Proterozoic lower crust	Mantle	Sediments	Units
Phase	1	2	3	4	5	6	7	
Lithology	wet quartz	strong wet anorthite	dry olivine	strong wet anorthite	Strong diabase	dry olivine	wet quartz smaller friction	
n	4	3	3	3	4.7	3	4	
A	$1.1.10^{-4}$	$4.0.10^2$	$7.0.10^3$	$4.0.10^2$	8	$7.0.10^3$	$1.1.10^{-4}$	$\text{MPa}^{-n} \cdot \text{s}^{-1}$
Q	223	356	510	356	485	510	223	$\text{kJ} \cdot \text{mol}^{-1}$
ρ_0	2800	2900	3335	2900	2900	3345	2400	kg/m^3
ϕ_0	30	30	30	30	30	30	30	°
ϕ_∞	10	10	10	10	10	10	10	
Co_0	20	20	20	20	20	20	20	MPa
Co_∞	1	1	20	1	10	20	1	MPa
References	G & T	R & D	G & E	R & D	M	G & E	G & T	

Table 1: Rheological parameters used in all experiments. References are from R & D (Rybacki and Dresen, 2000), G & T (Gleason and Tullis, 1995), G & E (Goetze and Evans, 1979) and M (Mackwell et al., 1998). $\alpha = 3.10^{-5} \text{ K}^{-1}$, $\beta = 1.10^{-11} \text{ Pa}^{-1}$, $\kappa_e = 5.10^{-7} \text{ m}^2 \cdot \text{s}^{-1}$, $\kappa = 1.10^{-6} \text{ m}^2 \cdot \text{s}^{-1}$, $\epsilon_{\min} = 0$, $\epsilon_{\max} = 1$, $C_p = 1000 \text{ J} \cdot \text{kg}^{-1} \cdot \text{K}^{-1}$, $H = 3.10^{-9} \text{ W} \cdot \text{kg}^{-1}$.

The vertical boundaries of the model have null vertical shear stress. Horizontal kinematic boundary conditions (Figure VI-5a) are either zero or their integral with time is zero. This second type of boundary conditions is used to simulate the effects of far field orogenic cycle. A sinusoidal variation with time period of 40 Myr peak to peak has been chosen as representative between two shortening events (Figure VI-5b). The amplitude of the signal 0.5 mm/Myr ($1.5e^{-11}s^{-1}$) ensures a minimal amount of shortening and stretching per cycle (10 km over 1600 km). Appendix B details the equations solved and the method.

6 Accretionary vs homogeneous lithosphere

We present eight different experiments grouped in 3 benchmarks aimed at characterizing how the presence of a thermal anomaly (3.1), far field tectonic forcing (3.2) and interplay between the two (3.3) is recorded in the different type of lithosphere. List of these inputs parameters for each models (A, P and M) are referenced in Table 2.

Models	Lithosphere type	Far field stresses (compression/extension alternation)	Thermal anomaly	Lateral sediment supply
A1	Homogeneous archean	no	yes	no
A2	Homogeneous archean	yes	no	no
P1	Homogeneous proterozoic	no	yes	no
P2	Homogeneous proterozoic	yes	no	no
M1	Heterogeneous archean/proterozoic	no	yes	no
M2	Heterogeneous archean/proterozoic	yes	no	no
M3	Heterogeneous archean/proterozoic	no	no	no
M4	Heterogeneous archean/proterozoic	yes	yes	no
M5	Heterogeneous archean/proterozoic	no	no	yes
M6	Heterogeneous archean/proterozoic	yes	yes	yes

Table 2: List of parameters inputs for each models. Notice that duration of each model is 250 Myrs.

6.1 Impact of thermal anomaly

The purpose of this first benchmark (Figure VI-6 and Figure VI-8) is to analyze the behavior of the three types of lithosphere, namely Proterozoic (P1), Archean (A1) and accretionary lithosphere (M1) in response to an initial thermal perturbation.

The two first tests (P1 and A1 in Figure VI-6), after 250 Myr, show the same features. That is the lack of deep sedimentary basins and an exponential decay in subsidence rate characteristic of thermal subsidence. Subsidence actually ceases after 150 Myr for both simulations (see P1 and A1 in Figure VI-7). On the contrary, the third experiment (M1) displays three bowl-shaped

basins created upon the 3 Proterozoic terranes, in our configuration i.e. two peripheral basins and one central basin, separated by basement inter-basins arches upon Archean terranes (Figure VI-8). The peripheral basins are 200 km width with a thickness of 1.25 km. The central basins are thinner (i.e. 0.8 km) and narrower (i.e. 140 km) than peripheral ones.

During the simulation, due to the relief creation, the uplifted Archean terranes get eroded and sediments are deposited upon Proterozoic ones. No sediments are deposited on Archean terranes (i.e. arches). The basins form topographic lows, which indicates that sedimentation rate does not compensate for accommodation space creation. The thickness of the different sedimentary layers increases towards the center of the basins and decrease progressively approaching arch forming growth strata. Truncations (M1 in Figure VI-9) show that the strata are successively eroded by the next deposits. Consequently, the width of the basins remains stable through time.

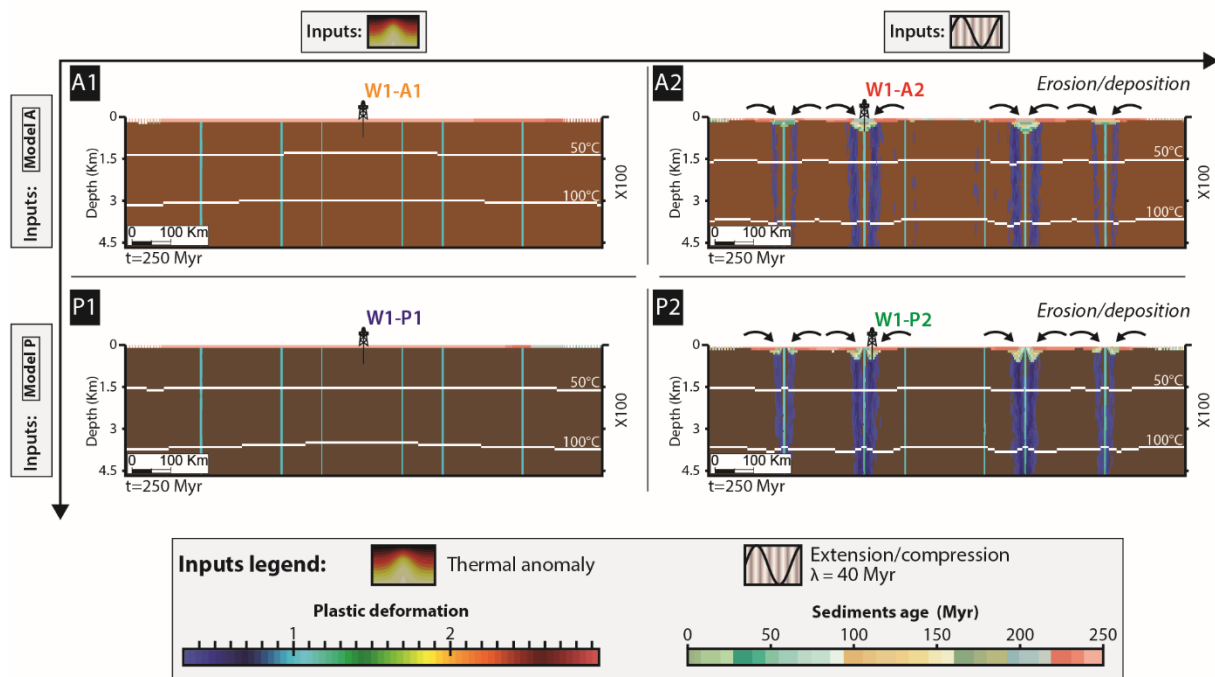


Figure VI-6: (A1) Model A with thermal anomaly shows no creation of basin. (P1) Model P with thermal anomaly shows no creation of basin. (P2) Model P with far field stresses shows the creation of eight narrow basins with chaotic stratigraphic architecture near shear zones. (A2) Model A with far field stresses displays the formation of four narrow basins with chaotic stratigraphic architecture above shear zones.

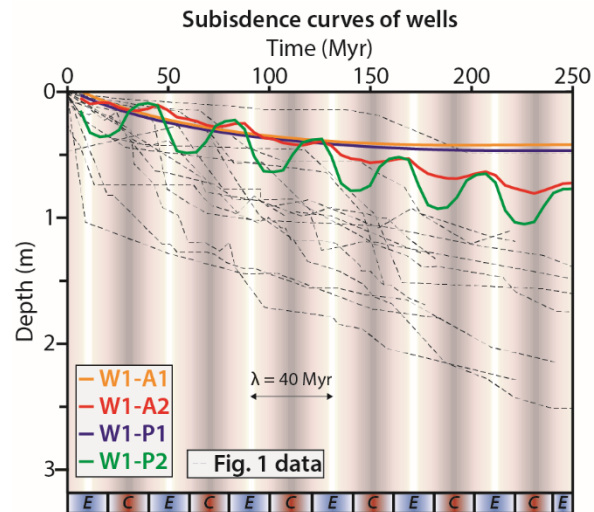


Figure VI-7: Subsidence curves from different models in Figure VI-6 (wells W1-A1 to W1-A2 and W1-P1 to W1-P2) associated with Figure 1 bibliographic data. The thermal subsidence of W1-A1 and W1-A2 is achieved after 150 Myr. The wells P1 and P2 show linear decay subsidence with deviations of different amplitude. Boundary conditions: E=Extension and C=Compression.

This first benchmark shows that thermal anomaly below homogenous lithosphere cannot explain the long-lived subsidence of intracratonic basins and so whatever are the lithosphere characteristics. In less than 50 Myr the equilibrium is reached. On the contrary, with a heterogeneous lithosphere, due for instance by the accretion of different ones, with initial isostasy disequilibrium, the morphology of the subsidence curve is very weakly bent indicating that the potential of subsidence is not over after 250 Myr (see M1 in Figure VI-9).

6.2 Impact of far field stresses (tectonics)

The purpose of this second benchmark (Figure VI-6 and Figure VI-8) is to analyze the behavior of the three types of lithosphere in response to far field tectonic periodic loading by comparing simulation P2, A2 and M2.

On one the hand, the two homogeneous models display a condensed and a complex sedimentation pattern, which does not fit any intracratonic basin geometry. In P2 test (Figure VI-6), eight mini-basins (i.e. about 25 km large and 280 to 770 m thick) are created on either side of the shear zones except the two central ones. The simulation A2 (Figure VI-6) displays four narrow basins (i.e. 50 km large and 280 to 720 m thick) located just above the shear zones. In these two runs, the maximum of strain (and of basin thickness) is concentrated on the second

shear zone starting from models boundaries. The subsidence curve morphologies show a linear decreasing trend with alternation of up and down deviations of amplitude of 110 m for P2 and 400 m for A2 (Figure VI-7).

On the other hand, the accretionary lithosphere model M2 display the formation of arches and basins, which are very similar at first order to the structural pattern obtained with simulation M1 (Figure VI-8). At second order, some dissimilarities are however to be noted. The bottom of the bowl-shaped basins of M2 is flat, with angular shape and with some weak undulations that does not happen in the purely thermally-driven model. Also, the main basins are formed in peripheral positions rather than in the center of the heterogeneous corridor.

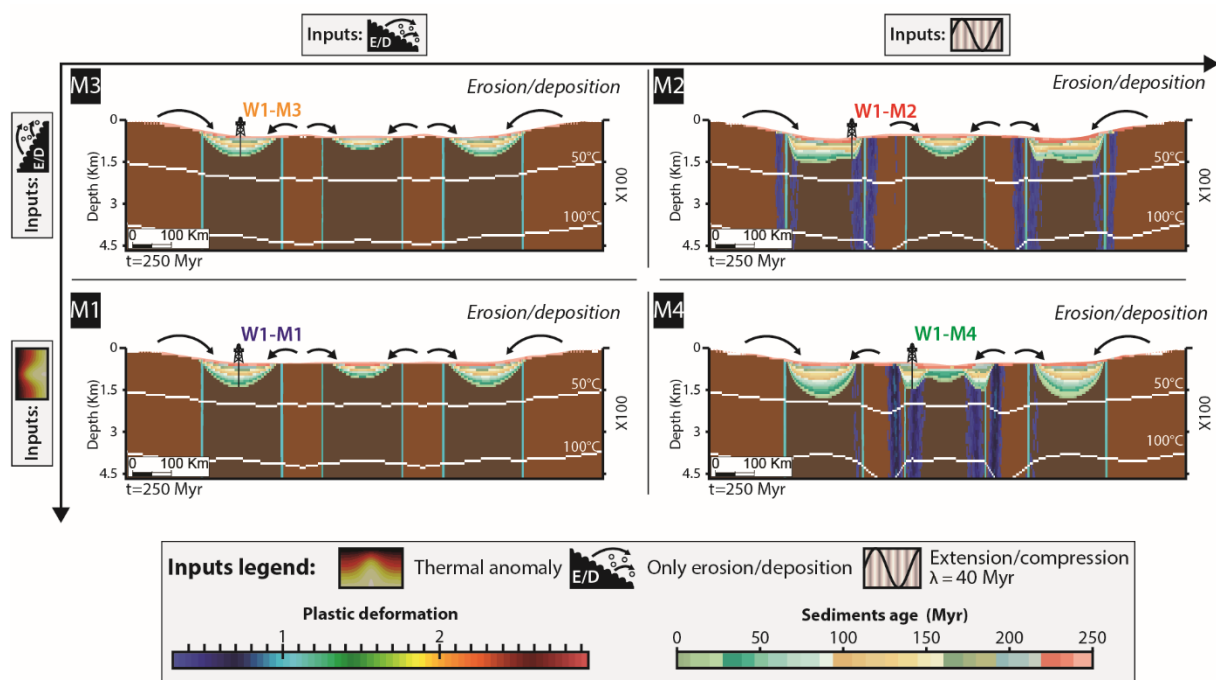


Figure VI-8: (M1) Model M with thermal anomaly displays the creation of arches and basins architecture (i.e. One central basin and two peripheral basins separated another by arches). (M3) Model M without thermal anomaly shows the same architecture of basins than M1 demonstrating the minor influence of thermal anomaly. (M2) Model M with far field stresses and without thermal anomaly modifies peripheral basins structural architecture by flattening the bottom. (M4) Model M with far field stresses and thermal anomaly modifies central basin structural architecture (i.e. formation of grabens above the shear zones).

This second benchmark demonstrates that for similar tectonic loading, homogenous lithosphere with faults remain stable, and only allow the formation of small basins at the apex of the shear zones. Their subsidence curves display a liner trends with deviations. Heterogeneous

lithosphere on the contrary forms basins and arches structures associated to inherited lithospheric heterogeneities in buoyancy and rheology that are very similar to the results obtained with a thermal anomaly. Yet, far field stresses cause period of acceleration, deceleration and inversion of the subsidence (Figure VI-9) that were identified on the data displayed in Figure VI-3. It also complexify the architecture of intracratonic basins.

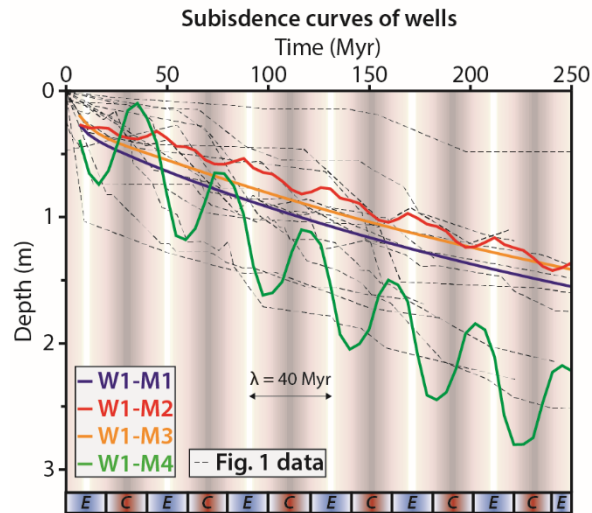


Figure VI-9: Subsidence curves from different models in Figure VI-8 (wells W1-M1 to W1-M4) associated with Figure 1 bibliographic data. The subsidence of W1-M1 and W1-M2 is constant after 250 Myr (i.e. still have a potential of subsidence). The wells W1-M2 and W1-M4 show linear decay subsidence with deviations of different amplitude. Boundary conditions: E=Extension and C=Compression.

6.3 Interplay between tectonic and thermal anomalies

Having shown that basins and arches only form and last for long in case of heterogeneous lithosphere, we now want to evaluate the relative effect of thermal anomaly and far field tectonics on the location and rate of subsidence. This third benchmark therefore aims (1) at dissociating the role of the thermal anomaly from the role of heterogeneous rock column (2) understanding the interplay between tectonic and thermal anomaly using two extra experiments M3 and M4. M3 has no thermal anomaly nor tectonic forcing, M4 has a thermal anomaly and tectonic forcing. Both models are displayed on Figure VI-8 together with M1 and M2.

After 250 Myr, M3 simulations show globally the same features as M1 (Figure VI-8). The peripheral basins are 200 km width and 1.5 km deep. The central basins are thinner (i.e. 1 km) and narrower (i.e. 160 km) than peripheral ones. This singularity can be explained by the larger

surface of erosion of the two end Archean blocks (i.e. the source of sediments is more important) directly feeding the peripheral basins (i.e. sedimentation rate varying according the different basins) and by the thermal doming of the central basin due to the initial thermal anomaly. The only difference between these two models is indeed a negative vertical shift of 125 m of subsidence curve of M3 as compared with M1 (Figure VI-9) that we interpret as initial thermal doming in M1.

After 250 Myr, M2 and M4, the two models subjected to tectonic forcing display more differences than M1 and M3 (Figure VI-8). While M2 displays the same overall distribution of depocenter as M1 and M3 and only differs by the flat angular base of the basins, M4 displays more complex distribution of depocenters. Central and boundary sub-basins are indeed separated by inter-basin arches, inter-basin arches secondary arch and intra-basin secondary arches. A specific structural framework has been described in Perron et al., (2018). Moreover, the maximum of deformation is localized in the peripheral basins for M2 and in the central basin, above the initial thermal anomaly, for M4.

The secondary arches and basins are controlled by steeply dipping conjugated normal faults (synthetic and antithetic), forming graben structures located from either side of terranes boundaries (and shear zones). These structures are repeatedly activated and re-activated during extensions and inversed during compressions due to far field tectonics (i.e. sinusoidal boundary conditions). The comparison between M2 and M4 demonstrates that the thermal anomaly can favor initial fault softening and control the strain intensity in the basins that are located above them. The subsidence curve morphologies are so impacted and show a linear decreasing trend with alternation of up and down deviations of amplitude of 280 m for M2 and 960 m for M4 (Figure VI-9). The deformation as well as the amplitude of deviations are much more significant under the central thermal anomaly.

The comparison of these four tests (Figure VI-8) clearly indicates that isostatic rebalancing between different accreted terranes with heterogenic rheological properties (Archean and Proterozoic) can be considered as a driving force for the creation of accommodation. Thermal or tectonic forcing are not necessary conditions for the creation of basins and their preservation through time. However, while thermal forcing alone does not induce very large changes in the distribution and shape of the basins, tectonic forcing is sensitive to the presence of thermal anomalies.

7 Architecture of basins in accretionary lithosphere

7.1 Covering the arches: Impact lateral sediment supply

None of the simulations presented so far have reached solutions in which sediments cover arches, as it is the case in the sub-Saharan platform (Perron et al., 2018). As surface processes permit the local isostatic reequilibration and controls its (M3 in Figure VI-8), we expect that variation in lateral (out-of-plane) sediment supply implemented as a source term might also affect the subsidence of the basins and arches. Thus, we compare the basins obtained with a heterogeneous lithosphere (model M) without lateral sediment supply (i.e. only local sediment supply by diffusive erosion/deposition processes; M3 in Figure VI-8) to a model with lateral sediment supply (M5 in Figure VI-10; see also Figure VI-11). The simulation M5 consists of bringing a constant lateral sedimentation flux on the external edges of the model (expected in a 3D model with the possibility of many sources). The sediments infill the accommodation created.

After 250 Myr, we observe the same configuration than the last simulations (M1 and M3 in Figure VI-8). The peripheral basins are characterized by a thickness of 3 km and the central basin by a thickness of 2.75 km. Contrary to all the previous models, we observe the presence of sediment on arches about 1.5 km thick. The width of the peripheral basins is about 350 km and 300 km for the central one (from the edge to the arches centers). The morphology of the curves displays an exponential decay trend and almost reach equilibrium after 250 Myr (Figure VI-10C). They show a differential subsidence between peripheral (W1), central basins (W3) and arches (W2). The average rate of subsidence is 12 m/Myr in peripheral basins (W1), 11 m/Myr in the central basin (W3) and 6 m/Myr on arches (W2).

During the simulation, the Proterozoic terranes and the Archean terranes are differentially subsiding one relative to each other. The addition of lateral sediment flux increases the temperature of the basins (<50 °C in simulations Figure VI-8 and >100°C in Figure VI-10A). We observe an unexpected rise up of the isotherms under Proterozoic terranes (i.e. basins) and a go down under Archean terranes (i.e. arches). It is caused by the slow burial of the radiogenic heat production of the basement that follows the relative uplift of the Archean terranes regarding the Proterozoic terranes (Figure VI-11).

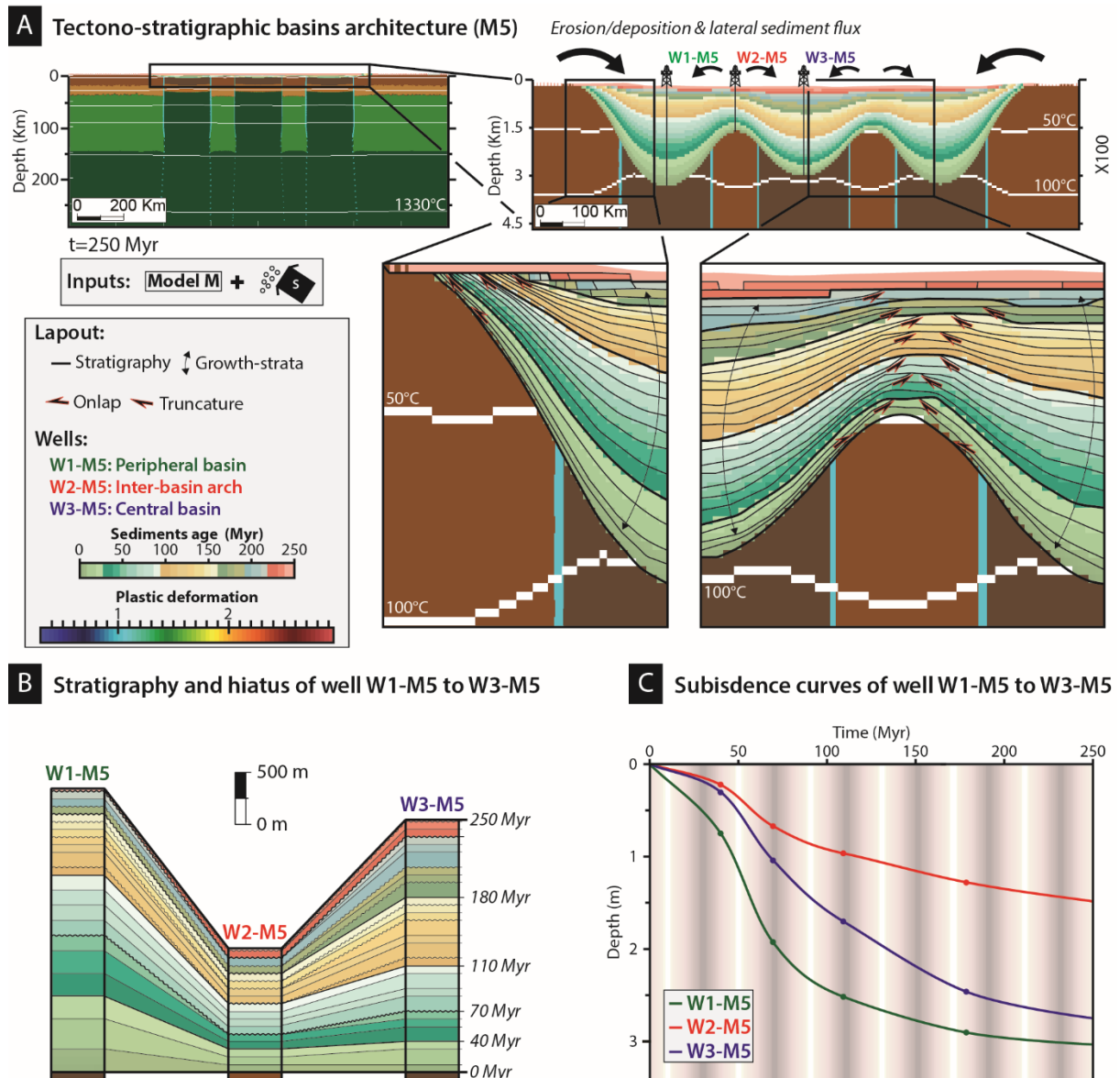


Figure VI-10: (A) Tectono-stratigraphic basins architecture and heat production of Model M5 without thermal anomaly shows stratigraphic lapout (i.e. onlap, truncatures and thickness variations) features when approaching the arches; (B) Stratigraphy and hiatus repartition between the wells W1-M5 to W3-M5; (C) Subsidence curves of well W1-M5 to W3-M5 are characterized by exponential decay shape.

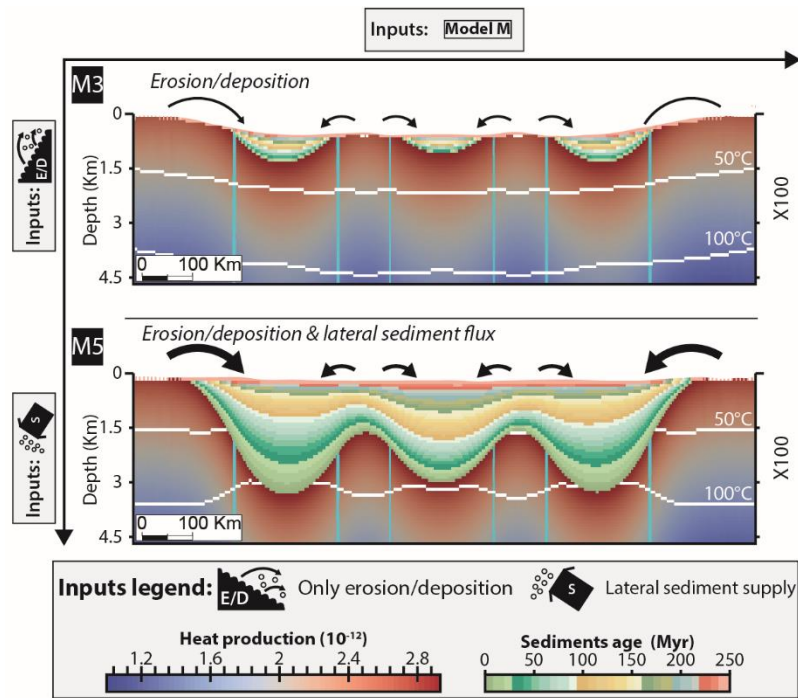


Figure VI-11: Comparison between model M3 and M5 showing increase of the temperature under the basins with lateral sediment supply due to heat production of the basement.

The analysis of these two simulations (M3 and M5) shows the importance of additional sediment supply rate as a forcing factor on the dynamics and filling of basins (loading). In our model these sources are lateral since the modeling is done in 2D. This parameter permits to rapidly reach the isostatic compensation by increasing subsidence rate. It also brings sediment on arches and enlarges the width of the basins. The high intensity of the external sediment flux reduces the duration of subsidence and also increases the thermal of the basin. The tectono-stratigraphic architecture of arches and basins is also well expressed.

7.2 More complex models

We have now circumscribed the first-order trend controlling the low long-lived subsidence rate and the architecture (arches and basins) of the intracratonic basins. Besides, the second-order trend featured by deviations with periods of acceleration, deceleration and inversion of the low subsidence rate can be explained by far field stresses alternating compressional/extensional pulses (i.e. changes in tectonic processes occurring at the adjacent plate margins). We now want to compare the results at smaller scale by comparing the internal architecture of M5, a pure isostatic model with lateral sedimentary influx, to M6, the same model submitted to both thermal anomaly and tectonic forcing.

In M5, the association of arches and basins (Figure VI-10) is evidenced by divergent onlaps (i.e. growth strata), truncatures and reduce thickness when approaching the arches (i.e. Archean terranes). The stratigraphic succession is featured by many hiatuses that can be followed on the model at the local scale (one basin) and the regional scale (three basins). The unconformities are particularly well expressed on arches where some entire stratigraphic units are missing and amalgamated. Besides, some stratigraphic units are present in central basin and not in peripheral basins.

Simulation M6 (Figure VI-12) displays the same sub-basins and sub-arches than M4, yet with more sediments due to the lateral sediment supply. The left peripheral basin and central basin are both characterized by a thickness of 4.8 km while the right peripheral is slightly less thick (4.25 km). We observe the presence of sediments on arches about 2.2 km. The maximum of thickness is in the central boundary basin where sediments reach nearly 5 km. The structural pattern similar to M4 localizes the strain in this latter fault related unit. The fault softening that results from the initial thermal perturbation gives its asymmetrical shape to the central basin.

The basins display divergent onlaps (i.e. growth strata), truncatures and reduction in thickness when approaching the different arches (i.e. inter-basins or intra-basins on Figure VI-12A). The stratigraphic succession features many unconformities. Some entire stratigraphic units are missing in the sub-basins, intra-basin arches and inter-basin secondary boundary arches while present in others (Figure VI-12B). The minimum of thickness and the maximum of amalgamated erosional surfaces are detected on the inter-basin principal arches (W5 in Figure VI-12). In the central boundary basins (W2 in Figure VI-12A), unconformities are observed in the depocenter (maximum thickness recorded in the model) where a continuous conformable stratigraphy would have been expected.

7.3 Basins evolution: key to deciphering past geodynamics

The far field stresses associated with thermal perturbation parameters bring specificities on the tectono-stratigraphic architecture of the basins (Figure VI-12). The arch and basin structural first-order pattern (Figure VI-10) is remodeled by the formation of grabens near terranes boundaries during extension, positively inverted during compression. It is defined by sub-basins, intra-basin arches and inter-basin secondary boundary arches a characteristic identified in the Saharan intracratonic basins (Perron et al., 2018).

In our case, the lithospheric heterogeneities associated with newly created faults on weaknesses zones by far field stresses control the compartmentalization and the tectonic kinematics. This individualization of the different structural units and the disparate propagation of the deformation through them explain the diachronism of the subsidence patterns (i.e. acceleration, deceleration and inversion) and the stratigraphic succession architecture between neighboring basins. For instance, we have highlighted that the layers present in the footwall can be eroded in the hanging wall where the maximum of thickness is usually expected.

First of all, the analysis of 1D well burial history shows that, the initial rate of subsidence in the center of the basins is greater in models with tectonics (W1-M6, 4 and 6 on Figure VI-12C) than in models without far field tectonics (W1-M5 and 3 on Figure VI-10C). Nevertheless, a clear tectonic signal is only recorded in the sedimentary architecture of the central basin at the onset of the models with tectonics. The peripheral basins do subside faster, but they do not display large temporal oscillations with 40 Myr cycle before 80 Myr. We infer that this delay reflects the reduced strength of the lithosphere at the apex of the thermal anomaly at the onset of the model. This thermal signal disappears after 80 Myr and tectonic deformation become distributed across the three basins.

This suggest that variations of the sedimentary record of tectonic oscillation in subsidence rate is a good indicator for lateral variation in strength of the lithosphere and that whether these variations are stable or not in time can be interpreted as local thermal (non-stationary) or chemical (stationary) weakening of the lithosphere.

Looking in more details at the sedimentary record of the far field tectonic sinusoidal loading, it is clear that the subsidence curve response is 1) not always sinusoidal and 2) different whether wells are located on arches (W5-M6, Figure VI-12A), intra-basin arches (W3-M6, Figure VI-12A), central boundary basins (W2-M6, Figure VI-12A), central basins (W4-M6, Figure VI-12A) or peripheral basins (W1-M6 and W6, Figure VI-12A).

First of all, tectonic loading sedimentary record is stronger in the central boundary basins (W2-M6, Figure VI-12C) than in any other well. To first order, these basins subside rapidly during extension and uplift in lesser amount during compression. Yet, in the details the phase of subsidence last longer than the phase of uplift. Indeed, subsidence starts during the slowing down of far field compression and last to the very end of the extension cycle. It is easier to understand how the system behaves by studying the effect of one tectonic cycle (see supplementary materials).

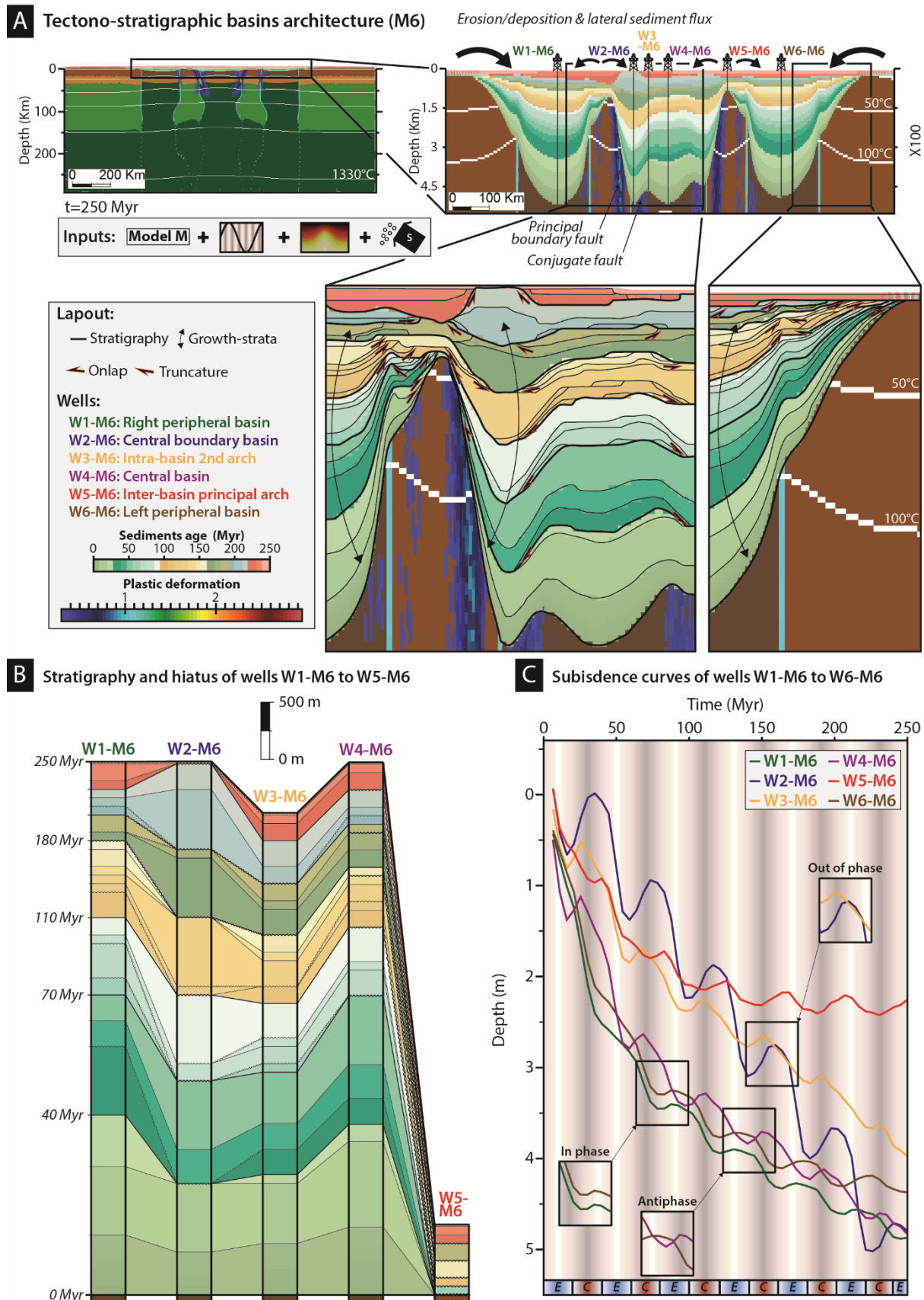


Figure VI-12: (A) Model M with far field tectonics, lateral sediment flux and thermal anomaly shows a complexification of the basins and arches architecture within Figure VI-10 with the

set-up of inter-basins boundary secondary arches and intra-basin secondary arches. The strain is concentrated in the central basin with creation of grabens above shear zones (i.e. limits of terranes); (B) Stratigraphy and hiatus repartition between the wells W1-M6 to W5-M6; (C) Subsidence curves of wells W1-M6 to W6-M6 displays an exponential decay with deviations of different amplitude depending on their localization (i.e. near maximum strain zones or not). Several type of diachronicity of the oscillations (antiphase, out of phase) are observed depending on the localisation and propagation of deformation. Boundary conditions: E=Extension and C=Compression.

The peripheral basins display very short periods of uplift, which corresponds to 1) maximum subsidence rate in the central boundary basins, 2) a marked increase in subsidence rate in the central basin, 3) maximum uplift of arches and 4) onset of subsidence in the central boundary basins. This short period of time corresponds to the period during which extension rate increases at the boundary. During that time period, the system behaves like a rift bordered by the external normal faults of the central boundary basins and where the arches and the peripheral basins behave like uplifting rift shoulder. As extension decelerates at the boundary, the central boundary basins (W2-M6) continue to subside but until extension ceased but the outer part of the system relaxes as shown by the subsiding trend of the arches (W5-M6) and the peripheral basins (W1-M6). The central basin (W4-M6) continues to subside at yet smaller rate than the central boundary basin (W2-M6), which highlights that the conjugate normal faults are active.

At the onset of compression, the peripheral basin (W1-M6) subsidence accelerates while the central basin (W4-M6) and the central boundary basin (W2-M6) mark a rapid uplift. This corresponds to a phase of tectonic inversion of the principal boundary faults. Yet, at the peak of compression, central basin and the central boundary basins start to subside together with the peripheral basins marking the end of tectonic activity on faults for the tectonic cycle. During that phase the system in buckling down as a whole.

To summarize, the principal faults that bounds the central boundary basins are active through all the extensional phase, whatever the rate, but the activity of the conjugate faults starts only towards the peak of extensional rate. During compression, principal boundary faults are only active with the acceleration of shortening. After the peak of compression, the system is locked and responds by downward buckling of the whole lithosphere. This asymmetric behavior between extension and compression phase is well explained by the fact that the lithosphere is stronger in compression than in extension (Brace and Kohlstedt, 1980).

These delays in inversion of the fault system versus global buckling may explain why during the a same tectonic event, both extensional or compressional structures can be locally identified in the different sub-basins (Perron et al., 2018).

8 Discussion

Low rate and long duration subsidences are an intriguing geological feature often described in the literature; several studies have attempted to explicate the first order mechanism of subsidence but generally without considering their particular architecture and intrinsic characteristics. Apart classical thermal cooling subsidence source after conventional phase of extension (McKenzie, 1978) suggested in different areas (Korsch et al., 1988; Lüning et al., 1999; de Oliveira and Mohriak, 2003; Thomas et al., 1999) or alternatively after a phase of compression (McKenzie and Priestley, 2016), some authors invoke thermal relaxation process by stretching of rifted basement at slow strain rate over long period of time (Allen and Armitage, 2011; Armitage and Allen, 2010; Cacace and Scheck-Wenderoth, 2016), by cooling and thickening of the lithosphere (Holt et al., 2010, 2015), by mantle delamination (Avigad and Gvirtzman, 2009), by phase changes (Baird et al., 1995; Eaton and Darbyshire, 2010; Gac et al., 2013; Hamdani et al., 1991; Kaus et al., 2005; Naimark and Ismail-Zadeh, 1995).

Yet, the cratonic studied area are often considered as “old”, “buoyant” “thick”, “cold” and “strong” lithosphere (Griffin et al., 2003; King, 2005; McKenzie and Priestley, 2008, 2016; Michaut et al., 2009; Nyblade and Pollack, 1993; Sleep, 2003, 2005) where thermal activity is reduced. With the current lithosphere characteristic, thermal anomalies allow indeed to explain lithosphere thinning during the rifting and then thickening (for aborted rift as for passive margin after the opening). Besides, our models show that thermal anomalies do not destabilize strong continental lithospheres (A1 and A2 in Figure VI-6) and that thermal subsidence is relaxed rapidly (see A1 and A2 in Figure VI-8), in less than 50 Myr as expected by computing the thermal relaxation of a lithosphere (see for instance Turcotte and Schubert, 2014). More over the existence of geological evidences for mantle flux, delamination, plume, thermal anomaly, rifting zone are not always obvious.

Here we find that contrast in rheologies and densities of Archean and Proterozoic terranes (all M models) are actually necessary and sufficient to drive slow long-term subsidence observed in intracratonic basins. The values of subsidence rate in our models (Figure VI-9) are coherent with the range of data (Figure VI-3) provided by the literature (Allen and Armitage, 2011; Xie

and Heller, 2009). Although, our subsidence curves can be described approximately by exponential decay, the diffusive process that causes the decay is the rate of basin infilling. High sedimentary rates cause a faster decay (Figure VI-10C).

In our models, the strength of the continental lithosphere keeps its integrity slowing down the isostatic compensation progression. The local differential strength between the terranes permits localized vertical movements and basins creation either by flexure or when far field loading occurs by buckling (in compression) or normal faulting (in extension). In the first case, feed and the preservation of subsidence are due to isostasy by coupling erosion/denudation of uplifted reliefs and deposition in depressions (Avouac and Burov, 1996; Moretti and Turcotte, 1985). In the second case, weaker lithosphere uplift by buckling during compressive events while rheological interfaces between terranes allows localized displacement to occur along normal faults during extensional events. Faults are found to play a more important role when the lithosphere is thermally weakened.

Various authors have suggested that far field stresses and intra-plate effects impact intra-cratonic basins (Klein and Hsui, 1987; Lambeck, 1983; Xie and Heller, 2009) more than can be reasonably accounted for by eustatic sea-level changes (Vail et al., 1977). Here we show that far field stresses forcing indeed allow explaining the second order trend characterized by the subsidence deviations pattern and complexification of the structural framework. The amplitude of variation in subsidence rate related to tectonic in our models (Figure VI-9) is coherent with the data range (Figure VI-3) provided by the literature (Allen and Armitage, 2011; Xie and Heller, 2009).

The different behavior of arches, sub-basins and sub-arches submitted to far field stress provides an alternative explanation to variation in dynamic topography (Burgess et al., 1997; Coakley and Gurnis, 1995) for the diachronicity of large regional unconformities documented in North America with the Michigan-Illinois basins (Allen and Armitage, 2011; Sloss, 1963; Watts et al., 2018), in South-America with the Parnaiba basin (Daly et al., 2018b; Watts et al., 2018) and in North Africa with peri-Hoggar basins (Beuf et al., 1971; Eschard et al., 2010; Perron et al., 2018).

9 Conclusions

Through a 2D thermo-mechanical modelling, we have applied basic internal (thermal anomaly, far field stresses) and external forcing factors (surface erosion/deposition and constant

sedimentation rate) to homogenous lithospheres and accretionary lithospheres (Archean and Proterozoic). From the analysis of the simulations, we can state that:

1. The presence of a thermal anomaly is not sufficient to create long-lived basins. Even with erosion sedimentation processes, thermal subsidence ceases after 150 Myr.
2. Arches and Basins can emerge from the amplification of the geometry of the terranes through vertical isostatic compensation of Archean/Proterozoic terranes (columns) with different rheologies/densities.
3. The sedimentation rates control the duration of subsidence, typically over 250 Myr in intra-continental context where there are no mountain ranges to provide large sediment supply.
4. Due to distance to the sources and to paleoclimatic changing (i.e. alternating arid and humid phases), the sedimentation rates may vary in these kinds of large subsiding intracontinental areas resulting in complex to interpret sedimentary features (time gap, truncation, onlap...) even if the boundary conditions are rather simple and the same for the various basins.
5. Lateral sedimentary influx is necessary to cover the arches and sufficient to both increase the thickness of basin and rise the temperature.
6. Far field stresses lead to more asymmetric basins and permit the formation intra-basins arches and inter-basin boundary secondary arches delimited by fault-related sub-basins (grabens). They can explain dissimilarities of sedimentary fillings between neighboring basins as well as the presence of unconformities in the deeper part of the basins.
7. The effect of tectonic is amplified when a deep-seated thermal anomaly weakens the lithosphere.

Taken as keys to interpret real dataset, we believe that the simulations presented here are simple but realistic enough to constitute a step forward in tectono-stratigraphic trap prediction and heat flux analysis in intracratonic basins.

10 Appendix A: Calculation of isostatic potential between Archean and Proterozoic terranes (cf. Figure VI-4)

sediments thickness basin = topography (t) \times ρ_{arche} \times arche sediments thickness

- (1) Initial state (no sedimentation on arches) with $t < 500$ m, $h_{\text{sa}}=0$, $h_{\text{sb}}=0$

$$(h_6 - h_0 + h_{sb}) \times \rho_6 + h_5 \times \rho_5 + h_4 \times \rho_4 + h_0 \times \rho_s + h_{sb} \times \rho_s$$

$$= (h_1 - h_{sb}) \times \rho_1 + h_2 \times \rho_2 + h_3 \times \rho_3 + h_{sb} \times \rho_6$$

$$= h_1 \times \rho_1 + h_2 \times \rho_2 + h_3 \times \rho_3 + h_{sa} \times \rho_s$$

$$= h_1 \times \rho_1 + h_2 \times \rho_2 + h_3 \times \rho_3 + h_{sa} \times \rho_s$$

$$h_{sa} \times \rho_s + P_a = h_{sb} \times \rho_s + P_p - t \times \rho_6 - h_{sb} + h_{sa} \times \rho_5$$

$$P_a - P_p = t \times \rho_6$$

(2) Initial state (basins filling) with $t=0$

$$P_a - P_p = -h_{sb} \times \rho_s + h_{sb} \times \rho_6 - h_{sa} \times \rho_6 + h_{sa} \times \rho_5 - t \times \rho_6$$

$$\text{positive constant} = h_{sb} \times (\rho_6 - \rho_5) - h_{sa} \times (\rho_6 - \rho_5) - t \times \rho_6$$

$$\text{positive constant} = (h_{sb} - h_{sa}) \times (\rho_6 - \rho_5)$$

$$(P_p - P_a) / (\rho_6 - \rho_5) = h_{sb} - h_{sa} - (t \times \rho_6) / (\rho_6 - \rho_5)$$

$$(t \times \rho_6) / (\rho_6 - \rho_5) = (500 \times 3345) / (3345 - 2400) = 1500 \text{ m}$$

(3) Final state (potential basins filling) with $t=\text{final}$

$$h = (P_a - P_p) / (2 \times \rho_6 - \rho_1 - \rho_s) = 7550 / (2 \times 3345 - 2800 - 2400) \sim 5 \text{ Km}$$

11 Appendix B: Numerical method.

In order to study the influence of accreted lithospheric heterogeneities on the architecture and the low long-lived subsidence of intracratonic basins, we use the thermo-mechanical numerical code pTatin (May et al., 2014) in its 2D version (Jourdon et al., 2017). The code relies on PETSc library Balay et al., (2017) to solve conservation of momentum

$$\nabla \cdot \sigma = \rho g$$

for an incompressible fluid flow described by its velocity \mathbf{v} such as

$$\nabla \cdot \mathbf{v} = 0,$$

using high order Q2P1 finite elements in parallel. This permits to model accurately the topography with a free surface. In order to avoid deformation of the mesh the lithologies are

tracked with ALE marker in cell approach (May et al., 2015). Markers are used to carry lithological inform and adjust the density with temperature T and pressure P using Boussinesq approximation

$$\rho = (1 - \alpha\Delta T + \beta P)\rho_0,$$

and to compute the stress and deformation rate. The fluid/rocks typically deform by dislocation creep

$$\sigma = A \frac{-1}{n} \exp\left(\frac{Q}{nRT}\right) e^{n\dot{\epsilon}} \dot{\epsilon}^{\frac{1-n}{n}}$$

where the viscosity depends on temperature T , lithology (A , n , Q see Table 1) and strain rate ($\dot{\epsilon}$). However, when viscous stress exceeds brittle frictional strength $\sigma^b = \sin\phi + C \cos\phi$ or maximum plastic strength σ^p the effective viscosity is adjusted to keep the stress on the yield cap $\sigma^y = \min(\sigma^b, \sigma^p)$ following

$$\eta = \frac{\sigma^y}{2e^{n\dot{\epsilon}}}$$

Conservation of momentum is coupled with conservation of heat

$$\frac{\partial T}{\partial t} = \nabla \cdot \kappa \nabla T + \frac{H}{Cp} - \nabla \mathbf{v} \cdot \nabla T$$

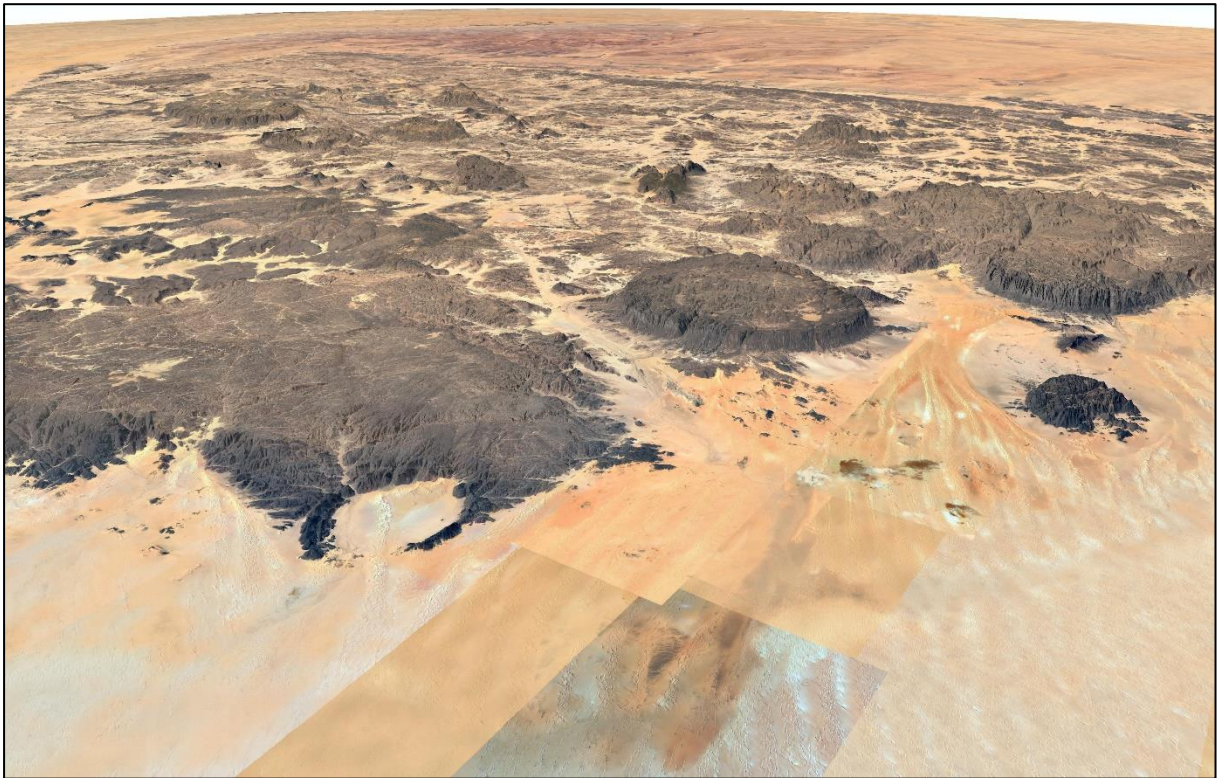
The heat diffusivity κ , heat production H and heat capacity Cp do not vary for the different simulations.

Sediment transport is simulated using advection diffusion of the topography in 1D

$$\frac{\partial h}{\partial t} = v_x + \frac{\partial}{\partial x} \left(\kappa_r \frac{\partial h}{\partial x} \right) + S - \frac{\partial v_x}{\partial x} \frac{\partial h}{\partial x}$$

with a source term S , which permits out-of-plane sediments inflow and outflow. Details about the implementation and tracking of the stratigraphy may be found in Jourdon et al., (2018).

**CHAPTER VII. DECIPHERING THE ORIGIN OF
FORCING FACTORS CONTROLLING THE
ARCHITECTURE OF PALEOZOIC INTRACRATONIC
PERI-HOGGAR BASINS: LINK WITH GEODYNAMIC
HISTORY – APPLICATION AND CLASSIFICATION**



Ring complex of the Air massif (Google-Earth view; 18°55'50" N, 9°06'39" E)



1 Summary and objectives

On the one hand, we have proposed a conceptual geological model integrating both the substrates nature and the tectono-sedimentologic architecture of the Arches-Basins (Chapter IV). On the second hand, we have developed a lithospheric thermomechanical numerical model testing several models with homogenous and heterogeneous lithospheres to forcing factors such as tectonics, sediment flux and thermal anomaly (Chapter VI). We have extracted several results explaining both the first and second order control of intracratonic basins as well as their arches and basins architecture.

This ending chapter attempts to link these two parts by calibrating and comparing geological data of peri-Hoggar Basins with our forward modelling results.

The different objectives of this chapter are the following:

- Application of the lithospheric thermo-mechanical numerical model to peri-Hoggar Basins;
- Comparison between the stratigraphic architecture, the thermal and the subsidence curves of forward modelling with geological data of peri-Hoggar Basins;
- Classification of the different peri-Hoggar Basins according to their factors forcing dominance (with numerical models standards).

2 Article in preparation

Abstract (Français)

La modélisation numérique thermomécanique d'échelle lithosphérique peut être utilisée comme un outil efficace pour identifier les différents forçages de la mise en place et du développement des bassins intracratoniques. En raison de leurs longues longueurs d'ondes et de leurs positions particulières dans des lithosphères stables à longue durée de vie, des paramètres inhabituels peuvent être prédominants contrairement à d'autres bassins considérés comme plus classiques (e.g. bassin d'avant-pays, rifts, marge passive...).

La comparaison des résultats de la modélisation avec les paléo-températures, les courbes de subsidences et l'architecture tectono-sédimentaire observées des bassins péri-Hoggar permet de mieux comprendre l'origine des mécanismes de subsidence et peut contraindre les forçages de

ces bassins intracratoniques et le lien avec les événements géodynamique. Une classification est proposée montrant les différents types de bassins intracratoniques basée sur les géométries et leur ressemblance architecturale des différents bassins péri-Hoggar.

Les principaux résultats de l'article :

La comparaison des résultats de la modélisation avec les données géologiques des bassins péri-Hoggar (Plateforme Saharienne) a permis de mettre en évidence la viabilité de la cohérence du modèle géologique conceptuel proposé (Perron et al., 2018) et l'hypothèse d'un déséquilibre isostatique entre les différentes terranes accrétées composant le substrat. La variabilité de densité dans la lithosphère, héritée des paléo-orogénèses, crée des colonnes non compensées qui seront conservées au fil du temps. L'équilibre entre ces entités sera atteint après une très longue durée.

Les principaux résultats de cette étude sont les suivants :

- Le modèle numérique thermomécanique mis au point est cohérent et viable pour expliquer la faible subsidence de longue durée (premier ordre) et les déviations associées du signal (second ordre) des bassins péri-Hoggar ;
- Les hétérogénéités de densité lithosphérique entre les terranes accrétées archéennes et protérozoïques contrôlent l'architecture en Arches et Basins ;
- La comparaison des données géologiques avec les modèles thermomécaniques numériques permet de classer chaque bassin péri-Hoggar en fonction de leurs forçages (à dominance tectonique, à dominance anomalie thermique et/ou à dominance flux sédimentaire externe). Ils sont définis par leur architecture (c'est-à-dire en forme de synclinal ou forme complexe), le ramollissement des failles/terranes et leur remplissage (c'est-à-dire, affamés ou comblés) ;
- Un très faible taux de contrainte (0,5 km/Ma) peut être transmis loin (plus de 1600 km) à l'intérieur du modèle et provoquer et/ou réactiver des failles, ce qui est cohérent avec la propagation des contraintes intraplaques lointaines mise en évidence par certains auteurs (Perron et al., 2018; Ziegler et al., 1995) ;
- Le diachronisme et les discordances entre les différents bassins péri-Hoggar sont bien expliqués par la propagation hétérogène de la déformation à travers le modèle.

En raison de la modélisation 2D, le flux de sédiments (c'est-à-dire l'apport de sédiments en amont) doit être simulé en apportant des sédiments externes aux extrémités des modèles. Par

ailleurs, la composante décrochante dans les mégas zones de cisaillement héritées, identifiée dans la plateforme saharienne, doit également être prise en compte (Haddoum et al., 2001, 2013; Perron et al., 2018; Zazoun, 2001, 2008). Par conséquent, la modélisation 3D devrait constituer une perspective intéressante afin de mieux contraindre ces bassins intracratoniques.

Abstract (English)

Lithospheric thermo-mechanical numerical modelling can be used as an efficient tool for deciphering different forcing factors of intracratonic basins. Because of their long wavelength feature and their particular position in long-lived stable lithosphere, unusual parameters can be predominant contrary to other classical basins (e.g. foreland basin, rifts, passive margin...).

Comparison of paleo-temperature, subsidence patterns and tectono-sedimentary architecture from the peri-Hoggar Basin with modeling results with provides new insight into the origin of the mechanism of subsidence and may constrains the forcing factors of these intracratonic basins, and the link with geodynamic events. A classification is proposed showing the different trends in regard with their geometries and architecture likeness with the peri-Hoggar Basins.

3 Introduction

The Paleozoic basins of the Northern part of the paleo-continent Gondwana, and more specifically the of Sahara platform, correspond to a series of syn-sedimentary synclinal with typical large wavelength of 75 to 620 km (sub-basins), strongly influenced by the structural inheritance of paleo-orogenies (Beuf et al., 1971; Coward and Ries, 2003; Perron et al., 2018). These basins are generally separated by structural highs of low amplitude (frequently named in the literature “arch”, “moles”, “ridges”, “highs”, “swells”) which were episodically reactivated during all Paleozoic and which are controlling the sedimentary architecture, and therefore their related specific petroleum system (Eschard et al., 2010; Perron et al., 2018). They represent the most prolific petroleum systems of the world (Boote et al., 1998; Eschard et al., 2010; Macgregor, 1996; MacGregor et al., 1998). They are classified as intracratonic basins (i.e. sag basin) and they are often referred as intercratonic or intercontinental basins (Holt, 2012; Holt et al., 2010).

The structural framework result from the subduction, accretion and collision of continental cratonic and oceanic island arc terranes/cores of various age and rheologies through a complex

geological history such as the Eburnean, the Kibaran and the Pan-African orogenic cycle (Bertrand and Caby, 1978; Black et al., 1994; Caby, 2003; Liégeois, 2019).

Perron et al., (2018) highlighted the influence of basement heterogeneity and anisotropy on the tectono-sedimentary architecture of the basins and arches in the Reggane, Ahnet, Mouydir and Illizi basins (i.e. North Hoggar area) through a multidisciplinary integrated approach. They have been exposed the specific distribution of the Paleozoic arches and basins framework of the Sahara with the different zonations of the accreted basement terranes (archean, paleoproterozoic and proterozoic). A conceptual geological model coupling the terranes natures and the tectono-sedimentary architecture was proposed, where the arches are preferentially situated upon Archean or Paleoproterozoic terranes and basins depocenter upon Meso-Neoproterozoic terranes.

Due to their sedimentary oval-bowl shaped arrangement around the large Saharan massifs, synsedimentary syncline geometry, low rate subsidence preserved over a long period, these basins cannot be linked to a classical rifting process, nor to a late-orogenic gravitational collapse process as documented in the literature (Morley et al., 1990; Pinet and Colletta, 1990; Séguret et al., 1989). The understanding of the geodynamic and structural evolution of these peri-Hoggar basins therefore requires a better knowledge of the dynamics of the lithosphere, on a regional scale.

Yet the process or processes that form these basins is still a matter of debate within the literature (Allen and Armitage, 2011). Especially, the difficulty is to explain their long-living polyhistory basin-fill feature. Owing to their extended history they are often formed by a combination of mechanisms. Besides, the forcing factors controlling the structural and stratigraphic framework related to arches-basins architecture is often misunderstood.

In Perron et al., (submitted), a numerical thermo-mechanical model was proposed to explain the mechanism of formation and evolution of these intracratonic basins by both reconciling their most enigmatic features such as the arches and basins architecture and the low-long-lived subsidence rate as well as the subsidence deviations patterns. Where for explaining subsidence source in our area, some modelling work has invoked a thermal cooling and thickening of the lithosphere (Holt et al., 2010) without constraining their architecture, the model proposed by Perron et al., (submitted) shows that an initial thermal anomaly is not necessary. Indeed, the hypothesis of an initial uncompensated isostatic heterogenic lithosphere inherited from accreted terranes with different densities column associated with basic erosion and deposition processes

and sedimentation flux can control the subsidence pattern of these basins. This lateral variation of lithospheric density will play a determining role in the structural evolution of the Pan-African mobile zone, in particular in the peri-Hoggar Basins.

The aim of this study is to decipher and better constraints the different processes of forcing factors controlling the peri-Hoggar basins through the Paleozoic time. For this purpose, we compare the architecture, the subsidence and the thermal pattern of the numerical thermo-mechanical model parametrized and tested in Perron et al., (submitted) with geological data compiled in the peri-Hoggar basins. For each peri-Hoggar Basins, a better-fit model with their geological data (architecture, morphologies, thermal and subsidence history) is proposed establishing a basin classification based on their forcing parameters combinations. We discuss the probable origins of these forcing factors such as far field stresses (plate boundary paleogeographic reconstruction), thermal anomaly (magmatic events), sediments flux (climato-eustatism) and their coherence and viability with the case of each peri-Hoggar Basins during the Paleozoic.

4 Geological and geophysical settings

The intracratonic basins of the Paleozoic Saharan platform (i.e. peri-Hoggar Basins) is characterized by an association of arches (anticlines) and basins (synclines) of different wavelengths from 75 to 620 km (Figure VII-1, Figure VII-2 and Figure VII-3). Stratigraphic hiatus, lateral facies variation (i.e. shallowing facies), thinning, wedges, erosion and condensation of series are highlighted when approaching the arches (Perron et al., 2018; Figure VII-2). These tectono-sedimentary structures are documented and dated by many studies (see Table 3 and Figure VII-1 for localization of different cross sections). It attests that the arches are representing structural highs that were preserved through time (i.e. slowly uplifting). The geometries of the intracratonic basins are featured by large circular, elliptical to oval-shaped in plan and saucer-shaped in cross section. They are characterized by low (5 to 50 m/Ma) and long periods of subsidence (>250 Ma) alternating periods of quiescence, acceleration and inversion due to compressional/extensional kinematics (Figure VII-4A). These periods are linked to regional tectonic pulses (e.g. Caledonian compression, Hercynian orogeny) or climate changes (e.g. Late Ordovician deglaciation featured by isostatic rebound) (Perron et al., 2018). The subsidence curves morphologies between the different basins can be in phase (i.e. synchronous curves), in antiphase and out phase (i.e. shifted curves) with these phases (Figure VII-4A). The

burial constrains the paleo-temperature history and so the maturity of the petroleum systems of these basins (Figure VII-4B).

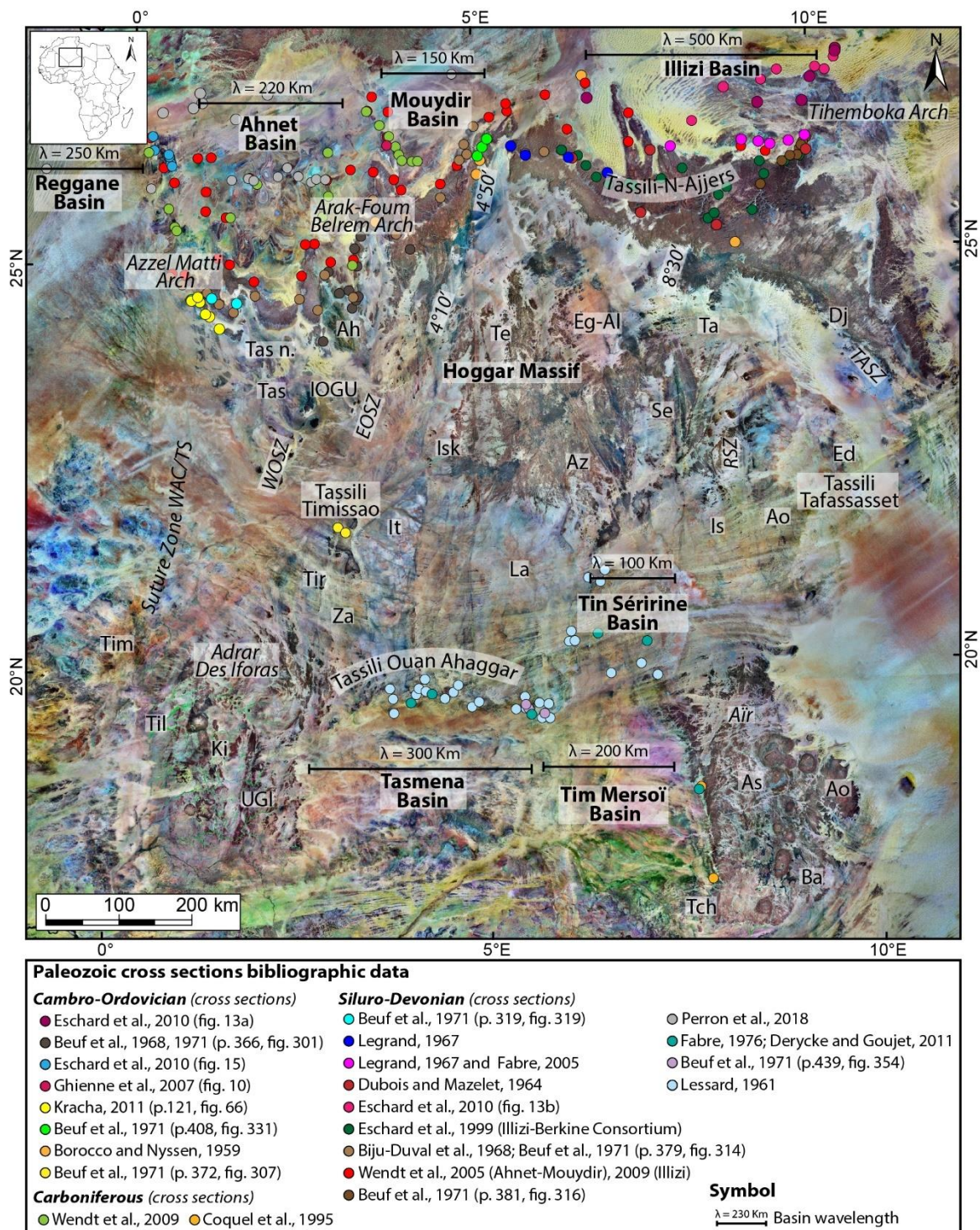


Figure VII-1: Satellite images of the Paleozoic peri-Hoggar basins (Landsat 7 ETM + from USGS database: <https://earthexplorer.usgs.gov/>) associated with the georeferenced different cross sections compiled from bibliography. See also Table 3 for reference.

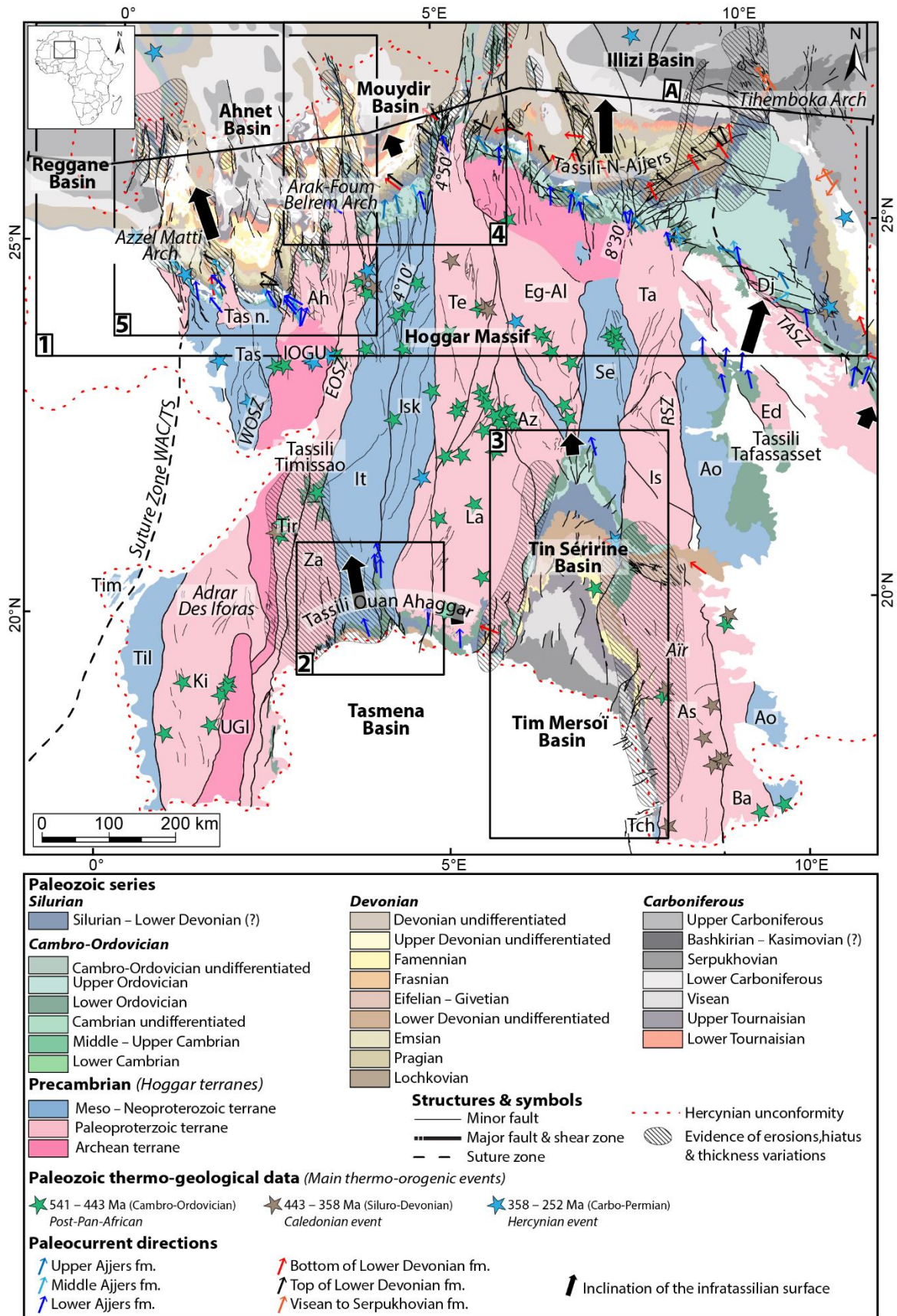


Figure VII-2: Geological map of the Paleozoic peri-Hoggar Basins (North Saharan Platform; North Gondwana) modified from Perron et al., (2018) showing evidence of erosion, hiatus,

thickness variations, paleocurrent directions, thermo-orogenic events and igneous activity data (<https://doi.org/10.5194/se-9-1239-2018-supplement>) compiled from bibliography (see Figure VII-1). Terrane names and abbreviations: Tassendjanet (Tas), Tassendjanet nappe (Tas n.), Ahnet (Ah), In Ouzzal Granulitic Unit (IOGU), Iforas Granulitic Unit (UGI), Kidal (Ki), Timétrine (Tim), Tilemsi (Til), Tirek (Tir), In Zaouatene (Za), In Teidini (It), Iskel (Isk), Tefedest (Te), Laouni (La), Azrou-n-Fad (Az), Egéré-Aleskod (Eg-Al), Serouenout (Se), Tazat (Ta), Issalane (Is), Assodé (As), Barghot (Ba), Tchilit (Tch), Aouzegueur (Ao), Edembo (Ed), and Djanet (Dj). Shear zone and lineament names and abbreviations: west Ouzzal shear zone (WOSZ), east Ouzzal shear zone (EOSZ), Raghane shear zone (RSZ), Tin Amali shear zone (TASZ), 4°100 shear zone, 4°500 shear zone, and 8°300 shear zone. A: Localization of cross section of Figure VII-3. 1: Figure VII-5; 2: Figure VII-11; 3: Figure VII-12; 4: Figure VII-13; 5: Figure VII-14.

The beginning of subsidence of these basins (i.e. Early Cambrian around 530 and 500 Ma) starts at the end of the Pan-African orogeny and was followed by an orogenic collapse (Ahmed and Moussine-Pouchkine, 1987; Boote et al., 1998; Bumby and Guiraud, 2005; Caby et al., 1985; Coward and Ries, 2003; Djellit et al., 2002; Fabre, 2005; Fabre et al., 1988). The whole was uplifted and peneplaned forming a wide polygenic planar “Infratassilian” surface unconformity (also called Pan-African unconformity) setting the place of a relatively typical stable cratonic platform tectono-stratigraphic history (Bennacef et al., 1971; Beuf et al., 1968b, 1971; Boissonnas et al., 1969; Fabre, 1988, 2005). The persistence of some low paleo-reliefs is identified preferentially localized on arches area (Beuf et al., 1971).

The two major tectonic events during the Phanerozoic (Hercynian and Late Eocene swell) are at the origin of the exhumation and the tilting of the Paleozoic series actually outcropping in the Saharan Platform (English et al., 2016b; Rougier, 2012; Rougier et al., 2013; Ye et al., 2017). These tectonic events allow to interpret in section the series visible in 2D maps (Figure V-8), showing the synsedimentary syncline-shaped architecture of the peri-Hoggar Basins defined in Perron et al., (2018).

The peri-Hoggar Basins were part of the Gondwana supercontinent formed by the assembly of several continental fragments and oceanic terranes during the Neoproterozoic Pan-African orogeny (Craig et al., 2008; Guiraud et al., 2005; Unrug, 1992). The origin of the structural framework emanates from the collision of the West African Craton (WAC) and the East Saharan Craton (ESC) also called the Saharan Metacraton (Abdelsalam et al., 2002), squeezing

the Tuareg Shield (TS) mobile belt (Craig et al., 2008; Guiraud et al., 2005; Unrug, 1992). It results heterogenic substrates inherited from proterozoic accreted mobile belt of different terranes (archean cratons and meso-neoproterozoic terranes) delimited by sub-vertical mega-shear zone (Black et al., 1994; Caby, 2003; Liégeois et al., 1994).

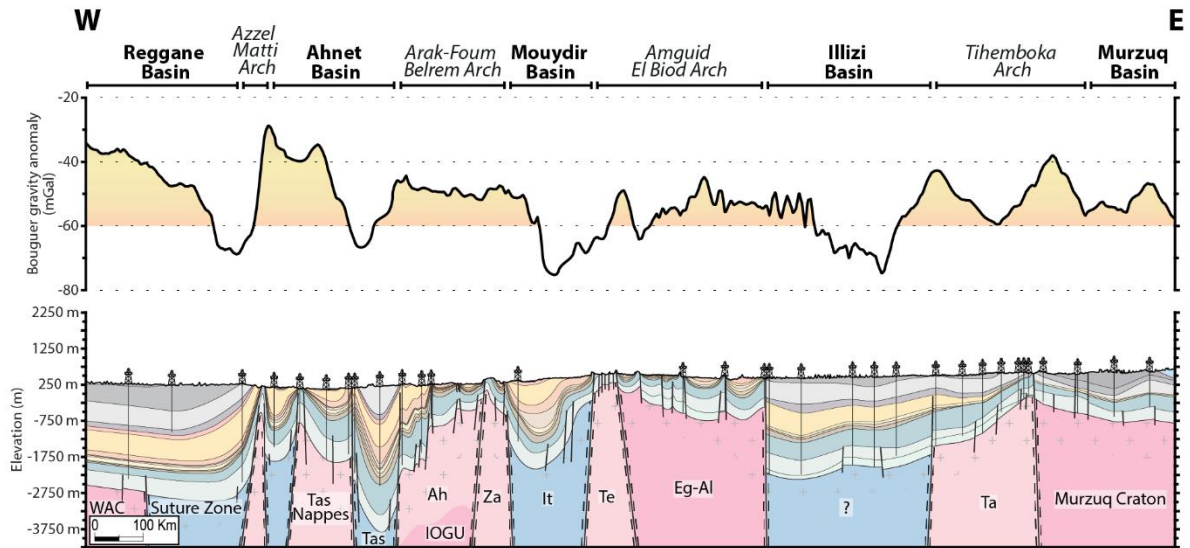


Figure VII-3: E–W cross-section of the Paleozoic peri-Hoggar basins (calibrated with wells) associated with the different terranes and the Bouguer anomaly extracted from Bouguer anomaly map (from International Gravimetric Bureau: <http://bgi.omp.obs-mip.fr/>). Notice the relation between arches with positive anomalies and syncline-shaped basins with negative anomalies. See Figure VII-2 and Figure VII-5 for legend and localization.

The sub-vertical mega-shear and suture zones indicating the boundaries between different terranes were first highlighted by Black et al., (1994). They were consecutively reactivated and/or inverted during the Phanerozoic tectonic events (Boote et al., 1998; Coward and Ries, 2003; Craig et al., 2008; Fabre, 1988, 2005; Guiraud et al., 2005; Perron et al., 2018). They are well constrained by aeromagnetic data (Figure VII-5) showing sigmoidal and SC shear fabrics (Perron et al., 2018). In addition, it was also used to decipher terranes structural geometries and the suture zones under the sedimentary cover (Bournas et al., 2003; Brahimi et al., 2018a; Perron et al., 2018). The existence of igneous or volcanic activity linked to these structures point out the lithospheric nature of these faults (e.g. Liégeois et al., 1994; Moreau et al., 1994; Nkono et al., 2018). This is supported by conductivity anomalies (i.e. an increase of the conductivity), showing the lithospheric scale of these structures (Bouزيد et al., 2008, 2015).

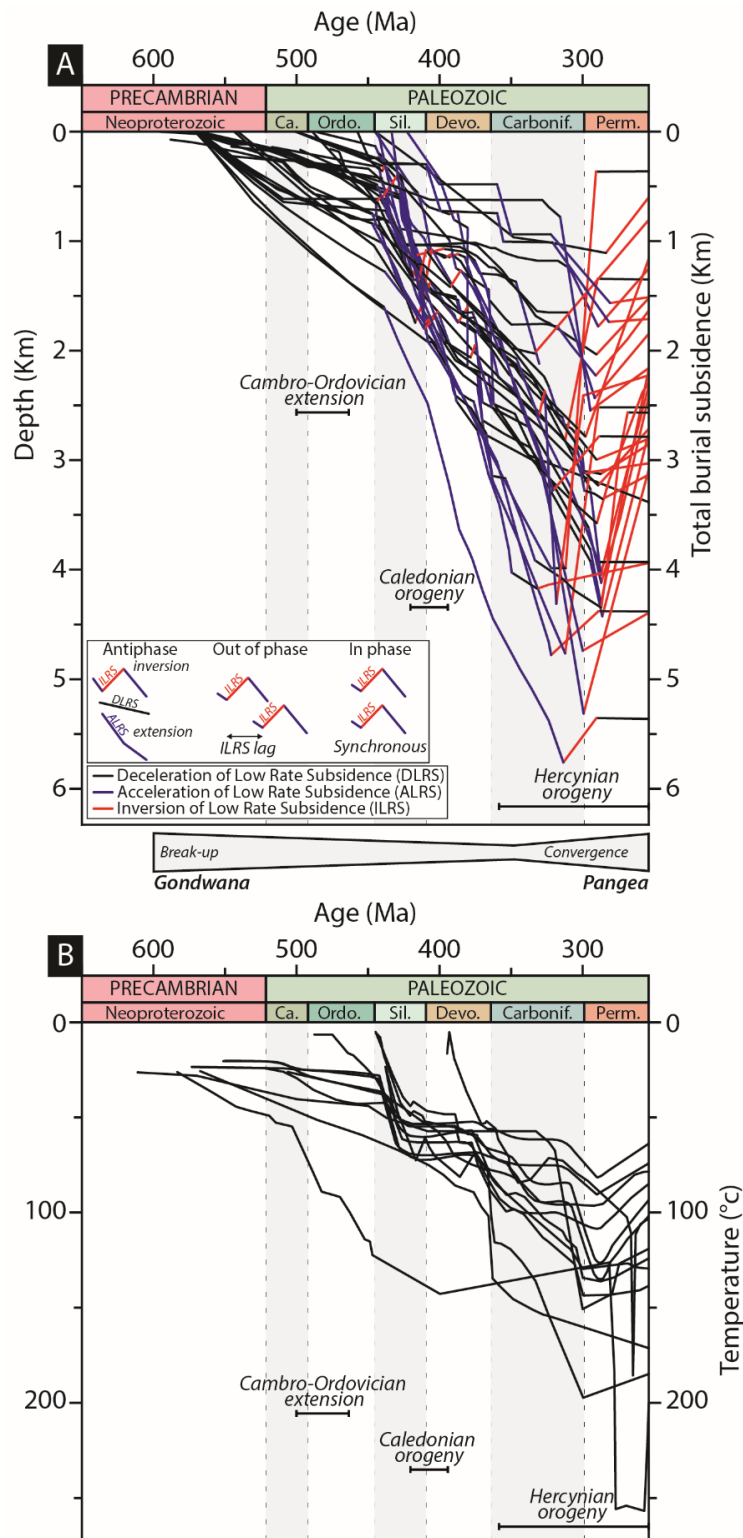


Figure VII-4: (A) Total burial subsidence curves of the Paleozoic North Saharan Platform (peri-Hoggar basins) compiled from literature: well W7 in Ahnet basin, well W21 in Mouydir basin (Perron et al., 2018); well W1, well W4, well W7 and well W9 in Ahnet basin (Kracha, 2011); well KB-2 in Timimoun basin, well ELA-1 in Ghadamès-Berkine basin (Kadi et al., 2013); well in the Illizi basin (Wells et al., 2018); wells model A and B in Ghadamès-Berkine

basin (Underdown et al., 2007); well LD-1 and well PDG-2 in Berkine-Ghadamès basin (Aissaoui et al., 2016); well F3-NC174, well H29-NC115, well AI-NC186, well AI-NC190 in Murzuq basin (Belaid et al., 2010); cross section in the southwestern Anti-Atlas (Burkhard et al., 2006); well OTRA-1 in the Sbâa basin, well RG-3 in the Reggane basin, well TEG-1 in the Timimoun basin (Logan and Duddy, 1998); Hassi Messaoud field (English et al., 2017); well in Sbâa basin (Tournier, 2010); well in Ghadamès-Berkine basin (Yahi, 1999); well RPL-101 in Reggane basin, well HAD-1 in Ghadamès basin, well REG-1 in Timimoun basin; well TGE-1 in Illizi basin, well TO-1 and well KA-1 in the Dahar depression (Makhous and Galushkin, 2003a, 2003b); well LT-1bis and well OTLA-1 in the Sbâa basin (Drid, 1989); well L1-1 in Murzuq basin (Galushkin and Eloghbi, 2014); well WT-1 in the Berkine basin (Yahi et al., 2001); well G and well A in the Illizi Basin (English et al., 2016a). The different curves morphologies showing antiphase, out of phase and in phase between basins. The data show low rate subsidence with periods of deceleration (Deceleration of Low Rate Subsidence: DLRS), acceleration (Acceleration of Low Rate Subsidence: ALRS), or inversion (Inversion of Low Rate Subsidence: ILRS) synchronous and correlated with regional tectonic pulses (i.e. major geodynamic events). (B) Thermal history curves of the Paleozoic North Saharan Platform (peri-Hoggar basins) compiled from literature: well in the Illizi basin (Wells et al., 2018); well model A and G in Ghadamès-Berkine basin (Underdown et al., 2007); well OTRA-1 in the Sbâa basin, well RG-3 in the Reggane basin, well TEG-1 in the Timimoun basin, well in the eastern Ahnet basin (Logan and Duddy, 1998); well F3-NC174, well H29-NC115, well NC-174, well NC-115, well NC-186, well NC-190 in Murzuq basin (Belaid et al., 2010); well A-76 well in Murzuq basin (Galushkin and Eloghbi, 2014).

Currently in the area, the negative gravity anomalies can be witnesses of Meso-Neo-Proterozoic oceanic terranes or suture zones composed of ophiolites, ultrabasic and basic rocks (Bayer and Lesquer, 1978; Roussel and Lesquer, 1991). While, the positive gravity anomalies can indicate Archean-Paleoproterozoic cratonic terranes composed of granulites and TTG rocks (Takherist, 1991).

In the Saharan basins, there is the existence of a good direct or inverse correlation between the sedimentary structure (structural depressions and arches) and Bouguer anomalies (Takherist, 1991). The gravimetric anomaly map (Figure VII-3 and Figure VII-5) shows that positive anomalies (> 66 mGal) are mainly associated with arches whereas negative anomalies are related to depressional basins (< 66 mGal). All this features highlighted by Perron et al., (2018) are interpreted as lithospheric mass disequilibrium related to density anisotropy between

different terranes. Knowing that, according to this same study there is a close relation between the Arches-Basins architecture and the underlying repartition of the terranes age.

Liégeois et al., (2005, 2013) have evidenced the rheological lithospheric heterogeneities and thickness between different entities (i.e. WAC, IOGU, LATEA, ESC) based on geological and tomography arguments (e.g. Fishwick and Bastow, 2011).

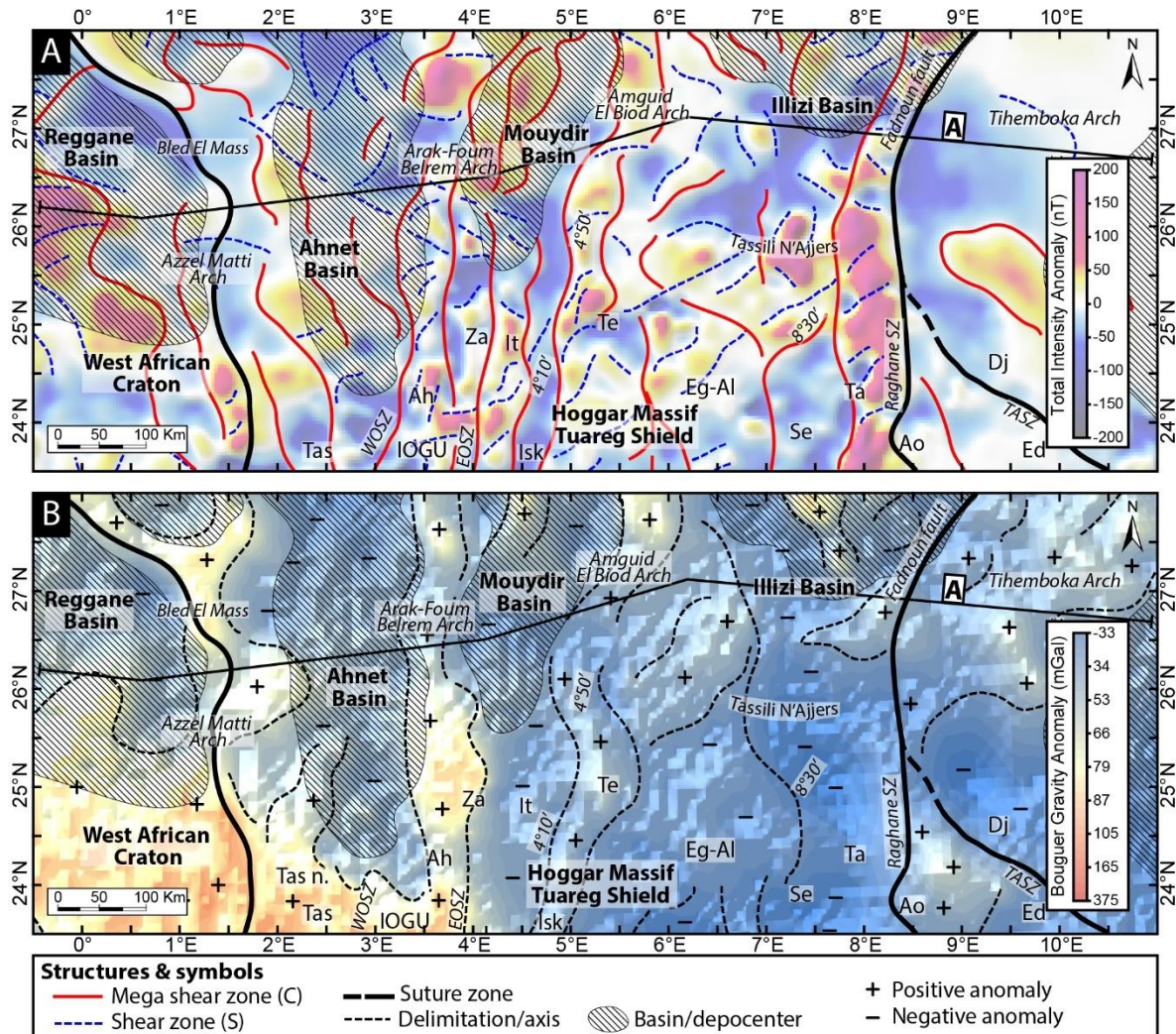


Figure VII-5: (A) Interpreted aeromagnetic anomaly map (EMAG2 from <https://www.geomag.us/>) of the Paleozoic peri-Hoggar basins (North Saharan Platform) showing the different terranes delimited by NS, NW-SE and NE-SW lineaments and mega-sigmoid structures (SC shear fabrics) from Perron et al., (2018); (B) Bouguer anomaly map (from International Gravimetric Bureau: <http://bgi.omp.obs-mip.fr/>) of the Paleozoic peri-Hoggar basins (North Saharan Platform) presenting evidence of positive anomalies under arches and negative anomalies under basins from Perron et al., (2018). A: Localization of cross section in Figure VII-3.

Events	References on the Saharan Platform	Magmatism & thermal activity
Eocene exhumation	English et al., 2016b; Galeazzi et al., 2010; Rougier, 2012; Rougier et al., 2013; Ye et al., 2017	
Hercynian compression	Abudeif, 2015; Boote et al., 1998; Carruba et al., 2014; Coward and Ries, 2003; Craig et al., 2008; Eschard et al., 2010; Follot, 1953; Haddoum, 2009; Haddoum et al., 2001; Najem et al., 2015; Wendt et al., 2009a; Zazoun, 2001, 2008. <u>Hiatus</u> : Coquel and Abdesselam-Rouighi, 2000; Wendt et al., 2009a	Bonhomme et al., 1996; Boote et al., 1998; Carpena et al., 1988; Chabou et al., 2007a; Derder et al., 2016; English et al., 2016b; Glover, 1999; Liégeois et al., 1991; Liégeois, 2019; Underdown et al., 2007
Famennian		
Frasnian unconformity	<u>Evidence</u> : Boudjema, 1987; Chaouchi et al., 1998; Henniche, 2002; Henniche et al., 2003a, 2003b. <u>No evidence</u> : Wendt et al., 2009b	
Frasnian hot shales	Lüning et al., 2003, 2004	
Middle to Late Devonian local compression	Perron et al., 2018	
Middle to Late Devonian extension	Abdesselam-Rouighi, 2003; Baïdder et al., 2008; Boumendjel et al., 1988; Brice and Latrèche, 1998; Chaumeau et al., 1961; Collomb, 1962; Craig et al., 2008; Eschard et al., 2010; Fabre, 2005; Fekirine and Abdallah, 1998; Frizon de Lamotte et al., 2013; Legrand, 1967a, 1967b; Lessard, 1961; Massa, 1988; Michard et al., 2008; Moreau-Benoit et al., 1993; Wendt, 1985; Wendt et al., 1997, 2006, 2009b	Belka, 1998; Derder et al., 2016; Frizon de Lamotte et al., 2013; Wendt et al., 1997
Emsian hiatus	Kermandji, 2007; Kermandji et al., 2003, 2008, 2009; Mehadjji Ouali et al., 2011; Wendt et al., 2006	
Pragian hiatus	Kermandji, 2007; Kermandji et al., 2003, 2008, 2009; Wendt et al., 2006	
Caledonian local compression	<u>Evidence</u> : Beuf et al., 1971; Biju-Duval et al., 1968; Boote et al., 1998; Boudjema, 1987; Boumendjel et al., 1988; Carruba et al., 2014; Chavand and Claracq, 1960; Coward and Ries, 2003; Dubois and Mazelet, 1964; Echikh, 1998; Eschard et al., 2010; Fekirine and Abdallah, 1998; Follot, 1950; Frizon de Lamotte et al., 2013; Ghienne et al., 2013; Gindre et al., 2012; Jäger et al., 2009; Legrand, 1967a, 1967b; Magloire, 1967; Najem et al., 2015. <u>No evidence</u> : Boumendjel, 2002; Fekirine and Abdallah, 1998; Kermandji, 2007; Kermandji et al., 2008, 2009; Ouanaïmi and Lazreq, 2008	Bertrand, 1974; Bonhomme et al., 1996; Denis, 2007; Derder et al., 2016; Fabre, 2005; Ferkous and Monie, 2002; Moreau et al., 1994; Picciotto et al., 1965
Caledonian extension	Perron et al., 2018	
Silurian sealing	Perron et al., 2018	
Silurian extension	Najem et al., 2015; Perron et al., 2018	
Silurian hot shales	Eschard et al., 2005, 2010; Lüning et al., 2000	
Glacial rebound and transgression	Beuf et al., 1971; Denis, 2007; Denis et al., 2007; Eschard et al., 2005, 2010; Ghienne et al., 2003; Girard et al., 2012, 2018; Konaté et al., 2003, 2006; Le Heron, 2010; Le Heron et al., 2006, 2007; Moreau, 2011. <u>Hiatus</u> : Beuf et al., 1971; Paris et al., 2000a; Remack-Petitot, 1960	
Upper Ordovician glaciation	<u>Glacial laout</u> : Le Heron, 2010; Najem et al., 2015; Smart, 2000a. <u>Syn-tectonic</u> : Beuf et al., 1971; Eschard et al., 2010; Ghienne et al., 2003, 2007b; Heron and Craig, 2008; Zazoun and Mahdjoub, 2011. <u>Glacio-tectonics</u> : Beuf et al., 1971; Denis, 2007; Denis et al., 2010; Ravier et al., 2014, 2015. <u>Architecture</u> : Deschamps et al., 2013; Hirst, 2012, 2016; Hirst et al., 2002; Lang et al., 2012	
Taconic	<u>Tectonics origin</u> : Bennacef et al., 1971; Beuf et al., 1968a, 1971; Echikh, 1998; Eschard et al., 2010; Fabre, 1988, 2005. <u>Eustatism origin</u> : Galeazzi et al., 2010. <u>Glaciotectonics/tectonics origin</u> : Zazoun and Mahdjoub, 2011	
Cambro-Ordovician extension	Bennacef et al., 1971; Beuf et al., 1968a, 1968b, 1971; Beuf and Montadert, 1962; Borocco and Nyssen, 1959; Claracq et al., 1958; Echikh, 1998; Eschard et al., 2010; Fabre, 1988, 2005; Ghienne et al., 2003, 2007b, 2013; Najem et al., 2015; Zazoun and Mahdjoub, 2011. <u>Hiatus</u> : Mélou et al., 1999; Oulebsir and Paris, 1995; Paris et al., 2000a; Vecoli et al., 1995, 1999	Azzouni-Sekkal et al., 2003; Liégeois et al., 2003; Liégeois, 2019
Pan-African peneplanation	Bennacef et al., 1971; Beuf et al., 1968a, 1971; Boissonnas et al., 1969; Fabre, 1988, 2005; Galeazzi et al., 2010	
Pan-African collapse	Abudeif, 2015; Ahmed and Moussine-Pouchkine, 1987; Bumby and Guiraud, 2005; Caby et al., 1985; Coward and Ries, 2003; Djellit et al., 2002; Fabre, 2005; Fabre et al., 1988; Najem et al., 2015; Oudra et al., 2005; Piqué et al., 1999; Soulaïmani et al., 2014	

Table 3: Synthesis of references highlighting evidence of hiatus, erosion and thickness variations related to geodynamic events on the Saharan Platform (preferentially documented at the vicinity of arches). See also bibliographic cross sections georeferenced in Figure VII-1.

All these observations helped by a large integrated multidisciplinary geological database show under the peri-Hoggar intracratonic Basins, the presence of an heterogenous accreted lithosphere with different nature, thickness and densities between terranes delimited by

subvertical lithospheric shear zones which seems isostatically uncompensated. These features are at the origin of the hypothesis developed and tested in model M (i.e. mixed) in Perron et al., (submitted).

5 Methods and modelling inputs

After the establishment of a geological conceptual model in Perron et al., (2018), highlighting the link between the repartition of the terranes age (archean, paleoproterozoic and meso-neoproterozoic) with the arches-basins system and the hypothesis of a lithospheric density heterogeneity related to this feature (according to authors such as Artemieva, 2009; Artemieva and Mooney, 2002; Djomani et al., 2001), we have constructed a numerical thermomechanical lithospheric model M (i.e. mixed) in consequence. The hypothesis and the coherency of the model in intracratonic settings were tested and validated by using a 2-D version of the code pTatin2d (Perron et al., submitted).

Then, this numerical model M which is featured by the collage of Archean and Proterozoic terranes is experienced to different inputs combinations (associating or not thermal anomaly, tectonics and sediment flux).

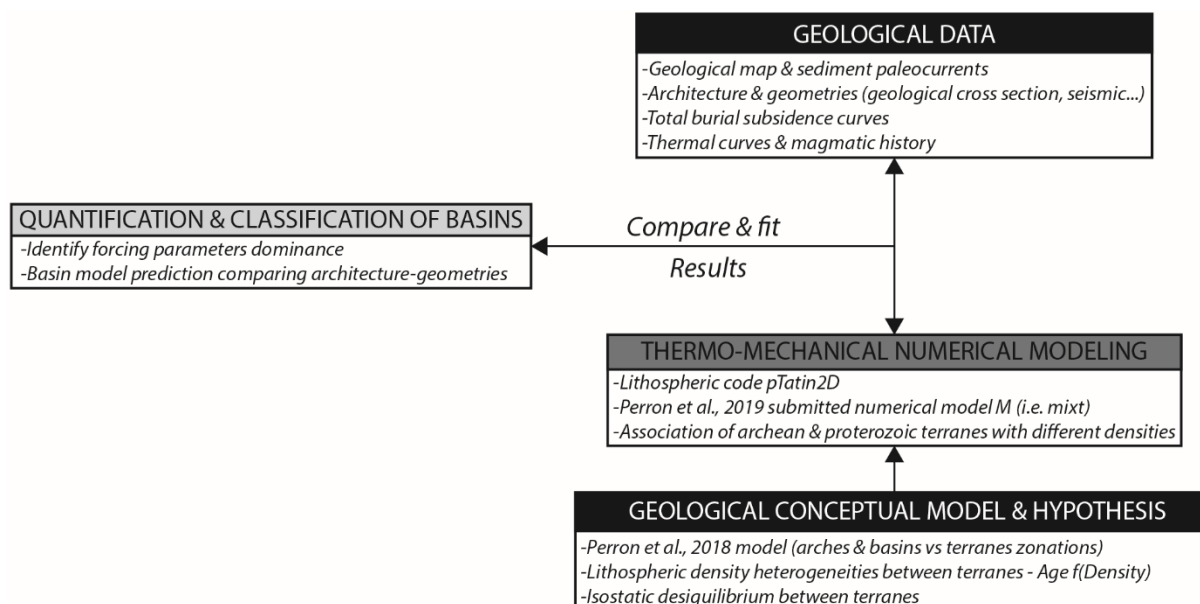


Figure VII-6: Method from construction of the numerical models to comparison, quantification and classification with the peri-Hoggar Basins.

In this study, results from these simulations are compared to geological data extracted from peri-Hoggar Basins (thermal and subsidence curves, cross sections, seismic data...) in order to

analysis some tendency and do a classification of these basins according to their forcing factors predominance (i.e. thermal dominated, sediment supply dominated, far field tectonic stresses dominated). The synthesis of this methodology is shown in Figure VII-6.

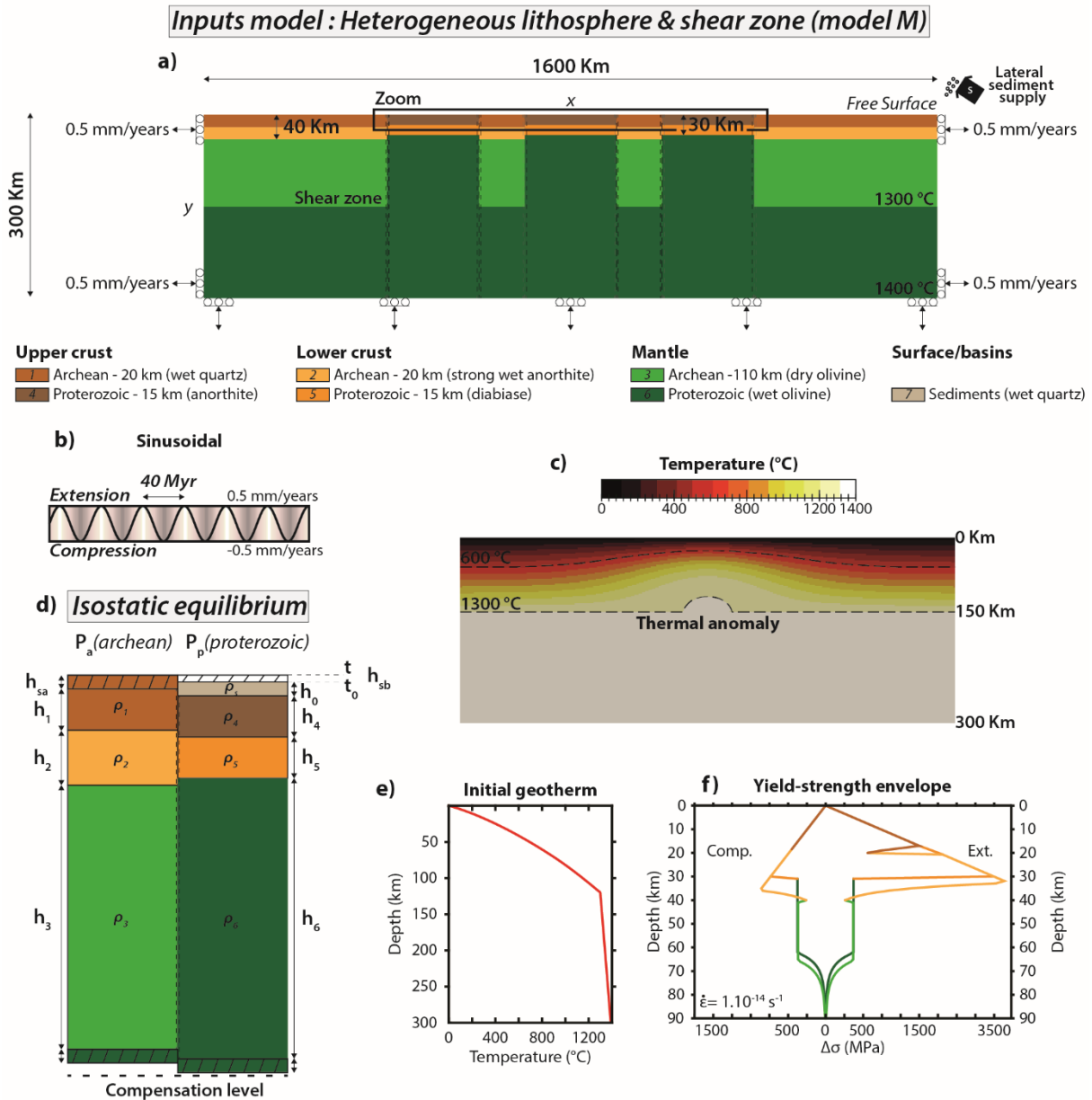


Figure VII-7: a) Inputs models of the simulations with the different parameters applied in experiments such as b) the far fields stresses (sinusoidal extension-compression 40 Myr) and c) the thermal anomaly. d) Isostasy equilibrium potential by an Airy calculation between archean and proterozoic terranes (see Appendix A). e) Initial temperature state of the lithosphere for all the simulations presented. f) Yield-strength envelopes of the simulated materials calculated for a strain rate of $1.5 \cdot 10^{-11} s^{-1}$. $\Delta\sigma$ represents the deviatoric stress, positive values under extension and negative values under compression.

The initial model setups, rheological parameters and boundary conditions are presented in Perron et al., (submitted). The model consists of three 200 km wide Proterozoic terranes separated by two Archean terranes of 100 km in width sandwiched in between two 400 km wide Archean cratons delimited by shear zones (i.e. softening corridors). It results therefore a local isostatic disequilibrium in the initial conditions that can be calculated based on a simple Airy isostatic balance model (e.g. Allen and Allen, 2013).

According to initial density parameters (Perron et al., submitted), initial model inputs (Figure VII-3) and an initial topography of 500 m, we estimated a potential basin filling of around 5 km, when the isostatic compensation is achieved (see Appendix A in Perron et al., submitted). The value of topography is chosen because of the planar characteristic of the “Infratassilian” unconformity where some low paleo-relief are described in the Saharan platform by Beuf et al., (1971). The maximum of basin thickness values observed in the Saharan platform are around 5 km (Figure VII-4).

6 Geological constrains of the numerical models M and link of forcing factors with geodynamics of peri-Hoggar Basins

The different models M are presented in Figure VII-8, Figure VII-9 and Figure VII-10 their inputs parameters compiled in Table 4. For each model M the tectono-stratigraphic architecture, the subsidence and thermal curves are extracted and visualizable. They are composed of three starved type basins (M3 in Figure VII-8A; M2 and M4 in Figure VII-9) and three filled type basins (M5 in Figure VII-8B; M6 and M7 in Figure VII-10). Two of them are featured by complex-shaped architecture (M4 and M6) and four by syncline-shaped architecture (M2, M3, M5 and M7). We defined as the complex-shaped architecture, the basin presenting intra-basin arches (i.e. intra-terrane deformations).

Before comparing the results of the model M from Perron et al., (submitted) to geological data of some singular peri-Hoggar Basins (i.e. Tasmena, Mouydir, Tim Mersoï and Ahnet Basins), we examine the general viability and the applicability of the different parameters of model M to case of the Saharan platform.

In Perron et al., (submitted), four main parameters were simulated and tested. They are the following: *lithosphere heterogeneities*, *thermal anomaly*, *far field tectonics* (i.e. low compression/extension tectonics alternation) *and surface processes intensity* (i.e. erosion/deposition and lateral sediment flux). All these inputs parameters can be deduced from

bibliographic synthesis of the Saharan platform (see Figure VII-2, Figure VII-3 and Table 3). The different link between inputs model parameters and geodynamic events on the Saharan platform is presented here.

Models	Limits conditions (compression/extension alternation)	Thermal anomaly	Lateral sediment supply	Duration (Myr)
M2	yes	no	no	250
M3	no	no	no	250
M4	yes	yes	no	250
M5	no	no	yes	250
M6	yes	yes	yes	250
M7	yes	no	yes	250

Table 4: Parameters inputs of different models M and runs.

6.1 Lithosphere heterogeneities: Control of long-lived low rate subsidence and Arches/Basins architecture

The choice of a model with lithosphere heterogeneities was first based on the singular zonation of terranes below the arches-basins architecture highlighted in the Saharan Platform by Perron et al., (2018). Where the Platform is characterized by the alternation of subsident zones (basin depocenter above Neo-Meso Proterozoic terranes) and elevated domains (arches above Archean/Paleoproterozoic craton) forming a "piano keys" configuration (Figure VII-2 and Figure VII-3).

The differential subsidence between arches and basins was explained by isostatic readjustment processes, where the high-density Proterozoic terranes are subsiding and the low-density Archean terranes are relatively uplifting (Perron et al., submitted). This structuring in "piano keys" was built in agreement with geophysical data available on the Saharan platform and with lithosphere models (e.g. Artemieva, 2009; Djomani et al., 2001), showing variations in average thicknesses and density of Archean (220 km, 3.31g/cc), Proterozoic (170 km, 3.33g/cc) and Phanerozoic (100 km, 3.36g/cc) lithospheres.

According to the model M3 proposed in Figure VII-8A, rose Archean terranes are strongly eroded and are the main sources of sediments. In contrast, the Proterozoic terranes, characterized by contrasting densities, are marked by gravitational instability. They present a structuration in relatively high (arches; Archean-Paleoproterozoic terranes) and low zones (basins; Neo-Meso-Proterozoic terranes). The Archean-Paleoproterozoic terranes are subject to erosion while the Neo-Meso-Proterozoic terranes are characterized by sedimentation. A constant horizontal transport of materials from the highs (hence the unconformities and reduce series) to the adjacent depocenters, which is compensated in the lithosphere for very long period of time. The global analysis of total burial (total subsidence) curves from the Sahara platform Basins during the Paleozoic (i.e. >250 Ma) shows depth reaching 0.5 to 6 km with an average rate ranging from 5 to 20 m/Ma (Figure VII-4A).

Both the long-lived low subsidence rate and arches-basins architecture are observed in the model M (Figure VII-8A-B). The subsidence values are in the same magnitude of model M3 and M5, respectively ranging from 5 m/Myr to 10 m/Myr (Figure VII-8C). They are more significant in model M6 and M7 (Figure VII-10)

The mechanism coupling erosions/sedimentation processes at the surface with the differential isostatic compensation in heterogeneous inherited accreted lithospheres control both the slow long-lived subsidence and the arches-basins architecture. This first order pattern observed in Perron et al., (submitted) for worldwide intracratonic basins can also be fitted to the mechanism of formation of the Paleozoic basins of the Sahara platform (Figure VII-8C).

Nevertheless, the non-presence of sediments on arches remains problematic in this model M3. Indeed, in the Saharan platform the arches are mainly recovered by sediments, even if they are rather thinner than in the rest of the platform (Perron et al., 2018)

This issue is corrected with the adding of lateral sediment supply presented in model M5 (Figure VII-8B). In this model M5, both the rate of subsidence is accelerated and reach more rapidly the isostatic equilibrium (W1-M5 in Figure VII-8C). It highlights the importance of sediment flux on the basin duration until the infilling of the basin. The quantity of sediments available controls the subsidence duration (Perron et al., submitted). Besides, the differential sediment supply could in some case explain the differential subsidence between the different basins (or sub-basins limited by arches) in the Saharan platform. A parameter that wasn't modelled and tested.

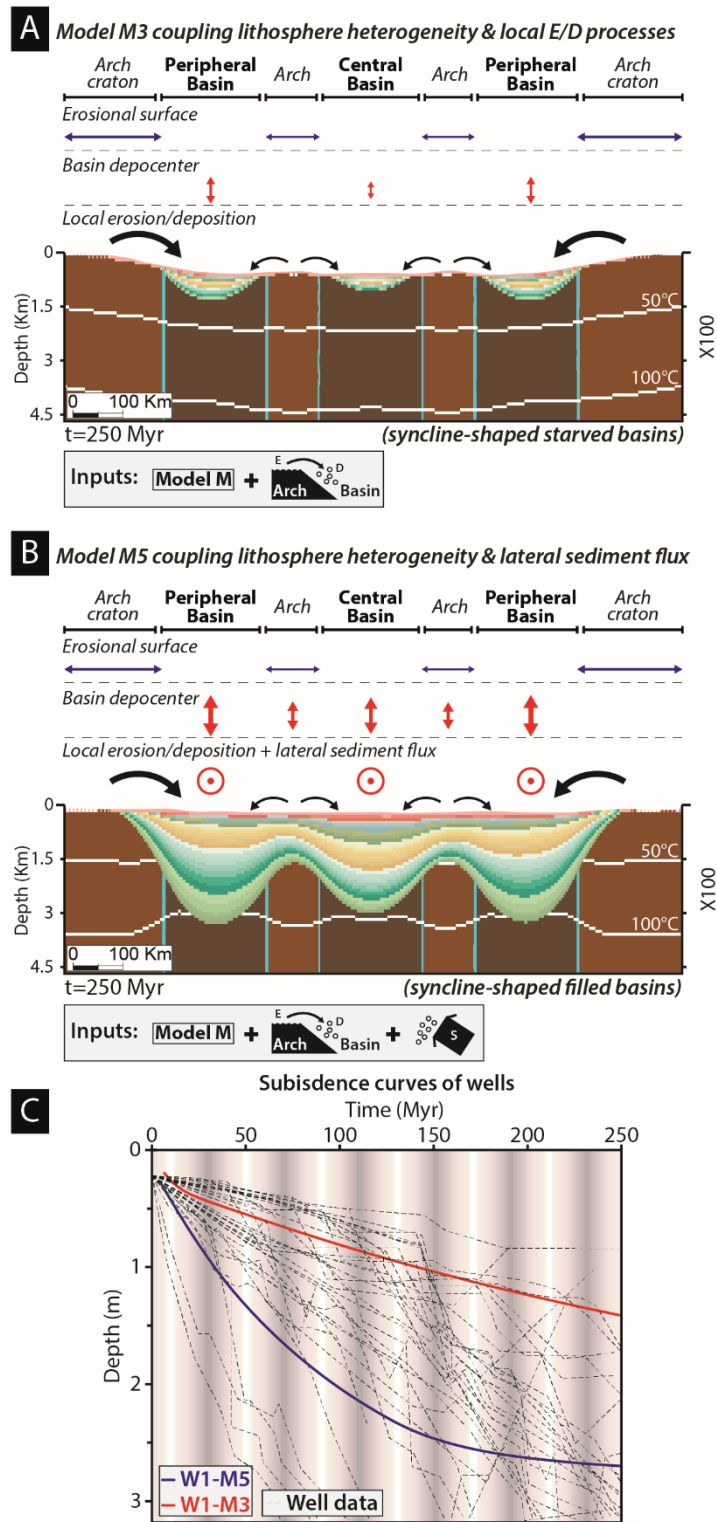


Figure VII-8: (A) Model M3 coupling lithosphere heterogeneity, local erosion/deposition and processes (syncline-shaped starved basins); Notice the impact of the size of the erosion surface on basins filling. Peripheral basins are thicker than the central basin. A link can be made with the WAC and the East Saharan craton two major sediment providers. (B) Model M5 coupling lithosphere heterogeneity and local erosion/deposition processes (syncline-shaped filled basins); Notice the impact of external sediment flux on basin architecture. (C) Subsidence

curves from the different models and comparison with literature curves (Well data: see Figure VII-4).

6.2 Far field tectonics: Impact on tectono-stratigraphic architecture

The integration of tectonics in the model helps to simulate the tectonic history of the Saharan platform, featured by an alternation of extensional and compressional periods during the Paleozoic (see references in Table 3). This tectonics is at the origin of the structural framework connected and nucleated to inherited mega-shear zone and characterized by large broad horst and graben systems re-activated and/or inversed during the Cambro-Ordovician extension, Caledonian compression, Late Devonian extension, Hercynian compression (Perron et al., 2018). In the literature (Craig et al., 2008; Frizon de Lamotte et al., 2013; Guiraud et al., 2005; Haddoum et al., 2001; Perron et al., 2018; Ziegler et al., 1995), the deformation observed during these events are considered as the results of intra-plate stresses caused by far field effects of distant tectonics such as orogenies (e.g. Caledonian compression), rifting and ocean spreading (e.g. Cambro-Ordovician extension). Therefore, in order to reproduce this effect, very weak strain of 0.5 km/Myr is applied over a model of 1600 km of large. Knowing that according to Ziegler et al., (1995) in continental craton compression stresses can be transmitted through distances of up to 1600 km from a collision front. The tectonic events of the Saharan platform are quantitatively well-registered in the subsidence pattern by the recording of deviations (defined as the second order pattern in Perron et al., submitted) with amplitude ranging from 0.25 to 3.5 km (Figure VII-4A). The subsidence rate can be inferior at +5 m/Ma during the periods of quiescence (DLRS), +150 m/Ma for periods of acceleration (ALRS) , and -150 m/Ma for inversion periods (ILRS) (Figure VII-4A). Notice that the exceptional high amplitude is essentially due to the Hercynian compression during the Carbono-Permian time.

In the simulation of models M where tectonics is activated, very weak strain (0.5 km/Myr) can be transmitted far away (over 1600 km) inside the model. The play of uplift and downlift called (oscillations) between the different units is diachronically set due to the heterogenic behavior of the lithosphere and the deformation transmission. It directly impacts the deposition or not of some layers depending on their location to the strain front. It is also materialized in the subsidence pattern between wells by out of phase and antiphase (Figure VII-9 and Figure VII-10). In the subsidence pattern of numerical models (Figure VII-9 and Figure VII-10), deviations amplitude are ranging from 0.3 to 1.3 km according to the well localization. The subsidence rate values of periods of quiescence (DLRS), periods of acceleration (ALRS) and

for inversion periods (ILRS) can be respectively inferior at +5 m/Myr, +110 m/Myr and -100 m/Ma.

All these results from models (Figure VII-9 and Figure VII-10) are coherent with the geological data values of Saharan Basins. Nevertheless, some high amplitude and high values of ALRS and ILRS in bibliographic data (Figure VII-4A) are due to Hercynian compression, which is a particular tectonically punctual intensive event (e.g. Boote et al., 1998; English et al., 2016a; Logan and Duddy, 1998). The model M difficulty fit with this major event. Higher compression/extension parameters could elucidate this singularity. We see that for actual boundary conditions (low deformation) the periods of acceleration and inversion of the subsidence is explained by tectonic activity. Fault and terranes rheologic softening through time also play an important role in the amplitude and the rate of these periods. In contrast, the periods of deceleration are explicated by a tectonic quiescence.

Concerning the stratigraphic architecture in the Saharan platform, many authors have documented the wide lateral extension and continuity of some facies during millions of years (Bennacef et al., 1971; Beuf et al., 1971; Coward and Ries, 2003; Fabre, 1988; Guiraud et al., 2005). The same shoreface or fluvial sequences can be correlated over tens to hundreds of kilometres even in the Illizi basin (Eschard et al., 2005, 2010). Such a continuity of the facies belts is also very specific to the Gondwana Saharan craton (Beuf et al., 1971) and is at the origin of the diachronous deposition of these sedimentary bodies. In low rate accommodation (or low rate subsidence basin) settings, relative sea-level fall either due to a tectonic uplift or to climato-eustatism can generate regional scale unconformities on the stratigraphic architecture of the Paleozoic succession. Many evidences of these regional widespread unconformities (bio-stratigraphic or stratigraphic), preferentially registered on arches, are register through the Saharan intracratonic platform during the Paleozoic (Table 3). They are often hard to temporally and spatially constrain.

The models M help to explain the stratigraphic continuity or the diachronicity of unconformities this heterogenic by the behavior of the lithosphere to far field stresses propagation below each basin and sub-basin highlighted by differential oscillation in the recording of subsidence pattern (Perron et al., submitted).

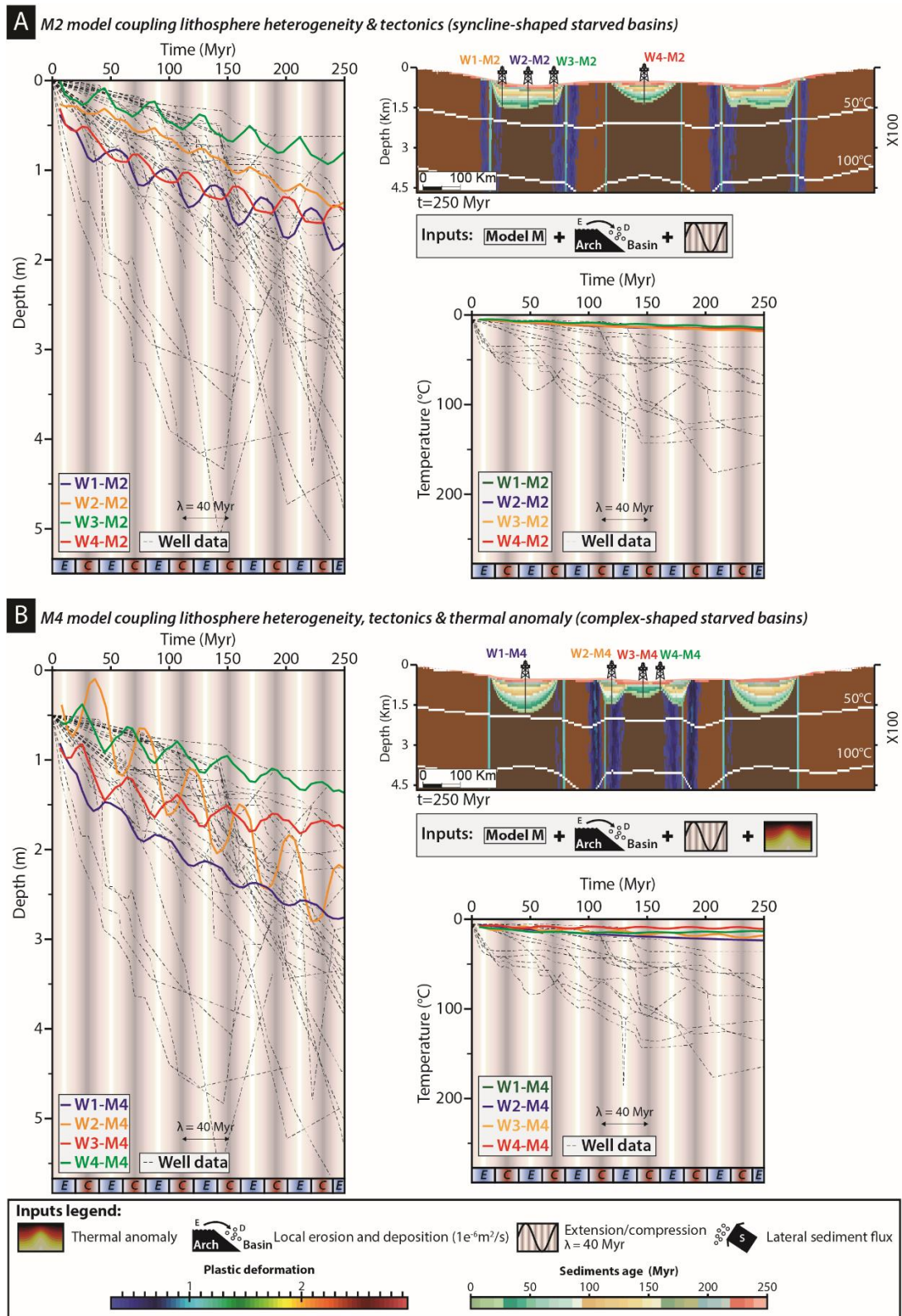


Figure VII-9: (A) Model M2 coupling lithosphere heterogeneity, local erosion/deposition processes and tectonics (syncline-shaped starved basins) with their burial and thermal history curves. (B) Model M2 coupling lithosphere heterogeneity, local erosion/deposition processes, tectonics and thermal anomaly (starved complex-shaped basins) with their burial and thermal

history curves. Well data: see Figure VII-4. See Figure VII-7c for localization of the thermal anomaly in the model (i.e. under the central basin).

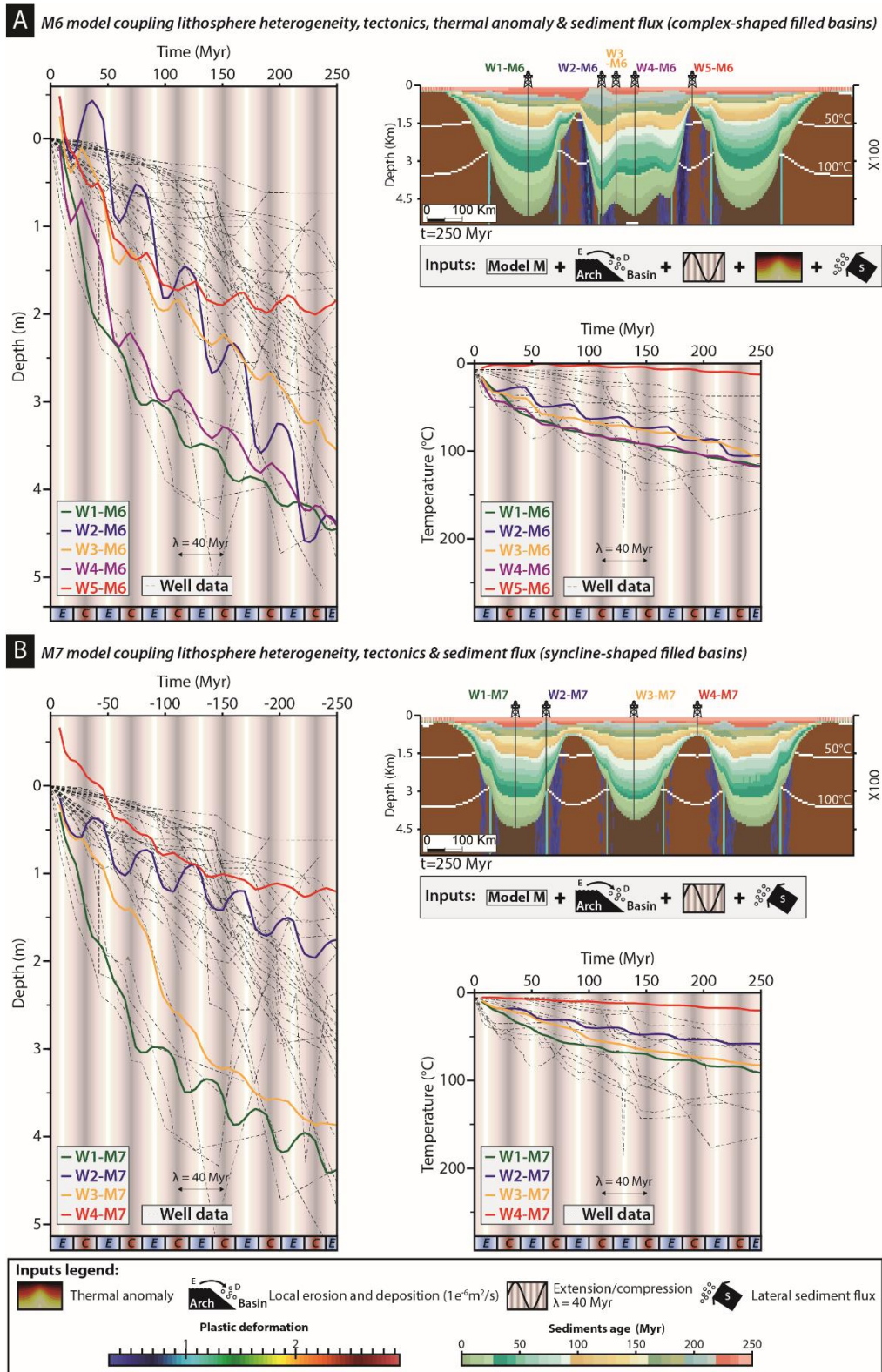


Figure VII-10: (A) Model M6 coupling lithosphere heterogeneity, local erosion/deposition processes, tectonics and lateral sediment flux (syncline-shaped filled basins) with their burial

and thermal history curves. (B) Model M7 coupling lithosphere heterogeneity, local erosion/deposition processes, tectonics, thermal anomaly and lateral sediment flux (complex-shaped filled basins) with their burial and thermal history curves. Well data: see Figure VII-4. See Figure VII-7c for localization of the thermal anomaly in the model (i.e. under the central basin).

6.3 Thermal activity, magmatism, and heat flux

The activation of thermal anomaly in the model results from the global analysis of the igneous and tectono-thermal history of the Saharan platform (see references in Table 3). It can be quantitatively documented by the global analysis of paleo-temperatures/thermal curves from bibliographic data (Figure VII-4B). These data show values at the end of the Permian ranging from 60°C to 250°C with the most ones around 130°C (Figure VII-4B). The amplitude of deviations of the temperature can reach 125°C. This high peak of temperature is mainly attained during the Carbono-Permian. The thermal maturation of the Paleozoic sedimentary infill of some Saharan basins (e.g. Ahnet, Mouydir and Illizi) is principally a product of burial (English et al., 2016a; Galeazzi et al., 2010; Zieliński, 2012). It has most probably been achieved during the Late Carboniferous prior to the Variscan (Hercynian) inversion and only locally during the Mesozoic and the Early Cenozoic (English et al., 2016a; Logan and Duddy, 1998; Zieliński, 2012). Burial temperature differences can be observed between neighboring basins as is observed in the model M7 between central and peripheral basins (W1-M7 and W3-M7 in Figure VII-10). The burial temperature range in the Ahnet basin (30-120°C) attest of lower values than in Mouydir (50-150°C) through the analysis of conodont color alteration index (CAI) during the Middle Devonian to the Lower Carboniferous (Zieliński, 2012).

Magmatic intrusion and thermal activity could have locally re-heated the basins (see Figure VII-2 and Table 3; e.g. Derder et al., 2016; Liégeois, 2019; Moreau et al., 1994, 2012; Zieliński, 2012). They are mainly associated to key tectonic events such as the Cambro-Ordovician extension, the Caledonian compression and the Hercynian compression (Figure VII-2 and Table 3). The different igneous intrusions (dolerites, plutons...) are predominantly aligned on shear zone (Figure VII-2), thus forming thermal drains.

Nevertheless, the majority of the plutons (constituting thermal source) are set during the Pan-African orogeny and older events (e.g. Liégeois, 2019), therefore, the initial thermal parameters of the lithosphere are rather “hot” for a cratonic area (see inputs in Perron et al., submitted).

The measurements of the modern heat flow in Algeria revealed the presence of an east-west trending zone with elevated heat values (90-130 mW/m²) across the Saharan basins (Lesquer et al., 1989, 1990; Takherist and Lesquer, 1989). High heat-flow average of 82± mW.m⁻² related to extensional Miocene-Pliocene-Quaternary volcanism and mantle thermal anomaly (Takherist and Lesquer, 1989)

In the numerical model M6, the 120°C maximum of temperature observed is achieved after 250 Myr in peripheral and central basins (W4-M6 and W1-M6; Figure VII-10A). In the model M7 temperature is featured by values lower around 90°C after 250 Myr (W1-M7; Figure VII-10B). This variance is correlated to the initial thermal anomaly in the model. The temperature on secondary boundary arches, intra-basin arches are a little colder than maximum ones. The temperature registered on arches is very low around 20°C. The amplitude of deviations is for the temperature smoother and damped (i.e. of the order of 10°C) than for subsidence curves observed previously.

The calculation of the heat flux from the initial parameters, we obtain values around 90 mW/m². Moreover, the thermal anomaly has a significant role on faults and terranes softening. It triggers the complexification of the basin architecture (see Perron et al., submitted; Chapter VI.6.3). Notice that temperature in model M2 and M4 (Figure VII-9) do not exceed 50°C. Nevertheless, they are in the range of temperature estimation of CAI during Devonian (Zieliński, 2012).

All these results from temperature curves and heat flow stay coherent between literature data and the model M. The temperature linked to simple burial dynamics as well as heat flow are in the same order magnitude. However, little dissimilarity can be observed:

The first major difference with the models M is the rapid and punctual peak of temperature (i.e. deviations) linked to the Hercynian orogeny associated to igneous/thermal intrusions (Figure VII-2). This major heating overprints the effects of heating caused by simple burial. The model proposed here cannot explain it. It could be triggered by an adiabatic decompression of the lithosphere (e.g. Latin and White, 1990). Probably insertion of other parameters (thermal anomalies, more important compression/extension...) should be added during the simulation.

The second variance is the low temperature registered on the arches (or at their vicinity). The diminution of the initial difference of density between Archean column and Proterozoic (and so initial paleo-topography) could be a response permitting a more significant burial (Figure VII-7b). Moreover, the increases of the surface radiogenic production (H) could also be a

solution. Even if, compared with younger continental crust, the Archaean craton has low heat flow (Nyblade and Pollack, 1993; Petitjean et al., 2006).

Moreover, alone thermal anomaly (i.e. without tectonics or/and sediments flux) has a small influence on subsidence intensity of the basins (see comparison between model M3 and M1 in Perron et al., submitted).

6.4 Sourcing of sediments: Impact of sediment flux and width of the erosional surface

The sedimentary external flux is modeled to simulate the detrital control parameters which can be considered as a sort of climatic proxy (see paleocurrents directions in Figure VII-2 attesting of lateral supply of sediments in the Saharan platform). Notice that for each models M basic local erosion and deposition processes are activated, defined by erosion of arches and deposition in basins depocenter. It is consistent with the presence of thin series with erosional unconformities on arches and conformal thick series in basins pointed out in Perron et al., (2018).

During the Paleozoic on the Saharan platform, the sediment is globally transported to the NNW shown by the general paleocurrent directions changes rather from NNW to NW (Figure VII-2; Bennacef et al., 1971; Beuf et al., 1969, 1971; Fabre, 1988, 2005; Fröhlich et al., 2010b; Le Heron et al., 2009). The platform shows a South to North deposition profile (i.e. respectively shallow to deep facies) and a general thickening of all units northwards (Beuf et al., 1971; Fabre, 1988, 2005; Garfunkel, 2002; Guiraud et al., 2005). The sources of sediments probably come from continental domains situated even further south, but their precise locations are still difficult to establish because the more proximal series have not been preserved towards the South (Beuf et al., 1971).

Besides, the presence of Paleozoic series and Precambrian series (crystalline rocks), put in outcrop by the exhumation of the Hoggar (Tuareg shield) which take place during the Late-Eocene (Rougier et al., 2013), indicate that this craton was not acting as a source of sedimentary material or as a barrier to sand drift in this region (Avigad et al., 2005; Beuf et al., 1971). The sourcing of sediments showed a distant and a local provenance (West African Craton, Tuareg Shield terranes, Cadomian terranes) mainly of Neoproterozoic ages (Altumi et al., 2013; Avigad et al., 2003, 2005, 2012; Linnemann et al., 2011; Meinhold et al., 2011, 2013; Morton et al., 2011). These studies have shown the significant role of width cratons such as the WAC in sediment supply.

The numerical model highlights the importance of sediment flux and the width of the erosion surface (i.e. related to the craton extension?) on both the thickness and the infilling rate of the basins until isostatic equilibrium (Figure VII-8; see also Perron et al., submitted). This result indicates that sourcing of sediments needs to be taken to account in the dynamics of the Saharan intracratonic basins.

The geological data enlighten here are coherent with the model M (Figure VII-8), which supplies laterally (far away) but also locally (i.e. by eroding cratons and arches) the sediments. Moreover, the differential quantity of sediment supply explains the variation of thickness between the peripheral basins and the central basin (Figure VII-8).

7 Application of the numerical models M to geological data of peri-Hoggar Basins

The latter part has shown the coherency of the applicability of the model M developed in Perron et al., (submitted) to the case the intracratonic basins of the Paleozoic Saharan platform.

The four main parameters tested, which are *lithosphere heterogeneities, thermal anomaly, far field tectonics* (i.e. low compression/extension tectonics alternation) *and surface processes intensity* (i.e. erosion/deposition and lateral sediment flux) are coherent with forcing factors occurring on the Saharan platform. They constitute proxies of these latter. Consequently, they can be applied to the singular case of some peri-Hoggar Basins.

The results of the different numerical models M are compared with geological/geophysical data of the peri-Hoggar basins such as total burial subsidence curves, thermal curves (compiled from the Saharan platform) and tectono-stratigraphic seismic or geological cross sections (e.g. Tasmena, Ahnet, Mouydir and Tim Mersoï Basins). Each of the peri-Hoggar Basins is controlled by one or several inputs parameters (tectonics, thermal anomaly and sediment flux).

7.1 The Tasmena Basin: Example of syncline-shaped starved Basin

Extracted geological data (satellite images and geological maps) from the Tasmena Basin are compared with our different numerical forward model M.

The Tasmena Basin forms a syn-sedimentary syncline-shaped structure associated with a horst and graben system where there is some highs and lows (Claret and Tempere, 1968; Lessard, 1961). The basin is delimited by sub-meridian major faults nucleated to ancient “basement

scars” at the edges where the series are reducing (Lessard, 1961). They are defined as terranes limits; hence, the wavelength of the basin is almost identical to that of the accreted Proterozoic oceanic domains (Figure VII-11A). The maximum of thickness in the basin reaches 1.5 km with decreases approaching arches (Claret and Tempere, 1968; Lessard, 1961). The essentially detritic filling of these basins is discordant on the Hoggar massif (Claret and Tempere, 1968; Lessard, 1961). Evidence of synsedimentary structures are highlighted northwards by Beuf et al., (1971) along the same lineament edging the Tasmena Basin in the Tassili Timissao (Figure VII-1). The paleocurrents directions are mainly oriented NNW (Figure VII-11A). They are more or less parallel to the major lineaments (Beuf et al., 1971). These observations are consistent with the general structural style observed on the Saharan platform (Perron et al., 2018).

In the area (Figure VII-2), there is no identified markers of major thermal and igneous activity during the Paleozoic, suggesting that they didn't had a key role in the basin dynamics. Besides, the intensity of deformation is low in regards of other basins closer to the WAC suture zone (Craig et al., 2008).

The best fit is found with the model M2 coupling lithosphere heterogeneity, local erosion/deposition processes and far field tectonics (Figure VII-11). In this numerical model M2 the maximum of thickness is about 1.5 km in peripheral basins. These basins form a syncline-shaped (with a flat angular bottom) limited by boundary faults. These basin architecture characteristics are similar to the geological observations in the Tasmena Basin.

In the light of these observations and conferring to the inputs of the model M2, we can advance that the main forcing factors of the Tasmena Basin are those gathering lithospheric heterogeneities, local erosion/deposition processes and low far field tectonics. In this case the lateral sediment flux didn't had a major role in supplying the basin.

Then, the basin is considered as starved and syncline-shaped (with a flat angular basement). Moreover, according to the inclination of the Infratassilian surface (to the NNW) and paleocurrents directions (Figure VII-11A), the Tasmena Basin was located upstream of the sediment source. The sedimentary supplies just passed through it and feed downstream basins with more accommodation space available such as the Ahnet and the Mouydir Basins. Indeed, these latter basins are featured by greater thicknesses.

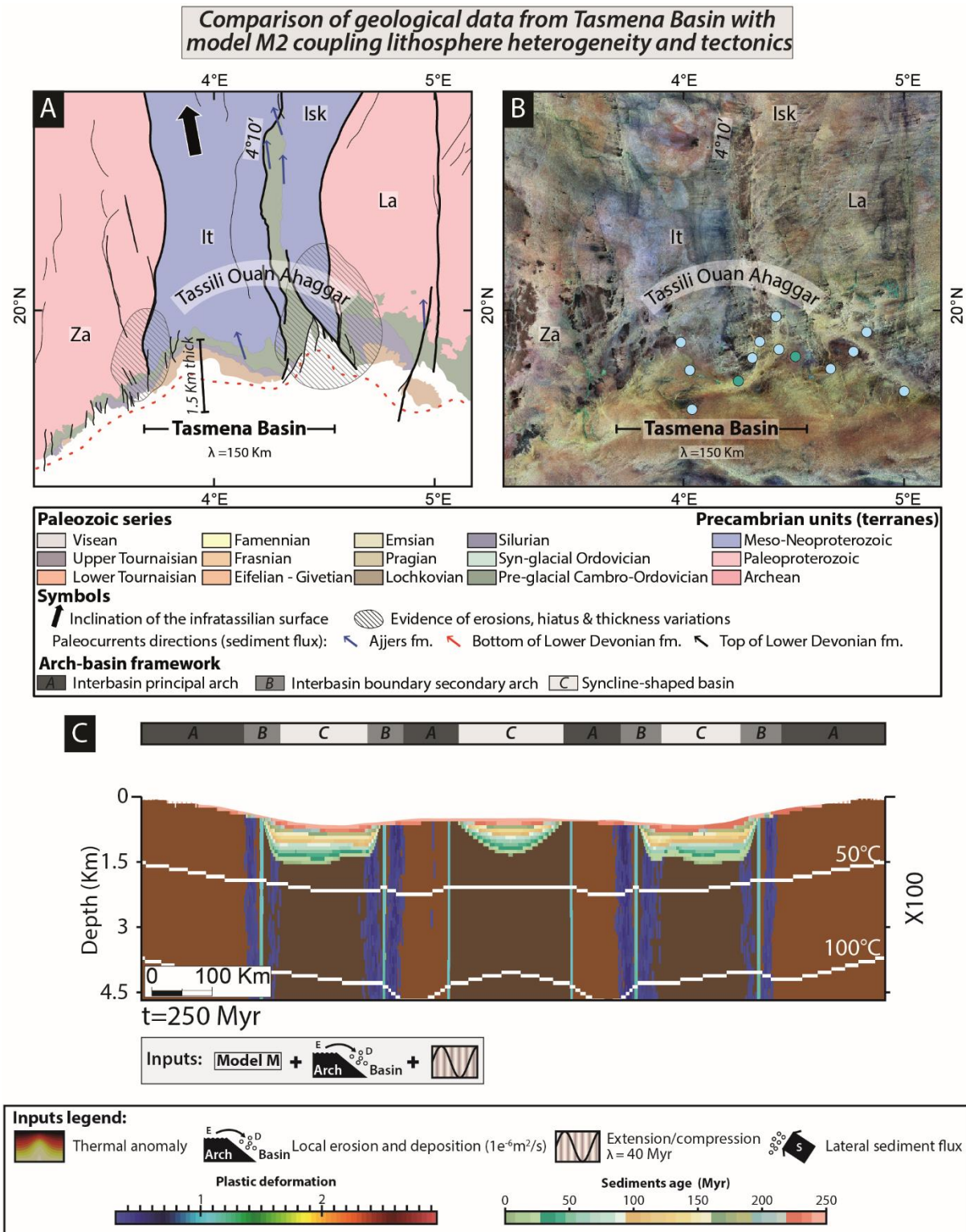


Figure VII-11: Comparison of the tectono-stratigraphic architecture of the Tasmena basin with thermo-mechanical numerical model M2. (A) Geological map of the Paleozoic series in the Tasmena basin showing the typical arch and basin architecture with diminution of series approaching arches. (B) Satellite images of the Paleozoic series in the Tasmena basin (Landsat 7 ETM +). (C) Cross section extracted from model M2 showing the similar arch-basin

architecture. Notice that we can compare our cross section with the 2D map (see explanation in the geological settings part). Thickness (1.5 km) of the model is coherent with thickness shown by Lessard, (1961).

7.2 The Mouydir and the Tim Mersoï Basins: Example of a syncline-shaped filled Basins

Extracted geological data (cross sections, seismic, satellite images, geological map, subsidence and thermal curves) from the Mouydir and the Tim Mersoï Basins were compared with the numerical forward model M (Figure VII-12 and Figure VII-13).

The Mouydir and Tim Mersoï basins show a syn-sedimentary synclinal geometry with a thickening of the Paleozoic series in the axial zone and a variations of facies, of paleocurrent directions (e.g. Beuf et al., 1968) as well as a thickness reduction in the vicinity of major accidents (i.e. arches), associated with onlaps (e.g. Figure VII-12A and B). They also display the migration of depocenters from North to south, associated with a gradual shift of Paleozoic series in the edges areas (particularly visible in the Tim Mersoï basin). This typical tectono-stratigraphic architecture in arches and basins (referenced as paleo-highs) was first described by Eschard et al., (2010) and renewed by Perron et al., (2018).

The depocenter of the Mouydir and Tim Mersoï basins is situated upon the accreted Proterozoic oceanic domains (Figure VII-12 and Figure VII-13). Divergent onlaps are visible on the Archean terranes as well as on the Paleoproterozoic Aïr terranes visible by satellite images and geological maps (Figure VII-12A-B). The essentially detritic filling of these basins is discordant on the Hoggar massif and on the Aïr basement (in the Tim Mersoï). In the Arlit region the maximum thickness of deposits is about 1800 m (Konaté et al., 2009; Yahaya and Lang, 2000). In the Mouydir the sedimentary succession can reach 1550 to 4800 m (Beuf et al., 1971; Conrad, 1984; Wendt et al., 2006, 2009a; Zieliński, 2012).

According to Zieliński, (2012), through the analysis of conodont color alteration index (CAI) during the Middle Devonian to the Lower Carboniferous, the burial temperature range from 50 to 150°C. Major igneous activity is described on the edges of the Tim Mersoï Basin, in the Aïr Massif (see Assodé terrane; Figure VII-1 and Figure VII-2), featured by giant Devonian ring complex mainly aligned on Raghane shear zone (Moreau et al., 1994). It highlights the role of faults as thermal drains.

During the Paleozoic, the structures of these basins are mainly controlled by N-S sinistral or dextral sub-vertical normal faults (i.e. transtension to transpression) forming horst and graben

network weakly inverted and/or reactivated through time (see tectonic calendar and stresses orientation in Haddoum et al., 2001; Konaté et al., 2009; Perron et al., 2018; Yahaya and Lang, 2000; Zazoun, 2001). Both in the Mouydir basin and in the Tim Mersoï, the sedimentary filling has the same tectono-stratigraphic features cited previously (Figure VII-12 and Figure VII-13). Besides, intensity of the deformation in these basins is lower than in the Ahnet Basin, situated near the WAC/TS suture zone (Craig et al., 2008; Haddoum et al., 2001).

These observations have shown a differential subsidence and sedimentary architecture between arches and basins through the Paleozoic. On arches (inter-basin principal arches, intra-basin arches) or approaching these ones (inter-basin boundary/peripheric secondary arches), singular sedimentary and strata geometries such as strata pinch out, wedges (i.e. divergent onlaps, strata growth), partitioning facies, diminution or erosion of series and condensation level can be identified during the Paleozoic (Perron et al., 2018). These evidences were also locally exposed by several authors elsewhere on the Saharan platform (Table 3).

The paleocurrents directions are globally oriented NNW which is more or less parallel to the major lineaments (Beuf et al., 1971). However, local variations of these directions can be observed during Cambro-Ordovician, Caledonian tectonics pulses (Figure VII-12A and Figure VII-13A; Beuf et al., 1968b, 1971; Wendt, 1995). They can be punctually oriented orthogonally to the main directions. They can be both evidence of lateral sediment flux from upstream and punctual local erosion/deposition processes during uplift of arches (i.e. archean terranes).

The geological data from Mouydir and the Tim Mersoï Basins particularly fit well with the geometry of the peripheral or central basins in the numerical model M7 coupling lithosphere heterogeneity, local erosion/deposition processes, tectonics and lateral sediment flux (Figure VII-13F and Figure VII-12D).

In M7, the maximum of thickness is registered in the central part of the basin covering Proterozoic terranes while wedges (divergent onlaps), diminution and erosion of series are observed when approaching arches associated with Archean terranes (Figure VII-12 and Figure VII-13). In addition, the total burial subsidence curve of well W21 (from Perron et al., 2018) well-fit with the curve of well W3-M7 (Figure VII-13E-F). Amplitude of deviations stays coherent between them. The strain is localized near terranes limits where local inversion zones associated with folding can be both observed on geological cross section (cf. interbasin boundary secondary arch; Figure VII-13C) and the model (Figure VII-12C). In the model M7,

truncatures and strata pinch out are highlighted in the limbs of the folding, features that were already observed in seismic (see Fig. 7 in Perron et al., 2018).

Consequently to this best fit found, we can advance that the main forcing factors of the Mouydir and Tim Mersoï Basins are those gathering both lithospheric heterogeneities, local erosion/deposition processes, tectonics and lateral sediment flux (Figure VII-12 and Figure VII-13). We can define it as a syncline-shaped filled basin with boundary secondary arches structures.

Notice that the Mouydir and Tim Mersoï Basins also fit well with peripheral basins in the numerical model M6 (Figure VII 10A or Figure VII 14D), which are situated away (i.e. on the edges) from the central basin submitted to the thermal anomaly (Figure VII 7c). This choice is more coherent with the magmatic and thermal activity identified in the Hoggar and Air Massif (e.g. Liégeois, 2019; Moreau et al., 1994).

In the arch of the Tim Mersoï Basin (i.e. edge of the basins), Moreau et al., (1994) have shown the establishment of the Air ring complex in the Assodé terrane, constituting a major thermal source during the Devonian. In the terranes under the Mouydir Basin, the “Taourirt” plutons are set between 539-523 Ma (i.e. Early Cambrian) according to Azzouni-Sekkal et al., (2003). After that few thermal re-heating activities are observed in granites aligned on shear zones (Figure VII-2). They are attributed to tectonic reactivation of the shear zones (e.g. Djouadi et al., 1997).

Consequently, thermal activity seems have occurred in these different basins, however at different degrees (it is the case of the majority of the basins in the Saharan platform because of the heritage of the Pan-African orogeny; e.g. Liégeois, 2019).

In the case of the Mouydir Basin thermal activity is weaker (or at least older) than in the Tim Mersoï Basin. In contrast, the intensity of tectonic activity is more significative in the Mouydir Basin than in the Tim Mersoï Basin. Indeed, the latter is farer from the different deformation front during the Paleozoic (Craig et al., 2008; Haddoum et al., 2001). These basins highlight either the coupling between high thermal anomaly/low tectonic stresses and low thermal anomaly/high tectonic stresses.

We have seen in Perron et al., (submitted) that thermal anomaly must be coupled to tectonics in order to have a major influence. Sensitive study should be led in order to decipher the balance gradient between tectonic and thermal intensity.

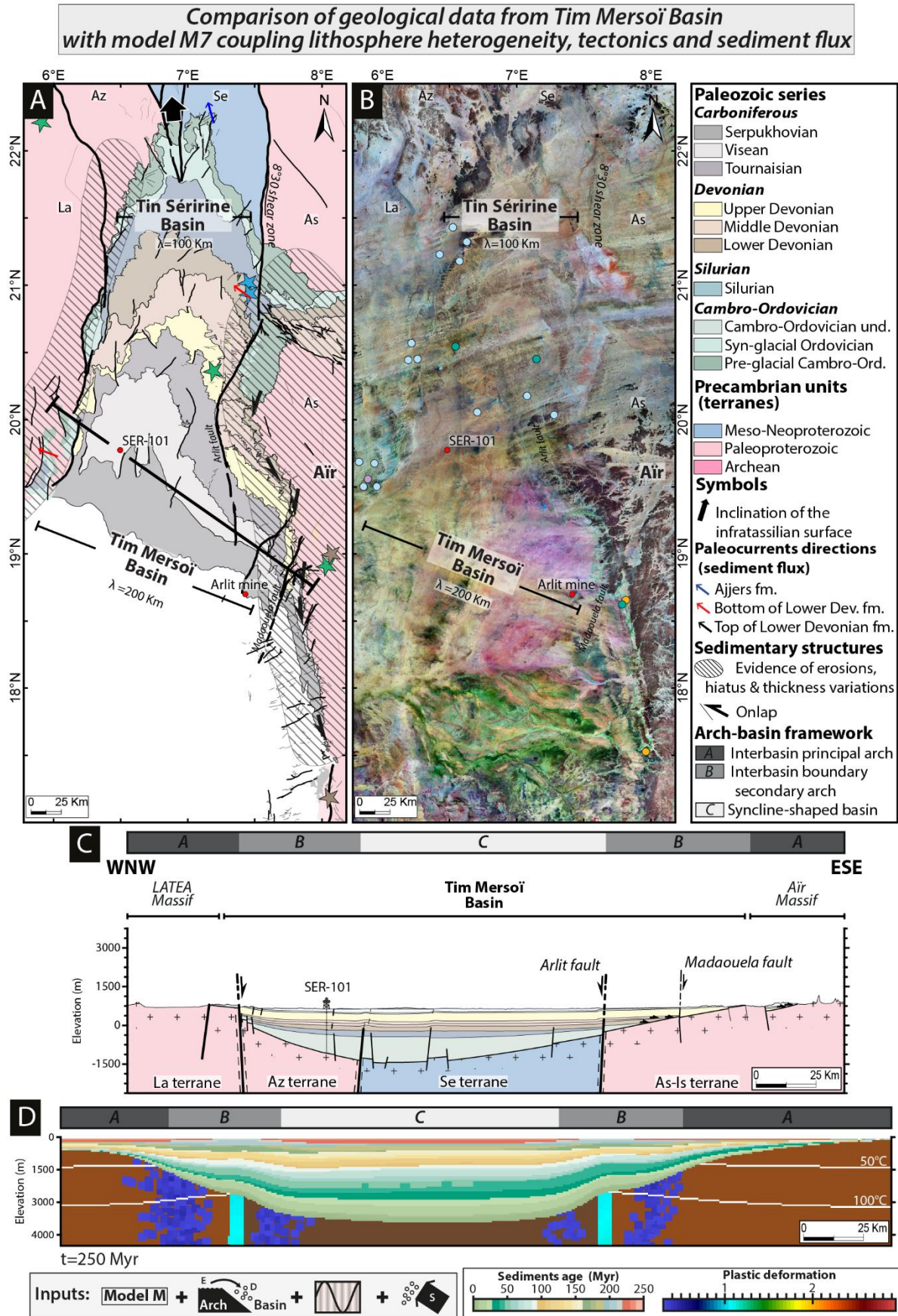


Figure VII-12: Comparison of stratigraphic architecture cross section in the Tim Mersoï basin with thermo-mechanical numerical model M7. (A) Geological map of the Paleozoic series in

the Tim Mersoï basin. (B) Satellite images of the Paleozoic series in the Tim Mersoï basin (Landsat 7 ETM+). (C) WNW-ESE cross section of the Tim Mersoï basin localized in Figure A showing the typical arche and basin architecture with diminution of series approaching arches. (D) Cross section extracted from model M7 showing the similar arch-basin architecture. Notice that this comparison is possible with peripheral basins in the numerical model M6.

7.3 The Ahnet Basin: Example of a complex-shaped filled Basin

Extracted geological data (cross sections, seismic, satellite images, geological map, subsidence and thermal curves) from the Ahnet Basin are compared with the numerical forward model M (Figure VII-14).

In the Ahnet Basin similar geological observations can be established than in the Mouydir and Tim Mersoï Basins such as differential thickness variations between arches and basins, and paleocurrents directions, (Figure VII-14A-B-C). Nevertheless, the main changes are in relation with the tectono-stratigraphic architecture. The presence of intra-arches structures complexify the global syncline-shaped architecture of the Ahnet Basin (Figure VII-14A-C; Perron et al., 2018). Besides, the thickness reaches 1.7 to 7.1 km in the Ahnet Basin which is on average higher than the Mouydir type basins (Beuf et al., 1971; Conrad, 1984; Wendt et al., 2006, 2009a; Zieliński, 2012). Evidence of thermal activity (Figure VII-14A) and the position of the Ahnet Basin near the WAC suture testify of a high tectonic and thermal activity. The tectonic history is featured by the pulsatile alternation of periods of compression and extension at origin of the formation of horst and graben systems inversed and/or reactivated through time (Perron et al., 2018). During the Paleozoic, the direction of shortening and stretching are mainly oriented NNE-SSW to NE-SW, E-W and NNW-SSE (Boudjema, 1987; Haddoum, 2009; Haddoum et al., 2001; Zazoun, 2001). According to numerous authors (Akkouche, 2007; Boote et al., 1998; Coward and Ries, 2003; Craig et al., 2008; Haddoum et al., 2001; Logan and Duddy, 1998; Zazoun, 2001) the tectono-thermal intensity in this area was very significant than elsewhere on the Saharan platform because of his position near the deformation front during the Hercynian orogeny (see Fig. 32 in Craig et al., 2008). Before this major event, during the Middle Devonian to the Lower Carboniferous, the burial temperature range in the Ahnet basin are from 30 to 120°C according to the analysis of CAI (Zieliński, 2012).

In the light of these observations, a good fit is found between the geological data from Ahnet Basin and the central basin in the numerical model M6 coupling lithosphere heterogeneity, local

erosion/deposition processes, tectonics, lateral sediment flux and thermal anomaly (Figure VII-14D).

Model M6 presents many similar features than the model M7. However, the main changes are observed in the singular complexification of the tectono-stratigraphic architecture (Figure VII-14D). As shown in Perron et al., (submitted), the thermal anomaly has a significant role on faults and terranes softening. It triggers the complexification of the basin architecture in the central part of the model where the strain is preferentially localized near terranes limits (Chapter VI.6.3). Indeed, the first-order structural pattern featured by arches-basins framework is overprinted by the formation of grabens near terranes boundaries during extension, positively inverted during compression. They are associated to major folding creating intra-basins arches and secondary boundary arches, a structural style well-defined in the Ahnet Basin (Perron et al., 2018). The sub-basins register the maximum of thickness which can reach 5 km. The total burial subsidence curve of well W7 (from Perron et al., 2018) and 1 to 4 from Kracha, (2011) well-fit with the curves of well W3-M6 and W4-M6 (Figure VII-14E-G). The thermal curve 5 from Logan and Duddy, (1998) and CAI data from Zieliński, (2012) are coherent with the model results (Figure VII-14F-H). In these two cases, both the slope and the amplitude of deviations of the curves stays in the same magnitude of data. Notice that the first part of the subsidence history from the Precambrian to the Early Silurian time of wells in the Ahnet Basin (Figure VII-14E) is more coherent with starved model M2 or M4 (Figure VII-9). In addition, according to the position of the wells (Figure VII-14A), the subsidence pattern between them can be in antiphase, in out of phase and in phase (Figure VII-14E). This differential oscillation of the subsidence curves is also noticeable between wells in Figure VII-14G. It is documented in Perron et al., (submitted) as the propagation of the deformation in a heterogeneous lithosphere.

The numerical model M6 globally reconcile the complex architecture, the thickness, subsidence and thermal history of the Ahnet Basin. So, the forcing factors of Ahnet Basin are those gathering lithospheric heterogeneities, local erosion/deposition processes, tectonics, lateral sediment flux and thermal anomaly. This basin is complex-shaped filled basin with intra-arches and boundary secondary arches structures.

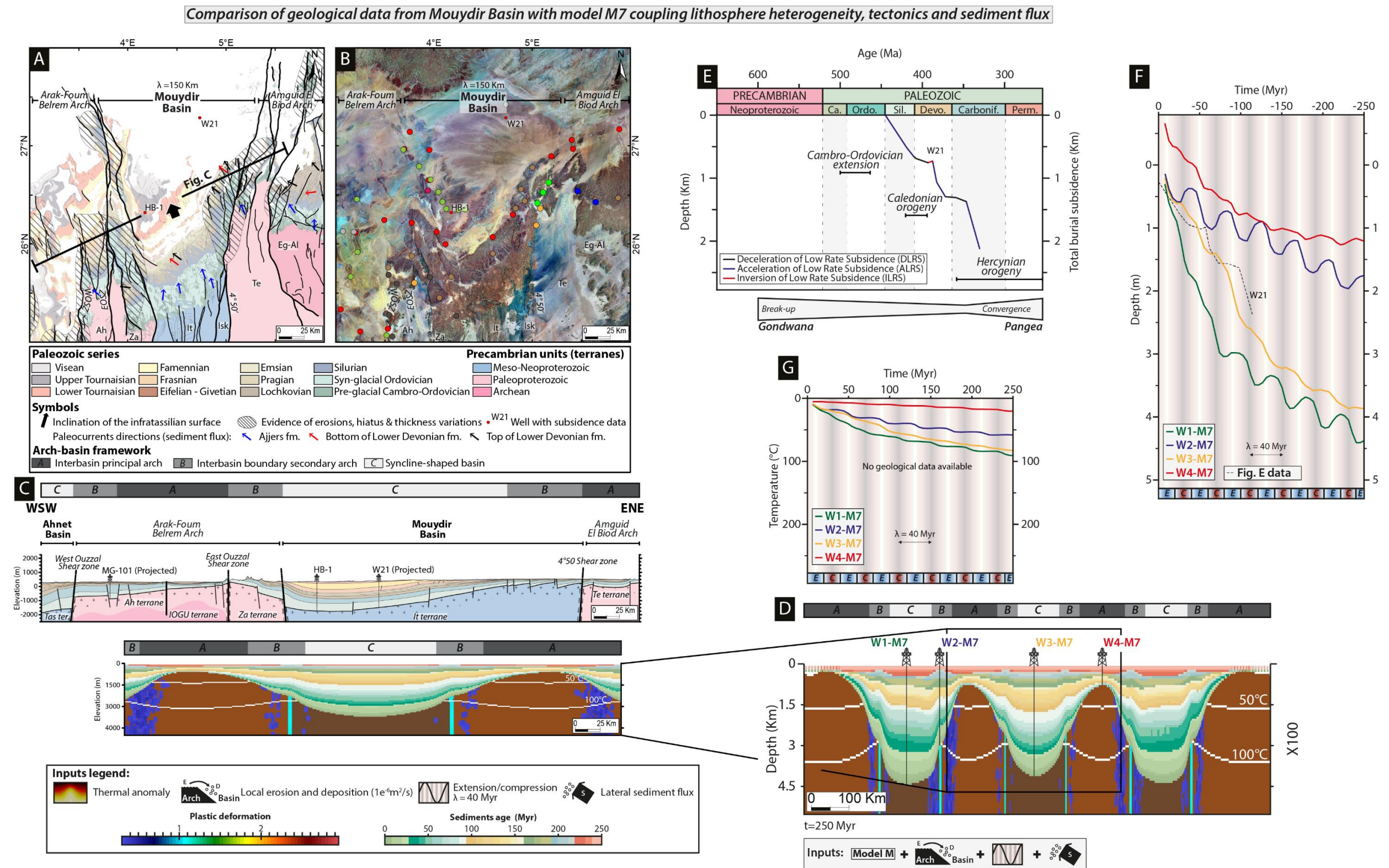


Figure VII-13: Comparison of tectono-stratigraphic architecture cross section and thermal subsidence curves in the Mouydir basin with thermo-mechanical numerical model M7. (A) Geological map of the Paleozoic series in the Mouydir basin. (B) Satellite images of the Paleozoic series in the Mouydir basin (Landsat 7 ETM+). (C) WSW-ENE cross section of the Mouydir basin localized in Figure A showing the typical arch and basin architecture with diminution of series approaching arches. (D) Cross section extracted from model M7 showing the similar arch-basin architecture. (E) Total burial subsidence of well W21 from bibliography (Perron et al., 2018). (F) Comparison of total subsidence in E with curve model M7. (G) Thermal curves extracted from the model M7. Notice that this comparison is possible with peripheral basins in the numerical model M6.

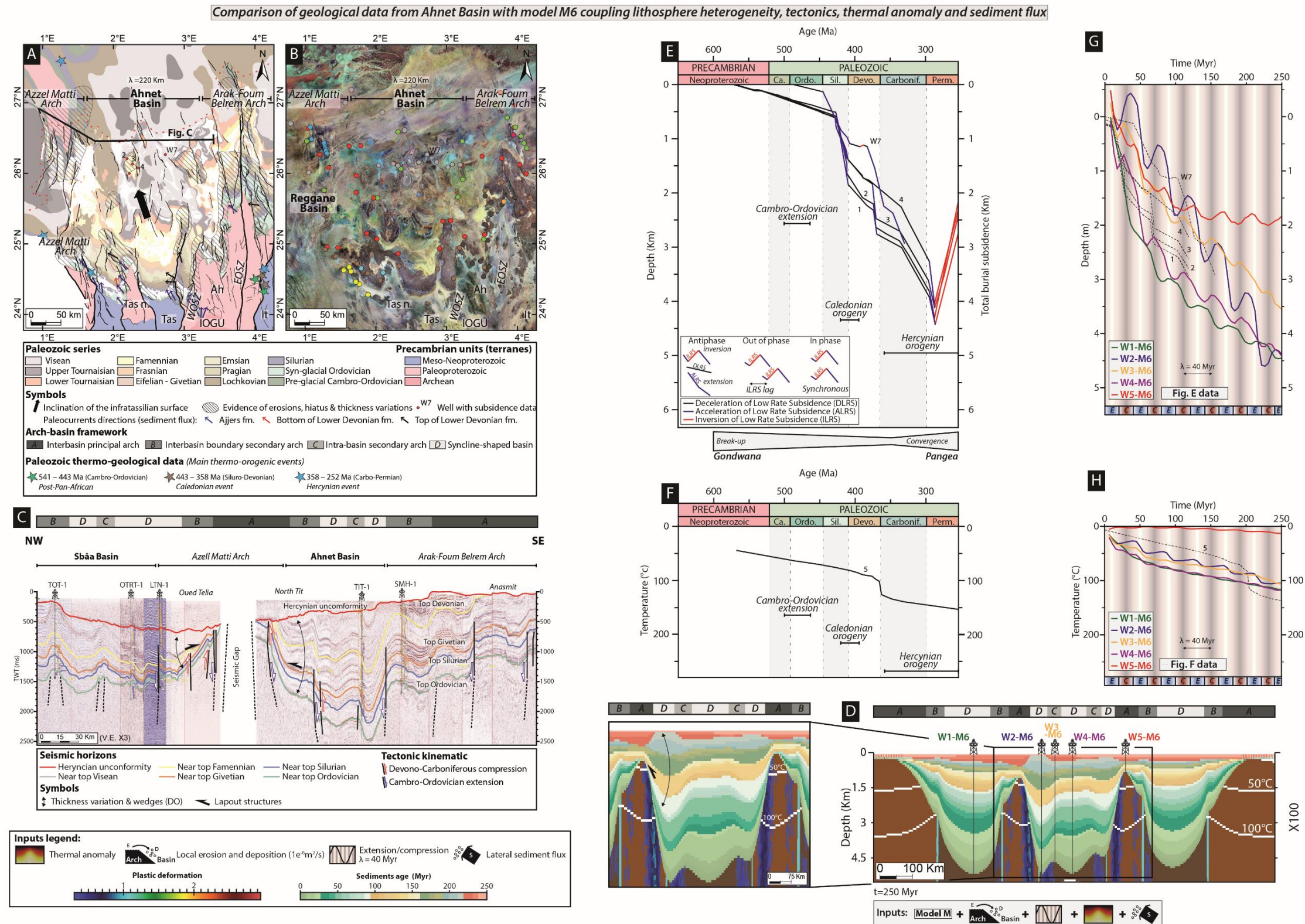


Figure VII-14: Comparison of tectono-stratigraphic architecture cross section and thermal subsidence curves in the Ahnet basin with thermo-mechanical numerical model M6. (A) Geological map of the Paleozoic series in the Ahnet basin. (B) Satellite images of the Paleozoic series in the Ahnet basin (Landsat 7 ETM+). (C) NW-SE seismic cross section of the Ahnet basin and Azzel Matti Arch localized in Figure A showing the typical complexification of arch and basin architecture with intra-arches structures. (D) Cross section extracted from model M6 showing the similar complexification of the arch-basin architecture with presence of intra-arches. (E) Total burial subsidence of well W7 from Perron et al., (2018) and well 1, 2, 3, 4 from Kracha, (2011). (F) Comparison of total subsidence curves of E with curve model M6. (G) Comparison of thermal curves extracted from the model M6 with 5 from bibliography (Logan and Duddy, 1998).

8 Classification of peri-Hoggar Basins in function of their forcing factors dominance

The comparison between geological data of the peri-Hoggar Basins and the different numerical thermo-mechanical models allows to classify the basins according to their forcing factors in a three pole diagram (Figure VII-15): Tectonic dominated (represented by the model M2), thermal dominated (represented by the model M1) and external sediment flux dominated (represented by the model M3).

In this classification, we can see the distribution of the different peri-Hoggar Basins according to their architecture (i.e. syncline-shaped, complex-shaped), their softening of the faults/terranes and their infilling (i.e. starved or filled).

The different main criteria needed in order to classify each basin are compiled in Table 5.

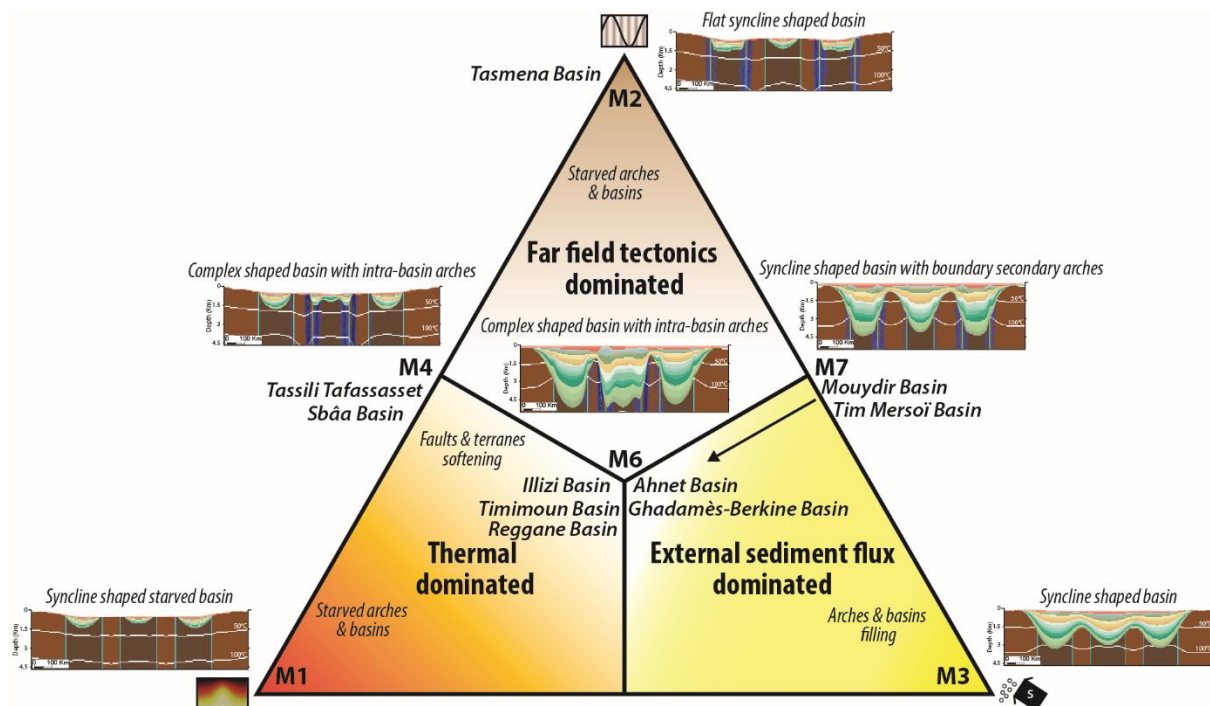


Figure VII-15: Classification of the different peri-Hoggar Basins based on the intensity of the three main modelled parameters from M1 to M7 (thermal anomaly, tectonics and sediment flux). Note that this classification is established by comparing the architecture, the geometries, the thermal and the subsidence curves between models and geological data. For each category local erosion/deposition process is active (i.e. erosion of arches and deposition in basins depocenter).

Models		M2	M3	M4	M5	M6	M7
Limits conditions (compression/extension alternation)		yes	no	yes	no	yes	yes
Thermal anomaly		no	no	yes	no	yes	no
Lateral sediment supply		no	no	no	yes	yes	yes
Duration (Myr)		250	250	250	250	250	250
Basins morphologies & typologies	Lateral basins	Flat angular syncline-shaped	Syncline-shaped	Syncline-shaped	Syncline-shaped	Syncline-shaped	Syncline-shaped
	Central basin	Syncline-shaped	Syncline-shaped	Complex-shaped	Syncline-shaped	Complex-shaped	Syncline-shaped
Arches structures identified		inter-basin arches, inter-basin 2nd boundary arches	only inter-basin arches	inter-basin arches, inter-basin 2nd boundary arches, intra-basin arches	only inter-basin arches	inter-basin arches, inter-basin 2nd boundary arches, intra-basin arches	inter-basin arches, inter-basin 2nd boundary arches
Basin filling		Starved	Starved	Starved	Infilled	Infilled	Infilled
Arches thickness max. (km)		no	no	no	1,5	2,2	1,8
Basin thickness max. (km)		1,9	1,4	2,8	3	5	4,5
Temperature max. (°C)		20	20	25	90	120	90
Global average subsidence rate (m/Myr)		8	6	11	12	20	18
Deviations highs (m)		5 to 400	no	400 to 1100	no	400 to 1400	5 to 500
Peri-Hoggar Basins best morphology fit		Tasmena Basin		Tassili Tafassasset, Sbâa Basin ?		Ahnet Basin, Illizi Basin?, Timimoun Basin, Ghadamès Basin, Mouydir Basin, Tim Mersoï Basin	Mouydir Basin, Tim Mersoï Basin

Table 5: Main criteria of classification of the different peri-Hoggar Basins.

9 Conclusion and perspective

Comparing results from forward modelling to geological data from the peri-Hoggar Basins (Saharan platform) has led to highlight the viability of the coherency of the conceptual geological model proposed (Perron et al., 2018) and the hypothesis of isostatic disequilibrium of the accreted terranes composing the substrate. The density variability in the lithosphere inherited from paleo-orogenies creates uncompensated entities that will be conserved through time. It will be achieved their equilibrium after a very long time.

The key results of this study are the following:

- The thermo-mechanical numerical model developed is coherent and viable to explain the first (i.e. long-lived low signal) and seconder (i.e. deviations) order subsidence pattern of the peri-Hoggar Basins;
- The lithospheric density heterogeneities between accreted Archean and Proterozoic terranes control the Arches-Basins architecture;
- Comparison of geological data with numerical thermo-mechanical models allows to classify each peri-Hoggar Basins related to their forcing factors (dominated tectonics, dominated thermal and dominated external sediment flux). They are defined by their architecture (i.e. syncline-shaped, complex-shaped), their softening of the faults/terranes and their infilling (i.e. starved or filled);
- Periods of acceleration of the low rate subsidence (ALRS) are well-correlated with temperature increasing during the Paleozoic, which have an impact on climate dynamic and so on sediment flux (considered as a proxy). Knowing that, the external sediment supply controls the total basin infill until reaching isostatic equilibrium. However, in some case, sediment supply only cannot explain ALRS, tectonics parameter has to be taken to account. It is a major forcing factor indispensable during inversion of the low subsidence rate (IRLS);
- Very low strain rate (0.5 km/Myr) can be transmitted far away (over 1600 km) inside the model and provoke or/and reactivate faulting, which is coherent with the propagation of far field stresses in plate interiors highlighted by some authors (Perron et al., 2018; Ziegler et al., 1995);
- Diachronism and unconformities between the different peri-Hoggar Basins is well explained by the heterogenic propagation of the deformation through the model.

Because of the 2D modelling, lateral sediment flux (i.e. sediment supply from upstream) has to be simulated by bringing external sediment supply at edges of the models. As well as strike slip kinematics through inherited mega-shear zone well identified in the Saharan platform (Haddoum et al., 2001, 2013; Perron et al., 2018; Zazoun, 2001, 2008) cannot be taken into account. Consequently, 3D modelling should be an interesting perspective in order better constrain these intracratonic basins.

CHAPTER VIII. CONCLUSION AND PERSPECTIVES



Sandstones bodies in the Tassili-N-Ajjers (Google-Earth view; 25°26'15" N, 8°14'15" E)



1 Temporal geological synthesis of the Paleozoic peri-Hoggar Basins

The sedimentation pattern of the Gondwana craton is characterized by a stable tectonic regime and very low sedimentation rate during the Paleozoic (Bennacef et al., 1971). These basins subside over very long periods of time with a low rate (Beuf et al., 1971; Coward and Ries, 2003; Eschard et al., 2010). A poly-history is represented by distinct phases of subsidence basin evolution, rhythmized by tectonic pulse (Perron et al., 2018). In intracratonic basin, the eustatic sea level variation strongly affects the sedimentary bodies organization because of slow subsidence (i.e. low accommodation space for sediment supplying) over hundreds of millions of years (Holt, 2012; Sloss, 1963). Consequently, in this context, glacio-eustatic variation might explain actual architecture (i.e. widespread unconformities, weak lateral facies variations) of the Saharan platform. In such geodynamical context, eustatic variations can be a main controlling factor of accommodation changes (third-order sequences), being amplified above the highs. The Paleozoic eustatic charts of Haq and Schutter (2008) show that the eustatic variations amplitude can be sufficient to provoke the emersion of the arches during the eustatic sea-level falls. Glacio-eustatic variation cannot be considered as a unique controlling factor.

If it had been the case arches structures would have disappeared through time by erosion and deposition leveling. Conversely, arches growth through time and keep their configuration from Cambrian to Devonian and Carboniferous (Perron et al., 2018). Therefore, an internal mechanism (i.e. tectonic) seems to maintain this configuration. According to Eschard et al., (2010), in such a cratonic context, the uplift rate of the highs is expected to be slow and constant. This organization seems similar between the different arches (Eschard et al., 2010). Nevertheless, acceleration or deceleration of subsidence can be noted during geodynamic event (Figure VIII-1B). Consequently, the analysis of subsidence histories should help to decipher the different forcing mechanisms during the Paleozoic in the peri-Hoggar Basins (NW Basins).

The subsidence curves analysis of the Paleozoic history of the peri-Hoggar Basins allows extracting three types of low subsidence pattern (ALRS: Acceleration of the Low Rate Subsidence, DLRS: Deceleration of the Low Rate Subsidence and IRLS: Inversion of the Low Rate Subsidence), linked to internal (tectonics) and/or external forcing (climate change and glaciation) (Figure VIII-1).

Two periods of DLRS (Deceleration of the Low Rate Subsidence) are mainly registered during the Late Cambrian and the Early Devonian with rate of subsidence comprising from 5 to 20 m/Ma. The

Late Cambrian shows a global increase of the temperature (high temperature) associated with a worldwide eustatic transgression trend (Figure VIII-1C and D). During these periods, evidence of unconformities is observed which are preferentially registered on arches (Table 3; Figure VIII-1A). Especially, the Emsian hiatus identified by many authors (Table 3) which is well correlated to a high peak of temperature and a worldwide eustatic regression (Figure VIII-1C and D). We observe for both stages, the deposition of principally continental fluvial dominated systems. This type of sedimentation in a context of low rate subsidence is consistent with denudation rates range (5 to 50 m/Ma) in low relief area (see Fig. 9.14 in Einsele, 2000) in stable tectonic regime. During these periods of tectonic quiescence, the sedimentation pattern seems to be mostly influenced by climatic and surface processes mechanism (erosion, weathering and low sediment flux).

This phase of quiescence is in agreement with the model M3, where basic surface processes eroding uplifted arches and depositing in subsided basins without tectonic parameters (Figure VII-8) control the basin dynamics and the low rate subsidence. The external sediment supply and surface processes are identified as the first order signal in these intracratonic basins (Perron et al., submitted).

Fourth periods of ALRS (Acceleration of the Low Rate Subsidence) are observed during the Early-Middle Ordovician, the Silurian, the Early Mid Devonian and the Late Devonian with rate of subsidence, which can reach 150 m/Ma. They are characterized by the deposition of marine dominated environments with rare hiatus rare and conformable series (Figure VIII-1A). These periods are linked to worldwide high (Early-Middle Ordovician) or increasing temperature (Silurian, Early Mid Devonian and the Late Devonian) permitting to enlighten a possible increase of sediment supply (Figure VIII-1D). They are associated to worldwide transgressions (Early-Middle Ordovician, Silurian and Early Mid Devonian) and regressions (Late Devonian). During these transgressions (Figure VIII-1C), the maximum of magnitude of sea level variation are about 50 m (Haq and Schutter, 2008), which is insufficient to alone explicate the subsidence acceleration.

Then, neither eustatic or/and climatic parameters only can explain this acceleration of the subsidence. Putting into perspective the results from numerical model M, the acceleration of the subsidence rate can be explained by the high sediments flux (climatic proxy) and/or extensional tectonics (far field stresses). Where, subsidence acceleration rate from high sediment flux are featured by lower values than from tectonics (see difference of slop between the curves M3 and M6). Consequently, external forcing factors have undoubtedly accentuated

or limited this trend, even if the tectonic seems to be the main controlling factor. In some case, it is possible because of the range of values that the acceleration of the subsidence rate can be related only to the increase of the sediment flux. Besides, globally the increases of temperatures and so the augmentation of detrital supply related is globally correlated with acceleration of the subsidence.

Three periods of ILRS (Inversion of the Low Rate Subsidence) are identified during the Late Ordovician, the Early Devonian, the Givetian and the Early Carboniferous with negative rate of subsidence comprise from -5 to -100 m/Ma. They are mainly featured by deposition of glacial (Late Ordovician), fluvial (Early Devonian) and shallow marine (the Givetian and the Early Carboniferous) systems. During these periods, evidence of many unconformities (e.g. glacial incision, Caledonian unconformity) is observed which are preferentially registered on arches (Table 3; Figure VIII-1A). They are associated with a negative (Hirnantian glaciation) or positive peak of temperature (Figure VIII-1D). They are associated to worldwide regression (Late Ordovician, Early Devonian, and Early Carboniferous) and transgression (Givetian). The maximum magnitude of sea level variation is going from 100 m for the Late Ordovician glaciation to 50 m for the Early Devonian regression (Figure VIII-1C). Decipher signature to isostatic and eustatic signals during glaciation/deglaciation events is difficult (Girard et al., 2018).

Comparison with our model allow to propose tectonic as the mechanism permitting to understand this inversion. Following these observations, these periods must be correlated to tectono-isostatic events. We can identify the early Silurian isostatic rebound from ice sheet melting and the far field stresses from the Early Devonian Caledonian orogeny, the Middle-Late Devonian event and the Carbo-Permian Hercynian orogeny (Figure VIII-1C).

To conclude, the temporal and spatial variation in subsidence and architecture within basins result from a complex balance between internal forcing (lithosphere heterogeneity, thermal anomaly, tectonics) and/or external forcing (local erosion/deposition, lateral sediment flux). The Saharan platform was alternatively flooded or emerged depending on the eustatic sea-level variations, sediments supply, the uplift rates and the global geodynamic deformation. Depending on the nature of the subsidence rate pattern (i.e. either DLRS, ALRS and IRSL), one or a combination of several of these forcing factors control the Paleozoic intracratonic basins of the Saharan platform.

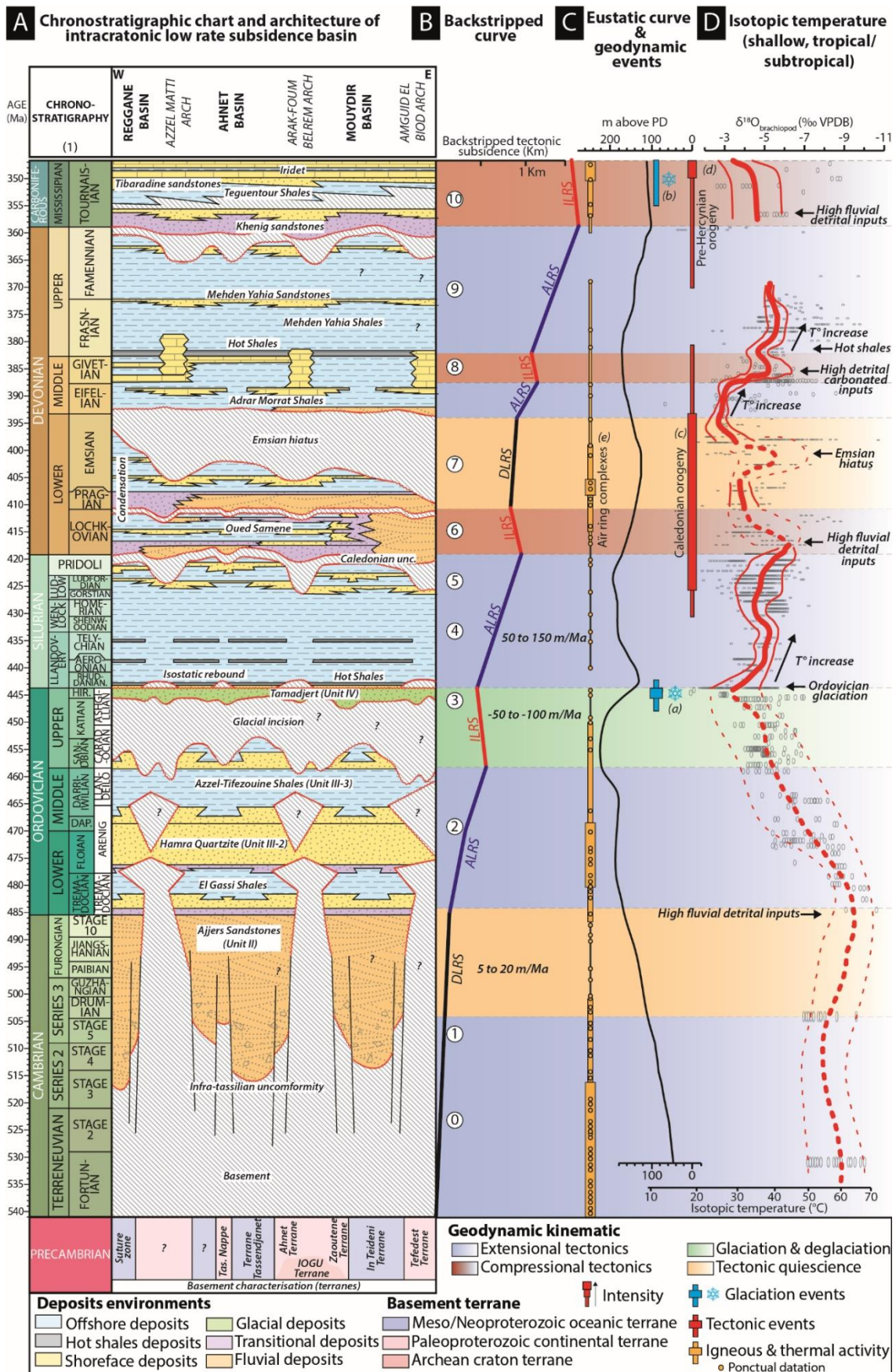


Figure VIII-1: (A) Chronostratigraphic chart and architecture of the Paleozoic intracratonic basins (Reggane, Ahnet, Mouydir) associated with their basement heterogeneities (i.e.

*terrane*s) drawn from literature (Eschard et al., 2010; Perron et al., 2018; Wendt et al., 2006); (B) Schematic characteristic backstripped curve of these basins; (C) Eustatic curve (Haq and Schutter, 2008) and geodynamic events: (a) Hirnantian glaciation, (b) Carboniferous glaciation, (c) Caledonian orogeny, (d) pre-Hercynian orogeny, (e) Devonian igneous intrusion; (D) Isostopic temperature (shallow, tropical/sub-tropical) during the Paleozoic (Prokoph et al., 2008). (0) Late Pan-African extensional collapse, (1) Pan-African peneplanation, (2) Cambro-Ordovician extension, (3) Upper Ordovician glaciation and deglaciation linked to isostatic rebound, (4) Silurian extension, (5) Silurian sealing, (6) Caledonian compression, (7) Early Devonian tectonic quiescence, (8) Middle Devonian compression, (9) Middle to Late Devonian extension, (10) Pre-Hercynian compression.

2 Conclusion (Question responses)

The aim of this thesis was to analyze the tectono-sedimentary architecture systems of the North Gondwanan Paleozoic platforms (peri-Hoggar basins), which are very large (in width and length) and have no current equivalent. Several questions were asked and introduced at beginning of this manuscript:

- (1) What are the working mechanisms of these slow subsidence basins?
- (2) How can we characterize crustal and lithospheric deformations?
- (3) What is the nature of the apparently permanent lithospheric & rheological heterogeneities through 250 Ma?
- (4) What is the control and trigger of the regular uplifts of inherited paleohighs/arches and extensive & coeval unconformities/hiatuses?
- (5) What are the controlling factors of the sedimentary record, the reservoir architecture and facies distribution?
- (6) What is the impact on the Silurian/Devonian Hot Shales and other source rocks deposits?

With the help of our multi-disciplinary integrated approach, we have tried to response to each of them:

(1) What are the working mechanisms of these slow subsidence basins?

Both the published paper (Chapter IV) and the submitted paper (Chapter VI) has permitted to response to this question. After the establishment of an integrated multi-disciplinary conceptual

geological model coupling both tectono-sedimentologic of the Arches-Basins architecture and the nature of the substrate, we have highlighted a specific distribution between the Arches-Basins framework and the age of the terranes. We have shown that “old” terranes (Archean and Paleoproterozoic) form preferentially substrates of the Arches and the “young” terranes (Meso-Neoproterozoic) constitute the substrates of the basin depocenter. This zonation is inherited from accreted, assembled and sutured terranes separated by major mega shear zone during several paleo-orogenies. Stating the hypothesis of isostatic disequilibrium between the different terranes because of differential densities of Achaean, Paleoproterozoic, Meso-Neoproterozoic entities based on published studies (Artemieva, 2009; Artemieva and Mooney, 2002; Djomani et al., 2001), led to the construction of a 2D numerical thermo-mechanical lithospheric model. We have seen that a combination of lithospheric heterogeneity assembled with terranes of different densities and basic surface processes can explain the first order mechanism at the origin of the low and long subsidence rate. It also reconciles the Arches-Basins architecture. Erosion and deposition of the different blocks associated with a progressive re-equilibration of the isostatic density anomalies in the lithosphere will maintain the subsidence dynamic through long geological time. As a consequence, the nature of the inherited uncompensated isostatic anomalies associated with basic surface processes (external forcing) can constrain and force the mechanism of slow subsidence (first order mechanism in intracratonic basins). This new numerical model developed in this study has shown by extracting and comparing forward modelling results with geological data that it is both coherent with peri-Hoggar Basins and other worldwide basins.

(2) How can we characterize crustal and lithospheric deformations?

The submitted paper (Chapter VI) has tried to response to this question. The new numerical model developed in this study (see model M) inspired and calibrated from geological data was subject to sinusoidal pulsatile tectonics alternating compressional and extensional kinematics (0.5 km/Myr with time period of 40 Myr). In our simulation, this very weak strain can be transmitted far away (over 1600 km) inside the model provoking or/and reactivating faults. A tectonic style coherent with the propagation of far field stresses in plate interiors highlighted by some authors (Coakley and Gurnis, 1995; Haddoum et al., 2001; Perron et al., 2018; Ziegler et al., 1995). Moreover, two type of deformations are identified, featured by classical faulting during extension implying the crustal scale and buckling mainly during compression evolving the whole lithosphere. During extension horst and grabens systems are created and concentrated at near terranes boundaries (i.e. shear zones). In contrast, during compression large scale

buckling is observed, characterized by the uplift of the Archean terranes and the downlift of the Proterozoic terranes. This asymmetric behavior between extension and compression phase is well explained by the fact that the lithosphere is stronger in compression than in extension (Brace and Kohlstedt, 1980). Delays in inversion of the fault system versus global buckling is also observed. It may explain why during the a same tectonic event, both extensional or compressional structures can be locally recognized in the different Arches and sub-basins (Perron et al., 2018). Moreover, the presence or not of a thermal anomaly (which can be related to both tectonics activity and igneous activity) is at the origin of fault and terranes softening and strain localization. It may be at the origin of the terrane response to lithospheric buckling. It can also influence the thermal activity of the basins and so the reservoirs (maturity of the source rock...).

(3) What is the nature of the apparently permanent lithospheric & rheological heterogeneities through 250 Ma?

Both the published paper (Chapter IV) and the submitted paper (Chapter VI) has helped to response to this question. The multidisciplinary approach integrating geophysical (aeromagnetic, Bouguer anomaly maps), geological and geochronological (U/Pb SHRIMP...) analysis of the Saharan platform, and especially of the exhumed Hoggar massif has allowed to establish a substrates geological model. It was the results of collage of portion of different terranes during paleo-orogenies with their own physico-chemical properties. A particular zonation of the terranes with the cover framework was highlighted, where the relation between these two seems to be the age and origin of the different terranes (i.e. Archean, Paleoproterozoic, Meso-Neoproterozoic). Through a 2D numerical thermo-mechanical modelling, we have shown that differential densities (dependent of age) between the terranes (in this case Archean and Proterozoic) in the lithosphere can be a viable hypothesis to explain the nature of the apparently permanent lithospheric and rheological heterogeneities through 250 Ma. Moreover, we have seen that in the simulation submitted to basic surface processes (erosion and deposition), the isostatic equilibrium isn't reach after 250 Myr. This argue in favor of a very long process maintaining the stability of the lithosphere coherency.

(4) What is the control and trigger of the regular uplifts of inherited paleohighs/arches and extensive & coeval unconformities/hiatuses?

Both the published paper (Chapter IV) and the submitted paper (Chapter VI) has helped to response to this question. In the first part (Chapter IV), we have seen that the vertical motions

of the platform produced several arches (also called domes, swells, highs, ridges) and basins (synclines shaped depressions) with different wavelengths going from several hundred to more than a thousand kilometres. This latter controlling spatially and temporally the deposition and the erosion dynamics. Several major erosion events significantly truncated the pre-existing sediments over wide areas, producing regional unconformities amalgamated approaching arches that separate the platformal cover into divisions. The persistence of a rather uniform pattern of vertical motions seems to control the architecture of these basins and the thickness variation at the vicinity of Arches. With the different simulations from the new developed models (Chapter VI), we have both explained the first order mechanism controlling the Arches-Basins architecture (described previously) as well as the second order mechanism directing the deviations of the subsidence signal. In our modelling, the lithospheric density heterogeneities are at the origin of the Arches-Basins framework; And the far field tectonics applied at the model boundaries are at the origin of the up and down deviations of the subsidence pattern and complexification of the stratigraphic architecture. The coupling of these two controls the stratigraphic distribution of unconformities/hiatuses which is coherent with geological data collected on the Saharan platform. They help to understand heterogenic propagation of the strain impacting the stratigraphic diachronism and the absence or presence of some layers between neighboring basins.

(5) What are the controlling factors of the sedimentary record, the reservoir architecture and facies distribution?

In order to totally response to the question a coupling with stratigraphic modelling (with DIONISOS software) should be led. However, a beginning of response at this question can be realized with the two last chapters (Chapter VI and Chapter VII). Apart all the controlling factors needed to explain the first and second order mechanism of control already cited previously that constrain the tectono-stratigraphic architecture, we have seen that sediment flux is predominant factor in the duration of subsidence (until isostatic equilibrium achievement) of the basins. It also constrains the presence of sediment on arches. Besides, we have observed a close synchronization between climatic global warming and acceleration of the subsidence rate. This lateral sediment supply control the facies distribution and features (grain size, nature, origin...) depending on the source. We have shown that it could be both local (erosion of arches) and more distal/regional (cratons). Nevertheless, alone this parameter cannot explain the characteristic of these basins. A subtitle equilibrium between far field stresses, sediment flux and thermal anomaly has to be taken to account...

(6) What is the impact on the Silurian/Devonian Hot Shales and other source rocks deposits?

The thermo-mechanical models proposed in this study cannot alone response to this question. Further work should be pursued by a coupling with stratigraphic modelling (with DIONISOS software) in order to refine the study, especially on facies partitioning. This latter cannot be succeeded by our thermo-mechanical modelling. Nevertheless, actual model of deposition of hot shales on the Saharan platform is defined by their preferential deposition in depression or paleo-depressions (Lüning et al., 1999, 2000, 2004) essentially created by horst and grabens faulting and glacial systems (themselves controlled by fault network) during Hirnantian deglaciation (Clerc, 2012; Clerc et al., 2013; Denis et al., 2007; Ghienne et al., 2003; Girard et al., 2018; Ravier et al., 2014; Zazoun and Mahdjoub, 2011). Our models have shown that due to cyclic inversion (extensional and compressional kinematics) in the maximum basin depocenter important hiatus (truncatures of series) are observed which could be at the origin of the non-presence of the hot shales. This unexpected observation could have a no negligible impact on the petroleum systems and the repartition of the source rocks.

3 Perspectives and comparison with intracratonic basins possible analogues (Case of Paraná Basin)

Aside its potential (yet requested) use for a broader understanding of the Paleozoic intracratonic basins, the multidisciplinary integrated method developed during this work may find other applications to answer diverse scientific questions.

Due to this approach involving different parameters as several scales, tools and domains (from geological analysis to numerical thermo-mechanical modelling), which is the main interest of the method, it might be used to help discriminate the influence of each distinct controlling parameter. It remains a first step in order to better constrain quality reservoirs predictions in intracratonic basins by coupling stratigraphic modelling (Dionisos).

At the light of the conclusion and results from this research work many opened perspectives and questions arise both from the geological analysis part (Chapter IV and Chapter V) and the modelling part (Chapter VI and Chapter VII) such as: (1) Can we export this model and approach to other worldwide basins? (2) Can we better constrain spatial paleogeographic environments of the Paleozoic succession? (3) What is the implication on modelled facies partitioning (Dionisos)? (4) Can a coupling between stratigraphic modelling and thermo-

mechanical modelling allow to better constrain quality reservoirs predictions of these intracratonic basins? (5) How can 3D thermo-mechanical modelling help the understanding of strike slip kinematics and sediments source supply of these basins? (6) Can other rheologic parameters than density control the differential subsidence?

Case of Paraná Basin:

A similar work can be achieved elsewhere. Indeed, a comparison of our forward numerical model with other worldwide basins can be allowed, especially with the South-American Basins (example of Paraná Basin in Figure VIII-2 and Figure VIII-3). These intracratonic basins were part of the Gondwana history (Rogers et al., 1995; Unrug, 1992), resulting from the same processes of accretion of heterogeneous terranes and cratonic cores described in this study (Figure III-17).

In this case, the basin depocenter is situated upon a different substrate than the edges of it, where the series are thinning and onlapping (Figure VIII-2A-B). The different substrates are separated by major shear zones (Figure VIII-2B). Besides, several authors (de Brito Neves et al., 1984; de Castro et al., 2012; Coelho et al., 2018; Rostirolla et al., 2003) have pointed out the influence of basement on the architecture of these basins. Geophysics anomalies are also highlighted and often related to basement structures (Cordani and Teixeira, 2007; Dallmeyer, 1989; Daly et al., 2014, 2018b; Heilbron et al., 2008; James and Assumpção, 1996; Mantovani et al., 2005; Nunn and Aires, 1988; Padilha et al., 2014; Pérez-Gussinyé et al., 2007; Tozer et al., 2017). They could be evidence of isostatic disequilibrium in the lithosphere between different terranes.

In view of our first observations (Figure VIII-2 and Figure VIII-3), both the architecture and the subsidence curves geological data of Paraná Basin seems coherent with the results of our models.

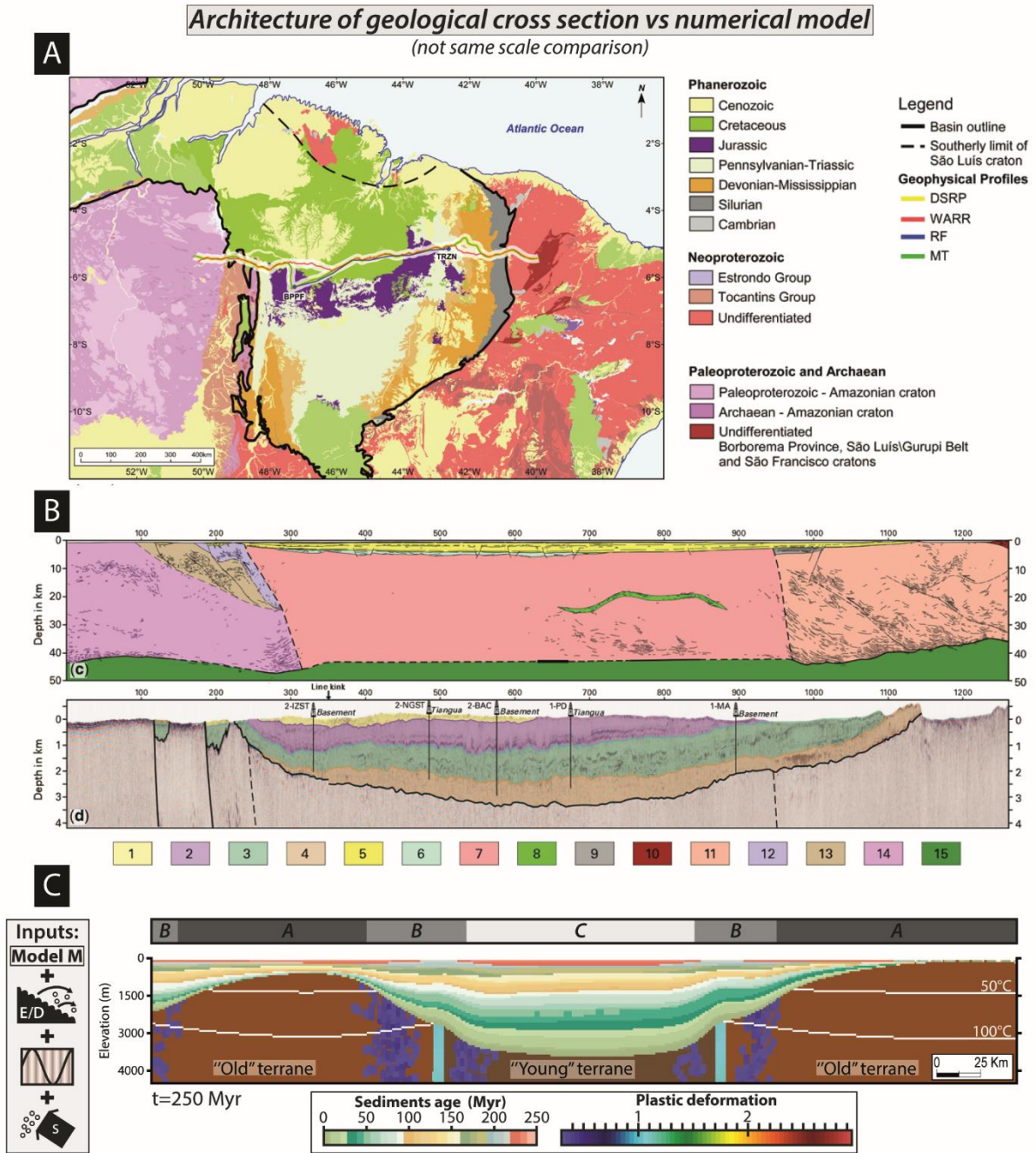


Figure VIII-2: Comparison of stratigraphic architecture cross section in the Paraná Basin with thermo-mechanical numerical model. (A) Geological map of the Paleozoic series in the Paraná Basin from Daly et al., (2018b). (B) Geoseismic interpretation of the deep seismic profile; And the same seismic data at a vertical exaggeration of 1:30 showing the cratonic megasequence and overlying Cretaceous section from Daly et al., (2018b). (C) Cross section extracted from model M7 showing the similar architecture. 1: Cretaceous Grajaú Group; 2: Upper carboniferous–Middle Triassic Balsas Group; 3: Middle Devonian–Lower Carboniferous Caninde Group; 4: Silurian–Lower Devonian Serra Grande Group; 5: Silurian–Triassic

cratonic basin megasequence; **6**: Late Neoproterozoic and Cambrian sedimentary remnants of the Riachão basin; **7**: Parnaíba Block crystalline basement; **8**: mid-crustal reflectivity; **9**: Cambrian volcanics and sediments of the Campo Maior graben; **10**: Neoproterozoic Cruzeta Complex of the Borborema Province; **11**: Neoproterozoic granitic gneisses of the Borborema Province; **12**: Neoproterozoic schists of the Estrondo Group; **13**: Neoproterozoic phyllites of the Tocantins Group; **14**: Paleoproterozoic Amazonian craton; **15**: lithospheric mantle.

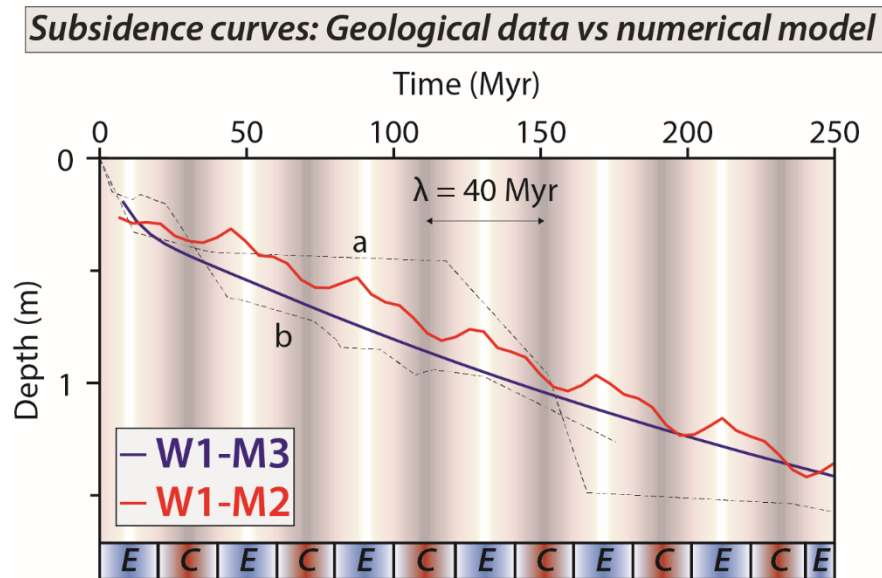


Figure VIII-3: Comparison of subsidence curves from geological data of Paraná Basin and numerical models (Model M2 and M3). **a**: Well CB-3 from Paraná Basin, Brazil, (Oliveira, 1987 from Allen and Armitage, 2011); **b**: Well from Paraná Basin (Zalan et al., 1990).

LIST OF FIGURES



*Fossil of Pingos in the Arak region of Mouydir Basin (Google-Earth view; 25°29'56" N,
3°57'42" E)*



CHAPTER I:

Figure I-1: Distribution of intracontinental basins on the continents surrounding the Atlantic Ocean, with typical cratonic basins highlighted. Other basins shown are commonly unequivocally associated with extensional tectonics. Selected basins are color-coded according to the timing of initiation. Source: Base map and basin outlines provided by Trond Torsvik from Allen and Armitage, (2011).	19
Figure I-2: Map showing the location of 24 cratonic basins overlain on a map of lithospheric thickness derived from surface wave tomography (Priestley and McKenzie, 2013). The basins are colour-coded by their age of initiation. 1: Southern West Siberian basin; 2: Hudson basin; 3: Williston basin; 4: Michigan basin; 5: Illinois basin; 6: Solimoes basin; 7: Amazon basin; 8: Parnaíba basin; 9: Paraná basin; 10: Chaco basin; 11: Congo basin; 12: Taoudenni basin; 13: Kufra basin; 14: Murzuq basin; 15: Illizi basin; 16: Ghadames basin; 17: Tindouf basin; 18: Ordos basin; 19: Sichuan basin; 20: Georgina basin; 21: Amadeus basin; 22: Officer basin; 23: Mporokoso basin; 24: Witswatersrand basin. Figure from published paper (Daly et al., 2018a).	20
Figure I-3: Localization and thickness of intracratonic basins in the world from Heine et al., (2008).	21
Figure I-4: Example of tectonic subsidence in intracratonic basins through the world modified from literature (Allen and Armitage, 2011; Xie and Heller, 2009). 1: Illinois Basin (Bond and Kominz, 1984); 2: Michigan Basin (Bond and Kominz, 1984); 3: Williston Basin, North Dakota (Bond and Kominz, 1984); 4: Williston Basin, Saskatchewan (Fowler and Nisbet, 1985); 5: Paraná Basin, Brazil, CB-3 well (Oliveira, 1987 from Allen and Armitage, 2011); 6: Northeast German Basin (Scheck and Bayer, 1999); 7: Southwest Ordos Basin (Xie, 2007 from Xie and Heller, 2006); 8: Paris Basin (Prijac et al., 2000); 9: West Siberian Basin, Russia, Urengoy well (Saunders et al., 2005); 10: West Siberian Basin, Russia, Samotlar-39 well (Saunders et al., 2005); 11: Paraná Basin (Zalan et al., 1990); 12: Well W17 in Ahnet Basin (Perron et al., 2018).	22
Figure I-5: Subsidence repartition in different types of basin modified from Lafont, (1994). t: basin duration of subsidence; T: thickness of the basin; λ : wavelength of the basin; v: range of subsidence rate. Values from Allen and Allen, (2013).	23
Figure I-6: (A) The three lithospheric processes account for subsidence. Any sedimentary basin subsidence results from one of these three processes or a combination of them (Allen and Allen,	

2013). (B) Different hypotheses for subsidence origin of intracratonic basins (Allen and Armitage, 2011).25

Figure I-7: The arch and syncline-shaped basin architecture, a common characteristic of intracratonic basins inspired from Seyfert, (1987).....26

Figure I-8: Relation between basins wavelength and the thickness of deformed unit. Characteristic sizes of some major types of sedimentary basins as a function of deformation intensity. Figure modified from Brun, (1999).....26

Figure I-9: Characteristics of lithospheric folding. (A) Poly-harmonic folding concept: due to rheological stratification, the lithosphere can develop different folding wavelength in response to tectonic compression. Surface topography will reflect superposition of different wavelengths. (B) Theoretically predicted wavelengths as function of thermo-tectonic age (for different lithospheric layers as well as whole-lithosphere folding. Model is compared to the observed wavelengths (Cloetingh et al., 1999). **1:** Tien Shan; **2:** Western Goby; **3:** Central Asia; **4:** Himalayan syntaxis belt; **5:** Central Australia; **6:** Russian platform; **7:** South Caspian Basin; **8:** Eastern Black Sea; **9:** Western Black Sea; **10:** Pannonian Basin System; **11:** NW European platform; **12:** Brittany; **13:** Iberia; **14:** Barents Sea; **15:** Canadian Arctic; **16:** Transcontinental Arch of North America; **17:** Laramide foreland (USA). Figure modified from Cloetingh and Burov, (2011). Paleozoic peri-Hoggar Basins based on this study data (last major thermotectonic event: Pan-African orogeny dated around 600 Ma e.g. Guiraud et al., (2005).27

Figure I-10: Schematic diagram illustrating the relationship between the duration of subsidence and the configurations of the lithosphere and of the sedimentary infill at specific intracontinental basins modified from Cacace and Scheck-Wenderoth, (2016). Lithospheric thickness data are after (Artemieva, 2006), sediment thickness after (Heine et al., 2008), and subsidence duration after (Xie and Heller, 2009). The observed lack of correlation between equilibrium lithospheric thickness (red circles) and subsidence duration strongly suggests that subsidence in these basins cannot be exclusively explained by differences in the initial lithospheric configuration of the respective basins. In contrast, preserved sediments thickness (light blue circles) provides a better fit to the duration of subsidence, thus supporting the existence of a dynamic and structural relation between sedimentation pattern and history and resulting subsidence history. Placement of some Paleozoic peri-Hoggar Basins based on this study data.28

Figure I-11: Schematic cross section illustrating different orogenic styles developed through time modified from Cagnard et al., (2011). (A) Archean domes and basins orogens, (B)

Paleoproterozoic accretionary orogens, (C) Modern cold orogens characterized by thrusting style tectonics. Example of regional-scale shear zone patterns and sigmoidal structures in accretionary Precambrian orogens. (D) The Eastern Goldfield province, Yilgam craton, Australia modified from Chardon et al., (2009); (E) The Birrimian orogen, West African Craton, Burkina Faso modified from Chardon et al., (2009).....	33
Figure I-12: Lithospheric thermal thickness versus geologic age of the continental lithosphere. The Archean lithosphere has bimodal thickness distribution centered at 350 and 220 km. Gray area shows the lithospheric thickness estimates derived from thermal data from Artemieva and Mooney, (2002). Key: Ar—Archean; ePt, mPt, lPt—early, middle and late Proterozoic, respectively; Pz—Paleozoic; Cz—Cenozoic. Placement of the West African Craton (WAC) and the Pan-African mobile belts (Central African) from Artemieva, (2006).....	35
Figure I-13: Secular variations in average physical properties of the continental lithospheric mantle (CLM) due to compositional and temperature variations modified from Artemieva, (2009): (a) forsterite content, (b) average temperature in the CLM, (c) density at standard, i.e. room, P–T conditions, (d) S-wave seismic velocity. Primitive mantle (of pyrolite composition) is shown for a comparison. Right column illustrates the effect of temperature on: (e) density, (f) seismic velocities, and (g) inverse seismic attenuation. Placement of Archean terranes (WAC: West African Craton, IOGU: In Ouzal Granulites Unit) and Proterozoic terranes (Se: Serouenout, It: In Teidini, Tas: Tassendjanet).....	36

CHAPTER II:

Figure II-1: Method of integrated multidisciplinary characterization of intracratonic basins used in this study. Notice that WP4 (Stratigraphic modelling) workflow is not under the scope of this manuscript. It represents an interesting perspective of work for the future.	43
Figure II-2: Methodology of satellite images analysis and re-interpretation from Landsat 7 ETM+ (USGS: https://earthexplorer.usgs.gov/) and geological maps (Bennacef et al., 1974; Bensalah et al., 1971).	45
Figure II-3: Methodology of well correlation and interpretation from wireline, cuttings, core and sedimentological studies (e.g. Eschard et al., 1999).....	47
Figure II-4: Example of biostratigraphical (Palynology) correlation in the Ordovician from internal (Eschard et al., 1999; Robertson, 2002) or published data (Kichou-Braïk et al., 2006; Oulebsir and Paris, 1995).....	48

Figure II-5: Example of biostratigraphical (Palynology) good to fair correlation in the Devonian from internal (e.g. Eschard et al., 1999) or published data (e.g. Abdesselam-Rouighi, 2003; Moreau-Benoit et al., 1993).....	49
Figure II-6: Compilation and integration of radiochronology data in a SIG project.	51
Figure II-7: Methodology characterizing the basement terranes.	52

CHAPTER III:

Figure III-1: Localization of peri-Hoggar basins and of the Paleozoic Saharan Platform, part of the North Gondwana (North Africa). The satellites images are from USGS Landsat 7 ETM+ (https://earthexplorer.usgs.gov/). Note the presence of outcropping Paleozoic series around the exhumed basement of the Hoggar Massif (800 km large).....	60
Figure III-2: Geological map of the Paleozoic North Saharan Platform (North Gondwana) georeferenced, compiled and modified from (1) Paleozoic subcrop distribution below the Hercynian unconformity geology of the Saharan Platform (Boote et al., 1998; Galeazzi et al., 2010); (2) Geological map (1/500,000) of the Djado basin (Jacquemont et al., 1959); (3) Geological map (1/200,000) of Algeria (Bennacef et al., 1974; Bensalah et al., 1971), (4) Geological map (1/50,000) of Air (Jouliia, 1963), (5) Geological map (1/2,000,000) of Niger (Greigertt and Pougnet, 1965), (6) Geological map (1/5,000,000) of the Lower Paleozoic of the Central Sahara (Beuf et al., 1971), (7) Geological map (1/1,000,000) of Morocco (Hollard et al., 1985), (8) Geological map of the Djebel Fezzan (Massa, 1988); Shear zone and lineament names: Suture Zone East Saharan Craton (SZ ESC), West Ouzzal Shear Zone (WOSZ), East Ouzzal Shear Zone (EOSZ), Raghane Shear Zone (RSZ), Tin Amali Shear Zone (TASZ), 4°10' Shear Zone, 4°50' Shear Zone, 8°30' Shear Zone. 1: Figure III-40; 2: Figure III-41; 3: Figure III-3; 4: Figure III-4 and Figure III-34.	62
Figure III-3: EW cross section of peri-Hoggar Basins (North Gondwana Platform, North Africa) modified from Craig et al., (2006). For localization see 3 in Figure III-2.....	63
Figure III-4: NS cross section of peri-Hoggar Basins (North Gondwana Platform, North Africa) modified from English et al., (2016b). For localization see 4 in Figure III-2.	64
Figure III-5: Chronological repartition of major important PhD thesis, publications and monographies (not exhaustive) in the Paleozoic Saharan platform through the 20 centuries. .	65
Figure III-6: Compilation of different directions of sedimentary flux and isopach maps during the Paleozoic. (1) Paleocurrent directions measured in the Ajjers formation i.e. Cambrian compiled from Beuf et al., (1971); (2) Paleocurrent directions in the Lower Devonian sandstones compiled from literature (Bennacef et al., 1971; Beuf et al., 1969, 1971); (3)	

Paleocurrent directions during Visean and Serpukhovian compiled from Fröhlich et al., (2010b); (4) Evidence of the inclination of the “infratassilian” surface (Pan-African surface) to the north according to the directions of the paleocurrents measured in the basic sandstones of the Cambrian compiled from Beuf et al., (1971); (5) Isopach map for the entire Lower Paleozoic in the North African platform compiled from Fabre, (1988); (6) Isopach map for the entire Devonian in the North African platform from Fabre, (1988).	68
Figure III-7: Backstripped subsidence curves of the Paleozoic North Saharan Platform (peri-Hoggar basins) compiled from literature: 1: well W17, 2: well W5 and 3: well W7 in Ahnet basin, 4: well W21 in Mouydir basin, 5: well W1 in Reggane basin (Perron et al., 2018); 6: well in Sbâa basin (Tournier, 2010); 7: well in Ghadamès-Berkine basin (Yahi, 1999); 8: well RPL-101 in Reggane basin, 9: well HAD-1 in Ghadamès basin, 10: well REG-1 in Timimoun basin, 11: well TGE-1 in Illizi basin (Makhous and Galushkin, 2003a, 2003b); 12: well L1-1, 13: Pseudowell, 14: well A1-76, 15: well F1-NC58, 16: well J1-NC101, 17: well A1-77, 18: well D1-NC58, 19: well H1-NC58, 20: well A1-67 in Murzuq basin (Galushkin and Eloghbi, 2014); 21: Well B1NC43 and 22: A1NC43 in Al Kufrah basin, 23: composite well in Ghadames basin (Holt et al., 2010).	69
Figure III-8: Total burial subsidence curves of the Paleozoic North Saharan Platform (peri-Hoggar basins) compiled from literature: 1: well W1, 2: well W4, 3: well W7 and 4: well W9 in Ahnet basin (Kracha, 2011); 5: well KB-2 in Timimoun basin, 6: well ELA-1 in Ghadamès-Berkine basin (Kadi et al., 2013); 7: well in the Illizi basin (Wells et al., 2018); wells model 8: A and 9: B in Ghadamès-Berkine basin (Underdown et al., 2007); 10: well LD-1 and 11: well PDG-2 in Berkine-Ghadamès basin (Aissaoui et al., 2016); 12: well F3-NC174, 13: well H29-NC115, 14: well A1-NC186, 15: well A1-NC190 in Murzuq basin (Belaid et al., 2010); 16: cross section in the southwestern Anti-Atlas (Burkhard et al., 2006); 17: well OTRA-1 in the Sbâa basin, 18: well RG-3 in the Reggane basin, 19: well TEG-1 in the Timimoun basin (Logan and Duddy, 1998); 20: Hassi Messaoud field (English et al., 2017); 21: well in Sbâa basin (Tournier, 2010); 22: well in Ghadamès-Berkine basin (Yahi, 1999); 23: well RPL-101 in Reggane basin, 24: well HAD-1 in Ghadamès basin, 25: well REG-1 in Timimoun basin; 26: well TGE-1 in Illizi basin, 27: well TO-1 and 28: well KA-1 in the Dahar depression (Makhous and Galushkin, 2003a, 2003b); 29: well LT-1bis and 30: well OTLA-1 well in the Sbâa basin (Drid, 1989); 31: well L1-1 in Murzuq basin (Galushkin and Eloghbi, 2014); 32: well WT-1 in the Berkine basin (Yahi et al., 2001); 33: well G and 34: well A in the Illizi Basin (English et al., 2016a).....	70

Figure III-9: Main rheological domain of Saharan Africa centered on the Saharan metacraton from Liégeois et al., (2013).....	75
Figure III-10: (A) Historical subdivision. (B) Actual Tuareg shield terrane mapped (Liégeois et al., 2003). (C) Proposed geodynamic evolution of western and central Hoggar between 900 and 520 Ma (Caby, 2003).....	76
Figure III-11: Interpretative sketch summarizing the geodynamic evolution of the Tassendjanet-Tidéridjaouine terrane (western part of the Hoggar Massif) deduced from data collected on eclogite and garnetamphibolites (Berger et al., 2014).....	77
Figure III-12: Tuareg Shield formation: terranes accretion modified from Liégeois et al., (2003). (A) 900 Ma: LATEA constitutes a passive margin without any applied stress; this is the period of the building of the Iskel island arc with the subduction plane dipping away from LATEA craton; the limits of the greater LATEA craton is inferred from available drillings (Latouche, pers. observations). (B) 870–850 Ma: accretion of the Iskel island arc onto the LATEA cratonic passive margin. (C) Accretion onto LATEA of juvenile terrains represented by eclogites, ophiolites and other various oceanic lithologies, including that studied here in the Tin Begane area. (D) Period of metacratonization of LATEA: LATEA is squeezed between the West African craton (WAC) to the east and the Saharan craton (SC) or metacraton (SmC) to the east. LATEA is dissected by mega-shear zones generating linear lithospheric delamination and asthenospheric uprise.....	79
Figure III-13: (A) Main rheological domains from North-West Africa with enhancement of the LATEA metacraton and of the Djanet and Edembo metacratonic terranes (Liégeois et al., 2013). (B) Schematic model section at 570–550 Ma of the Murzuq craton. Metacratonization resulted from the intracontinental convergence of the Murzuq craton, relaying a northern unknown continent push and the relatively stable Tuareg shield, leant against the West African craton (Fezaa et al., 2010; Liégeois et al., 2013).....	80
Figure III-14: Sketched E–W cross-sections through the Tuareg Shield showing terranes accretion (Liégeois, 2019).	81
Figure III-15 Lithospheric model based on geology and tomography showing differential lithospheric thickness between terranes and cratonic cores from Liégeois et al., (2005).	82
Figure III-16: Archean terrane of In Ouzzal structural style in "dome and basins" reactivated during the Paleoproterozoic Eburnean orogeny via the mega shear zones (Benbatta et al., 2016).	84
Figure III-17: (A) Evolution of North Africa during the Pan-African orogeny modified from Craig et al., (2008). (B) Paleogeographic reconstruction of the supercontinent Gondwana at the	

end of the Pan-African cycle relating the distribution of stable cratons and Pan-African mobile belts modified from Craig et al., (2008).	85
Figure III-18: Late-orogenic Panafrican molasses basins of In Semmen and of Ouallen (Ahmed and Moussine-Pouchkine, 1987).	87
Figure III-19: (A) Thickness and facies lateral variation of Cambro-Ordovician series on the Arak-Foum Belrem Arch (Beuf et al., 1968b). (B) Syn-tectonic conglomerates in Cambro-Ordovician series on the Arak-Foum Belrem Arch (Beuf et al., 1968b). (C) Syn-tectonic conglomerates in Cambro-Ordovician series on the Arak-Foum Belrem Arch (Beuf et al., 1971).	89
Figure III-20: (A) EW cross section on the Tihemboka Arch (Illizi Basin) showing variation of thickness, wedges strata in the Cambro-Ordovician series. (B) NNW-SSE cross section on the Azzel Matti Arch (Ahnet Basin) showing variation of thickness, wedges strata in the Cambro-Ordovician series. (C) Cross-section between in the Berkine Basin and the Ahara High, showing the stratigraphic pinchout of the Cambro-Ordovician succession on the northern flank of the Ahara High. (D) Seismic section on the southern flank of the Berkine Basin illustrating the onlap configuration of the Cambro-Ordovician, and the thickness reduction of the Silurian and Devonian succession. Images from published paper (Eschard et al., 2010).	90
Figure III-21: Geological section of the Ordovician formations in North Africa illustrating the gully associated with the Taconic unconformity (Echikh, 1998)	91
Figure III-22: Isopachs map of syn-glacial Tamadjert Formation in the Illizi basin. The geometry seems compatible with an NE–SW extensional direction resulted in a transtension along the N–S and NNW–SSE major lineaments and the formation of pull-apart basins during the deposition of the Tamadjert Formation (Zazoun and Mahdjoub, 2011).	92
Figure III-23: Constraints regime in Cambro-Ordovician series in the Illizi basin (Zazoun and Mahdjoub, 2011).	93
Figure III-24: Paleogeography of the Gondwana at the Upper Ordovician (Veevers, 2005). At that time, Gondwana is partly covered by a large ice cap. During the period of maximum ice extension, the ice cap covered more than half of the South American continent and the Arabian Peninsula, as well as almost the entire African continent.	94
Figure III-25: Palaeo-glaciological reconstructions of the Late Ordovician Saharan ice sheet modified from Heron and Craig, (2008) showing both Ice sheet configuration at glacial maximum position and during its stepwise recession.	95
Figure III-26: (A) EW cross section in the Illizi basin and the Tihemboka Arch showing variation of thickness, angular unconformities, wedges strata in the lower Devonian series	

(Eschard et al., 2010). (B) Correlation of the Devonian succession on the northern flank of the Ahara High where we observe the complete pinchout of the Gedinnian fluvial unit on the flank of the high (Eschard et al., 2010). (C) Cross-section showing the stratigraphic architecture of the Siluro-Devonian succession between the Ghadames Basin and the Gargaff Arch (Eschard et al., 2010).....97

Figure III-27: (A) EW cross section on the Tihemboka Arch (Illizi basin) showing variation of thickness, angular unconformities, wedges strata in the lower Devonian series (Beuf et al., 1971). (B) Thickness variation and sandy lense (Beuf et al., 1971). (C) EW cross section through the Ahnet and Mouydir basin in the Siluro-lower Devonian series showing variation of thickness near Azzel Matti and Arak-Foum Belrem Arches (Beuf et al., 1971) see also (Biju-Duval et al., 1968).98

Figure III-28: (A) Thickness and facies variations of Siluro-Devonian formations on the Idjerane axis (i.e. Arak-Foum belrem Arch) (Legrand, 1967a). (B) Thickness and facies variations of Siluro-Devonian formations in the Bled El Mass area (i.e. Azzel Matti Arch) (Legrand, 1967a). (C) EW cross section in the Illizi basin and the Tihemboka Arch showing variation of thickness, angular unconformities, wedges strata in the lower Devonian series (Legrand, 1967a).99

Figure III-29: (A) Pinch out of Middle-Upper Devonian series on the Tihemboka Arch (Chaumeau et al., 1961). (B) Pinch out of Middle-Upper Devonian series on the Tihemboka and Gargaf Arches (Fabre, 2005). (C) Pinch out of Middle-Upper Devonian series on the Ougarta chain, Djebel Heche, Touat, Azzel Matti and the Ahnet basin (Legrand, 1967a)... 101

Figure III-30: The structural context of the Bechar Basin (Algeria) (Frizon de Lamotte et al., 2013). (a) Line drawing illustrating the geometry of the Bechar Basin at depth; notice that the tilted blocks at depth were folded during the Variscan Orogeny together with the Upper Devonian (?)–Carboniferous infilling of the Bechar Basin. (b) Schematic diagram synthesizing the tectonic history of the Bechar Basin during the Paleozoic and Mesozoic. 102

Figure III-31: EW cross section in the Ahnet and Mouydir basins in the Carboniferous series showing variation of thickness near Azzel Matti and Arak-Foum Belrem Arches (Wendt et al., 2010b). 104

Figure III-32: Permo-Carboniferous intra-plate deformation of the Sahara Platform forming the foreland of the Mauretaniides-Atlas orogen. Arrows indicate axes of major Arches. Schematic evolutionary diagram of Ougarta trough modified from Dallmeyer and Lécorché, (1991); Ziegler et al., (1995). Ti = Tinduff basin, Ta = Taoudeni basin, Tm = Timimoun basin, Gh = Cihadames basin, MO = Mourzouk basin. (1) major faults, (3) rift, (4) Late Carboniferous

thrusting, (5) Lower Permian thrusting, (6) Lower Permian-Late Carboniferous folded chain, (7) major extruded Arches, (8) terminal Carboniferous shortening direction, (9) terminal Permian shortening direction.	105
Figure III-33: Main extension phases during the Tethys and Atlantic opening reactivating major ancient faults lineaments (Fairhead et al., 2013).	106
Figure III-34: Schematic structural section across the Hoggar Massif from the Berkine Basin in the north to the Iullemeden Basin in the south from English et al., (2016b). Note that the Hoggar had an earlier history of uplift with significant erosion of the Paleozoic sequence during the Hercynian orogeny. For localization see 4 in Figure III-2.	107
Figure III-35: Thermal history curves of the Paleozoic North Saharan Platform (peri-Hoggar basins) compiled from literature: 1 : well in the Illizi basin (Wells et al., 2018); 2 : well model A and 3 : G in Ghadamès-Berkine basin (Underdown et al., 2007); 4 : well OTRA-1 in the Sbâa basin, 5 : well RG-3 in the Reggane basin, 6 : well TEG-1 in the Timimoun basin, 7 : well in the eastern Ahnet basin (Logan and Duddy, 1998); 8 : well F3-NC174, 9 : well H29-NC115, 10 : well NC-174, 11 : well NC-115, 12 : well NC-186, 13 : well NC-190 in Murzuq basin (Belaid et al., 2010); 14 : well A-76 well in Murzuq basin (Galushkin and Eloghbi, 2014).	108
Figure III-36: Paleozoic litho-stratigraphic, sequence stratigraphy and tectonic framework of the Peri-Hoggar basins (North African Saharan Platform) compiled from (1) Chronostratigraphic chart (Ogg et al., 2016), (2) The Cambrian–Silurian (Askri et al., 1995) and the Devonian–Carboniferous stratigraphy of the Reggane basin (Cózar et al., 2016; Lubeseder, 2005; Lubeseder et al., 2010; Magloire, 1967; Wendt et al., 2006), (3) The Cambrian–Silurian (Paris, 1990; Wendt et al., 2006) and the Devonian–Carboniferous stratigraphy of the Ahnet basin (Beuf et al., 1971; Conrad, 1973, 1984; Legrand-Blain, 1985; Wendt et al., 2006, 2009a), (4) The Cambrian–Silurian (Askri et al., 1995; Paris, 1990; Videt et al., 2010) and the Devonian–Carboniferous stratigraphy of the Mouydir basin (Askri et al., 1995; Beuf et al., 1971; Conrad, 1973, 1984; Wendt et al., 2006, 2009a), (5) The Cambrian–Silurian (Eschard et al., 2005; Fekirine and Abdallah, 1998; Jardiné and Yapaudjian, 1968; Videt et al., 2010) and the Devonian–Carboniferous stratigraphy of the Illizi basin (Eschard et al., 2005; Fekirine and Abdallah, 1998; Jardiné and Yapaudjian, 1968), (6) The Cambrian–Silurian (Dubois, 1961; Dubois and Mazelet, 1964; Eschard et al., 2005; Henniche, 2002; Videt et al., 2010) and the Devonian–Carboniferous stratigraphy of the Tassili-N-Ajjers (Dubois et al., 1967; Eschard et al., 2005; Henniche, 2002; Wendt et al., 2009a), (7) The whole stratigraphy of the Murzuq basin (Echikh and Sola, 2000), (8) The whole stratigraphy of the Tim Mersoï basin (Coquel et al., 1995; Denis et al., 2007; Joulia, 1963), (9) 2 nd order sequence stratigraphy	

of the Saharan Platform (Carr, 2002; Eschard et al., 2005; Fekirine and Abdallah, 1998), **(10)** 3rd order sequence stratigraphy of the Saharan Platform (Djouder et al., 2018; Eschard et al., 2005; Fröhlich et al., 2010b; Lubeseder, 2005; Lubeseder et al., 2010; Wendt et al., 2006), **(11)** Eustatic and climatic chart (Haq and Schutter, 2008; Scotese et al., 1999), **(12)** Tectonic events (Boudjema, 1987; Coward and Ries, 2003; Craig et al., 2008; Guiraud et al., 2005; Lüning, 2005); **(A)** Infra-Tassilian (Pan-African) unconformity, **(B)** Intra-Arenig unconformity, **(C)** “Taconic” and glacial unconformity, **(D)** Isostatic rebound unconformity, **(E)** Caledonian unconformity, **(F)** Hercynian unconformity. ***16:** Conrad, (1984) and Wendt et al., (2009a) dated the formation Carboniferous; ***15:** Iridet Dalle dated Late Touraisian Early-Viséan by ammonoids (Korn et al., 2010a); ***14:** Orsine fm. dated Emsian by abundant microfauna (Eschard et al., 2005); ***13:** Unit C2 dated Pragian by palynomorphs (Eschard et al., 2005); ***12:** Oued Saret sandstones dated Lower Llandeilo (Oulebsir and Paris, 1993; Paris et al., 2000a); ***11:** Azzel-Tiferouine shales dated Arenig to Llandeilo (Paris et al., 2000a); ***10:** Ouargla sandstones dated Arenig (Oulebsir and Paris, 1993); ***9:** In Tahouite fm. dated Arenig by brachiopods and lamellibranches (Legrand, 1964); ***8:** Hamra’s Quartzite/Unit III-2 dated Arenig (Eschard et al., 2005); ***7:** El Gassi shales/Unit III-1 dated Tremadoc by Graptolites and Chitinozoan (Legrand, 1964; Paris et al., 2000a); ***6:** Vire du Mouflon dated Lower Ordovician by brachiopods and lamellibranches (Legrand, 1964); ***5:** Unit IV /Tamadjert fm. dated Late Ashgill (Oulebsir and Paris, 1993); ***4:** Unit B Dalle dated Pridoli (Henniche, 2002); ***3:** M’Kratte Dalle dated Late Ordovician (Oulebsir and Paris, 1993); ***2:** Graptolites shales dated from Llandovery to Upper Ludlow (Legrand, 1964); ***1:** Unit M dated Wenlock to Ludlow (Boumendjel et al., 1988; Henniche, 2002). 111

Figure III-37: Paleozoic plate reconstruction of the north Gondwana modified from Blakey, (2008). 114

Figure III-38: Cambro-Ordovician synthesis of biostratigraphic zonation compiled from bibliography. (1) Time slices. (2) Chitizonoan biozones of North Gondwana (Paris, 1990; Paris et al., 2000b; Videt et al., 2010). (3) Chitizonoan biozones of Illizi (Eschard et al., 1999; Paris et al., 2000b). (4) Miospores biozones (Richardson and McGregor, 1986). (5) Miospores biozones (Streel et al., 1987). (6) Miospores biozones (Richardson and McGregor, 1986). (7) Miospores biozones (Rubinstein and Steemans, 2002). (8) Miospores biozones (Kermandji, 2007, 2012; Kermandji et al., 2008, 2009). (9) Miospores biozones (Boumendjel, 1987). (10) Miospores biozones (Massa, 1988). (11) Miospores biozones (Moreau-Benoit et al., 1993). (12) Miospores biozones (Abdesselam-Rouighi, 1986, 2003, 2003). (13) Acritaches biozones

(Jardiné et al., 1974). (14) Graptolites biozones (Videt et al., 2010). (15) Conodontes biozones (Wendt et al., 2010b). (16) Ammonites zonations (Korn et al., 2007, 2010a, 2010b).	118
Figure III-39: Devono-Carboniferous synthesis of biostratigraphic zonation compiled from bibliography. (1) Time slices. (2) Chitizonoan biozones of North Gondwana (Paris, 1990; Paris et al., 2000b; Videt et al., 2010). (3) Chitizonoan biozones of Illizi (Eschard et al., 1999; Paris et al., 2000b). (4) Miospores biozones (Richardson and McGregor, 1986). (5) Miospores biozones (Streel et al., 1987). (6) Miospores biozones (Richardson and McGregor, 1986). (7) Miospores biozones (Rubinstein and Steemans, 2002). (8) Miospores biozones (Kermandji, 2007, 2012; Kermandji et al., 2008, 2009). (9) Miospores biozones (Boumendjel, 1987). (10) Miospores biozones (Massa, 1988). (11) Miospores biozones (Moreau-Benoit et al., 1993). (12) Miospores biozones (Abdesselam-Rouighi, 1986, 2003, 2003). (13) Acritaches biozones (Jardiné et al., 1974). (14) Graptolites biozones (Videt et al., 2010). (15) Conodontes biozones (Wendt et al., 2010b). (16) Ammonites zonations (Korn et al., 2007, 2010a, 2010b).	119
Figure III-40: Localization of different cross sections of north peri-Hoggar Basins georeferenced and compiled from bibliography. See Figure III-2 for geological legend and localization.	121
Figure III-41: Localization of different cross sections of south peri-Hoggar Basins georeferenced and compiled from bibliography. See Figure III-2 for geological legend and localization.	122

CHAPTER IV:

Figure IV-1: Fault drag of a central marker along normal and reverse (thrust) faults. Normal drag refers to markers that are convex in the direction of slip and reverse drag to markers that are concave in the direction of slip. The angle θ is the acute angle measured from the fault to the undeformed central marker (anticlockwise angles are positive). The presented work demonstrates that low angles favor normal drag and high angles favor reverse drag modified from Grasemann et al., (2005).	128
Figure IV-2: (A) Development of a syn-depositional syncline during extensional tectonics modified from Guiraud and Seguret, (1985). The syncline develops on a tilted basement block overlain by a competent-incompetent layer. (B) Fold and fault patterns associated with extensional/compressional forced folding modified from Patton and Fletcher, (1995) and Withjack et al., (1990). (1-2) normal, (3) vertical, and (4) reverse fault basement.	129
Figure IV-3: (A) Schematic diagram of a classical positive inversion structure; A, B and C are stratigraphic sequences. A, prerift; B, synrift; C, postrift sequence modified from Williams et	

al., (1989). (B) Deformation styles of shortened (inverted) normal fault systems: (1) normal fault localizing thrust-ramp; (2-3) thrust ramp decapitating an early normal fault modified from Bonini et al., (2012).....	130
Figure IV-4: Growth strata as records of fold kinematics (folding by progressive limb rotation) modified from Shaw et al., (2005).	132

CHAPTER V:

Figure V-1: Geological map of the Paleozoic North Saharan Platform (North Gondwana) showing the localization of geological map zooms, structural interpretations zooms and regional seismic cross sections. 1: Figure V-4; 2: Figure V-5; 3: Figure V-6; 4: Figure V-7; 5: Figure 5b in (Perron et al., 2018); 6: Figure V-14B; 7: Figure V-17A; 8: Figure VII-12; 9: Figure V-8. (a): Figure V-2A; (b): Figure V-2B; (c): Figure V-3A; (d): Figure V-3B. Ah. B.: Ahnet Basin; Mo. B.: Mouydir Basin.	177
Figure V-2: (A) EW seismic profile of Ahnet Basin showing Arches and basins architectures between Bahar El Hammar intra-arches and Fom Belrem interbasin boundary secondary arch. (B) NW-SE seismic cross section from Sbâa to Ahnet Basins going through the Azzel Matti Arch and Ara-Fom Belrem Arch. See (a) and (b) in Figure V-1 for localization.	178
Figure V-3: (A) SSW-NNE seismic cross section through the Reggane, the Sbâa and the Timimoun Basins showing Arches and basins architectures. (B) W-E seismic cross section from the Reggane to the Ahnet Basins separated by Azzel Matti Arch and Arak-Fom Belrem Arch. See (c) and (d) in Figure V-1 for localization.	179
Figure V-4: (A) Satellite images of the Reggane, Ahnet, and Mouydir Basins (Landsat 7 ETM + from USGS database). (B) Geological map of the Paleozoic of the Reggane, Ahnet, and Mouydir Basins associated with the different terranes. For the legend and references see Figure V-1. Localization of map 1: Figure VII-13 and Figure V-9. Localization of the interpreted seismic profiles a: Figure 7b in (Perron et al., 2018); b: Figure 7a in (Perron et al., 2018); c: Figure 7c in (Perron et al., 2018); d: Figure 7d in (Perron et al., 2018); e: Figure V-26; f: Figure V-19; g: Figure V-20; h: Figure V-21; i: Figure V-25; j: Figure V-18.	181
Figure V-5: Structural map of Amguid El Biod Arch. The blue and red colors corresponding respectively to Cambro-Ordovician structures and Devonian structures (to Carboniferous?). 1: Figure V-16A; 2: Figure V-14A. For localization of the map see Figure V-1.	182
Figure V-6: Structural map of Arak-Fom Belrem Arch. The blue, red and green colors corresponding respectively to Cambro-Ordovician structures, Devonian structures and Carboniferous (Hercynian). 1: Figure 5a in (Perron et al., 2018); 2: Figure V-15; 3: Figure V-13;	

4: Figure V-22; 5: Figure V-11A; 6: Figure 6d in (Perron et al., 2018); 7: Figure V-11B. For localization of the map see Figure V-1.....	183
Figure V-7: Structural map of Ahnet Basin and Azzel Matti Arch. The blue, red and green colors corresponding respectively to Cambro-Ordovician structures, Devonian structures and Carboniferous (Hercynian). 1: Figure V-12A; 2: Figure V-12B; 3: Figure V-23; 4: Figure V-24; 5: Figure V-17B. For localization of the map see Figure V-1.....	184
Figure V-8: Schematic structural section across the Hoggar Massif and the peri-Hoggar Basins showing in 2D map projection the architecture of the basins modified from English et al., (2016b). Note that the Hoggar had two history of uplift with significant erosion of the Paleozoic sequence during the Hercynian orogeny and the Late Eocene. For localization see Figure V-1.	185
Figure V-9: Example of Mouydir Basin a synsedimentary syncline-shaped basin delimited by arches showing maximum of thickness of series at the center and reduce approaching arches. See Figure V-4 for localization.	186
Figure V-10: (A) Thin-skinned vs thick-skinned tectonic style modified from Tozer et al., (2002); In (1) uplift and folding have resulted from thin-skinned thrusting and duplication of the stratigraphy at depth. In contrast, uplift in interpretation in (2) is due to reactivation of a pre-existing extensional fault that originally hosted an increased thickness of sediment. (B) Structural pattern of a dextral strike-slip fault (Riedel shear) modified from Sylvester, (1988). (C) Example of tectonic structures present in a strike slip zone modified from Guiraud, (1990); (1) Deformation of the sedimentary cover by folds arranged in echelon on a basement strike-slip fault; (2) Positive flower structures associated to strike-slip component in a fault zone. (D) Map and cross-sections of a generic strike-slip fault system, showing flower structures and duplexes; (1) Positive flower structure and (2) Negative flower structure modified from Woodcock and Fischer, (1986).	190
Figure V-11: (A) Normal fault associated with footwall anticline and hanging wall syncline (i.e. forced fold). (B) Syn-sedimentary normal fault in Mid-Upper Devonian inverted. For localization see 5 and 7 in Figure V-6.....	192
Figure V-12: (A) Syn-sedimentary normal fault in Cambro-Ordovician series and inversion of Lower Devonian on Silurian detachment layer. (B) Divergent onlaps over Azzel Matti basement (“series Pourprée”). For localization see 1 and 2 in Figure V-7.	193
Figure V-13: (A) Not interpreted Google Earth image (B) Interpreted Google Earth image showing NS normal sinuous and straight faults in Cambro-Ordovician series (C) 3D Google Earth image showing relief. For localization see 3 in Figure V-6.	194

Figure V-14: (A) Structural interpretation of Google earth satellites images of Aguelman area showing poly-historic paleo-reliefs (ancient normal fault escarpment associated to a footwall anticline and a hanging wall syncline) sealed by Silurian deposits. (B) Structural interpretation of Google earth satellites images showing growth strata (wedges) in Siluro-Devonian series. OTh: In Tahouite formation (Early to Late Ordovician, Floian to Katian), OTj: Tamadjert Formation (Late Ordovician, Hirnantian), sIm: Imirhou formation (Early Silurian), sdAt: Atafaïtafa formation (Middle Silurian), dTi: Tifernine formation (Middle Silurian). 1: Cambro-Ordovician extension, 2: Silurian sealing (horizontal drape). For localization see 2 in Figure V-5 for (A) and 6 in Figure V-1 for (B). 195

Figure V-15: (A) 3D Google Earth image of Arak-Foum Belrem Arch with localization of cross sections. (B) Google earth satellites images of Adrar Tiggad-N-Teghlamt (near Arak-Foum Belrem Arch, eastwards inter-basin boundary secondary arch). (C) Structural interpretation Google earth satellites images showing normal fault inverted structure associated with folding (tectonic transport from hanging wall to footwall), detachment layer in Silurian shales series; Strata geometries shows divergent onlap in Silurian series in the hanging wall. (SSi: Basement and infra-Cambrian series, CoAj: Ajers formation (Late Cambrian), OTh: In Tahouite formation (Early to Late Ordovician, Floian to Katian), OTj: Tamadjert Formation (Late Ordovician, Hirnantian), sIm: Imirhou formation (Early Silurian), sdAs1: Asedjrad formation 1 (Late Silurian to Early Devonian), dAs2: Asedjrad formation 2 (Early Devonian, Lochkovian), dSa: Oued Samene formation (Early Devonian, Pragian). 1: Cambro-Ordovician extension, 2: Siluro-Devonian reactivation (Caledonian event) to Herycnian (?). For localization see 1 and 2 in Figure V-6..... 196

Figure V-16: (A) Structural interpretation of Google earth satellites images near Oued In Rhlem (near Amguid El Biod Arch, inter-basin boundary secondary arch) showing normal fault; Strata geometries shows divergent onlap in Lower Devonian series in the hanging wall. For localization see 1 in Figure V-5. (B) Structural interpretation of Google earth satellites images of Djebel Idjerane in the Mouydir basin (near Arak-Foum Belrem Arch, eastwards inter-basin boundary secondary arch) showing a normal fault (footwall anticline and syncline hanging wall). Thickness variation of Imirhou formation (Early Silurian) between footwall and hanging wall. For localization see 1 in Figure V-22 and 4 in Figure V-6. OTj: Tamadjert Formation (Late Ordovician, Hirnantian), sIm: Imirhou formation (Early Silurian), sdAs1: Asedjrad formation 1 (Late Silurian to Early Devonian), dAs2: Asedjrad formation 2 (Early Devonian, Lochkovian), dSa: Oued Samene formation (Early Devonian, Pragian) d2b: Givetian, d3a: Meden Yahia formation (Late Devonian, Frasnian)..... 197

- Figure V-17: (A) Structural interpretation of Google earth satellites images near Tihemboka arch (inter-basin arch) showing angular unconformity in Upper Silurian-Lower Devonian series in the hanging wall. For localization see 7 in Figure V-1. (B) Structural interpretation of Google earth satellites images near Azzel Matti Arch (inter-basin boundary secondary arch) showing normal blind fault; Strata geometries shows onlap in Lower Devonian series in the hanging wall. For localization see 5 in Figure V-7. sIm: Imirhou formation (Early Silurian), sdAs1: Asedjrad formation 1 (Late Silurian to Early Devonian), dAs2: Asedjrad formation 2 (Early Devonian, Lochkovian), dSa: Oued Samene formation (Early Devonian, Pragian)..... 198
- Figure V-18: (A) NS seismic profile of near Djoua arch (inter-basin arch between the Ahnet and the Timimoun basins); (B) Interpreted seismic profile showing steeply-dipping basement normal blind faults associated to forced folding forming a horst; At the south, a structures is featured by reverse fault propagation fold (inversion); Strata lapout geometries shows Frasnian onlaps on top Givetian and diminution of Frasnian near the arch; Truncature of Paleozoic series by Mesozoic unit on Hercynian unconformity. For localization see j in Figure V-4..... 199
- Figure V-19: (A) West-East seismic profile in the Ahnet basin near Erg Teguentour (near Arak-Foum Belrem Arch, westwards inter-basin boundary secondary arch) (B) Interpreted seismic profile showing steeply-dipping westwards basement normal blind faults associated to forced folding; Strata lapout geometries shows lower Silurian onlaps on the top Ordovician, upper, onlaps and downlaps of Frasnian series on top Givetian unit. For localization see f in Figure V-4..... 200
- Figure V-20: (A) NW-SE seismic profile in the Ahnet basin near Erg Teguentour (near Arak-Foum Belrem Arch, westwards inter-basin boundary secondary arch) (B) Interpreted seismic profile showing steeply-dipping westwards basement normal blind faults associated to forced folding; Strata lapout geometries shows lower Silurian onlaps on the top Ordovician, glacial valley in intra-Ordovician series, onlaps and downlaps of Frasnian series on top Givetian unit. For localization see g in Figure V-4..... 201
- Figure V-21: (A) West-East seismic profile in the Ahnet basin near Erg Teguentour (near Arak-Foum Belrem Arch, westwards inter-basin boundary secondary arch). (B) Interpreted seismic profile showing steeply-dipping westwards basement normal blind faults associated to forced folding; Strata lapout geometries shows lower Silurian onlaps on the top Ordovician, upper, onlaps and downlaps of Frasnian series on top Givetian unit. For localization see h in Figure V-4..... 202
- Figure V-22: (A) Not interpreted Google Earth image with localization of maps; **1**: Figure V-16B; **2**: Figure 6f in Perron et al., (2018); **3**: Figure 6e in Perron et al., (2018). (B) Interpreted

Google Earth image showing NS echelons folds in Devonian series. (C) 3D Google Earth image showing relief. (D) Model of en echelon dextral folds. For localization see 4 in Figure V-6.203

Figure V-23: (A) Not interpreted Google Earth image. (B) Interpreted Google Earth image near Azzl Matti Arch showing echelon fold with a senestral strike slip movement in Devonian series. (C) 3D Google Earth image showing relief. (D) Model of en echelon senestral folds. For localization see 3 in Figure V-7.204

Figure V-24: (A) Not interpreted Google Earth image with localization of map; **1**: Figure 6e in (Perron et al., 2018). (B) Interpreted Google Earth image showing dextral strike slip fault associated to horse tails structures in Devonian series (C) 3D Google Earth image showing relief. (D) Model of horse tails strike slip. For localization see 4 in Figure V-7.205

Figure V-25: (A) West-East seismic profile of Bahar el Hammar in the Ahnet basin (Ahnet intra-basin arch); (B) Interpreted seismic profile showing steeply-dipping eastwards normal fault inverted structure associated with folding (convex drag in each part of the fault); Strata lapout geometries shows glacial valley in the Ordovician series, Silurian onlaps on top Ordovician, Silurian onlaps on top Ordovician; Frasnian onlaps on top Givetian; Polyphased events: Cambro-Ordovician extension and Devo-Carboniferous positive inversion (tectonic transport from hanging wall to footwall). For localization see i in Figure V-4.206

Figure V-26: (A) SN seismic profile near the Foug Belrem Arch. (B) Interpreted SN seismic profile near the Foug Belrem Arch showing glacial valley in the Ordovician series, Silurian onlaps on the top Ordovician limit, downlaps and onlaps structures in Frasnian series on the top Givetian, Pan-African unconformity, Pan-African paleo-thrusting. For localization see e in Figure V-4.208

Figure V-27: Comparison between classical extensional basin and peri-Hoggar intracratonic basins structural style. Notice that faults morphologies impact the sedimentation pattern.210

Figure V-28: Synthesis of structural model, stratigraphic lapout identified from satellite images and seismic profiles during the Paleozoic time on the Saharan Platform. (i), (ii), (iii) correspond to structural models proposed in Perron et al., 2018.213

Figure V-29: Geological map of the Paleozoic North Saharan Platform (North Gondwana) showing the localization of regional wells cross sections. **(a)**: Figure V-33; **(b)**: Figure V-32; **(c)**: Figure V-39; **(d)**: Figure V-35; **(e)**: Figure V-34; **(f)**: Figure V-36; **(g)**: Figure V-42; **(h)**: Figure V-37; **(i)**: Figure V-40; **(j)**: Figure V-38; **(k)**: Figure V-41. Sb. B.: Sbâa Basin; Ah. B.: Ahnet Basin; Mo. B.: Mouydir Basin.214

Figure V-30: Example of sequence stratigraphy limit with the depositional environments associated with their gamma-ray signature and well-logs patterns (i.e. electro-facies) in (A) the Ordovician series and (B) in the Devonian series. Example of representative electrofacies of Cambro-Ordovician and Devonian successions used as a pattern for regional well correlations of peri-Hoggar Basins.....	216
Figure V-31: Core sedimentologic description of well MSR-1 in Devonian series in Ahnet Basin. The palynological datation is from published paper (Kermandji et al., 2008) and the core description from internal study (Aissani and Bennamane, 2003).	217
Figure V-32: North EW wells cross section of North peri-Hoggar Basins (Reggane-Ahnet-Mouydir-Illizi Basins). Horizontalization on top Pragian transgression. For localization see Figure V-29.	219
Figure V-33: South EW wells cross section of North peri-Hoggar Basins (Reggane-Ahnet-Mouydir-Illizi Basins). Horizontalization on top Pragian transgression. For localization of the cross section see Figure V-29.	220
Figure V-34: EW cross wells section in the North part of the Ahnet Basin. Horizontalization on top Pragian transgression. For localization of the cross section see Figure V-29.....	221
Figure V-35: EW cross wells section in the central part of the Ahnet Basin. Horizontalization on top Pragian transgression. For localization of the cross section see Figure V-29.....	222
Figure V-36: NS wells cross section of North peri-Hoggar basins (Ahnet-Sbâa-Reggane Basins). Horizontalization on top Givetian transgression. For localization of the cross section see Figure V-29.	223
Figure V-37: NS wells cross section of North peri-Hoggar basins (Ahnet-Timimoun Basins). Horizontalization on top Pragian transgression. For localization of the cross section see Figure V-29.	224
Figure V-38: NS wells cross section of North peri-Hoggar basins (Mouydir-Timimoun Basins). Horizontalization on top Givetian transgression. For localization of the cross section see Figure V-29.	225
Figure V-39: EW wells cross section of North peri-Hoggar basins (Reggane-Sbâa-Timimoun Basins). Horizontalization on top Givetian transgression. For localization of the cross section see Figure V-29.	226
Figure V-40: NS wells cross section of North peri-Hoggar basins (Ahnet-Timimoun Basins). Horizontalization on top Givetian transgression. For localization of the cross section see Figure V-29.	227

Figure V-41: NS wells cross section of North peri-Hoggar basins (Timimoun Basin). Horizontalization on Lower Silurian transgression. For localization of the cross section see Figure V-29.....	228
Figure V-42: NS wells cross section of North peri-Hoggar basins (Sbâa-Timimoun Basins). Horizontalization on top Givetian transgression. For localization of the cross section see Figure V-29.....	229

CHAPTER VI:

Figure VI-1: Conceptual model of the subsidence mechanism between arches and basins depocenter extracted from geological observations in previous chapter.....	233
Figure VI-2: Example of idealize model ingredients for numerical physic calculation.....	234
Figure VI-3: Compilation of backstripped tectonic subsidence of intracratonic basins modified from literature (Allen and Armitage, 2011; Xie and Heller, 2009) showing periods of acceleration (ALRS), deceleration (DLRS) and inversion (ILRS) of the low rate subsidence. 1: Ghadames/Berkine Basin, Algeria (Yahi, 1999); 2: Illinois Basin (Bond and Kominz, 1984); 3: Michigan Basin (Bond and Kominz, 1984); 4: Williston Basin, North Dakota (Bond and Kominz, 1984); 5: Williston Basin, Saskatchewan (Fowler and Nisbet, 1985); 6: Paraná Basin, Brazil, CB-3 well (Oliveira, 1987 from Allen and Armitage, 2011); 7: Northeast German Basin (Scheck and Bayer, 1999); 8: Southwest Ordos Basin (Xie, 2007 from Xie and Heller, 2006); 9: Paris Basin (Prijac et al., 2000); 10: West Siberian Basin, Russia, Urengoy well (Saunders et al., 2005); 11: West Siberian Basin, Russia, Samotlar-39 well (Saunders et al., 2005); 12: Paraná Basin (Zalan et al., 1990); 13: A1NC43 Al Kufrah basin (Holt et al., 2010); 14: Ghadamès basin (Holt et al., 2010); 15: Well W17 in Ahnet Basin (Perron et al., 2018).....	238
Figure VI-4: Isostasy equilibrium potential by an Airy calculation between Archean and Proterozoic terranes (see Appendix A).....	241
Figure VI-5: a) Inputs models (model P, A and M) of the different simulations with the different parameters applied in experiments such as b) the far fields stresses (sinusoidal extension-compression 40 Myr) and c) the thermal anomaly. d) Yield-strength envelopes of the simulated materials calculated for a strain rate of $1.5 \cdot 10^{-11} \text{ s}^{-1}$. $\Delta\sigma$ represents the deviatoric stress, positive values under extension and negative values under compression. e) Initial temperature state of the lithosphere for all the simulations presented.....	242
Figure VI-6: (A1) Model A with thermal anomaly shows no creation of basin. (P1) Model P with thermal anomaly shows no creation of basin. (P2) Model P with far field stresses shows the creation of eights narrow basins with chaotic stratigraphic architecture near shear zones.	

(A2) Model A with far field stresses displays the formation of four narrow basins with chaotic stratigraphic architecture above shear zones.....	246
Figure VI-7: Subsidence curves from different models in Figure VI-6 (wells W1-A1 to W1-A2 and W1-P1 to W1-P2) associated with Figure 1 bibliographic data. The thermal subsidence of W1-A1 and W1-A2 is achieved after 150 Myr. The wells P1 and P2 show linear decay subsidence with deviations of different amplitude. Boundary conditions: E=Extension and C=Compression.....	247
Figure VI-8: (M1) Model M with thermal anomaly displays the creation of arches and basins architecture (i.e. One central basin and two peripheral basins separated another by arches). (M3) Model M without thermal anomaly shows the same architecture of basins than M1 demonstrating the minor influence of thermal anomaly. (M2) Model M with far filed stresses and without thermal anomaly modifies peripheral basins structural architecture by flattening the bottom. (M4) Model M with far field stresses and thermal anomaly modifies central basin structural architecture (i.e. formation of grabens above the shear zones).	248
Figure VI-9: Subsidence curves from different models in Figure VI-8 (wells W1-M1 to W1-M4) associated with Figure 1 bibliographic data. The subsidence of W1-M1 and W1-M2 is constant after 250 Myr (i.e. still have a potential of subsidence). The wells W1-M2 and W1-M4 show linear decay subsidence with deviations of different amplitude. Boundary conditions: E=Extension and C=Compression.	249
Figure VI-10: (A) Tectono-stratigraphic basins architecture and heat production of Model M5 without thermal anomaly shows stratigraphic lapout (i.e. onlap, truncatures and thickness variations) features when approaching the arches; (B) Stratigraphy and hiatus repartition between the wells W1-M5 to W3-M5; (C) Subsidence curves of well W1-M5 to W3-M5 are characterized by exponential decay shape.	252
Figure VI-11: Comparison between model M3 and M5 showing increase of the temperature under the basins with lateral sediment supply due to heat production of the basement.....	253
Figure VI-12: (A) Model M with far field tectonics, lateral sediment flux and thermal anomaly shows a complexification of the basins and arches architecture within Figure VI-10 with the set-up of inter-basins boundary secondary arches and intra-basin secondary arches. The strain is concentrated in the central basin with creation of grabens above shear zones (i.e. limits of terranes); (B) Stratigraphy and hiatus repartition between the wells W1-M6 to W5-M6; (C) Subsidence curves of wells W1-M6 to W6-M6 displays an exponential decay with deviations of different amplitude depending on their localization (i.e. near maximum strain zones or not). Several type of diachronicity of the oscillations (antiphase, out of phase) are observed	

depending on the localisation and propagation of deformation. Boundary conditions: E=Extension and C=Compression.256

CHAPTER VII:

Figure VII-1: Satellite images of the Paleozoic peri-Hoggar basins (Landsat 7 ETM + from USGS database: <https://earthexplorer.usgs.gov/>) associated with the georeferenced different cross sections compiled from bibliography. See also Table 2 for reference.270

Figure VII-2: Geological map of the Paleozoic peri-Hoggar Basins (North Saharan Platform; North Gondwana) modified from Perron et al., (2018) showing evidence of erosion, hiatus, thickness variations, paleocurrent directions, thermo-orogenic events and igneous activity data (<https://doi.org/10.5194/se-9-1239-2018-supplement>) compiled from bibliography (see Figure VII-1). Terrane names and abbreviations: Tassendjanet (Tas), Tassendjanet nappe (Tas n.), Ahnet (Ah), In Ouzzal Granulitic Unit (IOGU), Iforas Granulitic Unit (UGI), Kidal (Ki), Timétrine (Tim), Tilemsi (Til), Tirek (Tir), In Zaouatene (Za), In Teidini (It), Iskel (Isk), Tefedest (Te), Laouni (La), Azrou-n-Fad (Az), Egéré-Aleskod (Eg-Al), Serouenout (Se), Tazat (Ta), Issalane (Is), Assodé (As), Barghot (Ba), Tchilit (Tch), Aouzegueur (Ao), Edembo (Ed), and Djanet (Dj). Shear zone and lineament names and abbreviations: west Ouzzal shear zone (WOSZ), east Ouzzal shear zone (EOSZ), Raghane shear zone (RSZ), Tin Amali shear zone (TASZ), 4°100 shear zone, 4°500 shear zone, and 8°300 shear zone. **A:** Localization of cross section of Figure VII-3. **1:** Figure VII-5; **2:** Figure VII-11; **3:** Figure VII-12; **4:** Figure VII-13; **5:** Figure VII-14.271

Figure VII-3: E–W cross-section of the Paleozoic peri-Hoggar basins (calibrated with wells) associated with the different terranes and the Bouguer anomaly extracted from Bouguer anomaly map (from International Gravimetric Bureau: <http://bgi.omp.obs-mip.fr/>). Notice the relation between arches with positive anomalies and syncline-shaped basins with negative anomalies. See Figure VII-2 and Figure VII-5 for legend and localization.273

Figure VII-4: (A) Total burial subsidence curves of the Paleozoic North Saharan Platform (peri-Hoggar basins) compiled from literature: well W7 in Ahnet basin, well W21 in Mouydir basin (Perron et al., 2018); well W1, well W4, well W7 and well W9 in Ahnet basin (Kracha, 2011); well KB-2 in Timimoun basin, well ELA-1 in Ghadamès-Berkine basin (Kadi et al., 2013); well in the Illizi basin (Wells et al., 2018); wells model A and B in Ghadamès-Berkine basin (Underdown et al., 2007); well LD-1 and well PDG-2 in Berkine-Ghadamès basin (Aissaoui et al., 2016); well F3-NC174, well H29-NC115, well A1-NC186, well A1-NC190 in Murzuq basin (Belaid et al., 2010); cross section in the southwestern Anti-Atlas (Burkhard et al., 2006);

well OTRA-1 in the Sbâa basin, well RG-3 in the Reggane basin, well TEG-1 in the Timimoun basin (Logan and Duddy, 1998); Hassi Messaoud field (English et al., 2017); well in Sbâa basin (Tournier, 2010); well in Ghadamès-Berkine basin (Yahi, 1999); well RPL-101 in Reggane basin, well HAD-1 in Ghadamès basin, well REG-1 in Timimoun basin; well TGE-1 in Illizi basin, well TO-1 and well KA-1 in the Dahar depression (Makhous and Galushkin, 2003a, 2003b); well LT-1bis and well OTLA-1 in the Sbâa basin (Drid, 1989); well L1-1 in Murzuq basin (Galushkin and Eloghbi, 2014); well WT-1 in the Berkine basin (Yahi et al., 2001); well G and well A in the Illizi Basin (English et al., 2016a). The different curves morphologies showing antiphase, out of phase and in phase between basins. The data show low rate subsidence with periods of deceleration (Deceleration of Low Rate Subsidence: DLRS), acceleration (Acceleration of Low Rate Subsidence: ALRS), or inversion (Inversion of Low Rate Subsidence: ILRS) synchronous and correlated with regional tectonic pulses (i.e. major geodynamic events). (B) Thermal history curves of the Paleozoic North Saharan Platform (peri-Hoggar basins) compiled from literature: well in the Illizi basin (Wells et al., 2018); well model A and G in Ghadamès-Berkine basin (Underdown et al., 2007); well OTRA-1 in the Sbâa basin, well RG-3 in the Reggane basin, well TEG-1 in the Timimoun basin, well in the eastern Ahnet basin (Logan and Duddy, 1998); well F3-NC174, well H29-NC115, well NC-174, well NC-115, well NC-186, well NC-190 in Murzuq basin (Belaid et al., 2010); well A-76 well in Murzuq basin (Galushkin and Eloghbi, 2014).274

Figure VII-5: (A) Interpreted aeromagnetic anomaly map (EMAG2 from <https://www.geomag.us/>) of the Paleozoic peri-Hoggar basins (North Saharan Platform) showing the different terranes delimited by NS, NW–SE and NE–SW lineaments and megasigmoid structures (SC shear fabrics) from Perron et al., (2018); (B) Bouguer anomaly map (from International Gravimetric Bureau: <http://bgi.omp.obs-mip.fr/>) of the Paleozoic peri-Hoggar basins (North Saharan Platform) presenting evidence of positive anomalies under arches and negative anomalies under basins from Perron et al., (2018). A: Localization of cross section in Figure VII-3.....276

Figure VII-6: Method from construction of the numerical models to comparison, quantification and classification with the peri-Hoggar Basins.....278

Figure VII-7: a) Inputs models of the simulations with the different parameters applied in experiments such as b) the far fields stresses (sinusoidal extension-compression 40 Myr) and c) the thermal anomaly. d) Isostasy equilibrium potential by an Airy calculation between archean and proterozoic terranes (see Appendix A). e) Initial temperature state of the lithosphere for all the simulations presented. f) Yield-strength envelopes of the simulated materials calculated for

a strain rate of $1.5 \cdot 10^{-11} \text{ s}^{-1}$. $\Delta\sigma$ represents the deviatoric stress, positive values under extension and negative values under compression.279

Figure VII-8: (A) Model M3 coupling lithosphere heterogeneity, local erosion/deposition and processes (syncline-shaped starved basins); Notice the impact of the size of the erosion surface on basins filling. Peripheral basins are thicker than the central basin. A link can be made with the WAC and the East Saharan craton two major sediment providers. (B) Model M5 coupling lithosphere heterogeneity and local erosion/deposition processes (syncline-shaped filled basins); Notice the impact of external sediment flux on basin architecture. (C) Subsidence curves from the different models and comparison with literature curves (Well data: see Figure VII-4).283

Figure VII-9: (A) Model M2 coupling lithosphere heterogeneity, local erosion/deposition processes and tectonics (syncline-shaped starved basins) with their burial and thermal history curves. (B) Model M2 coupling lithosphere heterogeneity, local erosion/deposition processes, tectonics and thermal anomaly (starved complex-shaped basins) with their burial and thermal history curves. Well data: see Figure VII-4. See Figure VII-7c for localization of the thermal anomaly in the model (i.e. under the central basin).286

Figure VII-10: (A) Model M6 coupling lithosphere heterogeneity, local erosion/deposition processes, tectonics and lateral sediment flux (syncline-shaped filled basins) with their burial and thermal history curves. (B) Model M7 coupling lithosphere heterogeneity, local erosion/deposition processes, tectonics, thermal anomaly and lateral sediment flux (complex-shaped filled basins) with their burial and thermal history curves. Well data: see Figure VII-4. See Figure VII-7c for localization of the thermal anomaly in the model (i.e. under the central basin).287

Figure VII-11: Comparison of the tectono-stratigraphic architecture of the Tasmena basin with thermo-mechanical numerical model M2. (A) Geological map of the Paleozoic series in the Tasmena basin showing the typical arche and basin architecture with diminution of series approaching arches. (B) Satellite images of the Paleozoic series in the Tasmena basin (Landsat 7 ETM +). (C) Cross section extracted from model M2 showing the similar arch-basin architecture. Notice that we can compare our cross section with the 2D map (see explanation in the geological sittings part; 0). Thickness (1.5 km) of the model is coherent with thickness shown by Lessard, (1961).293

Figure VII-12: Comparison of stratigraphic architecture cross section in the Tim Mersoï basin with thermo-mechanical numerical model M7. (A) Geological map of the Paleozoic series in the Tim Mersoï basin. (B) Satellite images of the Paleozoic series in the Tim Mersoï basin

(Landsat 7 ETM +). (C) WNW-ESE cross section of the Tim Mersoï basin localized in Figure A showing the typical arche and basin architecture with diminution of series approaching arches. (D) Cross section extracted from model M7 showing the similar arch-basin architecture. Notice that this comparison is possible with peripheral basins in the numerical model M6. .297

Figure VII-13: Comparison of tectono-stratigraphic architecture cross section and thermal subsidence curves in the Mouydir basin with thermo-mechanical numerical model M7. (A) Geological map of the Paleozoic series in the Mouydir basin. (B) Satellite images of the Paleozoic series in the Mouydir basin (Landsat 7 ETM +). (C) WSW-ENE cross section of the Mouydir basin localized in Figure A showing the typical arche and basin architecture with diminution of series approaching arches. (D) Cross section extracted from model M7 showing the similar arch-basin architecture. (E) Total burial subsidence of well W21 from bibliography (Perron et al., 2018). (F) Comparison of total subsidence in E with curve model M7. (G) Thermal curves extracted from the model M7. Notice that this comparison is possible with peripheral basins in the numerical model M6.300

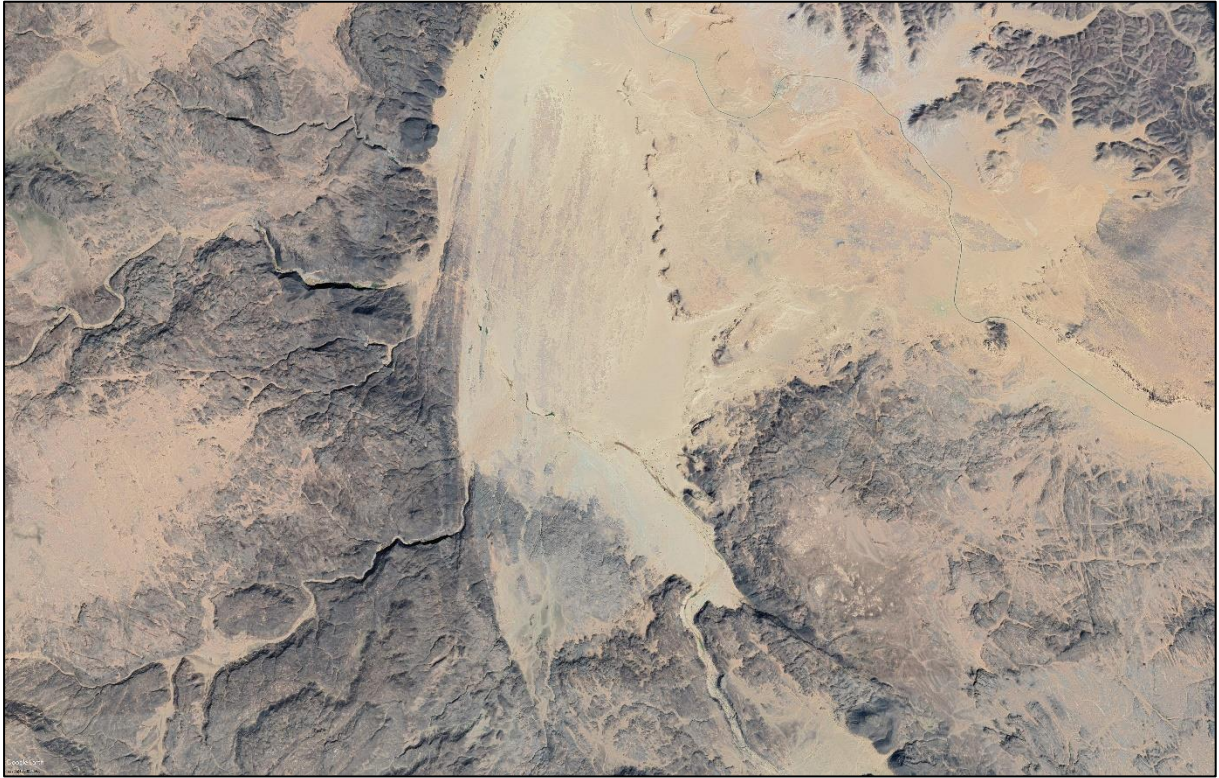
Figure VII-14: Comparison of tectono-stratigraphic architecture cross section and thermal subsidence curves in the Ahnet basin with thermo-mechanical numerical model M6. (A) Geological map of the Paleozoic series in the Ahnet basin. (B) Satellite images of the Paleozoic series in the Ahnet basin (Landsat 7 ETM +). (C) NW-SE seismic cross section of the Ahnet basin and Azzel Matti Arch localized in Figure A showing the typical complexification of arche and basin architecture with intra-arches structures. (D) Cross section extracted from model M6 showing the similar complexification of the arch-basin architecture with presence of intra-arches. (E) Total burial subsidence of well W7 from Perron et al., (2018) and well 1, 2, 3, 4 from Kracha, (2011). (F) Comparison of total subsidence curves of E with curve model M6. (G) Comparison of thermal curves extracted from the model M6 with 5 from bibliography (Logan and Duddy, 1998).301

Figure VII-15: Classification of the different peri-Hoggar Basins based on the intensity of the three main modelled parameters from M1 to M7 (thermal anomaly, tectonics and sediment flux). Note that this classification is established by comparing the architecture, the geometries, the thermal and the subsidence curves between models and geological data. For each category local erosion/deposition process is active (i.e. erosion of arches and deposition in basins depocenter).302

CHAPTER VIII:

- Figure VIII-1: (A) Chronostratigraphic chart and architecture of the Paleozoic intracratonic basins (Reggane, Ahnet, Mouydir) associated with their basement heterogeneities (i.e. terranes) drawn from literature (Eschard et al., 2010; Perron et al., 2018; Wendt et al., 2006); (B) Schematic characteristic backstripped curve of these basins; (C) Eustatic curve (Haq and Schutter, 2008) and geodynamic events: **(a)** Hirnantian glaciation, **(b)** Carboniferous glaciation, **(c)** Caledonian orogeny, **(d)** pre-Hercynian orogeny, **(e)** Devonian igneous intrusion; (D) Isostopic temperature (shallow, tropical/sub-tropical) during the Paleozoic (Prokoph et al., 2008). **(0)** Late Pan-African extensional collapse, **(1)** Pan-African peneplanation, **(2)** Cambro-Ordovician extension, **(3)** Upper Ordovician glaciation and deglaciation linked to isostatic rebound, **(4)** Silurian extension, **(5)** Silurian sealing, **(6)** Caledonian compression, **(7)** Early Devonian tectonic quiescence, **(8)** Middle Devonian compression, **(9)** Middle to Late Devonian extension, **(10)** Pre-Hercynian compression.310
- Figure VIII-2: Comparison of stratigraphic architecture cross section in the Paraná Basin with thermo-mechanical numerical model. (A) Geological map of the Paleozoic series in the Paraná Basin from Daly et al., (2018b). (B) Geoseismic interpretation of the deep seismic profile; And the same seismic data at a vertical exaggeration of 1:30 showing the cratonic megasequence and overlying Cretaceous section from Daly et al., (2018b). (C) Cross section extracted from model M7 showing the similar architecture. **1:** Cretaceous Grajaú Group; **2:** Upper carboniferous–Middle Triassic Balsas Group; **3:** Middle Devonian–Lower Carboniferous Caninde Group; **4:** Silurian–Lower Devonian Serra Grande Group; **5:** Silurian–Triassic cratonic basin megasequence; **6:** Late Neoproterozoic and Cambrian sedimentary remnants of the Riachão basin; **7:** Parnaíba Block crystalline basement; **8:** mid-crustal reflectivity; **9:** Cambrian volcanics and sediments of the Campo Maior graben; **10:** Neoproterozoic Cruzeta Complex of the Borborema Province; **11:** Neoproterozoic granitic gneisses of the Borborema Province; **12:** Neoproterozoic schists of the Estrondo Group; **13:** Neoproterozoic phyllites of the Tocantins Group; **14:** Paleoproterozoic Amazonian craton; **15:** lithospheric mantle.317
- Figure VIII-3: Comparison of subsidence curves from geological data of Paraná Basin and numerical models (Model M2 and M3). **a:** Well CB-3 from Paraná Basin, Brazil, (Oliveira, 1987 from Allen and Armitage, 2011); **b:** Well from Paraná Basin (Zalan et al., 1990).318

LIST OF TABLES



Late Ordovician ice stream near Ghat area (Google-Earth view; 24°32'20" N, 10°12'17" E)



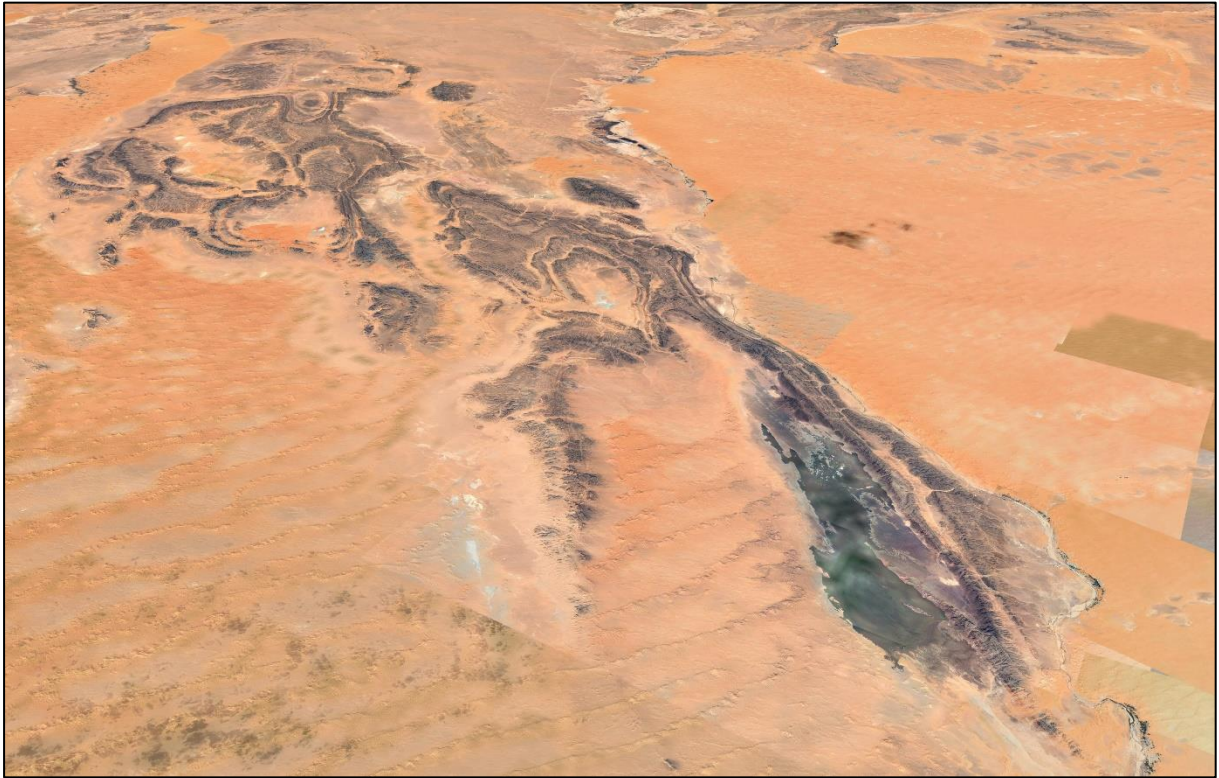
CHAPTER VI:

Table 1: Rheological parameters used in all experiments. References are from R & D (Rybacki and Dresen, 2000), G & T (Gleason and Tullis, 1995), G & E (Goetze and Evans, 1979) and M (Mackwell et al., 1998). $\alpha = 3.10^{-5} \text{ K}^{-1}$, $\beta = 1.10^{-11} \text{ Pa}^{-1}$, $\kappa e = 5.10^{-7} \text{ m}^2 \cdot \text{s}^{-1}$, $\kappa = 1.10^{-6} \text{ m}^2 \cdot \text{s}^{-1}$, $\epsilon_{\min} = 0$, $\epsilon_{\max} = 1$, $C_p = 1000 \text{ J} \cdot \text{kg}^{-1} \cdot \text{K}^{-1}$, $H = 3.10^{-9} \text{ W} \cdot \text{kg}^{-1}$	244
Table 2: List of parameters inputs for each models. Notice that duration of each model is 250 Myrs.....	245

CHAPTER VII:

Table 3: Synthesis of references highlighting evidence of hiatus, erosion and thickness variations related to geodynamic events on the Saharan Platform (preferentially documented at the vicinity of arches). See also bibliographic cross sections georeferenced in Figure VII-1.	277
Table 4: Parameters inputs of different models M and runs.	281
Table 5: Main criteria of classification of the different peri-Hoggar Basins.	303

BIBLIOGRAPHIC REFERENCES



Paleozoic folding in the Ougarta range (Google-Earth view; 25°20' N, 2°05' W)



- Abdelsalam, M. G., Liégeois, J.-P. and Stern, R. J.: The saharan metacraton, *J. Afr. Earth Sci.*, 34(3), 119–136, 2002.
- Abdelsalam, M. G., Gao, S. S. and Liégeois, J.-P.: Upper mantle structure of the Saharan Metacraton, *J. Afr. Earth Sci.*, 60(5), 328–336, doi:10.1016/j.jafrearsci.2011.03.009, 2011.
- Abdesselam, F.: Etude palynologique du Dévonien HFR-1 (Bassin de Rhadames), Sonatrach centre de recherche et de développement, Boumerdès., 1990.
- Abdesselam-Rouighi, F.: Etude palynologique du sondage Sebket El Melah (unpublished), Entreprise nationale Sonatrach division hydrocarbures direction Laboratoire central des hydrocarbures, Boumerdès., 1977.
- Abdesselam-Rouighi, F.: Premiers résultats biostratigraphiques (Miospores, Acritarches et Chitinozoaires) concernant le Dévonien moyen et supérieur du mole d'Ahara (bassin d'Illizi, Algérie), *Rev. Micropaléontologie*, 29(2), 87–92, 1986.
- Abdesselam-Rouighi, F.: Résultats de l'étude palynologiques des sondage Garet El Guefoul Bassin de l'Ahnet-Mouydir (unpublished), Entreprise nationale Sonatrach division hydrocarbures direction Laboratoire central des hydrocarbures, Boumerdès., 1991.
- Abdesselam-Rouighi, F.-F.: Biostratigraphie des spores, acritarches et chitinozoaires du Dévonien moyen et supérieur du bassin d'Illizi (Algérie), *Bull. Serv. Géologique Algérie*, 14(2), 97–117, 2003.
- Abdesselam-Rouighi, F.-F. and Boumendjel, K.: Biostratigraphie des spores, acritarches et chitinozoaires de la synéclyse Illizi Ghadamès, 1992.
- Abdesselam-Rouighi, F.-F. and Coquel, R.: Palynologie du Dévonien terminal-Carbonifère Inférieur dans le Sud-Est du bassin d'Illizi (Sahara algerien). Position des premières lycospores dans la série stratigraphique, *Ann. Société Géologique Nord*, 5, 47–58, 1997.
- Abudeif, A. M.: Seismotectonic analysis of Hamada oil pool, Libya, using Landsat and seismic data, *Arab. J. Geosci.*, 8(9), 6811–6834, doi:10.1007/s12517-014-1700-8, 2015.
- Ahmed, A. A.-K. and Moussine-Pouchkine, A.: Lithostratigraphie, sédimentologie et évolution de deux bassins molassiques intramontagneux de la chaîne Pan-Africaine: la Série pourprée de l'Ahnet, Nord-Ouest du Hoggar, Algérie, *J. Afr. Earth Sci.* 1983, 6(4), 525–535, 1987.
- Aïfa, T., Feinberg, H. and Pozzi, J.-P.: Devonian-Carboniferous paleopoles for Africa: Consequences for Hercynian geodynamics, *Tectonophysics*, 179(3), 287–304, doi:10.1016/0040-1951(90)90295-J, 1990.
- Aissani, F. and Bennamane, K.: Couvinian Reservoir Characterization of Ahnet-Timimoun Basin, AAPG Hedberg Conference, Algiers, Algeria., 2003.
- Aissaoui, M. N., Bédir, M. and Gabtni, H.: Petroleum assessment of Berkine–Ghadames Basin, southern Tunisia, *AAPG Bull.*, 100(03), 445–476, doi:10.1306/01141612083, 2016.
- Akkouche, M. M.: Application de la datation par traces de fission à l'analyse de la thermicité de bassins à potentialités pétrolières. Exemple de la cuvette de Sbaâ et du bassin de l'Ahnet-Nord (plate-forme saharienne occidentale, Algérie), Université Bordeaux 1., 2007.

Alekseev, A. S., Kononova, L. I. and Nikishin, A. M.: The Devonian and Carboniferous of the Moscow Syncline (Russian Platform): stratigraphy and sea-level changes, *Tectonophysics*, 268(1), 149–168, doi:10.1016/S0040-1951(96)00229-6, 1996.

Aliev, M.: Geological structures and estimation of oil and gas in the Sahara in Algeria, *SONATRACH.*, 1971.

Allegre, C. J. and Caby, R.: Chronologie absolue du Précambrien de l'Ahaggar occidental, *CR Acad Sci Paris*, 2095–2098, 1972.

Allègre, C. J. and Othman, D. B.: Nd–Sr isotopic relationship in granitoid rocks and continental crust development: a chemical approach to orogenesis, *Nature*, 286(5771), 335–342, doi:10.1038/286335a0, 1980.

Allen, P. A. and Allen, J. R.: *Basin analysis: Principles and applications*, Second Edition., Wiley-Blackwell, Chichester, West Sussex, UK., 2005.

Allen, P. A. and Allen, J. R.: *Basin analysis: principles and application to petroleum play assessment*, Third edition., Wiley-Blackwell, Chichester, West Sussex, UK., 2013.

Allen, P. A. and Armitage, J. J.: Cratonic Basins, in *Tectonics of Sedimentary Basins*, edited by C. Busby and A. Azor, pp. 602–620, John Wiley & Sons, Ltd., 2011.

Altumi, M. M., Elicki, O., Linnemann, U., Hofmann, M., Sagawe, A. and Gärtner, A.: U–Pb LA-ICP-MS detrital zircon ages from the Cambrian of Al Qarqaf Arch, central-western Libya: Provenance of the West Gondwanan sand sea at the dawn of the early Palaeozoic, *J. Afr. Earth Sci.*, 79, 74–97, doi:10.1016/j.jafrearsci.2012.11.007, 2013.

Armitage, J. J. and Allen, P. A.: Cratonic basins and the long-term subsidence history of continental interiors, *J. Geol. Soc.*, 167(1), 61–70, doi:10.1144/0016-76492009-108, 2010.

Artemieva, I. M.: Global $1^\circ \times 1^\circ$ thermal model TC1 for the continental lithosphere: implications for lithosphere secular evolution, *Tectonophysics*, 416(1–4), 245–277, 2006.

Artemieva, I. M.: The continental lithosphere: Reconciling thermal, seismic, and petrologic data, *Lithos*, 109(1–2), 23–46, doi:10.1016/j.lithos.2008.09.015, 2009.

Artemieva, I. M. and Mooney, W. D.: Thermal thickness and evolution of Precambrian lithosphere: A global study, *J. Geophys. Res. Solid Earth*, 106(B8), 16387–16414, doi:10.1029/2000JB900439, 2001.

Artemieva, I. M. and Mooney, W. D.: On the relations between cratonic lithosphere thickness, plate motions, and basal drag, *Tectonophysics*, 358(1–4), 21, doi:10.1016/S0040-1951(02)00425-0, 2002.

Artyushkov, E. V.: Role of crustal stretching on subsidence of the continental crust, *Tectonophysics*, 215(1), 187–207, doi:10.1016/0040-1951(92)90081-G, 1992.

Askri, H., Belmecheri, A., Benrabah, B., Boudjema, A., Boumendjel, K., Daoudi, M., Drid, M., Ghalem, T., Docca, A. M., Ghandriche, H. and others: Geology of Algeria, in *Well Evaluation Conference Algeria*, pp. 1–93, Schlumberger-Sonatrach., 1995.

- Aspler, L. B., Wisotzek, I. E., Chiarenzelli, J. R., Losonczy, M. F., Cousens, B. L., McNicoll, V. J. and Davis, W. J.: Paleoproterozoic intracratonic basin processes, from breakup of Kenorland to assembly of Laurentia: Hurwitz Basin, Nunavut, Canada, *Sediment. Geol.*, 141, 287–318, 2001.
- Attar, A., Fournier, J., Candilier, A. M. and Coquel, R.: Étude palynologique du Dévonien terminal et du Carbonifère inférieur du bassin d'Illizi (Fort-Polignac), Algérie, *Rev. Inst. Fr. Pétrole*, 35(4), 585–619, doi:10.2516/ogst:1980044, 1980.
- Audet, P. and Bürgmann, R.: Dominant role of tectonic inheritance in supercontinent cycles, *Nat. Geosci.*, 4(3), 184–187, doi:10.1038/ngeo1080, 2011.
- Avigad, D. and Gvirtzman, Z.: Late Neoproterozoic rise and fall of the northern Arabian–Nubian shield: The role of lithospheric mantle delamination and subsequent thermal subsidence, *Tectonophysics*, 477(3), 217–228, doi:10.1016/j.tecto.2009.04.018, 2009.
- Avigad, D., Kolodner, K., McWilliams, M., Persing, H. and Weissbrod, T.: Origin of northern Gondwana Cambrian sandstone revealed by detrital zircon SHRIMP dating, *Geology*, 31(3), 227, doi:10.1130/0091-7613(2003)031<0227:OONGCS>2.0.CO;2, 2003.
- Avigad, D., Sandler, A., Kolodner, K., Stern, R., McWilliams, M., Miller, N. and Beyth, M.: Mass-production of Cambro–Ordovician quartz-rich sandstone as a consequence of chemical weathering of Pan-African terranes: Environmental implications, *Earth Planet. Sci. Lett.*, 240(3–4), 818–826, doi:10.1016/j.epsl.2005.09.021, 2005.
- Avigad, D., Gerdes, A., Morag, N. and Bechstädt, T.: Coupled U–Pb–Hf of detrital zircons of Cambrian sandstones from Morocco and Sardinia: Implications for provenance and Precambrian crustal evolution of North Africa, *Gondwana Res.*, 21(2–3), 690–703, doi:10.1016/j.gr.2011.06.005, 2012.
- Avouac, J. P. and Burov, E. B.: Erosion as a driving mechanism of intracontinental mountain growth, *J. Geophys. Res. Solid Earth*, 101(B8), 17747–17769, doi:10.1029/96JB01344, 1996.
- Azzoune, N.: Analyse palynologique de trois (03) échantillons de carottes du sondages DTS-1, Sonatrach (unpublished), Entreprise nationale Sonatrach division hydrocarbures direction Laboratoire central des hydrocarbures, Boumerdès., 1999.
- Azzouni-Sekkal, A., Liégeois, J.-P., Bechiri-Benmerzoug, F., Belaidi-Zinet, S. and Bonin, B.: The “Taourirt” magmatic province, a marker of the closing stage of the Pan-African orogeny in the Tuareg Shield: review of available data and Sr–Nd isotope evidence, *J. Afr. Earth Sci.*, 37(3–4), 331–350, doi:10.1016/j.jafrearsci.2003.07.001, 2003.
- Badalini, G., Redfern, J. and Carr, I. D.: A synthesis of current understanding of the structural evolution of North Africa, *J. Pet. Geol.*, 25(3), 249–258, 2002.
- Badsì, M., Angelier, J. and Université Pierre et Marie Curie (Paris): Fracturation naturelle des roches application au bassin de l’Ahnet (Algérie), Atelier national de reproduction des thèses, Grenoble., 1999.
- Baidder, L., Raddi, Y., Tahiri, M. and Michard, A.: Devonian extension of the Pan-African crust north of the West African craton, and its bearing on the Variscan foreland deformation:

evidence from eastern Anti-Atlas (Morocco), *Geol. Soc. Lond. Spec. Publ.*, 297(1), 453–465, doi:10.1144/SP297.21, 2008.

Baird, D. J., Knapp, J. H., Steer, D. N., Brown, L. D. and Nelson, K. D.: Upper-mantle reflectivity beneath the Williston basin, phase-change Moho, and the origin of intracratonic basins, *Geology*, 23(5), 431–434, 1995.

Balay, S., Abhyankar, S., Adams, M., Brown, J., Brune, P., Buschelman, K., Dalcin, L. D., Eijkhout, V., Gropp, W., Kaushik, D., Knepley, M., May, D., McInnes, L. C., Munson, T., Rupp, K., Sanan, P., Smith, B., Zampini, S., Zhang, H. and Zhang, H.: PETSc Users Manual Revision 3.8, Argonne National Lab. (ANL), Argonne, IL (United States), 2017.

Baratoux, L., Metelka, V., Naba, S., Jessell, M. W., Grégoire, M. and Ganne, J.: Juvenile Paleoproterozoic crust evolution during the Eburnean orogeny (~2.2–2.0Ga), western Burkina Faso, *Precambrian Res.*, 191(1–2), 18–45, doi:10.1016/j.precamres.2011.08.010, 2011.

Bayer, R. and Lesquer, A.: Les anomalies gravimétriques de la bordure orientale du WAC suture panafricaine, *Bull. Société Géologique Fr.*, (6), 863–876, 1978.

Beaumont, C., Quinlan, G. and Hamilton, J.: Orogeny and stratigraphy: Numerical models of the Paleozoic in the eastern interior of North America, *Tectonics*, 7(3), 389–416, 1988.

Bechiri-Benmerzoug, F., Bonin, B., Bechiri, H., Khéloui, R., Talmat-Bouzeguela, S. and Bouzid, K.: Hoggar geochronology: a historical review of published isotopic data, *Arab. J. Geosci.*, 10(16), 351, 2017.

Beekman, F., Badsı, M. and van Wees, J.-D.: Faulting, fracturing and in situ stress prediction in the Ahnet Basin, Algeria—A finite element approach, *Tectonophysics*, 320(3), 311–329, 2000.

Beicip-Franlab: Etude de la cuvette de Sbâa, Beicip-Franlab & Sonatrach., 1996.

Bekkouche, D.: Le Silurien supérieur - Dévonien inférieur du bassin de Ghadamès (Sahara oriental Algérien): lithostratigraphie, sédimentologie et diagenèse des réservoirs gréseux, phdthesis, Université Joseph-Fourier - Grenoble I, 2 July. [online] Available from: <https://tel.archives-ouvertes.fr/tel-00759888/document> (Accessed 20 November 2016), 1992.

Belaid, A., Krooss, B. M. and Littke, R.: Thermal history and source rock characterization of a Paleozoic section in the Awbari Trough, Murzuq Basin, SW Libya, *Mar. Pet. Geol.*, 27(3), 612–632, doi:10.1016/j.marpetgeo.2009.06.006, 2010.

Belka, Z.: Early Devonian Kess-Kess carbonate mud mounds of the eastern Anti-Atlas (Morocco), and their relation to submarine hydrothermal venting, *J. Sediment. Res.*, 68(3), 368–377, 1998.

Bellahsen, N. and Daniel, J. M.: Fault reactivation control on normal fault growth: an experimental study, *J. Struct. Geol.*, 27(4), 769–780, doi:10.1016/j.jsg.2004.12.003, 2005.

Bellahsen, N., Leroy, S., Autin, J., Razin, P., d’Acremont, E., Sloan, H., Pik, R., Ahmed, A. and Khanbari, K.: Pre-existing oblique transfer zones and transfer/transform relationships in continental margins: New insights from the southeastern Gulf of Aden, Socotra Island, Yemen, *Tectonophysics*, 607, 32–50, doi:10.1016/j.tecto.2013.07.036, 2013.

- Bellini, E. and Massa, D.: A stratigraphic contribution to the Palaeozoic of the southern basins of Libya, *Geol. Libya*, 1, 3–56, 1980.
- Benbatta, A., Bendaoud, A., Cenko-Tok, B., Adjerid, Z., Lacène, K. and Ouzegane, K.: Ternary feldspar thermometry of Paleoproterozoic granulites from In-Ouzzal terrane (Western Hoggar, southern Algeria), *J. Afr. Earth Sci.*, doi:10.1016/j.jafrearsci.2016.08.005, 2016.
- Bennacef, A., Beuf, S., Biju-Duval, B., Charpal, O. de, Gariel, O. and Rognon, P.: Example of Cratonic Sedimentation: Lower Paleozoic of Algerian Sahara, *AAPG Bull.*, 55(12), 2225–2245, 1971.
- Bennacef, A., Attar, A., Froukhi, R., Beuf, S., Philippe, G., Schmerber, G. and Vermeire, J. C.: Cartes Géologiques d'Iherir-Dider (NG-32-IX), Iherir (NG-32-X), Illizi (NG-32-XV), Aharhar (NG-32-VIII), Oued Samène (NG-32-XIV), Erg Tihodaine (NG-32-VII), Tin Alkoum (NG-32-V), Djanet (NG-32-IV), Ta-N-Mellet (NG-32-XIII), Ta-N-Elak (NG-32-XIX), Fort Tarat (NG-32-XVI), Tilmas El Mra (NG-31-XXIV), Ers Oum El Lil (NG-31-XXII), Amguid (NG-31-XVIII), 1/200000 Sonatrach-Ministère de l'Industrie et des Mines, Algérie, 1974.
- Bensalah, A., Beuf, S., Gabriel, O., Philippe, G., Lacot, R., Paris, A., Basseto, D., Conrad, J. and Moussine-Pouchkine, A.: Cartes Géologiques de Khanguet El Hadid (NG-31-XVII), Ain Tidjoubar (NG-31-XVI), Oued Djaret (NG-31-XV), Aoulef El Arab (NG-31-XIV), Reggane (NG-31-XIII), Ifetessene (NG-31-IX), Arak (NG-31-X et NG-31-IV), Meredoua (NG-31-XIII), Tanezrouft (NG-31-VII et NG-31-I), In Heguis (NG-31-IX), Tin Senasset (NG-31-III), Ouallene (NG-31-II) 1/200000 Sonatrach-Ministère de l'Industrie et des Mines, Algérie, 1971.
- Berger, J., Ouzegane, K., Bendaoud, A., Liégeois, J.-P., Kiénast, J.-R., Bruguier, O. and Caby, R.: Continental subduction recorded by Neoproterozoic eclogite and garnet amphibolites from Western Hoggar (Tassendjanet terrane, Tuareg Shield, Algeria), *Precambrian Res.*, 247, 139–158, doi:10.1016/j.precamres.2014.04.002, 2014.
- Bertrand, J. M.: Evolution polycyclique des gneiss précambriens de l'Aleksod (Hoggar central, Sahara algérien): aspects structuraux, pétrologiques, géochimiques et géochronologiques, Theses, Université Montpellier II - Sciences et Techniques du Languedoc, February. [online] Available from: <https://tel.archives-ouvertes.fr/tel-00875170> (Accessed 21 November 2016), 1974.
- Bertrand, J. M. L. and Caby, R.: Geodynamic evolution of the Pan-African orogenic belt: A new interpretation of the Hoggar shield (Algerian Sahara), *Geol. Rundsch.*, 67(2), 357–388, doi:10.1007/BF01802795, 1978.
- Bertrand, J. M. L. and Lasserre, M.: Pan-African and pre-Pan-African history of the Hoggar (Algerian Sahara) in the light of new geochronological data from the Aleksod area, *Precambrian Res.*, 3(4), 343–362, 1976.
- Beuf, S. and Montadert, L.: Géologie-sur une discordance angulaire entre les unités II et III du Cambro-Ordovicien au sud-est de la plaine de Dider (Tassili des Ajjers), *Compte Rendus Hebd. Séances L'Académie Sci.*, 254(6), 1108–1109, 1962.
- Beuf, S., Biju-Duval, B., Mauvier, A. and Legrand, P.: Nouvelles observations sur le 'Cambro-Ordovicien' du Bled El Mass (Sahara central), *Publ. Serv. Géologique Algér. Bull.*, 38, 39–51, 1968a.

- Beuf, S., Biju-Duval, B., De Charpal, O., Gariel, O., Bennacef, A., Black, R., Arene, J., Boissonnas, J., Chachau, F., Guérangé, B. and others: Une conséquence directe de la structure du bouclier Africain: L'ébauche des bassins de l'Ahnet et du Mouydir au Paléozoïque inférieur, *Publ. Serv. Géologique L'Algérie Nouv. Sér. Bull.*, 38, 105–34, 1968b.
- Beuf, S., Biju-Duval, B., De Charpal, O. and Gariel, O.: Homogénéité des directions des paléocourants du Dévonien inférieur au Sahara central, *Comptes Rendus L'Académie Sci. Sér. D*, 268, 2026–9, 1969.
- Beuf, S., Biju-Duval, B., de Charpal, O., Rognon, P., Gabriel, O. and Bennacef, A.: Les grès du Paléozoïque inférieur au Sahara: Sédimentation et discontinuités évolution structurale d'un craton, Technip., Paris., 1971.
- Biju-Duval, B., de Charpal, O., Beuf, S. and Bennacef, A.: Lithostratigraphie du Dévonien inférieur dans l'Ahnet et le Mouydir (Sahara Central), *Bull Serv Géologique Algérie*, (38), 83–104, 1968.
- Bird, P. C., Cartwright, J. A. and Davies, T. L.: Basement reactivation in the development of rift basins: an example of reactivated Caledonide structures in the West Orkney Basin, *J. Geol. Soc.*, 172(1), 77–85, 2015.
- Black, R., Latouche, L., Liégeois, J. P., Caby, R. and Bertrand, J. M.: Pan-African displaced terranes in the Tuareg shield (central Sahara), *Geology*, 22(7), 641–644, 1994.
- Bladon, A. J., Clarke, S. M. and Burley, S. D.: Complex rift geometries resulting from inheritance of pre-existing structures: Insights and regional implications from the Barmer Basin rift, *J. Struct. Geol.*, 71, 136–154, 2015.
- Blakey, R. C.: Gondwana paleogeography from assembly to breakup—A 500 m.y. odyssey, in *Special Paper 441: Resolving the Late Paleozoic Ice Age in Time and Space*, vol. 441, pp. 1–28, Geological Society of America., 2008.
- Boissonnas, J., Borsi, S., Ferrara, G., Fabre, J., Fabries, J. and Gravelle, M.: On the Early Cambrian age of two late orogenic granites from west-central Ahaggar (Algerian Sahara), *Can. J. Earth Sci.*, 6(1), 25–37, 1969.
- Bond, G. C. and Kominz, M. A.: Construction of tectonic subsidence curves for the early Paleozoic miogeocline, southern Canadian Rocky Mountains: Implications for subsidence mechanisms, age of breakup, and crustal thinning, *GSA Bull.*, 95(2), 155–173, doi:10.1130/0016-7606(1984)95<155:COTSCF>2.0.CO;2, 1984.
- Bonhomme, M. G., Fabre, J. and Kaddour, M.: Datations K-Ar d'évènements varisques dans le Cambrien de l'Ougarta (Sahara occidental algérien), *Mem Serv Geol Alger*, 8, 117–125, 1996.
- Bonini, M., Sani, F. and Antonielli, B.: Basin inversion and contractional reactivation of inherited normal faults: A review based on previous and new experimental models, *Tectonophysics*, 522–523, 55–88, doi:10.1016/j.tecto.2011.11.014, 2012.
- Boote, D. R. D., Clark-Lowes, D. D. and Traut, M. W.: Palaeozoic petroleum systems of North Africa, *Geol. Soc. Lond. Spec. Publ.*, 132(1), 7–68, doi:10.1144/GSL.SP.1998.132.01.02, 1998.

- Borocco, J. and Nyssen, R.: Nouvelles observations sur les "gres inferieurs" cambro-ordoviciens du Tassili interne (Nord-Hoggar), *Bull. Société Géologique Fr.*, S7-I(2), 197–206, doi:10.2113/gssgfbull.S7-I.2.197, 1959.
- Bouche, P. M.: Repartition verticale des chitinozoaires du sondage HNE-1, Institut Française du Pétrole., 1963.
- Boudjema, A.: Evolution structurale du bassin pétrolier" triasique" du Sahara nord oriental (Algérie), Doctoral dissertation, Paris 11, France., 1987.
- Bouhallier, H., Choukroune, P. and Ballèvre, M.: Diapirism, bulk homogeneous shortening and transcurrent shearing in the Archaean Dharwar craton: the Holenarsipur area, southern India, *Precambrian Res.*, 63(1), 43–58, doi:10.1016/0301-9268(93)90004-L, 1993.
- Bouhallier, H., Chardon, D. and Choukroune, P.: Strain patterns in Archaean dome-and-basin structures: The Dharwar craton (Karnataka, South India), *Earth Planet. Sci. Lett.*, 135(1), 57–75, doi:10.1016/0012-821X(95)00144-2, 1995.
- Boumendjel, K.: Les chitinozoaires du silurien superieur et du devonien du sahara algerien (cadre geologique, systematique, biostratigraphie), Doctoral dissertation, Rennes 1, France., 1987.
- Boumendjel, K.: Nouvelles espèces de chitinozoaires du Silurien Supérieur et du Dévonien Inférieur du bassin de Timimoun (Sahara central, Algérie): New chitinozoan species from the Upper Silurian and Lower Devonian of the Timimoun basin (central Sahara, Algeria), *Rev. Palaeobot. Palynol.*, 118(1–4), 29–46, doi:10.1016/S0034-6667(01)00106-3, 2002.
- Boumendjel, K., Loboziak, S., Paris, F., Steemans, P. and Strel, M.: Biostratigraphie des Miospores et des Chitinozoaires du Silurien supérieur et du Dévonien dans le bassin d'Illizi (S.E. du Sahara algérien), *Geobios*, 21(3), 329–357, doi:10.1016/S0016-6995(88)80057-3, 1988.
- Bournas, N., Galdeano, A., Hamoudi, M. and Baker, H.: Interpretation of the aeromagnetic map of Eastern Hoggar (Algeria) using the Euler deconvolution, analytic signal and local wavenumber methods, *J. Afr. Earth Sci.*, 37(3–4), 191–205, doi:10.1016/j.jafrearsci.2002.12.001, 2003.
- Bouziid, A., Akacem, N., Hamoudi, M., Ouzegane, K., Abtout, A. and Kienast, J.-R.: Modélisation magnétotellurique de la structure géologique profonde de l'unité granulitique de l'In Ouzzal (Hoggar occidental), *Comptes Rendus Geosci.*, 340(11), 711–722, doi:10.1016/j.crte.2008.08.001, 2008.
- Bouziid, A., Bayou, B., Liégeois, J.-P., Bourouis, S., Bougchiche, S. S., Bendekken, A., Abtout, A., Boukhlof, W. and Ouabadi, A.: Lithospheric structure of the Atakor metacratonic volcanic swell (Hoggar, Tuareg Shield, southern Algeria): Electrical constraints from magnetotelluric data, in *Geological Society of America Special Papers*, vol. 514, pp. 239–255, Geological Society of America., 2015.
- Brace, W. F. and Kohlstedt, D. L.: Limits on lithospheric stress imposed by laboratory experiments, *J. Geophys. Res. Solid Earth*, 85(B11), 6248–6252, doi:10.1029/JB085iB11p06248, 1980.

- Brahimi, S., Liégeois, J.-P., Ghienne, J.-F., Munsch, M. and Bourmatte, A.: The Tuareg shield terranes revisited and extended towards the northern Gondwana margin: Magnetic and gravimetric constraints, *Earth-Sci. Rev.*, 185, 572–599, doi:10.1016/j.earscirev.2018.07.002, 2018a.
- Brahimi, S., Liégeois, J.-P., Ghienne, J.-F., Munsch, M. and Bourmatte, A.: The Tuareg shield terranes revisited and extended towards the northern Gondwana margin: Magnetic and gravimetric constraints, *Earth-Sci. Rev.*, 2018b.
- Brice, D. and Latrèche, S.: Brachiopodes du bassin d'Illizi (Sahara algérien oriental) près de la limite Givétien-Frasnien, *Geobios*, 31(4), 437–454, doi:10.1016/S0016-6995(98)80116-2, 1998.
- de Brito Neves, B. B., Fuck, R. A., Cordani, U. G. and Thomaz F^o, A.: Influence of basement structures on the evolution of the major sedimentary basins of Brazil: A case of tectonic heritage, *J. Geodyn.*, 1(3), 495–510, doi:10.1016/0264-3707(84)90021-8, 1984.
- Brun, J.-P.: Deformation of the continental lithosphere: Insights from brittle-ductile models, *Geol. Soc. Lond. Spec. Publ.*, 200(1), 355–370, doi:10.1144/GSL.SP.2001.200.01.20, 2002.
- Brune, S., Corti, G. and Ranalli, G.: Controls of inherited lithospheric heterogeneity on rift linkage: Numerical and analog models of interaction between the Kenyan and Ethiopian rifts across the Turkana depression, *Tectonics*, 36(9), 1767–1786, 2017.
- Buchanan, P. G. and McClay, K. R.: Sandbox experiments of inverted listric and planar fault systems, *Tectonophysics*, 188(1), 97–115, doi:10.1016/0040-1951(91)90317-L, 1991.
- Buiter, S. J. H. and Pfiffner, O. A.: Numerical models of the inversion of half-graben basins, *Tectonics*, 22(5), doi:10.1029/2002TC001417, 2003.
- Bumby, A. J. and Guiraud, R.: The geodynamic setting of the Phanerozoic basins of Africa, *J. Afr. Earth Sci.*, 43(1–3), 1–12, doi:10.1016/j.jafrearsci.2005.07.016, 2005.
- Burgess, P. M.: Phanerozoic evolution of the sedimentary cover of the North American craton, in *Sedimentary Basins of the World*, vol. 5, pp. 31–63, Elsevier., 2008.
- Burgess, P. M. and Gurnis, M.: Mechanisms for the formation of cratonic stratigraphic sequences, *Earth Planet. Sci. Lett.*, 136(3), 647–663, doi:10.1016/0012-821X(95)00204-P, 1995.
- Burgess, P. M., Gurnis, M. and Moresi, L.: Formation of sequences in the cratonic interior of North America by interaction between mantle, eustatic, and stratigraphic processes, *Geol. Soc. Am. Bull.*, 109(12), 1515–1535, 1997.
- Burke, K., MacGregor, D. S. and Cameron, N. R.: Africa's petroleum systems: four tectonic 'Aces' in the past 600 million years, *Geol. Soc. Lond. Spec. Publ.*, 207(1), 21–60, 2003.
- Burkhard, M., Caritg, S., Helg, U., Robert-Charrue, C. and Soulaïmani, A.: Tectonics of the Anti-Atlas of Morocco, *Comptes Rendus Geosci.*, 338(1–2), 11–24, doi:10.1016/j.crte.2005.11.012, 2006.

- Burov, E. and Cloetingh, S.: Controls of mantle plumes and lithospheric folding on modes of intraplate continental tectonics: differences and similarities, *Geophys. J. Int.*, 178(3), 1691–1722, doi:10.1111/j.1365-246X.2009.04238.x, 2009.
- Burov, E. B. and Diament, M.: The effective elastic thickness (T_e) of continental lithosphere: what does it really mean?, *J. Geophys. Res. Solid Earth*, 100(B3), 3905–3927, 1995.
- Butler, R. W. H.: The influence of pre-existing basin structure on thrust system evolution in the Western Alps, *Geol. Soc. Lond. Spec. Publ.*, 44(1), 105–122, doi:10.1144/GSL.SP.1989.044.01.07, 1989.
- Caby, R.: Terrane assembly and geodynamic evolution of central–western Hoggar: a synthesis, *J. Afr. Earth Sci.*, 37(3–4), 133–159, doi:10.1016/j.jafrearsci.2003.05.003, 2003.
- Caby, R. and Andreopoulos-Renaud, U.: Le Hoggar oriental, bloc cratonisé à 730 Ma dans la chaîne pan-africaine du nord du continent africain, *Precambrian Res.*, 36(3), 335–344, 1987.
- Caby, R., Andreopoulos-Renaud, U. and Lancelot, J. R.: Les phases tardives de l’orogénèse pan-africaine dans l’Adrar des Iforas oriental (Mali): Lithostratigraphie des formations molassiques et géochronologie U/Pb sur zircon de deux massifs intrusifs, *Precambrian Res.*, 28(2), 187–199, 1985.
- Cacace, M. and Scheck-Wenderoth, M.: Why intracontinental basins subside longer: 3-D feedback effects of lithospheric cooling and sedimentation on the flexural strength of the lithosphere: Subsidence at Intracontinental Basins, *J. Geophys. Res. Solid Earth*, 121(5), 3742–3761, doi:10.1002/2015JB012682, 2016.
- Cagnard, F., Barbey, P. and Gapais, D.: Transition between “Archaean-type” and “modern-type” tectonics: Insights from the Finnish Lapland Granulite Belt, *Precambrian Res.*, 187(1–2), 127–142, doi:10.1016/j.precamres.2011.02.007, 2011.
- Campbell, I. H., Griffiths, R. W. and Hill, R. I.: Melting in an Archaean mantle plume: heads it’s basalts, tails it’s komatiites, *Nature*, 339(6227), 697, 1989.
- Candilier, M.: Etude palynologique du Dévonien terminal et du Carbonifère inférieur du bassin d’Illizi (Fort-Polignac) Algérie, Université des sciences et techniques de Lille., 1979.
- Caravaca, G., Brayard, A., Vennin, E., Guiraud, M., Le Pourhiet, L., Grosjean, A.-S., Thomazo, C., Olivier, N., Fara, E., Escarguel, G., Bylund, K. G., Jenks, J. F. and Stephen, D. A.: Controlling factors for differential subsidence in the Sonoma Foreland Basin (Early Triassic, western USA), *Geol. Mag.*, 1–25, doi:10.1017/S0016756817000164, 2017.
- Carpena, J., Kienast, J.-R., Ouzegane, K. and Jehanno, C.: Evidence of the contrasted fission-track clock behavior of the apatites from In Ouzzal carbonatites (northwest Hoggar): The low-temperature thermal history of an Archean basement, *Geol. Soc. Am. Bull.*, 100(8), 1237–1243, 1988.
- Carr, I. D.: Second-Order Sequence Stratigraphy of the Palaeozoic of North Africa, *J. Pet. Geol.*, 25(3), 259–280, doi:10.1111/j.1747-5457.2002.tb00009.x, 2002.

Carruba, S., Perotti, C., Rinaldi, M., Bresciani, I. and Bertozzi, G.: Intraplate deformation of the Al Qarqaf Arch and the southern sector of the Ghadames Basin (SW Libya), *J. Afr. Earth Sci.*, 97, 19–39, doi:10.1016/j.jafrearsci.2014.05.001, 2014.

Casas, A. M., Gapais, D., Nalpas, T., Besnard, K. and Román-Berdiel, T.: Analogue models of transpressive systems, *J. Struct. Geol.*, 23(5), 733–743, doi:10.1016/S0191-8141(00)00153-X, 2001.

Casas-Sainz, A. M., Soto-Marín, R., González, Á. and José Villalaín, J.: Folded onlap geometries: implications for recognition of syn-sedimentary folds, *J. Struct. Geol.*, 27(9), 1644–1657, doi:10.1016/j.jsg.2005.05.005, 2005.

de Castro, D. L., Bezerra, F. H., Sousa, M. O. and Fuck, R. A.: Influence of Neoproterozoic tectonic fabric on the origin of the Potiguar Basin, northeastern Brazil and its links with West Africa based on gravity and magnetic data, *J. Geodyn.*, 54, 29–42, 2012.

Catuneanu, O., Abreu, V., Bhattacharya, J. P., Blum, M. D., Dalrymple, R. W., Eriksson, P. G., Fielding, C. R., Fisher, W. L., Galloway, W. E., Gibling, M. R., Giles, K. A., Holbrook, J. M., Jordan, R., Kendall, C. G. St. C., Macurda, B., Martinsen, O. J., Miall, A. D., Neal, J. E., Nummedal, D., Pomar, L., Posamentier, H. W., Pratt, B. R., Sarg, J. F., Shanley, K. W., Steel, R. J., Strasser, A., Tucker, M. E. and Winker, C.: Towards the standardization of sequence stratigraphy, *Earth-Sci. Rev.*, 92(1–2), 1–33, doi:10.1016/j.earscirev.2008.10.003, 2009.

Cawood, P. A., Ed.: *Earth accretionary systems in space and time*, Geological Soc, London., 2009.

Cawood, P. A., Kröner, A., Collins, W. J., Kusky, T. M., Mooney, W. D. and Windley, B. F.: *Accretionary orogens through Earth history*, *Geol. Soc. Lond. Spec. Publ.*, 318(1), 1–36, doi:10.1144/SP318.1, 2009.

Célérier, J., Sandiford, M., Hansen, D. L. and Quigley, M.: Modes of active intraplate deformation, Flinders Ranges, Australia, *Tectonics*, 24(6), 1–17, doi:10.1029/2004TC001679, 2005.

Chabou, M. C., Sebai, A., Féraud, G. and Bertrand, H.: Datation $^{40}\text{Ar}/^{39}\text{Ar}$ de la province magmatique de l'Atlantique central dans le Sud-Ouest algérien, *Comptes Rendus Geosci.*, 339(16), 970–978, doi:10.1016/j.crte.2007.09.011, 2007a.

Chabou, M. C., Bentalaa, S., Dib, N. and Sebai, A.: Les dolérites du bassin d'Illizi (Algérie) : manifestations d'un linéament du socle de direction E-W ?, 2007b.

Chaouchi, R., Malla, M. S. and Kechou, F.: Sedimentological evolution of the Givetian-Eifelian (F3) sand bar of the West Alrar field, Illizi Basin, Algeria, *Geol. Soc. Lond. Spec. Publ.*, 132(1), 187–200, 1998.

Chardon, D., Choukroune, P. and Jayananda, M.: Sinking of the Dharwar Basin (South India): implications for Archaean tectonics, *Precambrian Res.*, 91(1), 15–39, doi:10.1016/S0301-9268(98)00037-0, 1998.

Chardon, D., Gapais, D. and Cagnard, F.: Flow of ultra-hot orogens: A view from the Precambrian, clues for the Phanerozoic, *Tectonophysics*, 477(3–4), 105–118, doi:10.1016/j.tecto.2009.03.008, 2009.

- Chaumeau, J., Legrand, P. and Renaud, A.: Contribution a l'étude du Couvinien dans le bassin de Fort-de-Polignac (Sahara), *Bull. Société Géologique Fr.*, S7-III(5), 449–456, doi:10.2113/gssgfbull.S7-III.5.449, 1961.
- Chavand, J. C. and Claracq, P.: La disparition du Tassili externe à l'E de Fort-Polignac (Sahara central), *CR Soc Géol Fr*, 1959, 172–174, 1960.
- Cherepanova, Y. and Artemieva, I. M.: Density heterogeneity of the cratonic lithosphere: A case study of the Siberian Craton, *Gondwana Res.*, 28(4), 1344–1360, doi:10.1016/j.gr.2014.10.002, 2015.
- Cherepanova, Y., Artemieva, I. M., Thybo, H. and Chemia, Z.: Crustal structure of the Siberian craton and the West Siberian basin: An appraisal of existing seismic data, *Tectonophysics*, 609, 154–183, doi:10.1016/j.tecto.2013.05.004, 2013.
- Chevalier, F., Guiraud, M., Garcia, J.-P., Dommergues, J.-L., Quesne, D., Allemand, P. and Dumont, T.: Calculating the long-term displacement rates of a normal fault from the high-resolution stratigraphic record (early Tethyan rifting, French Alps), *Terra Nova*, 15(6), 410–416, doi:10.1046/j.1365-3121.2003.00508.x, 2003.
- Choukroune, P., Gapais, D. and Merle, O.: Shear criteria and structural symmetry, *J. Struct. Geol.*, 9(5–6), 525–530, doi:10.1016/0191-8141(87)90137-4, 1987.
- Choukroune, P., Bouhallier, H. and Arndt, N. T.: Soft lithosphere during periods of Archaean crustal growth or crustal reworking, *Geol. Soc. Lond. Spec. Publ.*, 95(1), 67–86, doi:10.1144/GSL.SP.1995.095.01.05, 1995.
- Claracq, P., Fabre, C., Freulon, J. M. and Nougarede, F.: Une discordance angulaire dans les “Grès inférieurs” de l'Adrar Tan Elak (Sahara central), *C. r. Somm. Séances Soc. Géologique Fr.*, 309–310, 1958.
- Claret, J. and Tempere, C.: Le Paléozoïque du Bassin du Tamesna (Sud del 'Ahaggar), *Z. Dtsch. Geol. Ges.*, 460–468, 1968.
- Clerc, S.: Modèles de dépôt sous-glaciaires et dynamique de remplissage des vallées tunnel. Exemple au Quaternaire (Bray, Irlande) et application à l'Ordovicien supérieur de l'Anti-Atlas (Alnif, Maroc)., Université de Bourgogne., 2012.
- Clerc, S., Buoncristiani, J.-F., Guiraud, M., Vennin, E., Desaubliaux, G. and Portier, E.: Subglacial to proglacial depositional environments in an Ordovician glacial tunnel valley, Alnif, Morocco, *Palaeogeogr. Palaeoclimatol. Palaeoecol.*, 370, 127–144, doi:10.1016/j.palaeo.2012.12.002, 2013.
- Cloetingh, S.: Intraplate Stresses: A New Element in Basin Analysis, in *New Perspectives in Basin Analysis*, edited by K. L. Kleinspehn and C. Paola, pp. 205–230, Springer New York, New York, NY., 1988.
- Cloetingh, S. and Burov, E.: Lithospheric folding and sedimentary basin evolution: a review and analysis of formation mechanisms, *Basin Res.*, 23(3), 257–290, doi:10.1111/j.1365-2117.2010.00490.x, 2011.

- Cloetingh, S., Burov, E. and Poliakov, A.: Lithosphere folding: Primary response to compression? (from central Asia to Paris basin), *Tectonics*, 18(6), 1064–1083, doi:10.1029/1999TC900040, 1999.
- Coakley, B. and Gurnis, M.: Far-field tilting of Laurentia during the Ordovician and constraints on the evolution of a slab under an ancient continent, *J. Geophys. Res. Solid Earth*, 100(B4), 6313–6327, 1995.
- Coelho, D. L. O., Julià, J., Rodríguez-Tribaldos, V. and White, N.: Deep crustal architecture of the Parnaíba basin of NE Brazil from receiver function analysis: implications for basin subsidence, *Geol. Soc. Lond. Spec. Publ.*, 472, SP472.8, doi:10.1144/SP472.8, 2018.
- Collomb, G. R.: Étude géologique du Jebel Fezzan et de sa bordure paléozoïque, *Compagnie française des pétroles.*, 1962.
- Condie, K. C.: Origin and early development of the earth's crust, *Precambrian Res.*, 11(3), 183–197, doi:10.1016/0301-9268(80)90064-9, 1980.
- Condie, K. C.: Episodic continental growth and supercontinents: a mantle avalanche connection?, *Earth Planet. Sci. Lett.*, 163(1), 97–108, doi:10.1016/S0012-821X(98)00178-2, 1998.
- Condie, K. C.: Accretionary orogens in space and time, in *Geological Society of America Memoirs*, vol. 200, pp. 145–158, Geological Society of America., 2007.
- Conrad, J.: La régression namurienne sur le Nord de la plate-forme africaine, *CR Acad Sci Paris*, 274, 2003–2006, 1972.
- Conrad, J.: Les grandes lignes stratigraphiques et sédimentologiques du Carbonifère de l'Ahnet-Mouydir (Sahara central algérien), *Rev. Inst. Fr. Pétrole*, 28, 3–18, 1973.
- Conrad, J.: Les séries carbonifères du Sahara central algérien: stratigraphie, sédimentation, évolution structurale, *Doctoral dissertation*, Université Aix-Marseille III, France., 1984.
- Conrad, J., Massa, D. and Weyant, M.: Late Devonian regression and Early Carboniferous transgression on the Northern African platform, *Ann. Société Géologique Belg.* [online] Available from: <http://popups.ulg.ac.be/0037-9395/index.php?id=2997> (Accessed 20 November 2016), 2010.
- Copper, P.: Frasnian/Famennian mass extinction and cold-water oceans, *Geology*, 14(10), 835–839, 1986.
- Coquel, R. and Abdesselam-Rouighi, F.: Révision palynostratigraphique du dévonien terminal-carbonifère inférieur dans le Grand Erg occidental (bassin de Béchar) Sahara Algérien, *Rev. Micropaléontologie*, 43(3), 353–364, doi:10.1016/S0035-1598(00)90182-X, 2000.
- Coquel, R., Lang, J. and Yahaya, M.: Palynologie du Carbonifère du Nord Niger et de la plate-forme saharienne—implications stratigraphiques et paléogéographiques, *Rev. Palaeobot. Palynol.*, 89(3), 319–334, doi:10.1016/0034-6667(95)00035-2, 1995.
- Cordani, U. G. and Teixeira, W.: Proterozoic accretionary belts in the Amazonian Craton, *Geol. Soc. Am. Mem.*, 200, 297–320, 2007.

- Cosgrove, J. W. and Ameen, M. S.: A comparison of the geometry, spatial organization and fracture patterns associated with forced folds and buckle folds, *Geol. Soc. Lond. Spec. Publ.*, 169(1), 7–21, 1999.
- Coward, M. P. and Ries, A. C.: Tectonic development of North African basins, *Geol. Soc. Lond. Spec. Publ.*, 207(1), 61–83, doi:10.1144/GSL.SP.2003.207.4, 2003.
- Cózar, P., Somerville, I. D., Vachard, D., Coronado, I., García-Frank, A., Medina-Varea, P., Said, I., Del Moral, B. and Rodríguez, S.: Upper Mississippian to lower Pennsylvanian biostratigraphic correlation of the Sahara Platform successions on the northern margin of Gondwana (Morocco, Algeria, Libya), *Gondwana Res.*, 36, 459–472, doi:10.1016/j.gr.2015.07.019, 2016.
- Craig, J., Rizzi, C., Thusu, B., Lüning, S., Asbali, A. I., Keeley, M. L., Bell, J. F., Durham, M. J., Eales, M. H., Beswetherick, S. and Bishop, C.: Structural Styles and Prospectivity in the Precambrian and Palaeozoic Hydrocarbon Systems of North Africa, 2006.
- Craig, J., Rizzi, C., Said, F., Thusu, B., Luning, S., Asbali, A. I., Keeley, M. L., Bell, J. F., Durham, M. J. and Eales, M. H.: Structural styles and prospectivity in the Precambrian and Palaeozoic hydrocarbon systems of North Africa, *Geol. East Libya*, 4, 51–122, 2008.
- Culling, W. E. H.: Theory of erosion on soil-covered slopes, *J. Geol.*, 73(2), 230–254, 1965.
- Dallmeyer, R. D.: Terranes in the Circum-Atlantic Paleozoic Orogens, Geological Society of America., 1989.
- Dallmeyer, R. D. and Lécorché, J. P., Eds.: The West African Orogens and Circum-Atlantic Correlatives, Springer Berlin Heidelberg, Berlin, Heidelberg., 1991.
- Daly, M. C., Chorowicz, J. and Fairhead, J. D.: Rift basin evolution in Africa: the influence of reactivated steep basement shear zones, *Geol. Soc. Lond. Spec. Publ.*, 44(1), 309–334, 1989.
- Daly, M. C., Andrade, V., Barousse, C. A., Costa, R., McDowell, K., Piggott, N. and Poole, A. J.: Brasiliano crustal structure and the tectonic setting of the Parnaíba basin of NE Brazil: Results of a deep seismic reflection profile, *Tectonics*, 33(11), 2102–2120, doi:10.1002/2014TC003632, 2014.
- Daly, M. C., Fuck, R. A., Julià, J., Macdonald, D. I. M. and Watts, A. B.: Cratonic basin formation: a case study of the Parnaíba Basin of Brazil, *Geol. Soc. Lond. Spec. Publ.*, SP472.20, doi:10.1144/SP472.20, 2018a.
- Daly, M. C., Tozer, B. and Watts, A. B.: Cratonic basins and the Wilson cycle: a perspective from the Parnaíba Basin, Brazil, *Geol. Soc. Lond. Spec. Publ.*, 470, SP470.13, doi:10.1144/SP470.13, 2018b.
- Denis, M.: Interactions entre glaciation deglaciation, déformation et enregistrement stratigraphique Application à l'Ordovicien supérieur-Silurien du bassin du Djado (Niger) et des bassins d'Afrique du Nord, Université de Bourgogne., 2007.
- Denis, M., Buoncristiani, J.-F., Konaté, M., Ghienne, J.-F. and Guiraud, M.: Hirnantian glacial and deglacial record in SW Djado Basin (NE Niger)., *Geodin. Acta*, 20(3), 177–195, doi:10.3166/ga.20.177-195, 2007.

- Denis, M., Guiraud, M., Konaté, M. and Buoncristiani, J.-F.: Subglacial deformation and water-pressure cycles as a key for understanding ice stream dynamics: evidence from the Late Ordovician succession of the Djado Basin (Niger), *Int. J. Earth Sci.*, 99(6), 1399–1425, doi:10.1007/s00531-009-0455-z, 2010.
- Derder, M. E. M., Smith, B., Henry, B., Yelles, A. K., Bayou, B., Djellit, H., Ait ouali, R. and Gandriche, H.: Juxtaposed and superimposed paleomagnetic primary and secondary components from the folded middle carboniferous sediments in the Reggane Basin (Saharan craton, Algeria), *Tectonophysics*, 332(4), 403–421, doi:10.1016/S0040-1951(00)00298-5, 2001.
- Derder, M. E. M., Maouche, S., Liégeois, J. P., Henry, B., Amenna, M., Ouabadi, A., Bellon, H., Bruguier, O., Bayou, B., Bestandji, R., Nouar, O., Bouabdallah, H., Ayache, M. and Beddiaf, M.: Discovery of a Devonian mafic magmatism on the western border of the Murzuq basin (Saharan metacraton): Paleomagnetic dating and geodynamical implications, *J. Afr. Earth Sci.*, 115, 159–176, doi:10.1016/j.jafrearsci.2015.11.019, 2016.
- DeRito, R. F., Cozzarelli, F. A. and Hodge, D. S.: Mechanism of subsidence of ancient cratonic rift basins, *Tectonophysics*, 94(1), 141–168, doi:10.1016/0040-1951(83)90014-8, 1983.
- Derycke, C. and Goujet, D.: Multicuspidate shark teeth associated with chondrichthyan and acanthodian scales from the Emsian (Devonian) of southern Algeria, *Geodiversitas*, 33(2), 209–226, doi:10.5252/g2011n2a1, 2011.
- Desaubliaux, G., Callot, J. P., Cacas, M. C., Eschard, R., Euzen, T. and Deschamps, R.: Sedimentology of the Cambro-Ordovician reservoir in the Sbâa Basin, Institut Française du Pétrole - GDF unpublished., 2005.
- Deschamps, R., Eschard, R. and Roussé, S.: Architecture of Late Ordovician glacial valleys in the Tassili N’Ajjer area (Algeria), *Sediment. Geol.*, 289, 124–147, doi:10.1016/j.sedgeo.2013.02.012, 2013.
- Dineley, D. L.: Arches and basins of the Southern Arctic Islands of Canada, *Proc. Geol. Assoc.*, 82(4), 411-IN5, doi:10.1016/S0016-7878(71)80019-6, 1971.
- Dixon, R. J., Patton, T. L. and Hirst, J. P. P.: Giant Sandwaves from the Late Ordovician of the Tassili N’Ager, Algeria, *Mar. River Dune Dyn.*, 2008a.
- Dixon, R. J., Patton, T. L., Hirst, J. P. P. and Diggins, J.: Transition from Subglacial to Proglacial Depositional Systems: Implications for Reservoir Architecture, Illizi Basin, Algeria, AAPG Annual Convention, San Antonio, Texas., 2008b.
- Dixon, R. J., Moore, J. K. S., Bourne, M., Dunn, E., Haig, D. B., Hossack, J., Roberts, N., Parsons, T. and Simmons, C. J.: Integrated petroleum systems and play fairway analysis in a complex Palaeozoic basin: Ghadames-Illizi Basin, North Africa, in *Petroleum Geology: From Mature Basins to New Frontiers—Proceedings of the 7th Petroleum Geology Conference*, pp. 735–760, Geological Society of London., 2010.
- Djellit, H., Henry, B. and Derder, M. E.: Sur la présence d’une série molassique (de type série pourprée) au Sud-Est de l’Ahaggar (In Guezzam, Ahaggar, Algérie), *Comptes Rendus Geosci.*, 334(10), 789–794, 2002.

- Djomani, Y. H. P., O'Reilly, S. Y., Griffin, W. L. and Morgan, P.: The density structure of subcontinental lithosphere through time, *Earth Planet. Sci. Lett.*, 184(3–4), 605–621, doi:10.1016/S0012-821X(00)00362-9, 2001.
- Djouadi, M. T., Gleizes, G., Ferré, E., Bouchez, J. L., Caby, R. and Lesquer, A.: Oblique magmatic structures of two epizonal granite plutons, Hoggar, Algeria: late-orogenic emplacement in a transcurrent orogen, *Tectonophysics*, 279(1), 351–374, 1997.
- Djouder, H., Boulvain, F., Da Silva, A.-C. and Lüning, S.: The Siluro-Devonian sedimentary record of the Tassili n'Ajjer (SE Algeria), *STRATA*. [online] Available from: <http://orbi.ulg.ac.be/handle/2268/188688> (Accessed 20 November 2016), 2015.
- Djouder, H., Lüning, S., Da Silva, A.-C., Abdallah, H. and Boulvain, F.: Silurian deltaic progradation, Tassili n'Ajjer plateau, south-eastern Algeria: Sedimentology, ichnology and sequence stratigraphy, *J. Afr. Earth Sci.*, 142, 170–192, 2018.
- Dokka, A. M.: Sedimentological core description WELL: W7, Block - 340, (District - 3) (unpublished), Core description, Sonatrach division exploration direction des opérations département assistance aux opérations service géologique, Algérie., 1999.
- Dooley, T. P. and Schreurs, G.: Analogue modelling of intraplate strike-slip tectonics: A review and new experimental results, *Tectonophysics*, 574–575, 1–71, doi:10.1016/j.tecto.2012.05.030, 2012.
- Doré, A. G., Lundin, E. R., Fichler, C. and Olesen, O.: Patterns of basement structure and reactivation along the NE Atlantic margin, *J. Geol. Soc.*, 154(1), 85–92, 1997.
- Drid, M.: Sur quelques aspects de la diagénèse organique et minérale dans le bassin de Timimoun et le sillon de Sbaa, Sahara central algérien, Bordeaux 3, 1 January., 1989.
- Dubois, P.: Stratigraphie du Cambro-Ordovicien du Tassili n'Ajjer (Sahara central), *Bull. Société Géologique Fr.*, S7-III(2), 206–209, doi:10.2113/gssgfbull.S7-III.2.206, 1961.
- Dubois, P. and Mazelet, P.: Stratigraphie du Silurien du Tassili N'Ajjer, *Bull. Société Géologique Fr.*, S7-VI(4), 586–591, doi:10.2113/gssgfbull.S7-VI.4.586, 1964.
- Dubois, P., Beuf, S. and Biju-Duval, B.: Lithostratigraphie du Dévonien inférieur gréseux du Tassili n'Ajjer, in *Symposium on the Lower Devonian and its limits: Bur. Recherche Geol. et Minieres Mem*, pp. 227–235., 1967.
- Durrheim, R. J. and Mooney, W. D.: Evolution of the Precambrian lithosphere: Seismological and geochemical constraints, *J. Geophys. Res.*, 99(B8), 15359, doi:10.1029/94JB00138, 1994.
- Eaton, D. W. and Darbyshire, F.: Lithospheric architecture and tectonic evolution of the Hudson Bay region, *Tectonophysics*, 480(1–4), 1–22, doi:10.1016/j.tecto.2009.09.006, 2010.
- Echikh, K.: Geology and hydrocarbon occurrences in the Ghadames basin, Algeria, Tunisia, Libya, *Geol. Soc. Lond. Spec. Publ.*, 132(1), 109–129, 1998.
- Echikh, K. and Sola, M. A.: Geology and hydrocarbon occurrences in the Murzuq Basin, SW Libya, in *Geological exploration in Murzuq Basin*, pp. 175–222, Elsevier., 2000.

- Einsele, G.: *Sedimentary Basins - Evolution, Facies, and Sediment Budget* | Gerhard Einsele | Springer. [online] Available from: <http://www.springer.com/us/book/9783540661931> (Accessed 5 January 2017), 2000.
- English, J. M., Finkbeiner, T., English, K. L. and Cherif, R. Y.: State of stress in exhumed basins and implications for fluid flow: insights from the Illizi Basin, Algeria, *Geol. Soc. Lond. Spec. Publ.*, 458(1), 89–112, doi:10.1144/SP458.6, 2017.
- English, K. L., Redfern, J., Corcoran, D. V., English, J. M. and Cherif, R. Y.: Constraining burial history and petroleum charge in exhumed basins: New insights from the Illizi Basin, Algeria, *AAPG Bull.*, 100(04), 623–655, doi:10.1306/12171515067, 2016a.
- English, K. L., Redfern, J., Bertotti, G., English, J. M. and Yahia Cherif, R.: Intraplate uplift: New constraints on the Hoggar dome from the Illizi basin (Algeria), *Basin Res.*, n/a-n/a, doi:10.1111/bre.12182, 2016b.
- Eriksson, P. G., Catuneanu, O., Nelson, D. R. and Popa, M.: Controls on Precambrian sea level change and sedimentary cyclicity, *Sediment. Geol.*, 176(1–2), 43–65, 2005.
- Eschard, R., Desaubliaux, G., Deschamps, R., Montadert, L., Ravenne, C., Bekkouche, D., Abdallah, H., Belhaouas, S., Benkouider, M., Braïk, F., Henniche, M., Maache, N. and Mouaïci, R.: *Illizi-Berkine Devonian Reservoir Consortium* (unpublished), Institut Française du Pétrole - Sontrach, unpublished, Algérie., 1999.
- Eschard, R., Abdallah, H., Braïk, F. and Desaubliaux, G.: The Lower Paleozoic succession in the Tassili outcrops, Algeria: sedimentology and sequence stratigraphy, *First Break*, 23(10), 27–36, 2005.
- Eschard, R., Braïk, F., Bekkouche, D., Rahuma, M. B., Desaubliaux, G., Deschamps, R. and Proust, J. N.: Palaeohighs: their influence on the North African Palaeozoic petroleum systems, *Pet. Geol. Mature Basins New Front. 7th Pet. Geol. Conf.*, 707–724, 2010.
- Eyer, J. A.: 20 - The Moscow Basin, in *Regional Geology and Tectonics: Phanerozoic Passive Margins, Cratonic Basins and Global Tectonic Maps*, edited by D. G. Roberts and A. W. Bally, pp. 730–751, Elsevier, Boston., 2012.
- Fabre, J.: *Introduction à la géologie du Sahara algérien et des régions voisines: La couverture phanérozoïque*, SNED., 1976.
- Fabre, J.: Les séries paléozoïques d’Afrique: une approche, *J. Afr. Earth Sci. Middle East*, 7(1), 1–40, doi:10.1016/0899-5362(88)90051-6, 1988.
- Fabre, J.: *Géologie du Sahara occidental et central*, Musée royal de l’Afrique centrale., 2005.
- Fabre, J., Kaci, A. A., Bouïma, T. and Moussine-Pouchkine, A.: Le cycle molassique dans le Rameau trans-saharien de la chaîne panafricaine, *J. Afr. Earth Sci.*, 7, 41–55, doi:10.1016/0899-5362(88)90052-8, 1988.
- Fairhead, J. D., Green, C. M., Masterton, S. M. and Guiraud, R.: The role that plate tectonics, inferred stress changes and stratigraphic unconformities have on the evolution of the West and Central African Rift System and the Atlantic continental margins, *Tectonophysics*, 594, 118–127, doi:10.1016/j.tecto.2013.03.021, 2013.

- Faure, J. L. and Chermette, J.-C.: Deformation of tilted blocks, consequences on block geometry and extension measurements, *Bull. Société Géologique Fr.*, 5, 3, 1989.
- Fekirine, B. and Abdallah, H.: Palaeozoic lithofacies correlatives and sequence stratigraphy of the Saharan Platform, Algeria, *Geol. Soc. Lond. Spec. Publ.*, 132(1), 97–108, doi:10.1144/GSL.SP.1998.132.01.05, 1998.
- Ferkous, K. and Monie, P.: Neoproterozoic shearing and auriferous hydrothermalism along the lithospheric N–S East In Ouzzal shear zone (Western Hoggar, Algeria, North Africa), *J. Afr. Earth Sci.*, 35(3), 399–415, 2002.
- Ferrara, G. and Gravelle, M.: Radiometric ages from Western Ahaggar (Sahara) suggesting an eastern limit for the West African craton, *Earth Planet. Sci. Lett.*, 1(5), 319–324, 1966.
- Fezaa, N., Ouabadi, A., Liégeois, J. P., Abdallah, N., De Waele, B. and Bruguier, O.: La terrane de Djanet: Géochronologie et géochimie de ses granites et sédiments; lien avec le métacraton Saharien, USTHB, Algiers, Algeria., 2006.
- Fezaa, N., Liégeois, J.-P., Abdallah, N., Cherfouh, E. H., De Waele, B., Bruguier, O. and Ouabadi, A.: Late Ediacaran geological evolution (575–555Ma) of the Djanet Terrane, Eastern Hoggar, Algeria, evidence for a Murzukian intracontinental episode, *Precambrian Res.*, 180(3–4), 299–327, doi:10.1016/j.precamres.2010.05.011, 2010.
- Fezaa, N., Liégeois, J. P., Abdallah, N., Bruguier, O., Laouar, R. and Ouabadi, A.: Origine du groupe métasédimentaire de Djanet (Hoggar Oriental, Algérie) Géochronologie et géochimie, *Bull Serv Géologique Natl*, 24, 3–26, 2013.
- Fishwick, S. and Bastow, I. D.: Towards a better understanding of African topography: a review of passive-source seismic studies of the African crust and upper mantle, *Geol. Soc. Lond. Spec. Publ.*, 357(1), 343–371, doi:10.1144/SP357.19, 2011.
- Follot, J.: Sur l'existence de mouvements calédoniens au Mouydir (Sahara Central), *Compte Rendus Hebd. Séances L'Académie Sci.*, 230(25), 2217–2218, 1950.
- Follot, J.: Sur les différentes phases tectoniques ayant affecté la bordure septentrionale du Hoggar, *Trav. Institut Rech. Sahariennes*, 9, 137–142, 1953.
- Fossen, H.: *Structural geology*, Cambridge University Press, Cambridge; New York., 2010.
- Fowler, A. and Osman, A. F.: Sedimentation and inversion history of three molasse basins of the western Central Eastern Desert of Egypt: Implications for the tectonic significance of Hammamat basins, *Gondwana Res.*, 23(4), 1511–1534, doi:10.1016/j.gr.2012.08.022, 2013.
- Fowler, C. M. R. and Nisbet, E. G.: The subsidence of the Williston Basin, *Can. J. Earth Sci.*, 22(3), 408–415, doi:10.1139/e85-039, 1985.
- François, T., Burov, E., Meyer, B. and Agard, P.: Surface topography as key constraint on thermo-rheological structure of stable cratons, *Tectonophysics*, 602, 106–123, doi:10.1016/j.tecto.2012.10.009, 2013.

- Frederiksen, A. W., Deniset, I., Ola, O. and Toni, D.: Lithospheric fabric variations in central North America: Influence of rifting and Archean tectonic styles, *Geophys. Res. Lett.*, 40(17), 4583–4587, 2013.
- Freulon, J. M.: Mouvements calédoniens dans l'est du Sahara central, *COMPTES RENDUS Hebd. SEANCES Acad. Sci.*, 241(25), 1965–1967, 1955.
- Freulon, J. M.: Étude géologique des séries primaires du Sahara central:(Tassili-n-Ájjer et Fezzan)., Centre national de la recherche scientifique., 1964.
- Frizon de Lamotte, D., Tavakoli-Shirazi, S., Leturmy, P., Averbuch, O., Mouchot, N., Raulin, C., Leparmentier, F., Blanpied, C. and Ringenbach, J.-C.: Evidence for Late Devonian vertical movements and extensional deformation in northern Africa and Arabia: Integration in the geodynamics of the Devonian world: Devonian evolution Northern Gondwana, *Tectonics*, 32(2), 107–122, doi:10.1002/tect.20007, 2013.
- Fröhlich, S., Petitpierre, L., Redfern, J., Grech, P., Bodin, S. and Lang, S.: Sedimentological and sequence stratigraphic analysis of Carboniferous deposits in western Libya: Recording the sedimentary response of the northern Gondwana margin to climate and sea-level changes, *J. Afr. Earth Sci.*, 57(4), 279–296, doi:10.1016/j.jafrearsci.2009.09.007, 2010a.
- Fröhlich, S., Petitpierre, L., Redfern, J., Grech, P., Bodin, S. and Lang, S.: Sedimentological and sequence stratigraphic analysis of Carboniferous deposits in western Libya: Recording the sedimentary response of the northern Gondwana margin to climate and sea-level changes, *J. Afr. Earth Sci.*, 57(4), 279–296, doi:10.1016/j.jafrearsci.2009.09.007, 2010b.
- Futyan, A., Croxton, C. and Miles, N.: Palynological analysis of the MLE-1 well (3099m to 4400m TD) for Anadarko Algeria corporation and LL&E Algeria Limited, Futyan Jawzi & Associates International Petroleum Consultancy., 1996.
- Gac, S., Huismans, R. S., Simon, N. S. C., Podladchikov, Y. Y. and Faleide, J. I.: Formation of intracratonic basins by lithospheric shortening and phase changes: a case study from the ultra-deep East Barents Sea basin, *Terra Nova*, 25(6), 459–464, doi:10.1111/ter.12057, 2013.
- Galeazzi, S., Point, O., Haddadi, N., Mather, J. and Druésne, D.: Regional geology and petroleum systems of the Illizi–Berkine area of the Algerian Saharan Platform: An overview, *Mar. Pet. Geol.*, 27(1), 143–178, doi:10.1016/j.marpetgeo.2008.10.002, 2010.
- Galloway, W. E.: Genetic Stratigraphic Sequences in Basin Analysis I: Architecture and Genesis of Flooding-Surface Bounded Depositional Units, *AAPG Bull.*, 73(2), 125–142, 1989.
- Galushkin, Yu. I. and Eloghbi, S.: Thermal history of the Murzuq Basin, Libya, and generation of hydrocarbons in its source rocks, *Geochem. Int.*, 52(6), 486–499, doi:10.1134/S0016702914060032, 2014.
- Gapais, D., Jaguin, J., Cagnard, F. and Boulvais, P.: Pop-down tectonics, fluid channelling and ore deposits within ancient hot orogens, *Tectonophysics*, 618, 102–106, doi:10.1016/j.tecto.2014.01.027, 2014.
- Garfunkel, Z.: Early Paleozoic sediments of NE Africa and Arabia: Products of continental-scale erosion, sediment transport, and deposition., *Isr. J. Earth Sci.*, 51 [online] Available from: <http://search.ebscohost.com/login.aspx?direct=true&profile=ehost&scope=site&authtype=cra>

- wler&jrnl=00212164&AN=14592281&h=OdLrhH3KzMb2pww3GATywxQNMBEAady8lzJdRECzPz5YyQLxfrOjIxbPZ99mYx3tiOKRYQVGWRoXzJQq1KM0Kw%3D%3D&crl=c (Accessed 24 November 2016), 2002.
- Gariel, O., de Charpal, O. and Bennacef, A.: Sur la sédimentation des grès du Cambro-Ordovicien (Unité II) dans l'Ahnet et le Mouydir (Sahara central): *Algerie, Serv. Geol, Bull N Ser*, (38), 7–37, 1968.
- Gaschnig, R. M., Vervoort, J. D., Lewis, R. S. and Tikoff, B.: Probing for Proterozoic and Archean crust in the northern U.S. Cordillera with inherited zircon from the Idaho batholith, *GSA Bull.*, 125(1–2), 73–88, doi:10.1130/B30583.1, 2013.
- Ghienne, J. F., Le Heron, D. P., Moreau, J., Denis, M. and Deynoux, M.: The Late Ordovician glacial sedimentary system of the North Gondwana platform, *Glacial Sediment. Process. Prod. Spec. Publ. Ed. Hambrey M Christoffersen P Glas. N Janssen P Hubbard B Siegert M*, 39, 295–319, 2007a.
- Ghienne, J.-F.: Late Ordovician sedimentary environments, glacial cycles, and post-glacial transgression in the Taoudeni Basin, West Africa, *Palaeogeogr. Palaeoclimatol. Palaeoecol.*, 189(3–4), 117–145, doi:10.1016/S0031-0182(02)00635-1, 2003.
- Ghienne, J.-F., Deynoux, M., Manatschal, G. and Rubino, J.-L.: Palaeovalleys and fault-controlled depocentres in the Late-Ordovician glacial record of the Murzuq Basin (central Libya), *Comptes Rendus Geosci.*, 335(15), 1091–1100, doi:10.1016/j.crte.2003.09.010, 2003.
- Ghienne, J.-F., Boumendjel, K., Paris, F., Videt, B., Racheboeuf, P. and Salem, H. A.: The Cambrian-Ordovician succession in the Ougarta Range (western Algeria, North Africa) and interference of the Late Ordovician glaciation on the development of the Lower Palaeozoic transgression on northern Gondwana, *Bull. Geosci.*, 183–214, doi:10.3140/bull.geosci.2007.03.183, 2007b.
- Ghienne, J.-F., Moreau, J., Degermann, L. and Rubino, J.-L.: Lower Palaeozoic unconformities in an intracratonic platform setting: glacial erosion versus tectonics in the eastern Murzuq Basin (southern Libya), *Int. J. Earth Sci.*, 102(2), 455–482, doi:10.1007/s00531-012-0815-y, 2013.
- Gindre, L., Le Heron, D. and Bjørnseth, H. M.: High resolution facies analysis and sequence stratigraphy of the Siluro-Devonian succession of Al Kufrah basin (SE Libya), *J. Afr. Earth Sci.*, 76, 8–26, doi:10.1016/j.jafrearsci.2012.08.002, 2012.
- Girard, F.: *Faciès, architecture et dynamique d'un système proglaciaire fini-ordovicien (Bassin de Murzuq, Libye sud-occidentale)*, Université de Strasbourg., 2011.
- Girard, F., Ghienne, J.-F. and Rubino, J.-L.: Channelized sandstone bodies ('cordons') in the Tassili N'Ajjer (Algeria & Libya): snapshots of a Late Ordovician proglacial outwash plain, *Geol. Soc. Lond. Spec. Publ.*, 368(1), 355–379, doi:10.1144/SP368.3, 2012.
- Girard, F., Deschamps, R., Ghienne, J.-F., Roussé, S. and Rubino, J.-L.: Tracking the isostatic and eustatic signals in an end Ordovician-early Silurian deglacial sedimentary record (Algeria - Libya border), edited by N. Eyles, *Sedimentology*, doi:10.1111/sed.12535, 2018.
- Gleason, G. C. and Tullis, J.: A flow law for dislocation creep of quartz aggregates determined with the molten salt cell, *Tectonophysics*, 247(1–4), 1–23, 1995.

- Glover, R. T.: Aspects of intraplate deformation in Saharan cratonic basins, Ph.D., University of Wales, Aberystwyth, [online] Available from: <https://ethos.bl.uk/OrderDetails.do?uin=uk.bl.ethos.404019> (Accessed 25 March 2019), 1999.
- Goetze, C. and Evans, B.: Stress and temperature in the bending lithosphere as constrained by experimental rock mechanics, *Geophys. J. R. Astron. Soc.*, 59(3), 463–478, doi:10.1111/j.1365-246X.1979.tb02567.x, 1979.
- Golonka, J.: Plate-Tectonic Maps of the Phanerozoic, [online] Available from: http://archives.datapages.com/data/sepm_sp/SP72/Plate-Tectonic_Maps_of_the_Phanerozoic.htm (Accessed 4 July 2017), 2002.
- Goodwin, A. M.: Principles of Precambrian geology, Acad. Press, London., 1996.
- Grasemann, B., Martel, S. and Passchier, C.: Reverse and normal drag along a fault, *J. Struct. Geol.*, 27(6), 999–1010, doi:10.1016/j.jsg.2005.04.006, 2005.
- Greigertt, J. and Pognet, R.: Carte Géologique du Niger, 1/2000000, BRGM, République du Niger, 1965.
- Griffin, W. L., O'Reilly, S. Y., Abe, N., Aulbach, S., Davies, R. M., Pearson, N. J., Doyle, B. J. and Kivi, K.: The origin and evolution of Archean lithospheric mantle, *Precambrian Res.*, 127(1–3), 19–41, doi:10.1016/S0301-9268(03)00180-3, 2003.
- Guiraud, M.: Mécanisme de formation du bassin sur décrochements multiples de la Haute-Bénoué (Nigéria): faciès et géométrie des corps sédimentaires, microtectonique et déformations synsédimentaires, Thèse HDR, 444, 1990.
- Guiraud, M. and Seguret, M.: A Releasing Solitary Overstep Model for the Late Jurassic-Early Cretaceous (Wealdian) Soria Strike-Slip Basin (Northern Spain), [online] Available from: http://archives.datapages.com/data/sepm_sp/SP37/A_Releasing_Solitary_Overstep_Model.html (Accessed 19 December 2016), 1985.
- Guiraud, R. and Bosworth, W.: Senonian basin inversion and rejuvenation of rifting in Africa and Arabia: synthesis and implications to plate-scale tectonics, *Tectonophysics*, 282, 39–82, doi:10.1016/S0040-1951(97)00212-6, 1997.
- Guiraud, R., Bosworth, W., Thierry, J. and Delplanque, A.: Phanerozoic geological evolution of Northern and Central Africa: An overview, *J. Afr. Earth Sci.*, 43(1–3), 83–143, doi:10.1016/j.jafrearsci.2005.07.017, 2005.
- Gwavava, O., Swain, C. J. and Podmore, F.: Mechanisms of isostatic compensation of the Zimbabwe and Kaapvaal cratons, the Limpopo Belt and the Mozambique basin, *Geophys. J. Int.*, 127(3), 635–650, 1996.
- Haddoum, H.: Les structures hercyniennes dans la couverture sédimentaire paléozoïque de l'Ahnet Occidental et de Bled El Mass (NO Hoggar, Algérie): une conséquence du rejeu des failles panafricaines, *Bull. Serv. Géologique Natl.*, 20, 221–243, 2009.
- Haddoum, H., Choukroune, P. and Peucat, J. J.: Evolution of the Precambrian In-Ouzzal block (Central Sahara, Algeria), *Precambrian Res.*, 65(1), 155–166, 1994.

- Haddoum, H., Guiraud, R. and Moussine-Pouchkine, A.: Hercynian compressional deformations of the Ahnet–Mouydir Basin, Algerian Saharan Platform: far-field stress effects of the Late Palaeozoic orogeny, *Terra Nova*, 13(3), 220–226, 2001.
- Haddoum, H., Mokri, M., Ouzegane, K., Ait-Djaffer, S. and Djemai, S.: Extrusion de l'In Ouzzal vers le Nord (Hoggar occidental, Algérie): une conséquence d'un poinçonnement panafricain, *J. Hydrocarb. Mines Environ. Res.* Vol., 4(1), 6–16, 2013.
- Hallett, D.: *Petroleum geology of Libya*: BV Elsevier, Amst. Neth., 2002.
- Hamdani, Y., Mareschal, J.-C. and Arkani-Hamed, J.: Phase changes and thermal subsidence in intracontinental sedimentary basins, *Geophys. J. Int.*, 106(3), 657–665, doi:10.1111/j.1365-246X.1991.tb06337.x, 1991.
- Haq, B. U. and Schutter, S. R.: A Chronology of Paleozoic Sea-Level Changes, *Science*, 322(5898), 64–68, doi:10.1126/science.1161648, 2008.
- Harris, L. B.: Structural and tectonic synthesis for the Perth basin, Western Australia, *J. Pet. Geol.*, 17(2), 129–156, 1994.
- Hartley, R., Watts, A. B. and Fairhead, J. D.: Isostasy of Africa, *Earth Planet. Sci. Lett.*, 137(1), 1–18, doi:10.1016/0012-821X(95)00185-F, 1996.
- Hartley, R. W. and Allen, P. A.: Interior cratonic basins of Africa: relation to continental break-up and role of mantle convection, *Basin Res.*, 6(2–3), 95–113, 1994.
- Hassan, A.: Etude palynologique Paléozoïque du sondage Razzal-Allah-Nord (unpublished), Entreprise nationale Sonatrach division hydrocarbures direction Laboratoire central des hydrocarbures, Boumerdès., 1984.
- Haxby, W. F., Turcotte, D. L. and Bird, J. M.: Thermal and Mechanical Evolution of the Michigan Basin, *Dev. Geotecton.*, 12, 57–75, doi:10.1016/B978-0-444-41549-3.50008-6, 1976.
- Heilbron, M., Valeriano, C. M., Tassinari, C. C. G., Almeida, J., Tupinambá, M., Siga, O. and Trouw, R.: Correlation of Neoproterozoic terranes between the Ribeira Belt, SE Brazil and its African counterpart: comparative tectonic evolution and open questions, *Geol. Soc. Lond. Spec. Publ.*, 294(1), 211–237, 2008.
- Heine, C., Dietmar Müller, R., Steinberger, B. and Torsvik, T. H.: Subsidence in intracontinental basins due to dynamic topography, *Phys. Earth Planet. Inter.*, 171(1–4), 252–264, doi:10.1016/j.pepi.2008.05.008, 2008.
- Henniche, M.: *Architecture et modèle de dépôts d'une série sédimentaire paléozoïque en contexte cratonique*, Rennes 1, France., 2002.
- Henniche, M., Eschard, R., Proust, J. N., Hamel, A. and Paris, F.: Depositional models and reservoir architecture of the Siluro-Devonian series in outcrops and subsurface of Illizi basin (Algeria), in AAPG Hedberg Conference: Paleozoic and Triassic Petroleum Systems in North Algeria, Algiers., 2003a.

- Henniche, M., Eschard, R. and Proust, J. N.: Sedimentary Architecture of the Siluro-Devonian Sequences in Illizi Basin, Algeria., 2003b.
- Henry, B., Bayou, B., Derder, M. E. M., Djellit, H., Ouabadi, A., Khaldi, A. and Hemmi, A.: Late Panafrican evolution of the main Hoggar fault zones: Implications of magnetic fabric study in the In Telloukh pluton (Tin Serririne basin, Algeria), *J. Afr. Earth Sci.*, 49(4–5), 211–221, doi:10.1016/j.jafrearsci.2007.09.004, 2007.
- Heron, D. P. L. and Craig, J.: First-order reconstructions of a Late Ordovician Saharan ice sheet, *J. Geol. Soc.*, 165(1), 19–29, doi:10.1144/0016-76492007-002, 2008.
- Hesselbo, S. P.: 23. Spectral gamma-ray logs in relation to clay mineralogy and sequence stratigraphy, Cenozoic of the Atlantic margin, offshore New Jersey, in *Proceedings of the Ocean Drilling Program: Scientific Results*, vol. 150, p. 411, The Program., 1996.
- Hillis, R. R., Sandiford, M., Reynolds, S. D. and Quigley, M. C.: Present-day stresses, seismicity and Neogene-to-Recent tectonics of Australia's 'passive' margins: intraplate deformation controlled by plate boundary forces, *Geol. Soc. Lond. Spec. Publ.*, 306(1), 71–90, doi:10.1144/SP306.3, 2008.
- Hirst, J. P. P.: Ordovician proglacial sediments in Algeria: insights into the controls on hydrocarbon reservoirs in the In Amenas field, Illizi Basin, *Geol. Soc. Lond. Spec. Publ.*, 368(1), 319–353, doi:10.1144/SP368.17, 2012.
- Hirst, J. P. P.: Ordovician shallow-marine tidal sandwaves in Algeria – the application of coeval outcrops to constrain the geometry and facies of a discontinuous, high-quality gas reservoir, *Geol. Soc. Lond. Spec. Publ.*, 436(1), 135–150, doi:10.1144/SP436.11, 2016.
- Hirst, J. P. P., Benbakir, A., Payne, D. F. and Westlake, I. R.: Tunnel Valleys and Density Flow Processes in the upper Ordovician glacial succession, Illizi Basin, Algeria: influence on reservoir quality, *J. Pet. Geol.*, 25(3), 297–324, 2002.
- Hoffman, P. F., Bally, A. W. and Palmer, A. R.: Precambrian geology and tectonic history of North America, *Geol. North Am. Overv.*, 447–512, 1989.
- Hollard, H., Choubert, G., Bronner, G., Marchand, J. and Sougy, J.: Carte géologique du Maroc, scale 1: 1,000,000, *Serv Carte Géol Maroc*, 260(2), 1985.
- Holt, P.: Subsidence Mechanisms of Sedimentary Basins Developed over Accretionary Crust, Doctoral, Durham University. [online] Available from: <http://etheses.dur.ac.uk/3584/> (Accessed 22 November 2016), 2012.
- Holt, P. J., Allen, M. B., van Hunen, J. and Bjørnseth, H. M.: Lithospheric cooling and thickening as a basin forming mechanism, *Tectonophysics*, 495(3–4), 184–194, doi:10.1016/j.tecto.2010.09.014, 2010.
- Holt, P. J., Allen, M. B. and van Hunen, J.: Basin formation by thermal subsidence of accretionary orogens, *Tectonophysics*, 639, 132–143, doi:10.1016/j.tecto.2014.11.021, 2015.
- Howell, P. D. and Pluijm, B. A. van der: Early history of the Michigan basin: Subsidence and Appalachian tectonics, *Geology*, 18(12), 1195–1198, doi:10.1130/0091-7613(1990)018<1195:EHOTMB>2.3.CO;2, 1990.

- Howell, P. D. and van der Pluijm, B. A.: Structural sequences and styles of subsidence in the Michigan basin, *Geol. Soc. Am. Bull.*, 111(7), 974–991, doi:10.1130/0016-7606(1999)111<0974:SSASOS>2.3.CO;2, 1999.
- Idres, M., Belabbes, S., Bourmatte, A., Haddoum, H. and Samai, S.: Proposition d'un modèle de morphologie du socle sous le bassin de Tindouf, Algérie, à partir de l'inversion 3D des données gravimétriques, *Bull. Serv. Géologique Natl.*, 22(1), 81–90, 2011.
- Jacquemont, P., Jutard, G., Plauchut, B., Grégoire, J. and Mouflard, R.: Etude du bassin du Djado, *Bur. Rech. Pétroles Rapp.*, 1215, 1959.
- Jäger, H., Lewandowski, E. and Lampart, V.: Palynology of the upper Silurian to middle Devonian in the Reggane Basin, southern Algeria, Ext. Abstr. DGMK-Tagungsbericht 2009-1 DGMKÖGEW Spring Meet. Celle, 47–51, 2009.
- James, D. E. and Assumpção, M.: Tectonic implications of S-wave anisotropy beneath SE Brazil, *Geophys. J. Int.*, 126(1), 1–10, 1996.
- Jardiné, S. and Yapaudjian, L.: Lithostratigraphie et palynologie du Dévonien-Gothlandien gréseux du Bassin de Polignac (Sahara), *Rev. L'Institut Fr. Pétrole*, 23(4), 439–469, 1968.
- Jardiné, S., Combaz, A., Magloire, L., Peniguel, G. and Vachey, G.: Distribution stratigraphique des acritarches dans le paléozoïque du sahara algérien, *Rev. Palaeobot. Palynol.*, 18(1), 99–129, doi:10.1016/0034-6667(74)90012-8, 1974.
- Jin, G. and Groshong, R. H.: Trishear kinematic modeling of extensional fault-propagation folding, *J. Struct. Geol.*, 28(1), 170–183, doi:10.1016/j.jsg.2005.09.003, 2006.
- Johnson, K. M. and Johnson, A. M.: Mechanical analysis of the geometry of forced-folds, *J. Struct. Geol.*, 24(3), 401–410, 2002.
- Joulia, F.: Carte géologique de reconnaissance de la bordure sédimentaire occidentale de l'Aïr au 1/500 000, Éditions BRGM Orléans Fr., 1963.
- Jourdon, A.: Déformation de la lithosphère continentale en convergence : de la tectonique paléozoïque à la réactivation cénozoïque intra-plaque dans le Tien Shan (Asie Centrale), thesis, Côte d'Azur, 8 September. [online] Available from: <http://www.theses.fr/2017AZUR4070> (Accessed 28 December 2018), 2017.
- Jourdon, A., Le Pourhiet, L., Petit, C. and Rolland, Y.: The deep structure and reactivation of the Kyrgyz Tien Shan: Modelling the past to better constrain the present, *Tectonophysics*, doi:10.1016/j.tecto.2017.07.019, 2017.
- Jourdon, A., Le Pourhiet, L., Petit, C. and Rolland, Y.: Impact of range-parallel sediment transport on 2D thermo-mechanical models of mountain belts: Application to the Kyrgyz Tien Shan, *Terra Nova*, 30(4), 279–288, doi:10.1111/ter.12337, 2018.
- Kaban, M. K., Tesauro, M., Mooney, W. D. and Cloetingh, S. A. P. L.: Density, temperature, and composition of the North American lithosphere—New insights from a joint analysis of seismic, gravity, and mineral physics data: 1. Density structure of the crust and upper mantle, *Geochem. Geophys. Geosystems*, 15(12), 4781–4807, doi:10.1002/2014GC005483, 2014.

- Kadi, B., Aït Ouali, R. and Zazoun, R. S.: Comparaison de l'histoire thermique des bassins de Timimoun et de Berkine : impact sur l'évolution des argiles et de la matière organique, *Bull. Serv. Géologique Algérie*, 24(3), 1–25, 2013.
- Kamel, F. E.: Géologie du paléozoïque des Rehamna nord-orientaux, Maroc. Évolution sédimentaire et structuration hercynienne d'un bassin dévono-carbonifère. Sédimentation et déformation des molasses post-orogénique, phdthesis, Université Paul Cézanne - Aix-Marseille III, 7 July. [online] Available from: <https://tel.archives-ouvertes.fr/tel-01015986/document> (Accessed 20 November 2016), 1987.
- Kaminski, E. and Jaupart, C.: Lithosphere structure beneath the Phanerozoic intracratonic basins of North America, *Earth Planet. Sci. Lett.*, 178(1–2), 139–149, 2000.
- Kane, K. E., Jackson, C. A.-L. and Larsen, E.: Normal fault growth and fault-related folding in a salt-influenced rift basin: South Viking Graben, offshore Norway, *J. Struct. Geol.*, 32(4), 490–506, doi:10.1016/j.jsg.2010.02.005, 2010.
- Kaus, B., Connolly, J., Podladchikov, Y. and Schmalholz, S.: Effect of mineral phase transitions on sedimentary basin subsidence and uplift, *Earth Planet. Sci. Lett.*, 233(1–2), 213–228, doi:10.1016/j.epsl.2005.01.032, 2005.
- Kermandji, A. M.: Silurian–Devonian miospores from the western and central Algeria, *Rev. Micropaléontologie*, 50(1), 109–128, doi:10.1016/j.revmic.2007.01.003, 2007.
- Kermandji, A. M. H.: Late Silurian-Middle Devonian Miospores, , doi:10.5772/35200, 2012.
- Kermandji, A. M. H., Kowalski, M. W. and Pharisat, A.: Palynologie et séquences de l'Emsien de la région d'In Salah, Sahara central Algérien, *Bull. Société D'Histoire Nat. Pays Montbél.*, 301–306, 2003.
- Kermandji, A. M. H., Kowalski, W. M. and Touhami, F. K.: Miospore stratigraphy of Lower and early Middle Devonian deposits from Tidikelt, Central Sahara, Algeria, *Geobios*, 41(2), 227–251, doi:10.1016/j.geobios.2007.05.002, 2008.
- Kermandji, A. M. H., Touhami, F. K., Kowalski, W. M., Abbés, S. B., Boularak, M., Chabour, N., Laifa, E. L. and Hannachi, H. B.: Stratigraphie du Dévonien Inférieur du Plateau du Tidikelt d'In Salah (Sahara Central Algérie), *Comun. Geológicas*, (t. 96), 67–82, 2009.
- Khalil, S. M. and McClay, K. R.: Extensional fault-related folding, northwestern Red Sea, Egypt, *J. Struct. Geol.*, 24(4), 743–762, 2002.
- Khier, S.: Résultats palynologiques du sondage Garet El Guefoul (unpublished), Entreprise nationale Sonatrach division hydrocarbures direction Laboratoire central des hydrocarbures, Alger., 1974.
- Kichou-Braïk, F., Samar, L., Fekirine, B. and Legrand, P.: Découverte de graptolites d'âge Caradocien dans quelques sondages du Tinrhert (Sahara algérien), *Comptes Rendus Palevol*, 5(5), 675–683, doi:10.1016/j.crpv.2005.11.001, 2006.
- King, S.: Archean cratons and mantle dynamics, *Earth Planet. Sci. Lett.*, 234(1–2), 1–14, doi:10.1016/j.epsl.2005.03.007, 2005.

- Kingston, D. R., Dishroon, C. P. and Williams, P. A.: Global Basin Classification System, AAPG Bull., 67(12), 2175–2193, 1983.
- Klein, G. deV and Hsui, A. T.: Origin of cratonic basins, *Geology*, 15(12), 1094–1098, doi:10.1130/0091-7613(1987)15<1094:OOCB>2.0.CO;2, 1987.
- Klemme, H. d.: Petroleum Basins-Classifications and Characteristics, *J. Pet. Geol.*, 3(2), 187–207, doi:10.1111/j.1747-5457.1980.tb00982.x, 1980.
- Konaté, M., Guiraud, M., Lang, J. and Yahaya, M.: Structuration extensive et évolution tectono-sédimentaire du bassin d'âge Ordovicien supérieur-Silurien inférieur de Kandi (Nord Bénin, Sud Niger), *Afr. Geosci. Rev.*, 10(1 & 2), 33–68, 2003.
- Konaté, M., Lang, J., Guiraud, M., Yahaya, M., Denis, M. and Alidou, S.: Un bassin extensif formé pendant la fonte de la calotte glaciaire hirnantienne: le bassin ordovico-silurien de Kandi (Nord Bénin, Sud Niger), *Afr. Geosci. Rev.*, 13(2), 157–183, 2006.
- Konaté, M., Denis, M., Yahaya, M. and Guiraud, M.: Structuration extensive et transtensive au Dévono-Dinantien du bassin de Tim Mersoï (Bordure occidentale de l'Aïr, Nord Niger), 2009.
- Koptev, A., Burov, E., Calais, E., Leroy, S., Gerya, T., Guillou-Frottier, L. and Cloetingh, S.: Contrasted continental rifting via plume-craton interaction: Applications to Central East African Rift, *Geosci. Front.*, 7(2), 221–236, doi:10.1016/j.gsf.2015.11.002, 2016.
- Korn, D., Bockwinkel, J. and Ebbighausen, V.: Tournaisian and Viséan ammonoid stratigraphy in North Africa, *Neues Jahrb. Für Geol. Paläontol. - Abh.*, 243(2), 127–148, doi:10.1127/0077-7749/2007/0243-0127, 2007.
- Korn, D., Ebbighausen, V. and Bockwinkel, J.: Ammonoids from the Dalle des Iridet of the Mouydir and Ahnet (Central Sahara) and the Formation d'Hassi Sguilma of the Saoura Valley (Late Tournaisian-Early Viséan; Algeria), *Foss. Rec.*, 13(1), 203–214, doi:10.1002/mmng.200900012, 2010a.
- Korn, D., Bockwinkel, J. and Ebbighausen, V.: The ammonoids from the Argiles de Teguentour of Oued Temertasset (early Late Tournaisian; Mouydir, Algeria), *Foss. Rec.*, 13(1), 35–152, doi:10.1002/mmng.200900010, 2010b.
- Korsch, R. J., Harrington, H. J., Wake-Dyster, K. D., O'Brien, P. E. and Finlayson, D. M.: Sedimentary basins peripheral to the New England Orogen: their contribution to understanding New England tectonics, in *New England Orogen, Tectonics and Metallogensis*, pp. 134–140, Department of Geology and Geophysics, University of New England., 1988.
- Kracha, N.: Relation entre sédimentologie, fracturation naturelle et diagénèse d'un réservoir à faible perméabilité application aux réservoirs de l'Ordovicien bassin de l'Ahnet, Sahara central, Algérie, Doctoral dissertation, Université des sciences et technologies de Lille, France., 2011.
- Kroner, A.: Evolution of the Archean continental crust, *Annu. Rev. Earth Planet. Sci.*, 13(1), 49–74, 1985.
- Kröner, A. and Layer, P. W.: Crust formation and plate motion in the early Archean, *Science*, 256(5062), 1405–1411, 1992.

al-Laboun, A. A.: Stratigraphy and Hydrocarbon Potential of the Paleozoic Succession in Both Tabuk and Widyan Basins, Arabia, , 131, 373–397, 1986.

Lachkar, N., Guiraud, M., Harfi, A. E., Dommergues, J.-L., Dera, G. and Durlet, C.: Early Jurassic normal faulting in a carbonate extensional basin: characterization of tectonically driven platform drowning (High Atlas rift, Morocco), *J. Geol. Soc.*, 166(3), 413–430, doi:10.1144/0016-76492008-084, 2009.

Lafont, F.: Influences relatives de la subsidence et de l'eustatisme sur la localisation et la géométrie des réservoirs d'un système deltaïque: Exemple de l'Eocène du bassin de Jaca, Pyrénées espagnoles, phdthesis, Université Rennes 1, 6 January. [online] Available from: <https://tel.archives-ouvertes.fr/tel-00653783/document> (Accessed 21 November 2016), 1994.

Lafosse, M., Boutoux, A., Bellahsen, N. and Le Pourhiet, L.: Role of tectonic burial and temperature on the inversion of inherited extensional basins during collision, *Geol. Mag.*, 153(5–6), 811–826, doi:10.1017/S0016756816000510, 2016.

Laggoun-Défarage, F.: Etude de la diagenèse organique des séries paleozoïques du bassin de Sbaa (Algérie). Approche géochimique et pétrologique., phdthesis, Université d'Orléans, 11 December. [online] Available from: <https://tel.archives-ouvertes.fr/tel-00322456/document> (Accessed 20 November 2016), 1987.

Lambeck, K.: The role of compressive forces in intracratonic basin formation and mid-plate orogenies, *Geophys. Res. Lett.*, 10(9), 845–848, doi:10.1029/GL010i009p00845, 1983.

Lang, J., Dixon, R. J., Le Heron, D. P. and Winsemann, J.: Depositional architecture and sequence stratigraphic correlation of Upper Ordovician glaciogenic deposits, Illizi Basin, Algeria, *Geol. Soc. Lond. Spec. Publ.*, 368(1), 293–317, doi:10.1144/SP368.1, 2012.

Latin, D. and White, N.: Generating melt during lithospheric extension: Pure shear vs. simple shear, *Geology*, 18(4), 327–331, doi:10.1130/0091-7613(1990)018<0327:GMDLEP>2.3.CO;2, 1990.

Latouche, L.: Les tectoniques superprisées dans la région des Gour Oumelalen (NE de l'Ahaggar, Algérie), *CR Acad Sci Paris D*, 275, 899–902, 1972.

Latouche, L. and Vidal, P.: Géochronologie du Précambrien de la région des Gour Oumelalen (Nord-Est de l'Ahaggar-Algérie) Un exemple de mobilisation du strontium radiogénique, *Bull Soc Géol Fr7*, XVI(2), 1974.

Latreche, S. and Coquel, R.: Stratigraphie, sédimentologie et palynologie de la Formation d'Illère (Dévonien-Carbonifère) du bassin d'Illizi (Sahara algérien), *Bull. Serv. Géologique Algérie*, 7(1), 87–107, 1996.

Le Guerroué, E. and Cobbold, P. R.: Influence of erosion and sedimentation on strike-slip fault systems: insights from analogue models, *J. Struct. Geol.*, 28(3), 421–430, doi:10.1016/j.jsg.2005.11.007, 2006.

Le Heron, D. P.: Late Ordovician glacial record of the Anti-Atlas, Morocco, *Sediment. Geol.*, 201(1–2), 93–110, doi:10.1016/j.sedgeo.2007.05.004, 2007.

- Le Heron, D. P.: Interpretation of Late Ordovician glaciogenic reservoirs from 3-D seismic data: an example from the Murzuq Basin, Libya, *Geol. Mag.*, 147(01), 28–41, doi:10.1017/S0016756809990586, 2010.
- Le Heron, D. P., Sutcliffe, O. E., Whittington, R. J. and Craig, J.: The origins of glacially related soft-sediment deformation structures in Upper Ordovician glaciogenic rocks: implication for ice-sheet dynamics, *Palaeogeogr. Palaeoclimatol. Palaeoecol.*, 218(1–2), 75–103, doi:10.1016/j.palaeo.2004.12.007, 2005.
- Le Heron, D. P., Craig, J., Sutcliffe, O. E. and Whittington, R.: Late Ordovician glaciogenic reservoir heterogeneity: An example from the Murzuq Basin, Libya, *Mar. Pet. Geol.*, 23(6), 655–677, doi:10.1016/j.marpetgeo.2006.05.006, 2006.
- Le Heron, D. P., Ghienne, J.-F., El Houicha, M., Khoukhi, Y. and Rubino, J.-L.: Maximum extent of ice sheets in Morocco during the Late Ordovician glaciation, *Palaeogeogr. Palaeoclimatol. Palaeoecol.*, 245(1–2), 200–226, doi:10.1016/j.palaeo.2006.02.031, 2007.
- Le Heron, D. P., Craig, J. and Etienne, J. L.: Ancient glaciations and hydrocarbon accumulations in North Africa and the Middle East, *Earth-Sci. Rev.*, 93(3–4), 47–76, doi:10.1016/j.earscirev.2009.02.001, 2009.
- Legrand, P.: Découverte de nouveaux gisements fossilifères dans les grès inférieurs du Tassili N'Ajjers, *Société Géologique Fr. C. r.*, 5, 100–101, 1964.
- Legrand, P.: Le Devonien du Sahara Algérien, *Can. Soc. Pet. Geol.*, 1, 245–284, 1967a.
- Legrand, P.: Nouvelles connaissances acquises sur la limite des systèmes Silurien et Dévonien au Sahara algérien, *Bull. Bur. Rech. Géologiques Minières*, 33, 119–37, 1967b.
- Legrand, P.: The lower Silurian graptolites of Oued In Djerane: a study of populations at the Ordovician-Silurian boundary, *Geol. Soc. Lond. Spec. Publ.*, 20(1), 145–153, doi:10.1144/GSL.SP.1986.020.01.15, 1986.
- Legrand, P.: Late Ordovician-early Silurian paleogeography of the Algerian Sahara, *Bull. Société Géologique Fr.*, 174(1), 19–32, 2003a.
- Legrand, P.: Silurian stratigraphy and paleogeography of the northern African margin of Gondwana, in *Silurian Lands and Seas: Paleogeography Outside of Laurentia*, edited by E. Landing and M. E. Johson, pp. 59–104, New York., 2003b.
- Legrand-Blain, M.: Dynamique des Brachiopodes carbonifères sur la plate-forme carbonatée du Sahara algérien: paléoenvironnements, paléobiogéographie, évolution, Doctoral dissertation, Université de Bordeaux 1, France., 1985.
- Leprêtre, R.: Evolution phanérozoïque du Craton Ouest Africain et de ses bordures Nord et Ouest, Paris 11. [online] Available from: <http://www.theses.fr/2015PA112057> (Accessed 21 November 2016), 2015.
- Leprêtre, R., Missenard, Y., Barbarand, J., Gautheron, C., Saddiqi, O. and Pinna-Jamme, R.: Postrift history of the eastern central Atlantic passive margin: Insights from the Saharan region of South Morocco: Postrift Evolution Moroccan Margin, *J. Geophys. Res. Solid Earth*, 120(6), 4645–4666, doi:10.1002/2014JB011549, 2015.

- Lesquer, A., Bourmatte, A., Ly, S. and Dautria, J. M.: First heat flow determination from the central Sahara: relationship with the Pan-African belt and Hoggar domal uplift, *J. Afr. Earth Sci. Middle East*, 9(1), 41–48, 1989.
- Lesquer, A., Takherist, D., Dautria, J. M. and Hadiouche, O.: Geophysical and petrological evidence for the presence of an “anomalous” upper mantle beneath the Sahara basins (Algeria), *Earth Planet. Sci. Lett.*, 96(3–4), 407–418, 1990.
- Lessard, L.: Les series primaires des Tassilis Oua-n-Ahaggar au sud du Hoggar entre l’Ar et l’Adrar des Iforas (Sahara meridional), *Bull. Société Géologique Fr.*, S7-III(5), 501–513, doi:10.2113/gssgfbull.S7-III.5.501, 1961.
- Lewis, M. M., Jackson, C. A.-L. and Gawthorpe, R. L.: Salt-influenced normal fault growth and forced folding: The Stavanger Fault System, North Sea, *J. Struct. Geol.*, 54, 156–173, doi:10.1016/j.jsg.2013.07.015, 2013.
- Lewis, M. M., Jackson, C. A.-L., Gawthorpe, R. L. and Whipp, P. S.: Early synrift reservoir development on the flanks of extensional forced folds: A seismic-scale outcrop analog from the Hadahid fault system, Suez rift, Egypt, *AAPG Bull.*, 99(06), 985–1012, doi:10.1306/12011414036, 2015.
- Liégeois, J. P., Sauvage, J. F. and Black, R.: The Permo-Jurassic alkaline province of Tadhak, Mali: Geology, geochronology and tectonic significance, *Lithos*, 27(2), 95–105, doi:10.1016/0024-4937(91)90022-D, 1991.
- Liégeois, J. P., Latouche, L., Boughrara, M., Navez, J. and Guiraud, M.: The LATEA metacraton (Central Hoggar, Tuareg shield, Algeria): behaviour of an old passive margin during the Pan-African orogeny, *J. Afr. Earth Sci.*, 37(3–4), 161–190, doi:10.1016/j.jafrearsci.2003.05.004, 2003.
- Liégeois, J.-P.: A New Synthetic Geological Map of the Tuareg Shield: An Overview of Its Global Structure and Geological Evolution, in *The Geology of the Arab World---An Overview*, edited by A. Bendaoud, Z. Hamimi, M. Hamoudi, S. Djemai, and B. Zoheir, pp. 83–107, Springer International Publishing, Cham., 2019.
- Liégeois, J.-P., Black, R., Navez, J. and Latouche, L.: Early and late Pan-African orogenies in the Air assembly of terranes (Tuareg Shield, Niger), *Precambrian Res.*, 67(1), 59–88, 1994.
- Liégeois, J.-P., Benhallou, A., Azzouni-Sekkal, A., Yahiaoui, R. and Bonin, B.: The Hoggar swell and volcanism: Reactivation of the Precambrian Tuareg shield during Alpine convergence and West African Cenozoic volcanism, *Geol. Soc. Am. Spec. Pap.*, 388, 379–400, doi:10.1130/0-8137-2388-4.379, 2005.
- Liégeois, J.-P., Abdelsalam, M. G., Ennih, N. and Ouabadi, A.: Metacraton: Nature, genesis and behavior, *Gondwana Res.*, 23(1), 220–237, doi:10.1016/j.gr.2012.02.016, 2013.
- Lindsay, J. F. and Leven, J. H.: Evolution of a Neoproterozoic to Palaeozoic intracratonic setting, Officer Basin, South Australia, *Basin Res.*, 8(4), 403–424, doi:10.1046/j.1365-2117.1996.00223.x, 1996.
- Linnemann, U., Ouzegane, K., Drareni, A., Hofmann, M., Becker, S., Gärtner, A. and Sagawe, A.: Sands of West Gondwana: An archive of secular magmatism and plate interactions — A

- case study from the Cambro-Ordovician section of the Tassili Ouan Ahaggar (Algerian Sahara) using U–Pb–LA-ICP-MS detrital zircon ages, *Lithos*, 123(1–4), 188–203, doi:10.1016/j.lithos.2011.01.010, 2011.
- Logan, P. and Duddy, I.: An investigation of the thermal history of the Ahnet and Reggane Basins, Central Algeria, and the consequences for hydrocarbon generation and accumulation, *Geol. Soc. Lond. Spec. Publ.*, 132(1), 131–155, 1998.
- Loi, A., Ghienne, J.-F., Dabard, M. P., Paris, F., Botquelen, A., Christ, N., Elaouad-Debbaj, Z., Gorini, A., Vidal, M., Videt, B. and Destombes, J.: The Late Ordovician glacio-eustatic record from a high-latitude storm-dominated shelf succession: The Bou Ingarf section (Anti-Atlas, Southern Morocco), *Palaeogeogr. Palaeoclimatol. Palaeoecol.*, 296(3–4), 332–358, doi:10.1016/j.palaeo.2010.01.018, 2010.
- Lubeseder, S.: Silurian and Devonian sequence stratigraphy of North Africa; Regional correlation and sedimentology (Morocco, Algeria, Libya), Doctoral dissertation, University of Manchester, UK., 2005.
- Lubeseder, S., Redfern, J., Petitpierre, L. and Fröhlich, S.: Stratigraphic trapping potential in the Carboniferous of North Africa: developing new play concepts based on integrated outcrop sedimentology and regional sequence stratigraphy (Morocco, Algeria, Libya), in *Geological Society, London, Petroleum Geology Conference series*, vol. 7, pp. 725–734, Geological Society of London., 2010.
- Lüning, S.: North African Phanerozoic, in *Phanerozoic in the Northern african basins*, *Encyclopedia of Geology*, pp. 152–172, Elsevier., 2005.
- Lüning, S., Craig, J., Fitches, B., Mayouf, J., Busrewil, A., Dieb, M. E., Gammudi, A., Loydell, D. and McIlroy, D.: Re-evaluation of the petroleum potential of the Kufra Basin (SE Libya, ne Chad): does the source rock barrier fall?, *Mar. Pet. Geol.*, 16(7), 693–718, doi:10.1016/S0264-8172(99)00013-6, 1999.
- Lüning, S., Craig, J., Loydell, D. K., Štorch, P. and Fitches, B.: Lower Silurian ‘hot shales’ in North Africa and Arabia: regional distribution and depositional model, *Earth-Sci. Rev.*, 49(1–4), 121–200, doi:10.1016/S0012-8252(99)00060-4, 2000.
- Lüning, S., Adamson, K. and Craig, J.: Frasnian organic-rich shales in North Africa: regional distribution and depositional model, *Geol. Soc. Lond. Spec. Publ.*, 207(1), 165–184, doi:10.1144/GSL.SP.2003.207.9, 2003.
- Lüning, S., Wendt, J., Belka, Z. and Kaufmann, B.: Temporal–spatial reconstruction of the early Frasnian (Late Devonian) anoxia in NW Africa: new field data from the Ahnet Basin (Algeria), *Sediment. Geol.*, 163(3–4), 237–264, doi:10.1016/S0037-0738(03)00210-0, 2004.
- Lyatsky, H., Friedman, G. M. and Lyatsky, V. B.: *Principles of Practical Tectonic Analysis of Cratonic Regions: With Particular Reference to Western North America*, Springer., 2006.
- Macgregor, D. S.: The hydrocarbon systems of North Africa, *Mar. Pet. Geol.*, 13(3), 329–340, doi:10.1016/0264-8172(95)00068-2, 1996.
- MacGregor, D. S., Moody, R. and Clark-Lowes, D. D., Eds.: *Petroleum geology of North Africa*, Geological Society ; AAPG Bookstore [distributor], London : Tulsa, OK., 1998.

- Mackwell, S. J., Zimmerman, M. E. and Kohlstedt, D. L.: High-temperature deformation of dry diabase with application to tectonics on Venus, *J. Geophys. Res. Solid Earth*, 103(B1), 975–984, 1998.
- Madritsch, H., Schmid, S. M. and Fabbri, O.: Interactions between thin-and thick-skinned tectonics at the northwestern front of the Jura fold-and-thrust belt (eastern France), *Tectonics*, 27(5), 1–31, doi:10.1029/2008TC002282, 2008.
- Magloire, L.: Étude stratigraphique, par la Palynologie, des dépôts argilo-gréseux du Silurien et du Dévonien inférieur dans la Région du Grand Erg Occidental (Sahara Algérien), *Can. Soc. Pet. Geol.*, 2, 473–491, 1967.
- Magloire, L. and Chennaux, G.: Etude palynologique, étude pétrographique HBH-1., 1965.
- Makhous, M. and Galushkin, Y. I.: Burial history and thermal evolution of the southern and western Saharan basins: Synthesis and comparison with the eastern and northern Saharan basins, *AAPG Bull.*, 87(11), 1799–1822, 2003a.
- Makhous, M. and Galushkin, Yu. I.: Burial history and thermal evolution of the northern and eastern Saharan basins, *AAPG Bull.*, 87(10), 1623–1651, doi:10.1306/04300301122, 2003b.
- Mantovani, M. S. M., Quintas, M. C. L., Shukowsky, W. and Brito Neves, B. B.: Delimitation of the Paranapanema Proterozoic block: a geophysical contribution, *Episodes-Newsmag. Int. Union Geol. Sci.*, 28(1), 18–22, 2005.
- Marante, A.: Architecture et dynamique des systèmes sédimentaires silico-clastique sur la “plate-forme géante” Nord-Gondwanienne L’Ordovicien moyen de l’Anti-Atlas Marocain, *Université Michel de Montaigne Bordeaux 3.*, 2008.
- Marchal, D., Guiraud, M., Rives, T. and van den Driessche, J.: Space and time propagation processes of normal faults, *Geol. Soc. Lond. Spec. Publ.*, 147(1), 51–70, doi:10.1144/GSL.SP.1998.147.01.04, 1998.
- Marchal, D., Guiraud, M. and Rives, T.: Geometric and morphologic evolution of normal fault planes and traces from 2D to 4D data, *J. Struct. Geol.*, 25(1), 135–158, doi:10.1016/S0191-8141(02)00011-1, 2003.
- Massa, D.: Paléozoïque de Libye occidentale: stratigraphie et paléogéographie, *Doctoral dissertation, Université de Nice, France.*, 1988.
- May, D. A., Brown, J. and Pourhiet, L. L.: pTatin3D: High-Performance Methods for Long-Term Lithospheric Dynamics, in *SC ’14: Proceedings of the International Conference for High Performance Computing, Networking, Storage and Analysis*, pp. 274–284., 2014.
- May, D. A., Brown, J. and Le Pourhiet, L.: A scalable, matrix-free multigrid preconditioner for finite element discretizations of heterogeneous Stokes flow, *Comput. Methods Appl. Mech. Eng.*, 290, 496–523, doi:10.1016/j.cma.2015.03.014, 2015.
- McKenzie, D.: Some remarks on the development of sedimentary basins, *Earth Planet. Sci. Lett.*, 40(1), 25–32, doi:10.1016/0012-821X(78)90071-7, 1978.

- McKenzie, D. and Priestley, K.: The influence of lithospheric thickness variations on continental evolution, *Lithos*, 102(1–2), 1–11, doi:10.1016/j.lithos.2007.05.005, 2008.
- McKenzie, D. and Priestley, K.: Speculations on the formation of cratons and cratonic basins, *Earth Planet. Sci. Lett.*, 435, 94–104, doi:10.1016/j.epsl.2015.12.010, 2016.
- Mckerrow, W. S., Niocaill, C. M. and Dewey, J. F.: The Caledonian Orogeny redefined, *J. Geol. Soc.*, 157(6), 1149–1154, doi:10.1144/jgs.157.6.1149, 2000.
- Mehadji Ouali, A., Racheboeuf, P., Elmi, S. and Mekahli, L.: Dynamique sédimentaire et cycles eustatiques de haute fréquence du niveau majeur de Marhouma au passage Dévonien inférieur-Dévonien moyen de la Saoura (Sahara Nord-Ouest, Algérie), *Bull. Serv. Géologique Natl.*, 22(1), 27–45, 2011.
- Meinhold, G., Morton, A. C., Fanning, C. M., Frei, D., Howard, J. P., Phillips, R. J., Strogon, D. and Whitham, A. G.: Evidence from detrital zircons for recycling of Mesoproterozoic and Neoproterozoic crust recorded in Paleozoic and Mesozoic sandstones of southern Libya, *Earth Planet. Sci. Lett.*, 312(1–2), 164–175, doi:10.1016/j.epsl.2011.09.056, 2011.
- Meinhold, G., Morton, A. C. and Avigad, D.: New insights into peri-Gondwana paleogeography and the Gondwana super-fan system from detrital zircon U–Pb ages, *Gondwana Res.*, 23(2), 661–665, doi:10.1016/j.gr.2012.05.003, 2013.
- Mélou, M., Oulebsir, L. and Paris, F.: Brachiopodes et chitinozoaires ordoviciens dans le NE du Sahara algérien: Implications stratigraphiques et paléogéographiques, *Geobios*, 32(6), 822–839, doi:10.1016/S0016-6995(99)80865-1, 1999.
- Mezlah, H.: Les mud-mounds du dévonien moyen du bassin de l’Ahnet et ses régions limitrophes (sud-ouest algérien) Sédimentologie-diagenèse, *École Nationale Supérieure des Mines de Paris*. [online] Available from: <https://pastel.archives-ouvertes.fr/pastel-00002484/> (Accessed 19 November 2016), 2006.
- Michard, A., Hoepffner, C., Soulaïmani, A. and Baidder, L.: The Variscan Belt, *Earth Sci.*, 2008.
- Michaut, C., Jaupart, C. and Mareschal, J.-C.: Thermal evolution of cratonic roots, *Lithos*, 109(1–2), 47–60, doi:10.1016/j.lithos.2008.05.008, 2009.
- Milani, E. J. and Zalan, P. V.: An outline of the geology and petroleum systems of the Paleozoic interior basins of South America, *Episodes*, 22, 199–205, 1999.
- Milton, N. J., Bertram, G. T. and Vann, I. R.: Early Palaeogene tectonics and sedimentation in the Central North Sea, *Geol. Soc. Lond. Spec. Publ.*, 55(1), 339–351, 1990.
- Mitrovica, J. X., Beaumont, C. and Jarvis, G. T.: Tilting of continental interiors by the dynamical effects of subduction, *Tectonics*, 8(5), 1079–1094, doi:10.1029/TC008i005p01079, 1989.
- Moreau, C., Demaiffe, D., Bellion, Y. and Boullier, A.-M.: A tectonic model for the location of Palaeozoic ring complexes in Air (Niger, West Africa), *Tectonophysics*, 234(1), 129–146, 1994.

- Moreau, J.: Architecture stratigraphique et dynamique des dépôts glaciaires Ordoviciens du bassin de Murzuq (Libye), Université Louis Pasteur, Strasbourg., 2005.
- Moreau, J.: The Late Ordovician deglaciation sequence of the SW Murzuq Basin (Libya): Late Ordovician deglaciation sequence, *Basin Res.*, 23(4), 449–477, doi:10.1111/j.1365-2117.2010.00499.x, 2011.
- Moreau, J., Ghienne, J. F. and Hurst, A.: Kilometre-scale sand injectites in the intracratonic Murzuq Basin (South-west Libya): an igneous trigger?: Sand injectites in the Murzuq Basin: an igneous trigger?, *Sedimentology*, 59(4), 1321–1344, doi:10.1111/j.1365-3091.2011.01308.x, 2012.
- Moreau-Benoit, A., Coquel, R. and Latreche, S.: Étude palynologique du dévoniendu bassin d'illizi (Sahara oriental algérien). Approche biostratigraphique, *Geobios*, 26(1), 3–31, doi:10.1016/S0016-6995(93)80002-9, 1993.
- Moretti, I. and Froidevaux, C.: Thermomechanical models of active rifting, *Tectonics*, 5(4), 501–511, 1986.
- Moretti, I. and Turcotte, D. L.: A model for erosion, sedimentation, and flexure with application to New Caledonia, *J. Geodyn.*, 3(1), 155–168, doi:10.1016/0264-3707(85)90026-2, 1985.
- Morley, C. K., Nelson, R. A., Patton, T. L. and Munn, S. G.: Transfer Zones in the East African Rift System and Their Relevance to Hydrocarbon Exploration in Rifts, *AAPG Bull.*, 74(8), 1234–1253, 1990.
- Morton, A. C., Meinhold, G., Howard, J. P., Phillips, R. J., Strogon, D., Abutarruma, Y., Elgadry, M., Thusu, B. and Whitham, A. G.: A heavy mineral study of sandstones from the eastern Murzuq Basin, Libya: Constraints on provenance and stratigraphic correlation, *J. Afr. Earth Sci.*, 61(4), 308–330, doi:10.1016/j.jafrearsci.2011.08.005, 2011.
- Mory, A. J., Zhan, Y., Haines, P. W., Hocking, R. M., Thomas, C. M. and Copp, I. A.: A paleozoic perspective of Western Australia, Geological Survey of Western Australia., 2017.
- Naimark, B. M. and Ismail-Zadeh, A. T.: Numerical models of a subsidence mechanism in intracratonic basins: application to North American basins, *Geophys. J. Int.*, 123(1), 149–160, doi:10.1111/j.1365-246X.1995.tb06667.x, 1995.
- Najem, A., El-Arnauti, A. and Bosnina, S.: Delineation of Paleozoic Tecto-stratigraphic Complexities in the Northern Part of Murzuq Basin-Southwest Libya, in SPE North Africa Technical Conference and Exhibition, Society of Petroleum Engineers., 2015.
- Nance, R. D., Gutiérrez-Alonso, G., Keppie, J. D., Linnemann, U., Murphy, J. B., Quesada, C., Strachan, R. A. and Woodcock, N. H.: Evolution of the Rheic Ocean, *Gondwana Res.*, 17(2–3), 194–222, doi:10.1016/j.gr.2009.08.001, 2010.
- Neumann, E.-R., Olsen, K. H., Baldrige, W. S. and Sundvoll, B.: The Oslo rift: A review, *Tectonophysics*, 208(1–3), 1–18, 1992.
- Neves, S. P., Tommasi, A., Vauchez, A. and Hassani, R.: Intraplate continental deformation: Influence of a heat-producing layer in the lithospheric mantle, *Earth Planet. Sci. Lett.*, 274(3–4), 392–400, doi:10.1016/j.epsl.2008.07.040, 2008.

- Nijman, W., Clevis, Q. and de Vries, S. T.: The waning stage of a greenstone belt: The Mesoarchaeon Mosquito Creek Basin of the East Pilbara, Western Australia, *Precambrian Res.*, 180(3–4), 251–271, doi:10.1016/j.precamres.2010.03.010, 2010.
- Nkono, C., Liégeois, J.-P. and Demaiffe, D.: Relationships between structural lineaments and Cenozoic volcanism, Tibesti swell, Saharan metacraton, *J. Afr. Earth Sci.*, 145, 274–283, doi:10.1016/j.jafrearsci.2018.05.022, 2018.
- Nunn, J. A.: Free thermal convection beneath intracratonic basins: thermal and subsidence effects, *Basin Res.*, 6(2–3), 115–130, 1994.
- Nunn, J. A. and Aires, J. R.: Gravity anomalies and flexure of the lithosphere at the Middle Amazon Basin, Brazil, *J. Geophys. Res. Solid Earth*, 93(B1), 415–428, doi:10.1029/JB093iB01p00415, 1988.
- Nunn, J. A. and Sleep, N. H.: Thermal contraction and flexure of intracratonic basins: a three-dimensional study of the Michigan basin, *Geophys. J. Int.*, 76(3), 587–635, doi:10.1111/j.1365-246X.1984.tb01912.x, 1984.
- Nunn, J. A., Sleep, N. H. and Moore, W. E.: Thermal Subsidence and Generation of Hydrocarbons in Michigan Basin, *AAPG Bull.*, 68, doi:10.1306/AD460A17-16F7-11D7-8645000102C1865D, 1984.
- Nyblade, A. A. and Pollack, H. N.: A global analysis of heat flow from Precambrian terrains: implications for the thermal structure of Archean and Proterozoic lithosphere, *J. Geophys. Res. Solid Earth*, 98(B7), 12207–12218, 1993.
- Ogg, J. G., Ogg, G. and Gradstein, F. M.: Introduction, in *A Concise Geologic Time Scale: 2016*, p. 3, Elsevier., 2016.
- de Oliveira, D. C. and Mohriak, W. U.: Jaibaras trough: an important element in the early tectonic evolution of the Parnaíba interior sag basin, Northern Brazil, *Mar. Pet. Geol.*, 20(3), 351–383, doi:https://doi.org/10.1016/S0264-8172(03)00044-8, 2003.
- Ouanaimi, H. and Lazreq, N.: The ‘Rich’ group of the Drâa Basin (Lower Devonian, Anti-Atlas, Morocco): an integrated sedimentary and tectonic approach, *Geol. Soc. Lond. Spec. Publ.*, 297(1), 467–482, doi:10.1144/SP297.22, 2008.
- Oudra, M., Beraaouz, H., Ikenne, M., Gasquet, D. and Soulaïmani, A.: La Tectonique Panafricaine du Secteur d’Igherm: Implication des dômes extensifs tardi à post-orogéniques (Anti-Atlas occidental, Maroc), *Estud. Geológicas*, 61(3–6), 177–189, 2005.
- Oulebsir, L. and Paris, F.: Nouvelles espèces de chitinozoaires dans l’Ordovicien inférieur et moyen du sud-est du Sahara algérien, *Rev. Micropaléontologie*, 36(3), 269–292, 1993.
- Oulebsir, L. and Paris, F.: Chitinozoaires ordoviciens du Sahara algérien: biostratigraphie et affinités paléogéographiques, *Rev. Palaeobot. Palynol.*, 86(1), 49–68, doi:10.1016/0034-6667(94)00098-5, 1995.
- Ouzegane, K., Kienast, J.-R., Bendaoud, A. and Drareni, A.: A review of Archaean and Paleoproterozoic evolution of the In Ouzzal granulitic terrane (Western Hoggar, Algeria), *J. Afr. Earth Sci.*, 37(3–4), 207–227, doi:10.1016/j.jafrearsci.2003.05.002, 2003a.

- Ouzegane, K., Liegeois, J.-P. and Kienast, J. R.: The Precambrian of Hoggar, Tuareg shield: history and perspective, *J. Afr. Earth Sci.*, 37(3–4), 127–131, doi:10.1016/j.jafrearsci.2003.10.002, 2003b.
- Padilha, A. L., Vitorello, Í., Pádua, M. B. and Bologna, M. S.: Electromagnetic constraints for subduction zones beneath the northwest Borborema province: Evidence for Neoproterozoic island arc–continent collision in northeast Brazil, *Geology*, 42(1), 91–94, doi:10.1130/G34747.1, 2014.
- Paris, F.: The Ordovician chitinozoan biozones of the Northern Gondwana domain, *Rev. Palaeobot. Palynol.*, 66(3–4), 181–209, doi:10.1016/0034-6667(90)90038-K, 1990.
- Paris, F., Bourahrouh, A. and Hérissé, A. L.: The effects of the final stages of the Late Ordovician glaciation on marine palynomorphs (chitinozoans, acritarchs, leiospheres) in well NI-2 (NE Algerian Sahara), *Rev. Palaeobot. Palynol.*, 113(1–3), 87–104, doi:10.1016/S0034-6667(00)00054-3, 2000a.
- Paris, F., Winchester-Seeto, T., Boumendjel, K. and Grahn, Y.: Toward a global biozonation of Devonian chitinozoans, 2000b.
- Patton, T. L. and Fletcher, R. C.: Mathematical block-motion model for deformation of a layer above a buried fault of arbitrary dip and sense of slip, *J. Struct. Geol.*, 17(10), 1455–1472, 1995.
- Peace, A., McCaffrey, K., Imber, J., van Hunen, J., Hobbs, R. and Wilson, R.: The role of pre-existing structures during rifting, continental breakup and transform system development, offshore West Greenland, *Basin Res.*, 30(3), 373–394, 2018.
- Pelletier, A., Gapais, D., Ménot, R.-P. and Peucat, J.-J.: Tectonique transpressive en terre Adélie au Paléoprotérozoïque (Est Antarctique), *Comptes Rendus Geosci.*, 334(7), 505–511, 2002.
- Pérez-Gussinyé, M., Lowry, A. R. and Watts, A. B.: Effective elastic thickness of South America and its implications for intracontinental deformation: Elastic thickness, *Geochem. Geophys. Geosystems*, 8(5), n/a-n/a, doi:10.1029/2006GC001511, 2007.
- Perron, P., Guiraud, M., Vennin, E., Moretti, I., Portier, É., Le Pourhiet, L. and Konaté, M.: Influence of basement heterogeneity on the architecture of low subsidence rate Paleozoic intracratonic basins (Reggane, Ahnet, Mouydir and Illizi basins, Hoggar Massif), *Solid Earth*, 9(6), 1239–1275, doi:https://doi.org/10.5194/se-9-1239-2018, 2018.
- Perrouty, S., Aillères, L., Jessell, M. W., Baratoux, L., Bourassa, Y. and Crawford, B.: Revised Eburnean geodynamic evolution of the gold-rich southern Ashanti Belt, Ghana, with new field and geophysical evidence of pre-Tarkwaian deformations, *Precambrian Res.*, 204–205, 12–39, doi:10.1016/j.precamres.2012.01.003, 2012.
- Petitjean, S., Rabinowicz, M., Grégoire, M. and Chevrot, S.: Differences between Archean and Proterozoic lithospheres: Assessment of the possible major role of thermal conductivity: Archean craton thickness, *Geochem. Geophys. Geosystems*, 7(3), n/a-n/a, doi:10.1029/2005GC001053, 2006.
- Petter, G.: Goniatices dévoniennes du Sahara, Service de la carte géologique de l'Algérie., 1959.

- Peucat, J. J., Capdevila, R., Drareni, A., Choukroune, P., Fanning, C. M., Bernard-Griffiths, J. and Fourcade, S.: Major and trace element geochemistry and isotope (Sr, Nd, Pb, O) systematics of an Archaean basement involved in a 2.0 Ga very high-temperature (1000° C) metamorphic event: In Ouzzal Massif, Hoggar, Algeria, *J. Metamorph. Geol.*, 14(6), 667–692, 1996.
- Peucat, J. J., Drareni, A., Latouche, L., Deloule, E. and Vidal, P.: U–Pb zircon (TIMS and SIMS) and Sm–Nd whole-rock geochronology of the Gour Oumelalen granulitic basement, Hoggar massif, Tuareg shield, Algeria, *J. Afr. Earth Sci.*, 37(3–4), 229–239, doi:10.1016/j.jafrearsci.2003.03.001, 2003.
- Peucat, J.-J., Capdevila, R., Drareni, A., Mahdjoub, Y. and Kahoui, M.: The Eglab massif in the West African Craton (Algeria), an original segment of the Eburnean orogenic belt: petrology, geochemistry and geochronology, *Precambrian Res.*, 136(3–4), 309–352, doi:10.1016/j.precamres.2004.12.002, 2005.
- Phillips, T. B., Jackson, C. A.-L., Bell, R. E. and Duffy, O. B.: Oblique reactivation of lithosphere-scale lineaments controls rift physiography – the upper-crustal expression of the Sorgenfrei–Tornquist Zone, offshore southern Norway, *Solid Earth*, 9(2), 403–429, doi:10.5194/se-9-403-2018, 2018.
- Picciotto, E., Ledent, D. and Lay, C.: Etude géochronologique de quelques roches du socle cristallophyllien du Hoggar (Sahara Central), *Sci. Terre*, X(3–4), 481–495, 1965.
- Pinet, B. and Colletta, B.: Probing into extensional sedimentary basins: comparison of recent data and derivation of tentative models, *Tectonophysics*, 173(1), 185–197, doi:10.1016/0040-1951(90)90216-U, 1990.
- Pinet, N., Lavoie, D., Dietrich, J., Hu, K. and Keating, P.: Architecture and subsidence history of the intracratonic Hudson Bay Basin, northern Canada, *Earth-Sci. Rev.*, 125, 1–23, doi:10.1016/j.earscirev.2013.05.010, 2013.
- Piqué, A., Bouabdelli, M., Soulaïmani, A., Youbi, N. and Iliani, M.: Les conglomérats du P III (Néoprotérozoïque supérieur) de l'Anti Atlas (Sud du Maroc): molasses panafricaines, ou marqueurs d'un rifting fini-protérozoïque?, *Comptes Rendus Académie Sci. - Ser. IIA - Earth Planet. Sci.*, 328(6), 409–414, doi:10.1016/S1251-8050(99)80107-4, 1999.
- Pohl, A., Donnadieu, Y., Le Hir, G., Ladant, J., Dumas, C., Alvarez-Solas, J. and Vandembroucke, T. R. A.: Glacial onset predated Late Ordovician climate cooling, *Paleoceanography*, 31(6), 800–821, doi:10.1002/2016PA002928, 2016.
- Pourhiet, L. L., Burov, E. and Moretti, I.: Rifting through a stack of inhomogeneous thrusts (the dipping pie concept), *Tectonics*, 23(4), doi:10.1029/2003TC001584, 2004.
- Priestley, K. and McKenzie, D.: The relationship between shear wave velocity, temperature, attenuation and viscosity in the shallow part of the mantle, *Earth Planet. Sci. Lett.*, 381, 78–91, doi:10.1016/j.epsl.2013.08.022, 2013.
- Prijac, C., Doin, M. P., Gaulier, J. M. and Guillocheau, F.: Subsidence of the Paris Basin and its bearing on the late Variscan lithosphere evolution: a comparison between Plate and Chabliss models, *Tectonophysics*, 323(1), 1–38, doi:10.1016/S0040-1951(00)00100-1, 2000.

- Prokoph, A., Shields, G. A. and Veizer, J.: Compilation and time-series analysis of a marine carbonate $\delta^{18}\text{O}$, $\delta^{13}\text{C}$, $^{87}\text{Sr}/^{86}\text{Sr}$ and $\delta^{34}\text{S}$ database through Earth history, *Earth-Sci. Rev.*, 87(3), 113–133, doi:10.1016/j.earscirev.2007.12.003, 2008.
- Purdy, E. G. and MacGregor, D. S.: Map compilations and synthesis of Africa's petroleum basins and systems, *Geol. Soc. Lond. Spec. Publ.*, 207(1), 1–8, 2003.
- Quinlan, G.: Models of Subsidence Mechanisms in Intracratonic Basins, and Their Applicability to North American Examples, , 463–481, 1987.
- Quinlan, G. M. and Beaumont, C.: Appalachian thrusting, lithospheric flexure, and the Paleozoic stratigraphy of the eastern interior of North America, *Can. J. Earth Sci.*, 21(9), 973–996, 1984.
- Ranalli, G.: Rheology of the crust and its role in tectonic reactivation, *J. Geodyn.*, 30(1–2), 3–15, doi:10.1016/S0264-3707(99)00024-1, 2000.
- Ratheesh-Kumar, R. T., Windley, B. F. and Sajeev, K.: Tectonic inheritance of the Indian Shield: New insights from its elastic thickness structure, *Tectonophysics*, 615–616, 40–52, doi:10.1016/j.tecto.2013.12.010, 2014.
- Ravier, E.: Structures de déformation induites par surpressions de fluide dans les environnements sous-glaciaires et marin profonds : implications paléoenvironnementales et réservoirs, Université de Bourgogne, 11 December., 2014.
- Ravier, E., Buoncristiani, J.-F., Guiraud, M., Menzies, J., Clerc, S., Goupy, B. and Portier, E.: Porewater pressure control on subglacial soft sediment remobilization and tunnel valley formation: A case study from the Alnif tunnel valley (Morocco), *Sediment. Geol.*, 304, 71–95, doi:10.1016/j.sedgeo.2014.02.005, 2014.
- Ravier, E., Buoncristiani, J.-F., Menzies, J., Guiraud, M., Clerc, S. and Portier, E.: Does porewater or meltwater control tunnel valley genesis? Case studies from the Hirnantian of Morocco, *Palaeogeogr. Palaeoclimatol. Palaeoecol.*, 418, 359–376, doi:10.1016/j.palaeo.2014.12.003, 2015.
- Reches, Z. and Eidelman, A.: Drag along faults, *Tectonophysics*, 247(1–4), 145–156, 1995.
- Remack-Petitot, M. L.: Contribution a l'étude des conodontes du Sahara (bassins de Fort-Polignac, d'Adrar Reggane et du J. Bechar); comparaison avec les Pyrenees et la Montagne Noire, *Bull. Société Géologique Fr.*, S7-II(2), 240–262, doi:10.2113/gssgfbull.S7-II.2.240, 1960.
- Reymer, A. and Schubert, G.: Phanerozoic addition rates to the continental crust and crustal growth, *Tectonics*, 3(1), 63–77, 1984.
- Riba, O.: Syntectonic unconformities of the Alto Cardener, Spanish Pyrenees: a genetic interpretation, *Sediment. Geol.*, 15(3), 213–233, doi:10.1016/0037-0738(76)90017-8, 1976.
- Richardson, J. B. and McGregor, D. C.: Silurian and Devonian spore zones of the Old Red Sandstone Continent and adjacent regions, Geological Survey of Canada, Ottawa, Canada., 1986.

- Richter, F. M.: A major change in the thermal state of the Earth at the Archean-Proterozoic boundary: consequences for the nature and preservation of continental lithosphere, *J. Petrol.*, (1), 39–52, 1988.
- Robert-Charrue, C.: *Géologie structurale de l'Anti-Atlas oriental, Maroc*, Université de Neuchâtel., 2006.
- Robertson: Regional synthesis of the Ordovician Saharan Platform, Algeria., 2002.
- Rodgers, J.: The taconic orogeny, *Geol. Soc. Am. Bull.*, 82(5), 1141–1178, 1971.
- Rogers, J. J. W. and Santosh, M.: Configuration of Columbia, a Mesoproterozoic Supercontinent, *Gondwana Res.*, 5(1), 5–22, doi:10.1016/S1342-937X(05)70883-2, 2002.
- Rogers, J. J. W., Unrug, R. and Sultan, M.: Tectonic assembly of Gondwana, *J. Geodyn.*, 19(1), 1–34, doi:10.1016/0264-3707(94)00007-7, 1995.
- Rostirolla, S. P., Mancini, F., Rigoti, A. and Kraft, R. P.: Structural styles of the intracratonic reactivation of the Perimbo fault zone, Paraná basin, Brazil, *J. South Am. Earth Sci.*, 16(4), 287–300, 2003.
- Rougier, S.: Interactions lithosphère-asthénosphère et mouvements verticaux: le cas du massif du Hoggar, Université Paris Sud-Paris XI. [online] Available from: <https://tel.archives-ouvertes.fr/tel-00788392/> (Accessed 21 November 2016), 2012.
- Rougier, S., Missenard, Y., Gautheron, C., Barbarand, J., Zeyen, H., Pinna, R., Liégeois, J.-P., Bonin, B., Ouabadi, A., Derder, M. E.-M. and Lamotte, D. F. de: Eocene exhumation of the Tuareg Shield (Sahara Desert, Africa), *Geology*, 41(5), 615–618, doi:10.1130/G33731.1, 2013.
- Roussel, J. and Lesquer, A.: Geophysics and the Crustal Structure of West Africa, in *The West African Orogens and Circum-Atlantic Correlatives*, pp. 9–28, Springer, Berlin, Heidelberg., 1991.
- Rubinstein, C. and Steemans, P.: Miospore assemblages from the Silurian–Devonian boundary, in borehole A1-61, Ghadamis Basin, Libya, *Rev. Palaeobot. Palynol.*, 118(1–4), 397–421, doi:10.1016/S0034-6667(01)00124-5, 2002.
- Rybacki, E. and Dresen, G.: Dislocation and diffusion creep of synthetic anorthite aggregates, *J. Geophys. Res. Solid Earth*, 105(B11), 26017–26036, 2000.
- Sabaou, N., Ait-Salem, H. and Zazoun, R. S.: Chemostratigraphy, tectonic setting and provenance of the Cambro-Ordovician clastic deposits of the subsurface Algerian Sahara, *J. Afr. Earth Sci.*, 55(3–4), 158–174, doi:10.1016/j.jafrearsci.2009.04.006, 2009.
- Salomon, E., Koehn, D. and Passchier, C.: Brittle reactivation of ductile shear zones in NW Namibia in relation to South Atlantic rifting, *Tectonics*, 34(1), 70–85, 2015.
- Saunders, A. D., England, R. W., Reichow, M. K. and White, R. V.: A mantle plume origin for the Siberian traps: uplift and extension in the West Siberian Basin, Russia, *Lithos*, 79(3–4), 407–424, 2005.

Scheck, M. and Bayer, U.: Evolution of the Northeast German Basin — inferences from a 3D structural model and subsidence analysis, *Tectonophysics*, 313(1), 145–169, doi:10.1016/S0040-1951(99)00194-8, 1999.

Schlische, R. W.: Geometry and origin of fault-related folds in extensional settings, *AAPG Bull.*, 79(11), 1661–1678, 1995.

Sclater, J. G. and Christie, P. A. F.: Continental stretching: An explanation of the Post-Mid-Cretaceous subsidence of the central North Sea Basin, *J. Geophys. Res. Solid Earth*, 85(B7), 3711–3739, doi:10.1029/JB085iB07p03711, 1980.

Scotese, C. R., Boucot, A. J. and McKerrow, W. S.: Gondwanan palaeogeography and paleoclimatology, *J. Afr. Earth Sci.*, 28(1), 99–114, doi:10.1016/S0899-5362(98)00084-0, 1999.

Séguret, M., Séranne, M., Chauvet, A. and Brunel, A.: Collapse basin: A new type of extensional sedimentary basin from the Devonian of Norway, *Geology*, 17(2), 127–130, doi:10.1130/0091-7613(1989)017<0127:CBANTO>2.3.CO;2, 1989.

Serra, O. and Serra, L.: Well logging, facies, sequence and environment, in *Well logging and geology*, pp. 197–238, Technip Editions, France., 2003.

Seyfert, C. K.: Cratonic basins, domes, and arches, in *Structural Geology and Tectonics*, pp. 141–158, Springer Berlin Heidelberg, Berlin, Heidelberg., 1987.

Sharata, S., Röth, J. and Reicherter, K.: Basin evolution in the North African Platform, *Geotecton. Res.*, 97(1), 80–81, doi:10.1127/1864-5658/2015-31, 2015.

Shaw, J. H., Connors, C. D. and Suppe, J.: Recognizing growth strata, in *Seismic interpretation of contractional fault-related folds: an AAPG seismic atlas*, vol. 53, pp. 11–14, American Association of Petroleum Geologists, Tulsa, Okla., U.S.A., 2005.

Sleep, N. H.: Thermal Effects of the Formation of Atlantic Continental Margins by Continental Break up, *Geophys. J. R. Astron. Soc.*, 24(4), 325–350, doi:10.1111/j.1365-246X.1971.tb02182.x, 1971.

Sleep, N. H.: Survival of Archean cratonic lithosphere: Survival of cratons, *J. Geophys. Res. Solid Earth*, 108(B6), doi:10.1029/2001JB000169, 2003.

Sleep, N. H.: Evolution of the continental lithosphere, *Annu. Rev. Earth Planet. Sci.*, 33(1), 369–393, doi:10.1146/annurev.earth.33.092203.122643, 2005.

Sleep, N. H. and Snell, N. S.: Thermal contraction and flexure of mid-continent and Atlantic marginal basins, *Geophys. J. R. Astron. Soc.*, 45(1), 125–154, 1976.

Sloss, L. L.: Sequences in the cratonic interior of North America, *Geol. Soc. Am. Bull.*, 74(2), 93–114, 1963.

Smart, J.: Seismic expressions of depositional processes in the upper Ordovician succession of the Murzuq Basin, SW Libya, in *Geological Exploration in Murzuq Basin*, edited by M. A. Sola and D. Worsley, pp. 397–415, Elsevier Science B.V., Amsterdam., 2000.

Soares, P. C., LANDIM, P. M. B. and Fulfaro, V. J.: Tectonic cycles and sedimentary sequences in the Brazilian intracratonic basins, *Geol. Soc. Am. Bull.*, 89(2), 181–191, 1978.

Sola, M. A., Worsley, D., Mu'assasah al-Waṭaniyah lil-Naḡ (Libya) and Jāmi'at Sabhā, Eds.: Geological exploration in Murzuq Basin: the Geological Conference on Exploration in the Murzuq Basin held in Sabha, September 20-22, 1998, 1st ed., Elsevier Science B.V, Amsterdam ; New York., 2000.

Soto, R., Martinod, J. and Odonne, F.: Influence of early strike-slip deformation on subsequent perpendicular shortening: An experimental approach, *J. Struct. Geol.*, 29(1), 59–72, doi:10.1016/j.jsg.2006.08.001, 2007.

Soulaimani, A., Michard, A., Ouanaimi, H., Baidder, L., Raddi, Y., Saddiqi, O. and Rjimati, E. C.: Late Ediacaran–Cambrian structures and their reactivation during the Variscan and Alpine cycles in the Anti-Atlas (Morocco), *J. Afr. Earth Sci.*, 98, 94–112, doi:10.1016/j.jafrearsci.2014.04.025, 2014.

Stampfli, G. M. and Borel, G. D.: A plate tectonic model for the Paleozoic and Mesozoic constrained by dynamic plate boundaries and restored synthetic oceanic isochrons, *Earth Planet. Sci. Lett.*, 196(1), 17–33, 2002.

Stampfli, G. M., von Raumer, J. F. and Borel, G. D.: Paleozoic evolution of pre-Variscan terranes: from Gondwana to the Variscan collision, *Spec. Pap.-Geol. Soc. Am.*, 263–280, 2002.

Stel, H., Cloetingh, S., Heeremans, M. and van der Beek, P.: Anorogenic granites, magmatic underplating and the origin of intracratonic basins in a non-extensional setting, *Tectonophysics*, 226(1), 285–299, doi:10.1016/0040-1951(93)90123-2, 1993.

Stone, D. S.: Analysis of Scale Exaggeration on Seismic Profiles, *AAPG Bull.*, 75(7), 1161–1177, 1991.

Streel, M., Higgs, K., Loboziak, S., Riegel, W. and Steemans, P.: Spore stratigraphy and correlation with faunas and floras in the type marine devonian of the Ardenne-Rhenish regions, *Rev. Palaeobot. Palynol.*, 50(3), 211–229, doi:10.1016/0034-6667(87)90001-7, 1987.

Streel, M., Caputo, M. V., Loboziak, S. and Melo, J. H. G.: Late Frasnian–Famennian climates based on palynomorph analyses and the question of the Late Devonian glaciations, *Earth-Sci. Rev.*, 52(1), 121–173, 2000.

Suppe, J., T. Chou and C. Hook: Rates of folding and faulting determined from growth strata, , 105–121., 1992.

Sutcliffe, O. E., Dowdeswell, J. A., Whittington, R. J., Theron, J. N. and Craig, J.: Calibrating the Late Ordovician glaciation and mass extinction by the eccentricity cycles of Earth's orbit, *Geology*, 28(11), 967, doi:10.1130/0091-7613(2000)28<967:CTLOGA>2.0.CO;2, 2000.

Sylvester, A. G.: Strike-slip faults, *Geol. Soc. Am. Bull.*, 100(11), 1666–1703, 1988.

Takherist, D.: Structure crustale, subsidence mésozoïque et flux de chaleur dans les bassins nord-sahariens (Algérie): apport de la gravimétrie et des données de puits, Centre Géologique et Géophysique de Montpellier., 1991.

- Takherist, D. and Lesquer, A.: Mise en évidence d'importantes variations régionales du flux de chaleur en Algérie, *Can. J. Earth Sci.*, 26(4), 615–626, doi:10.1139/e89-053, 1989.
- Tavakoli-Shirazi, S., de Lamotte, D. F., Wrobel-Daveau, J.-C. and Ringenbach, J.-C.: Pre-Permian uplift and diffuse extensional deformation in the High Zagros Belt (Iran): integration in the geodynamic evolution of the Arabian plate, *Arab. J. Geosci.*, 6(7), 2329–2342, 2013.
- Taylor, S. R. and McLennan, S. M.: The geochemical evolution of the continental crust, *Rev. Geophys.*, 33(2), 241–265, 1995.
- Tesauro, M., Kaban, M. K. and Mooney, W. D.: Variations of the lithospheric strength and elastic thickness in North America: Lithosphere strength and TE variations, *Geochem. Geophys. Geosystems*, 16(7), 2197–2220, doi:10.1002/2015GC005937, 2015.
- Thomas, J. C., Cobbold, P. R., Shein, V. S. and Le Douaran, S.: Sedimentary record of late Paleozoic to Recent tectonism in central Asia — analysis of subsurface data from the Turan and south Kazak domains, *Tectonophysics*, 313(3), 243–263, doi:10.1016/S0040-1951(99)00208-5, 1999.
- Torsvik, T. H. and Cocks, L. R. M.: The Palaeozoic palaeogeography of central Gondwana, *Geol. Soc. Lond. Spec. Publ.*, 357(1), 137–166, doi:10.1144/SP357.8, 2011.
- Torsvik, T. H. and Cocks, L. R. M.: Gondwana from top to base in space and time, *Gondwana Res.*, 24(3–4), 999–1030, doi:10.1016/j.gr.2013.06.012, 2013.
- Torsvik, T. H., Van der Voo, R., Preeden, U., Mac Niocaill, C., Steinberger, B., Doubrovine, P. V., van Hinsbergen, D. J. J., Domeier, M., Gaina, C., Tohver, E., Meert, J. G., McCausland, P. J. A. and Cocks, L. R. M.: Phanerozoic polar wander, palaeogeography and dynamics, *Earth-Sci. Rev.*, 114(3–4), 325–368, doi:10.1016/j.earscirev.2012.06.007, 2012.
- Tournier, F.: Mécanismes et contrôle des phénomènes diagénétiques en milieu acide dans les grès de l'Ordovicien glaciaire du bassin de Sbaa, Algérie, Doctoral dissertation, Université de Paris 11, France., 2010.
- Tozer, B., Watts, A. B. and Daly, M. C.: Crustal structure, gravity anomalies, and subsidence history of the Parnaíba cratonic basin, Northeast Brazil, *J. Geophys. Res. Solid Earth*, 122(7), 5591–5621, doi:10.1002/2017JB014348, 2017.
- Tozer, R. S. J., Butler, R. W. H. and Corrado, S.: Comparing thin-and thick-skinned thrust tectonic models of the Central Apennines, Italy, *EGU Stephan Mueller Spec. Publ. Ser.*, 1, 181–194, 2002.
- Trompette, R.: Le Précambrien supérieur et le Paléozoïque inférieur de l'Adrar de Mauritanie (bordure occidentale du bassin de Taoudeni, Afrique de l'Ouest), un exemple de sédimentation de craton. Étude stratigraphique et sédimentologique - TOME 2 (Séries 2 et 3), phdthesis, Université de Provence - Aix-Marseille I, 1 October., 1973.
- von Tscharnier, M., Schmalholz, S. M. and Epard, J.-L.: 3-D numerical models of viscous flow applied to fold nappes and the Rawil depression in the Helvetic nappe system (western Switzerland), *J. Struct. Geol.*, 86, 32–46, doi:10.1016/j.jsg.2016.02.007, 2016.

- Turcotte, D. L. and Schubert, G.: *Geodynamics*, Third edition., Cambridge University Press, Cambridge, United Kingdom., 2014.
- Underdown, R., Redfern, J. and Lisker, F.: Constraining the burial history of the Ghadames Basin, North Africa: an integrated analysis using sonic velocities, vitrinite reflectance data and apatite fission track ages, *Basin Res.*, 19(4), 557–578, doi:10.1111/j.1365-2117.2007.00335.x, 2007.
- Unrug, R.: The supercontinent cycle and gondwanaland assembly: Component cratons and the timing of suturing events, *J. Geodyn.*, 16(4), 215–240, doi:10.1016/0264-3707(92)90011-G, 1992.
- Ustaszewski, K., Schumacher, M., Schmid, S. and Nieuwland, D.: Fault reactivation in brittle–viscous wrench systems—dynamically scaled analogue models and application to the Rhine–Bresse transfer zone, *Quat. Sci. Rev.*, 24(3–4), 363–380, doi:10.1016/j.quascirev.2004.03.015, 2005.
- Vail, P. R., Mitchum Jr, R. M. and Thompson III, S.: *Seismic stratigraphy and global changes of sea level: Part 3. Relative changes of sea level from Coastal Onlap: section 2. Application of seismic reflection Configuration to Stratigraphic Interpretation*, 1977.
- Vecoli, M., Albani, R., Ghomari, A., Massa, D. and Tongiorgi, M.: Précisions sur la limite Cambrien-Ordovicien au Sahara Algérien (Secteur de Hassi-Rmel), *Comptes Rendus Académie Sci. Sér. 2 Sci. Terre Planètes*, 320(6), 515–522, 1995.
- Vecoli, M., Tongiorgi, M., Abdesselam-Roughi, F. F., Benzarti, R. and Massa, D.: Palynostratigraphy of upper Cambrian-upper Ordovician intracratonic clastic sequences, North Africa, *Boll.-Soc. Paleontol. Ital.*, 38(2/3), 331–342, 1999.
- Veevers, J. J.: *Gondwanaland and Gondwana*, 2005.
- Vennin, E., Kolodka, C., Asghari, A., Thomazo, C., Buoncristiani, J. F., Goodarzi, H. and Desaubliaux, G.: Discussion on Palaeozoic discontinuities in the Kuh-e Surmeh area (Zagros, Iran), *Mar. Pet. Geol.*, 66, 1073–1092, doi:10.1016/j.marpetgeo.2015.05.019, 2015.
- Viallette, Y. and Vitel, G.: Geochronological data on the Amsinassene-Tefedest Block (Central Hoggar, Algerian Sahara) and evidence for its polycyclic evolution, *Precambrian Res.*, 9(3), 241–254, 1979.
- Vidal, M., Gumiaux, C., Cagnard, F., Pouclet, A., Ouattara, G. and Pichon, M.: Evolution of a Paleoproterozoic “weak type” orogeny in the West African Craton (Ivory Coast), *Tectonophysics*, 477(3–4), 145–159, doi:10.1016/j.tecto.2009.02.010, 2009.
- Videt, B., Paris, F., Rubino, J.-L., Boumendjel, K., Dabard, M.-P., Loi, A., Ghienne, J.-F., Marante, A. and Gorini, A.: Biostratigraphical calibration of third order Ordovician sequences on the northern Gondwana platform, *Palaeogeogr. Palaeoclimatol. Palaeoecol.*, 296(3–4), 359–375, doi:10.1016/j.palaeo.2010.03.050, 2010.
- Villeneuve, M. and Cornée, J. J.: Structure, evolution and palaeogeography of the West African craton and bordering belts during the Neoproterozoic, *Precambrian Res.*, 69(1), 307–326, doi:10.1016/0301-9268(94)90094-9, 1994.

- Viola, G., Odonne, F. and Mancktelow, N. S.: Analogue modelling of reverse fault reactivation in strike-slip and transpressive regimes: application to the Giudicarie fault system, Italian Eastern Alps, *J. Struct. Geol.*, 26(3), 401–418, doi:10.1016/j.jsg.2003.08.014, 2004.
- Vyssotski, A. V., Vyssotski, V. N. and Nezhdanov, A. A.: 21 - Evolution of the West Siberian Basin, in *Regional Geology and Tectonics: Phanerozoic Passive Margins, Cratonic Basins and Global Tectonic Maps*, edited by D. G. Roberts and A. W. Bally, pp. 754–801, Elsevier, Boston., 2012.
- Watts, A. B.: *Isostasy and Flexure of the Lithosphere*, Cambridge University Press, Oxford University., 2001.
- Watts, A. B., Tozer, B., Daly, M. C. and Smith, J.: A comparative study of the Parnaíba, Michigan and Congo cratonic basins, *Geol. Soc. Lond. Spec. Publ.*, 472, SP472.6, doi:10.1144/SP472.6, 2018.
- Wazir, I.: Contrôles sédimentaires et diagénétiques sur les propriétés pétrophysiques des réservoirs gréseux à gaz des bassins de Sbaa, Algérie, et des Palmyrides-Sud, Syrie, phdthesis, Université Paris Sud - Paris XI, 3 April. [online] Available from: <https://tel.archives-ouvertes.fr/tel-01018496/document> (Accessed 22 November 2016), 2014.
- Wells, M., Hirst, P., Bouch, J., Whear, E. and Clark, N.: Deciphering multiple controls on reservoir quality and inhibition of quartz cement in a complex reservoir: Ordovician glacial sandstones, Illizi Basin, Algeria, *Geol. Soc. Lond. Spec. Publ.*, 435(1), 343–372, doi:10.1144/SP435.6, 2018.
- Wendt, J.: Disintegration of the continental margin of northwestern Gondwana: Late Devonian of the eastern Anti-Atlas (Morocco), *Geology*, 13(11), 815–818, 1985.
- Wendt, J.: Facies Pattern and Paleogeography of the Middle and Late Devonian in the Eastern Anti-Atlas (Morocco), *Can. Soc. Pet. Geol.*, 1(14), 467–480, 1988.
- Wendt, J.: Shell directions as a tool in palaeocurrent analysis, *Sediment. Geol.*, 95(3), 161–186, doi:10.1016/0037-0738(94)00104-3, 1995.
- Wendt, J. and Kaufmann, B.: Mud buildups on a Middle Devonian carbonate ramp (Algerian Sahara), *Geol. Soc. Lond. Spec. Publ.*, 149(1), 397–415, doi:10.1144/GSL.SP.1999.149.01.18, 1998.
- Wendt, J., Belka, Z. and Moussine-Pouchkine, A.: New architectures of deep-water carbonate buildups: Evolution of mud mounds into mud ridges (Middle Devonian, Algerian Sahara), *Geology*, 21(8), 723–726, 1993.
- Wendt, J., Belka, Z., Kaufmann, B., Kostrewa, R. and Hayer, J.: The world's most spectacular carbonate mud mounds (Middle Devonian, Algerian Sahara), *J. Sediment. Res.*, 67(3), 424–436, doi:10.1306/D426858B-2B26-11D7-8648000102C1865D, 1997.
- Wendt, J., Kaufmann, B., Belka, Z., Klug, C. and Lubeseder, S.: Sedimentary evolution of a Palaeozoic basin and ridge system: the Middle and Upper Devonian of the Ahnet and Mouydir (Algerian Sahara), *Geol. Mag.*, 143(3), 269–299, doi:10.1017/S0016756806001737, 2006.

- Wendt, J., Kaufmann, B., Belka, Z. and Korn, D.: Carboniferous stratigraphy and depositional environments in the Ahnet Mouydir area (Algerian Sahara), *Facies*, 55(3), 443–472, doi:10.1007/s10347-008-0176-y, 2009a.
- Wendt, J., Kaufmann, B. and Belka, Z.: Devonian stratigraphy and depositional environments in the southern Illizi Basin (Algerian Sahara), *J. Afr. Earth Sci.*, 54(3–4), 85–96, doi:10.1016/j.jafrearsci.2009.03.006, 2009b.
- Wendt, J., Kaufmann, B., Belka, Z. and Korn, D.: Carboniferous stratigraphy and depositional environments in the Ahnet Mouydir area (Algerian Sahara): reply to the discussion by Legrand-Blain et al. (DOI: 10.1007/s10347-010-0214-4), *Facies*, 56(3), 477–481, doi:10.1007/s10347-010-0215-3, 2010a.
- Wendt, J., Kaufmann, B., Belka, Z. and Korn, D.: Carboniferous stratigraphy and depositional environments in the Ahnet Mouydir area (Algerian Sahara): reply to the discussion by Legrand-Blain et al. (DOI: 10.1007/s10347-010-0214-4), *Facies*, 56(3), 477–481, doi:10.1007/s10347-010-0215-3, 2010b.
- Williams, G. D., Powell, C. M. and Cooper, M. A.: Geometry and kinematics of inversion tectonics, *Geol. Soc. Lond. Spec. Publ.*, 44(1), 3–15, doi:10.1144/GSL.SP.1989.044.01.02, 1989.
- Williams, H., Hoffman, P. F., Lewry, J. F., Monger, J. W. H. and Rivers, T.: Anatomy of North America: thematic geologic portrayals of the continent, *Tectonophysics*, 187(1), 117–134, doi:10.1016/0040-1951(91)90416-P, 1991.
- de Wit, M. J. and Linol, B.: Precambrian basement of the Congo Basin and its flanking terrains, in *Geology and Resource Potential of the Congo Basin*, pp. 19–37, Springer., 2015.
- de Wit, M. J., de Ronde, C. E. J., Tredoux, M., Roering, C., Hart, R. J., Armstrong, R. A., Green, R. W. E., Peberdy, E. and Hart, R. A.: Formation of an Archaean continent, *Nature*, 357(6379), 553–562, doi:10.1038/357553a0, 1992.
- Withjack, M. O. and Callaway, S.: Active normal faulting beneath a salt layer: an experimental study of deformation patterns in the cover sequence, *AAPG Bull.*, 84(5), 627–651, 2000.
- Withjack, M. O., Olson, J. and Peterson, E.: Experimental models of extensional forced folds, *AAPG Bull.*, 74(7), 1038–1054, 1990.
- Withjack, M. O., Schlische, R. W. and Olsen, P. E.: Rift-basin structure and its influence on sedimentary systems, *Soc. Sediment. Geol. Spec. Publ.*, (73), 57–81, 2002.
- Woodcock, N. H. and Fischer, M.: Strike-slip duplexes, *J. Struct. Geol.*, 8(7), 725–735, doi:10.1016/0191-8141(86)90021-0, 1986.
- Woodcock, N. H. and Rickards, B.: Transpressive duplex and flower structure: Dent Fault System, NW England, *J. Struct. Geol.*, 25(12), 1981–1992, doi:10.1016/S0191-8141(03)00057-9, 2003.
- Xie, X. and Heller, P.: Plate tectonics and basin subsidence history, *Geol. Soc. Am. Bull.*, 121(1–2), 55–64, doi:10.1130/B26398.1, 2009.

- Yahaya, M. and Lang, J.: Évolution tectono-sédimentaire de l'unité d'Akokan au cours du Viséen dans le bassin de Tim Mersoï (région d'Arlit, Niger), *J. Afr. Earth Sci.*, 31(2), 415–431, doi:10.1016/S0899-5362(00)00097-X, 2000.
- Yahi, N.: Petroleum generation and migration in the Berkine (Ghadames) Basin, Eastern Algeria: an organic geochemical and basin modelling study, Doctoral dissertation, Forschungszentrum, Zentralbibliothek, Jülich., 1999.
- Yahi, N., Schaefer, R. G. and Littke, R.: Petroleum Generation and Accumulation in the Berkine Basin, Eastern Algeria, *AAPG Bull.*, 85(8), 1439–1467, doi:10.1306/8626CAD7-173B-11D7-8645000102C1865D, 2001.
- Ye, J., Chardon, D., Rouby, D., Guillocheau, F., Dall'asta, M., Ferry, J.-N. and Broucke, O.: Paleogeographic and structural evolution of northwestern Africa and its Atlantic margins since the early Mesozoic, *Geosphere*, GES01426.1, doi:10.1130/GES01426.1, 2017.
- Zalan, P. V., Wolff, S., Astolfi, M. A. M., Vieira, I. S., Concelcao, J. C. J., Appi, V. T., Neto, E. V. S., Cerqueira, J. R. and Marques, A.: The Parana Basin, Brazil: Chapter 33: Part II. Selected Analog Interior Cratonic Basins: *Analog Basins*, , 134, 681–708, 1990.
- Zazoun, R. S.: Hercynian deformation in the western Ahnet Basin and Bled El-Mass area, Algerian Sahara: a continuous strain, *J. Afr. Earth Sci.*, 32(4), 869–887, 2001.
- Zazoun, R. S.: The Fadnoun area, Tassili-n-Azdjer, Algeria: Fracture network geometry analysis, *J. Afr. Earth Sci.*, 50(5), 273–285, doi:10.1016/j.jafrearsci.2007.10.001, 2008.
- Zazoun, R. S. and Mahdjoub, Y.: Strain analysis of Late Ordovician tectonic events in the In-Tahouite and Tamadjert Formations (Tassili-n-Ajers area, Algeria), *J. Afr. Earth Sci.*, 60(3), 63–78, doi:10.1016/j.jafrearsci.2011.02.003, 2011.
- Zhao, G., Wilde, S. A., Cawood, P. A. and Sun, M.: Archean blocks and their boundaries in the North China Craton: lithological, geochemical, structural and P–T path constraints and tectonic evolution, *Precambrian Res.*, 107(1–2), 45–73, 2001.
- Ziegler, P. A., Cloetingh, S. and van Wees, J.-D.: Dynamics of intra-plate compressional deformation: the Alpine foreland and other examples, *Tectonophysics*, 252(1), 7–59, doi:10.1016/0040-1951(95)00102-6, 1995.
- Ziegler, P. A., van Wees, J.-D. and Cloetingh, S.: Mechanical controls on collision-related compressional intraplate deformation, *Tectonophysics*, 300(1–4), 103–129, doi:10.1016/S0040-1951(98)00236-4, 1998.
- Zielinski, M.: Reconstruction of thermal history of the Ahnet and Mouydir basins (southern Algeria), Adam Mickiewicz University, Poznan., 2011.
- Zieliński, M.: Conodont thermal alteration patterns in Devonian and Carboniferous rocks of the Ahnet and Mouydir basins (southern Algeria), *Mar. Pet. Geol.*, 38(1), 166–176, 2012.



Titre : Tectonique et architecture des bassins intracratoniques Paléozoïques : Impact sur l'enregistrement sédimentaire et la géométrie des réservoirs associés. Exemple de la marge Nord Gondwanienne

Mots clés : Plate-forme saharienne, Bassins péri-Hoggar, Arches-Bassins structures, héritages structuraux précambriens, hétérogénéité de la lithosphère, terranes, thermo-mécaniques, champs de contraintes lointaines, densité, potentiel isostatique.

Résumé : La plate-forme Saharienne paléozoïque, comprenant les bassins péri-Hoggar (Murzuq, Illizi, Mouydir, Ahnet, Reggane et Tim Mersoï) sont définies comme des bassins intracratoniques. Ils ont été dominés par des mouvements verticaux lents et à grande longueur d'onde, conduisant à de faible vitesse de subsidence (c'est-à-dire environ 10 m/Ma à 50 m/Ma) et à l'accumulation d'une couverture sédimentaire étendue de type plate-forme (environnements de dépôts peu profonds), rythmée par des périodes pulsatiles d'augmentation et de diminution du taux de subsidence probablement déclenchées par des événements géodynamiques régionaux. Les mouvements verticaux de la plate-forme ont créé plusieurs arches également appelés dômes, paléo-topographies (par exemple les arches de la Tihemboka, d'Amguid El Biod, d'Arak-Foum Belrem et de l'Azzel Matti) et des bassins (en forme de synclinal) de différentes longueurs d'onde allant de plusieurs centaines à plus de milliers kilomètres. La persistance d'un ensemble assez uniforme de mouvements verticaux semble contrôler l'architecture des bassins, ce qui semble indiquer un contrôle à grande échelle (i.e. lithosphérique). Ce dernier contrôle spatialement et temporellement la dynamique sédimentaire de dépôt et d'érosion. Plusieurs périodes d'érosion majeures ont considérablement tronqué les sédiments préexistants sur de vastes zones, produisant des discordances régionales, restreintes et amalgamées sur les arches, qui séparent la couverture sédimentaire de la plateforme. À travers une approche intégrée multidisciplinaire originale allant d'une analyse géologique de bassin, associant le substrat et l'architecture de bassin à une modélisation thermomécanique numérique de la lithosphère, cette étude a permis de décrypter les facteurs de forçage des bassins intracratoniques de la plate-forme saharienne (bassins péri-Hoggar).

La plate-forme Saharienne paléozoïque, comprenant les bassins péri-Hoggar (Murzuq, Illizi, Mouydir, Ahnet, Reggane et Tim Mersoï) sont définies comme des bassins intracratoniques. Ils ont été dominés par des mouvements verticaux lents et à grande longueur d'onde, conduisant à de faible vitesse de subsidence (c'est-à-dire environ 10 m/Ma à 50 m/Ma) et à l'accumulation d'une couverture sédimentaire étendue de type plate-forme (environnements de dépôts peu profonds), rythmée par des périodes pulsatiles d'augmentation et de diminution du taux de subsidence probablement déclenchées par des événements géodynamiques régionaux. Les mouvements verticaux de la plate-forme ont créé plusieurs arches également appelés dômes, paléo-topographies (par exemple les arches de la Tihemboka, d'Amguid El Biod, d'Arak-Foum Belrem et de l'Azzel Matti) et des bassins (en forme de synclinal) de différentes longueurs d'onde allant de plusieurs centaines à plus de milliers kilomètres. La persistance d'un ensemble assez uniforme de mouvements verticaux semble contrôler l'architecture des bassins, ce qui semble indiquer un contrôle à grande échelle (i.e. lithosphérique). Ce dernier contrôle spatialement et temporellement la dynamique sédimentaire de dépôt et d'érosion. Plusieurs périodes d'érosion majeures ont considérablement tronqué les sédiments préexistants sur de vastes zones, produisant des discordances régionales, restreintes et amalgamées sur les arches, qui séparent la couverture sédimentaire de la plateforme. À travers une approche intégrée multidisciplinaire originale allant d'une analyse géologique de bassin, associant le substrat et l'architecture de bassin à une modélisation thermomécanique numérique de la lithosphère, cette étude a permis de décrypter les facteurs de forçage des bassins intracratoniques de la plate-forme saharienne (bassins péri-Hoggar).



Title : Architecture and tectonic of Paleozoic intracratonic Basins : Impact on the sedimentary record and associated geometries. Example of peri-Hoggar Basins (North Gondwana)

Keywords : Saharan platform, peri-Hoggar Basins, Arches-Basins, Precambrian structural heritages, lithosphere heterogeneity, terranes, thermo-mechanical, far field stresses, density, potential isostatic equilibrium.

Abstract : The Paleozoic Saharan platform including the peri-Hoggar Basins (i.e. Murzuq, Illizi, Mouydir, Ahnet, Reggane and Tim Mersoï basins) are defined as intracraonic basins. Their histories have been dominated by slow long-wavelength vertical motions leading to overall low subsidence rate (i.e ca. 10 m/Ma to 50 m/Ma) and accumulation of an extensive cover of platformal sediments (i.e. shallow deposits environments), rhythmized by pulsatile periods of increasing and decreasing rate probably triggered by regional geodynamic events. The vertical motions of the platform produced several arches also called domes, swells, highs, ridges (e.g. the Tihemboka, Amguid El Biod, Arak-Foum Belrem and Azzel Matti Arches) and basins (syncline-shaped) with different wavelengths going from several hundred to more than a thousand kilometres. The persistence of a rather uniform pattern of vertical motions seems to control the architecture of the basins indicating a large-scale control (i.e. lithospheric). This latter controls spatially and temporally the deposition and the erosion dynamics. Several major erosion events significantly truncated the pre-existing sediments over wide areas, producing regional unconformities, especially restricted and amalgamated on arches, which separate the platformal cover into divisions. Through an original multidisciplinary integrated approach going from a geological basin analysis, coupling the substrate and the basin architecture to a numerical thermo-mechanical modelling of the lithosphere, this study has led to decipher the forcing factors of the intracratonic basins of the Saharan platform.

The Paleozoic Saharan platform including the peri-Hoggar Basins (i.e. Murzuq, Illizi, Mouydir, Ahnet, Reggane and Tim Mersoï basins) are defined as intracraonic basins. Their histories have been dominated by slow long-wavelength vertical motions leading to overall low subsidence rate (i.e ca. 10 m/Ma to 50 m/Ma) and accumulation of an extensive cover of platformal sediments (i.e. shallow deposits environments), rhythmized by pulsatile periods of increasing and decreasing rate probably triggered by regional geodynamic events. The vertical motions of the platform produced several arches also called domes, swells, highs, ridges (e.g. the Tihemboka, Amguid El Biod, Arak-Foum Belrem and Azzel Matti Arches) and basins (syncline-shaped) with different wavelengths going from several hundred to more than a thousand kilometres. The persistence of a rather uniform pattern of vertical motions seems to control the architecture of the basins indicating a large-scale control (i.e. lithospheric). This latter controls spatially and temporally the deposition and the erosion dynamics. Several major erosion events significantly truncated the pre-existing sediments over wide areas, producing regional unconformities, especially restricted and amalgamated on arches, which separate the platformal cover into divisions. Through an original multidisciplinary integrated approach going from a geological basin analysis, coupling the substrate and the basin architecture to a numerical thermo-mechanical modelling of the lithosphere, this study has led to decipher the forcing factors of the intracratonic basins of the Saharan platform.